EVALUATING CARBON DIOXIDE STORAGE IN A VARIETY OF SOUTH AFRICAN COALS TO ESTIMATE THE POTENTIAL FOR ENHANCED METHANE RECOVERY

By

Kasturie Premlall

A Thesis submitted to the Faculty of Engineering and the Built Environment, University of the Witwatersrand, in fulfilment of the requirements for the degree of Doctor of Philosophy

in the

School of Chemical and Metallurgical Engineering

UNIVERSITY OF WITWATERSRAND

Johannesburg, 2019

DECLARATION

I, Kasturie Premlall, declare that the thesis entitled:

“EVALUATING CARBON DIOXIDE STORAGE IN A VARIETY OF SOUTH AFRICAN COALS TO ESTIMATE THE POTENTIAL FOR ENHANCED METHANE RECOVERY”

is my own work and that all sources I have used or quoted have been indicated and acknowledged by means of a comprehensive reference list.

Signature: ……

Date: ……...

ABSTRACT

Due to the energy- and carbon-intensive economic structure of South Africa (SA), the country has become one of the biggest contributors to greenhouse gas emissions, emitting more CO_2 than any other African country. The ratio of greenhouse gas emissions compared to per capita economic benefit, the so called carbon intensity of the economy, is amongst the highest in the world.

Carbon capture and storage (CCS) seems to be the most immediate form of action that can be implemented with the possibility of instantaneous reduction of CO_2. The injection of CO_2 into deep-unmineable coal seams, although not commercially viable for coal production, is a possible mitigation option under CCS for permanent underground storage of CO_2. As a spin-off, useful coal-bed CH_4, referred to as enhanced coal bed CH_4 (ECBM), could be extracted from the coal seam following CO_2 injection. In SA it has been estimated that approximately 1.2 Gt of CO_2 could be stored in the coalfields. Although not currently the preferred option for geological storage, coalfields provide the largest onshore CO_2 storage possibility.

The current research project aimed to study the fundamental differences in CO_2 adsorption in a variety of SA coal samples in order to access the CO_2 sorption capacities and secondly to evaluate the potential CH_4 characteristics of SA coals. The investigation aimed to identify the fundamental differences around the effects of increased pressure under simulated in-seam conditions including super-critical pressures up to ~90 bar for gaseous and supercritical CO_2 injection. The effects on CO_2 adsorption with regard to the difference in coal moisture contents, simulated in the range from ~0.5 – 4.4% and the influence of increased temperatures in the range of 35 to 55 ˚C were carried out on ten (10) SA coals taking into consideration differences in coal properties, samples with varying rank, ash and maceral compositions were sourced for this research. Then secondly, to evaluate the desorption potential of CH_4 for seven (7) selected SA coals. A High Pressure Volumetric adsorption system (HPVAS) was successfully designed and constructed in order to conduct experimental tests to generate the adsorption isotherms for the various parameters tested.

Results presented show comparable results with published literature in terms of the degree of variance in coal properties (with respect to rank, maceral and mineral content, ash

contents and the effects of moisture, and temperature variance) and the uptake of CO_2. Higher rank coals have a greater CO_2 absorption propensity, whereas lower rank bituminous coals tend to exhibit lesser CO_2 uptake, however, this is dependent on the coals' petrographic composition. It was clear that samples in the range greater than a vitrinite reflectance of 0.7% (R_oV_{mr}) exhibited increased CO_2 uptake due to larger macro, increasing meso porosity and micro-pore volumes. Findings related to coal properties; revealed that coals with a higher ash content exhibited a negating effect with regard to enhanced CO_2 adsorption. On average, for a 1% increase in ash content in HRC and MRC coals, a decrease of CO_2 adsorption capacity of 1.1 mmol/g and 0.018 mmol/g is observed respectively. While for maceral composition these findings suggest that a specific or ideal ratio between *only* the maceral components, in similar rank coals, is the controlling factor for best CO_2 adsorption required.

In terms of addressing the adsorption parameters, such as super-critical pressure, temperature and moisture variations inherent in natural coal seams, etc., it was determined that with increased pressure, more adsorption takes place for most coal types. A very positive correlation was found to exist between adsorption of CO_2 and desorption of CH_4, with increased pressure injections, ranging from sub-critical to super critical pressures, exhibiting increased sorption results, irrespective of coal moisture or temperature effects.

From these findings for simulated conditions regarding the effects of coal seam moisture and temperature variations, it has been concluded that results displayed an obvious decrease in CO_2 sorption ranging from sub-critical to supercritical pressures overall. The decrease in CO_2 sorption was as much as 77% from dry (0%) to the maximum moisture simulated value of ~4.4%. Sorption decreased almost linearly for every 1% of coal moisture increase, until the maximum coal saturation was approached at around 4%. Sorption results relating to increased temperature also displayed an inverse relationship, and hence lower overall CO_2 sorption capacities were calculated. The heats of adsorption for these coals were found to be between 21.9 and 39.9 kJ/mol confirming the nature of adsorption to be physical. Results confirm that the calculated heat of adsorption (KJ/mol) and the adsorption capacity (mmol/g) are positively correlative.

For investigations pertaining to CH_4 desorption for CH_4 saturated simulated coals (CH_4 added to and then removed from coal samples due to the unavailability of freshly cored coal samples), it was observed that CO_2 uptake by pressurized injection for low - high pressures certainly enhances CH_4 desorption rate. Results revealed that incremental CO_2 injection pressures yielded higher CH_4 desorption rates, for both the HRC and MRC coals.

Generally there was an observed increase in the rate of CH_4 desorbed for all coals tested at 55 ^oC as compared to 35 ^oC. This can as well be attributed to the fact that the increase in temperature causes the adsorbed CH_4 molecules to vibrate more due to the increased kinetic energy of the molecules. This consequently leads to ease of desorption when CO_2 is pumped under pressure into the coal structure, which clearly favours ECBM potentials.

Some very good findings have been highlighted in the thesis from a SA coal perspective, and certainly serve as a very good starting point for further investigations pertaining to CO_2, CH_4, and coal interactions. However, from the vast literature already published globally, it can be seen that much more needs to be done in terms of addressing coal-CO_2-CH_4 research from a SA perspective, and indeed CCS in SA in general. It is apparent that the results and sum of the key findings presented in this thesis, are of importance for the selectivity and technical modelling for CO_2 onshore coalbed storage and ECBM projects to be implemented in SA in the near future so as to meet the demands required to reduce CO_2 emissions in SA as part of the global community.

CONTRIBUTIONS FROM THIS STUDY

Conference presentations and papers emanating from this research:

1. **Premlall, K.** and Wagner, N., J**.,** 2015. *Laboratory experiments to determine best potential for cyclic supercritical CO_2 injections in SA coals to evaluate CH_4 desorption for ECBM potential*, ICCS&T (International Conference on Coal Science & Technology), Hosted by: Engineers Australia and IChemE, 27th September – 2nd October 2015, Melbourne, Australia.

2. **Premlall, K.** and Wagner, N., J*.,* 2015. *Laboratory experiment to determine the feasibility of cyclic CO_2 injections in SA coals to evaluate CH_4 desorption for ECBM potential*, 3rd APOEEC (African Publics Officials Energy and Environment Conference 2015), 3rd – 5th June 2015, St. Georges Hotel and Convention Centre, Hosted by CEEP (Centre for Electric Energy and Power), Tshwane University of Technology, Pretoria, South Africa, Proceedings [*ISBN: 978-0-620-65945-1].*

3. **Premlall, K.,** Wagner, N. J., 2014, *Evaluating sorption capacity of a myriad of South African Coal types: Comparative study of sub-critical to supercritical pressures*, *Energy Procedia: Journal, peer review SINTEF Energi AS*; 51: pp: 299-307. DOI: 10.1016/j.egypro.2014.07.036. [ISBN: 978-1-63439-249-5].

4. **Premlall, K.** and Wagner, N., J**.,** 2013. ***'****Evaluating Sorption capacity of a myriad of South African Coal types: Comparative Study of Sub-critical to Supercritical pressures*', ICCS&T: International Conference on Clean Coal Technology, 29th September – 3rd October 2013, Penn Stater Hotel, Pennsylvania State University, USA.

5. **Premlall, K.** and Wagner, N., J**.,** 2013**. *'Evaluating Sorption capacity of a myriad of South African Coal types: Comparative Study of Sub-critical to Supercritical pressures*', 7th Trondheim Conference on CCS (Carbon Capture & storage) (HOST: SINTEF), 4th – 9th June 2013, Trondheim, Norway.

6. **Premlall, K** and Mabuza, MM, 2012. *Comparing CO_2 uptake capacity for different South African coal types for low-high pressure adsorption*, 5th International Conference of Appropriate Technology (ICAT) HOST(S), Department of Science and Technology: Republic of South Africa, 20th to 24th November 2012, St. George Hotel and Convention Centre, Pretoria, South Africa.

7. **Premlall, K.**, Mabuza, M. M and Wagner, N. J., 2011. *Adsorption capacity of CO_2 on moisture simulated SA Bituminous coal type,* SACCS Week (South African carbon Capture & Storage), Gallagher Convention Centre, 24th – 28th October 2011, Pretoria, South Africa.

8. **Premlall, K.** and Mahlobo, M., 2011. *Adsorption of CO_2 to simulate ECBM (Enhanced Coalbed Methane),* SACCS Week (South African Carbon Capture & Storage), Gallagher Convention Centre, 24th – 28th October 2011, Pretoria, South Africa.

ACKNOWLEDGEMENTS

The authors' sincere gratitude and appreciation goes to the following people and organizations for their assistance during the course of this research work:

- Prof. J. H. Potgieter for the constant support and motivation he has given me over the past 15 years that I have known him, as HOD and supervisor. He is truly a great inspiration and I can truly say that I would have not come this far without his encouragement, guidance and advice.

- Prof. Nicola, J. Wagner (WITS), for all the motivation, lots and lots of patience and incredible and abundant supervision she has given me during this project. Also for her expertise in conducting the petrographic analysis on my samples. I am eternally grateful for this opportunity and for her having introduced me to an exciting and very current, yet pertinent research field, which is so complex and ever evolving.

- To my HOD, Prof Maurice S. Onyango (TUT) for support and encouragement, thank you and my most sincere gratitude to you for inspiration throughout this study!

- Mr M. M. Mabuza for continued support and assistance with running equipment, laboratory maintenance and his commitment to the success of CCS research at TUT. He has certainly motivated many students through his dedication to his work.

- Undergraduate students: Mr. MGH Mahlobo, Mr. MG Shongwe, Mr. K. Masima, Mr. TT Manjoro and Ms KDT Lukhele from TUT.

- SANERI (South African Energy Research Institute) for the funding rendered for the first part of this project. (Project AFF-06/07-138).

- NRF (National Research Foundation – R-I-T) for funding received towards capacity building and training at TUT and for all funding received ensuring the successful completion of this project.

- IEA Greenhouse Gas Association for awarding me an opportunity and sponsoring the 2008 Summer School held in Vancouver Island, Canada, 21st – 28th August, 2008.

- The Faculty of Engineering and the Built Environment: Tshwane University of Technology for granting start-up funds towards this research project.

- Dr W. Augustyn (CHEMVAK) for his assistance with the design, construction and commissioning of the High pressure adsorption test equipment, as well as continued equipment upgrades and service.

- Prof Hein Neomagus, Mr. Burgert Hattingh and Mr. Mok Roberts for supplying certain coal samples and Mr. G. Okolo for conducting BET analysis on coals, all from North-West University (NWU), School of Chemical and Minerals Engineering for their assistance.

- Mr Johann De Lange from the Department of Mechanical Engineering, Tshwane University of Technology, for assistance with welding and securing of gas cylinders.

- Mr Gerhard Swanepoel (AFROX) for assistance with gas requirements at short notice.

- Mr Johannes De Vries, (FSATIE – TUT) for assistance with digital conversion of equipment – data logging system.

- Mr Eric Botes (WIKA) for assistance with supply and installation of pressure transducers, readout equipment for the High Pressure Volumetric Adsorption System (HPVAS).
- Mr Japie Stoltz (UIS) for coal sample analysis, proximate and ultimate.

- Mr Kevin Reeves (ChromeSpec) for supply, installation and training of the SRI Gas Chromatograph (GC).

- The library staff at TUT (Arcadia Campus), Mrs. Maria Malete and Mrs. Maggie Mashilo (Pretoria Campus) and Mr. Mishack Modiba (Pretoria Campus) for their dedicated assistance with literature searches.

- The Department of Chemical, Metallurgical and Materials Engineering, in the Faculty of Engineering and the Built Environment at Tshwane University of Technology for the use of laboratory space, equipment and materials during the course of this research project.

- The School of Chemical & Metallurgical Engineering, University of Witwatersrand, for the use of equipment and materials during the course of this project. Wits URC and SPARC Fund, and The School of Chemical and Metallurgical Engineering, Wits, for supporting the project.

- The Department of Chemistry, in the Faculty of Sciences at Tshwane University of Technology for the use of equipment (TGA) during the course of this research project.

Table of Contents

LIST OF FIGURES

Page

LIST OF TABLES

Page

NOMENCLATURE

T_c	critical temperature	K
P_c	critical pressure	bar
ΔG_{ad}	free energy change	kJ/mol
ΔH_{ad}	change in enthalpy	kJ/mol
T	temperature	K
ΔS	entropy change	kJ/mol.K
V_{gas}	volume of adsorbed gas	cm^3
P_{gas}	gas pressure	bar
V_g	volume of the gas	cm^3
T	thickness	m
adb	Air dried basis	adb
daf	Dry ash free	daf
mmf	Mineral matter free	mmf
n^{σ}	amount of gas adsorbed	mmol
$\rho(z)$	density profile	g/cm^3
ρ_b	bulk phase density	g/cm^3
V_a	adsorbed phase volume	cm^3
n^s	total mass confined in the adsorbed phase	g
ρ_a	adsorbed phase density	g/cm^3
σ_{ff}	intermolecular distance	nm
P	pressure	bar
n_t	total amount of gas adsorbed	mmol/g-coal
M	molecular weight	g/mol
P_s	saturation pressure	bar
D	pore diameter	nm
$d_0{}^a$	pore width for slit-type or the pore diameter for cylindrical pore	nm
T_s	surface temperature	K
P^0	saturation pressure	bar
N_s	amount of gas adsorbed	mmol/g-coal
N_{sm}	monolayer coverage	mmol/g-coal
V_m	maximum amount of adsorption	cm^3/g-coal
B	Langmuir constant	bar^{-1}
Y	mole fraction	dimensionless
P_0	saturation pressure	bar

v_m	monolayer adsorbed gas quantity	cm^3/g-coal
C	BET constant	
V	adsorbed gas quantity	cm^3/g-coal
W	volume of adsorbed gas at equilibrium	cm^3
W_0	micropore volume	cm^3
B	sorbate affinity coefficient	
E	characteristic energy	
V_x	valve number s	
R	universal gas constant	cm^3.bar/mol.K
N	small integer	
R_0	Vitrinite Reflectance	Vol%
R_oV_{mr}	Mean vitrinite reflectance	Vol%
N	number of moles	mol
Z	gas compressibility factor	dimensionless
P_i	initial pressure	bar
P_f	final pressure	bar
$V_{sample.Cell}$	volume of the sample cell	cm^3
V_{sample}	volume of the sample	cm^3
V_{void}	void volume	cm^3
ρ_s	density of the sample	g/cm^3
Ms	sample mass	g
D	Diffusion coefficient	m^2/s
n_{sorbed}^{excess}	excess amount of adsorbed gas	mmol/g-coal
n_{total}	total amount of gas present in the system (injected)	mmol
ρ_{eq}	molar equilibrium density of the gas	mmol/cm^3
ρ_{gas}	molar density of the gas	mmol/cm^3
$n_{sorbed}^{absolute}$	absolute adsorbed amount of gas	mmol/g-coal
$\rho_{adsorbed}$	molar adsorbed phase density	mmol/cm^3
$n_{adsorbed}$	moles of gas adsorbed	mmol
C_{inj}	concentration of gas injected	g/cm^3
C_{unad}	unadsorbed concentration of gas	g/cm^3

ACRONYMS

CCS	Carbon Capture and Storage/Sequestration
CCUS	Carbon Capture, Utilisation and Storage
BET	Brunauer-Emmett-Teller
D-A	Dubinin-Astakhov
D-R	Dubinin-Radushkevich
BOM	Bureau of Meteorology

GCCSI	Global Carbon Capture and Storage Institute
GC	Gas Chromatograph
IPCC	Intergovernmental Panel on Climate Change
EU	European Union
EC	European Commission
FTIR	Fourier Transmission Infra-red
HPVAS	High Pressure volumetric Adsorption System
GHG	Greenhouse Gas
IP	Industrial Processes
CDM	Clean Development Mechanism
JI	Joint Implementation
UNFCCC	United Nations Framework on Convention on Climate Change
LTMS	Long Term Mitigation Scenarios
USA	United States of America
COP	Conference of the Parties
DAI	Dangerous Anthropogenic Interference
IEA	International Energy Agency
UN	United Nations
UNIDO	Industrial Development Organization
EOR	Enhanced Oil Recovery
MMV	Measuring, Monitoring and Verifying
ICCS	Industrial Carbon Capture and Sequestration
LPG	Liquefied Petroleum Gas
CBM	Coalbed Methane
CO2CRC	Cooperative Research Centre for Greenhouse Gas Technologies
ECBM	Enhanced Coalbed Methane
FTIR	Fourier Transform Infrared Spectroscopy
NMR	Nuclear Magnetic Resonance
TEM	Transmission Electron Microscopy
ICCP	International Climate Change Partnership
VOC	Volatile Organic Compound
IUPAC	International Union of Pure and Applied Chemistry
GSC	Gas Sorption Capacity
HPVAS	High Pressure CO_2 Volumetric Adsorption System
GC	Gas Chromatograph
ISO	International Organization for Standardization
SABS	South African Bureau of Standards
WEC	World Energy Council

TUT	Tshwane University of Technology
WITS	University of Witwatersrand

UNITS

ppm	parts per million
Gt	Gigatonne
%	Percentage
°C	degree celcius
Mt	Megaton
yr^{-1}	per year
vol%	volume percentage
MTPA	million tonnes per annum
Tg	Teragram
Kg	Kilogram
MPa	Megapascal
m^3	cubic meter
g/cm^3	Density
GtC	gigatonne of carbon
Scm	standard cubic meter
Km	Kilometre
Atm	Atmosphere
m	Meter
pH	potential hydrogen
mD	Millidarcy
Scf	standard cubic foot
m^2	square meter
nm^2	square nanometer
mmol	Milli mole
mg	Milligram
mm	Millimetre
Mm	Micrometer
cm^3	cubic centimetre
G	Gram
Min	Minutes
hrs	Hours
mL	Millilitre
L	Litre

CHEMICAL FORMULAE

CO_2	Carbon dioxide
CH_4	Methane
CO	carbon monoxide
N_2	Nitrogen
O_2	Oxygen
S	Sulphur
NO_x	oxides of nitrogen
SO_2	sulphur dioxide
HCl & HF	hydrogen halides
H_2	Hydrogen
C	Carbon
H_2O	Water
H_2S	hydrogen sulphide
He	Helium

CHAPTER 1

1. INTRODUCTION

Background and Motivation

For more than a century, scientists have measured a steady build-up of greenhouse gases in the atmosphere as a result of the burning of fossil fuels. The accumulation of these gases in the upper atmosphere traps solar radiation, which then increases Earth's atmospheric and oceanic temperatures. There is an extensive amount of evidence indicating that the Earth's climate has warmed during the past century, outside of the normal variability of temperature changes over the last thousand years (Weubbles and Jain, 2001). Increasing global greenhouse gas levels have led to "global climate change" (previously referred to as "global warming"). Many research studies indicate that a continued rise in average global temperatures will adversely affect the Earth's climate, which could lead to dramatic—even catastrophic—changes in weather patterns around the world (Weubbles and Jain, 2001). Globally weather patterns indeed appear to become more extreme.

Carbon dioxide (CO_2) is a major greenhouse gas (GHG), and increasing concentrations in the atmosphere will result in increased temperatures. CO_2 levels have been shown to be rapidly increasing relative to historical trends, specifically over the last few decades. This has largely been attributed to the burning of fossil fuels, including coal, oil, and natural gas. The current estimated amount of CO_2 in the atmosphere is approximately more than 400 ppm, compared to 260 ppm during the preindustrial era (Halmann and Steinberg, 1999). Methane (CH_4), another GHG, is a fraction of the amount of CO_2, but is approximately 25 times more (over a 100 year span) effective as a GHG than CO_2, and thus is also an important GHG affecting climate change (Weubbles and Jain, 2001).

The World Energy Council (WEC) study on "*World Coal Perspectives to 2030"* concluded that coal will continue to be an expanding, cheap foundation for economic and social development (globally). According to the South African Mining Institute (SAMI 2005/2006), coal will continue to make a significant contribution to eradicating energy poverty due to the vast and well distributed resource base. In addition, coal will become increasingly clean at a bearable cost in terms of technological sophistication and at little cost in terms of

international technology transfer and research and development in CO_2 sequestration (SAMI, 2005/2006).

In SA, coal is the predominant form of energy, and, due to abundant coal reserves, this is likely to remain so for the foreseeable future. Over 90% of SA's primary needs are met by coal; those of electricity generation from coal, petrochemical products from coal gasification, cement works, oil refineries, iron and steel production, are all dependant on coal feedstocks. All of these industrial processes emit large amounts of CO_2 gas. According to the DEAT (Department of Environmental Affairs and Tourism) reporting, the energy sector accounted for 91.1% of the total CO_2 emissions in 1994, and showed a slight increase in a study done in 2007 (DEAT, 2007).

Although SA is still considered a developing country, it is amongst the world's high CO_2 emitters, currently ranked at number 12 in the world. The country emits over 400-million tons of CO_2 a year, which represents 1% of total CO_2 emissions on a global scale (Hietkamp *et al.,* 2004 and Viljoen *et al.,* 2010). With the likes of SASOL coal-to–liquid processes and the advent of new coal-fired electricity generating stations built by ESKOM (Medupi and Kusela), SA's emissions are more than likely to rise still further. South Africa is predicted to respond negatively to climate change, specifically due to changes in rainfall patterns.

Due to the potentially disastrous consequences of global climate change, the global scientific community has proposed a number of mitigation scenarios to reduce CO_2 emissions. One of these methods is CO_2 sequestration, or CO_2 capture, utlisation and storage (CCUS), by means of capturing and utilizing, or storing CO_2. Carbon dioxide storage is defined as the placement of CO_2 into a repository in such a way that it will remain stored (or sequestered) permanently. The Inter-governmental Panel for Climate Change (IPCC, 2005) defines CO_2 capture as a process consisting of the separation of CO_2 from industrial and energy-related sources (major point sources), transport to a storage location for long term isolation from the atmosphere. CCS is done as an attempt to mitigate against the effects of released CO_2 on the atmosphere, thus stabilizing atmospheric greenhouse gas concentrations. Put simply, it involves storing emissions of CO_2 securely underground rather than releasing it to the atmosphere (Holloway, 1993; IEA GHG, 2007). This method

of geological storage is estimated to hold the CO_2 in place for geologically significant periods of time, as depicted in Figure 1.1.

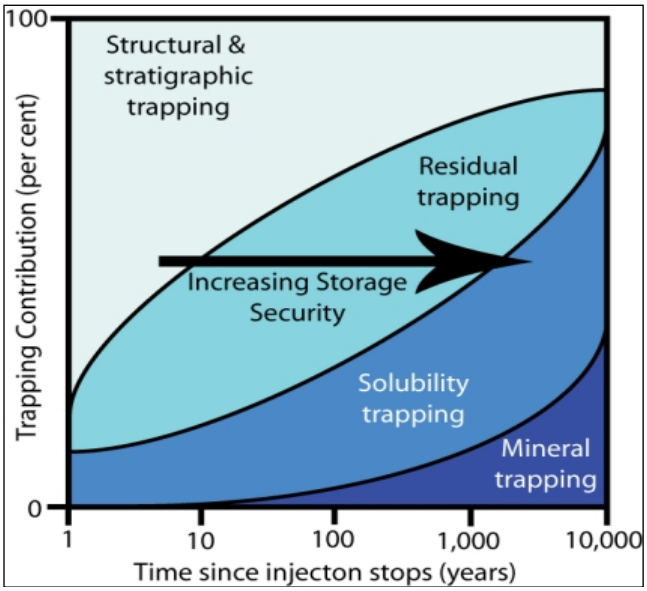

Figure 1.1 CO_2 Storage Mechanism showing integrity of long term storage capability.
(IPCC, 2005)

In terms of CCUS options, deep ocean floors, terrestrial ecosystems, and geological formations (such as deep saline formations, depleted oil and gas reservoirs and coal seams) are being considered as suitable CO_2 sinks globally (Chemical Technology, 2006). CO_2 storage in oil, gas, and coal reserves has potential value added benefits for enhanced oil recovery (EOR) and coal-bed CH_4 (ECBM) extraction. These are the only proposed mechanisms for CO_2 storage that would produce an economically valuable product and thus offset the costs of CCS.

The successful storage of CO_2 in geological formations has been demonstrated over a period of 20 years, with or without economic benefit. The largest application for EOR in North America, which involved approximately 30 million tons of CO_2 per year and several major CO_2 pipelines (Simbeck, 2004). Currently 70 000 tons of CO_2 per year are injected in a deep coal seam in the United States, and, a similar project, at a smaller scale was also developed in Canada (Stevens & Gale, 2000). The European RECOPOL project has demonstrated the technical feasibility of CO_2 injection into typical European Carboniferous

coal seams, which, in conjunction with a follow up project by Delft University of Technology (The Netherlands) and RWTH Aachen University (Germany) within RECOPOL and the national CO2TRAP project, have provided fundamental information on the interaction of Northern-Hemisphere coals with CO_2 and CH_4 under in-situ conditions (Goodman *et al.,* 2004).

A successful demonstration project in Africa (the only one currently) is that of the In Salah CH_4 Gas for Electricity Generation project in Algeria, where 1 million tonnes of CO_2 per year (equivalent to the emissions from a quarter of a million cars!) is being stored in a producing gas field. The natural gas produced from the deep rock formations is a mixture of CH_4 and CO_2; CO_2 is separated and re-injected underground. The cap-rock that kept the natural gas in the rock formation for millions of years keeps the liquid CO_2 stored in the underground reservoir (IEA Greenhouse Gas R&D Programme, 2007).

The injection of CO_2 into deep-unminable coal seams not commercially viable for future coal production, is a possible mitigation option under CCUS for permanent underground storage of CO_2. This sequestration option does not compete with agriculture, forestry, or other industries (Bachu, 2000; Bachu, 2003). In addition, it is the only significant sink-orientated option that is available to landlocked major producers of CO_2, such as several industrial provinces in South Africa. Krooss *et al.* (2002) concluded that CO_2 can access the finest porosity and absorb firmly to coal, with minimal chances of its later release. However, there remains generally a lack of fundamental understanding as to the actual uptake and retention mechanisms by the various components in coal.

There is generally a lack of CO_2 adsorption data on SA coals; most of the adsorption data currently available pertain to CO_2 adsorption studies for Northern Hemisphere and Australian coals (Bustin *&* Clarkson, 1996; Gentzis, 2000; Reeves *et al*., 2003; Busch *et al*., 2002(a) and Busch *et al*., 2002(b); Krooss *et* al., 2002; Busch *et al*., 2003; Good man *et al.,* 2007; Chalmers & Bustin, 2007; Faiz *et* al., 2007; Saghafi *et al*., 2007; Saghafi *et al*., 2008; Day *et al.,* 2008; Day *et al*., 2008(a); Day *et* al., 2008(b); Gensterblum *et al.,* 2009; Ozdemir & Schroeder, 2009; Florentin *et al*., 2009; Gensterblum *et al*., 2010; Perera *et al*., 2011; Masterlez *et al*., 2012). In order to develop the potential for CCUS in SA coal seams, there is a need to conduct studies on the CO_2 uptake behaviour of South African coals.

This aspect is the focus of the current research, and will aid in expanding the CO_2 CCUS database that is already being created for South Africa (Viljoen *et al.,* 2010).

Carbon dioxide can be stored in coal seams without extraction, but there is no revenue to offset the costs of CCS in this instance, and the coal seam would be sterilized, potentially rendering it useless for future extraction. Whilst coal-bed CH_4 (CBM) recovery technology is commercially available and is currently being practiced in some localities globally to produce electricity or heating fuel, ECBM extraction using CO_2 is still at a demonstration stage on the African continent (Ecoal, 2002). Obviously there are several key geological requirements to ensure the success of CO_2 storage with ECBM recovery as a commercial sequestration option, including 1) the depth and permeability of the coal seam; 2) the porosity of the coal; and 3) the CH_4 saturation levels.

From experimental research conducted internationally, it is generally accepted that coal can absorb more CO_2 than CH_4, and that CO_2 is preferentially absorbed onto the coal structure over CH_4 (Masterlez *et al.,* 2004). As reported in a Chemical Technology (2006) article, at least two to three molecules of CO_2 are sequestered for each molecule of CH_4 extracted, and provided the coal is never mined, the CO_2 should be sequestered permanently. Saghafi *et al.* (2006) concluded that the CO_2 storage capacity for the Australian coals tested is about twice that of CH_4 and six times that of N_2, and the diffusivity of CO_2 in coal is about twice that of CH_4, in moles per gram of coal tested. The maximum quantity of gas that can be stored in a given coal is mainly a function of its absorption capacity, although pressure can significantly increase the amount of gas absorbed, as was shown by Mazumder (2007). However, the sorption process can only be successful if the pores are not saturated with water (Saghafi *et al.*, 2007); CBM and ECBM processes pump significant amounts of water to surface prior and during CH_4 gas extraction.

Key research and development questions pertaining to CCUS are discussed in the Chemical Technology (2006) article, including the long-term stability of stored CO_2, lack of fundamental understanding of CO_2 uptake and retention mechanisms by various components in the coal, and quantities of CH_4 that can be potentially released. Many researchers do not provide a precise answer to the question as to how sorption of mixtures of CO_2 and CH_4 might proceed, or which of these two gases will dominate in a desorbed

gas. For this reason the possibility to predicate CH_4 recovery from coal seams based on the current knowledge of sorptive-diffusive properties of coals and on the competitive sorption of CO_2, CH_4, and / or mixtures of these two gases seem a most interesting subject for study, especially from a South African perspective. These issues and questions, amongst others, need to be addressed by means of extensive research in relation to the South African context for CCUS in coal seams, and potential ECBM. It is crucial that these findings be made available in order to realize the potential that the application of such technology holds. This project is thus extremely relevant considering the number of challenges that SA is facing pertaining to CO_2 emissions and climate change.

From a legal standpoint, as a further motivation for this research project, in March 2002 SA became one of the countries to sign the agreement to meet the KYOTO PROTOCOL (the only legally binding agreement for GHG emissions worldwide). The agreement is based on the reduction of CO_2 emissions by 5.2% before 2012 (for signatures in the A group). SA is in the early stages of developing climate change mitigation policy, with only policy intentions and directions existing at this stage. The major components of this policy direction include: the First and Second National Communications to the United Nations Framework Convention on Climate Change (UNFCCC); 2004 Climate Change Response Strategy; the 2005 Technology Needs Assessment; the Long Term Mitigation Scenarios (LTMS) process; the African National Congress (ANC)'s 2007 Polokwane Resolution on Climate Change; the 2008 Cabinet Response to the LTMS, outlining a strategic mitigation vision based on a 'peak, plateau and decline' trajectory; the March 2009 Climate Policy Summit Discussion Document; and the international commitments made at the 2009 Copenhagen Conference of the Parties (COP) to the Kyoto Protocol (Winkler *et al.,* 2010).

In November 2011, UNFCCC COP 17 was held in Durban, South Africa. South Africa and thirty seven other countries signed for a second commitment period of the KYOTO PROTOCOL starting January 2012 to 2017 or 2020 (decided at COP 18 in Qatar) which further commits to working towards emission reduction globally (Groenewald, 2011). The ***National White Paper on Climate Change Response*** was also recently gazetted, which will look at the monitoring and evaluation of carbon emission and the execution of mitigating emissions in South Africa. The White Paper makes a bold leap and states that after 2025

SA emissions will level out for 10 years before declining in absolute terms by 2036 (Groenewald, 2011).

UNFCCC COP 19 was held in Warsaw, Poland from 11 to 23 November 2013 (http://unfccc.int/meetings/warsaw_nov_2013/session/7767.php). This was then followed by COP 20, which was held in Lima, Peru from 1- 14 December 2014, which featured the first-ever "multilateral assessment" of mitigation efforts by developed countries, part of a new set of transparency procedures established under the 2010 Cancún Agreements. Seventeen developed country parties, including the United States, the European Union, several EU member states, and New Zealand, provided brief presentations to the Subsidiary Body on Implementation (SBI) on progress toward achieving their 2020 emission pledges, and fielded questions from other parties (http://www.c2es.org/international/negotiations/cop-20-lima/summary).

COP 21 was held in Paris in December 2015 (Røkke, 2015) and more recently COP 22 concluded its meeting in Marrakech, Morocco, from the 7-18 November, 2016, with a range of decisions around implementing the Paris Agreement. Following the new global agreement last December, the threshold of signatories for it to enter into force was passed less than 12 months after being agreed and far earlier than expected. This has added pressure to quickly develop the necessary rules and procedures to support the Agreement. Morocco saw meetings under the Convention, as well as the Kyoto Protocol, and for the first time, the Paris Agreement. It was finalized that further decisions relating to "global stocktake" process looking at long term goals, market mechanisms and implementation relating to timelines, duration and output for individual country compliance will be reviewed at the next COP 24 to be held in Poland November 2018 (IPIECA, 2016).

1.1 Project Justification

Reducing the atmospheric CO_2 concentration is believed to have a great impact on stabilizing the world's climate that has been under siege of global climate change effects being experienced globally. Geological carbon sequestration of CO_2 is an immediate solution, hence capture and storage research is being done to be better informed on the

feasibility of CCUS in coal beds. The conditions at which CO_2 is adsorbed in the coal beds of SA needs to be well known before the commercialization of the idea. This motivated the study of the CO_2 adsorption volumes for possibly CH_4 saturated coal beds at supercritical conditions in SA, with other research work running parallel to this investigation. Currently, 14 countries have been identified as having the largest reserves of CBM in the world, including: Russia, China, United States, Australia, Canada, Indonesia, SA, Ukraine, Turkey, and India, amongst others (IPPC 2005, IEA, 2010).

South Africa, having been listed as one of the countries with large reserves of CBM, opens up channels for recovery of the natural gas and thus reduces importation of the commodity from Mozambique, for example. The recovery of the gas can be enhanced by injection of CO_2 into the coal beds and this is further supported by previous research in other countries that reported 100% increase in CH_4 recovery by CO_2 injection (Masterlez *et al.,* 2004; Fitzgerald *et al*., 2005; Sakurovs *et al*., 2007; Ottiger *et al*., 2008; Mazzotti *et al*., 2009; Gaucher *et al.,* 2011).

As a contribution to this endeavour of ECBM recovery this research will therefore help in showing amounts of CH_4 that can be recovered at supercritical conditions with the injection of CO_2. Ratios of CO_2 adsorbed per volume of CH_4 desorbed will also be determined for different SA coals.

Furthermore, the revenues generated from the additional CH_4 recovered could offset the cost of CO_2 sequestration in the CCUS chain, potentially making this process economically feasible. Enhanced recovery can also make marginal coal reserves, which are low in gas content, or those which have already undergone primary depletion, an attractive target for CO_2 sequestration and CH_4 production.

1.2 Research Aims and Objectives

The current research aims to explore the CO_2 adsorption capacity of a variety of South African coals, with a consideration for CH_4 desorption, at a laboratory scale. This project is

extremely large, and involved a number of sub-projects, described in the separate objectives.

Specific objectives include:

1. To design and construct a High pressure CO_2 adsorption system.
2. To measure the adsorption isotherms and sorption capacities of CO_2 (pure) on coal under simulated in-seam conditions including pressures up to ~90 bar and temperature in the range of 35 to 55 ˚C for gaseous and supercritical CO_2.
3. To identify fundamental differences in CO_2 adsorption in different South African coal samples; for example, to determine if there is a correlation between coal rank or coal type and CO_2 adsorption behaviour.
4. To determine the impact of moisture on CO_2 adsorption at a laboratory scale.
5. To determine the permeability and the sorption capacity using crushed coal samples to ensure accuracy and reproducibility of isotherm data.
6. To obtain representative equilibrium and kinetic data with respect to the gas adsorption process; this can then be used effectively for reservoir modelling for CO_2 storage (not covered in this study).
7. To determine the CH_4 release rate relative to CO_2 adsorption and determine the maximum amount of CH_4 that can be extracted from some selected South African coals.
8. To determine if there will be an increase in CH_4 recovery from coal by injecting CO_2 at incremental pressures.
9. To evaluate the ratio of adsorption and desorption of CO_2/CH_4 respectively in different coals with regard to variable coal properties.
10. To understand the implications for CH_4 desorption from these results.
11. To compare the findings on these selected SA coals to international data and establish how they differ from those previously reported in literature.

1.3 Key research questions, as outlined below, are addressed in the conclusions of this report:

1. Can fundamental differences in CO_2 adsorption be observed in the different South African coal samples?
2. Is there a correlation between coal rank and the ability to adsorb CO_2 gas in South African coals?
3. Do inertinite-rich coals have the ability to adsorb a greater amount of CO_2 than vitrinite-rich coals?
4. Does the mineral composition in coal have an impact on the CO_2 adsorption capacity of the coal?
5. How does coal moisture and temperature affect CO_2 adsorption capacity?
6. What is the CH_4 release rate relative to CO_2 adsorption rate?
7. What are the implications for CH_4 desorption from these results?
8. Do the findings on South African coals differ from those previously reported in literature?

1.4 Hypotheses

1. CO_2 has a very high affinity for coal, especially with increased pressures; hence greater CO_2 sorption above supercritical pressures will be achieved.
2. A very definite correlation exists between coal rank and other coal properties (maceral and mineral matter ratios) and CO_2 sorption capacity as well as CH_4 desorption.
3. Different coal types will have varying CO_2 adsorption and CH_4 desorption rates, with regard to their respective mineral and maceral matter content.
4. Parameters such as low pressure, increased temperature and coal moisture content markedly hinder CO_2 sorption.
5. CH_4 recovery will increase with injection of CO_2 at supercritical conditions.

6. CO_2 volume stored will not be the same compared to the volume of CH_4 displaced for different coal types (as per detailed in 4 above).
7. CH_4 desorption from coals is significantly enhanced by continued pressurised injection of supercritical CO_2.

1.5 Outline of the thesis

This thesis is structured as follows:

In Chapter 1, previous related research is introduced. A comprehensive background and the motivation of this research is presented. Details of research questions and hypotheses are defined.

Chapter 2 gives an overview of global climate change, CO_2 emissions globally and in SA, considers the available sequestration options internationally and locally, and the various CCS technologies in current practice. Coal formation and its composition is explained and the advantages of CO_2 storage in coals is highlighted. The adsorption principles (physi and chemisorption) and techniques applied for sequestration are defined. The different gas adsorption measurement techniques are discussed. The various types of sorption isotherms are explained in conjunction to the numerous adsorption theoretical models generally used. A comprehensive review of previous studies conducted concerning CO_2 adsorption in coal are documented; specifically in relation to the effects of coal rank and composition, effects of particle size, effects of pressure (low – high) and temperature, effects of coal moisture content, the effects of swelling or structural deformation and the effects of mixed gas adsorption and CH_4 desorption.

Chapter 3, outlines the details of the experimental methodologies carried out; the type of SA coals used, characterisation methods, sample preparation methods, together with the experimental set-up (HPVAS) and test procedures used for supercritical pure CO_2 sorption investigations. It further provides detail of the procedures used to prepare coals as simulated conditions to determine the influence of moisture equilibrated coals, the effects of temperature variation on the outcome of CO_2 sorption capacity. It addition, the chapter

details the sample preparation methods for CH_4 simulated saturation methods for ambient desorption tests and the expanded CO_2 adsorption versus CH_4 desorption for saturated simulated samples at supercritical pressures. Details of the experimental methodology used for CO_2 cyclic injection for supercritical experimental tests of the method are explained. Flowsheet, Figure 3.10, summarises the details of all the experimental methods and technical programme described in the chapter.

Chapter 4 details the results and discussions of the various coal characterisation (petrographic, proximate and ultimate) data tests. Discussions of the CO_2 adsorption experimental test results that were undertaken occur; these include the effect of pressure (low – high), effect of coal rank, coal type/ composition i.e. maceral and mineral matter, ash composition, the effects of coal moisture content and the effects of temperature on CO_2 adsorption capacity. Modelling of the experimental CO_2 desorption data was undertaken using traditional theoretical Langmuir, Freundlich and Temkin adsorption models to establish the sorption mechanism to validate the experimental data obtained.

Results for pure CH_4 desorption tests from supercritical cyclic injection with CO_2 are detailed and explained. A comparison is made between CO_2 adsorption results obtained on dried and degassed coals and is compared to CH_4 saturated samples. The results include the effect of increased injection pressure, effect of coal rank, coal type/ composition i.e. maceral and mineral matter, effect of ash composition and effect of temperature for cyclic CH_4 desorption and CO_2 adsorption is also presented and discussed. Modelling of the experimental CH_4 desorption data was undertaken using traditional theoretical Langmuir, Freundlich and Temkin adsorption models to models to establish the sorption mechanism and validate the experimental data obtained for both, isothermal and temperature difference, experimental data sets.

Chapter 5 gives an overall summary and the final conclusions made with regard to the key findings of this work for all investigated sections as per Chapter 4.

Chapter 6 outlines the suggested recommendations made from this study that can be integrated and continued for future work in this field.

Detailed references that have been used and cited in assembling the research work of this thesis are compiled.

The appendices are extensive and include the following:
Appendix A; Detailed petrographic data of SA coals, Appendix B; Coal densities determined by volume displacement, Appendix B2; BET detailed sample reports, Appendix C; Isosteric adsorption line in the adsorption process, Appendix D; CO_2 adsorption - experimental and modelling data, Appendix E; CO_2 sorption modelling data: Regression plots, Appendix F; CO_2 sorption modelling data: Moisture, Appendix G; CO_2 sorption modelling data: Temperature.

For CH_4 saturated samples - Appendix H1; Cyclic injection of CO_2, Appendix H2; dried and de-gassed vs CH_4 saturated samples, and H3; Modelling data for CH_4 desorption during CO_2 cyclic injection, both for isothermal and temperature difference.

CHAPTER 2

2. LITERATURE REVIEW

An overview of global climate change, CO_2 emissions globally and in SA will be explained, as well as, the available sequestration options internationally and locally, and the various CCS technologies in current practice. Coal formation and its composition is explained and the advantages of CO_2 storage in coals is highlighted. Theoretical adsorption principles (physi and chemisorption) and techniques applied for sequestration are detailed. The different gas adsorption measurement techniques are discussed. The various types of sorption isotherms are explained in conjunction to the numerous adsorption theoretical models generally used. A comprehensive review of previous studies conducted concerning CO_2 adsorption in coal are documented; specifically in relation to the effects of coal rank and composition, effects of particle size, effects of pressure (low – high) and temperature, effects of coal moisture content, the effects of swelling or structural deformation and the effects of mixed gas adsorption and CH_4 desorption.

2.1 Global Warming and Climate Change

The greenhouse effect and carbon cycle are two issues that have been affected by anthropogenic activities. Presently, the atmosphere of the Earth is composed of about 0.04 percent CO_2 (Viljoen *et al*., 2010). The terms **global warming** and **climate change** are often used interchangeably, but the two phenomena are different.

Global warming is the rise in global mean temperature. It may be due to an increase of heat-trapping greenhouse gases such as CO_2 and CH_4 in the atmosphere (Figure 2.1). Based on surface and atmospheric temperatures from thousands of locations, and from satellites worldwide, it has been determined that the global mean temperature has risen 0.8 ^oC since 1880 (Blakemore, 2017).

Climate change is a more general term that refers to changes in many climatic factors (such as temperature and precipitation) from the global to the local scale. These changes

are happening in response to global warming and other factors at different rates and in different ways.

Atmospheric concentrations of CO_2 have increased from a pre-industrial concentration of 278 ppm. Very recent data recorded 410.03 ppm of CO_2 in the atmosphere (Figure 2.1). The graph shows the monthly mean atmospheric carbon dioxide at Mauna Loa Observatory, Hawaii, measured since 1958.

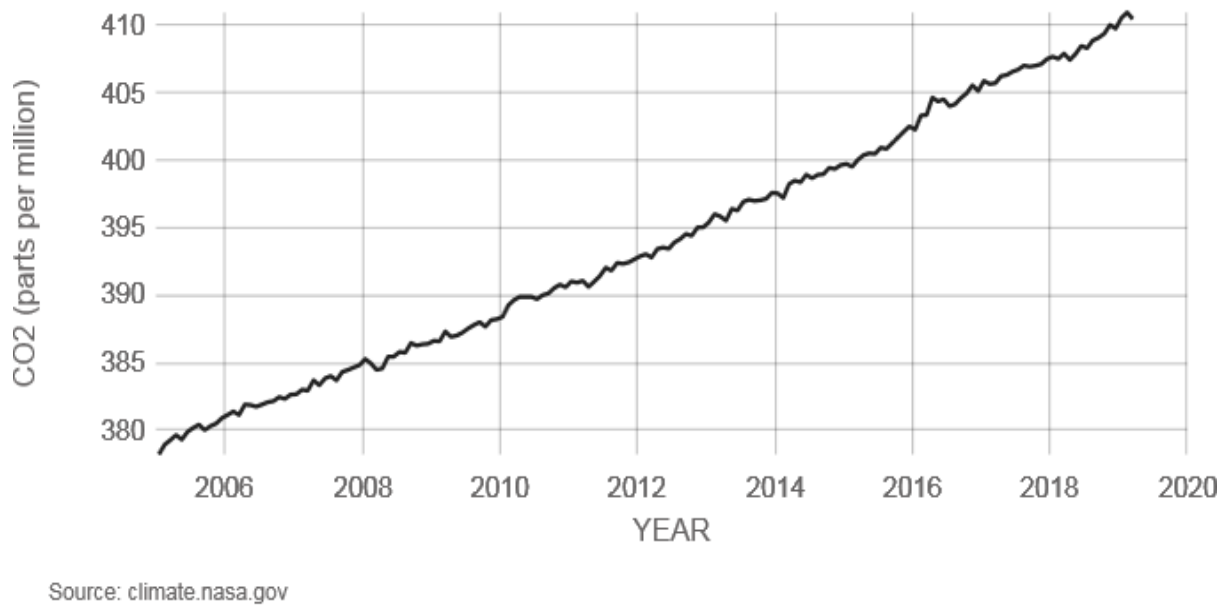

Figure 2.1 Global Concentrations of CO_2
Source: NASA's Global Climate Change newsletter

The rapid increase of atmospheric CO_2 is estimated to produce an increase of approximately 1.5–4.5 ºC surface warming based on climate data and models, with uncertainties mainly from cloud–climate feedback. Approximately 60% of the nearly 50 Gt per year of GHG emissions are CO_2 from fossil fuel combustion (McCoy, 2008).Unabated fossil fuel burning could lead to between two and three times this warming (Hoffert and Caldeira, 2004). Not only have CO_2 emissions from fossil fuel emissions have been growing steadily, but the largest single contributor to CO_2 emissions is electricity generation (McCoy, 2008). Given past growth in CO_2 emissions, future growth in global population, and increasing global average income per capita, it is almost certain that total CO_2

emissions will continue to grow in the absence of a rapid decrease in the carbon intensity of the worlds' primary energy supply (McCoy, 2008). Based on the Intergovernmental Panel on Climate Change (IPCC) summary, achieving the European Union (EU) target of no more than a 2 ºC temperature increase would require an emissions reduction of between 85% and 50% from 2000 levels by 2050. Achieving long term stabilization at a doubling of pre-industrial levels (approximately 550 ppm CO_2), would require emissions to be approximately the same as in 2000 or lower despite any growth that would otherwise occur, and would result in a warming of 2.8 to 3.3 ºC (McCoy, 2008).

2.2 Greenhouse Effect and Gases

The greenhouse effect is a naturally occurring process that aids in heating the Earth's surface and atmosphere. It causes the atmosphere to trap more heat energy at the Earth's surface and within the atmosphere by absorbing and re-emitting long wave energy, as shown in Figure 2.2. Certain atmospheric gases, collectively referred to as GHG (CO_2, water vapor, nitrous oxide (N_2O), CH_4, halocarbons, and ozone (O_3)) are able to change the energy balance of the planet by being able to absorb long wave radiation from the Earth's surface (Hassan, 2005). As energy from the sun passes through the atmosphere, a number of phenomena take place. A portion of the energy (26% globally) is reflected back to space by clouds and particles. Clouds, gases (like O_3), and particles in the atmosphere absorb about 19% of the available energy. Of the remaining 55% of the solar energy passing through the Earth's atmosphere, 4% is reflected from the surface back to space (Hassan, 2005).

Thus, on average about 51% of the sun's radiation reaches the surface. This energy is then used in number of processes including: the heating of the ground surface, the melting of ice and snow, and the evaporation of water and plant photosynthesis. The heating of the ground by sunlight causes the Earth's surface to become a radiator of energy in the long-wave band called infrared radiation. This emission of energy is generally directed to space (Hassan, 2005).

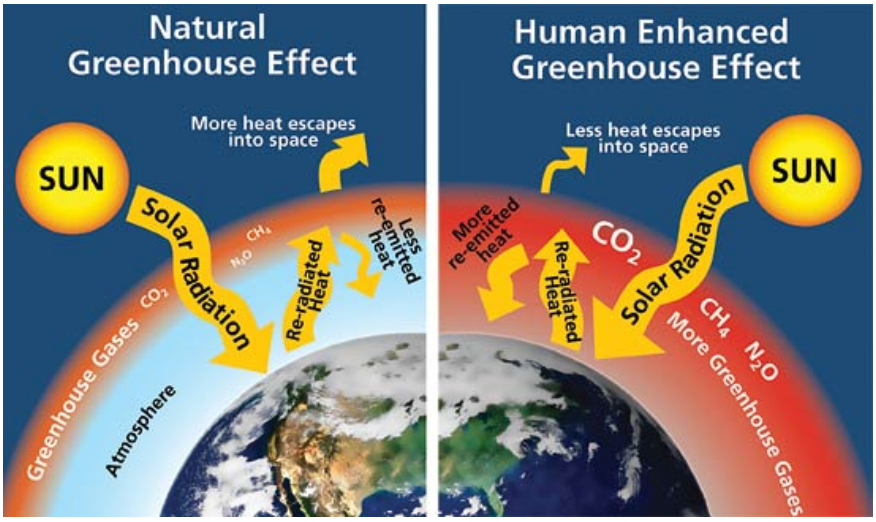

Left - Naturally occurring greenhouse gases—carbon dioxide (CO_2), methane (CH_4), and nitrous oxide (N_2O)—normally trap some of the sun's heat, keeping the planet from freezing. **Right** - Human activities, such as the burning of fossil fuels, are increasing greenhouse gas levels, leading to an enhanced greenhouse effect. The result is global warming and unprecedented rates of climate change.

Figure 2.2: The Greenhouse Effect
Source: Elder (2012)

However, only a small portion of this energy actually makes it back to space. The majority of the outgoing infrared radiation is absorbed by the greenhouse gases. Absorption of this energy causes additional heat energy to be added to the Earth's atmospheric system. The now warmer atmospheric greenhouse gas molecules begin radiating long-wave energy in all directions. Over 90% of this emission of long-wave energy is directed back to the Earth's surface where it once again is absorbed by the surface. The heating of the ground by the long-wave radiation causes the ground surface to once again radiate, repeating the cycle described above, again and again, until no more long-wave is available for absorption. The net result of the greenhouse effect is the addition of extra heat energy to the earth's atmosphere and ground surface. The amount of heat energy added to the atmosphere by the greenhouse effect is controlled by the concentration of GHG in the Earth's atmosphere (Hassan, 2005).

South Africa's GHG emissions from industrial processes recorded since 1970 are shown in Figure 2.3.

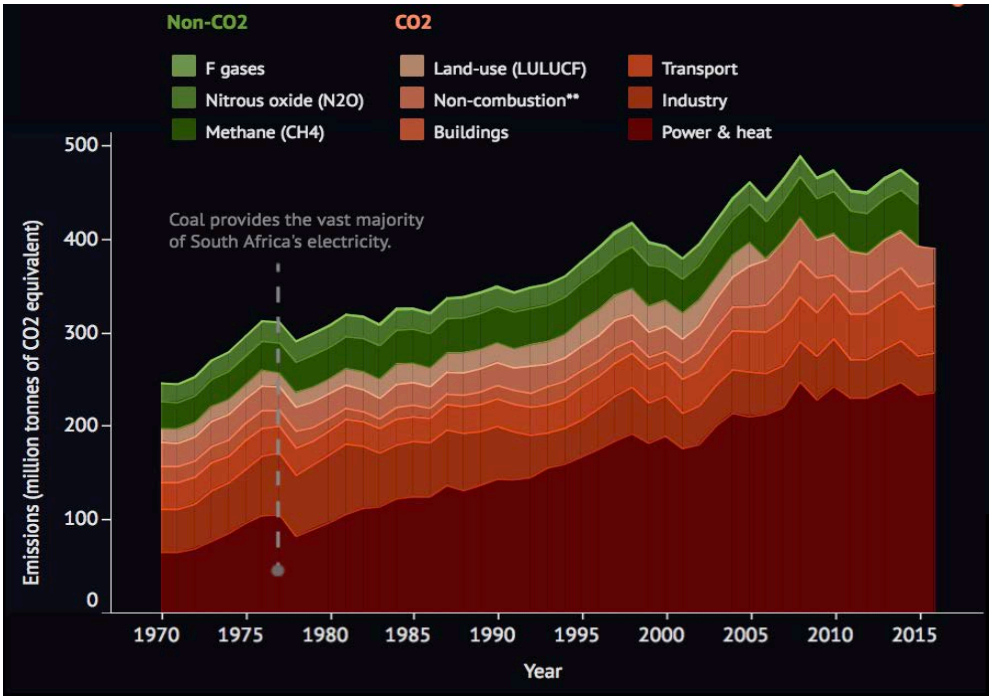

Figure 2.3: South Africa's Greenhouse Gas Emissions from Industrial Processes
Source: Carbon Brief (2018)

2.3 CO_2 Sequestration Technologies

Carbon dioxide sequestration refers to the long-term storage of CO_2 to reduce the amount of CO_2 in the atmosphere (Pires *et al.*, 2011). One of the methods of CO_2 sequestration is carbon capture, storage and utilisation (CCUS). Carbon capture includes several processes beyond the scope of the current research, but essentially involves capturing (using amines for example) and increasing the concentration of CO_2 to above 90% from a flue gas stream. The captured CO_2 is then compressed and transported to a storage site for injection. Following the capture and transport process, CO_2 needs to be stored, so that it will not be emitted into the atmosphere. Several key criteria must be applied to the storage method (Herzog and Golomb, 2004):

- the storage period should be prolonged, preferably hundreds to thousands of years;
- the cost of storage, including the cost of transportation from the source to the storage site, should be minimized;
- the risk of accidents should be eliminated;
- the environmental impact should be minimal;

- the storage method should not violate any national or international laws and regulations.

Typically, the long term storage options are grouped into three categories: 1) geological storage; 2) ocean storage; 3) or mineralization (Pires *et al.*, 2011). Geological storage includes CO_2 storage in depleted oil and gas reservoirs, EOR, deep saline formations (sub-terranean and sub-seabed), and unmineable coal seams (Hietkamp *et al.*, 2004), and is discussed further below. The latter storage options are referred to as conventional storage sites, but SA may need to look towards unconventional storage, such as in porous sandstone, basalts, and so on.

2.3.1 Geological Storage

Figure 2.4 depicts a number of conventional geological storage sites. Together, these can hold hundreds to thousands of gigatons of carbon (GtC), and the technology to inject CO_2 into the ground is well established. CO_2 is stored in geologic formations by a number of different trapping mechanisms, with the exact storage mechanism depending on the formation type. These storage mechanisms can take the form of either; structural, residual or mineral trapping, as is further discussed in Section 2.7.2 (Herzog and Golomb, 2004).

The formations shown in Figure 2.4 have the capacity, structure, seals, porosity and other properties (i.e. dissolving of CO_2 in groundwater), that make them amenable to decades or centuries worth of CO_2 storage. Such methods should be environmentally effective, socially acceptable, and economically feasible, but will each have their own weaknesses and strengths (Hietkamp *et al.*, 2004).

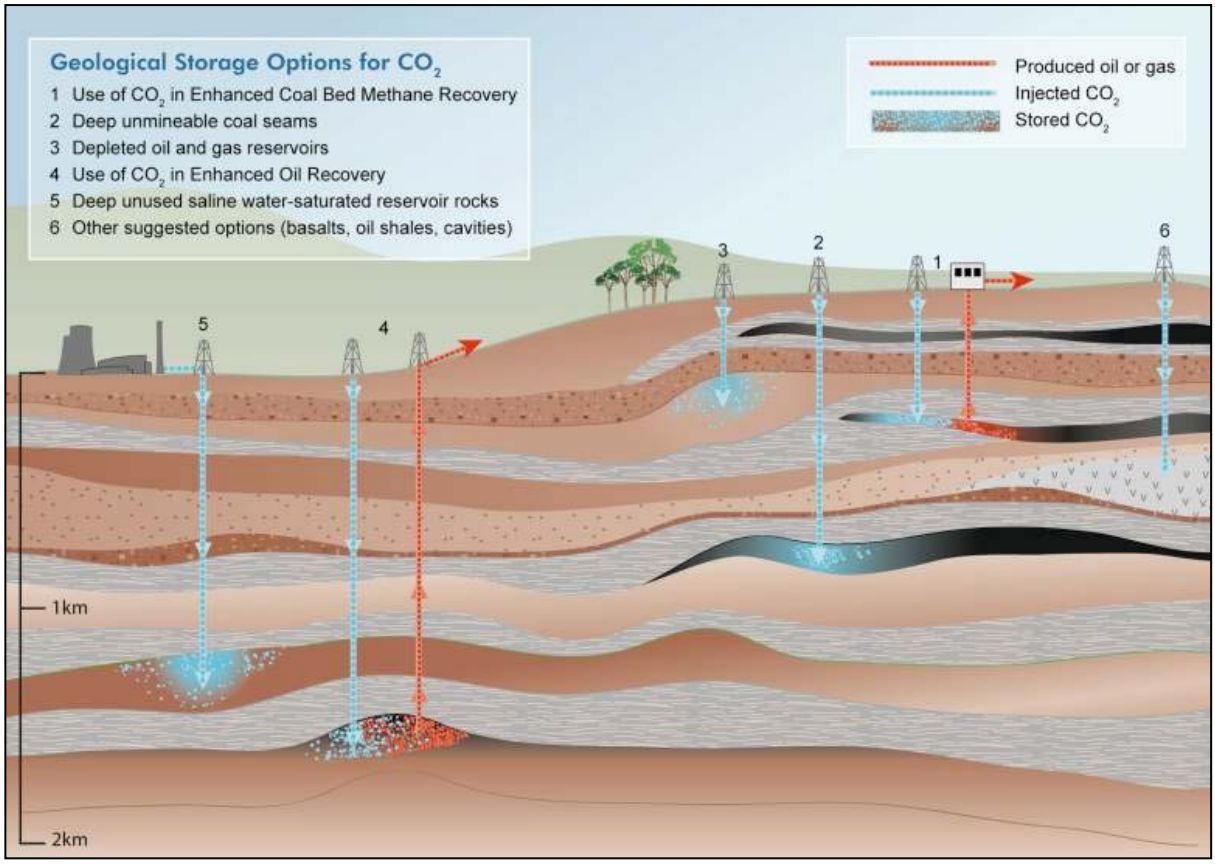

Figure 2.4: Possible sites for geological storage of CO_2 *(Metz et al., 2005)*

It is important to develop a good understanding of the reservoir performance, uncertainties and risks that are associated with geological storage. After Korre *et al.* (2007), the sources of uncertainty in risk assessment related to CO_2 storage in coal include:

- *Measurement uncertainty and variability*, accounting for the lack of accurate knowledge and representation of heterogeneity in the measured data.
- *Model parameter uncertainty,* i.e. variables, which are used to represent the physical processes in the models assessing the performance of a reservoir as a CO_2 sink. Frequently, there are large spatial and temporal variations in some of these parameters (e.g. porosity, sorption capacity, permeability, diffusion coefficients, etc.).
- *Modeling uncertainty,* which has to do with the true knowledge and understanding of the physics of the storage process and its representation in the mathematical models used (e.g. different sorption and/or diffusion models; accounting for stress, matrix shrinkage/swelling effects on permeability and/or injectivity).

- *Risk scenario uncertainty,* which is related to the long-term future of the reservoir and includes long-term processes.

(i) Depleted Oil and Gas Reservoirs

Though a relatively new idea in the context of climate change mitigation, injecting CO_2 into depleted oil and gas fields has been practiced for many years. The major purpose of these injections was to disposing of "acid gas," a mixture of CO_2, H_2S, and other by-products of oil and gas exploitation and refining. In 2001, nearly 200 million cubic meters of acid gas was injected into formations across Alberta and British Columbia at more than 30 different locations (Herzog and Golomb, 2004). Acid gas injection became a popular alternative to sulfur recovery and acid gas flaring, particularly in Western Canada. Essentially, acid gas injection schemes remove CO_2 and H_2S from the produced oil or gas stream, compress and transport the gases via pipeline to an injection well, and re-inject the gases into a different formation for disposal (Herzog and Golomb, 2004).

Proponents of acid gas injection claim that these schemes result in less environmental impact than alternatives for processing and disposing of unwanted gases. In most of these schemes, CO_2 represents the largest component of the acid gas, typically up to 90% of the total volume injected for disposal. Successful acid gas injection requires a nearby reservoir with sufficient porosity, amply isolated from producing reservoirs and water zones. Historically, depleted and producing reservoirs have proven to be extremely reliable containers of both hydrocarbons and acid gases over time (Herzog & Golomb, 2004).

(ii) Enhanced Oil Recovery (EOR)

CO_2 injection into geological formations for EOR is a mature technology (Herzog and Golomb, 2004). CO_2 is already pumped into oil reservoirs for EOR (e.g. Weyburn CO_2 Flood Project (Canada), Kaarsto (Norway), Teesside (UK)), although most of the CO_2 currently used for EOR comes from natural sources, and existing EOR practices are not implemented with a view to storing CO_2. The largest application currently for EOR is in

North America, which involves approximately 30 million tons of CO_2 per year and several major CO_2 pipelines (Simbeck, 2004). However, it would be possible to modify CO_2 EOR to emphasize CO_2 storage while at the same time improving oil recovery. Although CO_2 EOR could not provide accommodation for more than a very small fraction of the volume of CO_2 currently emitted, it does provide a field laboratory for technologies required for routine sequestration, driven by the commercial incentive to improve recovery of the oil from older reservoirs. Moreover, in a world where CO_2 is much more readily and cheaply available, there will be an incentive to use CO_2 earlier in the oil-recovery stage to better exploit dwindling resources (Metz *et al.*, 2005).

In most CO_2-EOR projects, much of the CO_2 injected into the oil reservoir is only temporarily stored. This is because the decommissioning of an EOR project usually involves the "blowing down" of the reservoir pressure to maximize oil recovery. This blowing down results in CO_2 being released, with a small but significant amount of the injected CO_2 remaining dissolved in the immobile oil (Herzog and Golomb, 2004).

(iii) Deep Saline Formations

Deep saline formations, both sub-terranean and sub-seabed, may have the greatest CO_2 storage potential. These reservoirs are the most widespread and have the largest volumes. These water reservoirs are very distinct from the more familiar reservoirs used for fresh water supplies (Herzog and Golomb, 2004).

The density of CO_2 depends on the depth of injection, which determines the ambient temperature and pressure. The CO_2 must be injected below 800 m, so that it is in a dense phase (either liquid or supercritical). When injected at these depths, the specific gravity of CO_2 ranges from 0.5 to 0.9, which is lower than that of the ambient aquifer brine. Therefore, CO_2 will naturally rise to the top of the reservoir, and a trap is needed to ensure that it does not reach the surface. Geological traps overlying the aquifer immobilize the CO_2 (Herzog and Golomb, 2004). In the case of aquifers with no distinct geologic traps, an impermeable cap-rock above the underground reservoir is needed. This forces the CO_2 to be entrained in the groundwater flow and is known as hydrodynamic trapping. Two other very important

trapping mechanisms are solubility and mineral trapping. Solubility and mineral trapping involve the dissolution of CO_2 into fluids, and the reaction of CO_2 with minerals present in the host formation to form stable, solid compounds like carbonates. If the flow path is long enough, the CO_2 might all dissolve or become fixed by mineral reactions before it reaches the basin margin, essentially becoming permanently trapped in the reservoir (Herzog and Golomb, 2004).

The first commercial-scale project dedicated to geologic CO_2 storage is in operation at the Sleipner West gas field, operated by Statoil, located in the North Sea about 250 km off the coast of Norway. The natural gas produced at the field has a CO_2 content of about 9%. In order to meet commercial specifications, the CO_2 content must be reduced to 2.5% percent. At Sleipner, the CO_2 is compressed and injected via a single well into the Utsira Formation, a 250 m thick saline aquifer located at a depth of 800 m below the seabed. About one million metric tons of CO_2 have been stored annually at Sleipner since October 1996, equivalent to about 3% of Norway's total annual CO_2 emissions. A total of 20 Mt of CO_2 is expected to be stored over the lifetime of the project (Herzog and Golomb, 2004).

(iv) Unmineable Coal Seams and CBM

Abandoned or uneconomic (not profitable) coal seams are another potential storage site. CO_2 diffuses through the pore structure of coal and is physically adsorbed to it. This process is similar to the way in which activated carbon removes impurities from air or water. The exposed coal surface has a preferred affinity for adsorption of CO_2 than for CH_4, with a ratio of 2:1 (Herzog and Golomb, 2004). Thus, CO_2 can be used to enhance the recovery of coal bed CH_4 (CBM). In some cases, this can be very cost effective or even cost free, as the additional CH_4 removal can offset the cost of the CO_2 storage operations. CBM production has become an increasingly important component of natural gas supply in the United States during the last decade (e.g. Powder River Basin, Illinois Basin, Arkoma Basin). In 2000, approximately 40 billion standard cubic meters (scm) of CBM was produced, accounting for about 7% of the nation's (US) total natural gas production (Herzog and Golomb, 2004).

The most significant CBM production, some 85% of the total, occurs in the San Juan basin of southern Colorado and northern New Mexico. Another 10% is produced in the Black Warrior basin of Alabama, and the remaining 5% comes from rapidly developing Rocky Mountain coal basins, namely the Uinta basin in Utah, the Raton basin in Colorado and New Mexico. Significant potential for CBM exists worldwide. A number of coal basins in Australia, Russia, China, India, Indonesia, South Africa and other countries have also been identified as having a large CBM potential. The total worldwide potential for CBM is estimated at around two trillion scm, with about 7.1 billion tons of associated CO_2 storage potential (Herzog & Golomb, 2004).

2.4 Summary of published CO_2 projects internationally

As already mentioned, the option of using geological storage for CO_2 is carried out internationally, CCS technology is proven and in use around the world. There are 21 large-scale CCS projects in operation or under construction globally. The combined CO_2 capture capacity of these 21 projects is around 40 million tonnes per annum (Mtpa) (Global Status of CCS 2016. There are variety of large scale projects, which have been started a while back, like Weyburn (conducted by Encana) in Saskatchewan, Canada, the Sleipner offshore gas field development project (conducted by STATOIL) in the Norwegian North Sea, In-Salah in Algeria; and on a smaller scale the Otway Project in Australia (conducted by CO_2CRC), and other projects in North America linked to EOR. These are just some of the projects receiving international attention that have already stored millions of tonnes of CO_2 underground, and there are many more that have already been planned. The IEA CCS Roadmap indicates that 3400 storage projects are required by 2050 to meet the target of 10Gt stored CO_2; 10Gt is the required amount of CO_2 that needs to be removed to meet average temperature targets.

With regard to CO_2 storage in coal seams, the Allison unit, operated by Burlington Resources in the USA has been conducting a commercial pilot application of CO_2 injection since 1996. While it was intended to test ECBM recovery primarily, the pilot also sequesters CO_2 as part of its routine operation, and is by far the most successful CBM development in the world, with per-well gas production averaging over 23,000 m^3/day of

CH_4 (Reeves *et al.,* 2003). The coal in this basin varies from sub-bituminous in the southern region to medium volatile bituminous in the north central area. The coal is extremely well cleated and faulting is minimal. Permeability ranges from 1 to 100 milliDarcy, averaging 20 milliDarcy. Coal seam thickness averages 20 m at a depth of about 1000 m (Reeves *et al.,* 2003; Stevens *et al.*, 2000).

Estimates of global storage capacity indicate that 675 – 900 Giga tonnes CO_2 ($GtCO_2$) can be stored in oil and gas fields, 3 - 200 $GtCO_2$ in unmineable coal seams, and 1000 – 10000 $GtCO_2$ in deep saline formations. This means that the storage capacity for CO_2 in geological formations is much higher than the global annual CO_2 emissions, which was reported in 2004 as 26 $GtCO_2$ 2004 (World Energy Outlook, 2006) and has been reported to be at 34 billion tonnes of CO_2 emitted globally for 2011 (Environmental and Energy Management News, 2011). The main CO_2 contributors being:

- China (29 %)
- The United States (16 %)
- The European Union (11 %)
- India (6 %)
- The Russian Federation (5 %)
- Japan (4 %)

International projects have been published by the Global Institute for CCS Global Status of CCS 2016) are summarised here. All projects were then in construction (five) and are now in preliminary operational stage as of the end of 2017, widening the range of countries, industries and technologies represented. This compares with less than 10 large-scale operational projects at the beginning of this decade.

- There are another 6 large-scale CCS projects at the most advanced stage of development planning, the Concept Definition (or Define) stage, with a total CO_2 capture capacity of around 8 Mtpa. A further 11 large-scale CCS projects are in earlier stages of development planning (the Evaluate and Identify stages) and have a total CO_2 capture capacity of around 21 Mtpa.
- One key CCS project has been launched in 2017, with one large-scale and one demonstration-scale key CCS projects launched in 2016:

- The Petra Nova Carbon Capture Project in Texas (CO2 capture capacity of approximately 1.4 Mtpa) has been launched on 10 January 2017. This project is the world's largest post-combustion CO2 capture project at a power station.
- The Abu Dhabi CCS Project, Phase 1 being the Emirates Steel Industries (ESI) CCS Project, was launched on 5 November 2016. This project represents the world's first application of CCS to iron and steel production. It involves the capture of approximately 0.8 Mtpa of CO_2 from the direct reduced iron (DRI) process used at the ESI plant in Abu Dhabi and its use for enhanced oil recovery (EOR).
- The Tomakomai CCS Demonstration Project commenced its CO_2 injection in April 2016. The capture system (using emissions from a hydrogen production facility at Tomakomai port) is processing CO_2 at a rate of at least 100,000 tonnes per annum; this CO_2 is then injected into near-shore deep geologic formations.
- The Illinois Industrial Carbon Capture and Storage Project (CO_2 capture capacity of approximately 1 Mtpa) began operations early in 2017. This project is the world's first large-scale bioenergy CCS project, as well as the first CCS project in the US to inject CO_2 into a deep saline formation at a scale of 1 Mtpa (Global Status of CCS 2018).

2.5 CO_2 Emissions and sequestration potential in South Africa

Upon joining the Carbon Sequestration Leadership Forum (CSLF), South Africa undertook a first step investigation to establish whether there were sources and possible sinks for CCS in the country. That study indicated potential carbon sources and storage sites (Hietkamp *et al.*, 2004). CO_2 emissions were found to be concentrated in the central industrial region (around Gauteng), associated with coal-fired electricity generation (ESKOM being the main electricity generator in SA), and the synthetic-liquid fuel plants (SASOL and PETROSA). Sasol's coal conversion technology provides half South Africa's liquid fuels requirements. The concentration of CO_2 emissions in the central region can be seen in Figure 2.5.

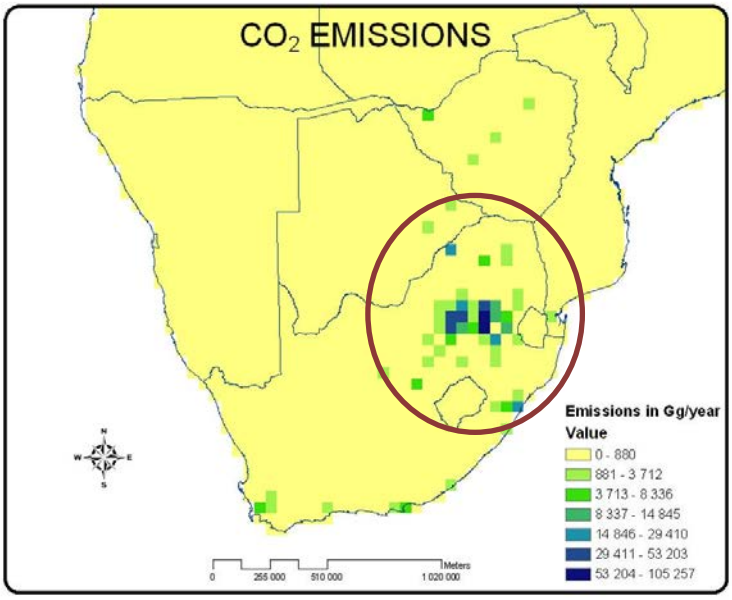

Figure 2.5 CO_2 emissions in South Africa *(Hietkamp et al., 2004).*

In comparison with other countries, SA unfortunately lacks conventional world-class storage reservoirs (oil or gas bearing fields, or an abundance of saline aquifers. From the recently published carbon storage atlas (Viljoen *et al*., 2010), the estimated capacity of geological storage in South Africa is at least 150 Gt (150 000 Mt) of CO_2. The largest storage volume (~98 % of the total storage potential of South Africa) is present in the Mesozoic basins along the coast of South Africa (Viljoen *et al.*, 2010). The storage potential lies mainly in the capacity of saline formations associated with the oil- and gas-bearing sequences in the Outeniqua, Orange and Durban/Zululand basins; these are all offshore. Slightly more than 2 % of the estimated storage capacity of South Africa occurs onshore: ~0,46 Gt for the onshore Zululand Basin; ~0,40 Gt for the onshore Algoa Basin, and ~1,2 Gt for the coalfields of South Africa as indicated in Figure 2.5 (Viljoen *et al.*, 2010).

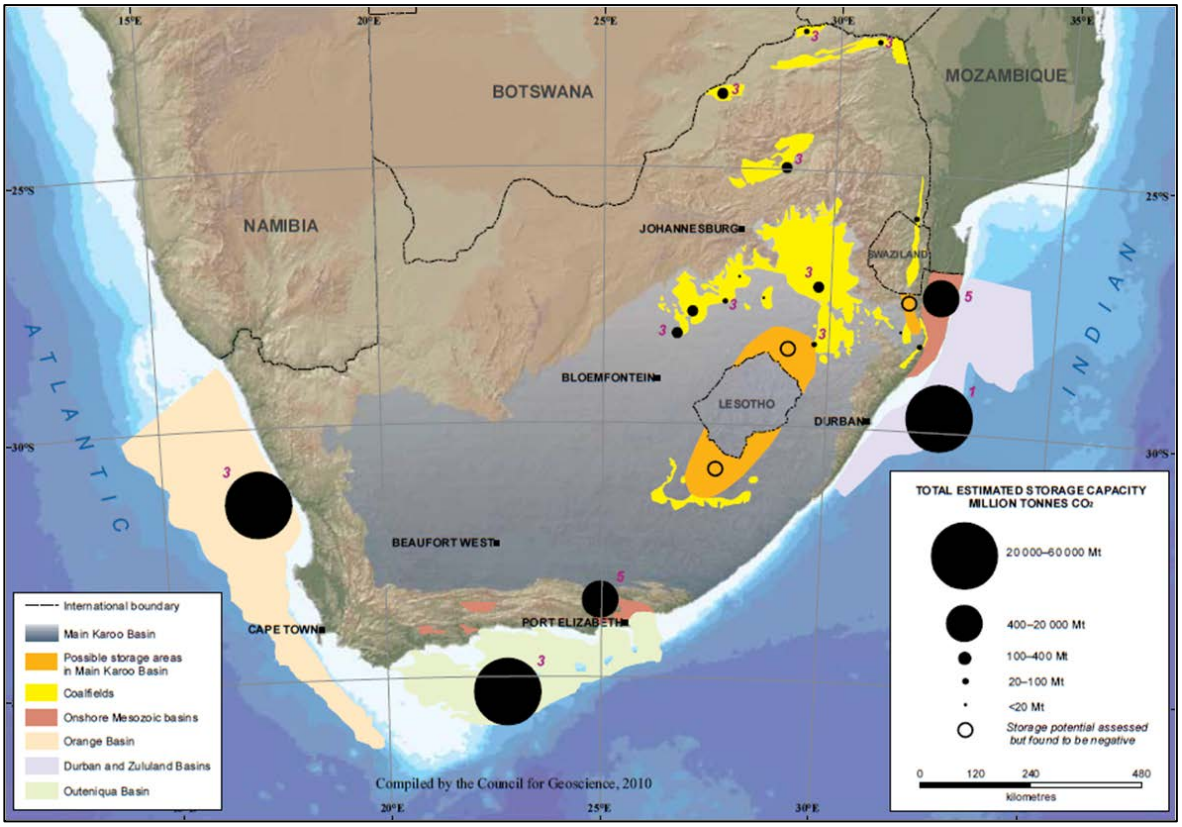

Figure 2.6 South African Available CO_2 Storage Potential (*Viljoen et al., 2010)*.

The option of CO_2 storage in coal seems viable, and is possibly one of the best options for SA, with the potential opportunity of ECBM, due to large coal resources. However, it must be borne in mind that ECBM may not be achievable due to low CH_4 occurrence and permeability, and that unmineable coalfields may become mineable in the future with changes in the economy, technology, and energy demands. In addition, the advent of underground gasification may decrease the estimated potential CO_2 storage capacity in coal seams, or it may be beneficial, (unfortunately this discussion is beyond the scope of the current report, but certainly makes for an interesting topic requiring further research and development).

As the scope of this research concerns CO_2 storage capacity estimations in SA coals, the following section gives further details on the storage capacity in deep unmineable coal seams in South Africa.

2.5.1 Storage Capacity in Deep Unmineable Coal Seams

Coal is found in South Africa in 19 coalfields (Figure 2.7), located mainly in KwaZulu-Natal, Mpumalanga, Limpopo, and the Free State, with lesser amounts in Gauteng, the North West Province and the Eastern Cape. The main coal mining areas are presently in the Witbank-Middelburg, Ermelo and Standerton-Secunda areas of Mpumalanga, around Sasolburg-Vereeniging in the Free State/Gauteng and in north-western KwaZulu-Natal where smaller operations are found. Single, although large, collieries are found near Ellisras and Tshipise (Jeffrey, 2005). This could mean that, in terms of storage of CO_2 in coal, with the added benefit of ECBM, there are many viable potential sites in SA. The latest Minerals Bureau estimate sets the coal reserves at *33.8 billion tons*, considered to last until around 2050 (Jeffrey, 2005), with an estimated CBM resource of 0.14 – 0.28 trillion m^3 (as reported in Viljoen *et al*., 2010).

The main criteria for the storage of CO_2 in coal seams are that the coal seams should be deeper than 300 m (in order not to sterilize mineable coal seams and not to influence potable groundwater). The critical depth at which CO_2 remains in supercritical phase is ideally between 750 – 900 m (the maximum depth for coalbeds to be considered for CO_2 storage is where the permeability becomes less than 1 millidarcy (mD)), and with a minimum thickness of 1 m (Viljoen *et al.*, 2010).

For effective storage, the coal should have the same properties that are necessary for the production of CBM, which are:

- Good permeability (30–50 mD), although it can be enhanced (hydraulic fracturing) if lower
- Depth - optimally between 200 and 800 m, thus leading to an increased pore pressure and gas content without adversely affecting its porosity and permeability
- Thickness (at least 1.0 m)
- High vitrinite content
- Bituminous coal.

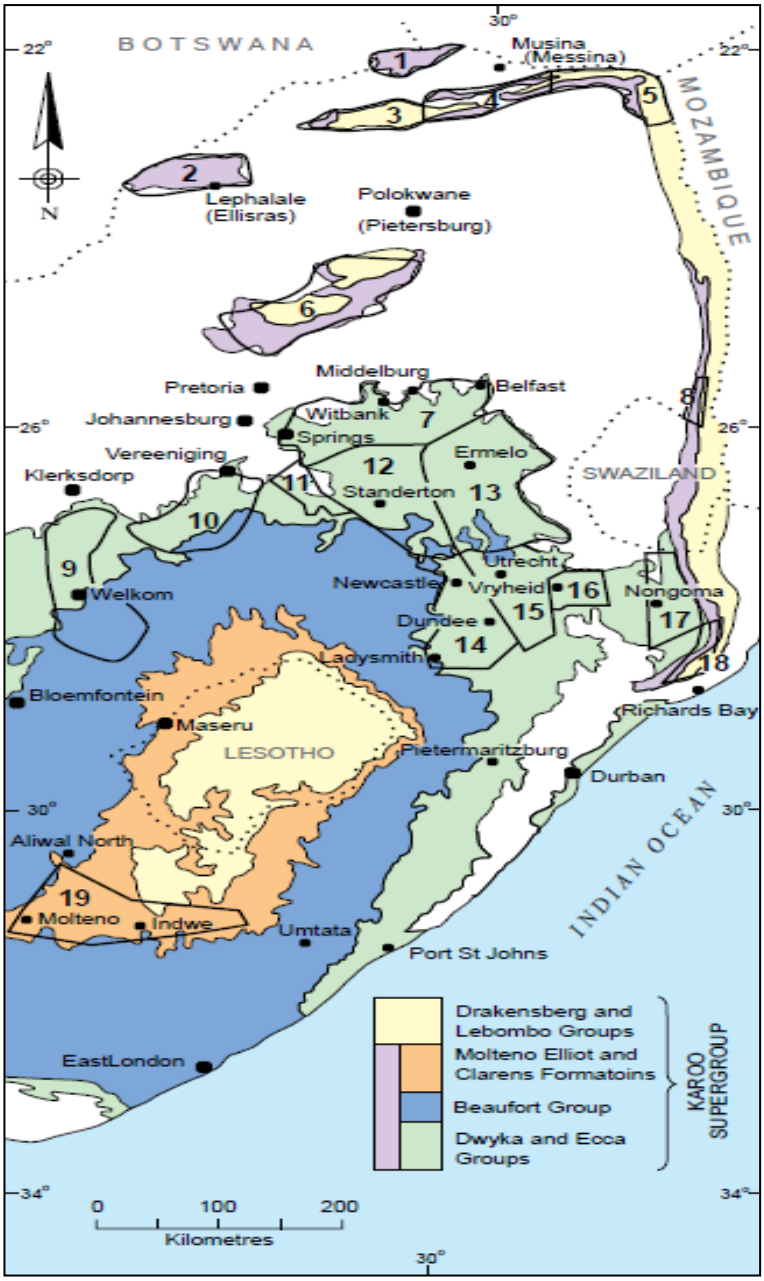

Figure: 2.7 The localities of the South African coal fields 1–Tuli, 2–Ellisras, 3–Mopane, 4–Tshipise, 5–Pafuri, 6–Springbok Flats, 7–Witbank, 8–Kangwane, 9–Free State, 10–Vereeniging/ Sasolburg, 11–South Rand, 12–Highveld, 13–Ermelo, 14–Klip River, 15–Utrecht, 16–Vryheid, 17–Nongoma, 18–Somkele, 19–Molteno/Indwe (Viljoen et al., 2010).

Not all the data necessary to calculate the CO_2 storage potential of the coal seams were available for the SA CO_2 Storage Atlas (Viljoen *et al*., 2010), and some generalizations had to be made. In many cases, the intrusive dolerite dykes and sills have displaced strata in the various coal fields, causing discontinuities in the coal seams. In addition, the elevated temperatures emanating from the intrusive caused extensive devolatilisation of the coal

seams over considerable areas, particularly in the eastern (KwaZulu-Natal) and northern (Witbank) coal fields of the Main Karoo Basin and in the Tshipise and Tuli basins. The western coal fields of the Main Karoo Basin and those of the Springbok Flats and Ellisras basins are far less affected by dolerite intrusives (Viljoen *et al.*, 2010). Table 2.1 gives estimated storage capacities as per coal basin as well as details of seam thickness, depth and possible adsorption capacities.

Table 2.1 Estimated CO_2 storage capacity in the coal fields of South Africa
(Viljoen et al., 2010)

Basins/ areas	***Area (m^2)***	***Coal thickness (m)***	***Depth interval (m)***	***CO_2 adsorption capacity/tonnes of coal (m^3)***	***CO_2 storage capacity (M tonnes)***
Amersfoort/Utrecht	3 600 x 10^6	2	300-550	22–27	331.8
Ellisras	800 x 10^6	10	300-800	17–22	293.4
Welkom/ Hennenman	1 440 x 10^6	3	300-550	17–21	154.4
Kroonstad	936 x 10^6	3	300-550	17–21	100.3
Springbok Flats	2 300 x 10^6	1	300-800	17–22	84.4
Somkele	360 x 10^6	5	300-800	22–27	82.9
Pafuri	420 x 10^6	3	300-800	22–26	56.9
Kangwane	195 x 10^6	6	300-800	22–26	52.8
Newcastle/ Ladysmith	936 x 10^6	1	300-550	22–27	43.1
Edenville	360 x 10^6	2	300-550	17–21	25.7
Tuli	150 x 10^6	3	300-550	22–27	20.7
Heilbron	288 x 10^6	1	300-550	17–21	10.3
Frankfort	216 x 10^6	1	300-550	22–27	10
Nongoma	75 x 10^6	1.5	300-550	22–27	5.2
Total estimated CO_2 storage capacity in the coal fields (million tonnes)					**1 271.9**

2.5.2 Storage Capacity in Deep Coal Seams versus high CH_4 content in SA

A considerable diversity of coal types (organic composition), grades (mineral matter composition) and rank (maturity) is found within the coal measures in SA. This is elaborated on further in Section 2.6. However, from Figure 2.8, a study of SA's most promising CH_4 emission seams have been identified and categorized according to their gas bearing content in cubic meters per ton (m^3/t).

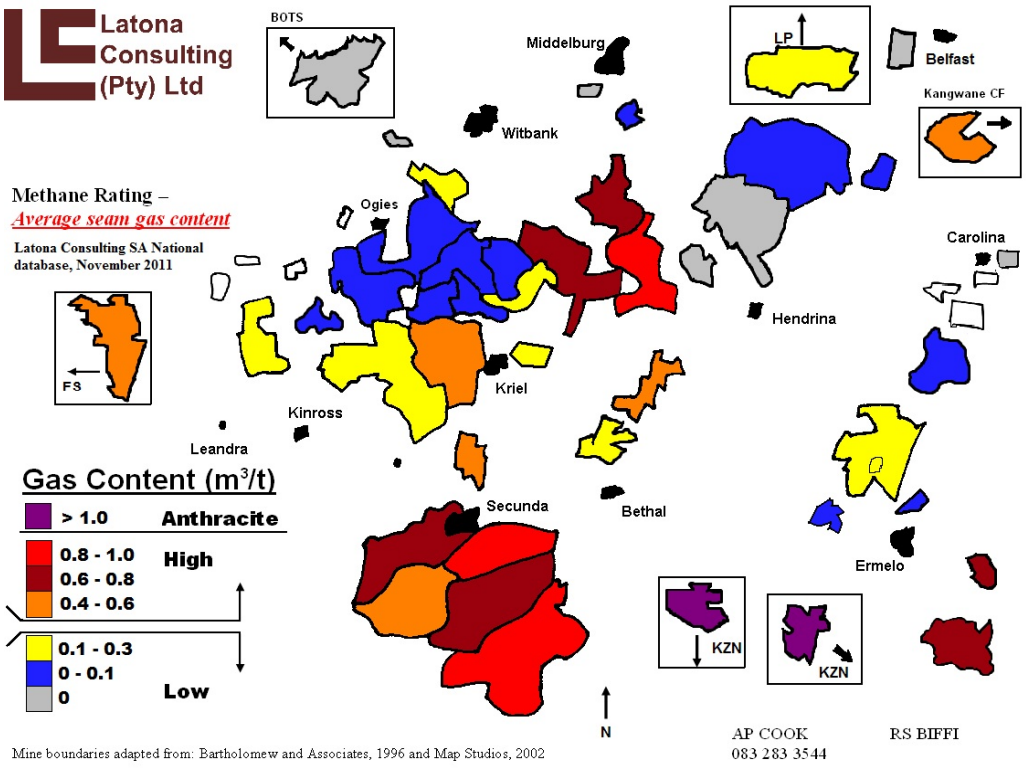

Figure 2.8: SA Mine Boundaries for CH_4 highest emissions
Source: (Latona Consulting (Pty) Ltd. 2011)

Of interest is data produced by Latona (Pty) Ltd for CH_4 rich seams in SA (provided by Mr. A. Cook), which shows the greatest CH_4 potential of coal seams across SA depicted in Figure 2.8 above. CH_4 rich fields are ideally located in the areas with high CO_2 emissions, namely: Secunda (Sasol) and close to Eskom power stations like Hendrina and Kriel. This information shows that ECBM could very well be undertaken in SA.

2.6 Coal

In order to understand the CO_2 adsorption potential in coal, it is necessary to have an understanding of coal and its composition. The origin and formation of coal is briefly considered, as well as coal composition and classification.

2.6.1 Origin and Formation of Coal

Coal is an extremely heterogeneous material consisting of organic matter, mineral matter, moisture, and a complex pore network. It is generally accepted that the organic portion of coal was formed from concentrated deposits of swampy organic matter originally derived from terrestrial plants. Plant structures (leaf, stems, roots, spores, etc.) were converted into coal through complex biological, chemical, and geochemical processes driven initially by selective microbial action and later by the temperature and pressure generated by overlaying sediments over several hundred millions of years (Ozdemir, 2004). The coal thus reflects primarily condition of climate, water level, and water chemistry in the mire. The plant source material in the swamp ultimately determines the petrographic composition of the coal (Meyers, 1982).

Coals formed in the peat swamp environment are autochthonous or *in situ* in origin. Some peat and even coal seams may be re-deposited in a fluvial system and are known as allochthonous in origin. Coal deposits formed from accumulation of driftwood are included in this category (Meyers, 1982). Any region where conditions were favourable for the accumulation of peat, was a potential region for coal formation. The back swamps of floodplains, lake margins, lagoons, coastal plains where tidal fluctuation is low, and glaciated regions with poor drainage, are all good environments for peat accumulation. The conditions for producing thick layers of coal are that the region must be constantly subsiding, or the groundwater level must be rising slowly but steadily, and the accumulation of plant debris must keep pace with rising water level (Zeng, 1997).

The process referred to as coalification, involves the physical and chemical transformation from peat through lignite and subbituminous coal, to bituminous coal, and through

bituminous coal to anthracite and metaanthracite, and approaching graphite. Coal rank is measured by a progressive decrease in moisture and volatile functional groups with a consequent increase in the carbon content, vitrinite reflectance, and calorific value (although the latter slightly decreases at high ranks) of the coal (van Krevelen, 1993; O'Keefe *et al*., 2013).

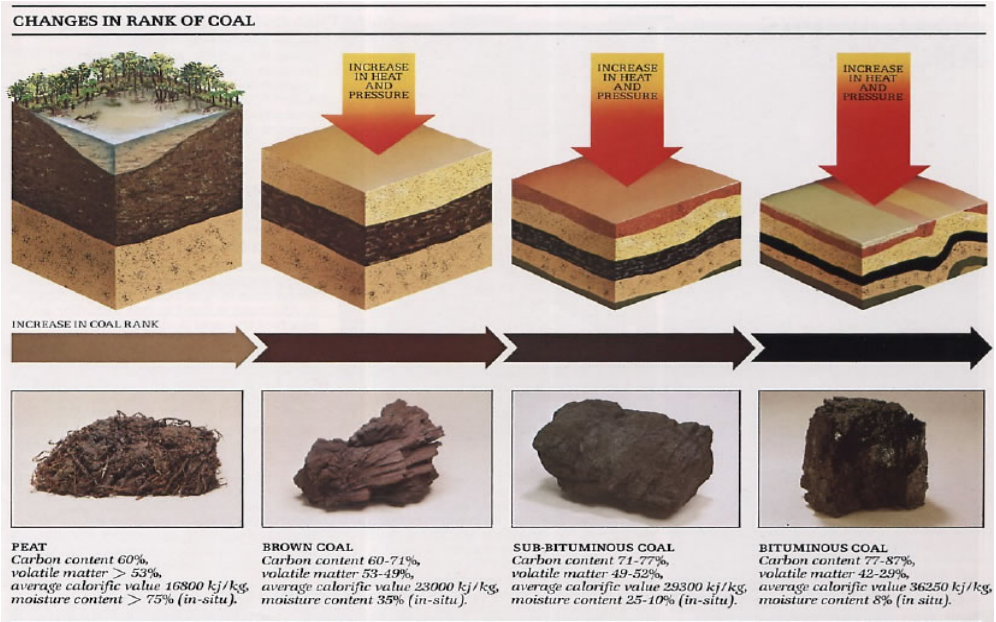

Figure 2.9: The coalification process: from swamp to coal
(*Gertenbach, 2009*)

2.6.2 Coal Composition

Coal is a combustible black or brownish-black sedimentary rock usually occurring in rock strata in layers or veins called coal beds or coal seams. The harder forms, such as anthracite coal, can be regarded as metamorphic rock because of later exposure to elevated temperature and pressure (coalification). Coal is composed primarily of carbon along with variable quantities of other elements, chiefly hydrogen, sulphur, oxygen, and nitrogen, (Meyers, 1981). It is commonly accepted that the coal is a macromolecule built of condensed aromatic rings joined by ether, alkoxy and sulfur bridges, and having hydroxyl groups, methoxyl groups and carboxyl groups attached to the aromatic nuclei (O'Keefe *et al*., 2013).

2.6.2.1 Types of Coal

Coal types typically fall in to two categories: humic coals, developed from peat, and sapropelic coals, developed from organic mud. Either type may be allocthonous or autochthonous, and within types, further refinement of depositional environment can be made (O'Keefe *et al*., 2013). The classification of coal is generally based on the content of volatiles. However, the exact classification varies between countries. The ranks defined by the ISO standard represent the "degree of metamorphism" or progressive alteration in the natural series from lignite to anthracite. Coal rank refers to the changes in geochemistry and resultant changes in reflectance caused by increasing thermal maturity of the coal. While, very differently, coal type refers solely to coals' depositional origin and the maceral–mineral admixture resulting from that origin (O'Keefe *et al*., 2013). These two classification methods are independent and orthogonal; therefore, within certain limits, any type of coal can be found at any rank (Neavel, 1981). South African coals are typically medium rank C bituminous coals (Gertenbach, 2009).

- Peat: Considered to be a precursor of coal, has industrial importance as a fuel in some regions, for example, Ireland and Finland. In its dehydrated form, peat is a highly effective absorbent for fuel and oil spills on land and water. It is also used as a conditioner for soil to make it more able to retain and slowly release water.
- Lignite/brown coal: This is the lowest rank of coal and used almost exclusively as fuel for electric power generation. Lignite is sometimes polished and has been used as an ornamental stone.
- Sub-bituminous coal: Coal, whose properties that range from those of lignite to those of bituminous coal. It is used primarily as fuel for steam-electric power generation and is an important source of light aromatic hydrocarbons for the chemical synthesis industry.
- Bituminous coal: Dense sedimentary rock, usually black, but sometimes dark brown, often with well-defined bands of bright and dull material. It is used primarily as fuel in steam-electric power generation, with substantial quantities used for heat and power applications in manufacturing and to make coke.
- Anthracite: considered to be the highest rank of coal, is a harder, glossy black coal used primarily for residential and commercial space heating.

- Graphite: technically the highest rank coal, is difficult to ignite and is not commonly used as fuel. It is mostly used in pencils and, when powdered, as a lubricant. Figure 2.11 depicts the various ranks of coal according to increasing carbon content.

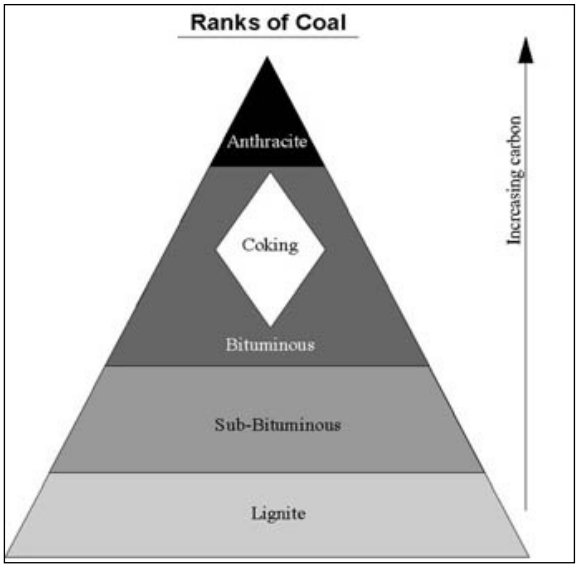

Figure 2.10: Different Ranks of Coal
(Source: Alberta Energy, 2011)

2.6.2.2 Coal Macerals

Coal is not homogenous; it is made up of organic and inorganic components. Coal macerals are the building blocks of the carbonaceous component of coal. They are microscopically recognizable components of coal and have different chemical compositions and different physical properties. Macerals are distinguished from each other on the basis of their morphology, hardness, optical properties and chemical characteristics (Stach *et al.*, 1982). Coal macerals owe their differences to the parent plant matter and conditions of deposition of the plant matter. They are analogous to minerals in inorganic rocks, but they differ from minerals in that they have no fixed chemical composition and lack a definite crystalline structure. Macerals change progressively both chemically and physically as the rank of coal advances. The three coal maceral groups are: vitrinite,

inertinite and liptinite. Vitrinite is a product of the decomposition of cellular plant material, while inertinite is a product of fossilized charcoal and liptinite is a product of decayed leafy matter, spores, pollen and algal matter (Stach *et al.*, 1982; Meyers, 1982; Falcon & Falcon, 1987).

2.6.2.3 Physical Properties of Vitrinite and Inertinite Groups

Basically there are two characteristics that influence the use of coal: its composition and its rank. Coal composition is in turn represented by two essentially independent factors: type (nature of the organic components) and grade (extent of dilution by mineral matter) (Suárez-Ruiz and Ward, 2008). The technique of coal petrology is used to express the fundamental parameters, which include:

- The nature of organic constituents in terms of macerals or maceral groups (an indicator of coal type).
- The mineral matter, including the major elements in the coal or oxides in the ash, the minerals in the coal, the forms of sulphur, and trace elements that may also be present (indicators of coal grade), and
- The vitrinite reflectance (which is usually taken as an indicator of coal rank (Suărez-Ruiz and Crelling, 2008)). Ro max is the maximum vitrinite reflectance is a measure of the maximum reflectance value obtained when rotating the stage 360°, using polarized light. Within the bituminous coal rank (Ro = approximately 0.5 to 1.5), directional anisotropy develops and increases with rank. For higher-rank coals, the minimum and maximum reflectance values are commonly measured. Table 2.2 provides a formal classificatin of the relation of coal rank to vitrinite reflectance values (R_oV_{mr} %).

Table 2.2: Classification of coals of coals by rank and organic maturity (ASTM 1981).

Coal rank		Vitrinite reflectance (random)	Volatile matter[1] (wt.% dmmf)	Bed moisture (wt %)	Calorific value MJ/kg (moist,mmf)	Hydro-carbon generation
Class	Group					
Anthracitic[2]	Meta-anthracite		2			Dry Gas
	Anthracite	2.50	8			
	Semianthracite	1.92	14			
Bituminous	Low volatile bituminous	1.51	22			Wet Gas
	Medium volatile bituminous	1.12	31			—
	High volatile A bituminous	0.75			32.6	
	High volatile B bituminous	0.50-0.75			30.2	Oil and Gas
	High volatile C bituminous					
Subbituminous	Subbituminous A[3]	0.50 ?		8-10	26.8	—
	Subbituminous B			25	24.4	
	Subbituminous C				22.1	
Lignitic	Lignite A	0.42		35	19.3	Early Gas
	Lignite B				14.7	
	Peat			75		

Optically homogeneous discrete organic material in coal is termed macerals (derived from the Latin macerare, to macerate, to separate) (Zeng, 1997). The macerals are the microscopically distinct areas in coal and are classified as (Ozdemir, 2004):

(i) Vitrinite (huminite)

(ii) liptinite (exinite)

(iii) inertinite

Vitrinite is very brittle, that is it fractures angularly and conchoidally, leaving a glossy or pitchy lustre on the fractured surface. Under pressure it fractures to form rectangular prisms or cubes and also forms splinters which are normally found concentrated in the coal

fines. Fissures and cleats caused by shrinkage and tectonic forces can be seen under the microscope. The density of vitrinite varies between 1.3 and 1.8g/cm^3, depending on the rank of coal. The resistance to polishing decreases with increasing rank. The pore volume of vitrinite also decreases with increasing coal rank. The reflectance of vitrinite is intermediate compared with other maceral groups. It increases with coal rank and hence it is used as a rank indicator (Stach *et al.*, 1982; Falcon & Falcon, 1987).

The inertinite group of macerals is also formed from the decomposition of cellulose and lignin from plant material. The difference to vitrinite is that the plant matter undergoes fusinisation either before deposition or on the peat surface. Fusinisation can include a number of material degradation processes such as charring, oxidation, mouldering and fungal attack. These processes produce substances that have very high carbon content, low hydrogen content and a high O to C ratio. During the coalification process inertinites alter very little because they are already degraded before deposition. These macerals are less reactive than liptinite and vitrinite. During coalification inert macerals may lose the remnant oxygen and hydrogen becoming more enriched in carbon. Inertinite maceral group comprises fusinite (pyrofusinte, degradofusinte, rank and primary fusinite), micrinite, sclerotinite, and semi-fusinite [and inertodetrinite, macrinite], and inertodetrinite, which are all rich in carbon [due to primary oxidation from smoldering or charring] (Stach *et al.*, 1982; (O'Keefe *et al*., 2013). In South African coals, a range of semi-fusinite[1] macerals occur, subdivided into reactive and inert semi-fusinite, based on the observed shade of grey relative to vitrinite; reactive semi-fusinite is ≤0.3% higher in reflectance than the maximum vitrinite reflectance (slightly lighter shade of gray, with definite structure, and a mottled appearance under crossed-polars) and inert semi-fusinite has a brighter appearance, but with a lower reflectance than fusinite (O'Keefe *et al*., 2013).

Liptinite macerals are considered to be produced from decayed leaf matter, spores, pollen and algal matter. Resins and plant waxes can also be part of liptinite macerals. Liptinite macerals tend to retain their original plant form, i.e., they resemble plant fossils. These are hydrogen rich and have the highest calorific values of all coal macerals. Macerals of

[1] Reactive semifusinite has been shown to be as reactive as vitrinite under certain conditions in South African coals (Falcon, 1986), and may explain why some inertinite-rich coals behave in a comparable manner during coking compared to vitrinite-rich coals of a comparable rank (O' Keefe, 2013).

liptinite are sporinite, cutinite, resinite, alginite (telalginite and lamalginite), liptodetrinite, fluorinite, and bituminite (Meyers, 1982).

The different coals are subdivided into a variety of macerals, sub-macerals, and maceral varieties on the basis of their reflectance, degree of destruction/preservation of original material, presence of cellular structure, gelification, and morphological features. The three maceral groups differ in both chemical composition and optical property, and their names conventionally end in *–inite* (Suárez-Ruiz and Ward, 2008).

When the processes of biochemical degradation ceased and the organic material was buried at great depths in the sedimentary environment, geochemical coalification occured over a long period of time, and under conditions of high temperature and pressure. As a result, the sediment of the original peat swamp was transformed and passes through the progressive evolutionary stages of lignite, sub-bituminous, and bituminous coal to anthracite and meta-anthracite. Throughout theses stages the physicochemical characteristics of the coal as well as its technological properties are modified (Suárez-Ruiz and Ward, 2008).

Figure 2.11 gives a general indication of the amounts of biogenic gases that was possibly generated during the coalification period for various coal types. The volume of the by-product gases increases with the rank of the coal, and is highest for anthracite, where the formation of every tonne of coal produces approximately 765 m^3 of CH_4 (Thakur *et al.,* 1994).

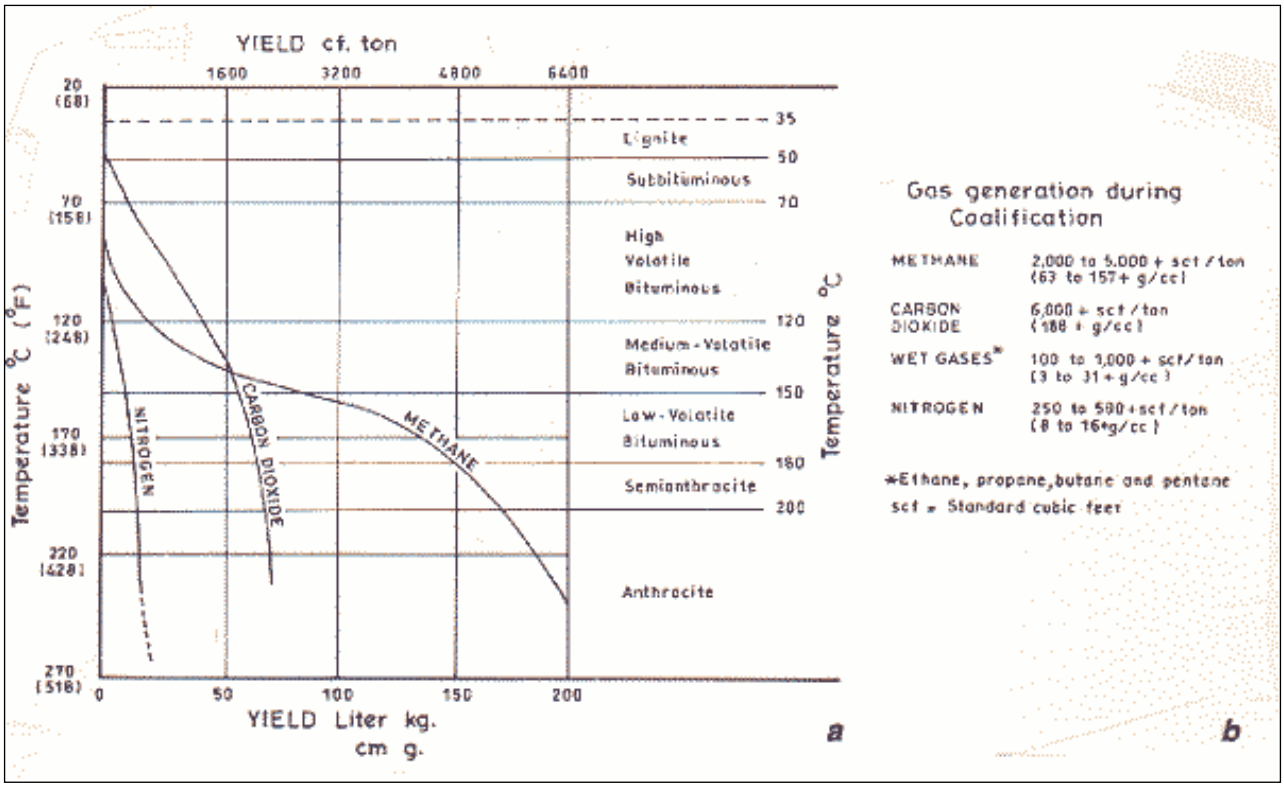

Figure 2.11: Gas Generation during coalification for different ranks of coal and temperature variants (*Thakur et al., 1994*)

2.7 Why does CO_2 stay underground?

There a number of reasons why CO_2 has a good potential to be sequestered in geological media such as coal seams for the purpose of CCS or for the prospective of ECBM. The following sub-sections highlight the various advantageous chemical and physical properties of CO_2. The benefit of the nature and make-up of the coal medium as a remarkable sorption media is detailed with regards to the permeability, porosity and diffusivity of various coal types.

2.7.1 CO_2 as a super-critical fluid

Carbon dioxide is a colourless and odourless gas at standard temperature and pressure, with a density of around 1.98 kg/m^3, (i.e. slightly more than 1.5 times the density of air) (Viljoen *et al.*, 2010). At temperatures below -78 °C, CO_2 condenses into a white solid

called ‘dry ice’. When warmed, dry ice vaporizes directly from a solid to CO_2 gas in a process called ‘sublimation’. CO_2 has several commercial applications, such as bubbles in soft drinks and beer, dry ice for cooling, and in fire extinguishers where it displaces the oxygen the fire needs to burn) (Viljoen *et al.*, 2010). Figure 2.12 outlines the phase diagram for CO_2 showing the distinct changes that CO_2 undergoes at various temperatures and pressures.

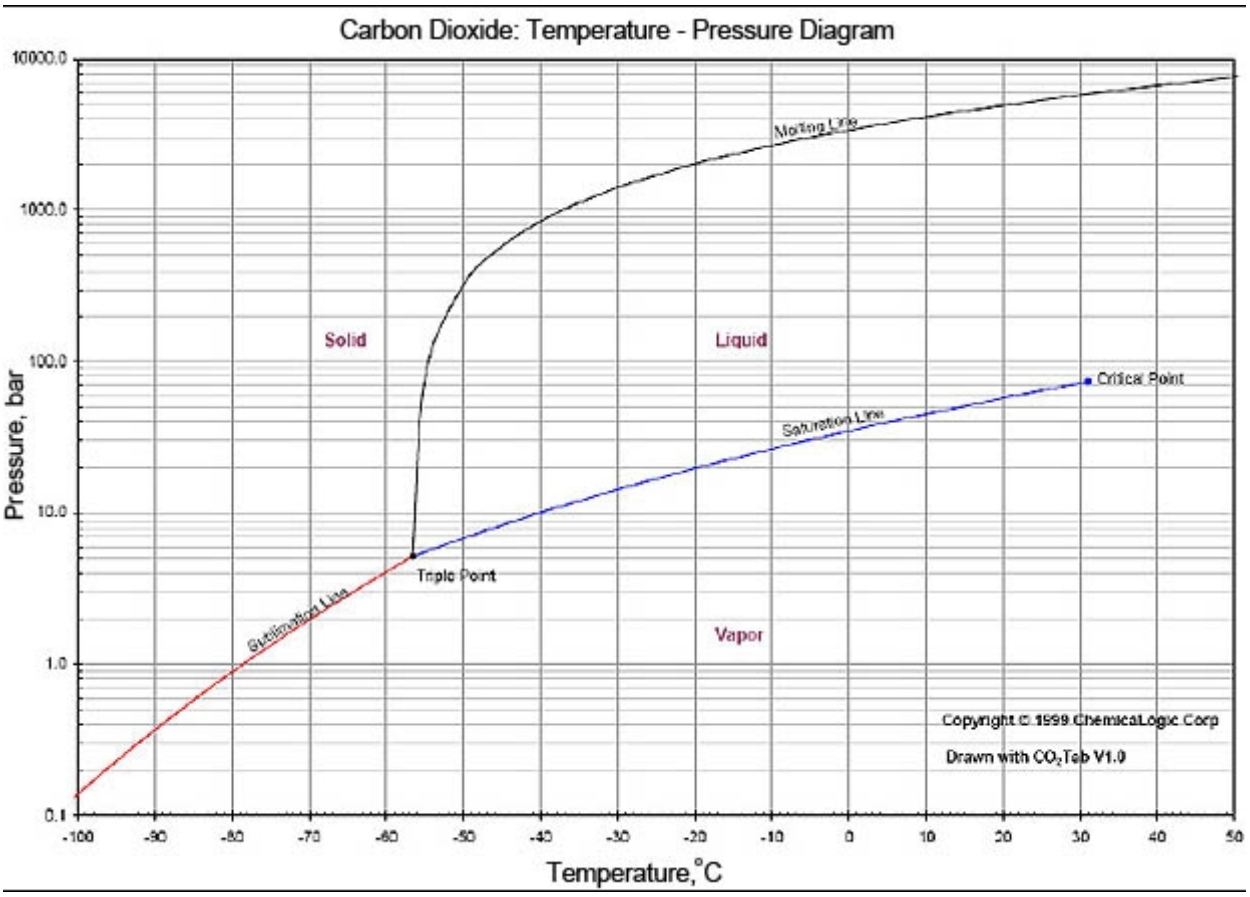

Figure 2.12 CO_2 phase diagram: Temperature – Pressure
(*Source: Global CCS Institute, 2012*)

With enough added pressure, liquid CO_2 can also be formed, which is essentially immiscible with water. Only a small amount of CO_2 is soluble in formation waters (Ennis-King and Paterson, 2000), forming a weak acid (carbonic acid) in the process. CO_2 solubility decreases with an initial increase in temperature and salinity, but increases with an increase in pressure. At very high temperatures, and especially in a high-pressure

environment, i.e. a deep pressurized basin, CO_2 solubility in water increases again (Viljoen *et al.*, 2010).

The thermodynamic critical point of CO_2 is at 31.1 °C and 7.38 MPa (Bachu 2000; Holloway & Savage 1993; Nalawade *et al.* 2006 and van der Meer, 1993). At temperatures and pressures in excess of this point, CO_2 occurs in the supercritical phase. In the supercritical phase, CO_2 has characteristics typical of both a gas and a fluid (Figure 2.12).

It can diffuse through solids like a gas, and dissolve materials like a liquid. It occurs as a fluid and its density approaches that of a liquid; it can have a density in the range 150 to 1 060 kg/m^3. In Figure 2.13, note that above the critical depth, CO_2 is in gaseous state (balloons); below the critical depth it is in liquid-like state (droplets). Volumetric relationship is shown by blue numbers (e.g. 100 m^3 of CO_2 at surface would occupy 0.32 m^3 at a depth of 1 km) (CO2CRC, 2008).

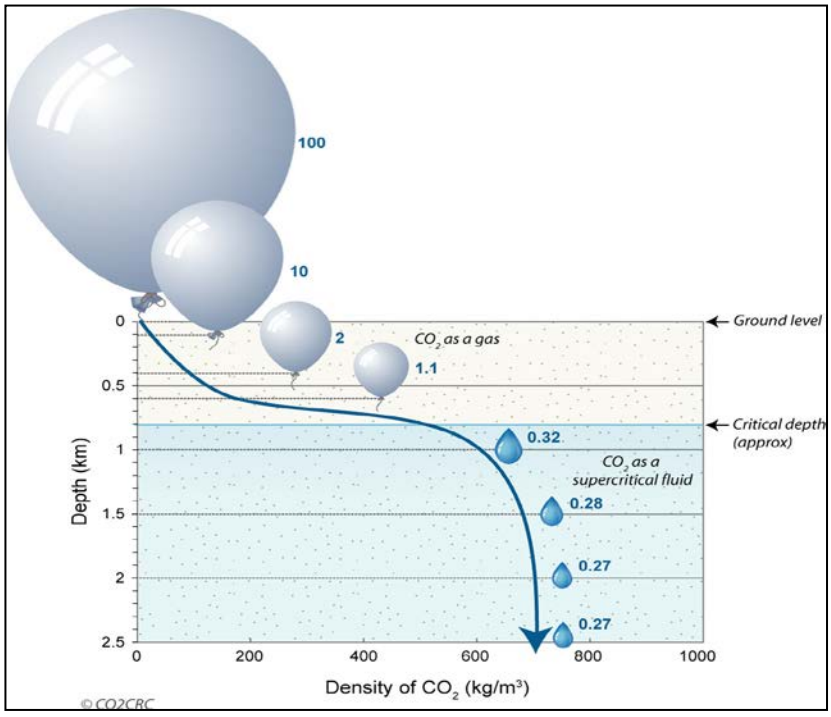

Figure 2.13 CO_2 Density Change with Depth *(CO2CRC, 2008)*

Considering average geothermal gradients and hydrostatic pressure conditions, it is assumed that a burial depth of at least 800 m is needed to achieve a high enough

temperature and pressure for CO_2 to occur in the supercritical phase (IPCC, 2005 and Figure 2.13). Below 800 m (under normal sedimentary basin conditions), supercritical CO_2 is 30–40 % less dense than a typical saline formation water under the same conditions (Ennis-King & Paterson, 2001). This means that the lighter CO_2 will naturally rise upwards by buoyancy through the reservoir rock until trapped by various physical, hydrodynamic or geochemical trapping mechanisms (although in the longer term — hundreds to thousands of years — the CO_2 dissolved will sink as it goes into solution, due to density changes (CO2CRC, 2008).

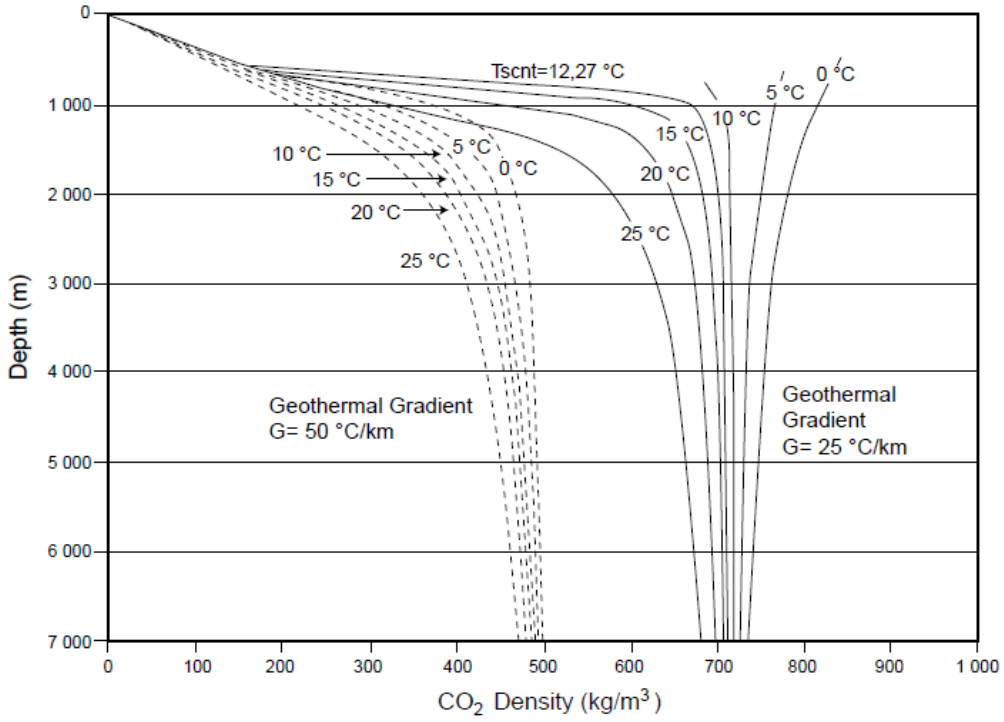

Figure 2.14 CO_2 density as a function of depth [additionally indicating the effect of geothermal gradient (G) and surface temperature (Ts)] *(Bachu, 2003)*

For CO_2 storage in coal seams, where adsorbed CO_2 may be in the adsobed phase (i.e. not supercritical), CO_2 density will be substantially less and more variable with respect to change in geothermal gradient. Figure 2.14 indicates that, in the depth range 300–800 m, which is the depth interval where CO_2 storage could be considered given permeability and safety issues, CO_2 (gaseous phase) has a density range of 60–270 kg/m^3 in the case of a 50 °C/km geothermal gradient. In the case of a 25 °C/km geothermal gradient, however,

CO_2 density varies between 60 and 820 kg/m^3 over the same depth range (Viljoen *et al.*, 2010).

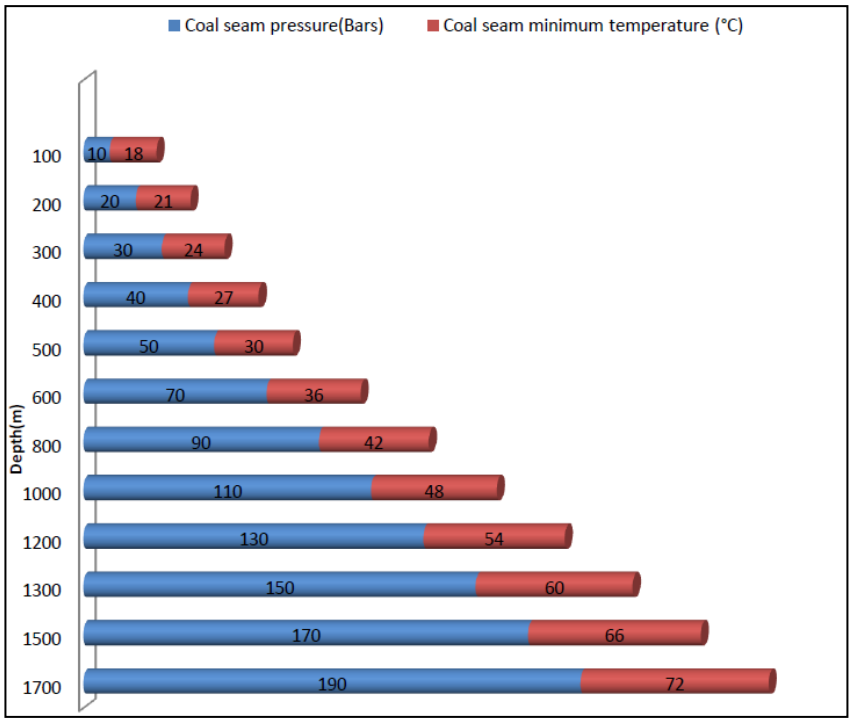

Figure 2.15 A bar chart showing the changes in pressure and temperature with depth to 1700m *(Qing-Ling, 2008)*

A supercritical fluid acts as neither a gas nor a liquid. Carbon dioxide stored in deep saline aquifers, depleted petroleum reservoirs, or unmineable coal seams, will preferentially be injected as a supercritical fluid. Based on worldwide average geothermal and hydrostatic pressure conditions, this equates to an approximate minimum subsurface depth of about 800 m (Figure 2.15) (Holloway and Savage, 1993; van der Meer, 1993). In its supercritical form, CO_2 is much denser than gaseous CO_2 and therefore a greater volume of CO_2 can be stored in the pore space available (CO2CRC, 2008). The CO_2 storage potential could be extremely high for supercritical CO_2 at pressures higher than 7.5MPa (75 Bar) (Hamelinck, 2000).

2.7.2 CO_2 Storage Mechanisms

2.7.2.1 Residual Storage

Reservoir rocks act like a tight, rigid sponge. Air on a sponge is residually trapped and the sponge usually has to be squeezed in water several times to replace the air with water. When supercritical liquid CO_2 is pumped and injected under pressure into a rock formation, it displaces fluid as it moves through the porous rock causing much of it to becomes "stuck" due to binding forces within the pore spaces of the storage medium and does not move. This is known as residual trapping (Figure 2.16).

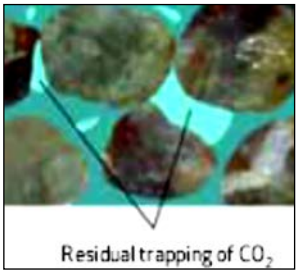

Figure 2.16: Residual Trapping mechanism of CO_2

(IEA, 2007)

2.7.2.2 Mineral Storage

Carbon dioxide dissolved in salt water is weakly acidic and can react with the minerals that are present in the surrounding rocks, which then go on to form new minerals, as a coating on the rock (much like shell-fish use calcium and carbon from sea water to form their shells). This process can be rapid or very slow (depending on the chemistry of the storage media) and it effectively binds the CO_2 and will keep it in place for an infinite period of time.

High concentration CO_2 from a capture step in industrial processes and flue gas systems is brought into contact with metal oxide bearing materials with the purpose of fixing the CO_2 as carbonates. This carbonation can be done in-situ where the CO_2 stream is injected into geological formations rich in alkaline base metal oxides or ex-situ in a chemical processing plant during the pre-treatment of silicates and industrial residues like fly ash from the steel industry (Lasaga and Berner 1998) (Figure 2.17).

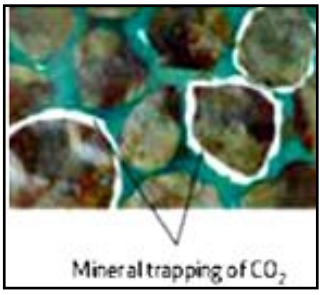

Figure 2.17: Mineral Trapping mechanism of CO_2

(IEA, 2007)

2.7.2.3 Sorption in Coals and Advantages

Coal is able to store a significant amount of gas due to its highly porous nature, having micro, macro (fractures and cleats) and meso pores. According to Day *et al.* (2007) the advantages of coal for CO_2 sorption by storing CO_2 into deep unminable coal seams is an attractive option from a sequestration point of view for the following reasons:

1. Coal has a fractured microporous structure and therefore a high internal surface area.
2. Coal can physically adsorb and absorb large amounts of CO_2.

Gas is kept in coal beds in four ways:

- adsorption upon internal surfaces (in micropores and mesopores)
- absorption into the molecular structure of coal
- as free gas in voids, cleats, and fractures; and as a solute in groundwater present within the coal seam.

3. Deep coal seams generally contain significant quantities of CH_4, and this is displaced when CO_2 is injected into the coal seam.
4. Recovery of the displaced CH_4 (i.e. ECBM), via CO_2 sequestration in coal seams, could offset some of the revenue costs of the CO_2 sequestration process.

The relatively high excess sorption capacity exhibited by coal for CO_2 (typically 6-10% by weight) is what makes coal a good sequestration target (Sakurovs *et al.,* 2008). These so called unmineable coals are generally too thin, too deep or too high in sulphur and mineral

matter content to be of economic benefit to be mined. Recovery of CBM or ECBM would be the most economic option as well as a method for permanent storage of the CO_2 in the coal seams.

Adsorption isotherms are one of the most important tools for the characterisation of solid adsorbent materials, such as coal. Adsorption isotherms are affected by the nature of the coal itself and environmental parameters, as depicted in Figure 2.18. The variables that affect the CO_2-coal interactions need to be investigated in order to develop an efficient method for CO_2 sequestration (Ozdemir, 2004).

Studies of the high-pressure adsorption/desorption isotherms of CO_2 is important for determining the coals ultimate CO_2 sequestration capacity. The information provided by the adsorption/desorption isotherms is used as one of the primary inputs to the simulations of coalbed sequestration processes. The CO_2 when injected into the coal seams is taken up into the coal structure in two ways: by adsorption and absorption. The relative proportions of adsorbed and absorbed gas in coal are unknown and therefore the collective term 'sorption' can be used to encompass the two modes of gas retention as described above.

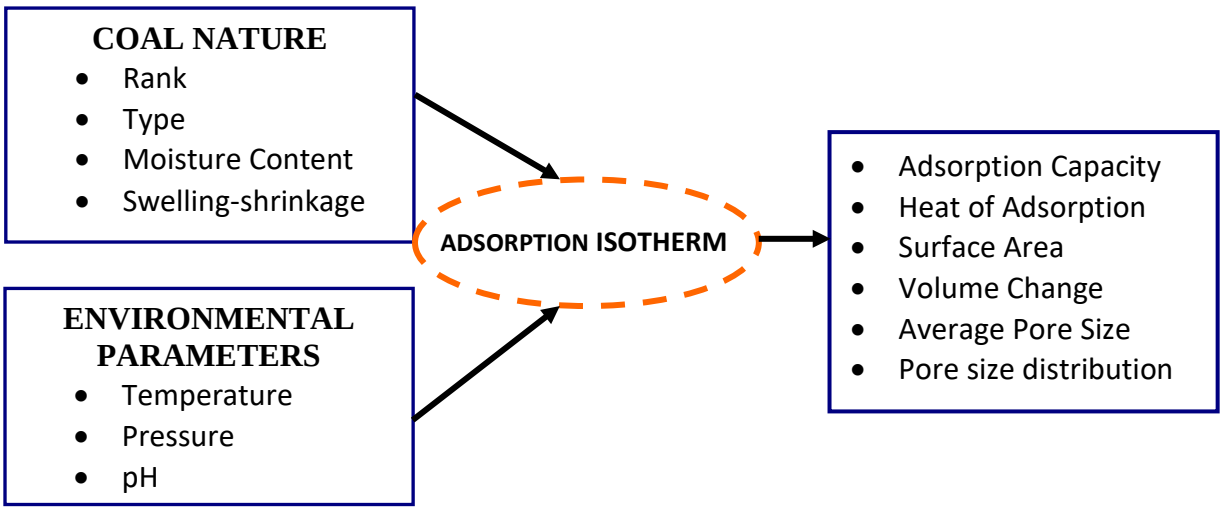

Figure: 2.18 Parameters that affect the adsorption isotherm, adsorption capacity and stability of CO_2 adsorbed on coal *(Ozdemir, 2004)*

The nature of good adsorption and desorption of CO_2 and CH_4 in coal is largely due to their individual molecular structures. CO_2 molecules are small and have a low activation energy and can easily penetrate pores inaccessible to other gases. The CO_2 molecule has a non-polar nature, hence it does not have a dipole moment and has a linear structure. The CH_4 molecule is tetrahedral in shape (a rectangular tetrahedron). The molecule is chemically stable as the bonds are weakly polarized with a lack of free electrons (Zarębska & Ceglarska-Stefańska, 2008). This has promoted interest into furthering investigations into the use of coal as an absorbent for CO_2 storage, and CH_4 recovery. It is necessary to gain an understanding with regards to the different sorption actions, and to distinguish how the different coal properties and CO_2 will interact over time.

2.7.2.4 Coal Porosity

The most important property of adsorbent materials, the property that is decisive for the adsorbent's usage, is the pore structure. The total number of pores, their shape, and size determine the adsorption capacity and even the dynamic adsorption rate of the material. Generally, pores are divided into macro-, meso-, and micro pores. According to IUPAC, pores are classified as shown in Table 2.3 (Inglezakis & Poulopoulos, 2006).

Table 2.3 The classification of pores according to their size
(Inglezakis & Poulopoulos, 2006).

Type	**Pore diameter *d* (nm)**
Macrospores	$d > 50$
Mesopores	$2 \leq d \leq 50$
Microspores	$d < 2$
Ultramicropores	$d < 0.7$
Supermicropores	$0.7 < d_0^a < 2$

d_0^a is the pore width for slit-type or the pore diameter for cylindrical pores.

Porosity is a property of solids that is attributed to their structure and is evident by the presence of pores between internal super-molecular structures. It is not considered to be an intrinsic property of the solids, but depends on the treatment of the materials. The porosity can be developed by the aggregation of particles as well as by the detachment of a part of the mass of the solid. The pores shaped during the second process are comparable in shape and size with the particles detached (Inglezakis & Poulopoulos, 2006).

Adsorptive molecules transport through macro-pores to the meso-pores and finally enter the micro-pores. The micro-pores usually constitute the largest portion of the internal surface and contribute the most to the total pore volume. The attractive forces are stronger and the pores are filled at low relative pressures in the micro porosity, and therefore, most of the adsorption of gaseous adsorptive occurs within that region. Thus, the total pore volume and the pore size distribution determine the adsorption capacity (Inglezakis & Poulopoulos, 2006).

2.8 Adsorption Principles

The term “sorption” is used to describe every type of capture of a substance from the external surface of solids, liquids, or mesomorphs, as well as from the internal surface of porous solids or liquids (Inglezakis and Poulopoulos, 2006). Depending on the type of bonding involved, sorption can be classified as follows:

a) physical sorption (physisorption)
b) chemical sorption (chemisorption)
c) electrostatic sorption (ion exchange) (Inglezakis and Poulopoulos, 2006).

In this research, focus will only be on physical and chemical sorption, which will be discussed in more detail later on in this chapter.

The term “adsorption” includes the uptake of gaseous or liquid components of mixtures from the external and/or internal surface of porous solids. In chemical engineering, adsorption is called the separation process during which specific components of one phase

of a fluid are transferred onto the surface of a solid adsorbent (Inglezakis & Poulopoulos, 2006) (Figure 2.19).

When the species of the adsorbate travel between the atoms, ions, or the molecules of the adsorbent, the phenomenon of “absorption” takes place; this discriminates absorption from the main phenomenon of adsorption that takes place on the interface. The adsorption of various substances from solids is due to the increased free surface energy of the solids due to their extensive surface. According to the second law of thermodynamics, this energy has to be reduced. This is achieved by reducing the surface tension via the capture of extrinsic substances (Inglezakis and Poulopoulos, 2006).

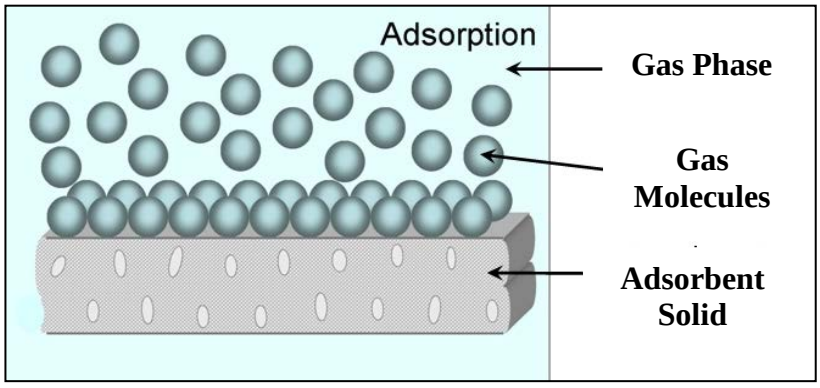

Figure 2.19: Surface Adsorption Phenomenon *(Li, 2011)*

When any clean solid surface is exposed to a gas, the latter may adsorb on the solid surface to varying degree. It has been observed that gas adsorption on solid surfaces does not stop at a monolayer state and that more than one layer (multilayer) adsorption will take place only if the pressure is reasonably high (For CO_2 this equates to supercritical state). Experimental data show this when the volume of gas adsorbed, V_{gas}, is plotted against P_{gas} (Birdi, 2010).

2.8.1 Chemisorption

Chemisorption (or chemical adsorption) is adsorption in which the forces involved are valence forces of the same kind as those operating in the formation of chemical compounds. The problem of distinguishing between chemisorption and physisorption (see below) is basically the same as that of distinguishing between chemical and physical interaction in general (Everett and Koopal, 2001). No absolutely sharp distinction can be made and intermediate cases exist, for example, adsorption involving strong hydrogen bonds or weak charge transfer. Chemisorption generally has a high enthalpy of adsorption, typically; ∆Hadsorption is 200-400KJ/mol.

2.8.2 Physisorption

Physisorption (or physical adsorption) is adsorption in which the forces involved are intermolecular forces (van der Waals forces) of the same kind as those responsible for the imperfection of real gases and the condensation of vapours, and which do not involve a significant change in the electronic orbital patterns of the species involved (Everett and Koopal, 2001). Physical Adsorption takes place with formation of multilayer of adsorbate on adsorbent. It has low enthalpy of adsorption i.e. ΔHadsorption is 20-40KJ/mol. It takes place at low temperature below boiling point of adsorbate. As the temperature increases in, process of Physisorption decreases (Zheng *et al*., 2009).

2.8.3 Surface Excess and Absolute Adsorption

Adsorption itself is, according to Gibbs formalism, an excess quantity. The situation at the gas/solid interface is schematically represented in Figure 2.20. As consequence of the adsorption potential, the average number of molecules in an element volume near the surface is larger than in an element volume of equal size in the bulk gas. Both molecular simulation of adsorption and experimental proof reveal that this density profile vanishes over quite a short range.

Therefore, the layer on the solid surface, where adsorbate molecules are concentrated, is referred to as the "adsorption space" or "adsorbate phase". It thus assumes a definite thickness (τ) for the adsorbed phase (Zhou, 2001).

Although the density profile can be determined by molecular simulation, it can hardly be both intermolecular distances decrease linearly with temperature and intersect at a point, which gives the value of $\sigma_{ff} = 0.34\,\mathrm{nm}$, the distance between molecules when the Leonard-Jones potential reaches minimum (Zhou, 2001).

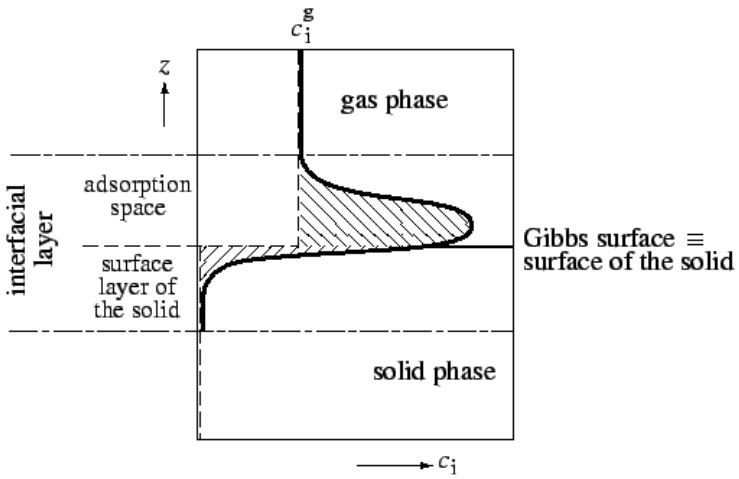

Figure 2.20 ***Schematic of a gas-solid adsorption system. The solid-line curve indicates the density profile (ρ) as a function of distance (z) normal to the surface in the real system; the broken line is in the case without adsorption, and dashed-dotted line is the boundary between phases. The shadowed area marks the excess amount of adsorbed substance*** *(Everett & Koopal, 2001).*

2.8.4 Supercritical Adsorption

Supercritical adsorption is the adsorption at above-critical temperatures and pressures, but it is sometimes referred to as the adsorption of supercritical fluids. However, there are different tacit understandings of supercritical fluids. For example, "a fluid is said to be 'supercritical' when its temperature and pressure exceed the temperature and pressure at the critical point" (Savage *et al.*, 1995). In the supercritical extraction studies, however,

"supercritical fluid" is especially applied for a narrow temperature region of (1-1.2)T_c or T_c + 10K, which is sometimes called the supercritical region (Findenegg, 1984). According to the adsorption behavior, the adsorption of gases on solids can be classified in three typical temperature ranges relative to the critical temperature (Zhou, 2001):

(i) Subcritical region ($T < T_c$)
(ii) Near –critical region ($T_c < T < T_c + 10$)
(iii) The region $T > T_c + 10$

It is, therefore, reasonable to assume that the adsorbate in the adsorbed phase is largely in the liquid state, based on which different adsorption and thermodynamic theories as well as their applications were developed. It seems that no upper limit applied for pressure and, hence "high-pressure adsorption" is synonymous with "supercritical adsorption".

2.9 Gas Adsorption Measurement Methods

The measurement of pure-gas isotherms is rather straightforward. The amount adsorbed at equilibrium can be determined by two commonly used methods: (1) the volumetric method, where the pressure-drop before and after adsorption in a closed system is measured, and (2) where the gravimetric method, in which the amount adsorbed is directly determined by the weight gain in a flow system. For mixed-gas isotherms, additional measurements are necessary for determining the compositions of both gas and adsorbed phases (Yang, 1997). It should be mentioned that the accuracy of each method strongly depends on the careful design of the measurement apparatus and experimental conditions (Ozdemir, 2004).

2.9.1 Volumetric Adsorption (Manometric) Methods

The volumetric method is the most widely used technique for determining gas sorption capacities on coal (Busch *et al*., 2003, 2004, 2007; Belmabkhout *et al*., 2004; Clarkson and Bustin, 1999; Chaback *et al*., 1996; DeGance *et al*., 1993; Harpalani et al., 2006;

Joubert *et al*., 1973; Krooss *et al*., 2002; Laxminarayana and Crosdale, 1999(b); Li *et al*., 2010; Mastalerz *et al*., 2004; Mavor *et al*., 1990; Nodzenski, 1998; Prinz *et al*., 2001; Siemons and Busch, 2007; Dutta *et al*., 2008; Zarębska and Ceglarska-Stefańska, 2008; Pone *et al*., 2009; Dutta *et al*., 2011; Merkel *et al*., 2015 and Li *et al*., 2016, to name a few). The setups are either custom made, or designed in-house, and consist typically of calibrated reference and sample cells (Figure 2.21).

In the volumetric procedure, defined amounts of gas are successively transferred from a calibrated reference volume into the sample cell containing a sample, coal for example. Pressure and temperature transducers are either connected to the sample cell only or to both reference and sample cell. To analyse sorption from gas mixtures (combination of usually N_2, CH_4 and CO_2) the gas composition has to be determined by using a gas chromatograph (GC) equipped, for instance, with a Thermal Conductivity Detector (TCD). Prior to the sorption experiment, the void volume (Vvoid) of the sample cell is determined by expansion of a “non-sorbing” gas, which is typically helium (He). Helium densities are calculated using the equation of state (EOS) or using the van der Waals equation with the; *a* and *b* parameters. This procedure also provides the skeletal volume (V sample) and the skeletal density (ρ sample) of the sample.

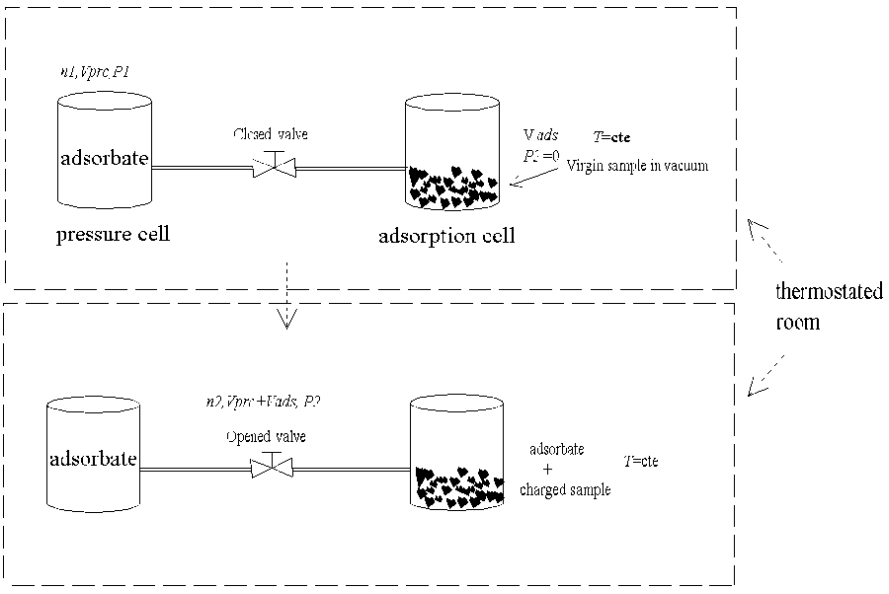

Figure 2.21 Schematic of the volumetric apparatus *(Belmabkhout et al., 2004)*

For gas sorption isotherms, the void volume multiplied by the density of the gas (or supercritical) phase ($V_{void} \cdot \rho CO_2(T,p)$), yields the "non-sorption" reference mass, i.e. the amount of gas (supercritical fluid) that would be accommodated in the measuring cell if no sorption takes place. Densities are calculated using the corresponding EOS for CO_2, CH_4, N_2, or their binary and ternary mixtures (Peng and Robinson, 1976; Setzmann and Wagner, 1991; Span and Wagner, 1996). The excess sorption mass (m excess CO_2) is the difference between the mass of gas that has been transferred into the measuring cell up to a given pressure step and the "non-sorption" reference mass.

The difficulty involved in the volumetric method lies in the slow attainment of equilibrium, caused by the diffusion resistance in the adsorbent bed as well as in the small-diameter tubing's. Thus, the time required for equilibration in a static system is usually in the order of days. The equilibration time can be substantially reduced to below one hour by circulating the gas mixture through the sample by using a circulating pump (Yang, 1997).

A volumetric system is used in this research, with pure CO_2 gas for adsorption measurements and CH_4 desorption measurements (Detailed in chapter 3, section 3.4).

2.9.2 Gravimetric Gas Adsorption Methods

Whilst this technique was not used in the current research, a short discussion is included to describe the method that has been used by some researchers (Humayun and Tomasko, 2000; Ozedemir, 2004; Faiz *et* al., 2007; Ottiger *et* al., 2008; Bae *et al*., 2009). In the gravimetric technique, only the measurement of the total amount of adsorbate is required. The adsorbate composition can be calculated by a rigorous thermodynamic technique suggested by Van Ness, using the Gibbs adsorption isotherm (Yang, 1997). A sensitive microbalance is used to measure the adsorption isotherm. Its sensitivity is very high, since only the difference in weight change is measured. These microbalances can measure weight differences in the range of nanograms to milligrams. With such extreme sensitivity, it is possible to measure the weight change caused by the adsorption of a single monolayer on a solid if the surface area is large.

The schematic is depicted in Figure 2.22. The normal procedure is to expose the sample to the adsorbate gas at a certain pressure, allowing sufficient time for equilibrium to be reached, and then determining the mass change. This is repeated for a number of different pressures, and the number of moles adsorbed as a function of pressure is plotted to give an adsorption isotherm (Belmabkhout *et al*., 2004; Birdi, 2010). Microbalances (stainless steel) can be made to handle pressures as high as 120 MPa (120 atm) since gases that adsorb weakly or boil at very low pressures can still be used (Birdi, 2010).

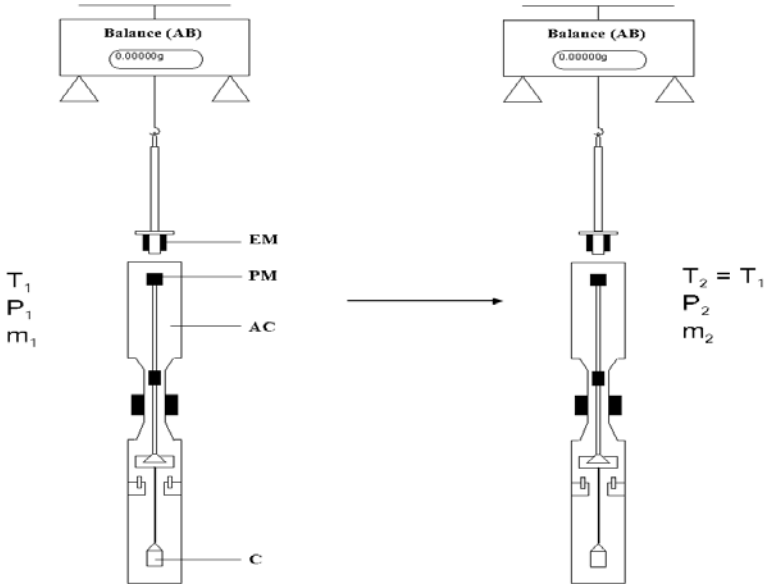

Figure 2.22 Schematic diagram of the principle of the gravimetric measurements
(Belmabkhout et al., 2004)

2.10 Gas Adsorption Isotherms

The amount of gas adsorbed by a solid sample is a function of the mass of the sample, the temperature and pressure, and the nature of both the solid and the gas (Gregg and Sing, 1982). The adsorption of a given gas on a particular solid can be represented by an adsorption isotherm, which is a plot of the amount adsorbed as a function of pressure at constant temperature. The shape of adsorption isotherms can provide information about the adsorption process, and the porosity as well as the surface area of the adsorbent. According to the IUPAC classification (IUPAC 1972), there are six significantly different

adsorption isotherms describing the physical adsorption as shown in Figure 2.24 (Gregg and Sing, 1982; Birdi, 2010).

- A Type I isotherm generally occurs when a monolayer of adsorbate molecules is adsorbed on a non-porous solid or when adsorption is dominated by a micro pore filling process. This type of isotherm is often called a Langmuir type isotherm.
- Type II is displayed by a nonporous or macroporous adsorbent. This isotherm is characterized by an inflection point, which represents the completion of the monolayer and the beginning of the formation of multilayers.
- Type III adsorption isotherm is typical for a non-porous or macroporous adsorbent and is observed for weak adsorbent-adsorbate interactions.
- The type IV isotherm which is similar to the Type II is typical for a mesoporous adsorbent. It displays a hysteresis loop due to capillary condensation.
- Type V is typical for non-porous or macroporous adsorbents and is observed for weak adsorbent-adsorbate interactions. Type VI isotherms or stepped isotherms are included in the classification although they are rare (Florentin *et al*., 2009).

Because coal is a heterogeneous, microporous solid, the adsorption isotherms of gases, including N_2, CH_4, and CO_2, would be expected to follow a Type I isotherm. However, various isotherms have been reported in the literature for CO_2 adsorption on coals. These deviations could be attributed to the influences of either variance in pressure, temperature and most possibly due to coal type. The other factor to consider, would be with regard to the nature of sorption type; i.e. physi, chemi or supercritical sorption mechanisms which affect the rate of sorption kinetics (Gregg and Sing 1982; Zhou, 2001; Everett and Koopal, 2001 and Birdi 2010). It is due to these many factors that adsorption experimental data needs to be mathematically modelled and fitted to theoretical adsorption models to evaluate the mechanism(s) of adsorption that occurs as depicted in Figure 2.23 and is expanded on further in section 2.11 which details the theoretical mathematical adsorption models and their different assumptions that have been applied to determine the sorption mechanism(s) of a specific sorbent.

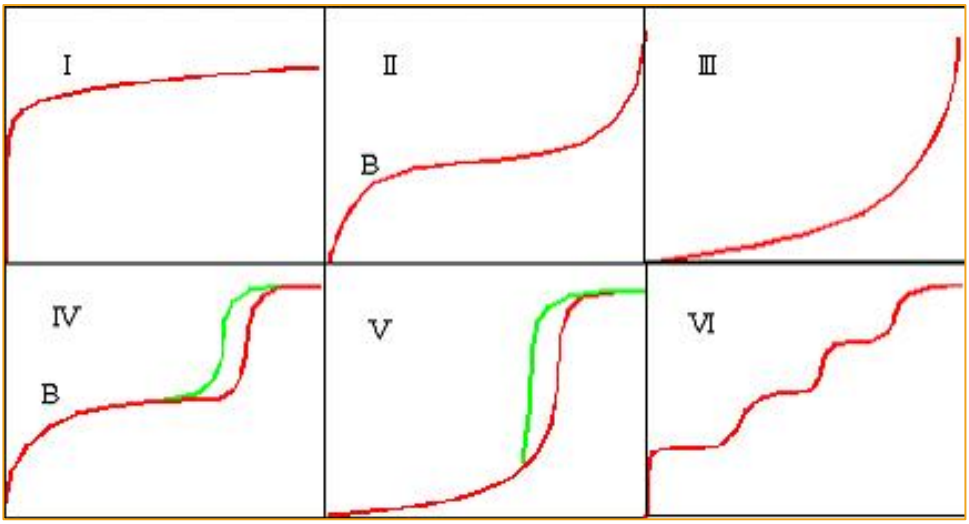

Figure 2.23 Depicting typical Adsorption isotherms:
Type I: Langmuir Monolayer, Type II &III: BET multilayer, Type IV & V: Dubinin pore-filling,
Type VI: Nonporous & uniform solid surfaces (*Birdi, 2010)*

2.11 Theoretical Adsorption Models

Adsorption isotherms simulate the amount of a gas in this case CO_2 adsorbed on coal at different pressures and isothermal conditions. Experimental data that is generated for the entire adsorption process is used and fitted to the most popularly used theoretical models outlined below.

2.11.1 Langmuir Model

The classical theory used to describe this isotherm for micro porous materials is based on the Langmuir equation. This isotherm displays a steep increase in the volume adsorbed at low pressures due to enhanced adsorption between the adsorbate molecules. The isotherm then flattens out into a plateau region at higher pressures, which is believed to be caused by the completion of the formation of a monolayer of adsorbed gas (Yu *et al.,* 2007).

The Langmuir model assumes that a state of dynamic equilibrium is established between the adsorbate vapor and the adsorbent surface and that adsorption is restricted to a single monolayer. The adsorbent surface is thought to be composed of a regular array of

energetically homogeneous adsorption sites, upon which an adsorbed monolayer is assumed to form. The rate of condensation is assumed to be equal to the rate of evaporation from the adsorbed monolayer at a given relative pressure and constant temperature. At high pressures, all sites available on the adsorbent are occupied by the adsorbate. Hence, beyond a certain pressure, the adsorbent can no longer adsorb adsorbate. This pressure is called the saturation pressure.

The Langmuir equation correctly expresses the adsorption behavior for a wide range of pressures. The pressure constant is a measure of the isotherm curvature (Yu *et al.,* 2007). This model will be used to model the experimental data generated from the current study.

2.11.2 Freundlich Model

Freundlich isotherm is the earliest known relationship describing the non-ideal and reversible adsorption, not restricted to the formation of monolayer. This empirical model can be applied to multilayer adsorption, with non-uniform distribution of adsorption heat and affinities over the heterogeneous surface (Foo & Hameed, 2010). The amount adsorbed is the summation of adsorption on all sites (each having bond energy), with the stronger binding sites are occupied first, until adsorption energy are exponentially decreased upon the completion of adsorption process. At present, Freundlich isotherm is widely applied in heterogeneous systems especially for organic compounds or highly interactive species on activated carbon and molecular sieves. The slope ranges between 0 and 1 is a measure of adsorption intensity or surface heterogeneity, becoming more heterogeneous as its value gets closer to zero (Foo & Hameed 2010). It is for this reason that this model was used to fit the experimental data generated in this study.

2.11.3 Temkin model

Temkin isotherm is the early model describing the adsorption of hydrogen onto platinum electrodes within the acidic solutions. The isotherm contains a factor that explicitly taking

into the account of adsorbent–adsorbate interactions. By ignoring the extremely low and large value of concentrations, the model assumes that heat of adsorption (function of temperature) of all molecules in the layer would decrease linearly rather than logarithmic with coverage. As implied in the equation, its derivation is characterized by a uniform distribution of binding energies (up to some maximum binding energy).

The Temkin isotherm equation is based on the following assumptions:

1. The heat of adsorption of all the molecules in layer decreases linearly with coverage due to adsorbent-adsorbate interactions, and that the adsorption is characterized by a uniform distribution of the bonding energies, up to some maximum binding energy (Oladoja *et al.*, 2008).
2. Like the Langmuir equation, its derivation assumes that all the sorption sites are identical but, unlike the Langmuir equation, it also assumes that, due to the influence of the particles sorbed at neighbouring sites, the sorption energy of each unoccupied site decreases proportionally with the increase in q_e, see equation (2.13) This assumption implies that when all the sites are occupied, the distribution of sorption energies is uniform on the interval (Vega *et al.*, 2011).
3. Additionally, it is assumed that q_e does not approach either zero or unity (Vega *et al.*, 2011).

The Temkin equation is excellent for predicting the gas phase equilibrium (when organization in a tightly packed structure (as synonymous with coal) with identical orientation is not necessary) (Kim *et al.*, 2004), and for this reason was used to model experimental data from this study.

A summary of all the three isotherm adsorption models containi4g their plots together with mathematical linear and nonlinear forms is shown in Table 2.4 (Foo & Hameed 2010). Adsorption CO_2 experimental data will be fitted to these three (3) theoretical adsorption models to evaluate the mechanism of adsorption type, either mono-layer, multi-layer or pore filling that occurs for the various SA coals tested.

Table 2.4 Summary of Theoretical Isotherm Models *(Foo & Hameed 2010)*

ISOTHERM	NON-LINEAR FORM	LINEAR FORM	PLOT
Langmuir	$q_e = \frac{Q_o b C_e}{1 + bC_e}$	$\frac{1}{q_e} = \frac{1}{Q_o} + \frac{1}{bQ_o C_e}$	$\frac{1}{q_e}\ Vs\ \frac{1}{C_e}$
Freundlich	$q_e = K_F C_e^{\frac{1}{n}}$	$logq_e = logK_F + \frac{1}{n} logC_e$	$\log q_e\ Vs\ logC_e$
Temkin	$q_e = \frac{RT}{b_T} lnA_T C_e$	$qe = \frac{RT}{b_T} lnA_T + \left(\frac{RT}{b_T}\right) lnC_e$	$q_e\ Vs\ lnC_e$

Where:

A_T -Temkin isotherm equilibrium binding constant (L/g)

b - Langmuir isotherm constant ($L.mol^{-1}$)

b_T- Temkin isotherm constant

C_{e-} equilibrium concentration (mol/L)

C_{o-} adsorbate initial concentration (mol/L)

K_F -Freundlich isotherm constant (mg/g) (dm^3/g) related to adsorption capacity

K_L -Langmuir isotherm constant (mol/g)

K_T- Temkin equilibrium binding constant

q_{e-} amount of adsorbate in the adsorbent at equilibrium (mg/g)

q_{s-} Theoretical isotherm saturation capacity (mg/g)

Q_{o-} maximum monolayer coverage capacities (mg/g)

R- Universal gas constant (8.314 J/mol K)

T- Temperature (K)

2.12 Review of previous studies concerning CO_2 adsorption in coal

2.12.1 Effect of coal rank and composition on CO_2 adsorption

Long term effects of sequestration are dependent on the interactions of CO_2 with coals and the effects of CO_2 on coals' properties. CO_2 transport in coal is dependent on a myriad of coal properties, including coal composition (e.g. rank, permeability, macerals, minerals, lithotypes, etc.), pore structure, grain size, and moisture content of the coal. Coals dominant chemical composition is a mixture of carbon, hydrogen, oxygen, nitrogen, and sulphur. The general groups of macerals are vitrinite, liptinite, and inertinite; liptinite is richer in hydrogen and inertinite is richer in carbon than vitrinite (Meyers, 1982; Stanton *et al.,* 2009).

The effect of coal carbon content,, which relates to the coal rank on the coals gas adsorption capacity, has been noted by many researchers having a specific correlation, Gan *et* al., 1972; Bustin & Clarkson, 1998; Walker *et al*., 1998; Ozdemir, 2004; Faiz *et al.,* 2007; Sakurovs *et al.*, 2009; Ceglarska-Stefańska and Zarębska; 2005; Saghafi *et al*., 2007; Day *et* al., 2008; Pini *et al*., 2010; Li *et* al., 2010 and Dutta *et al*., 2011). According to all of these studies, their findings showed that the gas sorption capacity follows a specific "U"-shaped trend variation with carbon content, where the medium volatile bituminous coal with around approximately 83.5% fixed carbon content is at the bottom of that U-shape (Figures 2.24 (a & b)). This reduction of gas adsorption capacity with carbon content up to medium volatile bituminous coal has been observed and according to them, is due to the regular laminar, liquid-type structure of the medium volatile bituminous coal which causes it to have minimal open porosities, resulting in lower gas adsorption capacities.

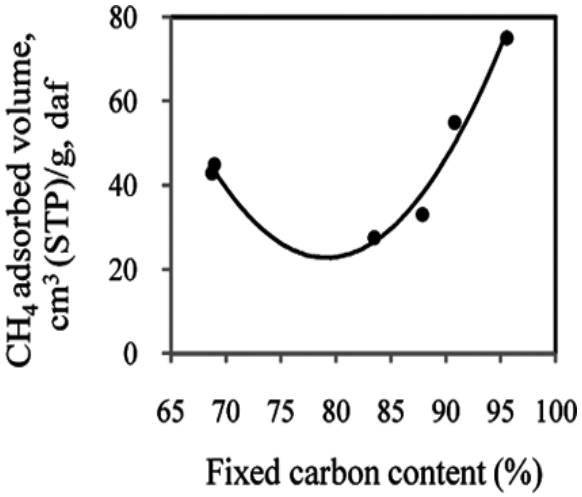

Figure 2.24(a) Variation of gas sorption
(From: Gan et al., 1972)

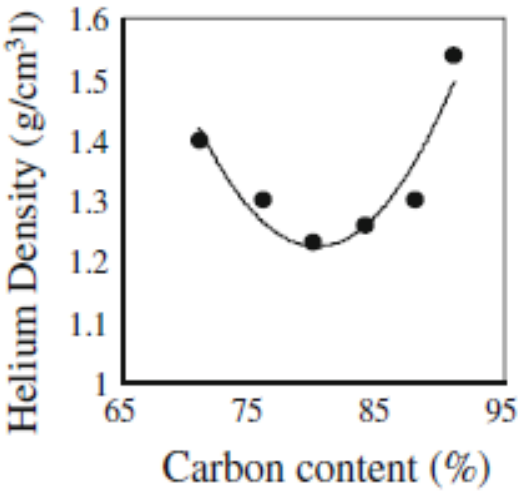

Figure: 2.24(b) Variation of average coal density
(From: Bustin & Clarkson, 1998)

Inter-laboratory comparisons were presented for CO_2 adsorption isotherms measured on dried coals (Goodman, *et al.,* 2004) and moisture-equilibrated coals (Goodman *et al.,* 2007). The data for dry coals indicated that the largest variations of measured CO_2 adsorption were correlated with coal rank. It was also evident from findings by Larsen (2004), who reported that more CO_2 is dissolved as the rank of coal decreases. Other studies investigating coal rank conducted by Stanton *et al*. (2001) indicate that the ratio of 2:1 of CO_2 preferential uptake as compared to CH_4 can vary quite significantly, from >10 in low rank coals (lignite and sub-bituminous coal), to <2 in medium and bituminous coals of low volatile content.

The effect of coal rank and depth of coal seam on the adsorption capacity of carbon dioxide was conducted on coal from the Sydney Basin in Australia. Results show that the deepest and highest rank coal had the highest adsorption capacity. The shallowest coal, which was not necessarily the lowest rank, exhibited the lowest adsorption capacity (Saghafi *et al*., 2007).

Zhang *et al.* (2011) conducted adsorption tests on bituminous Chinese coals using volumetric method and temperature range, 35, 50 and 60^oC using pressures of 120 – 160 bars. They concluded that the preferential adsorption ratio (CO_2:CH_4) decreased as the rank increased from 0.47 – 1.35% R_oV_{mr}. But, for the anthracite, this was not true, when

compared to the bituminous results; at lower pressures, the preferential ratio is lower than that of the bituminous coals tested, and that further increasing the pressure the preferential ratio is greater than for the bituminous coal.

Thus, it can be seen that the rank dependence of the preferential adsorption ratio is not a monotonic correlation. This was also noted by Faiz *et al.,* (2007), who stated that the total open porosity and internal surface area of coal decreases with increases in rank from high volatile bituminous (R_oV_{mr} ~ 1.4%) to medium volatile bituminous (R_oV_{mr} ~ 0.7%), and with further increases in rank the sorption potential increased. The adsorption capacity is both the function of the amount and reactivity of surface area contained in pores and possibly fractures. The determination of the dependence of maximum adsorption capacity of CO_2 on coal rank is vital for the selection of suitable coal seams for the CO_2-ECBM process. It is therefore important to have an understanding of the relationship of adsorption of CO_2 and the coal rank.

As coal rank increases, the density of the coal initially decreases from lignite to high volatile bituminous coal, as a result of expulsion of water, compaction, and the formation of micro-pores. In low rank coals (lignite and sub-bituminous ranks), which are less than 75% carbon (on a dry, ash-free (daf) basis), surface areas have been interpreted as primarily contained in the macro-pores > 20 nm. Pores in higher rank coals are primarily micro-pores (<2 nm) and to a lesser extent transitional pores (2-20 nm) (Stanton *et al.,* 2009*)* Investigations by Gürdal & Yalçin*.* (2001) indicated that the micro-pore volume of coal decreases with an increase of R_oV_{mr} up to a value of 1.0 – 1.1%. However, with further increases in R_oV_{mr}, the micro-pore volume was seen to increase again. Rank is known to have an effect on the amount of CO_2 that can be adsorbed into the coal porosity (Gan *et al.,* 1972).

Also, important, for enhanced gas transport in coals seams is the permeability. This property is mainly due to cleat network system in coal seams. Cleat density and cleat spacing are related inversely. Cleats are natural opening-mode fractures formed in coal. Cleats usually occur in two sets that are, in most instances, mutually perpendicular and also perpendicular to bedding (Laubach *et al.,* 1998). They account most of the

permeability and much of the porosity of coal bed gas reservoirs and serve as permeability avenues for Darcy flow of fluids (gas and water) to the wellbore during production (Laubach *et al.,* 1998). It has been noted that cleat spacing varies with coal type and ash content. Bright coal lithotypes vitrain, generally have smaller cleat spacing's than do dull coal lithotypes; durain. Also, that coals with low ash content tend to have smaller cleat spacing's than do coals with high ash content (Stach *et al*., 1982; Laubach *et al.,* 1998). The coal rank is said to be a key factor, as due to progressive coalification, the cleavage of cross-linked, oxygen bearing functional groups in the coal structure results in additional shrinkage and hence increased cleat development (Levine, 1993).

In addition, to the effects of porosity and permeability due to coalification, the primary composition of the coal has a significant influence on the pore structure and therefore on the sorption capacity. Adsorption properties of CO_2 differ with the chemical composition of various coal beds, because of the inherent differences in the origin of various macerals as the source materials differ from seam to seam. Gases should be adsorbed mostly by vitrain-rich facies that contain low amounts of minerals (Clarkson and Bustin, 1997). This was also noted by Karacan and Mitchell (2003), who reported that vitrinite–rich coals were more microporous than inertinite-rich coals. Faiz *et al.* (2007) also highlighted several earlier studies that concluded that vitrinite contains higher volumes of micro-pores than inertinite at a given rank. However, in contrast, the investigation by Faiz *et al.* (2007) showed no systematic differences between gas sorption capacities of vitrinite- and inertinite- rich coals. Laxminarayana and Crosdale (2002) concluded that the difference in source material results in different porosity, pore structure and therefore, also different sorption rates. Water may compete with gases for adsorption sites in maceral pores. In the case of CO_2, it may be dissolved in water and /or displace water and CH_4 in adsorption sites (Gentzis, 2000).

Research carried out by Crosdale *et al.* (1998) concluded that maceral composition significantly affects both adsorption and desorption properties of coals. They also concluded that micro pore structure also plays a significant role, and this related to type and rank of coal. While Walker *et al*. (1998) determined that CO_2 uptake occurs in open and closed micro-pores, Ceglarska-Stefańska and Zarębska (2005) observed that the capillary structure of hard coals is heterogeneous, and differences between pores lie in

their shape and size. Pore dimensions range over several orders of magnitude, from cracks of the order of several microns to openings that remain inaccessible even to helium at room temperatures. Investigations of pore volumes in coals displaying a variable degree of metamorphism lead to the following conclusions by Ceglarska-Stefańska and Zarębska (2005):

- In coals with carbon content less than 75%, porosity is related to the macro-pore volume.
- In coals with 75-86% carbon content, porosity is chiefly attributed to the presence of transition pores and macro-pores.
- In coals with medium degree of metamorphism (85-91%) micro-porosity seems to be the predominant factor.
- In anthracites (%C>91%) micro-porosity tends to be predominate.

Ceglarska-Stefańska and Zarębska's (2005) sorption experiments, conducted on various sorbates and in highly varied conditions, demonstrated the concept that higher rank coals have the most highly developed micro-pore systems. A large proportion of these micro-pores are comparable in size to molecules of absorbed / adsorbed substances. It is a well-established fact that the macro and meso-pore contribution to the sorption capacity of coals is a minor factor, although they play a role in the processes of diffusion and gas migration. Hence, HR (high rank) coals are regarded as heterogeneous sorbents. Their structural heterogeneity is as a result of changes to the original organic matter during coalification. This is closely associated with the chemical content and properties of the coal deposit, being the consequence of the presence of reactive oxygen groups and the differences in the elemental compositions of macerals of vitrinite, liptinite, and fusinite. Thus, the structural parameters of coal are closely related to its maceral content (Larsen and Wernett, 1988; Karacan and Okadan, 2000). Micropores tend to predominate in vitrinite, while meso-pores and macro-pores predominate in inertinite.

With regard to ash content, many researchers have found that the sorption capacity of coal for CO_2 is negatively correlated with increasing ash content (Bustin and Clarkson, 1998; Faiz *et al*., 2007; Laxminarayana and Crosdale, 1999; Wang, 2007; Perera, *et al.,* 2011) as shown in Figure 2.25(a) and 2.25(b). This is a well-known inverse relationship which is due to the fact in coal beds nearly all gas is adsorbed on the organic surfaces rather that

the inorganic surfaces (Gürdal & Yalçin, 2000, Crosdale *et al*., 1998 and Clarkson & Bustin, 1997). It has been suggested from these studies that ash acts as a diluent hence reducing gas sorption capacity.

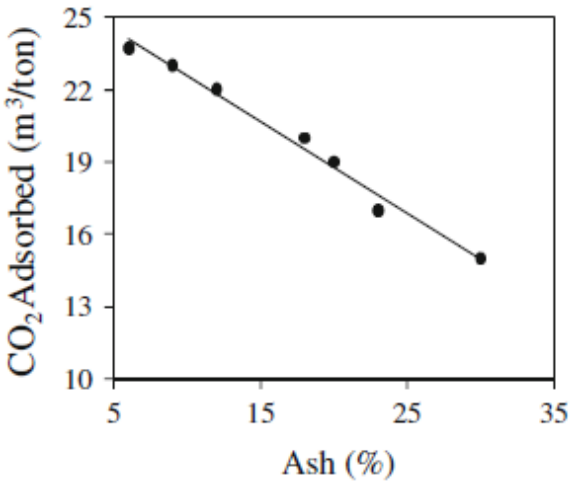

Figure 2.25(a): Influence of Ash on CO_2 adsorbed
(Source: Wang, 2007).

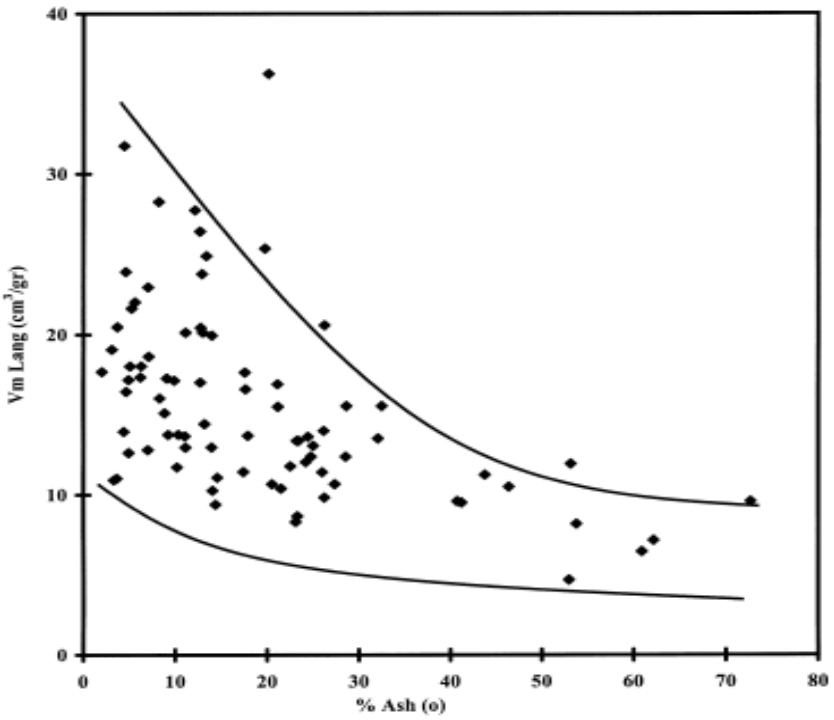

Figure 2.25(b): Relationship between ash content and Langmuir gas adsorption capacity *(Source: Gürdal & Yalçin, 2000).*

It has been shown that carboniferous coals with an ash content in the range of 50 – 60% generally have an adsorption capacity in the range of 0.24 – 0.4 mmol/g (Gürdal & Yalçin, 2000), while sorption experiments conducted by Soares *et al.* (2007) gave lower capacities in the range of 0.089 – 0.186 mmol/g for coal having ash content of 59.92 and 53.3 % respectively. Studies conducted by Gürdal & Yalçin (2000) determined a correlation between the ash content and Langmuir gas adsorption capacity for Turkish coals (figure 2.25(b)), but could not conclude which of the other controlling parameters (such as maceral composition, coal rank and carbon content) dominated due to scattered results.

2.12.2 Effect of particle size on CO_2 adsorption

Most published literature to date discusses results obtained using fine coal fractions, that is powdered or crushed coal (Ohga *et al.,* 2003; Soares *et al.,* 2007; Shi *et al.,* 2008; Jessen *et al.,* 2008). The fine size is probably used in order to minimize equilibration time of the experimental runs (Mazzotti *et al*., 2009). Very little work has been carried out on intact coal core samples to assess the effect of CO_2 adsorption or desorption capacity, and more especially relating to research involving CO_2-CH_4 counter-diffusion and competitive sorption (focus areas of this research).

Reported data from Bush *et al.* (2004) and Solano-Acosta *et al.* (2004), shows that CO_2 adsorption occurs much faster in fine-grained fractions. It was concluded that increased adsorption in finer fractions is perhaps a result of an increased surface area. These results suggest that coal particle size will play an important role in determining both the effective rate and capacity of CO_2 sequestration in coalbed.

Recent findings by Gruszkiewicz *et al.* (2009) showed that, for their studies on three size fractions (45-150 μm, 1-2 mm and 5-10 mm) of crushed coal at 40 ^oC and 35 ^oC over a pressure range of 14 – 16.9 bar using the volumetric method, adsorption was significantly faster for the 45-150 μm size fraction compared to the more coarser fractions. They too were in agreement with Bush *et al.* (2004) and Solano-Acosta *et al.* (2004), concluding that increased CO_2 adsorption in finer fractions are probably as a result of an increased surface area, enabling better CO_2 interaction with the coal, and hence will have an increased CO_2

uptake. However, this data cannot be used to simulate in-situ coal seams with regards to adsorption-desorption “real time” data. Thus, cores or “lump” coal samples, from a practical point of view, will give a better representation of what can be expected in-situ. It would probably be more statistically reliable to determine CO_2 adsorption parameters and capacities and CH_4 desorption data from representative bore core samples in order to simulate in-situ coal seam conditions more accurately.

2.12.3 Effect of Pressure on CO_2 adsorption

In this section, both low and high pressure studies for CO_2 sorption experiments are considered. For ease of comparison between published literature and the data presented from the current experimental set-up, all pressure data will be reported in the units of Bar.

There is a large amount of published data concerning CO_2 adsorption in coals at low temperatures and pressures (ambient temperature and pressure conditions). It has become widely accepted that the CO_2 isotherm obtained at lower pressures (<6MPa) could be extrapolated to high pressures. However, this may not be accurate as it does not give a true reflection of the actual in-situ parameters that could be expected in deep coal seams, and thus increased pressures, as previously discussed. Hydrostatic coalbed pressure is approximately 20-30 bar, while a pressure of approximately 40 – 50 bar represents elevated injection pressure that is less than fracture pressure, while the critical pressure is about 73.8 bar (Jessen *et al.*, 2008).

(i) *Low Pressure Sorption Studies*

Investigations were carried out by Soares *et al.* (2007) on high volatile C bituminous rank Brazilian coals with a high ash content at low pressures (<1 bar) to evaluate kinetics and equilibrium of sorption of CO_2. Adsorption equilibrium isotherms were measured at room temperature (30^oC) through a static method with a fixed-bed adsorption column containing granular coal (particle size of 0.8, 2.4 and 4.8 mm). Results showed that the Freundlich model fitted the data better than the Langmuir model; however, both worked reasonably

well to describe the equilibrium experimental results. It was found that the sorption capacity of Brazilian coals is in the range of 0.089-0.186 mmol CO_2/g, which are typical values for coals with high ash content. However, the gas adsorption capacity of CO_2 was found to decrease with the ash content of the coals (Soares *et al.,* 2007), which is a well-known inverse relationship due to the fact that, in coal, almost all gas is adsorbed on the organic surfaces, rather than on the inorganic surfaces (Gurdal *et al.*, 2000). Jessen *et al*. (2008) found that they could attain a maximum CO_2 adsorption capacity of 1.73 mol/kg for an experimental pressure of 57.9 bar.

Ohga *et al.* (2003) conducted fundamental test work on CO_2 sequestration into seven main coal seams in Japan. Their research involved laboratory tests which included adsorption tests for CO_2, N, and CH_4, replacement tests of CH_4 by CO_2, and gas mixtures and adsorption tests of coal samples treated by CO_2 under supercritical condition. The coal samples were crushed and screened to between 4 and 8 mesh size (approximately 2-4 mm). From their results (Ohga *et al.,* 2003), it is evident that there was a big difference in the adsorption volume of CH_4, but that there was no difference in CO_2 adsorption volume at low pressures. The adsorption volume of CO_2 was found to be three (3) times as much as the CH_4 adsorption volume, and the adsorption volume of N is half of the CH_4 adsorption. The results for the replacement tests showed that a higher ratio of sequestration to coal can be obtained when the lower concentration of CO_2 is injected, while CH_4 replacement ratio decreases with a decrease of CO_2 concentration, but there was no difference between CO_2 sequestration ratios (Ohga *et al.,* 2003).

(ii) ***High Pressure Sorption Studies***

During the last decade, interest in and a need for high-pressure adsorption data to simulate in-situ coal seam pressure has increased. But, to date, very little work has been published on CO_2 sorption using supercritical CO_2 at high pressures > 50 - 80 bar i.e. using supercritical CO_2 (Siemons and Busch, 2007).

In considering the storage of CO_2 by adsorption on coals, it is necessary to identify the most appropriate filling pressure which will lead to values of storage capacities that can be compared to the classical compressed natural gas storage. It is generally recognized that high-pressure adsorption measurements are more difficult to achieve than low-pressure ones, due to difficulties and high costs related with experimental set-up's for both volumetric and gravimetric methods, and the high potential of leaks that occur in very high pressure systems.

Busch *et al*. (2004) demonstrated that at a temperature of 45 ^oC using the volumetric method to a maximum pressure of 250 bar CO_2 was always adsorbed preferentially to CH_4, although preferential sorption of CH_4 was observed in some instances at lower pressures. Other results (Prusty, 2008) of preferential adsorption on dry moisture equilibrated coals of different rank under identical conditions indicated that adsorption is a function of coal type, moisture, content and pressure. Busch *et al*. (2004) also showed commonly, gas transport in coal is considered to occur at two scales: (1) laminar flow through the cleat system, and (2) diffusion through the coal matrix. Flow through the cleat system is pressure-driven and may be described by Darcy's Law, whereas the flow through the coal matrix is assumed to be concentration-driven and is modeled using Fick's Law of diffusion (Busch *et al.,* 2004).

Findings by Larsen (2004) showed that an increased CO_2 dissolution was possible with an increase in pressure. Larsen (2004) concluded that not only does CO_2 dissolve in coals, but also that at high pressures dissolution was found to exceed adsorption. These findings regarding coal deformation are further discussed in Section 2.12.6.

Table 2.5 gives a summary of some of the reviewed published CO_2 adsorption data to date. Some variances in the reported adsorption data have been noted, with differences in units reported, which makes comparing data difficult; however the trends exhibited can be clearly noted. A very good trend of adsorption capacities can be seen between Southern and Northern hemisphere results. The ranges of minimum to maximum sorption capacities are a good fit across the board.

Table 2.5: Summary of published data on CO_2 adsorption in coal (low and high pressure)

Publication	Coal type	Coal Rank	Ash/ Mineral	Particle type	Test conditions		CO_2 adsorption capacity(mmol/g)
Clarkson & Bustin (2000)	Canadian (British Columbia)	Medium Volatile Bituminous	Low	powder	60 bar, 30°C		34 ml/g*
			High				16 ml/g*
Gurdal & Yalcin (2001)	Turkish (Zonguldak Basin)	High volatile C bituminous	Low	powder	0.01 – 1.00#, 0.02 25 °C		5 – 37 cm^3/g*
Kroos *et al.* (2002)	Dutch/Netherlands			powder	60 bar, 40 - 80°C		21-17 cm^3/g*
					80-100 bar, 40-80°C		<5 cm^3/g*
Schroeder *et al.* (2002)	US (Argonne Premium coals)**	Low-high vol. bit.	Low - Medium	powder	40 bar, 22 - 55°C		0.9-1.7
Shimada *et al.* (2005)	Japanese (Akabira)	Bituminous rank B		powder	60 bar, 35°C		1.65
Busch *et al*. (2003)	US (Argonne Premium)**	High & medium volatile C bituminous	Low - Medium	powder	73.8 bar, 22 °C		1.05 – 2.31
Ceglarska-Stefanska & Zarebska (2005)	Polish	Hard coal B	Medium	powder	40 bar, 25°C,		22
		Hard coal M	Low				26
Bae & Bhatia (2006)	Australian (Bowen Basin)	High vol. bit.	Medium	powder	200 bar	313K	0.033-0.06
						323K	0.034.-039
						333K	0.019-0.026
Soares *et al.* (2007)	Brazilian	High volatile C bituminous	High	powder	<1 bar, 30°C 30°C		0.089-0.186
Goodman *et al*. (2007)	US (Argonne Premium coals)**	Low vol. bit.	Low	powder	150 bar, 55°C		0.44 – 9.07
		High vol. bit.	Medium				0.733-0.909
		Lignite	Low				0.68-1.476
Prusty (2008)	Indian	Seam 1	Medium	Powder	45°C	34 bar	22.2ml/g*
		Seam 2	Low		25°C		23ml/g*
		Seam 3	Low		23.5°C		25ml/g*
Jessen *et al*. (2008)	USA (Powder River Basin)	High vol. bit.	Low	powder	~58 bar		1.73
Yu *et al.,* (2008)	Chinese (Qinshui Basin)		Low	powder	~60 bar, 28°C		0.97 – 1.3
Zhang (2008)	Chinese	High – medium Volatile bituminous A	Low – Medium	unknown	10-190 bar, 18-72 °C		1.89 – 33.55 cm^3/g*
Dutta *et al.* (2008)	USA (Illinois)	High Volatile bituminous A	Medium	powder	50 bar, 28.6°C		0.929
		High Volatile					0.998-1.198

		bituminous B				
Publication	**Coal type**	**Coal Rank**	**Ash/ Mineral**	**Particle type**	**Test conditions**	**CO_2 adsorption capacity(mmol/g)**
Gruszkiewicz *et al. (*2009)	US (Lower Pennsylvania)	Lack Warrior	Low – medium	powder	22-34 bar, 35 – 40^oC	0.7-0.82
Gertenbach (2009)	South Africa (Highveld, Waterberg)	Low Rank A- Medium Rank C	Low-medium	powder	50 bar,	0.3-1.5
Charriére *et al.* (2009)	France	High Volatile Bituminous B	Low	powder	10 – 50 bar, 10 – 60 ^oC	0.34 – 1.55
Pone *et al*. (2009)	USA (Kentucky)	Bituminous	Low	powder	69 bar,	1.17
Ozdemir & Schroeder (2009)	Argonne Premium coals	Low Volatile B	Low	powder	30 bar, 22 ^oC	1.25
		Med Volatile B	Medium			1.07
		High Volatile B	Low-high			1.17-1.65
		Sub bituminous	Low			1.97
		Lignite	Low			1.72
Charriére *et al.* (2010)	France	High Volatile Bituminous B	Low	powder	150 bar, 23 ^oC	0.05 – 1.55
Li *et al.* (2010)	Chinese	Anthracite	Low, Medium	powder	250 bar, 35 ^oC	3.03
		Medium Volatile Bituminous				2.02
		Sub-bituminous				4.36
He *et al.* (2010)	Korean	Anthracite	Medium -high		152 bar, 25 - 45^oC	1.4 – 1.5
Garnier *et al.* (2011)	French	High-Medium Volatile Bituminous	low	powder	1-50 bar, 25 ^oC	0.5 – 2
Zhang *et al.* (2011)	Chinese	Bituminous	Low, Medium	powder	60 bar, 35^oC	2.2, 1.0
			Low, Medium		120 bar, 50^oC	1.6, 1.23
Dutta *et al.* (2011)	Indian (Gondwana)	Medium Volatile Bituminous	Low, medium	powder	58 bar, 30^oC	12 – 36 mL/g*
Pini, *et al.* (2012)	Swedish	Medium Volatile Bituminous	Low, medium	powder	190 bar, 45^oC	0.75 – 1.31
Weniger *et al.* (2012)	Silesia	Medium Volatile Bituminous	Low, medium	powder	55 bar, 20 ^oC	1.07 – 1.36
Mabuza (2013)	South Africa	High & medium	Medium - High	crushed	90 bar, 35^oC	1.08 – 2.58

		volatile C bituminous					
Publication	**Coal type**	**Coal Rank**	**Ash/ Mineral**	**Particle type**	**Test conditions**		**CO_2 adsorption capacity(mmol/g)**
Gensterblum *et al*. (2013)	Australian (Queensland)	Sub bituminous A	Low	crushed	150 bar	45 ºC	0.023
						61 ºC	0.011
						76 ºC	0.007
Gensterblum *et al*. (2013)	German (Ruhr)	High Volatile bituminous	Low	crushed	150 bar	45 ºC	0.007
						61 ºC	0.010
						76 ºC	0.012
Ramasamy *et al*. (2014)	Australian	Low, med, high volatile bituminous &, sub-bituminous	Medium	crushed	65 bar, 45.5 ºC		~1.0

**Conversion to units of mmol/g cannot be undertaken – unknown sample masses (g).*
***Selection of coal samples obtained from seven states comprise of the Argonne Premium Coal Samples.*
 # Relative Pressure (P/Po)

2.12.4 Effects of Temperature on CO_2 adsorption

Gas sorption (adsorption and / absorption) is an exothermic process and therefore once equilibrium is reached at a given pressure the sorption capacity decreases with increase in temperature (Gregg and Sing, 1982).

Sakurovs *et al.* (2008) demonstrated that the calculated sorption capacity of coals and charcoals is strongly temperature-dependant, and therefore inconsistent with simple mono-layer models like the Langmuir model. Their data showed that the sorption capacity of coals tends to decrease strongly with increasing temperature. This is inconsistent with expectations from the Langmuir models for coal adsorption, which predict that sorption capacities are independent of temperature. They did, however, suggest that a pore-filling approach could explain the temperature dependence. Their isotherm data was successfully fitted using a modified Dubinin-Radushkevich equation that uses gas density rather than the gas pressure. A simple pore filling model that assumes there is a maximum pore width that can be filled in supercritical conditions and that this maximum pore width decreases with increasing temperature. A pore-filling process suggests that CO_2 motion across the coal surface is relatively free and that there is no need to invoke sites on the coal that are specific for CO_2. Kaneko and Murata (1997) found that, with a fixed temperature for supercritical gases, this pore width tends to a maximum value with

increasing pressure; this is unlike the situation for sub-critical gases where this width decreases with increasing temperature above the critical temperature.

The thermal experiments for the coals of low rank shows that temperature plays an insignificant role in storage capacity because absolute differences between all the isotherms were found to be small (Crosdale *et al*., 2008). For coals of higher rank, it was found that adsorption capacity decreases significantly with increasing temperature (Saunders and Yang, 1985; Krooss et al., 2002; Ozdemir, 2004). Similar results were found for bituminous coals by a number of authors (Levy *et al*., 1997, Azmi *et al*., 2006) showing adsorption capacity of the coal samples had an inverse response to an increase in temperature in the adsorption environment for all test work conducted. Temperature dependence was also studied by Qing-ling *et al.,* (2008). This is depicted from the bar graph as outlined in Figure 2.12; the bar chart shows the changes in pressure and temperature with depth to 1700 m.

Azmi *et al*. (2006) conducted the adsorption studies on the Malaysian coal samples. Their studies involved CO_2 adsorption profiles of coal samples of varying mean size distributions ranging from1000μm to 2000μm. They observed that the coal samples having smaller mean particle size distribution of 1000μm show a better rate of adsorption compared to the 2000 μm size distribution. These Malaysian coal samples were studied for CO_2 adsorption at varying temperatures (24.6°C, 30°C, 40^0C and 50°C). The adsorption capacity of the coal samples showed an inverse response to temperature change for all test work conducted.

The classical Joule-Thomson experiment was focused on the cooling effect on gas injectivity. It was found that temperature can drop over 20°C due to gas expansion, which has a negative effect on injectivity (Oldenburg, 2007; Sakurovs *et al.,* (2008). There is a general agreement that the rate of sorption of CO_2 strongly depends on pressure and temperature. Experiments on CO_2 sorption kinetics performed on dried coal at a temperature range between 10°C and 60°C showed that the adsorption rate of CO_2 is positively correlated with temperature, and an increase in pressure and temperature causes a decrease in equilibrium time i.e. the time take to reach stability in the sorption cell (Charrière *et al*., 2010). Similar results were reported where the equilibration time was

found to decrease with an increase in temperature due to the increase of diffusion rate (Deishad *et al*., 2009).

The apparent excess adsorption of CO_2 on dry activated carbon at 45°C reaches a maximum at about 8 bars and then decreases linearly with increasing gas density (Sudibandriyo *et al.*, 2003; Sakurovs *et al.,* 2008). Coal is also known to swell in the presence of CO_2 and this may be significant with respect to interpreting data (Vyacheslav, *et al.*, 2005).

Ozdemir (2004) conducted the adsorption test on Argonne premium coal samples using a manometric technique. They studied the sorption characteristics at different temperatures (22°C, 30°C, 40°C and 50°C). They observed that adsorption capacity of coal samples shows an inverse response with temperature. This is attributed to decrease in the adsorption equilibrium capacity with increasing temperature because higher temperatures increasingly favour the gas phase due to T*S entropy term in the free energy expression. Every *et al*. (1972), conducted experiments to find the ability of CO_2, He and air to displace CH_4 from crushed coal. Their data showed that CO_2 was able to displace 90 percent CH_4 under laboratory conditions. CO_2 was three times more effective than air, and five times more effective than He in displacing CH_4 from coal.

Qing-Ling (2008) found that there is a definite regularity between temperature and pressure in the strata. Starting from the surface, for every 100 m increase in depth of the strata, the temperature increases by 3 °C and the reservoir pressure by 1 MPa (10 bar). Given this regularity, adsorption tests were conducted using temperatures and pressures corresponding to the coal reservoirs at various depths, for each of the different ranks. Adsorption isotherms were also conducted using the same samples and results were compared with the ones for variable temperature. The first finding was that when the temperature of the variable temperature and pressure tests is lower than the temperature of the isothermal adsorption test at 30 °C, the amounts of gas adsorbed at the various temperatures and pressure of the anthracite, lean coal and coking coal are larger than the amounts of isothermal adsorption at the same pressure. The adsorption curves of the variable temperature and pressure adsorption tests are above the isothermal adsorption test curve at 30 °C. The amount of gas adsorbed by the “longflame” coal at the variable

temperatures and pressure was always larger than the amount of isothermal adsorption at the same pressure. The variable temperature and variable pressure adsorption curve was always above of the isothermal adsorption test curve at 30 °C.

2.12.5 Effect of Moisture on CO_2 adsorption

Deep coal seams are naturally wet and will undergo recharge from surface water more rapidly during CO_2 sequestration as a result of drilling operations, fracturing of the coal bed and over-lying strata, and the injection of flue gas which may contain residual water of combustion. Thus, an aqueous phase will be present and will vary in composition according to its source and the nature of the coal bed and the surrounding minerals with which it is in contact (Joubert *et a*l., 1973; Levy *et al*., 1997; Ozdemir, 2004; Day *et al*., 2008; Kim *et al*., 2011).

Although many projects have been undertaken globally, like the European RECOPOL, MOVECBM, CATO and CO_2TRAP which have provided fundamental information, CO_2 research is still regarded as being in its infancy. Many researchers noted that are considerable problems regarding repeatability of supercritical CO_2 sorption (Goodman *et al*., 2004; Goodman *et al*., 2007); an inter-laboratory comparison on high-pressure sorption of CO_2 on Argonne Premium coals was undertaken. The first inter-laboratory tests compared sorption isotherms of CO_2 on dry coals at temperatures from 295K – 328K and with pressure of 70 bar, using five types of coal; these experiments were conducted at five individual laboratories. The preparation procedure involved drying of samples for 36 hours at 353K under vacuum. However, large deviations were observed in the results for medium-to-low rank coals; this was attributed to varying moisture contents, and it was recommended that further studies were done with well-defined procedures to improve repeatability of results. The sorption isotherms on high-rank coals were considered to be sufficiently accurate (Goodman *et al*., 2004).

The second inter-lab study (Goodman *et al*., 2007) compared sorption isotherms of CO_2 on moisture-equilibrated coals at 328K and pressures up to 150 bar, conducted at six different laboratories. It was found that sorption data showed good agreement for

pressures up to 80 bar, but great deviation was found for higher pressures, and again the variation in results were attributed to variations in moisture contents. This lead Gensterblum *et al*. (2009) to continue with CO_2 sorption studies which were conducted to assess and improve the quality of high-pressure sorption isotherms of CO_2 on coals. They attempted to do this by performing inter-laboratory results comparisons of sorption experiments which were performed at 318K up to 160 bar simulating typical conditions for coalbeds suitable for CO_2 storage, with pressures ranging from 60 – 150 bar and temperatures between 300 and 330K. They used both manometric and volumetric methods to determine sorption data. Samples were prepared by some laboratories drying their samples in the measuring cell to avoid contact with atmospheric air after drying, while other laboratories degassed the samples (mass between 5-7g) at 473K, the samples were then placed into a heating sleeve and then heated to 473K under vacuum (10^{-2}) for 24 hours. All results obtained showed very good agreement with a deviation of less than 5%. Excess sorption values measured in this study were consistently higher than those generally reported in literature. It was also observed that the three-parameter excess sorption function based on a Langmuir-type absolute sorption function was found to be adequate to represent the experimental data most favourably.

Gas adsorption measurements on dry coals with pure gases can be routinely performed up to pressures of 200 bar and more. However, sorption of CH_4 and particularly supercritical CO_2 on moisture equilibrated coals is at present not well researched and hence poorly understood (Busch *et al*., 2003). Documented literature shows that all adsorption measurements for wet coals have much less CO_2 uptake than for tests with dry coals, which is due to competitive water adsorption. Most studies using wet coals have highlighted much difficulty with regard to techniques for the measurement of adsorption isotherms as compared to dry samples, which are well established. To date, inter-laboratory studies using different techniques has shown unsatisfactory reproducibility of CO_2 adsorption data on wet coal, especially for supercritical CO_2 tests conducted exceeding 60-80 bar (Krooss *et* al., 2002; Goodman *et al*., 2007; Goodman *et al*., 2004; Day *et al*., 2008; Day *et al*., 2008(b)).

Day *et al*. (2008b) conducted tests on moist coals at super-critical pressures, and their adsorption measurement results showed that in general wet coal uptakes less CO_2 than

dry coals. Coal containing 3% moisture, corresponding to a relative humidity of 50%, was found to adsorb around 30% less CO_2 than the corresponding dry one.

In contradiction, Faiz *et al* (2007) are of the opinion, that low rank coals, which contain high amounts of moisture as well as numerous hydroxyl and carboxyl groups, are more ionic than higher rank coals and, therefore, the contribution from electrostatic forces to CO_2 sorption is likely to be greatest. Furthermore, low rank coals that contain very high moisture contents, CO_2 may also be stored in solution especially at high pressures. The higher sorption capacity may also be related to the strong polarity of CO_2 (permanent quadrupole) and the electrostatic forces may be a significant contributor to gas sorption.

2.12.5.1 Effects of Changes in pH of moist coals

The change of pH can affect the coal and CO_2 sequestration process in coal seams in several ways. A decrease of pH can dissolve and extract mineral matter associated with the coal. Change in pH can alter the surface charge of the coal, which, in turn, can affect the intermolecular interactions responsible for the 3-dimentional structure of the macromolecular network (Sakanishi *et al*., 2001). Because the aperture size of a pore in the coal is important for gases to access within the pores and because the maximum adsorbed amount is related to the pore volume, all of these may affect the storage capacity of the coal and the stability of the adsorbed CO_2 (Ozdemir, 2004).

Injected CO_2 into a coal seam can decrease the pH and dissolves and extracts the mineral matter. Mineral matter in coal takes two forms: inherent mineral matter and extraneous mineral matter. Inherent mineral matter is found in relatively minor amounts in the coal. These minerals, once present as nutrients in the original plant matter, were trapped in microscopic amounts during the coalification process and, as a result, have become part of the organic matrix (Meyers, 1982). The inherent mineral matter is generally found embedded within the micro-pore system of the coal, associated with the organic matrix, and cannot be easily removed. The second type of mineral matter is referred to as extraneous mineral matter. These minerals have entered the seam via aqueous seepage during the coalification process. Because they tend to fill larger cleats and fissures,

extraneous deposits can range in size from a few hundred microns to several cubic feet. The bulk of extraneous mineral matter is composed mainly of pyrite, calcite, quartz, and alumina silicate clays. With the possible exception of quartz, these minerals are affected by either acidic or basic surroundings through dissolution or ion-exchange. Calcite is particularly sensitive to acidic aqueous surroundings (Falcon & Falcon, 1987; Zeng, 1997; Ozdemir, 2004 and Suárez-Ruiz and Ward, 2008).

In addition to the extraction of mineral matter, changes in pH can alter the overall surface charge of coals. It is well known that solids in contact with solutions with a pH above their isoelectric point acquire a net negative surface charge; those in contact with solutions with a pH below their isoelectric point acquire a net positive surface charge. The isoelectric point was reported to be about pH ≈ 3.8 for coals. The isoelectric point for demineralised coal is lower 55 than that of its mineral matter (Labuschagne, 1986). Consequently, the untreated coal in the presence of mineral matter is more hydrophilic than the carbonious coal. The CO_2 sequestration in water-saturated coal seam will certainly decrease the pH in the sequestration environment. Thus, the acidic pH would replace the carboxylic salts with the R-CO_2H form. Similarly, less reactive, and less common, phenolic groups in the coal matrix would be affected, transforming Ar-O-M to Ar-OH. Ubiquitous nitrogen-containing groups, which are almost always found in heterocyclic forms, usually take the form of basic pyridine groups in higher-rank coals, and acidic pyrrole derivatives in lower ranks.

Sulphur also plays a role in the organic matrix; however, most of it is in the form of –SH groups (Joseph and Forrai, 1992). Nitrogen and organic sulphur groups typically do not interact with mineral matter in coal and therefore cannot be removed by acid or base treatment although their chemical attributes can be changed. The properties of surface of a coal may change due to inherent surface charge and the chemical composition of coal. The three dimensional structure of coal is mainly maintained by the covalent bonding as well as the secondary forces such as hydrogen bonding, van der Waals interaction, electrostatic forces, and ionic interactions. Disturbances in such interactions may alter the 3-D structure of coals (Chen *et al*, 1998).

The sudden decrease in pH during the CO_2 injection may enhance the CO_2 storage. For instance, removal of inorganic matter from coals by acid treatment brings about random and significant changes in surface areas measured by adsorption of N_2 and CO_2 (Chen *et al*, 1998). Changes in surface areas of raw coals have been attributed to physical removal of inorganic matter from the aperture cavity system. It has been documented that CO_2 adsorption on demineralised coal increases proportionally to the concentration of carboxylic groups present on the coal's surface (Nishino, 2001). Nevertheless, studies of the effects of acidic and basic solutions on coal have frequently focused on the demineralization of the coals (Sakanishi *et al*., 2001). Most of these investigations have involved leaching the mineral matter in coal with concentrated acid and base solutions at elevated temperatures. Results gathered from these studies are of questionable applicability to carbon sequestration science because the coals have been exposed to more extreme pH values than they would be in a natural sequestration setting (Sakanishi *et al*., 2001).

2.12.6. Effect of coal swelling / stress / deformation

In order to successfully sequestrate CO_2 in coal beds and produce ECBM, more detailed knowledge of coal structural properties and their variation under simulated in-situ conditions need to be known (Holloway, 1997; White *et al*., 2005; Wang *et al*., 2007), in addition to knowing the best sequestration parameters for pressure, temperature, coal type, etc. Coals are glassy, strained, cross-linked, macromolecular systems, because the intermolecular segments are "frozen" in place. They do not have freedom to move except for small-scale rotations, vibrations, etc. when warmed to a temperature such that the thermal energy is greater than the intermolecular interaction energy, and the "polymer" becomes rubbery. This makes large scale molecular motion possible and internal viscosities are liquid like. The best evidence is that unplasticized coals remain glassy up to the temperatures at which they begin to thermally decompose (Opaprakasit and Painter, 2003). Coals are also not in their lowest energy state (Larsen *et al.,* 1997), and therefore the effect of CO_2–coal interaction must be studied as well, since the influence of coal heterogeneities and resultant strain distributions is complex due to the physical and chemical processes that transpire during CO_2 sorption. From an ECBM point, the

magnitude of swelling due to the CO_2 uptake combined with the shrinkage effects from the CH_4 desorption also need to be accounted for.

At low pressures (<1 bar), CO_2 dissolution does not seem to be a problem; however, high pressures are necessary for CO_2 sequestration (Pressure > 50 bar) (Soares *et al.,* 2007). It was previously assumed that CO_2 is only adsorbed (physi-sorption process) and does not dissolve in coal. It is now also known that when CO_2 dissolves in coals (chemi-sorption process), it swells them slightly. The dissolved CO_2 seems to act as a plasticizer, which enables physical structure rearrangements and lowers the coal's softening temperature (Larsen, 2004). For adsorption tests it was shown that the extent of swelling increases monotonically with pressure up to a few percent for adsorbing gases, with CO_2 swelling the coal more than CH_4 and N_2, whereas for He (a non-adsorbing gas) volume changes were found to be negligible (Mazzotti *et al*., 2009). Although CO_2 adsorption on coal is almost instantaneous, this is followed by a much slower diffusion of the molecules into the coal matrix. Reucroft and Patel (1986) reported that CO_2 dissolved in coals and swelled them in addition to adsorbing on the coal surface. Evidence that CO_2 absorption results in a change in the coal structure was also noted by Hsieh and Duda (1987). This was also confirmed by results obtained by Busch *et al*. (2003) which suggest strong volumetric effects to their results and concluded that it was most probably due to coal swelling.

With regard to coal swelling, in static experiments it is very difficult to distinguish between adsorption and a mixture of adsorption and absorption, because the latter follows the former (Larsen, 2004), the only truly measurable quantity accounts for the effect of both absorption and sorption, which is very difficult to differentiate between (Ozdemir *et al*., 2004; Romanov *et al*., 2006; Ottiger *et al*., 2008; Mazzotti, *et al*., 2009). It is important to understand the effects of coal swelling, as the volume changes of coal during ECBM operations are of key importance, because they affect coalbed permeability, which in turn controls injection pressure and gas production (Mazzotti *et al*., 2009). This decrease in coal permeability can be explained due to two effects: the external lithostatic pressure tends to press the matrix elements together, and to reduce porosity, while the gas adsorption swells the coal matrix elements and therefore consumes the space between them, thus further reducing the porosity (Cui *et al*., 2007).

Day *et al* (2008a) concluded from their experiments that the process of coal swelling is a reversible process, with coal samples returning to its original size when the pressure is released. They also found that the swelling due to CO_2 is typically between 1 - 2% for bituminous coals, but can be greater for lower rank coals. However, most of the gas-coal systems data regarding swelling and plasticity to date has been conducted on powdered, unconfined coal samples.

In findings from Milligan *et al*. (1997); Karacan (2003); Mazumder *et al.* (2005); Kelemen *et al*. (2006); Karacan, (2007) and Day *et al*. (2008b), it has been observed that there is indeed a relationship between coal swelling and the amount of CO_2 adsorbed by the coal. At pressures below a few atmospheres, swelling is low and generally unaffected by the amount of gas adsorbed. But at elevated pressures (>150 bar), swelling increases nearly linearly with the amount of CO_2 adsorbed. Depending on the rank of coal, maximum volumetric swelling induced by CO_2 in unconfined samples is generally within the range of 1 to 5%, with the highest swelling occurring in lower rank coals (Day *et al.,* 2012). Day *et al.* (2012) recently confirmed this with results from four Australian coals that showed volumetric swelling for CO_2 in the range of 1.9 – 5.5% and swelling for CH_4 in the range of 1.0 – 2.5% for bituminous and sub-bituminous coal types.

Coal is a very heterogeneous material because it is composed of various macerals and mineral matter (“ash”). Different macerals and ash components show different swelling behaviour (Gensterblum *et al.,* 2010). Above about 80 bar the relationship is no longer linear: adsorption continues to increase but the coal matrix volume remains constant (no swelling) (Kelemen *et al*., 2006). Additionally, the intensity of swelling changes with coal rank (Siemons and Busch, 2007).

Work by Pone *et al.* (2010) focused on characterization of lithotype specific deformation and strain behaviour during CO_2 sorption at simulated in-situ conditions, which included the evaluation of three-dimensional strain induced by confining stress, the sorption and desorption of CO_2 in coal. Pone *et al.* (2010) used X-ray computed tomography to characterize deformation of bituminous coal confined cores (2.54 cm diameter and 6.35 cm in length) under hydrostatic stress. A depth of 300 m was simulated using a confining stress pressure of 68 bar, hydraulically applied axially and longitudinally. Carbon dioxide

gas injection pressure was kept constant at 31 bar for 26 days of multi-injection in small increments. The cumulative excess sorption of 0.85 mmol/g for CO_2 was achieved. They concluded that a total average volumetric swelling of 0.44% was noted for the CO_2 adsorption, and after desorption an average volumetric compression of 0.33%, which showed that the deformation of the coal structure due to CO_2 sorption is irreversible. This is in contrast to findings made by Day *et al*. (2008). From their data, it is evident that average CO_2 sorption-induced strain is relatively low compared to other reported values. Alternating positive and negative strain values attained during compression, sorption, and desorption respectively emphasized that both compression/compaction and expansion of coal will occur during CO_2 sorption. It was also noted that some of the lithotype bands in coal were compressed or compacted to accommodate the swelling of an adjacent lithotype (Pone *et al*., 2010).

2.12.7 Adsorption of CO_2, CO_2 mixtures, and desorption of CH_4

Various studies already conducted internationally has proven that coal can absorb more CO_2 than CH_4, and that it is preferentially absorbed onto the coal structure over CH_4 (Masterlez *et al.,* 2004). Coal seams can thus store at least 5 to 10 times more the quantity of gas that is traditionally contained within it (Gaucher *et al.,* 2011). The relatively high excess sorption capacity exhibited by coal for CO_2 (typically 6-10% by weight) is what makes coal a good sequestration target (Sakurovs *et al.,* 2008). While most CH_4 / CO_2 adsorption isotherm studies on coals samples give adsorption behaviour, adsorption ratios, and other influential factors for ECBM and CO_2 sequestration, it must be noted that they only provide static characteristics. The sorption isotherms generated from the data do not provide information on pressure-driven and concentration-driven data during gas recovery and the CO_2 injection processes (Belmabkhout *et al.,* 2004). Typical pure CO_2 and CH_4 adsorption isotherms provide an estimate of the coalbed capacity for CO_2 storage, and of the maximum theoretical amount of coalbed CH_4, that is the so-called maximum gas in place, GIP_{max} respectively (Mazzotti *et al*., 2009).

Sorption on hard coal (i.e. a sorbent with a non-rigid structure) involves two processes whereby penetrative sorbate molecules overcome the cohesion forces (absorption), and

deposit the sorbate in sub-micro pores utilizing adhesion forces (adsorption). Increased sorption of single gas studies on coal shows a straight forward correlation between the coal structure of a sorbed substance and the identity and the chemical structure of the sorber substance and the conditions enabling structural developments to take place.

Studies undertaken by Shimada *et al.* (2005) established adsorption isotherms for Akabira coals (rank bituminous B, having moisture content 0.7%, ash 1.82%, volatile material 41.57%, and fixed carbon 55.91%), for pure CO_2, CH_4 and N_2 gases, using pressure ranges of 10-30 bar. Results indicated that the ratio of adsorption capacity for these individual gases (CO_2, CH_4 and N_2) were 8.5:3.5:1 at lower pressure of 12 bar, but when gas pressure was raised to 60 bar, the ratio of the above pure gases adsorption was 5.5 : 2 : 1. They also conducted CH_4 replacement tests using partially saturated CH_4 coal sample pressurized at 24 bar. A range of replacement tests including pure CO_2 and then using binary gas mixtures of CO_2:N_2 (35%:65% and 10%:90%) was conducted using pressure ranges 30, 40, 50 and 60 bar. The results were found to indicate that CO_2 was preferential sorbed as compared to CH_4 and N_2 alone, which is in agreement with other studies.

Another significant point raised was that the extended Langmuir model was not able to successfully model the experimental data for sorbed CH_4 as it was for CO_2 alone, and this was attributed to the coal swelling / dissolution. The EL (extended Langmuir) was able to predict the more strongly sorbed component more accurately. This is mainly due to the assumption that for the EL model, all gases are competitively adsorbed on all sites of the coal. However, it is known now, that CO_2 behaves preferentially in sorption characteristics as compared with both CH_4 and N_2. This can be explained due to the relatively small kinetic diameter and may be blocked. Also another factor could be due to CO_2 dissolving on the coal structure, and hence this effect will increase with pressure causes swelling and plasticity of the coal matrix (Larsen, 2004). Shimada *et al.* (2005) proposed that the EL equation for CO_2 be modified to accommodate the following assumptions:

1. The amount of CO_2 adsorbed preferentially at partial pressure in a mixed gas environment is equal to amount at the same pressure in single gas environment.

2. When injecting CO_2 at 30 bar, the actual experimental value of CH_4 is assumed to be equal to the predicted value using EL model. Based on this the Langmuir coefficient K (CO_2) in EL equation was obtained.
3. When injecting CO_2 at 30 bar, the actual experimental value of CO_2 is assumed to be equal to the sum of preferentially absorbed value and the calculated value using EL model. Based on this assumption, the amount of saturated adsorption of CO_2 Q_{max} (CO_2) in the EL equation was obtained.

Other experimental work investigating the adsorption kinetics of CO_2, CH_4, and equimolar mixtures was conducted by Gruszkiewicz *et al.* (2009). They tested three size fractions (45-150 μm, 1-2 mm and 5-10 mm) of crushed coal at 40 ^oC and 35 ^oC over a pressure range of 14 – 16.9 bar in order to simulate coalbed CH_4 recovery, using the volumetric method.

Their findings revealed: 1) CO_2 adsorption on both dry and water-saturated coal is much more rapid than CH_4 adsorption; 2) water saturation decreases the rates of CO_2 and CH_4 adsorption on coal surfaces, but it appears to have minimal effects on the final magnitude of CH_4 and CO_2 adsorption if the coal is not previously exposed to CO_2; 3) retention of adsorbed CO_2 on the coal surface is significant even with extreme pressure cycling.

Gas mixture adsorption experiments were conducted by Busch *et al*. (2003) at pressures up to 250 bar at a temperature of 45 ^oC using the volumetric method. Results of preferential adsorption on dry moisture equilibrated coals of different rank under identical conditions indicated that adsorption is a function of coal type, moisture content and pressure. They also showed that at pressures above 50 bar, CO_2 was always adsorbed preferentially to CH_4, although preferential sorption of CH_4 was observed in some instances at lower pressures. In general, excess sorption isotherms of lignite and sub-bituminous coals (0.25-0.46% R_oV_{mr}) exhibited a monotonous increase over the entire experimental pressure range (up to ~ 50 bar), while higher rank coals tended to approach a saturation level corresponding to a Langmuir isotherm.

When N_2 gas is used as part of the gas mixture, it was found for ECBM, it tends to yield incremental recovery response quite rapidly (Zhu *et al*., 2003). Jessen *et al.* (2008)

undertook studies to evaluate the CO_2-CH_4 adsorption-desorption rates using gas mixtures of CO_2 and N_2. It was found that injection of mixtures with large fraction of CO_2 reduces the initial recovery rate, but increases the breakthrough time as well as decreases the total amount of injectant needed to sweep out the CH_4. Jessen *et al.* (2008) also established that, in all cases, the CH_4 recovery was greater than 94%. For field studies and detailed simulations, it has also been shown that CO_2 injection allows for a complete displacement of CH_4 at a higher rate, through a broad injection front (the so called “shock front”), and its recovery as a pure gas, thanks to the stronger CO_2 adsorptivity. On the contrary, injection of N_2 rich gas mixture displaces CH_4 at a higher rate, through a broad injection front (the so-called “simple wave). As a drawback, the produced gas is a mixture of N_2 and CH_4. It can then be concluded that for mixtures of CH_4 and N_2, the CO_2 component yields a reduction in permeability and injectivity, while the N_2 injection component leads to a much more rapid breakthrough, thus reducing the product purity (CH_4 purity).

Other studies conducted by Sakurovs *et al*. (2007) using a mixture of CO_2, CH_4, and N_2, concluded that, for the coals tested, more CO_2 was adsorbed than CH_4, and more CH_4 adsorbed than N_2 for ternary gas mixture. This is also in agreement with conclusions made by other researchers (Fitzgerald *et al*., 2005, Bae and Bhatia, 2006 and Ottiger *et al*., 2008).

In recent work conducted by Dutta *et al.* (2011), fourteen Indian Gondwana coals with a mean vitrinite reflectance (%R_oV_{mr}) from 0.61 to 1.94% were tested using the volumetric method to establish sorption isotherm characteristics for CH_4 and CO_2 in relation to the influence of coal rank and macerals. Using dry, powdered coal samples, and an experimental pressure of 78 bar and 58 bar for CH_4 and CO_2 respectively, they found a decrease in the CO_2 to CH_4 ratios with an increase in experimental pressure, with the overall variation being between 4:1 and 1.5:1 for most samples tested.

2.12.8 Summary of the literature review

From the vast expanse of literature available it is evident that there are many variables that need to be considered when establishing the sorption capacity for coal. In addition to the

variances in coal composition (mineral and maceral (type) contents), moisture content, the sorption parameters also need further consideration. Most research only focuses on isothermal adsorption experimental investigations, using a fairly randomly chosen temperature, which is not also representative of the actual “in-situ” conditions. The thermal gradient of the coal seam needs to also be considered, in addition to the moisture and other characteristics of the seam.

Sorption data reported over the last two decades differs from researcher to researcher. This is also evident in the varied methodologies that are used to undertake the sorption determinations. Although attempts have been made to compare sorption data as produced from different experimental sets, i.e. volumetric, manometric and gravimetric, there is still some slight deviation in the adsorption isotherms for any given set of coal types. This was apparent with the round-robin trials conducted (Goodman *et al*., 2007, Gensterblum *et al*., 2009). Most commonly these errors could be attributed to cell volume determination, coal helium density evaluations, swelling and the adsorbed phase density used to calculate the excess sorption term. An added complication that is noted, is with regard to the diverse calculation methods that are employed by each researcher. Some prefer to determine the sorption data using gas density data, while others use CO_2 gas compressibility factors to conduct the calculations for the CO_2 sorption capacities.

It is difficult to do comparisons; however, with the methodology currently in place, and with consistent tests, a very applicable data set for SA coals could be determined and used as a data set to establish best SA coals adsorption capacities. Aspects relating to injection pressure, moisture content, sorption temperature and most importantly coal type and composition need much more investigation and verified repeatability of the initial data that has been established to date. The relation to coal deformation; swelling and /or shrinkage of the coal matrix needs extensive investigation and verification in combination of the other factors mentioned above.

CHAPTER 3

3. METHODOLOGY – Materials and Methods

3.1 Coal Samples

A number of coal samples were obtained from collieries around South Africa. The intention was to obtain as many samples as possible, with variations in rank, type, and grade, but this proved difficult in many aspects, despite approaching a number of coal mines. Coal samples used in this study are shown in Table 3.1. Due to the manner by which the samples were obtained, it cannot be stated that the samples were in carefully controlled conditions prior to testing. However, as each coal tested was crushed, air-dried and evacuated under vacuum prior to undertaking the CO_2 adsorption experiments, the conditions prior to crushing are unlikely to be of concern.

Table: 3.1. SA Coal Sample identification

Coal	***Coal ID***	***Coalfield /seam***	***Estimated composition (%C, db)***	***Estimated rank***
Anthracite	AN	KZN /unknown	82.0	High Rank C
Anthracite	SL	Unknown	84.9	High Rank B
Semi-Anthracite	SM	Unknown	73.7	High Rank C
Bituminous	EM	Unknown	60.3	Medium Rank C
Bituminous	BL	Unknown	64.3	Medium Rank C
Bituminous	GN	Witbank /#5	69.8	Medium Rank C
Bituminous	IN	Witbank /#2	66.8	Medium Rank C
Bituminous	SF	Highveld /#4	59.5	Medium Rank C
Bituminous	TN	Unknown	69.0	Medium Rank B
Bituminous	WG	Unknown	48.3	Medium Rank C

3.2 Sample Preparation and Handling

As all samples were received in 5 – 10 kg bags in particles far larger than suitable for the research tests; all samples underwent cone and quartering, and crushing to ensure even particle size distribution was attained. Brief summaries of these steps are included below.

3.2.1 Coning and Quartering

All coal samples were divided using the cone and quartering method. This is an old technique which is often used in dividing samples of material. It consists of pouring the material into a conical heap and relying on its radial symmetry to give four identical samples when the heap is flattened and divided by a cross-shaped metal (Wills, 1997) which ensures that each portion is representative of the parent sample.

3.2.2 Particle Sizing

The technique of sieve analysis was used to conduct sample particle size analysis (i.e. separation based on size or some other physical characteristic (Jillavenkatesa *et al.*, 2001). The method consists of shaking (agitating) the sample through a stacked series of sieves with decreasing mesh size. The mesh with the largest aperture is at the top, and that with the smallest aperture is at the bottom of the stack. (Jillavenkatesa *et al.*, 2001). The product was sieved, separating over-size, undersize and the desired fraction, the over-size product returned to the mill was for further milling and the undersize discarded. The process was repeated until 500 g samples of +4.75 -5 mm particles were obtained.

3.3 Coal Sample Characterisation

3.3.1 Proximate and Ultimate Analysis

The characterisation of the coal was undertaken to establish the analytical qualities of the different coal samples. Ultimate (determination of carbon, hydrogen, nitrogen, sulphur and oxygen by difference) and proximate analysis (determination of volatile matter, ash, moisture, and fixed carbon) were conducted, along with maceral analysis and vitrinite reflectance for all coal samples used. Proximate and Ultimate analysis was outsourced to, UIS Laboratories in Centurion, Pretoria, an SABS ISO accredited laboratory using the standard methods: ISO 11722:2013, ISO 1171:2010, ISO 562: 2010 and ISO 17247:2013 and ISO 19579: 2006.

3.3.2 Petrographic Analysis

All coal samples were petrographically analysed at the University of the Witwatersrand where a standard petrography procedure was used (ISO 7404:2009). Coals were crushed to -1 mm, set in epoxy resin, allowed to harden, and ground and polished to a final 0.05 alumina oxide finish (as per ISO 7404 part 2). The maceral analysis was undertaken on a Leica DMP4500 polarising microscope at a magnification of x500 under internal reflected light oil immersion, following procedures in ISO standard 7404 part 4. Mineral matter was counted as well as the organic components vitrinite, liptinite, and inertinite, which were further subdivided into maceral types (for detailed results see Table A1, Appendix A). Vitrinite reflectance analysis was undertaken on the same petrographic microscope fitted with a J&M spectrolytic system capable of determining reflectance. Standards were used to calibrate the system, and 100 points were determined on telocollinite, following ISO 7404 part 3.

3.3.3 Density Determination

Initial densities of all the coal samples were determined using a simple volume displacement method using de-ionised water as displacement medium in order to do the adsorption capacity calculations (details outlined in section 3.4.2.6). Second measurements were carried out using a standard model of manually operated stereopycnometer, which offers a choice of two interchangeable sample cells used in conjunction with a single reference volume. A sample is placed in the sample cell and degassed by purging with a flow of dry gas, by vacuum, or by a series of pressurization cycles. The standard analysis is performed by pressurizing the sample cell to approximately 17 psi (117.21 kPa) and recording the value. The selector valve is rotated so the gas expands into the reference or added volume and that lower pressure is recorded. From these two readings, the sample volume can be quickly and accurately calculated (Qi, 2007).

Density displacement measurements were carried out three times for each sample and the averaged density was used and compared with Helium Stereo-pycnometer results to calculate the standard deviation (see Appendix B1).

3.3.4 BET (Brunauer, Emmett and Teller) Analysis

BET analysis was carried out for all tested samples used to determine and compare the sorption properties of the different coals. The determination of the CO_2 surface areas and porosity properties of the coals were conducted on a Micromeritics ASAP 2020 (ASAP, 2000) surface area and porosity analyser. The samples (about 0.20 g each) were degassed under vacuum (10 lm Hg) at 90 ^oC for 2880 min on the degassing port of the equipment prior to adsorption analysis (0 ^oC in an ice bath for CO_2 and at 196 ^oC (77 K). These specific coal properties include determination of: surface area, micro-pore surface area, and pore volume. They were calculated from low pressure adsorption isotherms produced for the coal. The isotherms were determined up to a relative pressure of approximately 0.03 (experimental pressure/saturation pressure). Approximately 0.2 g of sample was analysed and results were calculated on a 66 per mass basis. The adsorption

data were automatically acquired by the ASAP 2020 v4.0 software in the relative pressure range: 0 < P/P0 6 0.032 for CO_2 The analysis was conducted using facilities at North West University (NWU), School of Chemical and Minerals Engineering, Potchefstroom campus.

The coal surface area was calculated by three different methods (BET, Langmuir and Single point), the micro-pore surface area, calculated by two different methods (Dubinin-Radushkevich and Dubinin-Astakhov), and the pore and micro-pore volumes. Table 4.2 is a summary reporting of the BET analysis results which can be found in section 4.2.2. (Detailed BET reports can be found in Appendix B2 – sample reports for two coals: SL and SM).

3.4 Experimental Set-up

3.4.1 High Pressure Volumetric adsorption system (HPVAS)

A volumetric sorption apparatus was designed in order to perform experiments to evaluate the sorption capacities of the coal types that were studied. A picture of the High Pressure CO_2 Volumetric Adsorption System (HPCVAS) is shown in Figure 3.1, and a schematic diagram of the system in shown in Figure 3.2. Each component of the HPCAS is described in Table 3.2, and the suppliers are also stated. The system was designed and constructed in SA by Chemvac, a company based in Pretoria specialising in designing and constructing specialised laboratory systems. The system built and used could only achieve pressures not higher than 100 bar and was built as to this specification to reduce costs.

The set-up consists of a reservoir cell, a sorption cell, a sample drying vessel, and a digital control system for temperature and pressure control and monitoring. The reservoir and sorption cells were made from stainless steel and have volumes of 467.2 cm^3 and 64.89 cm^3, respectively. After necessary modification, these volumes changed to 467.2 cm^3 and 43.79 cm^3 respectively. These changes are corrected for all subsequent CO_2 sorption experimental test data. The interconnecting manifold was made of stainless steel tubes and valves and was designed to be used at high pressures. The pressure in the reservoir and adsorption cells is controlled by a WIKA digital control system (Model A-10) via

accurate pressure sensors. Each cell can be controlled individually with an error less than 0.025 bar.

The major advantages of this HPCVAS apparatus are:

- The adsorption and desorption isotherms can be measured at pressures up to 100 bar,
- It can be used for either gas phase or in supercritical phase adsorption and desorption isotherms.
- It was designed to retroactively fit a GC (Gas Chromatograph) for online gas sampling, as well as an online data logger.
- It is relatively simple to use and maintain.

The costs were moderate to inexpensive for this type of equipment, due to the sourcing of second hand and / or SA parts, and the use of a local agent to construct the system

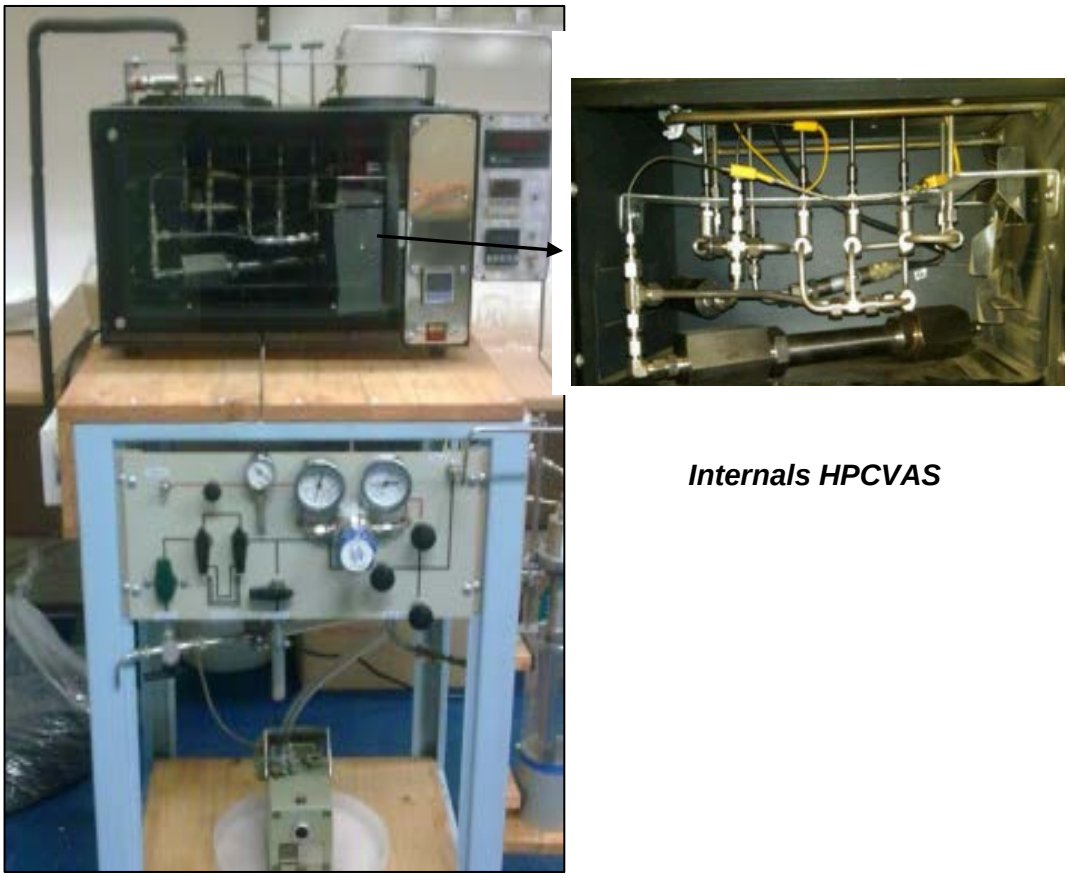

Internals HPCVAS

Figure 3.1 HPCVA

Schematic of the high pressure volumetric system (HPVAS) is depicted in Figure 3.2.

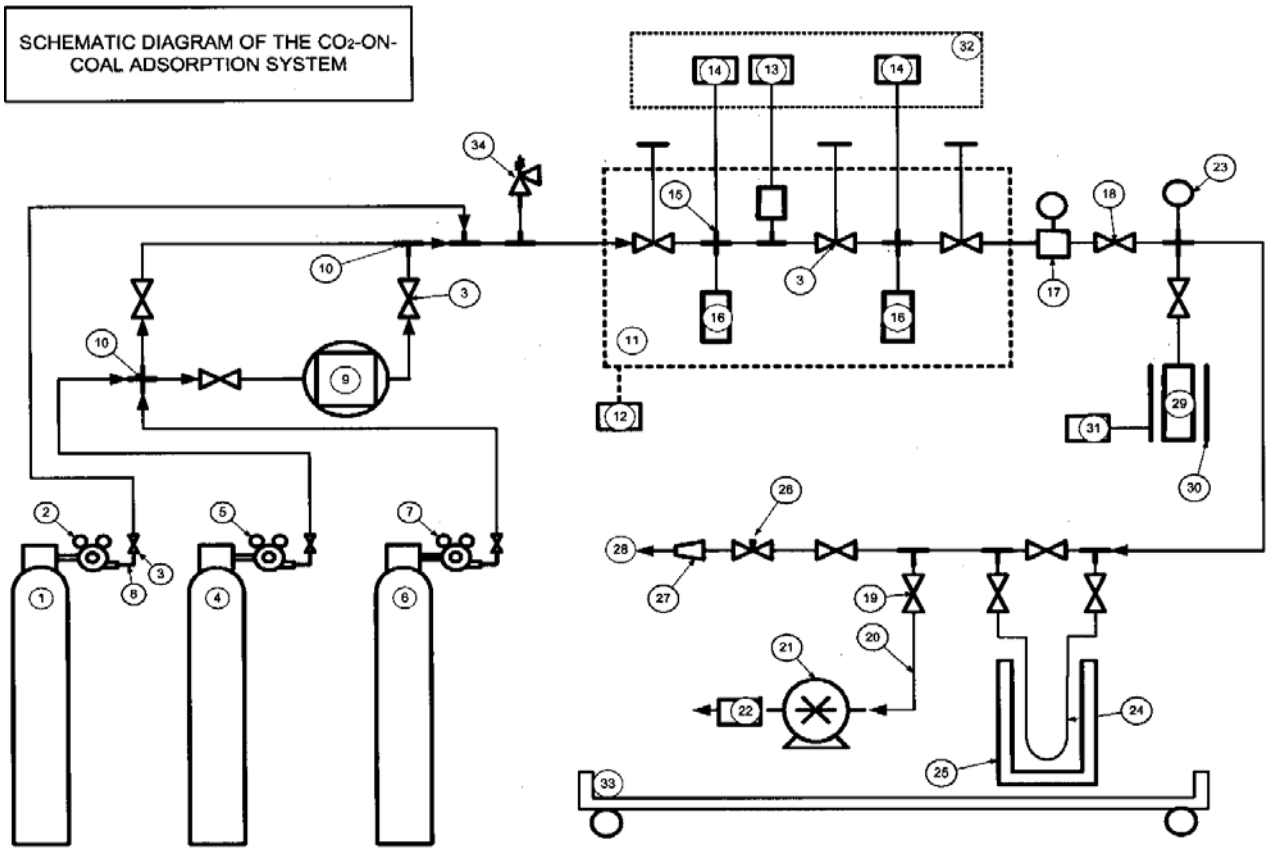

Figure 3.2: Schematic of the High Pressure CO_2 Volumetric Adsorption System Refer to Table 3.2 for numerical identification

Table 3.2: The components and description of the High Pressure CO_2 Volumetric Adsorption System

No.	*Component*	*Company*
1	N_2 gas cylinder	Afrox
2	N_2 pressure regulator	Afrox
3	¼" SS bellows seal valves	Chemvak
4	CO_2 cylinder	Afrox
5	CO_2 pressure regulator	Afrox
6	Flue gas cylinder	Afrox
7	Flue gas pressure regulator	Afrox
8	¼" SS tubing	Chemvak
9	Compressor	Chemvak
10	Swagelok ¼" SS unions	Chemvak
11	Used GC oven	Chemvak
12	Temperature control and Power Supply	Chemvak
13	0-200 bar pressure transducer + digital readout + PS WIKA (Model A-10)	Chemvak
14	Thermocouple (2) + digital readout + switch	Chemvak
15	Thermocouple SS couplings	Chemvak
16	Reference and Sample Cells	Chemvak
17	Single-stage, in-line pressure regulator + couplings	Chemvak
18	SS ¼" shut-off valves	Chemvak
19	NW 16 vacuum valve	Chemvak
20	NW 16 vacuum line + couplings + O-rings + clamps	Chemvak
21	2 m^3/h sliding vane fore-vacuum pump	Chemvak
22	Outlet oil mist trap	Chemvak
23	Mechanical vacuum gauge	Chemvak
24	U-tube volatiles trap	Chemvak
25	Liquid N_2 dewar (small)	Chemvak
26	SS ¼" Needle valve	Chemvak
27	SS reducer to GC	Chemvak
28	Gas chromatograph	Restek
29	Clamp-on heater	Chemvak
30	Clamp-on heater	Chemvak
31	Temperature controller (basic) + Thermocouple + PS	Chemvak
32	Instrument panel	Chemvak
33	Trolley	Chemvak
34	Pressure release valve	Chemvak

A Gas Chromatograph (GC) is attached to the HPCVAS setup, and is used to measure the gas composition after the adsorption/desorption tests. Figure 3.3 shows a SRI Model 8610C GC which was used for this project, supplied by Restek Chromagraphy. The GC consists of an injection block, a column, and two detectors. An inert gas (He) flows through the system as the carrier gas. The injection chamber is a heated cavity which serves to volatilize the compounds. The sample is injected by syringe into this chamber through a port which is covered by a rubber septum. Once inside, the sample becomes vaporized

and is carried out of the chamber and onto the column by the carrier gas. The two detectors that have been employed for this work, namely: TCD (Thermal Conductivity Detector), and FID (Flame Ionization Detector).

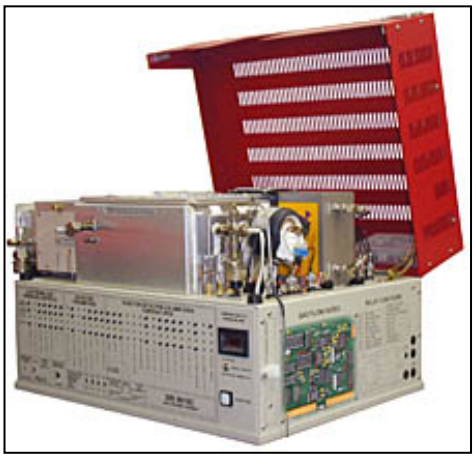

Figure 3.3: SRI Gas Chromatograph

3.4.1.1 Leak Testing

The key to best sorption performance results' is to ensure that a very precise leakage test be performed, because of the very small volumes used in this experimental setup. A leak test was conducted so as to ensure a hermetic seal of the entire apparatus. A leak test was conducted by introducing He to the system at the pressure of 45 bar and temperature of 35 ºC. The pressure was recorded and monitored at constant temperature for a period of 48 hours. Any leak occurred was detected by the decline in the 40 bar helium pressure in the system. In the case when the pressure dropped with time, a stream of Snoop liquid leak detector was applied to the pressurized connections. Formation of bubbles at a specific connection indicated leakage, and the nuts were tightened further, or the seals replaced. Concerns over leaks are the major reason for inaccurate results from a volumetric system, as discussed in Section 2.

3.4.1.2 Experimental Procedure: Sample Preparation

3.4.1.2.1 Sample drying and degassing

Since the adsorption capacity could be affected by the presence of moisture within the coal sample (Goodman *et al.*, 2004; Ozdemir, 2004), each coal sample was dried to remove residual moisture before the CO_2 adsorption measurements could take place.

For degassing to remove all surface moisture and any adsorbed gases present in the coal, ~5 g of sample was subjected to vacuum at a pressure of -0.7 bar and at a temperature of 110 ºC for 2 hours on a hot plate (Figure 3.4). The degas temperature range of 80-110ºC (353-378K) as has been suggested from most literature cited, as it ensures that the coal's physical and chemical structures remain unchanged with heat introduction, while the physically adsorbed moisture (most of the inherent moisture that interferes with gas adsorption) is driven off successfully (Bae & Bathia, 2006).

Figure 3.4: Degassing Set-up: vacuum pump, hot-plate and glassware

3.4.1.2.2 Determination of the Reference Cell and the Sample Cell Volumes

When using a volumetric apparatus for adsorption measurement, it is imperative to accurately determine the volumes of the reference (chamber B) and sample (chamber C)

cells. The empty volumes of the sample and reference cells were determined by a series of Helium expansions from reference cell to the sample cell when the sample cell was empty. The expansions were carried out in several steps to pressures up to 9 bar at room temperature (~25 ºC). A total of nine (9) incremental pressure steps were carried out for each test.

Figure 3.5 shows a simplified diagram of the HPCVAS with a standard (dozing) cell. The green section in Figure 3.5 represents the standard cell volume (chamber A), V_A, the yellow section represents the reference cell volume, V_B, and the red section represents the sample cell volume, V_C.

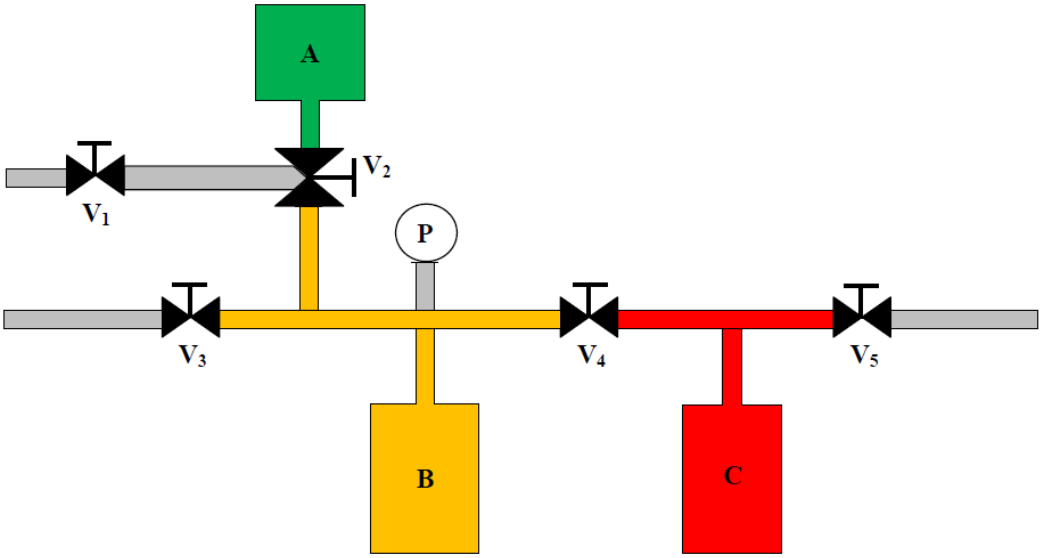

Figure 3.5 Simplified HPCVAS Diagram for Determining the Reference and Sample Cells Volumes (with a standard cell)

The standard cell volume, V_A, is known, and was connected to the system only when determining chamber B and C's volume, and was removed after that. P represents the pressure transducer connected directly to the reference cell, while V_1, V_2, V_3, V_4 and V_5 are the system valves.

It was assumed that for a given number of moles (n) of a gas, in this case He, the product of the pressure (P) and the volume (V) is constant at constant temperature. This

assumption was made on a basis that He acts as an ideal gas at room temperature and low pressures, and is inert. Therefore:

$$PV = nRT \qquad (3.1)$$

hence

$$PV = \text{constant} \qquad (3.2)$$

In equation 3.1 above, *R* is the gas constant whose value is 8.31441 J mol^{-1} K^{-1} (Geankoplis, 2003) given in SI units.

The following procedure was used to determine the volumes of the reference and sample cells:

1. Initially, the system was evacuated with valves V_2, V_4 and V_5 open, with valves V_1 and V_3 closed.
2. After 60 seconds of evacuation, all valves were closed.
3. The standard cell was then charged with *n* moles of He, with valves V_1 and V_2 open. The pressure *P* was recorded as P_1.
4. Valves V_1 and V_2 were closed and the system was evacuated.
5. Valve V_2 was open so that helium could expand from the standard cell, V_A, to the reference cell, V_B. After He expansion to the reference cell, the new volume is (V_A+V_B). The pressure obtained was recorded as P_2. Based on the assumption made in equation

$$PV = \text{constant} \qquad (3.3),$$

the following expression was obtained:

$$P_1 V_A = P_2(V_A + V_B) \qquad (3.4)$$

above, all variables (P_1, P_2, and V_A) are known except for V_B. Since V_B is the only unknown, it can now be determined as follows:

$$V_B = \frac{P_1 V_A}{P_2} - V_A \qquad (3.5)$$

or

$$V_B = V_A\left(\frac{P_1}{P_2} - 1\right) \qquad (3.6)$$

The system was again evacuated for 60 seconds, as in step 1 and step 2. Step 3 was repeated but pressure *P* was recorded as P_3. At this stage, V_A and V_B are combined and made one volume, (V_A+V_B), and their pressure *P* is P_3. Valve V_4 was open so that He could expand from the standard and reference cells, (V_A+V_B), to the reactor cell, V_C. After helium expansion to the reactor cell, the new volume is (V_A+V_B+V_C). The pressure obtained was recorded as P_4, hence the following expression was produced:

$$P_3(V_A + V_B) = P_4(V_A + V_B + V_C) \qquad (3.7)$$

In equation above, all variables (P_3, P_4, V_A, and V_B) are known except for V_C. Since V_C is the only unknown, it can now be determined as follows:

$$V_C = \frac{P_3(V_A + V_B)}{P_4} - V_A - V_B \qquad (3.8)$$

or

$$V_C = \left(\frac{P_3}{P_4} - 1\right)(V_A + V_B) \qquad (3.9)$$

The same procedure was repeated for pressures up to 6 bar.

3.4.1.2.3 Placement of the Coal Sample in the Sample Cell

After degassing the coal sample, the sample was re-weighed so as to get a definite mass (5 g). The sample was then placed inside the sample cell. The sample was then put under vacuum for 60 s, and the system was leak tested.

3.4.1.2.4 Estimation of the Void Volume in the Sample Cell

Before the adsorption test could commence, by introducing the adsorbate gas (CO_2) into the sample cell, the void volume within the sample cell was determined using the He expansion technique. The void volume is the available volume to the gas-phase in the sample cell (Ozdemir, 2004), the volume not occupied by the solid sample (Krooss *et al.*, 2002). Since He has a very small molecular size, it can be utilized to determine the void volume in the sample cell.

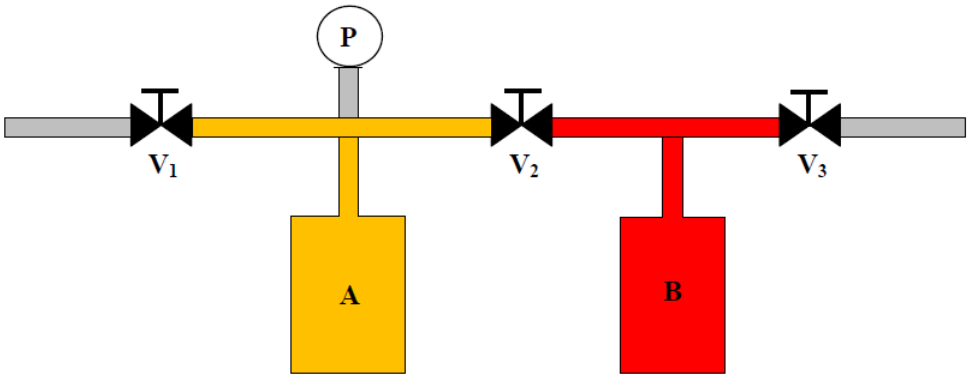

Figure 3.6 Simplified HPCVAS Diagram for Determining the Reference and Sample Cells Volumes (without the standard cell)

The following procedure was used to estimate the void volume of the sample cell:

1. Initially, the system was evacuated with valves V_2 and V_3 open, with valves V_1 closed.
2. After 60 seconds of evacuation, all valves were closed.
3. The reference cell, V_A, was then charged with n moles of He, with valve V_1 open. The pressure P was recorded as P_i.
4. Valve V_2 was open so that He could expand from the reference cell, V_A, to the sample cell, V_B. The pressure obtained was recorded as P_f. Using the recorded data, the following expressions used by Sudibandriyo (2010) were also used in this study to determine the void volume in the sample cell:

$$V_{void} = n_{He}\left(\frac{z_{He}RT}{P}\right) \qquad (3.10)$$

where number of moles of He injected into cell is

$$n_{He} = \frac{V}{RT}\left(\frac{P_i}{z_{He,i}} - \frac{P_f}{z_{He,f}}\right) \qquad (3.11)$$

V is the volume of the dozing cylinder, P_f and P_i represent final and initial pressure of that cylinder respectively, *R* is universal gas constant and *z* is the compressibility factor. The void volume was measured several times to reduce the uncertainty of this value (Sudibandriyo, 2010).

The He compressibility factor was evaluated using the Peng-Robinson equation of state. The He compressibility factor is given by:

$$z_{He} = 1 + \frac{\left(1.471\times10^{-3} - 4.779\times10^{-6}T + 4.92\times10^{-9}T^2\right)}{P} \qquad (3.12)$$

where *T* is in Kelvin and *P* is in atmospheres. This expression is based on the experimental data from National Bureau of Standards Technical Note 631 for He (McCarty, 1972).
The same procedure was repeated for pressures up to 6 bar.

3.4.1.3 Estimation of the Sample Volume

It is essential that the sample volume is known when dealing with the volumetric adsorption method. Busch *et al*. (2004) used the following expression to determine the sample volume, which was also used for this purpose of this research:

$$V_{sample.Cell} = V_{sample} + V_{void} \qquad (3.13)$$

In equation above, all variables ($V_{sample.Cell}$ and V_{void}) are known, $V_{sample.Cell}$ obtained from equation

$$V_C = \left(\frac{P_3}{P_4} - 1 \right) (V_A + V_B) \tag{3.14}$$

and V_{void} obtained from equation:

$$V_{void} = n_{He} \left(\frac{z_{He} RT}{P} \right) \tag{3.15}$$

except for V_{sample}. Since V_{sample} is our only unknown, it can be determined as follows:

$$V_{sample} = V_{sample.Cell} - V_{void} \tag{3.16}$$

The gas phase has a substantially lower specific density than the adsorbed phase and the volume of the latter can be neglected. In this case, the evaluation scheme results in the so called ‘‘excess sorption’’ or Gibbs sorption (Busch *et al.*, 2004).

3.4.1.4 Estimation of the Sample Density

The approximate density of a solid having a definite geometrical form may be determined by a volumetric method. The weight of the solid is obtained in a convenient manner. The density of a solid determined by this method is probably accurate to about 1 percent (Hidnert & Peffer, 1950). The expression used for determining the sample density is as follows:

$$\rho_s = \frac{m_s}{V_s} \tag{3.17}$$

Where:, ρ_s is the density of the sample, m_s is the mass of the sample, and V_s is the volume of the sample inside the sample cell.

Knowing V_s from equation and m_s from section 3.4.1.2.3 the sample density can then be computed using equation

$$V_{sample} = V_{sample.Cell} - V_{void} \quad (3.18)$$

Three samples per coal type were used to determine the coal densities with the displacement method and the average of them taken as the density. Appendix B outlines the manual density determinations for all coal samples used. Density values of each coal type where also verified using a Helium Stereo-pycnometer.

3.4.2 Experimental procedure: Simulated Coal Conditions

3.4.2.1 Moisture Simulation method

In order to compare the effect that moisture may have on the CO_2 sorption capacity, moisture simulation of a few chosen coals (TN, SL and EM) were conducted before the high pressure CO_2 adsorption tests were conducted. Coal samples of similar mass ~10g and particle size ~4.75 mm were dried and de-gassed (described in section 3.4.1.3) in order to remove excess inherent moisture and any adsorbed gases to aid in opening up the pores of the coal samples in preparation for absorption of de-ionised water. The samples were weighed again and then soaked in beakers of de-ionised water for different time periods in order to allow them to absorb some moisture at different percentages. The pre-determined moisture percentages were in the range of dry (representing 0%) to ~4.4%. After the soaking period, each sample was weighed again. The percentage moisture of each sample was calculated using equation 3.19, to determine the mass difference of the sample before and after it was soaked. The results were then compared to findings using a moisture balance (Figure 3.7).

$$\%\boldsymbol{moisture} = \frac{\boldsymbol{wet\ mass - dry\ mass}}{\boldsymbol{wet\ mass}} * 100 \quad (3.19)$$

Prepared samples were immediately transferred to the HPVAS and then run under a chosen set of varying increasing pressures up to 95 bar and temperature of 35 ^{o}C as for dried and degassed samples.

Figure 3.7: Shimadzu Moisture balance

3.4.2.2 Temperature simulated method: Isosteric Heat of Adsorption calculation

Isosteric heat of adsorption, also called differential heat of adsorption, is the heat released as the infinitesimal CO_2 molecules are adsorbed, with the adsorption capacity being constant. It is the enthalpy change at the moment of adsorption. Isosteric heat of adsorption is expressed as q^{st}, calculated with Clausius-Clapeyron equation 3.20 (Lu *et al*., 2014; Zheng *at al*., 2009; Ma *et al*., 2014).

$$\frac{\mathrm{d}\ln P}{\mathrm{d}T} = \frac{q^{st}}{RT} \qquad (3.20)$$

Where:

q^{st} =isosteric heat of adsorption; P = pressure; T = absolute temperature; R for gas constant = 8.314.

Integrating equation (3.20) yields:

$$\ln P = -\frac{q^{st}}{RT} + C \qquad (3.21)$$

Calculation process: ln*P* correlates with *n*, adsorption capacity (mmol/g); fit ln*P* − *n* data and get ln*P* − *n* relation. Several fixed *n* (mmol/g), and the corresponding ln*P* can be got with fitting formulas. Then, do a plot of ln*P* with 1/*T* at fixed adsorption capacity and have linear fitting, so adsorption isostere is achieved, based on this the slope of isosteric heat of adsorption is calculated.

3.4.2.3 Methane Saturation method of coals

Tests to investigate CH_4 desorption using a GC were conducted. In order to simulate a CH_4 saturated coal a low pressure stainless steel cylinder (maximum pressure specification of 2.5 bar) was used, Figure 3.8. Pure CH_4 was flushed into an empty stainless steel pressure cylinder at 2.3 bar for 4 hours to determine if any possible leak existed in it. This was done to ensure accurate results as any leak on the cylinder would eventually give less accurate results. Because there is no sample (adsorbent) inside the cylinder, the pressure must remain at 2.3 bar which symbolizes that no CH_4 molecules are being adsorbed or escaping the cylinder. If this is achieved for a very long time then there is no leaking on the cylinder.

Figure 3.8: Stainless Steel Pressure Cylinder

Crushed samples to the required size fraction (-5 mm + 4.75 mm); ~10g of each sample different coal sample types collected from the sieve screen were packed in labelled plastic sample bags for use.

Each of the prepared samples was degassed in an air tight conical flask connected to a suction vacuum pump, with the flask standing on a hot plate at temperatures of about 110^{o}C (as described in section 3.4.1.3). The coal sample was thereafter pressurized with pure CH_4 gas at a pressure of 2 bars, and left overnight so that the CH_4 adsorbs into the coal. This CH_4 uptake was indicated by the decrease of pressure monitored on the cylinder pressure gauge (see Figure 3.8). These CH_4 saturated samples were then used to undertake CH_4 desorption tests and CO_2 injection into saturated coals to test for CH_4 desorption versus CO_2 adsorption capacity for selected SA coals.

3.4.3 Determination of CO_2 Adsorption Isotherms: Dried-degassed, Temperature for CH_4 simulated tests

In order to address research objectives numbered two (2) to six (6) outlined in section 1.2 the following test methodology was undertaken:

The reservoir cell was first pressurized with CO_2. Ten minutes were allowed to achieve thermal equilibrium, although a stable temperature reading was achieved following 3 - 5 minutes. A portion of the gas was then transferred from the reference cell into the sample cell. Pressure and temperature were monitored in both cells to verify thermal and kinetic equilibration. In initial tests of up to 20 hours, it was found that 20-30 min was sufficient for the adsorption of CO_2 to reach equilibrium. The amount of CO_2 in gas phase within both the reference and sample cell was calculated using the real gas law, which accounts for the gas compressibility. The compressibility factor for CO_2 was calculated using Span and Wagner (1996) equation of state. The excess adsorbed amount was calculated from the mass balance between the reference and sample cells at each gas expansion step using Equation 3.6.

The system oven was set to a temperature of 35 ºC to ensure that a predefined isothermal temperature was established. 15 minutes were allowed to achieve thermal equilibrium in the system oven even though 10 minutes was sufficient to reach a stable temperature reading.

The reference cell was charged with CO_2 to a desired pressure by opening valve V_1, with valves V_2 and V_3 closed, see Figure 3.6. Valve V_1 was then closed to isolate the reference cell from the CO_2 gas cylinder. The pressure in the reference was allowed to stabilize for 5 minutes even though in some instances much less time was taken for the pressure to be stable. The data logger was started on the computer so that it could start recording the pressure and temperature data of the whole test run. Then, a portion of the gas was transferred from the reference cell into the sample cell by opening valve V_2. Pressure and temperature were monitored in both cells to verify thermal and kinetic equilibration. In the initial (trial) tests of up to 24 hrs, it was found that 4-6 hours was sufficient for the adsorption of CO_2 to reach equilibrium.

The most fundamental operational procedure to quantify gas adsorption is the Gibbs approach. Here the amount of adsorbed gas (n_{sorbed}) is defined as the difference between the total amount of gas (n_{total}) present in the system and the amount occupying the void volume (V_{void}), i.e. the volume not occupied by the solid sample. The Gibbs excess sorption method assumes a constant ratio of condensed phase volume and void volume throughout the experiment and requires no further assumptions (Krooss *et al.*, 2002). The excess amount of CO_2 adsorbed was calculated from the mass balance between the reference and sample cells at each gas expansion step using the Gibbs approach as expressed in the following expressions:

$$n_{sorbed}^{excess} = \frac{n_{total} - \rho_{eq} V_{void}}{m_s} \qquad (3.22)$$

Or

$$n_{sorbed}^{excess} = \frac{n_{total} - \rho_{eq} \left(V_{Sample.Cell} - V_{Sample} \right)}{m_s} \qquad (3.23)$$

where n_{sorbed}^{excess} is the excess amount adsorbed (mmol/g), n_{total} is the total amount injected into the system (mmol), ρ_{eq} is the density of the gas (mmol/cm^3) (in this case CO_2), and V_{void} is the void volume of the sample cell as expressed in equation

$$V_{void} = n_{He}\left(\frac{z_{He}RT}{P}\right) \tag{3.24}$$

The total amount injected into the system (n_{total}) can be expressed as follows:

$$n_{total} = \rho_{gas}(T,P)V_{void} \tag{3.25}$$

where ρ_{gas} the gas density at a given temperature (T) and pressure (P). The CO_2 densities (ρ_{eq} and ρ_{gas}) at a given T and P in the gas phase were obtained from the NIST (2007) website.

Now, knowing all variables and parameters of equation (3.16) the excess amount of CO_2 adsorbed n_{sorbed}^{excess} can be determined. Furthermore, the amount of gas adsorbed can be expressed in the absolute form as follows:

$$n_{sorbed}^{absolute} = \frac{n_{sorbed}^{excess}}{1 - \rho_{gas}/\rho_{adsorbed}} \tag{3.26}$$

where n_{sorbed}^{excess} is the absolute adsorbed amount of CO_2 (mmol/g), $\rho_{adsorbed}$ is the gas adsorbed phase density (in this case CO_2) (mmol/cm^3).

The adsorbed phase density is usually assumed to be constant across the experimental range (Kim *et al.*, 2011). Some authors have previously applied it successfully in their work (Fitzgerald *et al.* 2005; He *et al.,* 2010; Kim *et al.,* 2011; Sakurovs *et al.*, 2007). The adsorbed-phase density estimates do, however, affect the calculated absolute adsorption

isotherm (Fitzgerald *et al.*, 2005). In this study the value of 22.6 mol/ℓ, which is equivalent to 22.6 mmol/cm^3 for CO_2 was applied to the model.

3.4.4. CH_4 Desorption Tests

In order to address research objectives numbered 7, 8 and 9 as outlined in section 1.2. it was necessary to determine the CH_4 release rate relative to CO_2 adsorption and determine the maximum amount of CH_4 that can be extracted from some selected SA coals (using set-up depicted in Figure 3.9), desorption tests were undertaken using the method of cyclic super-critical CO_2 injection. The following tests were carried out:

Figure 3.9: GC connected to online PC

- Samples now with a CH_4 potentiality (as prepared according to details outlined in section 3.4.4.1) were fed to the HPVAS reactor and CO_2 was injected into the reactor at different pressure steps ranging from 10-90 (sub to super-critical) bars at an isothermal temperature of 35^{o}C.

- The adsorption system was connected to a computer installed with operative data logging software that captured the pressure gradients in the system reactor over injection time and was also connected to GC that was used to analyze the gas

concentrations (ppm) from the adsorption system reactor at hourly intervals after each CO_2 pressure injection step.

- As with the ambient CH_4 desorption trials, here to, the SRI 8610C Gas Chromatographer (GC) was connected to a PC with PEAK Simple software to capture the gas concentrations after every pressure step of injected CO_2. The quantity of CH_4 gas in the gas from the reactor cell supplied to the GC at every pressure interval indicates the amount of CH_4 gas desorbed by the coal sample for that pressure step.

- The gas in the GC line was evacuated by use of a vacuum pump at the beginning of every pressure step to ensure no build-up of the desorbed gases were trapped in the gas line, as this would affect the values of the CH_4 desorbed per each incremental CO_2 injection step.

- Desorption isotherms were constructed using the captured experimental data from data logging and GC PEAK Simple software.

The experimental methods described and used, as well as the technical programme followed, as was detailed in this Chapter 3, can be summarised by the flow chart as depicted in Figure 3.10.

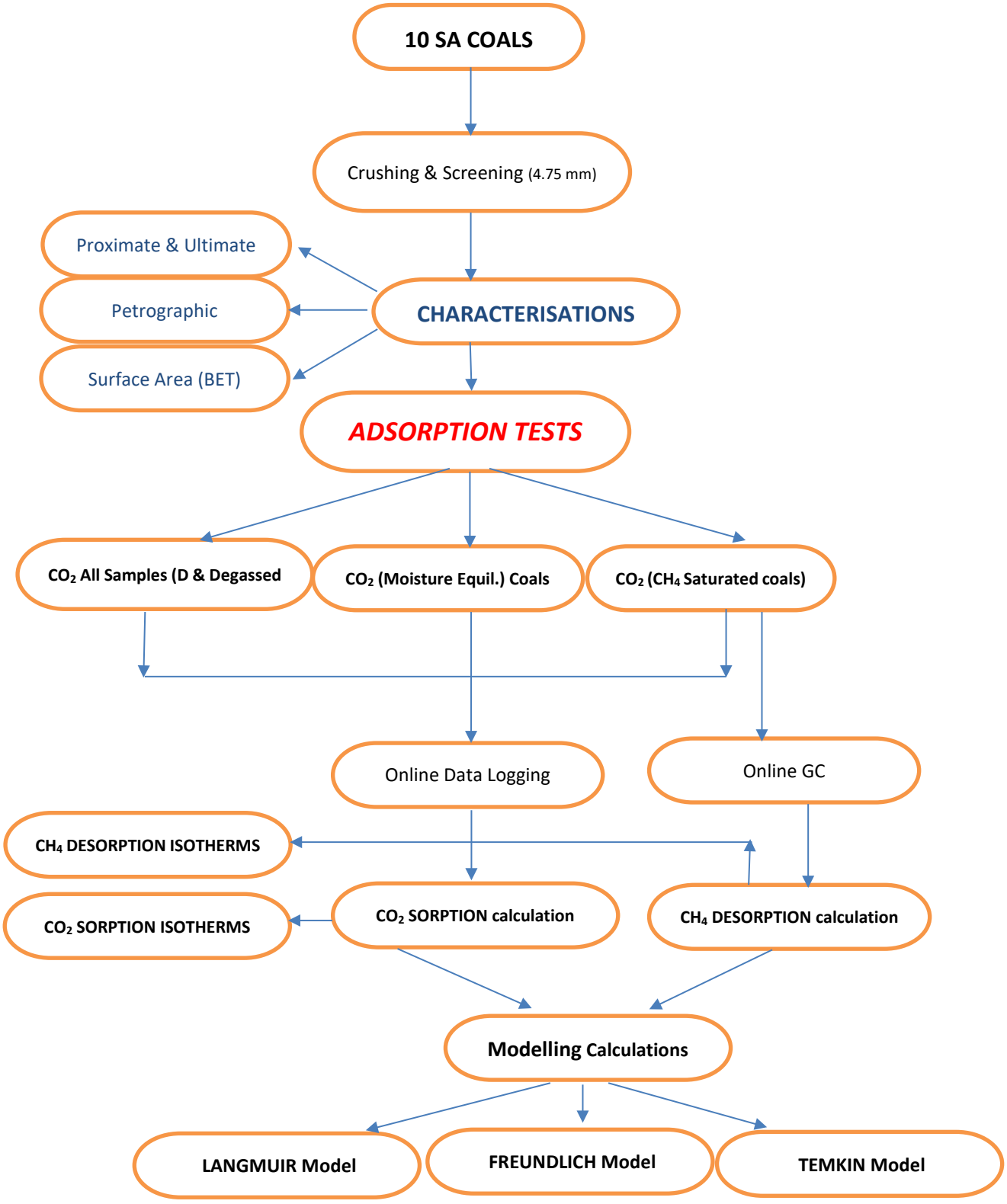

Figure 3.10: Flowsheet of experimental methods and technical programme

CHAPTER 4
RESULTS and DISCUSSION

4.1 INTRODUCTION

The main aim of this investigation was to determine CO_2 adsorption capacities and CH_4 desorption potential of a variety of different South African coal types using pure CO_2 and with CH_4 saturated coals using CO_2 injection to simulate and evaluate the different coal type's potential for ECBM. A number of South African coals (10) as outlined in Table 3.1 were tested to evaluate their ability to adsorb CO_2 and the potential to desorb CH_4, according to their respective properties of rank, coal type including, differences in maceral content, and mineral matter. This was further evaluated by investigating what the effects of pressure, varied temperature and different inherent moisture contents would have on the CO_2 sorption with the different coal types.

It is well known that the amount of CO_2 adsorbed on the coal depends on a number of factors (refer to Section 2.12.1 – 2.12.7). Coal contains a wide variety of organic and inorganic mineral phases in a complex, porous, three-dimensional macroporous and microporous network, which varies from one coal deposit to another, and between various seams. The organic part of the coal is believed to capture CO_2 using surface adsorption, pore-filling, and solid solution. The nature of the coal seam itself is a very important variable to be considered, addressing fractures, cleats, pore characteristics (open and closed), pore types; meso-macro and micro pores, to some extent ultra-pores and potential of swelling effects, which is beyond the scope of the current investigation.

Ultimately it is believed that the nature of the coal will determine the maximum adsorption capacity under a given set of conditions, be it for set coal seam pressure and temperature variables. The amount of CO_2 adsorbed as well as the amount of CH_4 desorbed for the given coal will depend on the physical and chemical reactions between coal and CO_2. Parameters such as temperature, pressure, particle size, and presence of moisture are expected to have reasonable to large influence on the adsorption capacity of CO_2 on the coal. Furthermore, the sorption of CO_2 and CH_4 also depends on another two important parameters: porosity/permeability and inherent surface area.

Research method and equipment background

The determination of sorption isotherms, sorption capacities and rates has become a standard approach for investigating coal performance with respect to CO_2 adsorption and CH_4 desorption. In this study, the volumetric (manometric) method (as detailed in Section 2.91 and Section 3.4) for recording both the CO_2 and CH_4 sorption isotherms was conducted. Using published data sets and theoretical considerations, the CO_2 sorption is discussed in detail to ascertain the best CO_2 adsorbing SA coal type available for testing. The sorption isotherms were recorded for as received, dry and degassed, crushed coals, for ease of preparation and testing. However, these coal samples are not ideally a representation of *in situ* conditions; attempts have been made to test coals with increased pressures and temperatures effects (representative of potential coalbed depths), different coal moisture contents (simulating inherent coal seam moisture), and finally with CH_4 saturated coals using CO_2 injection to simulate and evaluate the different coal types potential for ECBM.

The volumetric system (HPVAS) experienced significant delays during construction, and leaks have been problematic. Sudden pressure drops and difficulties in attaining higher CO_2 super-critical pressures hindered reliable results, and initial tests were undertaken in the sub-critical range. In addition, the methodology for experimental methods and coal sorption calculation, methods varied from article to article in published literature. Trial and error tests had to be conducted to determine the most reliable calculation method, which was time consuming. The data analysis method that was found to be more representative of CO_2 adsorption principles, and has since been adopted for the tests carried out (using gas density data, NIST, 2007). The adsorption (CO_2) and desorption (CH_4) tests were conducted from sub-critical (~9 bar) to super-critical (~90 bar) CO_2 injection pressure range. All pure CO_2 adsorption measurements were performed on 5 g samples with a grain size of -5+4.75 mm. All CH_4 saturated samples investigating CO_2 adsorption and CH_4 desorption results (detailed in Sections 4.9) used 10g and sample grain size -5+4.75 mm. Due to time constraints (as a result of equipment down time), not all samples were analysed repeatedly for CO_2 adsorption. However, leak tests conducted for some coals showed very good repeatability's were achieved, (Section 4.4) and hence all final results presented could be deemed completely valid.

4.2 Proximate, Ultimate and Petrographic, characterisation of coal samples

Table 4.1 provides the full suite of data for the selected South African coals used in this study pertaining to the main chemical, proximate and ultimate analyses, and petrographic characteristics for the total number of (10) coals used in this research study.

Data is presented on dry basis (db%) (i.e., as was received from the outsourced coal analysis laboratory using the ISO standards as outlined in Section 3.3.1) and was then used in order to compute the dry ash free basis (daf%) data using equation 4.1 as per guidelines (World Coal Institute, 2007).

$$\text{daf (\%)} = \text{db (\%)} \times (100)/(100\text{-Ash\%}) \qquad (4.1)$$

Detailed petrographic data can be found in Appendix A (Table A1), where all the respective maceral data (vitrinite, inertinite & liptinite, vol%) is reported as mineral matter free (mmf) volume percent (vol%). Density (g/cm^3) of coals as per Stereo pycnometer analysed data is presented in Appendix B (Table B1). The location of some samples is known, but other samples are simply referred to as bituminous or anthracite; all coals are from active SA coal mines.

Table 4.1: Proximate, Ultimate and Petrographic data of SA Coals

Sample ID:	***AN***		***SL***		***SM***		***TN***		***BL***		***SF***		***GN***		***IN***		***EM***		***WG***	
	db	*daf*	*Db*	*daf*	*db*	*daf*	*db*	*daf*	*db*	*daf*	*db*	*daf*	*db*	*daf*	*db*	*daf*	*db*	*daf*	*db*	*daf*
PROXIMATE DATA																				
Moisture %	1.4		1.5		1.1		0.7		3.8		5.0		3.4		2.0		4.5		1.1	
Vol. matter %	5.2	5.7	5.4	5.8	7.7	9.9	17.9	22.2	24.8	29.1	24.3	30.1	32.3	36.0	23.3	28.6	39.0	47.5	25.2	41.6
Ash %	8.8	9.6	6.1	6.5	18.2	22.2	19.5	24.2	14.7	17.2	19.3	23.9	10.3	11.5	18.4	22.5	17.9	21.9	39.4	64.9
Fixed C %	84.6	92.8	87.2	92.9	72.9	89.1	61.8	76.8	56.7	66.5	51.4	63.7	53.9	60.1	56.3	69.0	27.8	33.9	32.6	53.8
ULTIMATE DATA																				
Sample ID:	***AN***		***SL***		***SM***		***TN***		***BL***		***SF***		***GN***		***IN***		***EM***		***WG***	
C %	82.0	89.9	84.9	90.4	73.7	90.1	69.0	85.7	64.3	75.4	59.5	73.7	69.8	77.8	66.8	81.9	60.3	73.5	48.3	79.7
H %	3.1	3.4	3.0	3.2	3.3	4.1	4.1	5.0	4.2	5.0	3.7	4.6	4.9	5.5	4.0	4.9	3.7	4.5	2.9	4.7
N %	1.9	2.1	2.1	2.2	1.6	2.0	1.5	1.9	1.4	1.7	1.5	1.9	1.8	2.0	1.6	1.9	1.5	1.9	1.1	1.9
O%	3.3	3.7	1.9	2.0	2.5	3.1	5.3	6.6	14.9	17.5	14.5	18.0	12.7	14.2	8.3	10.2	15.9	19.4	7.3	12.1
S %	0.9	1.0	2.1	2.2	0.6	0.8	0.6	0.7	0.4	0.5	1.4	1.8	0.5	0.5	0.9	1.1	0.5	0.6	1.0	1.7
Total	100.0		100.0		100.0		100.0		100.0		100.0		100.0		100.0		100.0		100.0	
PETROGRAPHIC DATA																				
Sample ID:	***AN***		***SL***		***SM***		***TN***		***BL***		***SF***		***GN***		***IN***		***EM***		***WG***	
Vitrinite vol%[a]	33.4		56.1		88		71.6		32.2		20.8		51.4		50.2		13.9		5	
Inertinite vol%[a]	66.6		43.9		12		28.1		62.3		76.7		43.9		47.3		82.2		90.8	
Liptinite vol%[a]	0		0		0		0.3		5.5		2.5		4.7		2.5		3.6		4.3	
Mineral Mat. vol%	4.6		1.5		4.5		8.3		6.2		12.4		11.2		10.4		9.8		43.6	
R_oV_{mr} vol%[b]	2.91		3.49		2.24		1.26		0.7		0.65		0.7		0.81		0.64		0.51	
Coal Rank	***HRC***		***HRB***		***HRC***		***MRB***		***MRC***		***MRC***		***MRC***		***MRC***		***MRC***		***MRC***	
Density (g/cm^3)	1.59		1.55		1.8		1.47		2.23		1.59		1.48		1.47		1.64		2.31	

Highest value
Lowest value

db: air dried basis (%)
daf; dry ash free basis (%)

[a] – mmf; mineral matter free
[b] – Mean vitrinite reflectance in oil

4.2.1 Proximate and Ultimate analyses

Table 4.1 shows the proximate and ultimate analyses results of the ten (10) coal samples. These values reported are very typical of South African coals (Smith *et al*., 1983; Saghafi *et al*., 2008; Van Niekerk & Mathews, 2010; Maphala, 2012 and Hattingh *et al*., 2013). The coals were found to have fixed carbon contents in the range of 27.8 – 87.2 wt% and some coals having relatively high ash yields (6.1–39.4 wt%). Ash yield (air dried basis) ranges from 6.1% (SL) being the lowest to the highest being 39.4% (WG). The moistures (IM) were found to be in the range from 0.7 – 5.0 %. Figure 4.1 shows a plot for carbon % (daf %) to moisture content (%). It is clear that, MRC WG (1.06%) exhibited very low moisture, while having a high carbon content (79.7%), this is also noted for sample EM having a high moisture 4.5% and high carbon content (73.5%) (daf) basis. For all other MRC samples it was observed that moisture content decreases gradually with increase in rank (thermal maturity). While moistures for HRC coals were observed to be very low (<1.5%), as was expected (Stach *et al*., 1982; Meyers, 1982; Unsworth *et al*., 1989).

Volatile matter yields were very varied, ranging from 5.8 – 47.5 wt%, (daf) basis, exhibiting a notable decrease with increasing carbon content i.e. coal rank increase (as seen in Figure 4.2). The higher volatile matter content of coals GN (36.0 wt %), EM (47.5 wt %), WG (41.6 wt %) could possibly be attributed to higher liptinite contents (GN: 4.7%), (EM: 3.6%), WG (4.3%) (Smith *et al*., 1983). Although very different in maceral content, these coals displayed quite similar carbon contents. Alternatively it could very well be due to lower rank levels of these coals (EM and WG), while for GN it could be due to the higher vitrinite content (51.4%).

The elemental carbon contents ranged between 48.3% and 90.4% (daf) basis; while the elemental oxygen contents were comparatively lower for HRB sample SL (2.0%) followed by HRC samples SM (3.1%), AN (3.7%) than for the other samples (MRC) whereas, it was notably higher for samples SF (18%) and EM (19.4%) o dry ash free basis (daf). Both elemental nitrogen and total sulphur contents (daf) were low for nine (9) of the ten coals, at approximately <1.8%, with the exception of sample SL being at 2.2% for both nitrogen and sulphur respectively. While hydrogen ranged from 2.9 – 5.5%.

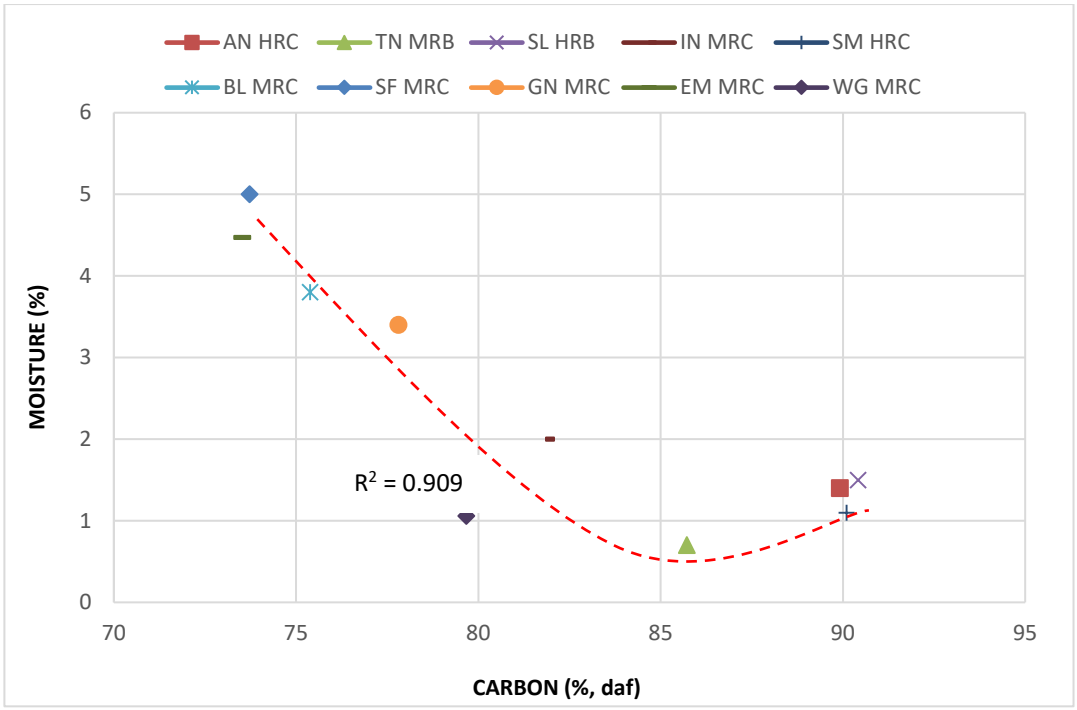

Figure 4.1: Comparison of Carbon (%, daf) to moisture (%)

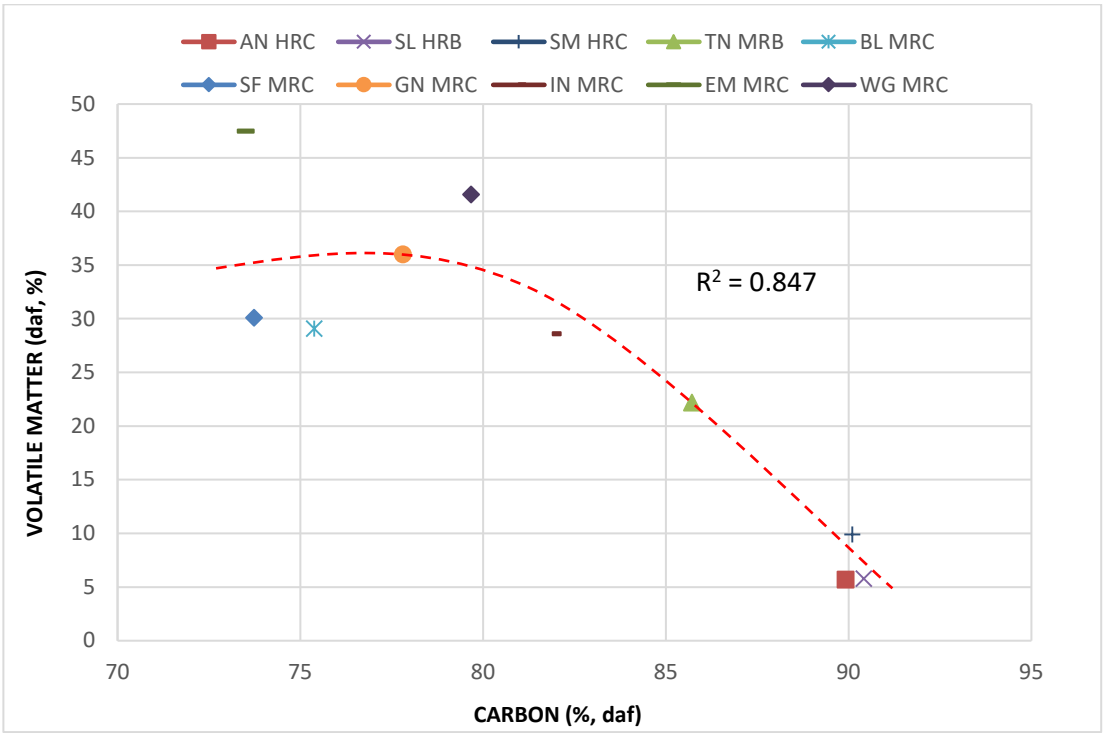

Figure 4.2: Comparison of Carbon (%, daf) to volatile matter (%, daf)

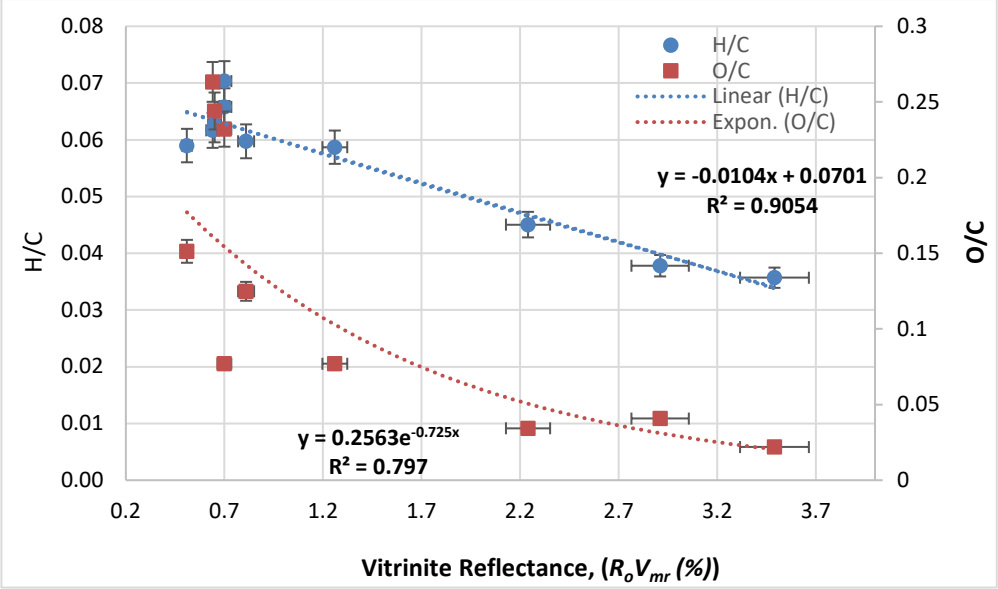

Figure 4.3(a): Correlation of atomic ratio: H/C & O/C versus vitrinite reflectance [R_oV_{mr} (%)] for all coals (10) of different ranks

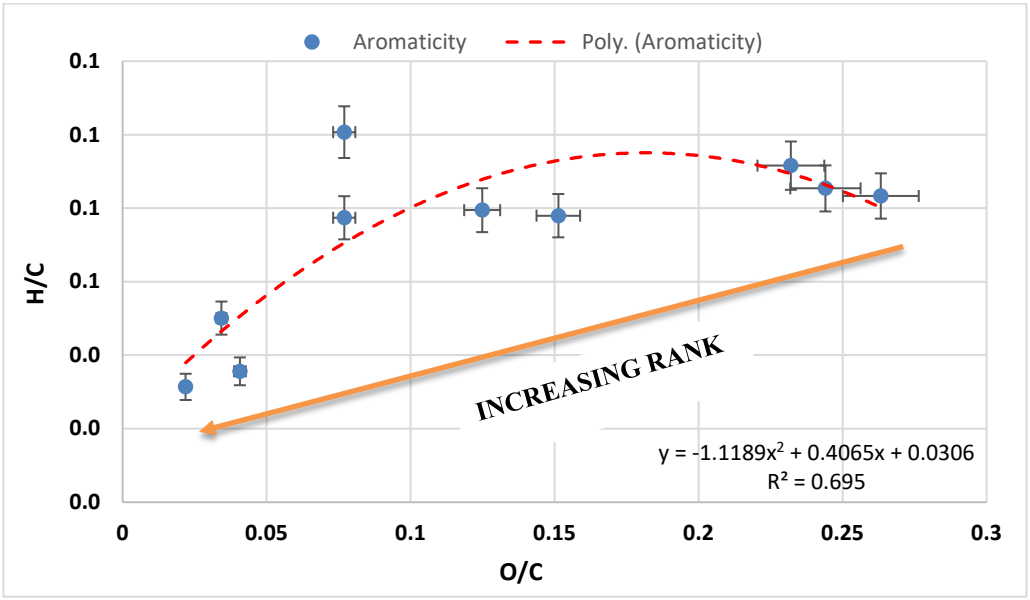

Figure 4.3(b): Correlation of atomic ratio: H/C versus O/C for all coals (10) of different ranks

Figure 4.3(a) shows the correlation of atomic hydrogen to carbon (H/C) and oxygen to carbon (O/C) against vitrinite reflectance (coal rank parameter) and Figure 4.3(b) shows the correlation for the ratio of atomic H/C versus atomic oxygen to carbon (O/C). It is obvious, from both graphical representations, that the progression from high to low H/C

and O/C values reflects the influence of severe metamorphic alteration; in other words, coals toward the lower-H/C-and-O/C end of the band are higher in rank. In other words, coal increases both its aromatic carbon and aromatic hydrogen, while its aliphatic hydrogen decreases during coalification (Neavel, 1981; Orrego-Ruiz *et al*., 2011; Odeh, 2015). As expected, the atomic mass ratio of H/C increases as the coal rank decreases, with the MRC coal samples (IN, BL, SF, GN, WG and EM) having a ratio in the range from 0.06 – 0.07, while the HRC coals, AN and SM, report ratios of 0.04 and 0.05, respectively. And HRB coal SL reported 0.04 and MRB coal TN reported 0.06. The trend obtained for the aromaticity was consistent for all coal samples used, in that the aromaticity was increasing with the increase in the coalification temperature.

It has been presumed that all carbon atoms present in coal are either aliphatic or aromatic in nature, neglecting the contribution that comes from the carbon in carboxylic acids (Orrego-Ruiz *et al*., 2011). Data set illustrating H/C ratio to vitrinite reflectance trend follows a linear regression fitting (R^2=0.91). While the O/C ratio data set follows the exponential regression having R^2 = 0.8. The fact that this data set does not follow a linear progression, implies that there is not a simple scale that defines the rank progression (Neavel, 1981).

4.2.2 Petrographic Analyses

The reflectance analysis indicates that most samples are Medium Rank C coals (BL, SF, GN, IN, EM and WG) with mean vitrinite reflectance (R_oV_{mr}%) ranging from 0.51 – 0.81% following the international ECE-UN In seam coal classification scheme, with two samples falling in the anthracite High Rank C category (AN and SM) having R_oV_{mr}% of 2.91% and 2.24% respectively, another (SL) in the High Rank B category having R_oV_{mr}% of 3.49%, while one other sample (TN) in the Medium Rank B has R_oV_{mr}% of 1.26%. Figure 4.4(a) illustrates the relationship between volatile matter (daf %) versus the vitrinite reflectance (R_oV_{mr}, %) as analysed petrographically. A distinct decrease in R_oV_{mr}, (%) can be observed as volatile matter increases as coal rank decreases. This is observed by a good polynomial trend showing a well fit regression analysis of R^2 = 0.9575. Giving good indication relating to other data sets. While the inverse can be seen for Figure 4.4(b) showing relationship between carbon (%) and the vitrinite reflectance (R_oV_{mr}, %).

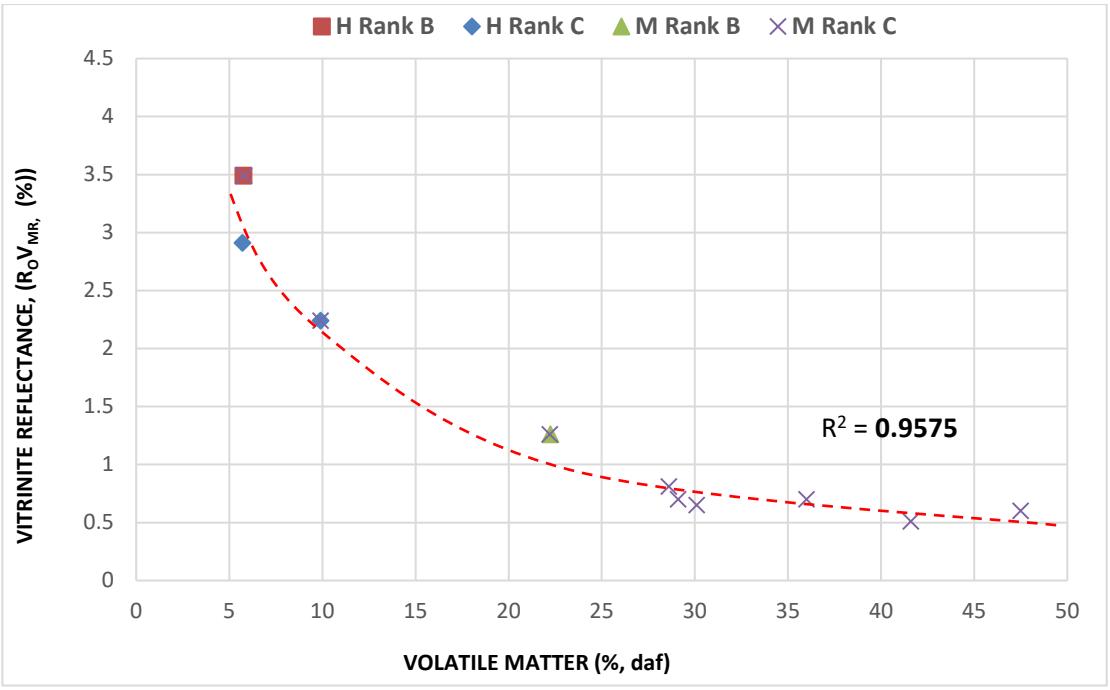

Figure 4.4(a): Comparison of Volatile Matter (%, daf) to Vitrinite Reflectance (R_oV_{mr}, %)

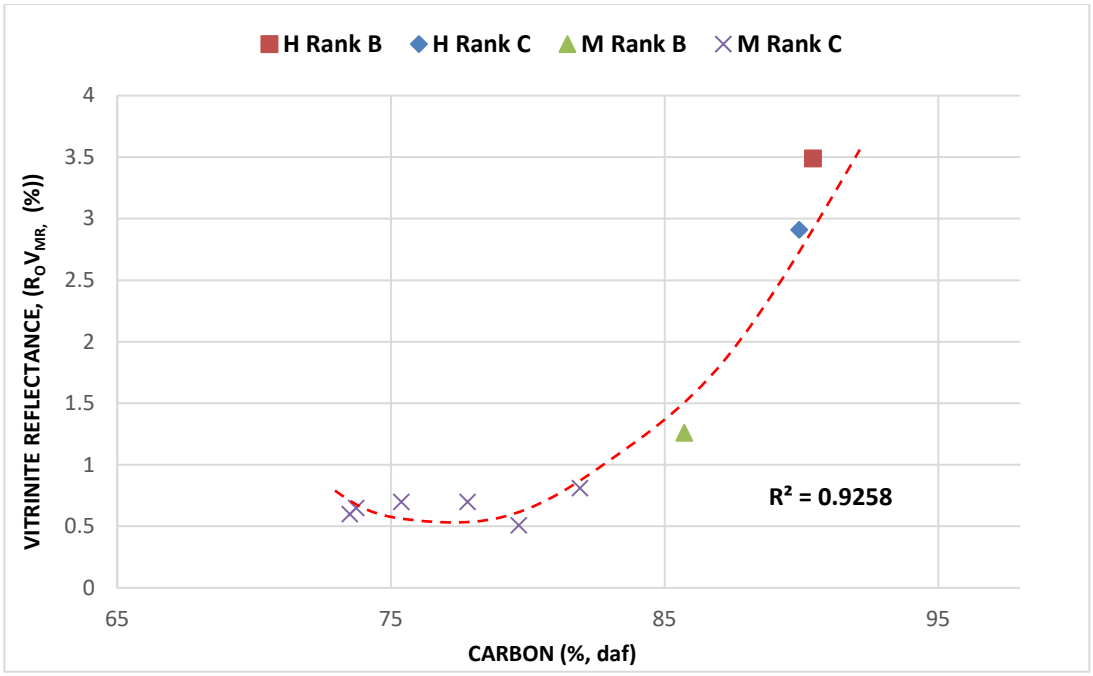

Figure 4.4(b): Comparison of Volatile Matter (%, daf) to Vitrinite Reflectance (R_oV_{mr}, %)

The samples have variable vitrinite contents, which is likely to impact on CO_2 absorptivity at the same rank (as detailed and discussed in the literature review). The anthracite (AN) and bituminous (BL) sample have comparable maceral and mineral matter contents, but

different ranks; thus, it will be useful to compare the CO_2 adsorption behaviour of these two coal samples. The other samples from specific locations have variable properties, but are essentially iso-rank (although the IN sample is slightly higher in terms of vitrinite reflectance). For all these samples, the differences in their maceral matter content need to be noted, where ratios of vitrinite to inertinite content are vastly different.

For example, the two high rank C coals (AN and SM) show very similar vitrinite reflectance (2.91%; 2.24%), mineral matter content (4.6%; 4.5%), however, the vitrinite to inertinite ratios are vastly different. Coal AN, has vitrinite (33.4%) to inertinite (66.6%) content having ratio of 1:2, while SM has a vitrinite (88%) to inertinite (12%) content having a ratio of 1:7. It would be interesting to compare the CO_2 sorption similarity between the two coals. Liptinite matter content was non-existent in the high rank coals; AN, SM, SL and only very minimal in MRB coal TN (0.3%), while SF, IN and WG were found to be in the range of 2.5; 2.5%, and 4.3% respectively. The MRC that exhibited the highest liptinite content was BL (5.5%).

For the ten SA samples used, it is noted that mineral matter ranges from 1.5% (SL) for high rank B being the lowest going up to 43.6% (WG) for MRC coal being the highest. The MRB sample, TN reported 8.3%, while the two high rank C coals (AN and SM) are respectively, 4.6 and 4.5%. With the exception of WG (43.6%), the other MRC coals (SF: 12.4%, GN: 11.2%, IN: 10.4% and EM: 10.2%) exhibit similar mineral matter values. As expected, the overall mineral matter content values show the general trend of increasing in volume percent (vol %) as the rank of coal decreases.

Coal density is highly variable and dependant on coal type and rank. The densities reported in Table 4.1 are in the range from 1.47 to 2.31 g/cm^3. Densities of minerals are significantly higher than that of organic matter, so the content and composition of the minerals in coals has a significant influence on the coal density hence here coal WG (43.6% mineral matter) reports the highest density of 2.31g/cm^3, while coal SL (1.5% mineral matter) had a lower density of 1.55 g/cm^3. The density also correlates to the ash content in the same way. Again coal WG (39.35% ash) has highest density while coal SL (6.1% ash) has lowest density. This variation in coal properties will definitely make for an interesting interpretation of the CO_2 sorption and CH_4 desorption results. These

petrographic results compare well to the reported results of other investigators on other bituminous and anthracitic coals of SA (Smith *et al*., 1983; Saghafi *et* al., 2008; Van Niekerk & Mathews, 2010; Maphala, 2012; Hattingh *et al*., 2013 and Matjie *et al.,* 2016).

4.2.2.1 Petrographic Images

Figures 4.5 (a) – (d) below show some petrographic (microscope) images of a few samples from this suite of SA coals tested. Namely: coals AN, BL and IN. All photographs were taken under reflected light with an oil immersion lens at a magnification of X500 as described fully in section 3.3.2. A scale bar is included for reference.

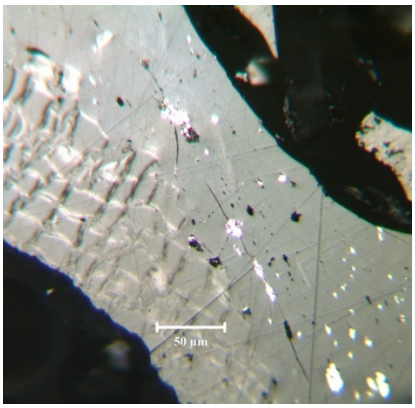

Figure 4.5 (a): Coal AN showing vitrinite & high rank

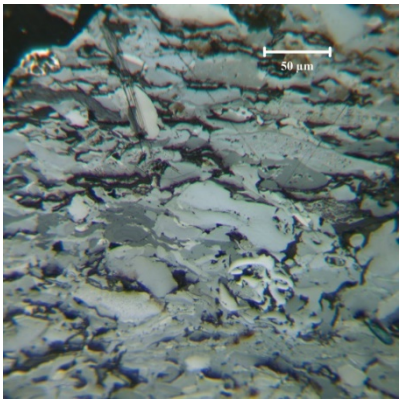

Figure 4.5 (b): Coal IN showing inertodetrinite

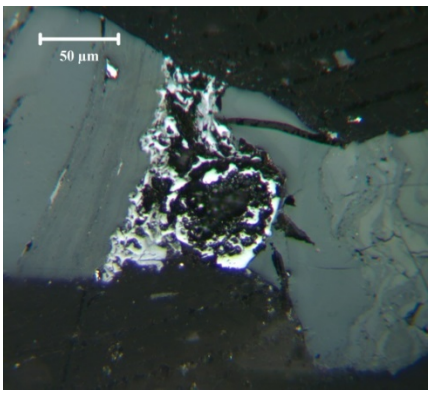

Figure 4.5 (c): Coal BL showing fusinite in centre with vitrinite on left

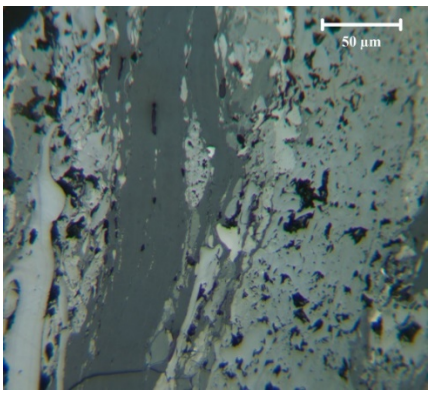

Figure 4.5 (d): Coal BL showing banding vitrinite & inertinite

Figure 4.5 (a) shows this high rank C coal (AN) contains vitrinite, fusinite, and pyrite (shows as bright spots) which can also be clearly seen in this sample. Also, to be noted that, this sample contains natural graphite, this was counted as “other”. Figure 4.5 (b): for this MRC coal (IN), inertodetrinite was observed. Figures 4.5 (c) and 4.5 (d) also for a MRC coal (BL), show images of fusinite and banded coal. The fusinite identified here can be described as very porous in nature.

The vitrinite in the coals is represented mainly by relatively thick bands of collotelinite (also known as telinite), depicted in figure 4.5(e) and lesser amounts of vitrodetrinite (with the exception of coals AN and EM) (0 vol%)). Collodetrinite (also known as desmocollinite) as depicted by figure 4.5(f) (Wang *et al*., 2016) occurs in very minor proportions, typically as a structure-less matrix containing other maceral components, only for coals IN, SF and GN, MRC coals.

The principal inertinite maceral is fusinite, with minor proportions of inertodetrinite, macrinite, and semi-fusinite as depicted in Figure 4.5(g). Sporinite can be seen in figure 4.5(h), this maceral and cutinite are the only liptinite macerals present, with sporinite being especially abundant in the liptinite-rich coals represented by samples EM, GN and BL (Matjie *et al.,* 2016 and Wang *et al*., 2016).

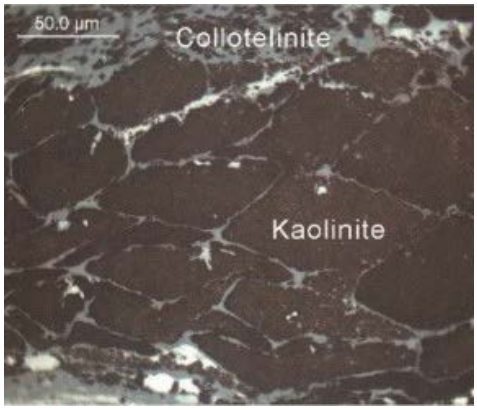

Figure 4.5 (e): Telinite with kaolinite

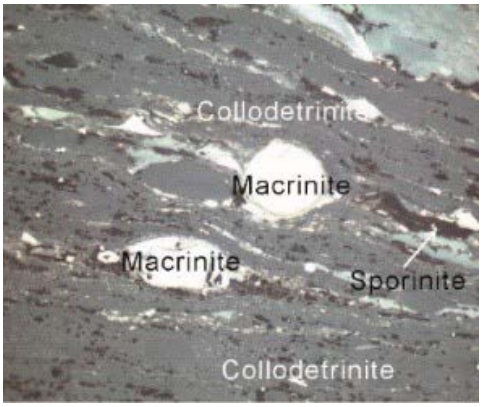

Figure 4.5 (f): Collodetrinite, macrinite and sporinite

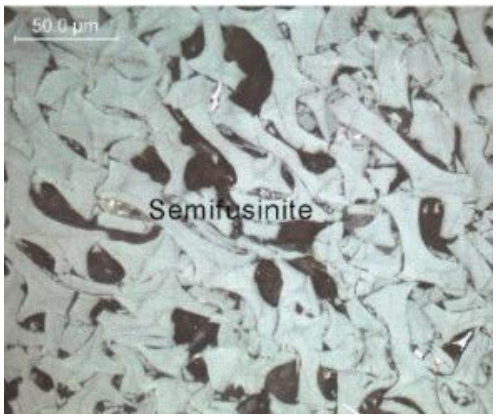

Figure 4.5 (g): Fusinite

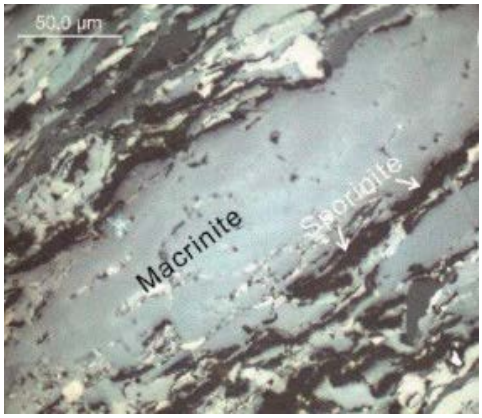

Figure 4.5 (h): Macrinite and sporinite

The minerals or mineral-rich components visible under the microscope are mainly disseminated clays, with minor carbonate and traces of quartz and pyrite. Stony particles (shale) are also present in the crushed coal grain mounts, especially in the mineral-rich coal of samples IN, GN and SF. It should be noted that the percentages in Table 1-Appendix A are all volume percentages; since minerals such as silicates, sulphides, carbonates, quartz and clays typically have densities around twice those of the macerals in coal, the weight percentages of mineral material would be significantly higher, as a fraction of the coal, than the volume percentages (Matjie *et al.,* 2016). Figures 4.5 (a) – (h) clearly demonstrate visually the vast differences of maceral and mineral contents, and as such the varying porosity and inherent surface areas that make the nature of coals so very diverse. As discussed, the impact of variable maceral types and mineral contents play a vital role in the sorption capacity of CO_2, as well as the maximum gas (CH_4) content of the specific coal. The ratios in which these organic and inorganic species exist, are found to be extremely varied in the different coal types, and need to be fully examined and taken into account with regard to the specific coals sorption and desorption characteristics.

4.3 BET (Brunauer, Emmett and Teller) Results

The micro-pore surface areas (m^2/g) of the samples were determined from low pressure CO_2 adsorption data (detailed in section 3.3.4) using the Dubinin-Raduschkevich (D-R) method. The maximum micro-pore volume or monolayer capacity (cm^3/g) and average micro-pore diameter were determined from the CO_2 adsorption results following the

Horvath-Kawazoe method (H-K method) (ASAP, 2010) as summarised in Table 4.2. The range of pore sizes (effective average micro-pore diameter) were found to be in the region of 3.7 Å ≤ d_p ≤ 4.2 Å.

Table 4.2: Summary of BET results for SA coals tested in this study

No.	*Sample I.D*	*Coal Rank*	*R_oV_{mr} (%)*	*Micro-pore surface area (m^2/g)*	*Surface area (m^2/g)*		*Monolayer volume (cm^3/g)*	*Ave micro-pore diameter (Å)*	*Max pore volume (cm^3/g)*
Method used				**D-R**	**Langmuir**	**BET**	**D-R**	**H-K**	**H-K**
1	AN	HRC	2.91	199	135	128	44.19	3.78	0.046
2	SL	HRB	3.49	171	115	109	37.52	3.80	0.039
3	SM	HRC	2.24	183	122	114	39.81	3.90	0.040
4	TN	MRB	1.26	108	70	65	21.23	4.13	0.019
5	BL	MRC	0.70	150	100	94	31.88	3.88	0.034
6	SF	MRC	0.65	154	102	96	31.72	3.83	0.035
7	GN	MRC	0.70	154	100	94	31.39	3.89	0.034
8	IN	MRC	0.81	130	85	80	26.65	3.93	0.028
9	EM	MRC	0.64	124	82	78	25.76	3.84	0.028
10	WG	*No sample available to conduct BET test*							

HRC: High Rank C; HRB: High Rank B; MRC: Medium Rank C

Figure 4.6 shows the trend of average pore sizes in angstroms (Å) determined from low pressure CO_2 BET analysis, compared to vitrinite reflectance data ($R_oV_{mr,}$ %). An increase in average pore size is noticed as R_oV_{mr} % increases from 0.64% (EM MRC) to a maximum of 1.26% (TN MRB) and then a continued decline in average pore size is noticed with increasing R_oV_{mr} % content towards the high rank samples, SM, AN and SL, respectively. Figure 4.6 demonstrates the relationship between effective surface areas, for both obtained, BET and Langmuir areas (m^2/g), while Figure 4.7 shows the relationship between obtained maximum pore volume (m^3/g) and micro pore surface area (m^2/g) for coals with increasing R_oV_{mr}%.

These graphical representations for SA coals are in agreement with the comparisons of Gürdal & Yalçin (2001) and others (Bustin & Clarkson, 1998; Walker *et al*., 1998; Ozdemir,

2004) who found a similar trend at R_oV_{mr} ~1.1 – 1.3%. The BET and Langmuir surface area data shows a trend exhibiting a decrease from R_oV_{mr}% from 0.65 – 1.26% and then increased for high rank coal to 2.91% (AN), thereafter decreases for HRC of SM (3.49%) from the BET tests (i.e. very low pressure CO_2 adsorption) conducted on dried, degassed and milled coal samples. The surface area is minimum (170.67 m^2/g) for high rank SL sample (HRB), at a carbon content of 87.2 %, although it has a large pore volume (0.039 cm^3/g) and average (3.80 Å) pore diameter, this is in agreement with reporting's from Xie (2015) on Chinese coals. The TN (MRB) sample shows the least / much lower values for Langmuir (70.16 m^2/g) and BET surface area (65.16 m^2/g) estimates (Figure 4.7), as well as for maximum pore volume (cm^3/g) and DR micro-pore surface area (m^2/g) estimation (Figure 4.8) as compared to MRC coals, numbered five (5) to nine (9) outlined in Table 4.2. Although it has the greatest average pore size, of 4.13 Å (Figure 4.6) in comparison to all other samples, it also exhibited the lowest maximum pore volume estimate of 0.019 cm^3/g.

This is in agreement with conclusions made by Gürdal & Yalçin (2001), who indicated that a decrease in micro-pore volume, Langmuir volume and specific surface area are noticed for coals around a maturity of this value (1.26%) and also observed for coals that are "in-between" rank. This could only mean that TN has mainly macro-and meso-pores with very limited micro-pores. Micro-pores are seen to increase as R_oV_{mr} % increases beyond 2% (AN & SM) and then is found to decrease at approximately 3.5% R_oV_{mr} % (SL).

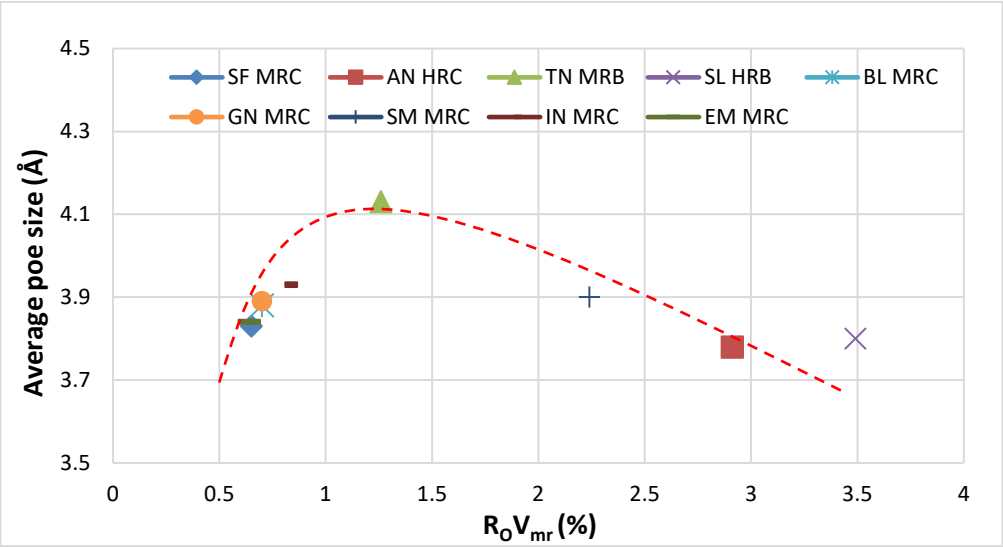

Figure 4.6: Average pore size diameter (Å) versus vitrinite reflectance, R_ov_r, (%

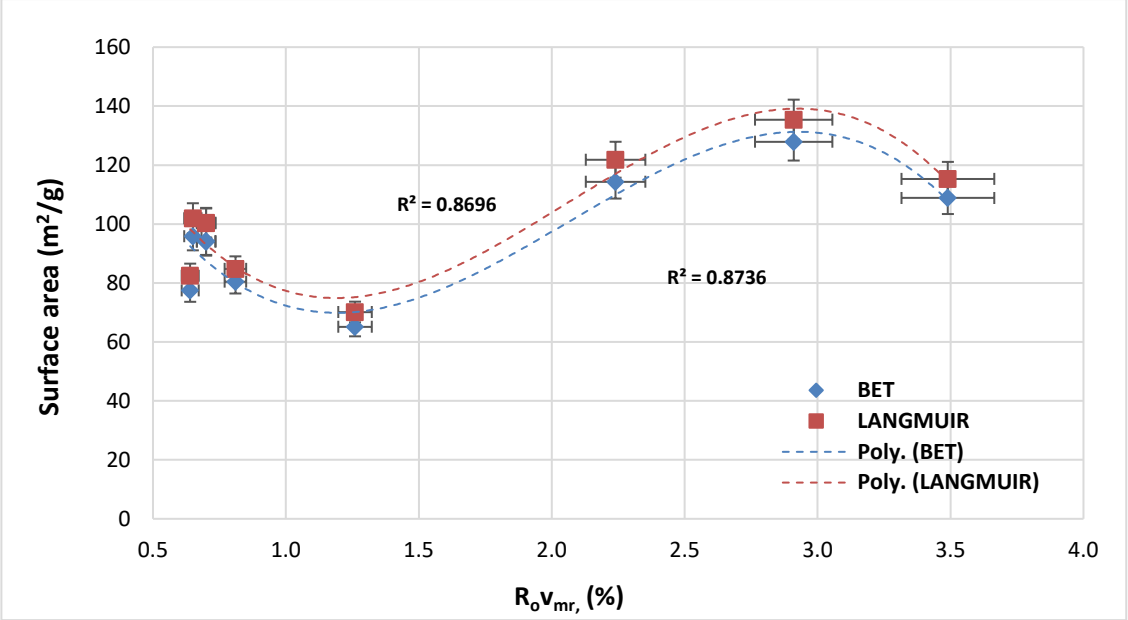

Figure 4.7: BET & Langmuir surface areas versus vitrinite reflectance, R_oV_{mr} (%)

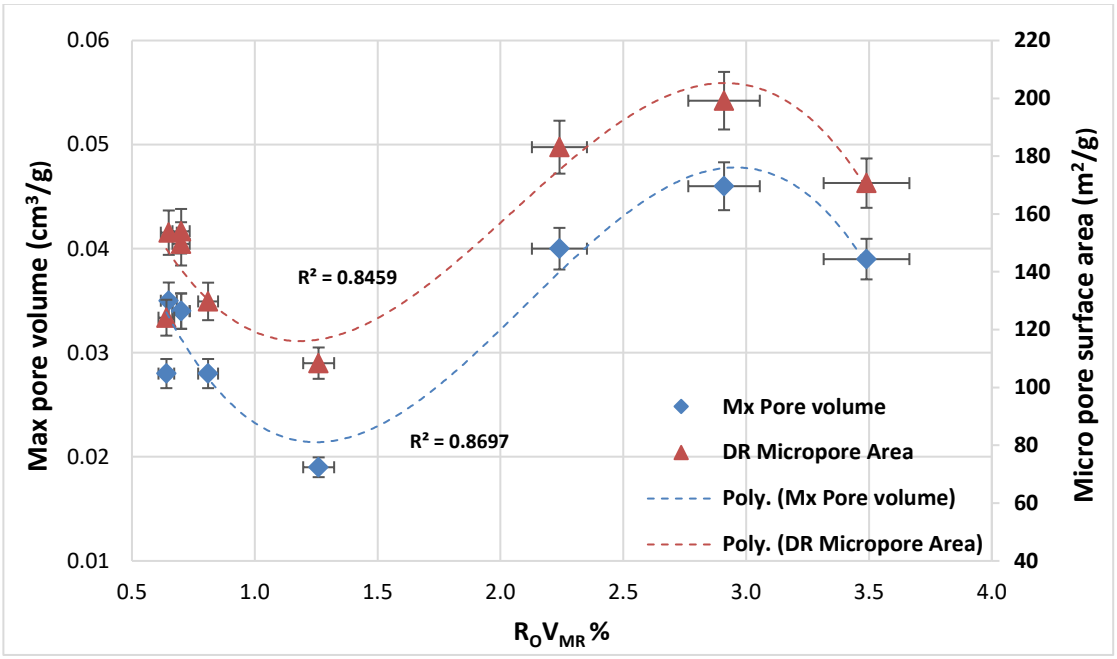

Figure 4.8: Max Pore volume (cm^3/g) & micro-pore surface area (m^2/g) versus vitrinite reflectance, R_oV_{mr} (%)

Overall, these BET results seem to be consistent and in agreement with previous findings mentioned, showing a trend exhibited for higher rank coals having greater potential for good sorption, specifically looking at the trend for each rank, showing decreasing potential

sorption capacity with diminishing coal rank. Experimental evidence has shown that coal porosity and pore size distribution varies with the degree of maturity of coal as are measured by the proxy indicators: carbon content and vitrinite reflectance (Okolo *et al*., 2015; Clarkson and Bustin, 1997; Karacan and Mitchell, 2003; Saghafi *et al*., 2007; Ceglarska-Stefańska and Zarębska, 2005 and Goodman *et al.,* 2007).

4.4 System Leak Tests and Repeatability Results

Due to the nature of high pressure work and the reliability of results needed for the sorption by pressure difference calculations, the system was subjected to a number of leak tests. Five bituminous (same coal) samples were prepared and subjected under pressure for a number of days, as per Figure 4.9. Unfortunately some of the tests were stopped at different intervals (for some of the trial tests) due to testing, modification requirements, and installation of a new automated data logging system. This was also necessary due to the long adsorption test times noted. Results below are indicative of manual pressure and time recordings.

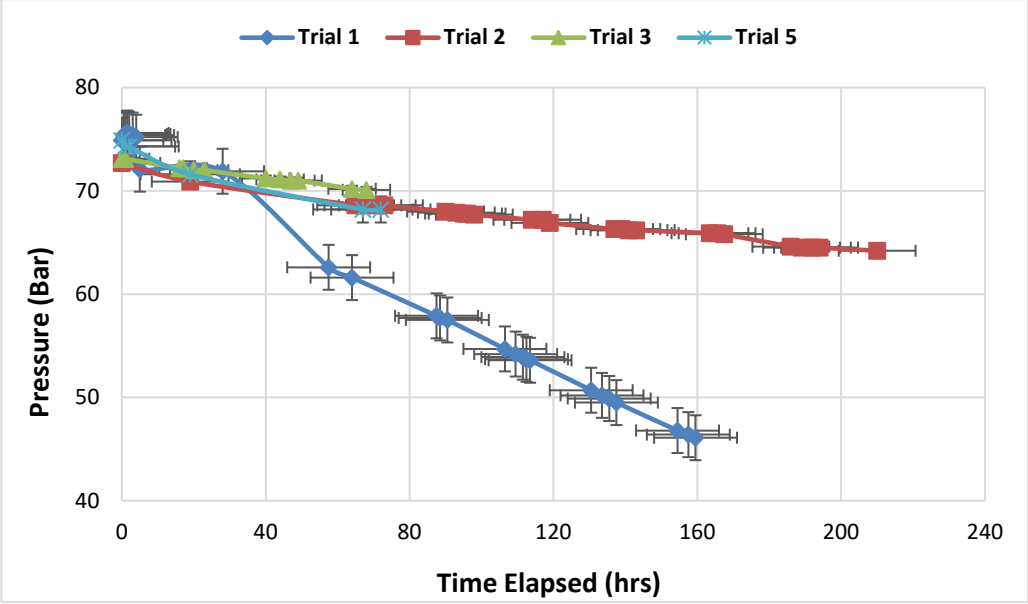

Figure 4.9 Pressure Leakage tests

As seen in Figure 4.10, a good comparison for trial runs for tests 2, 3, and 5 showed evidence of good repeatability for a specific coal type. This was considered to be an acceptable starting point for further test work, and eliminated concerns regarding system leaks at super-critical conditions:

- Trial 2 run for 67.8 hrs ~ 3 days
- Trial 3 run for 68 hrs = ~ 3 days
- Trial 5 run for 72hrs = ~ 3 days

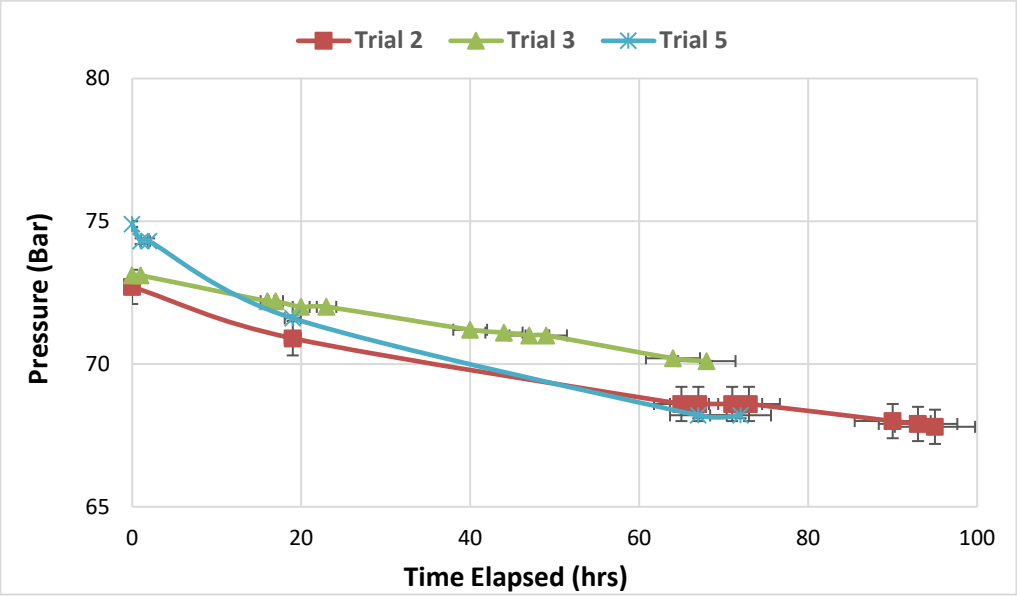

Figure 4.10 Three repeatability trial tests

After inclusion of the data logging system, further leak tests were conducted. The adsorption system was again also checked for leaks to ensure that there were no pressure drops inside the reactor as this would influence the CO_2 adsorption results. The leak test was done by conducting a blank experiment where the pressure in the empty reactor was raised to approximately 98 bars, then the equipment was left overnight (12 hours or longer). It was expected that due to the temperature drops at night a slight pressure drop of small magnitude would take place. A significantly large pressure drop would indicate leakages in the system, possibly around the pipe fittings and valves. The results of the leak test on the HPVAS are presented in Figure 4.11.

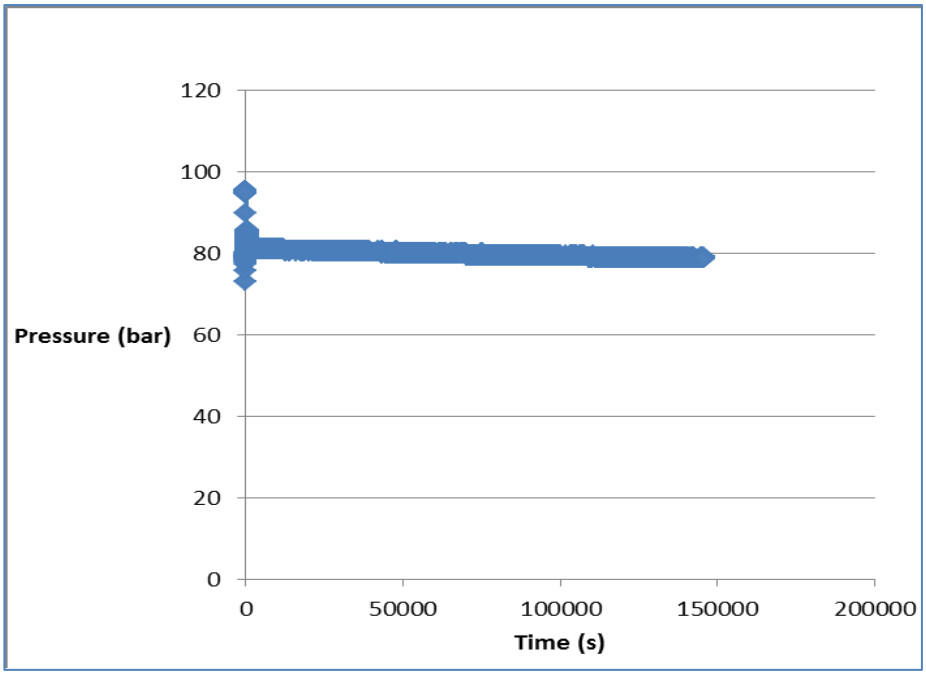

Figure 4.11: Leak test results on adsorption data logging system

From data logged results of leak tests undertaken, it can be noted, that insignificant pressure drop was experienced from the HPVAS. This confirmed that the CO_2 sorption data acquired gave confident results presented here forth.

4.5 CO_2 ADSORPTION RESULTS: COMPARISON OF ALL COALS TESTED

Figure 4.12 shows adsorption isotherm comparisons of the ten (10) locally available SA coals tested at an isothermal temperature of 35^{o}C and determined sample fraction of +4.75 mm -5 mm to generate adsorption isotherms in pure CO_2, measured using the pressure step method up, to a maximum attainable pressure of ~80 - 85 bar (super-critical ranges for CO_2 achieved). These sorption isotherms at 35^{o}C are typically representative of coal seam depth at approximately 600 m (Qing-Ling, 2008) and characteristically exhibit a maximum sorption potential in the 55--83 bar range depending on the rank of sample. Table 4.3 summarises the total amount of maximum CO_2 adsorbed for each of the ten (10) samples tested and the final pressure attained to the end of experiments.

Each coal sample was run for a total of ~8-9 hours with incremental pressures of CO_2. Most work reported in literature over the last two decades have followed this pressure step technique to obtain experimental data for generating gas adsorption isotherms (Reucroft & Patel, 1986; Clarkson *et al*., 1997; 1999; Bustin & Clarkson, 1998; Laxminarayana & Crosdale, 1999; Humayun & Tomasko, 2000; Gürdal & Yalçin, 2000; 2001; Krooss *et al*., 2002; Busch *et al*., 2003; 2004; Ozdemir, 2004; Larsen, 2004; Shimada, 2005; Bae & Bhatia, 2006 ; Azmi, 2006; Faiz *et al*., 2007; Goodman, 2007; Cui, *et al*., 2007; Ceglarska-Stefańska & Zarębska, 2008; Sakurovs, 2008; Day & Sakurovs, 2008(a), 2008(b); Gensterblum *et al*., 2009; 2010; Pone *et al*., 2009; Dutta, *et al*., 2011; Busch & Gensterblum, 2011; Kim *et al.,* 2011; Day, 2012; Qu, 2012; Weniger 2012; Wang *et al.*, 2014; Merkel *et al*., 2015; to name a few). The method that is proven to be more accurate in terms of in-situ comparisons is possibly still debatable, but the pressure-step method has been adopted for all the test work in this study for high pressure (CO_2) sorption and (CH_4) de-sorption investigations.

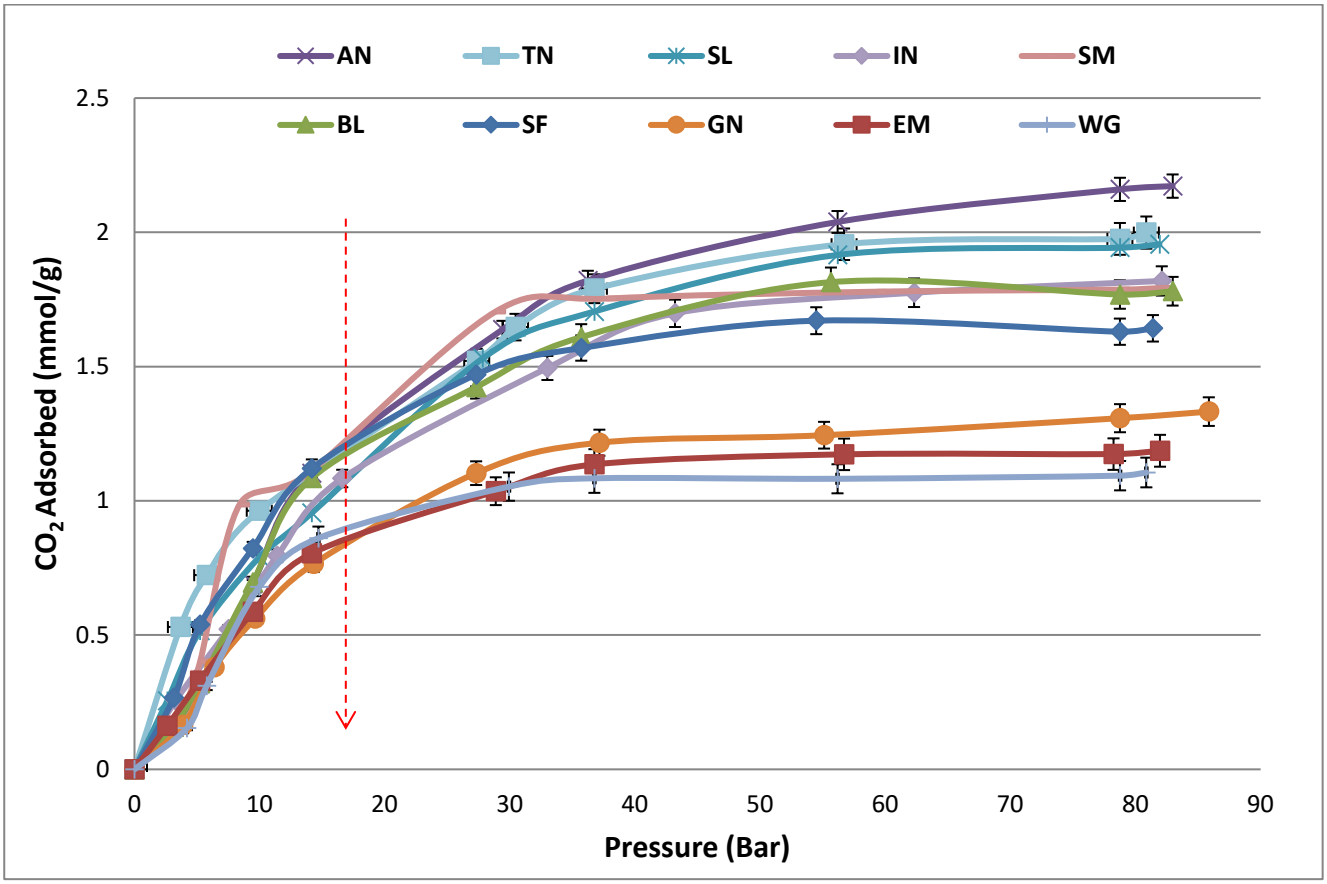

Figure 4.12: Adsorption Isotherms: Comparison of all SA 10 coals tested

Table 4.3: Summary of CO_2 Adsorption data for SA coals

No.	*Sample ID*	*Rank*	*R_oV_{mr} (%)*	*Carbon (daf,%)*	*CO_2 (mmol/g)*	*Pressure (bar)*
1	AN	HRC	2.91	89.9	2.17	83
2	TN	MRB	1.26	85.7	1.99	81
3	SL	HRB	3.49	90.4	1.95	82
4	IN	MRC	0.81	81.9	1.82	82
5	SM	HRC	2.24	90.1	1.79	82
6	BL	MRC	0.70	75.4	1.78	83
7	SF	MRC	0.65	73.7	1.64	81
8	GN	MRC	0.70	77.8	1.33	86
9	EM	MRC	0.64	73.5	1.19	82
10	WG	MRC	0.51	79.7	1.10	81

All coals essentially show comparable adsorption profiles at much lower pressures, some of the samples show steady increasing sorption nature while the others seem to have attained saturation or nearing saturation at the final point of the pressure range. While initial specs show the lines beginning to diverge after ~15 bar. At 30 bar, the anthracites (AN, SM, SL, TN) samples suddenly showed a sharp uptake of CO_2. The MRC (IN & BL) samples also showed the beginning of a sharp intake at around 44 bar. The results expressed in Figure 4.12 indicate that adsorption is lower at lower pressures, but with increasing CO_2 injections at higher pressures, moving away from sub-critical level, more CO_2 is essentially adsorbed, as expected.

Although the shape of the isotherms across the entire suite of SA coals was similar (Type I), what was possibly not expected are the changes in the slopes of the isotherms, showing that adsorption is not linear and for the lower ranked coals, sorption trend seems to stabilise as it moves into the supercritical range from around ~60 bar onwards, indicating that the CO_2 saturation rate has started to be achieved and that no further CO_2 sorption can be accommodated in those coals after reaching the maximum sorption at a range of ~80 – 85 bar. Results presented (Figure 4.11), show no evidence of the anomalous behaviour as has been observed by some investigators, where a sharp maxima followed by a minima have been reported at pressures above about 7 MPa (i.e. 70 bar) (Krooss *et al*., 2002 & Tschino *et al*., 2003).

The adsorption isotherms of these SA coals generated here, are clearly classified as the Type I: Langmuir isotherm according to the IUPAC classifications (Gregg & Sing, 1982; Birdi, 2010). This type of adsorption isotherm in mathematical form is presented as a non-standard hyperbola. It can be seen that the curve of the adsorbed volume of CO_2 versus the gas pressure exhibits a steep start and then slowly flattens above the sub-critical range of ~45 bar. The maximum capacity that can be seen from ~75 bar onwards, is due to the steep increase in the specific density of supercritical CO_2 in this pressure range (Gensterblum *et al*., 2009; Bae and Bhatia, 2006). This specific type of isotherm generally corresponds to micro porous media such as coal. It indicates that for the majority of pores, the diameter of a pore is only a few times larger than the diameter of the adsorbate (CO_2) molecules, and micro-pores are possibly the main gas storage space, over and above macro and meso-pores. At higher, supercritical pressures, the micro-pores fill completely with the CO_2 and thereafter possibly form mono and multi-layers, and the isotherm curves can then be seen to reach its plateau (Ozdemir, 2004; Saghafi *et al*., 2008; Gensterblum *et al*., 2010; Dutta, *et al*., 2011).

Although it can be deduced that pore filling, mono-layer and possibly multi-layer sorption methods are most definitely occurring for these coals with increasing pressure, it must however also be highlighted that, the noted difference in the adsorption capacities (mmol/g) is most likely due to the variations and ratios of specific coal properties which will be discussed further in the following sections of this chapter. Some general data correlations, namely, positive and negative relationships, have been derived from the experimental data generated (using eye fitting envelopes as well as regression data) in this study between the sorption capacity, coal rank and type, pressure, temperature and moisture effects. Some limited repetition will appear in discussing specific coal characteristics, but this is unavoidable due to the complexity and extremely interrelated properties of the coal and is done so in order to maintain a degree of completeness in explanations of the findings.

4.5.1 The Effect of Coal Rank

Figure 4.13 depicts the relationship between the experimentally obtained excess CO_2 (mmol/g) adsorption with regard to coal maturity represented in terms of petrographic

(visually determined) vitrinite reflectance (R_oV_{mr} %), as is summarised in Table 4.3, for this suite of SA coals. From some previous studies, it has been concluded that increasing coal rank or coal maturity, is the defining factor to elevated sorption of CO_2 at increased super-critical pressures to coal adsorbent/storage medium (Bustin & Clarkson, 1998; Laxminarayana & Crosdale, 1999; Chalmers & Bustin, 2007). The R_oV_{mr} % values as compared to the CO_2 adsorbed data, shows a rectilinear trend which indicates a very steep increase in sorption from R_oV_{mr} % of 0.51% until 0.81% for the MRC samples; WG, EM, GN, SF & IN. From samples TN, SM & AN, (for this SA suite) approximately from the R_oV_{mr} % range of 1.26, 2.24 – 2.91%, a relative "flattening out" with respect to CO_2 sorption is indicated. Data clearly shows an increase in CO_2 sorption capacity with increasing R_oV_{mr}, i.e. from a lower rank (MRC) to a higher rank (HRB, MRB, HRC) to a minimum, absolute range of vitrinite reflectance value. What is not expected here, was the decreased sorption capacity (1.79 mmol/g) at the R_oV_{mr} % of 2.24% for the SM (HRC) sample as compared to the equivalently ranked AN (HRC) having lower R_oV_{mr} % of 2.91 but a greater sorption of 2.17 mmol/g.

But generally, it can be seen, that a trend informing increased adsorption capacity follows suitably well, as the R_oV_{mr} % increases for the MRC coals to a relatively stable range in maturity, with rank increase to HRB, MRB & HRC, which reflects clearly in Figure 4.13.

However, the trend observed (Figure 4.13), is at odds to the typical "U-shaped" trend as has been discussed in section 2.12.1, relating to works that have been published by many author's reporting's; Gan *et al*. (1972); Bustin & Clarkson (1998); Walker *et al*. (1998); Ozdemir (2004); Faiz *et al*. (2007); Sakurovs *et al*. (2009); Ceglarska-Stefańska and Zarębska (2005); Saghafi *et al*. (2007); Day *et* al. (2008); Pini *et al*. (2010); Li *et al*. (2010) and Dutta *et al*. (2011). Day *et al.* (2008), who found that CO_2 sorption capacity tended to reduce with rank to reach a minimum that corresponded to a R_oV_{mr} of ~1.2%, after which it began to increase. It was hypothesised that increasing hydrogen content of the coal tended to result in a decrease in sorption capacity.

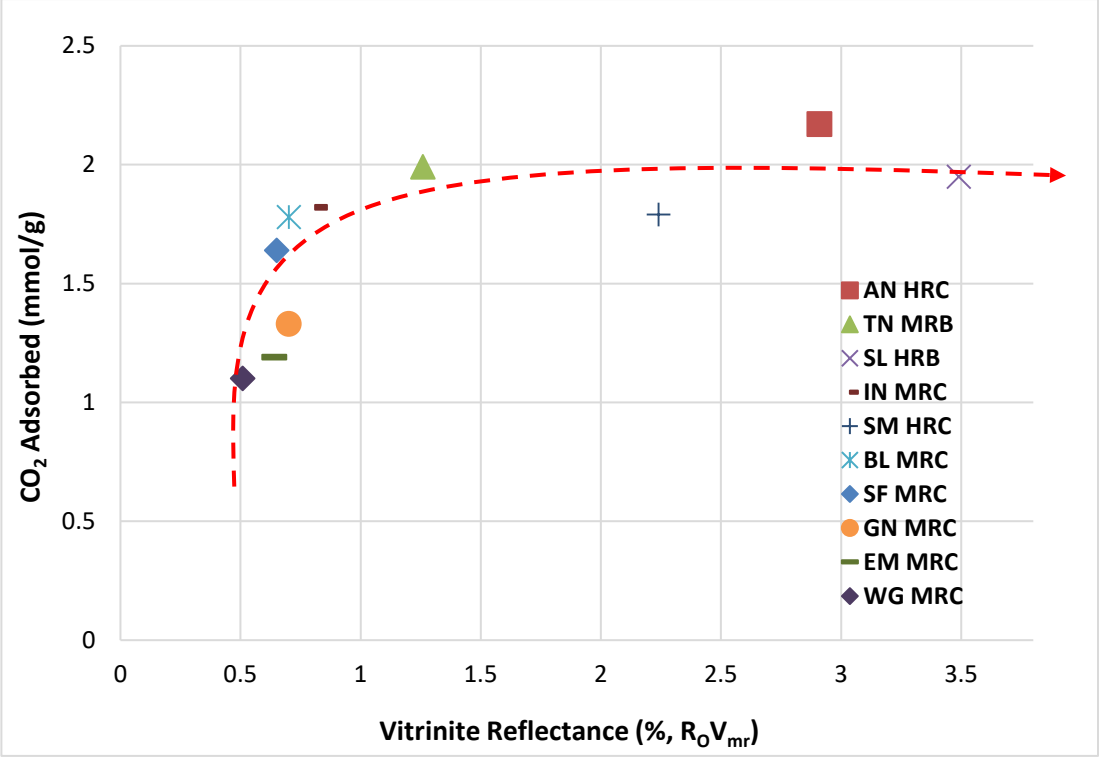

Figure 4.13: Comparison of R_oV_{mr} to CO_2 adsorbed (mmol/g) for different coals & ranks

Similarly, Prinz and Littke (2005), covering a wide range of ranks and pressures, also found that CO_2 adsorption exhibited a minimum range in coals with R_oV_{mr} % around 1.2 – 1.4%. Also, the general reduction in adsorption capacity with increasing rank was noticed by Ozdemir *et al*. (2004) at R_{max} value of about 1.2%, which corresponds to a total carbon content of about 85% (daf), there appears to be a broad minimum after which the sorption capacity starts to increase again. In contrast, the Saghafi study (2007) did not present this finding, they examined coals ranging in R_oV_{mr} from about 0.7 to 1.5%, a somewhat narrower range than the range used here in this current study. This, combined with the scatter in their data, which appears to be inherent in most of the studies, may have masked the presence of a minimum sorption capacity as observed by the others. This group also compared the sorption capacity with vitrinite reflectance but did not find any definite correlation. This was also not the case for findings, from Stanton *et al.* (2002), Siemons & Busch (2007) and Busch & Gensterblum (2011), who could not find any specific correlation or trend between CO_2 sorption capacity and coal rank at all.

Since, this “U-shaped” trend could not be seen from Figure 4.13 to use the petrographically determined R_oV_{mr} %, it was then decided to use the determined coal carbon content (C %) to identify if this relationship also applies to these SA coals. As it is possible that restrictions may occur causing erroneous reporting’s of R_oV_{mr} %, as it is done using the human eye of the petrographer, and observations may differ slightly from person to person (Li *et al*., 2010). It is well known that the C content in coal increases steadily with increasing coal rank (Stach *et al*., 1982; Meyers, 1982; Li *et al*., 2010) and is still the leading and most accurate parameter among other chemical characteristics for evaluation of coal rank advance despite some few limitations (Vassilev *et al*., 2010).

Perera *et al*. (2010) presented sorption data against coal maturity in terms of carbon content (%, daf). Author’s used the coals’ determined fixed carbon content (%) to show rank evolution which is determined as carbon content increases compared to respective sorption capacity of sorbent. Levy *et al*. (1997) found that the adsorptive capacity varied according to coal rank and showed a minimum at around 85–90% total carbon (%). These authors suggested that the minimum in adsorption capacity may correspond to a coalification “jump” which occurs at around ~87% carbon or comparatively to R_oV_{mr} % around 1.1 – 1.4% (Ozdemir *et al*., 2004; Perera *et al*., 2010). This “jump” is characterised by a reduction in the oxygen content (i.e. the loss of oxygen functional groups) of the coal and evolution of CO_2 and water. It is believed that an important aspect of the coal structure, which relates to rank, exhibits a change of both the meso and macro porosity in the said range of ~1.1–1.4% R_oV_{mr} (Stach *et al*., 1982; Prinz *et al*., 2004).

Figure 4.14 illustrates the relationship between the experimentally obtained excess CO_2 (mmol/g) adsorption with regard to coal maturity, represented in terms of carbon content (C %) dry ash free basis, which is summarised in Table 4.3. Here the claisc “u”-shape can be observed. It can be seen that a steady linear increase in CO_2 sorption capacity, as the C% increases from MRC coals towards the anthracitic level, namely, for coals SM and AN and then shows slight decline with higher rank (HRB) SL sample, as was also noted in Figure 4.14. This finding is in favour with reporting’s from Faiz *et al.,* (2007), who found that the rank dependence of the preferential adsorption ratio is not a monotonic correlation. The adsorption capacity is both the function of the amount and reactivity of surface area

contained in all pores, macro, meso and both micro and ultra-pores, and possibly the cleats and fractures inherent in the coal.

From the plot of R_oV_{mr} (Figure 4.14) no specific or appreciable indication of this decline can be seen in the R_oV_{mr} range 1.1-1.4% for the SA coal in this range; TN (1.26%). The noted trend may, however, be possibly displayed if a set of SA MRC samples in this R_oV_{mr} range can be evaluated in future studies.

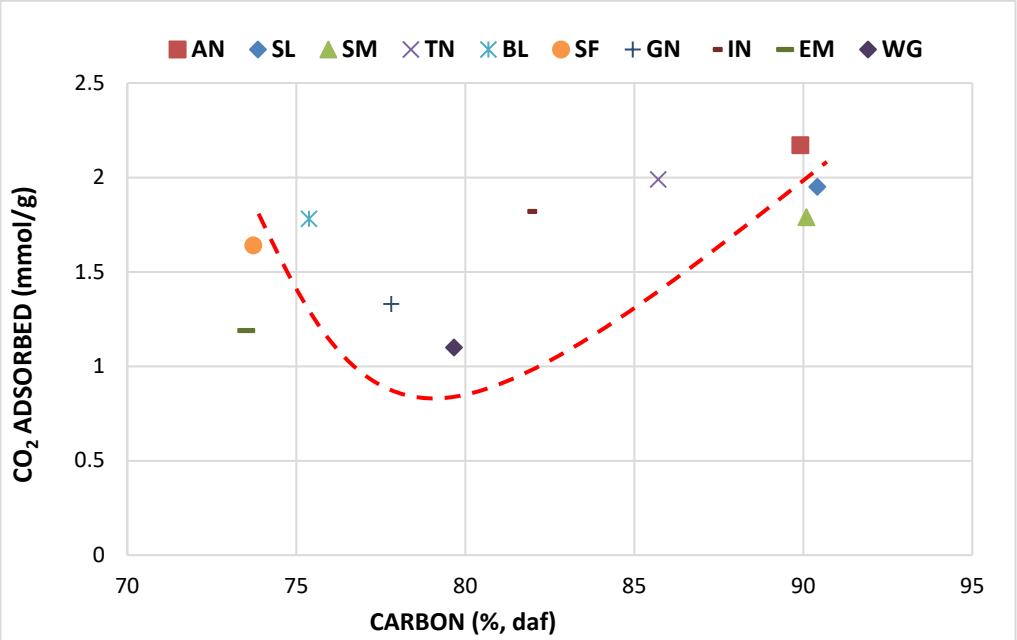

Figure 4.14: Comparison of carbon (%) to CO_2 adsorbed (mmol/g) for all coals & ranks

For simplicity, Figure 4.14 was re-plotted as Figure 4.15, which clearly identifies and highlights the coals by the specific rank *only*. This graph shows, very obviously, that an increase in coal rank most definitely shows an increased CO_2 sorption capacity. Although, the MRC samples do show a somewhat small scatter, the variations will be looked at in terms of more specific coal properties to try and identify the differences between these iso-rank coals.

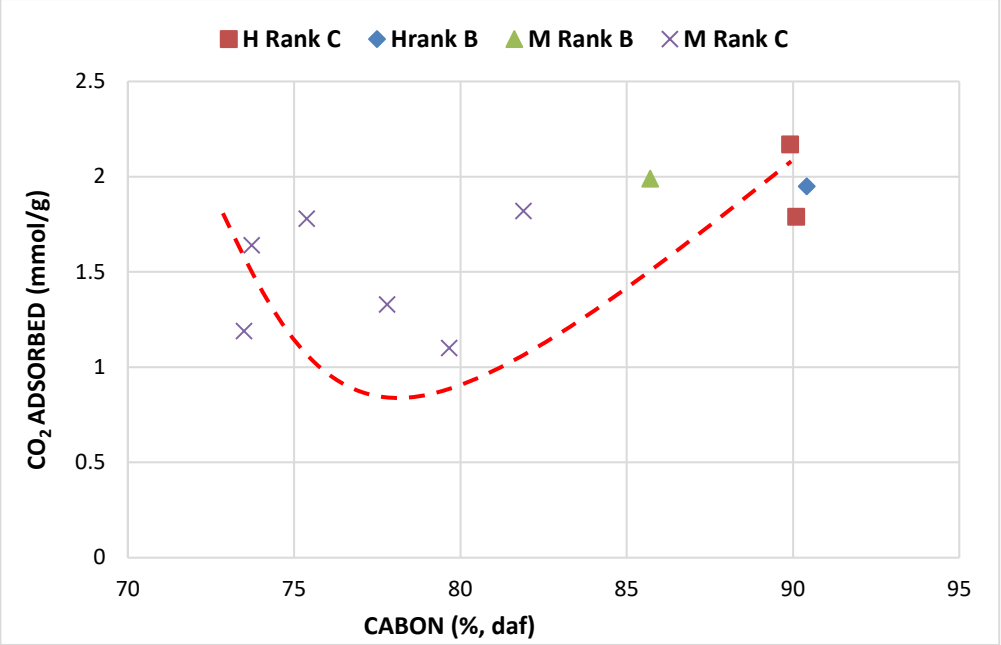

Figure 4.15: Comparison of carbon (%) to CO_2 adsorbed (mmol/g) for all coals: showing distinctive coal ranks

The two HRC samples also show a slight discrepancy in the sorption values attained, however, the reduced sorption value (1.79 mmol/g) is noted for the HRC SM sample with a higher value of R_oV_{mr} (3.49%). This finding seems to be consistent with reporting's of Laxminarayana and Crosdale (1999), who noted a decrease of Langmuir volume with increasing coal rank. They attributed this finding to the homogenization of the pore space during coalification. In addition, this finding could also possibly be due to heavy hydrocarbon molecules (volatile matter) occluded in the micro-pores being generated as a by-product of coalification in coals of similar rank which cause the subsequent blocking of pore mouths or throats creating physical constrictions and activation energy barrier, which may account for the decreased sorption of CO_2 (Levine, 1993; Faiz *et al*., 2007; Bae *et al*., 2009). This is clearly observed from Figure 4.16, where the determined volatile matter (%, mmf) across all ranks of coals is expressed against CO_2 sorption data acquired for this SA data set of coals. It is clear that an increasing volatile composition shows a definite decrease (good linear correlation: $R^2 = 0.784$) in CO_2 sorption capacity (mmol/g) overall for these samples.

However, it has been noted that for lower rank coals, pores, including macro, meso-pores and large micro-pores (>1 nm), are not as significantly affected by pore mouth constrictions due to volatile matter, as compared to higher ranked coals having significantly smaller micro-pores due to coalification (Bae *et al.*, 2009). It is observed that, increased volatile matter release due to increasing coalification, the coal pore diameter decreases significantly, creating fine pores, i.e., the micro-pore proportion increases and hence pore porosity, and the physical structure of the coal gradually becomes more compact having a greater surface area (Zhao *et al*., 2014), in this case depicted here by the three high rank SA coals: AN (HRC), SM (HRC) & SL (HRB) as is observed from Figure 4.16.

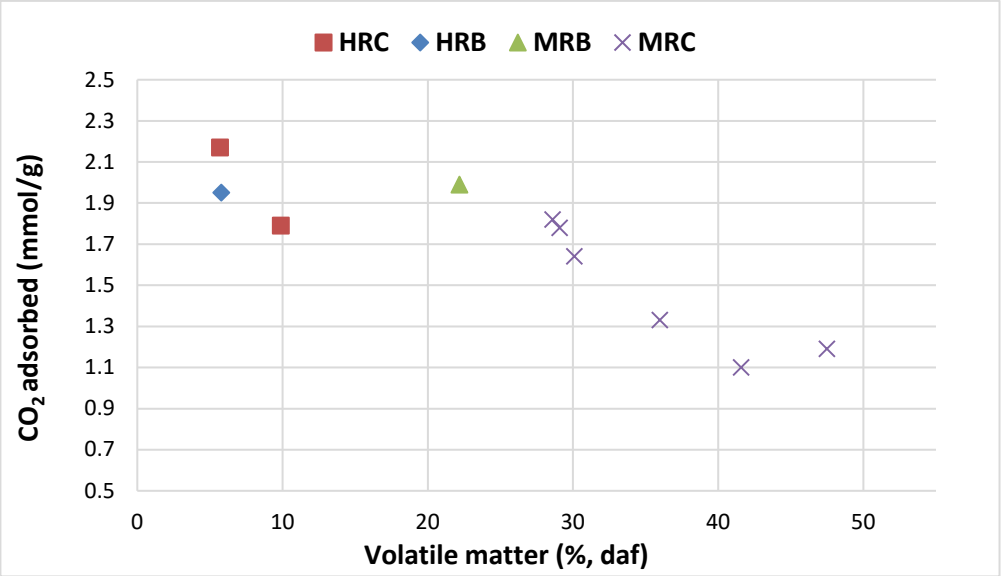

Figure 4.16: Comparison of volatile matter (%, mmf) versus CO_2 adsorbed (mmol/g)

4.5.1.1 Comparing High and Low Rank Coals

From data tabulated in Table 4.4, the high rank coal SL, having a carbon content of 90.4%, but with relatively equal amounts of vitrinite and inertinite matter, reported an adsorbed amount of CO_2 of 1.95 mmol/g at maximum pressure. The second high rank coal, (AN), reported the highest adsorption of 2.17 mmol/g and while having vitrinite to inertinite ratio of roughly 1:2. The medium rank B coal (TN) showed good adsorption behaviour as

compared to the MRC bituminous coals (excluding the WG and EM samples), having a maximum adsorbed amount of 1.99 mmol/g at maximum pressure and having a vitrinite to inertinite ratio of approximately 2.5:1. Figure 4.17 shows a comparison of the adsorption isotherms of the different high and low rank coals.

Table 4.4: Comparison between the different rank samples and CO_2 adsorbed

Coal sample	*Coal Rank*	*R_oV_{mr} (%)*	*Vitrinite (vol%, mmf)*	*Inertinite (vol%, mmf)*	*CO_2 adsorbed (mmol/g)*	*Pressure (bar)*
AN	HRC	2.91	33.4	66.6	2.17	83
TN	MRB	1.26	71.6	28.1	1.99	82
SL	HRB	3.49	56.1	43.9	1.95	82
BL	MRC	0.70	32.2	62.3	1.78	83
EM	MRC	0.64	13.9	82.2	1.19	82
WG	MRC	0.51	5.0	90.8	1.10	81

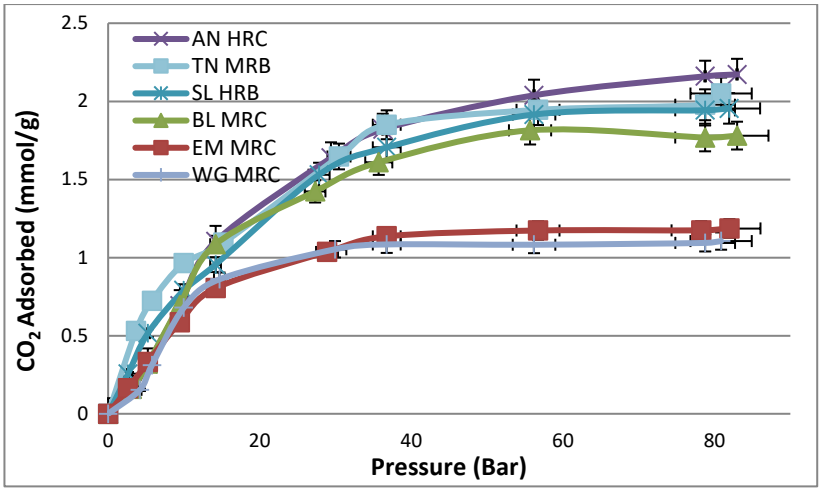

Figure 4.17: Adsorption isotherms: Comparison of CO_2 adsorbed (mmol/g) for high - low coal rank

4.5.1.2 Comparing ISO-Rank (MRC) Coals

Comparing the five (5) iso-ranked (MRC) coals, the IN, BL, SF, GN and EM samples; the basic coal properties and adsorption values are included in Table 4.5, while Figure 4.18

shows the adsorption isotherms obtained. A comparison cannot be accurately made, as the coal properties differ between them slightly. The difference in the ash and maceral composition most likely accounts for differences in adsorption behaviour between these iso-ranked coals.

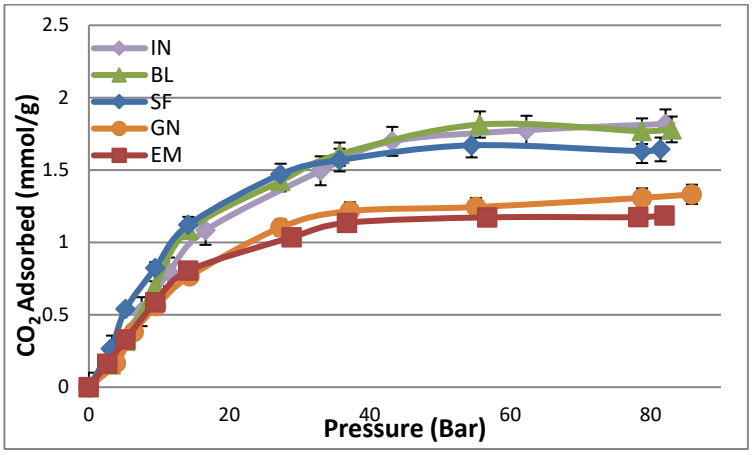

Figure 4.18: Adsorption Isotherms: Comparison of CO_2 adsorbed (mmol/g) bituminous MRC samples

Table 4.5: Comparison between the Iso-rank: MRC samples and CO_2 adsorbed

Coal sample	*Coal Rank*	*R_oVmr (%)*	*Ash (%)*	*Vol. Matter (%)*	*Vitrinite (vol%, mmf)*	*Inertinite (Vol%, mmf)*	*CO_2 adso. (mmol/g)*	*Pressure (bar)*
IN	MRC	0.81	22.5	28.6	45.0	42.4	1.82	82.1
SF	MRC	0.65	23.9	30.1	18.2	67.2	1.64	81.4
BL	MRC	0.70	17.2	29.1	30.2	58.4	1.78	82.9
GN	MRC	0.70	11.5	36.0	45.6	39.0	1.33	85.8
EM	MRC	0.64	21.9	47.5	12.5	77.6	1.19	81.9

The ash content for IN (22.5%) and SF (23.9%) are very close in value, and the volatile matter data for both are also very close in comparison, IN (28.6%) and SF (30.1%). However, the adsorption data shows that IN adsorbs approximately 20% less CO_2 as compared to SF. IN has almost equal ratios of vitrinite (50.2%) to inertinite (47.3%), while the inertinite content for IN is almost half the SF sample; this definitely suggests that there exists a significant relationship between the balance or ratios of these macerals in the sorption competition factor for CO_2.

Beamish *et al*. (1998) concluded that micro-porosity in coals is decreased by the presence of volatile components blocking the micro-pore structure. Hence, the more volatile matter a coal contains, the more micro-pore structure blockages there will be. This was clearly depicted in Figure 4.16. Evident for samples GN (36.0%) and EM (47.5), both have higher volatile matter than the other three (3) MRC samples (IN, SF and BL, all three samples have similar volatile matter compositions: IN – 28.6%, SF – 30.1% and BL – 29.1%) and can be seen to exhibit the lowest CO_2 sorption capacity of 1.33 and 1.19 mmol/g, respectively, although being of the same rank. This is most certainly due to the micro-pore structural blockages due to increased volatile matter.

The ash content is seen to be almost equivalent in SF and IN but slightly lower in BL, yet IN reported higher sorption at 1.82 mmol/g than the SF sample. Sample EM yielded the lowest sorption of 1.19 mmol/g as depicted in Figure 4.17. It is interesting to note, that it also has the greatest inertinite content, having a ratio of vitrinite to inertinite of approximately 1:6. From the differences observed in sorption capacities for these MRC samples, only the ratio of vitrinite to inertinite content between the samples can be noted for the possible deviation in sorption capacities.

4.5.1.2 Summary: Effect of coal rank

In summary, according to the results from this study, higher rank coals adsorbed more CO_2 than lower rank coals. Higher rank coals: AN, (HRC), TN (MRB), and SL (HRB) recorded higher adsorption capacities compared to the lower MRC; GN, IN, BL, EM, SF and WG samples. This observation is in agreement with Saghafi *et al*. (2007) who investigated the effect of coal rank and depth on CO_2 adsorption capacity with coal samples from the Sydney Basin, Australia. They observed that the deepest and highest rank coal samples adsorbed more CO_2 than the shallower lower rank samples. In contradiction, according to Crosdale *et al.* (1998), coal rank and composition do not appear to be the critical factors in controlling gas sorption, but rather the influence they exert over pore structure development; this was in agreement with sorption results from Ceglarska-Stefańska and Zarębska's (2005) and Stanton *et al.* (2009). It is clear that samples in the range greater

than 0.7% R_oV_{mr} exhibits increased CO_2 uptake due to larger macro, increasing meso porosity and possibly very limited micro-pore volumes.

4.5.2 The Effect of Ash content

4.5.2.1 All samples (10) compared

Adsorption capacity of CO_2 (mmol/g) indicates a very gradual decline as ash content increases, The WG and EM samples showed the lowest adsorption potential; the WG sample has a very high ash content (64.9%), which may explain this result. Although the WG coal has a greater ash content than the EM coal (more than double), very little difference in adsorbed amount of CO_2 can be noted from this study (Figure 4.19). While the two coals with the lowest ash%, AN (9.6%) and SL (6.5), reported higher CO_2 sorption values at 2.17 and 1.95 mmol/g. Of interest, TN adsorbed 1.99 mmol/g, only marginally higher than SL, even though it has a relatively higher ash% of 24.2%, approximately four times more than SL sample.

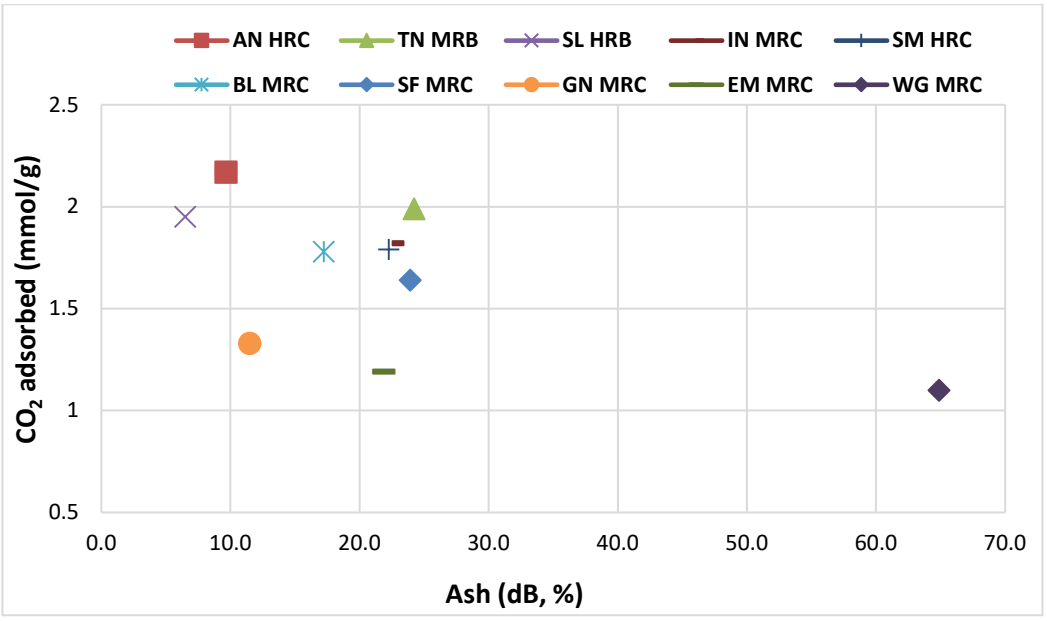

Figure 4.19: Comparison of Ash content (%) versus CO_2 adsorption (mmol/g)

Figure 4.20 shows the trend of decreasing CO_2 adsorption prolife versus the ash content as presented on db% for all 10 SA coals.

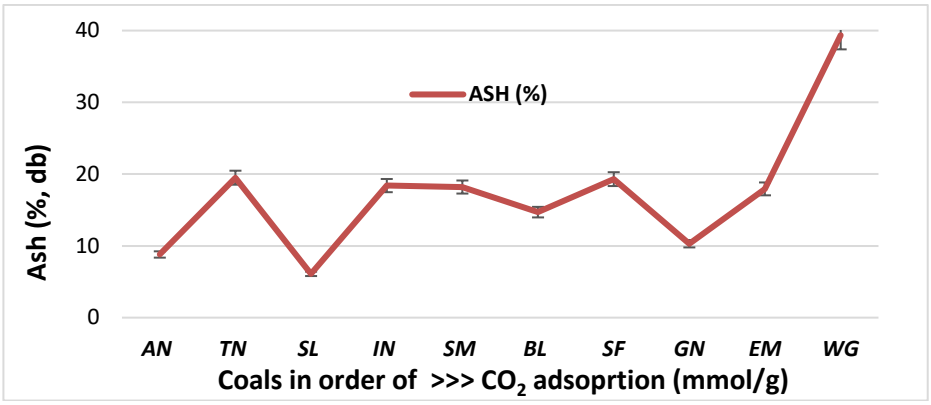

Figure 4.20: Comparison of coals with decreasing CO_2 adsorption versus Ash content (%)

The observed fluctuation is believed to be due to the "mix" of coals, i.e. different ranks compared together. On presenting high rank coals and medium (lower) rank coals separately, (Figure 4.21(a) and 4.21(b)), it can be seen that, HR coals' exhibit a very large variation in ash%. High rank coals presented here are; 1 HRB, 1 MRB and two HRC samples, which makes for a disseminated comparison. The MRC coals do exhibit more or less of a steady projection in the range of 10 – 19% ash content, having a range of R_oV_{mr} of 0.65 – 0.81%, with the exception of WG (39.35% and R_oV_{mr} of 0.51%).

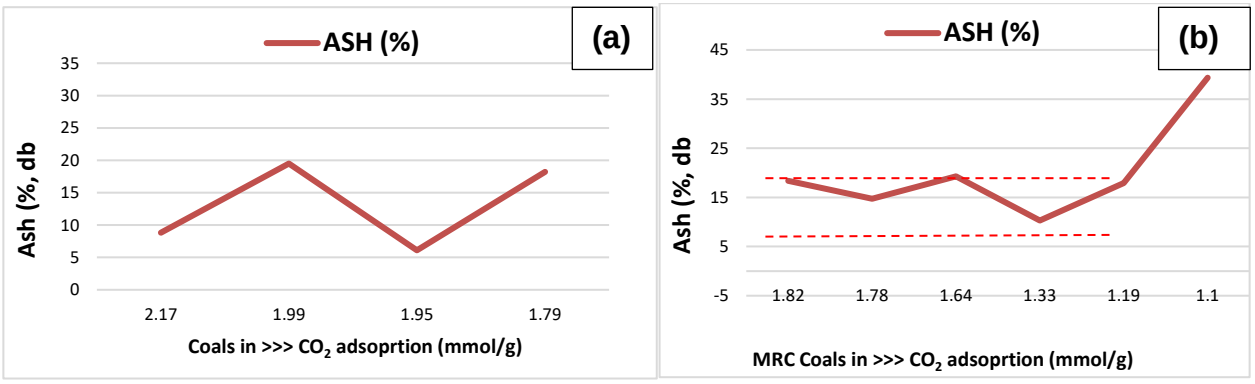

Figure 4.21(a: HRC's) and 4.21(b: MRC): Comparison of coals with decreasing CO_2 adsorption versus Ash content (%)

There is generally a negative correlation with ash content to sorption capacity, as can be seen in Figure 4.22(a) for the plot of the two HRC & HRB and 4.22(b) for MRC coals, a linear decrease is observed. From regression analysis it can be seen, that on average, for a 1% increase in ash content in HRC and MRC coals, a decrease of CO_2 adsorption capacity of 1.1 mmol/g and 0.018 mmol/g is observed respectively.

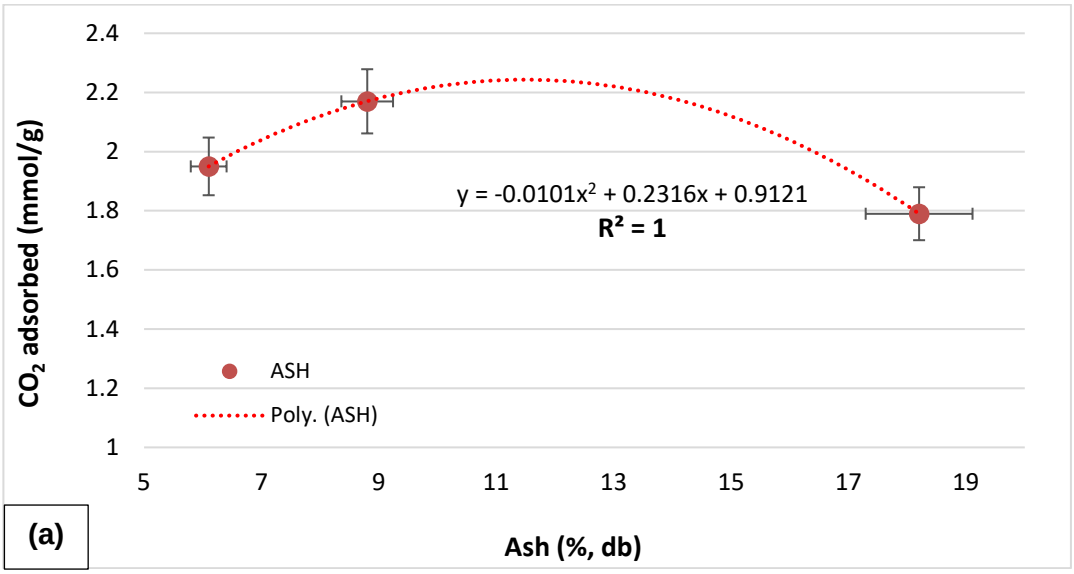

Figure 4.22(a): Comparison of CO_2 adsorption: HRB & HRC coals versus Ash content (%)

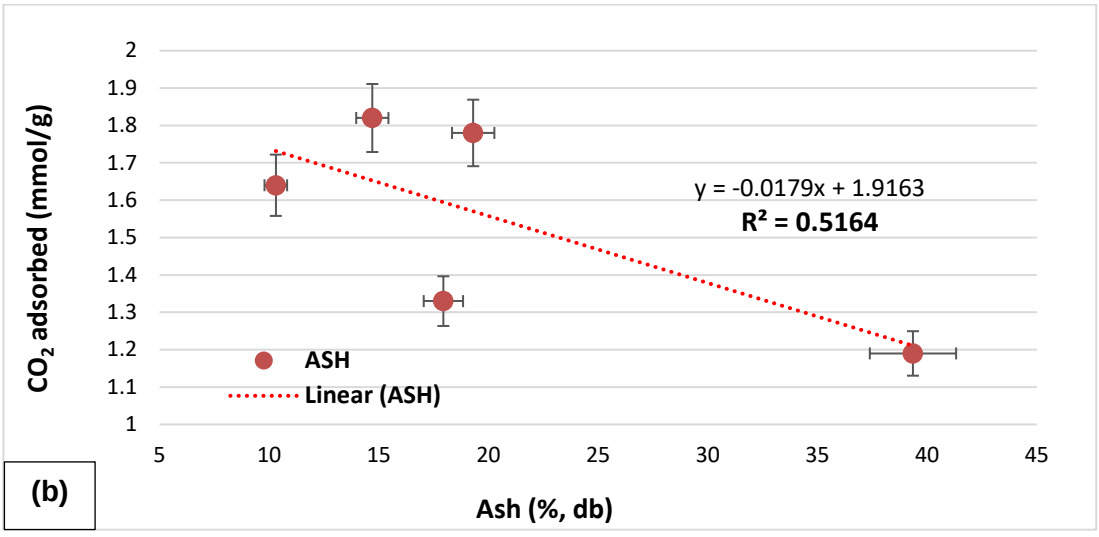

Figure 4.22(b): Comparison of CO_2 adsorption for MRC coals versus Ash content (%)

The overall observed negative trend, is in agreement with results from many previous studies, reporting decreased sorption capacity for both CO_2 and CH_4 trials (Bustin & Clarkson, 1998; Laxminarayana and Crosdale, 1999; Clarkson and Bustin, 2000; Laxminarayana and Crosdale, 2002; Gürdal & Yalçin, 2000; Gürdal & Yalçin, 2001; Faiz *et al*., 2007 and Weniger *et al*., 2010).

4.5.2.2 Analogous ash content samples compared

Four (4) of the most comparable ash content coal samples are compared for further evaluation. The coal samples listed in Table 4.6 show approximately the same ash content (range of 18.2 – 19.5%), but have varying adsorption capacity and large differences in their vitrinite contents (considered to be moderate to high in vitrinite).

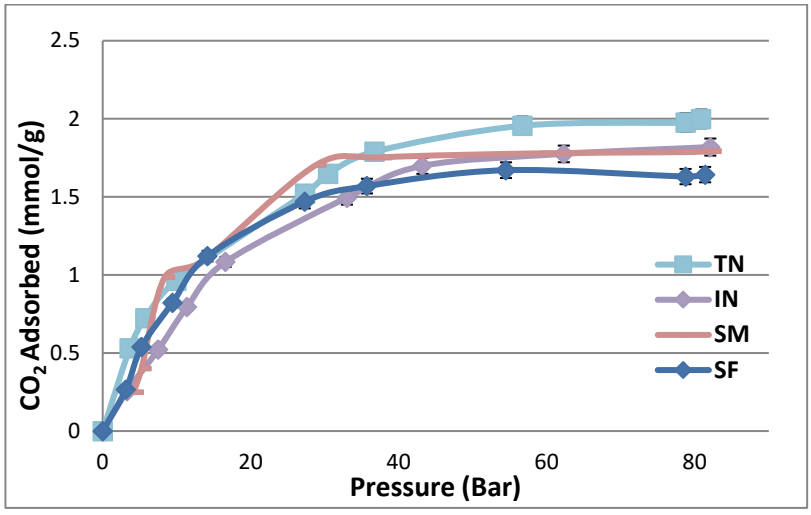

Figure 4.23: CO_2 Adsorption Isotherms: Comparison of comparable Ash (%)

Table 4.6: Ash and vitrinite content and CO_2 adsorbed for select high ash coals

Coal sample ID	*Ash (wt%)*	*Vitrinite (vol%, mmf)*	*CO_2 adsorbed (mmol/g)*	*Pressure (bar)*
TN	24.2	71.6	1.99	82.0
IN	22.5	50.2	1.82	82.1
SM	22.2	88.0	1.79	82.3
SF	23.9	20.8	1.64	81.4

Coals IN (18.4%) and SM (18.2%) report comparable ash values (a difference of only 0.2% between them), the difference in the sorption capacity is 0.03 mmol/g. Vitrinite contents of SM is almost double that of IN sample. The same trend can be seen for samples TN (19.5%) and SF (19.3%), having a difference of 0.2% in ash content but a difference in sorption capacity is seen to be 0.34 mmol/g. TN has three times the vitrinite contents of SF. These evaluations in differences leads to the possibility that ash content is not the only critical factor when evaluating coals' sorption capacity. This seems to be a clear indication that gas is adsorbed mostly by the organic matter (mostly vitrinite and to some extent in inertinite as well) only and not by the inorganic matter which act as diluents of the available organic carbon in the coal (Gürdal & Yalçin, 2001; Masterlez *et al*., 2004; Weniger *et al*., 2010; Dutta *et al*., 2011).

4.5.3 The Effect of Mineral and Maceral matter content

Gensterblum *et al*. (2011) suggested that the controlling factors that most possibly affect the preferential sorption behaviour of coal could be directly related to coal maceral and mineral matter content. Although the role of coal type (maceral composition) on gas adsorption is not fully established from most literature reviewed, various studies have reported that coal macerals (coal composition) influence the GSC (gas sorption capacity) of coal to some extent (Clarkson & Bustin, 1996; Crosdale *et al*., 1998; Clarkson & Bustin, 2000; Stanton *et al.*, 2001; Krooss *et al.*, 2002; Masterlez *et al*., 2004; Faiz *et al.,* 2007; Yu *et al.*, 2008).

Figure 4.24 shows an overall comparison between vitrinite, inertinite, liptinite and observable mineral matter (as determined petrographically) versus the total amount of CO_2 adsorbed (mmol/g) for all ten (10) SA coals tested. A fairly negative correlation exists between mineral matter, liptinite, inertinite content and adsorption capacity which is in agreement with many previous studies (Clarkson and Bustin, 1997; Ozdemir, 2004). Mineral matter and maceral matter will be looked at separately in the following sections.

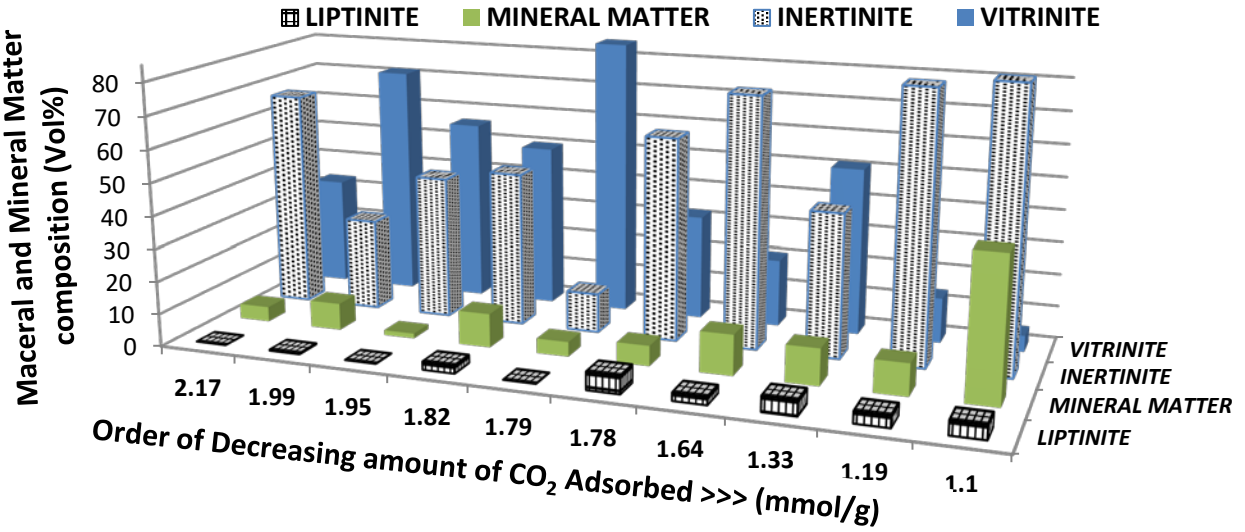

	2.17	1.99	1.95	1.82	1.79	1.78	1.64	1.33	1.19	1.1
LIPTINITE	0	0.3	0	2.5	0	5.5	2.5	4.7	3.6	4.3
MINERAL MATTER	4.6	8.3	1.5	10.4	4.5	6.2	12.4	11.2	9.8	43.6
INERTINITE	66.6	28.1	43.9	47.3	12	62.3	76.7	43.9	82.2	90.8
VITRINITE	33.4	71.6	56.1	50.2	88	32.2	20.8	51.4	13.9	5

Figure 4.24 Comparison of Macerals and observable Mineral Matter (Vol%)

4.5.3.1 Mineral Matter

On average, it can be seen that higher adsorption capacities were obtained in samples with very low mineral matter content while samples with increasing mineral matter content exhibited decreasing CO_2 adsorption capacities (Figure 4.24). Closer inspection of mineral matter *only*, (Figure 4.25), a distinction is made between the ranges of high and low rank coals and their respective mineral matter content. An exception to the trend is seen here, with the MRC BL sample, which seemingly falls out of the range as observed for the rest of the MRC samples (~8-13 %). This could most certainly be explained in relation to specific maceral composition ratios which need further investigation. Of interest, the SF and EM samples have similar mineral matter values (~10-12%), compared to the WG sample (43.6%). But again, the absorptive behaviour does not appear to be affected by the high mineral matter content, or the very low vitrinite content of the WG sample, in comparison to the other samples. These samples reported the lowest adsorptive capacity as summarised in Table 4.3.

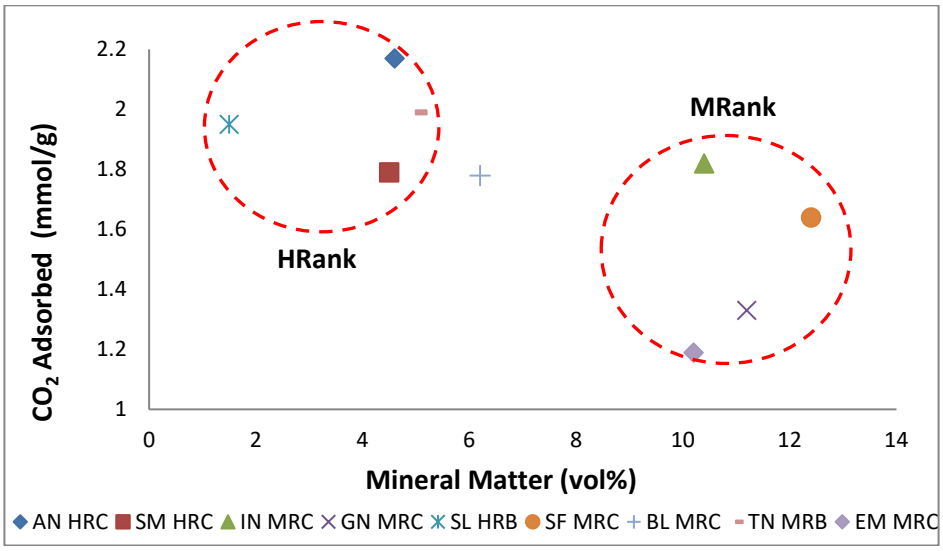

Figure 4.25 Comparison of observable Mineral matter content (Vol%) by rank versus CO_2 adsorption capacity (mmol/g)

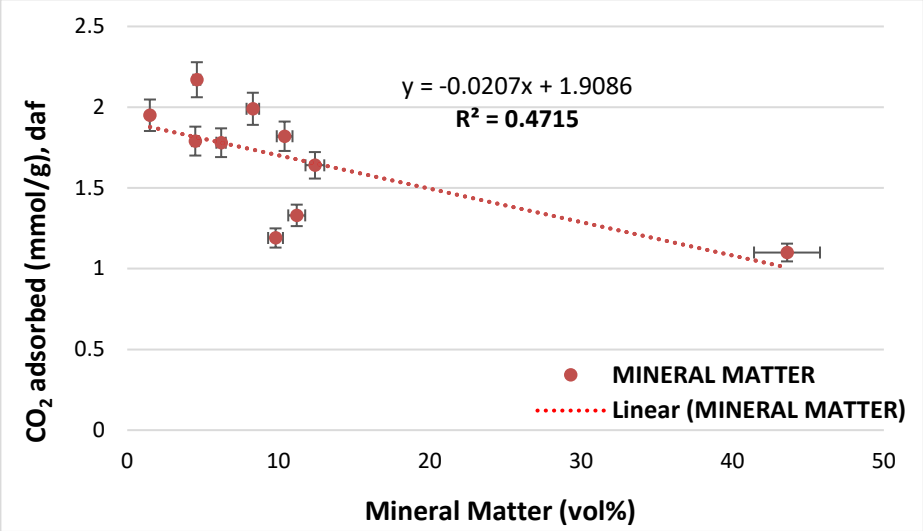

Figure 4.26 Comparison of observable Mineral Matter content versus CO_2 adsorption

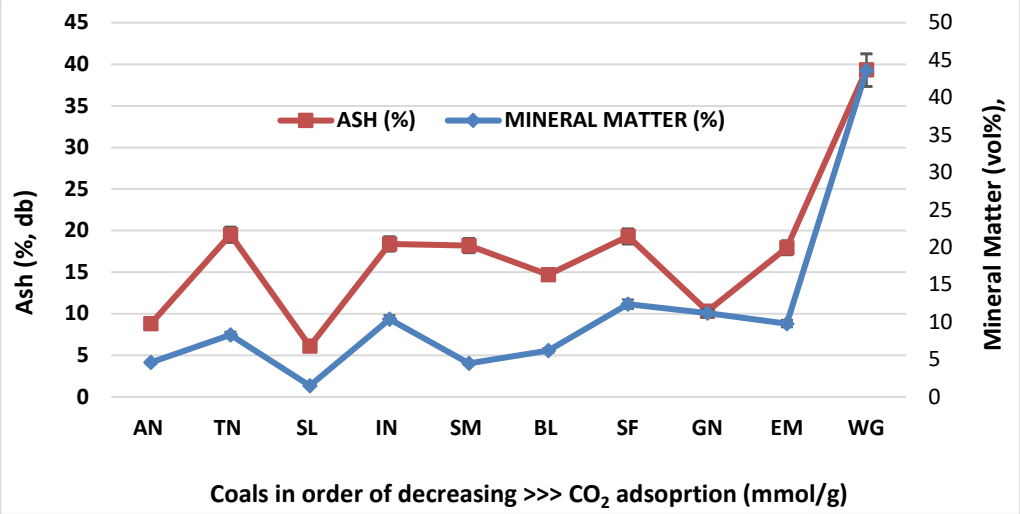

Figure 4.27 Comparison of ash content & observable mineral matter versus CO_2 adsorption

There is generally a negative relationship with mineral matter content to CO_2 sorption capacity, as can be seen in Figure 4.26, a linear decrease is observed which is in agreement with other investigators (Ward, 2002; Gürdal & Yalçin, 2001; Weniger *et al*., 2010; Dutta *et al*., 2011). Regression analysis shows, that on average, for a 1% increase in mineral matter content in coal, a decrease of CO_2 adsorption capacity of ~0.02 mmol/g is expected. This ties in well with the ash analysis data in section 4.5.2.1, showing a good consistency between proximate and petrographic data, which is evident from Figure 4.27 comparing both.

4.5.3.2 Maceral Matter

From studies across the globe (both Northern to Southern Hemisphere) presented thus far, detail pertaining to specific detailed maceral components have been sorely overlooked, and could very well be the contributing factor to various coals uptake of CO_2 and CH_4 desorption.

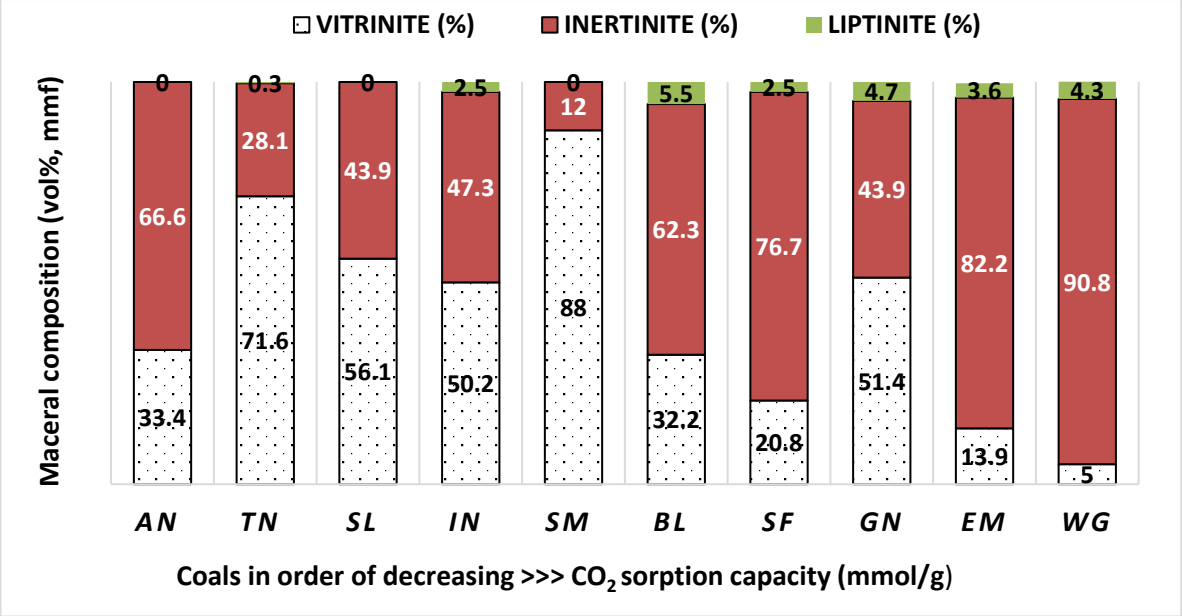

Figure 4.28 Comparison of Maceral matter (Vol%, mmf) versus decreasing CO_2 adsorption capacity

Figure 4.28 shows the overall comparison of the maceral groups (Vol%, mmf); vitrinite, inertinite and liptinite versus the excess CO_2 adsorption capacity (mmol/g) for all SA coals tested in this study. No apparent, direct relationship, can be observed from these results presented with relation to decreased CO_2 sorption potential.

The increasing liptinite content of coals; BL, GN, EM & WG, does however, correlate to a decrease with the CO_2 sorption capacity. The variation between the vitrinite and inertinite amounts fluctuate across the spectrum. Regression analysis for all coals (Figure 4.29) shows a very weak linear trend for both vitrinite (R^2= 0.3384) and inertinite (R^2 = 0.2946) contents comparing the decreasing CO_2 sorption capacity (mmol/g) for all coals across the different ranks. It does, however, faintly appear that as the vitrinite content decreases, and the inertinite content increases, a total decrease in sorption capacity is noted, but with the exception of coals; TN (MRB), SM (HRC) and GN.(MRC)

Clarkson & Bustin (1997) concluded that the heterogeneity of the micro-pore system increases with decreasing vitrinite and increasing inertinite content. This might be resulted from higher abundance of micro-pores in vitrinites as compared with inertinites (Crosdale *et al*., 1998; Unsworth *et al*., 1989). Vitrinite was found to be mainly micro- and

mesoporous. However, vitrinite-rich coals were found to have larger sized pores compared to vitrinite-poor coals, for the same rank of coal (bituminous coals and anthracites) (Zhao *et al.,* 2014). Inertinite, the most porous maceral group, was found to be mainly mesoporous and macro porous. Also, inertinite tends to contain more oxygen functional groups, and thus more hydrophilic sites (Unsworth *et al*., 1989), while liptinite, the least porous maceral group, was found to be only macroporous (Masterlez *et al*., 2004; Chalmers & Bustin, 2007).

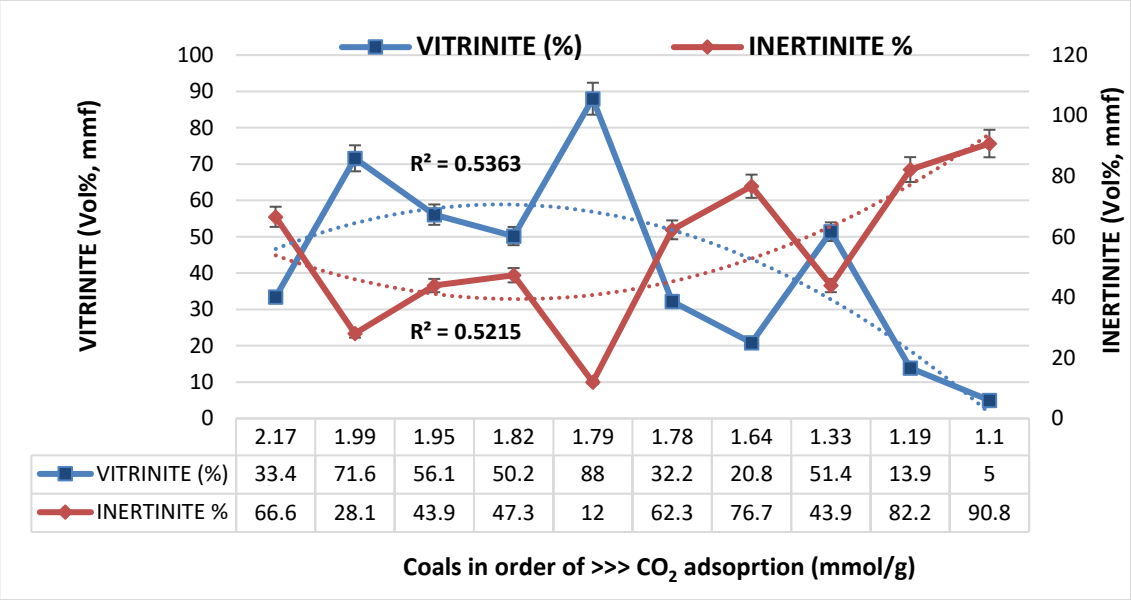

	2.17	1.99	1.95	1.82	1.79	1.78	1.64	1.33	1.19	1.1
VITRINITE (%)	33.4	71.6	56.1	50.2	88	32.2	20.8	51.4	13.9	5
INERTINITE %	66.6	28.1	43.9	47.3	12	62.3	76.7	43.9	82.2	90.8

Figure 4.29 Comparison of vitrinite & inertinite (Vol%, mmf) versus decreasing CO_2 adsorption capacity

From Figure 4.29, it is observed that, the AN sample starts off at the highest sorption (2.17 mmol/g) despite having lower vitrinite content (33.4%) than TN (MRB) (71.6%). Another exception is noted, with the SM (HRC) sample having a decreased sorption (1.79 mmol/g), although having the greatest vitrinite content (88%), which is more than two and a half times the content for the highest sorbing coal (AN). SM also, in comparison to all other coals tested, has the very least inertinite matter (12%) and no liptinite, so should theoretically be the best sorbing coal. While coals SL (56.1: 43.9%) and GN (51.4: 43.9%) have very comparable vitrinite to inertinite contents, however, a difference of 0.62 mmol/g is noted between them. The same is noted for coals AN (33.4: 66.6%) and BL (32.3: 62.3%), having comparable vitrinite to inertinite ratios, however reporting a sorption

difference of 0.39 mmol/g. The two lowest sorbing coals, EM and WG had the highest inertinite content, 82.2 and 90.8%, respectively. In addition they also had the very least vitrinite contents, 13.9 and 5% respectively, which could be the reason for very little sorption reported.

Also to note, coals, BL, GN, EM and WG (lower sorbing coals) have higher liptinite contents. The BL (5.5%) sample has the highest liptinite content of all coals tested, with GN (4.7%), followed by the WG sample (4.3 %), and then the EM sample (3.6%). Not many researchers have focused on the probability and influence of liptinite; however, by process of elimination here, it could be a possible reason for the differences considering all other coal characteristics and the fact that it the least porous maceral group (Masterlez *et al*., 2004). Chalmers and Bustin (2007) found contrasting CO_2 sorption processes occur between liptinite-rich samples (solution gas) and liptinite-poor coals (physical sorption), and therefore concluded that liptinite-rich samples need to be independently assessed for sorption ECBM potential. It was also found by Chalmers and Bustin (2007) that larger particle size fractions tested had a higher liptinite content than smaller size fractions. Hence further investigation into the influence of maceral composition and correlation between their ratios in coals must be accounted for with regard to CO_2 sorption capacity.

As mentioned, the coals used in this study originate from various coal basins. Coals from different basins are difficult to compare, all together, since the coal basin evolution (e.g. degree of metamorphism) and the organic precursors are very different (Siemons & Bush, 2007; Ceglarska-Stefańska & Zarębska, 2008; Prinz, 2004; Stach *et al*., 1982).

It has been observed by others, that seams with higher V/I ratio, have high cleat density as well as high permeability (Stach *et al*., 1982; Laubach *et al*. 1998). The comparison between the vitrinite to inertinite ratio (V : I) for the HR and MRC coals, to both the coal maturity, R_oV_{mr} and total amount of CO_2 adsorbed (mmol/g) are illustrated Figures 4.30(a: HR) and 4.30(b: MRC).

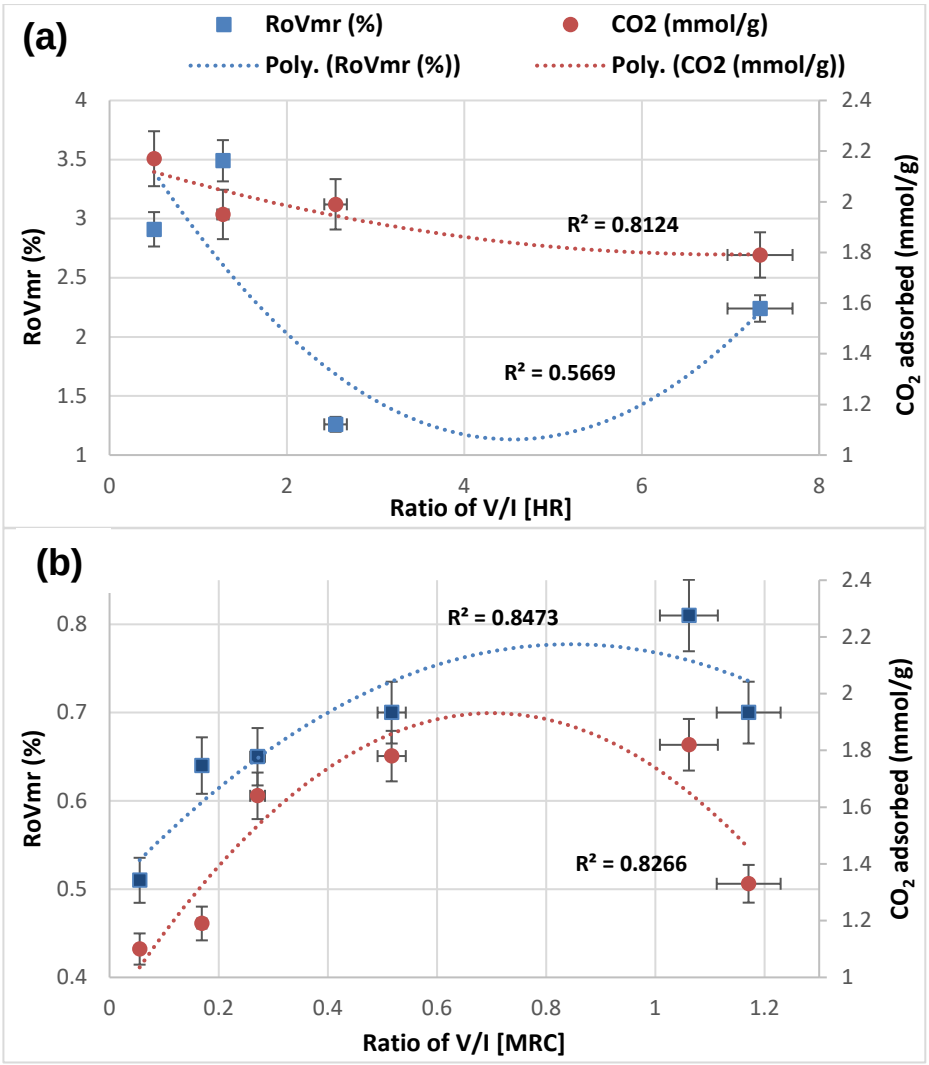

Figure 4.30(a: HR) & 4.30(b; MRC): Comparison of vitrinite to inertinite ratio (V:I) to vitrinite reflectance (R_oV_{mr} (%)) and CO_2 adsorbed (mmol/g)

The association of V:I ratio to R_oV_{mr} shows a negative relationship for HR coals (R^2=0.5669) from Figure 4.30(a), while an increasing V:I correlates to an increase in R_oV_{mr}%, as noted for the MRC coals up to a maximum of ~1.06% (V:I ratio) and 0.81 R_oV_{mr}%, which is in agreement with results from Sen & Banerjee (2015). Thereafter a decline with further increase in V:I ratio takes place. Although second order polynomial regression fit shows good fitting to validate this trend (R^2= 0.8124), the conflicting findings between HR and MRC coals is most likely due to the fact that, vitrinite reflectance i.e. rank of the coal is not controlled solely by petrographic (maceral) composition (Faiz *et al*., 2007; Masterlez *et* al., 2004; Sen & Banerjee, 2015).

The amount of total adsorbed CO_2 decreases very gradually with a decline in the V: I ratio for HR coals (Figure 4.30(a)). The R_oV_{mr} (%) versus V:I curve shows a very sharp decline (Coal TN @ R_oV_{mr} of 1.2%), this was also observed in previous studies and is proposed that it indicates that, spacing remains relatively constant only at vitrinite reflectance values above 1.5% (Meyers, 1982; Levine 1993; Laubach *et al*. 1998).

While for the MRC coals (Figure 4.30(b), an increasing V:I ratio (up to ~1.08%) shows a steady increase and thereafter a small drop in sorption capacity for V:R ratio of 1.06 to 1.17. This bell-shaped trend has also been established by a number of others (Stach *et al*., 1982; Laubach *et al*. 1998; Levine, 1993). This suggests that there exists an optimal ratio between vitrinite and inertinite maceral groups for best sorption capacity. Good regression results were obtained for the second order polynomial fit for both HR (R^2 =0.8124) and MRC (R^2 =0.8266).

In order to try and distinguish the effect of each maceral group separately, vitrinite content *only* (Figure 4.31(a)) and inertinite content *only* (Figure 4.31(b)), are plotted against CO_2 adsorption, comparing both the high rank coals (HRC; squares) and MRC (triangles) coals separately, to try and establish more of a trend with respect to vitrinite and inertinite composition. Linear regression fits show very improved configurations with respect to vitrinite and inertinite content for separately presented coal ranks versus CO_2 adsorption data as compared to that found from Figure 4.29.

It is clear that sorption capacity decreases steadily with a decrease in vitrinite content for HR coals, AN, TN, SL & SM (R^2=0.8603), while increasing vitrinite content for MRC (R^2= 0.8566) coals exhibit increasing sorption potential (Figure 4.31(a)). Whereas, from Figure 4.31(b), it can be noted, that as the inertinite content increases for HR coals, the CO_2 sorption is observed to also increase. While the opposite is noted for MRC coals, as inertinite decreases, the sorption also shows a decrease. GN is the only coal that is seen as an exception from both trends noted. Again this could be related to the fact that inertinite has been found to contain more macro-porosity (30 nm to 10 µm pore diameter) than vitrinite (Unsworth *et al*., 1989), and this demonstrates some agreement with higher inherent moisture content as observed for MRC (BL, SF, EM) coals tested here.

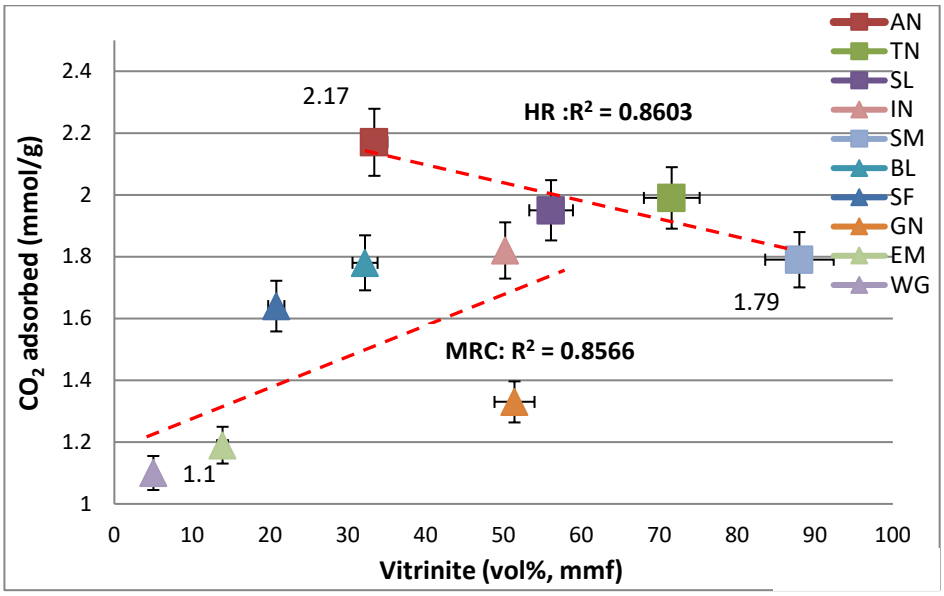

Figure 4.31(a): Comparison of vitrinite (Vol%, mmf) versus CO_2 adsorption capacity

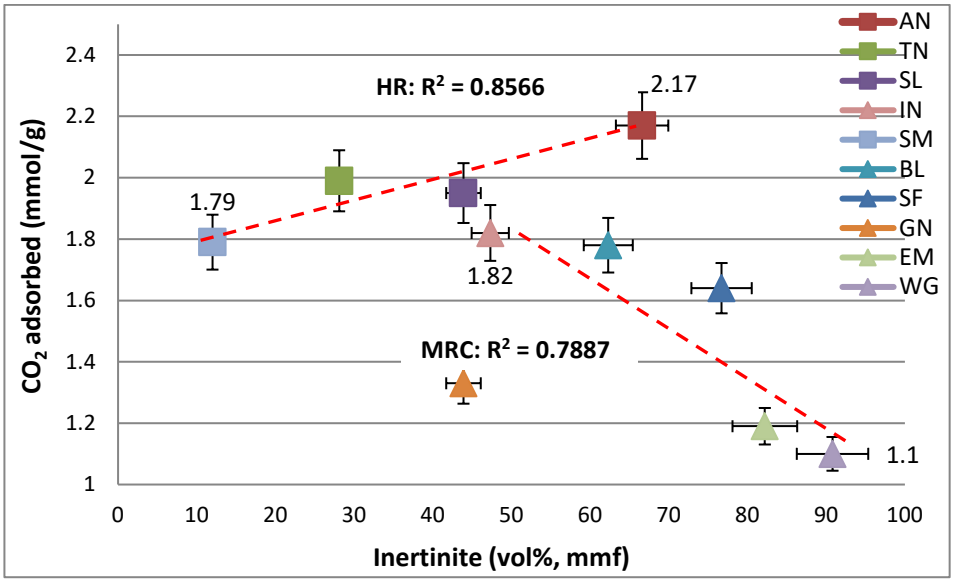

Figure 4.31(b): Comparison of inertinite (Vol%, mmf) versus CO_2 adsorption capacity

Although a higher adsorption rate for higher rank coals has been observed as with previous studies as well as in this study (discussed in Section 4.5.1), it must be noted that previous studies have also concluded that best sorption was noted mostly for vitrain-rich facies in high rank coals that contain low amounts of minerals (Clarkson and Bustin, 1997; Karacan

and Mitchell, 2003). It is well known that porosity is related to maceral composition, i.e. vitrinite predominantly contains microporous, whereas inertinite contains mesoporous and macroporous structures (Stach *et al.,* 1982; Falcon & Falcon, 1987). Among the different maceral groups, studies have found that vitrinite group macerals have more affinity for CO_2 compared to inertinite group macerals of similar rank coal and have demonstrated that vitrinite contains higher volumes of micro-pores than inertinite at a given rank (Unsworth *et al.,* 1989; Faiz, 1993; Crosdale *et al.,* 1998; Clarkson & Bustin, 1999; Masterlez *et al.,* 2004; Dutta, 2008; Prusty, 2008).

Early studies done by, Ettinger *et al.* (1966), Gregg & Sing (1982), Unsworth *et al.* (1989) and Bustin & Clarkson (1996), suggested that there is a distinct difference in the adsorption capacity of vitrinite-rich *versus* inertinite-rich coals. However, they concluded that inertinite rich coals had higher adsorption capacities than the vitrinite rich coals. Busch *et al*. (2006) observed for Dutch samples, that a stronger preferential adsorption of CO_2 was observed for the high inertinite content coal, with degree of preference for CO_2 adsorption increases with increasing inertinite. Results from Karacan and Mitchell (2003) show similar result and trends; they concluded that inertinite-rich samples exhibited the highest CO_2 adsorption rate compared to vitrinite-rich samples. No details of the constituents of maceral components were provided, which could lead to the further understanding and evaluation of the CO_2 sorption uptake. Adsorption experiments reported from various sources, including Australia, Poland, U.S.A, Germany and New Zealand show similar results concerning inertinite to vitrinite ratios. According to Day *et al*., (2007), the highest adsorption capacity observed was for a sample with a 23.9 % vitrinite, 74.5 % inertinite and 1.6 % liptinite. While the vitrinite-rich sample with a vitrinite-content of 95.5 % had the lowest adsorption capacity for the set of samples tested. While very recent findings for Chinese coals show that the order of the maceral surface areas exhibit a trend of inertinite > liptinite > vitrinite (Xie *et al*., 2015).

However, in contrast, other authors' found no correlation or systematic differences between gas sorption capacities of vitrinite- and inertinite-rich coals (Laxminarayana & Crosdale, 2002; Carroll & Pashin, 2003; Faiz *et al.,* 2007). The study by Busch *et al*. (2006) on Silesian Basin coals also did not indicate any distinct relationship between the preferential sorption behaviour and maceral composition or rank. Chalmers and Bustin (2007)

concluded that, the medium volatile bituminous rank coals with lower non-reactive inertinite contents showed a greater gas sorption capacity, because of higher micro-pore volumes. It was suggested that reactive inertinite should be considered when assessing low ranked coals as an adsorption media for ECBM resource.

It has been reported that although the Southern Hemisphere coals are known to be very rich in inertinite, they have been found to also exhibit a much higher reactivity than their Northern Hemisphere counterparts. The inertinite-rich coals from the Gondwana show partly reactive constituents compared with their northern Hemisphere counterparts with their propensity to react when heated. Individual macerals responsible for this behaviour in this group are the reactive semifusinite and reactive inertodetrinite (Falcon & Ham 1988; Smith *et al.*, 1983; Roberts *et al.*, 2015). This could possibly be the reason for the higher adsorption rates reported here for some of these SA coals with higher / increasing inertinite content.

Although conflict between the vitrinite and inertinite has been seen from widespread results from research across the globe, it seems evident on comparing current SA coal data, from Figure 4.31(a) and (b), that results presented here show that the vitrinite seems to be more of a controlling parameter than the inertinite for MRC coals, while the inertinite content increase seems to be more of a controlling factor for HR coal samples, (inverse to MRC coals). This suggests that a comparison of sorption capacities of coals having similar ranks and variable maceral group composition, indicate that rank has a dominating effect over any effects of organic matter type (Faiz *et al.,* 2007). But it is quite obvious as well that, the difference in source material results in different porosity, pore structure and therefore also in different adsorption rates (Laxminarayana & Crosdale, 2002). It is most likely that each maceral has a specific and distinctive set of physical and chemical properties that control the adsorptive behaviour of coal. This could mean that a specific or ideal ratio between *only* the maceral components, in similar rank coals, is the controlling factor for best CO_2 adsorption required, providing however that mineral matter / ash content (as discussed in Sections 4.5.2 and 4.5.3.1) are at the lowest possible. Thus, the next section 4.5.3.3, will look into comparing the detailed maceral compositions of these SA coals and identifying a possible correlation to the sorption capacity of CO_2 from the results presented.

4.5.3.3 Evaluation of detailed coal maceral composition on CO_2 adsorption

Lithotypes and microlithotypes[2] in coals can be distinguished from one another on the basis of their physical properties, either macroscopically and/or microscopically (Stach *et al*., 1982). However, even when optically homogenous, they may have variable elemental and molecular chemistry not only across different ranks, but also in iso-rank coals (Suárez-Ruiz & Crelling, 2008; Holuszko & Masterlez, 2015). Thus, indicating that the different macerals of the same coal can have different structural parameters (Xie, 2015). In this study, all coals show very variable reactive inertinite and vitrinite contents, as well as ratios of them. These variations in maceral chemistry may have significant impact on the sorption of CO_2 and may also complicate predictions of the coals' behaviour.

For the coals tested here, there is definitely a pronounced competing nature between macerals of inertinite and vitrinite components, as discussed in Section 4.5.3.2., which may explain the slight difference in adsorption behaviour, with the more reactive sample reporting a slightly higher level of CO_2 adsorption. SA coals studied here are most certainly multimodal, with respect to pore volume distribution, in addition to the rank difference, they obviously have varying proportions of micro-, meso-, and macro-porosity due to differing maceral compositions (Clarkson & Bustin, 1999).

Table 4.7 gives details of the respective compositions of individual macerals (vol%, mmf) (summarised from the detailed petrographic data presented in Appendix A). Correlating the detailed individual macerals of the vitrinite group are graphically represented in Figures 4.32 (a): vitrodetrinite, (b): corpogelinite & gelinite, (c) collotelinite and (d): pseudovitrinite. Figure 4.33, shows the comparison of individual inertinite maceral compositions on CO_2 adsorption; (a) Fusinite (b) Inertodetrinite, (c) Semi-fusinite, while Figure 4.34 depicts the comparison of liptinite maceral compositions; (a) sporinite and (b) cutinite, respectively, with regards to the CO_2 adsorption (mmol/g) capacities of the ten coals tested in this study.

[2] Further reading regarding details of litho and micro-lithotype petrographic characteristics of shape and size: Stach, *et al.,* 1982; Meyers *et al*., 1982; Suarez-Ruiz & Crelling, 2008.

Table 4.7: Details of Possible Impacting Maceral components: Vitrinite - Inertinite – Liptinite groups

PETROGRAPHIC DATA OF SA COALS: Individual Macerals										
Sample ID:	***AN***	***TN***	***SL***	***IN***	***SM***	***BL***	***SF***	***GN***	***EM***	***WG***
Vitrinite (vol%)#	**33.4**	**71.6**	**56.1**	**50.2**	**88.0**	**32.2**	**20.8**	**51.4**	**13.9**	**5.0**
Collotelinite	33.4	47.8	42.9	39.3	57.3	27.3	13.7	32.9	8.6	3.2
Collodetrinite	0.0	20.2	12.2	1.1	30.6	0.0	4.1	4.5	5.0	0.7
Corp* + Gelinite	0.0	0.0	0.0	2.0	0.0	2.1	1.6	6.1	0.0	1.1
Pseudovitrinite	0.0	3.6	1.0	4.7	0.0	1.7	0.0	3.6	0.3	0.0
Inertinite (vol%)#	**66.6**	**28.1**	**43.9**	**47.3**	**12**	**62.3**	**76.7**	**43.9**	**82.2**	**90.8**
Fusinite	6.1	12.3	5.3	7.8	6.3	13.2	4.8	20	9.7	3.5
Semi-fusinite **	46.8	9.6	35.0	15.4.3	4.7	17.7	25.1	17.1	20.9	34.7
I SF*	46.8	8.2	35.0	14.1	4.7	14.1	22.6	10.1	17.8	29.4
Inertodetrinite	13.4	4.6	3.0	19.2	0.8	25.4	42.5	4.1	39.2	48.6
Liptinite (vol%)#	**0.0**	**0.3**	**0.0**	**2.5**	**0.0**	**5.5**	**2.5**	**4.7**	**3.6**	**4.3**
Cutinite	0.0	0.0	0.0	0.2	0.0	1.3	0.2	1.1	0.6	0.7
Sporinite	0.0	0.3	0.0	2.0	0.0	3.8	2.3	3.6	3.1	2.1
Mineral M (vol%)	**4.6**	**8.3**	**1.5**	**10.4**	**4.5**	**6.2**	**12.4**	**11.2**	**9.8**	**43.6**
R_oV_{mr} (%)	2.91	1.26	3.49	0.81	2.24	0.7	0.65	0.7	0.64	0.51
Coal Rank	HRC	MRB	HRB	MRC	HRC	MRC	MRC	MRC	MRC	MRC

***R SF - Reactive Semi-Fusinite** ***I SF - Inert Semi-Fusinite** ***Corp – Corpogelinite**
*** = R.SF + I.SF**
 # -mmf (mineral matter free)

4.5.3.3.1 Effect of Vitrinite macerals

Vitrinites are classified into telinite (with remnant cellular structure) and collotelinite (no visible signs of cellular structure), Collodetrinite, vitrodetrinite, corpogelinite, gelinite and pseudovitrinite. Telinite and vitrodetrinite content are approximated to be almost neglible (0%) for this suite of SA coals, with the exception of GN (3.2% and 1.1%, respectively), and hence will not be examined.

- **Collodetrinite:**

Collodetrinite is identifiable as a mottled vitrinitic groundmass binding other coal components (ICCP, 1998). From Figure 4.32(a) it is observed that decreasing CO_2 sorption capacities (mmol/g) for both the HR and MRC coals are related to increasing vitrodetrinite values. There is a very clear distinction in amounts of vitrodetrinite for AN (0%), as compared to both SL (12.2%) and for TN (20.2%), which is 20 times the amount of the AN sample. One exception to this trend is noted for MRC WG (0.7%), it has the least vitrodetrinite and also reported the least CO_2 sorption (1.1 mmol/g), of all coals. This, however, could be attributed to the fact that it exhibited an exceptionally high mineral matter content of 43.6 vol% (discussed in Section 4.5.3.1).

- **Gelovitrinite (Corpogelinite & gelinite)**

Gelinite results from humic solutions that diffuse into cracks and other voids as a gel-like material, and is homogenous and structure-less with a slightly higher reflectance than the other vitrinite macerals. Corpogelinite has the same characteristics of gelinite, but the precipitated gel fills void spaces in cell walls, forming ovoid bodies i.e., discrete amorphous bodies representing cell infillings (ICCP, 1998; Taylor *et al.,* 1998).

The same decreasing trend is found for increasing gelovitrinite content (vol%) for both the HRC and MRC exhibit reduced sorption capacity (Figure 4.32 (b)). Of interest is the comparison of MRC IN and GN samples. Although they have very similar vitrinite contents, 50.2% and 51.4% respectively, the sorption capacity of GN (1.33 mol/g) was much lower than IN (1.82 mmol/g). GN (6.1%) reports much greater gelovitrinite as compared to IN (2%). This certainly demonstrates that these gel-filled bodies (infillings) have a very negating effect by reducing the coal porosity and is the reason for the decreased sorption capacity.

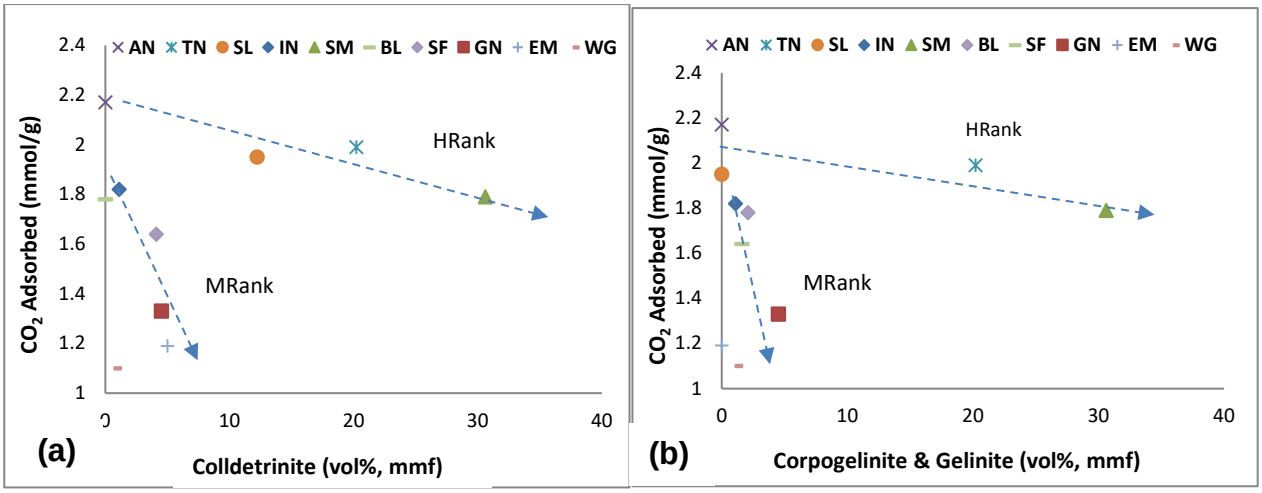

Figure 4.32: Comparison of vitrinite individual macerals' compositions on CO_2 adsorption; (a): Collodetrinite & (b): corpogelinite & gelinite

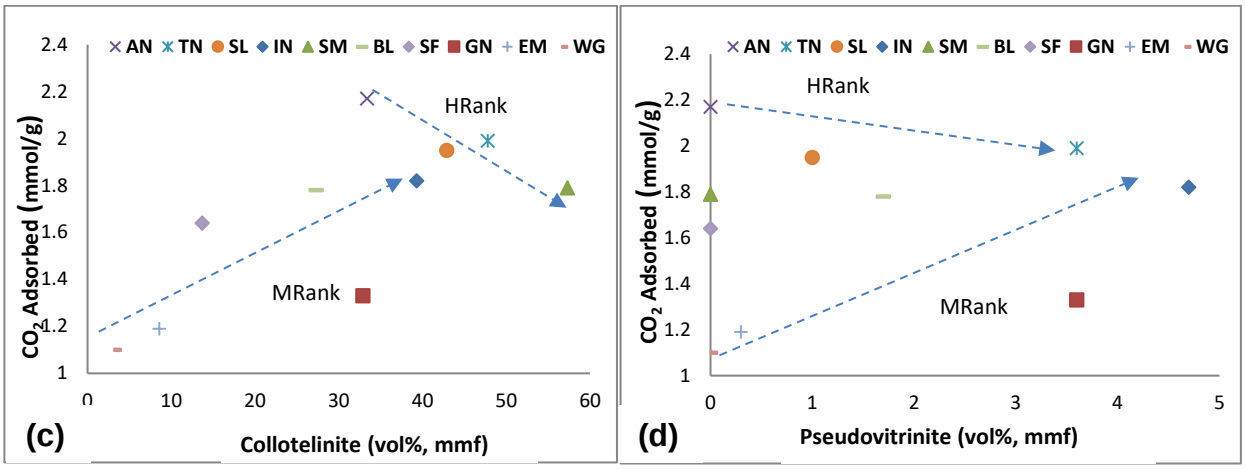

Figure 4.32: Comparison of vitrinite individual maceral compositions on CO_2 adsorption: (c): collotelinite & (d): pseudovitrinite

- **Collotelinite**

Collotelinite maceral is representative of the greatest percentage in the vitrinite group for both HRC and MRC cooals. Compared to collodetrinite, collotelinite has a higher degree of homogenization, lacks textural continuity, i.e. has no visible signs of cellular structure. For a given rank level, the collotelinite, has the lowest carbon and highest oxygen contents (Meyers, 1982; Suárez-Ruiz & Crelling, 2008). Figure 4.32(c) shows a conflicting correlation, revealing a trend of decreasing soprtion for HRC coals with increasing collotelinite maceral content was observed. The HRC SM sample, reporting the lowest

sorption of 1.79 mmol/g, had the highest collotelinite content (57.3%), while the highest sorbing coal, AN (33.4%) had the lowest percentage of all HR coals. This observation is contrary to reportings of Chalmers & Bustin (2007), who concluded that higher sorption capacities were found in high-rank vitrinite-rich coals with higher telovitrinite (collotelinite & telinite) content.

The inverse was observed for the MRC coals. The highest sorbing MRC coal IN (1.82 mmol/g) had the highest collotelinite value (39.3%) followed by BL (27.3%) and SF (13.7%) This outcome needs further study with more samples to make a more concise deduction.

- **Pseudovitrinite**

Pseudovitrinite is characterized by the slit structure and slightly enhanced reflectance when compared to other vitrinite of the same coal and is frequently observed in SA Permian-age coals. It is devoid of any pyrite inclusions and is considered to be an inert to semi-inert maceral. It is believed to have an origin similar to collotelinite (Meyers, 1982; O'Keefe *et al*., 2013).

Only two of the HR coals reported pseudovitrinite contents, i.e. coals SL (1%) and TN (3.6%). From Figure 4.32(d), it is evident that this maceral does not seem to have any negative effect on the total sorption capacity for high ranking coals. However, more samples need to be further examined to make a conclusive decision.

Although, very noticeable, trends have been identified for these selected vitrinite macerals, it must be mentioned that in iso-rank coals, vitrinite with the same textural and optical characteristics might not be homogeneous with respect to its chemical properties (Jimenez.*et al*., 1998).

4.5.3.3.2 Effect of Inertinite macerals

The inertinite-rich coals from the Gondwana coals in the Southern Hemisphere show partly reactive constituents compared with their northern hemisphere counterparts. Individual macerals responsible for this behaviour in this group are reactive semi-fusinite and reactive inertodetrinite (Smith *et al.,* 1983; Falcon & Ham, 1988). Gas sorption capacity of much of the semi-fusinite in SA coals is believed to be very comparable to vitrinite, such that no significant difference in gas sorption capacity is observable between the vitrinite and inertinite-rich coals, at a given rank (Lamberson and Bustin, 1993). Inertinite is classified into fusinite, semi-fusinite and inertodetrinite (Stach *et al*., 1982; Meyers, 1982; ICCP, 1998).

- **Fusinite**

Fusinite is close to the highest stage of coalification, it has a charcoal-like structure, has the least volatile matter (Xie, 2015) and displays well preserved cellular structures, reflective of its rapid origin during combustion events. It is the highest reflecting maceral and it does not change morphology or reflectance significantly during coalification (O'Keefe *et al*., 2013). While fusinite values (Figure 4.33(a)) for both AN (6.1%) and SM (6.3%) were similar, their sorption amounts differed by 0.38 mmol/g. The TN sample (12.3%) reported more than double those amounts and showed a decreased sorption. MRC coals showed on average an increasing sorption as fusinite increased, but these results are somewhat scattered, no definitive trend regarding the role of fusinite in sorption process can be made here. Fusinite has been found to have no micro porosity due to complete loss of volatile matter (CIarkson & Bustin, 1996), hence HRC coals, having very diminished volatile matter display decreased sorption potential.

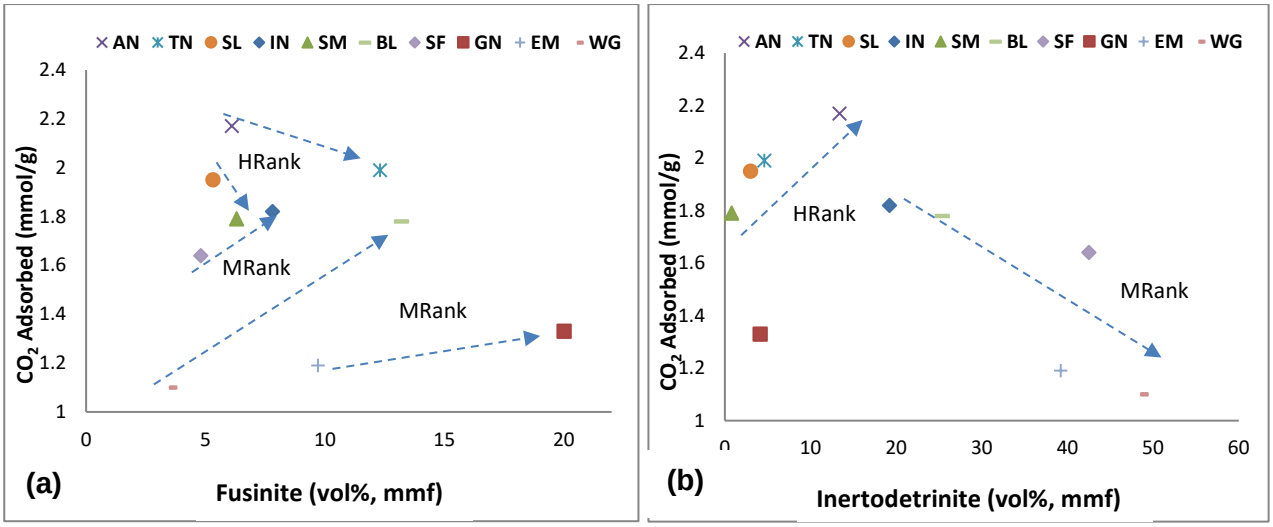

Figure 4.33: Comparison of inertinite macerals' compositions on CO_2 adsorption; (a) fusinite (b) inertodetrinite

- **Inertodetrinite**

Reactive inertodetrinite was found to be 0% for most coals, and in very low proportion for TN (0.5) and EM (7.5%) coals. Inert inertodetrinite is more dominant, ranging from 4.1 - 42.5%. Reactive inertodetrinite and inert inertodetrinite data have therefore, been combined (for simplicity of comparison and are presented in figure 4.33(c). The inertodetrinite maceral (figure 4.33(b)) seems to be more domineering for HR coals, having increase sorption capacity, with sample AN, at 13.4%, while the SL and TN were approximately less than 4.6% with SM (0.8%) reporting the least percentage. Inertodetrinite has the highest carbon and lowest oxygen contents (Suárez-Ruiz & Crelling, 2008). Applying these comparisons to the other high rank coal, SM (HRC), which had low sorption of 1.79 mmol/g, it can also be noted as discussed earlier, that the presence of a very high collodetrinite (30.6%) and extremely small inertodetrinite (0.8%) content seem to be the reasons or factors controlling the lower sorption of CO_2 for these coals ranging with high R_oV_{mr} values as compared in Figure 4.13.

MRC coals show a decreased sorption potential with increasing inertodetrinite content, with the exception of GN. (4.1%) having the lowest amount. But this, however, could be

attributed to other discussed macerals such as the high proportion of corpogelinite and gelinite content.

- **Semi-fusinite**

Semi-fusinite has very similar cell texture and general features of fusinite except that it is of lower reflectance. In fact, semi-fusinite has the largest range of reflectance of any of the various coal macerals going from the upper end of the pseudovitrinite range to fusinite. It is also the most abundant of the inertinite macerals. (Stach *et al.*, 1982; Meyers, 1982; ICCP, 1998).

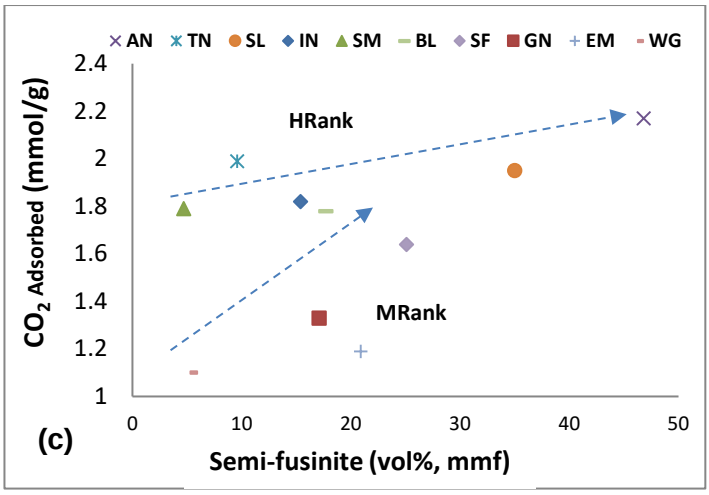

Figure 4.33: Comparison of inertinite macerals' compositions on CO_2 adsorption: (c) semi-fusinite

Reactive semi-fusinite (RSF) is found to be in very low proportion for all coals, ranging from 0-3%, with the only the exception of GN (7%). ISF (inert semi-fusinite) is more dominant, ranging from 10 – 46.8%. RSF and ISF data have therefore been combined (for simplicity of comparison) and are presented in Figure 4.33(c). As semi-fusinte content increases in HRC coals, there is a linear increase in the CO_2 sorption amount. It can be observed that the AN sample, had a very high semi-fusinite (46.80%) content as compared to both SL and TN (8.2%). CIarkson & Bustin (1996) hypothesised that, the loss of volatile matter as a result of partial charring during the formation of semi-fusinite may open up the pore

structure, allowing additional adsorption. It is believed to occur, whereby micro porosity is created by the removal of walls between adjacent micro pores through coalification process and creates additional micro porosity in semi fusinite. This theory is supported here by the fact that HRC coals, AN and SL, having the lowest volatile matter (as presented in Section 4.2.1, Figure 4.2) had the greatest total number of micro pore surface areas, 199.19, 170.67 m^2/g, respectively (as determined from BET determinations discussed in section 4.3), even though they do not have the highest total vitrinite contents (AN: 33.4% and SL: 56.1%).

While the inverse is noted for MRC coals (Figure 4.33(c)). A decline in semi-fusinite exhibits a decrease in sorption for MRC coals (Figure 4.33(c)). Coal IN (MRC) being the highest sorbing coal had the least semi-fusinite (15.4%).

4.5.3.3.3 Effect of Liptinite macerals:

The liptinite group includes components that are chemically more resistant to physical and chemical degradation than other macerals and are enriched in hydrogen, owing to a greater amount of aliphatic components (Holuszko & Masterlez, 2015). The main liptinite macerals examined in this study are classified as sporinite and cutinite. In general an increased liptinite content seems to relate to a decrease in CO_2 uptake. For this suite of SA coals, other macerals in this group are considered negligible as percentages is at zero.

- **Sporinite**

As sporinite dominates the liptinite maceral group, it could be assumed, that it is solely responsible for decreased sorption. This was observed for the HRB and MRC and coals (Figure 4.34(a)). Coal BL seems to be at odds with this trend.

Comparing MRC IN and WG samples, although they have very similar sporinite contents, 2% and 2.1% respectively, the sorption capacity of IN (1.82 mmol/g) was much greater

than WG (1.1 mmol/g), this, however, could be attributed to the fact that it exhibited an exceptionally high mineral matter content of 90.8 vol% (discussed in Section 4.5.3.1).

- **Cutinite**

Cutinite maceral is non-existent in the HRC coals (0%). For MRC coals, a decrease in cutinite, generally seems to correlate to a decrease in sorption, however, an exception is noted for coals BL and GN. However, these coals, exhibited greater collotelinite, fusinite and semi-fusinite values as compare to the other MRC coals.

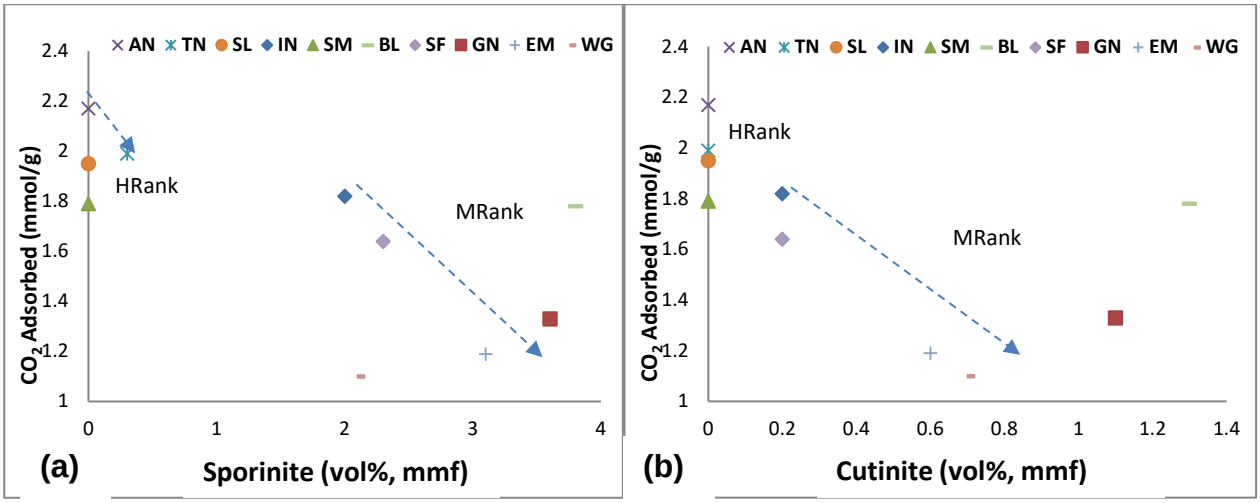

Figure 4.34: Comparison of liptinite macerals' compositions on CO_2 adsorption; (a) sporinite (b) cutinite

4.5.3.3.4 Summary of maceral component effect

These comparative correlations relating different macerals to CO_2 sorption capacity do indeed show, that details of maceral compositions are essential and need to be identified and considered as well when evaluating the sorption capacity of the coal. It can be noted that a certain ratio of maceral components to the inert ones in terms of petrographic composition is pertinent when gas sorption processes are to be considered (Holuszko &

Masterlez, 2015). It is evident that only selected maceral constituents are seemingly responsible for gas transport and movement in the coal matrix.

Although, very noticeable, trends have been identified for these selected vitrinite macerals, it must be mentioned that in iso-rank coals, vitrinite with the same textural and optical characteristics might not be homogeneous with respect to its chemical properties (Jimenez.*et al*., 1998). This is because variations are not only affected by rank but also by paleo environmental conditions and post-sedimentary history (Jimenez.*et al*., 1998).

4.6 RESULTS FOR MOISTURE DIFFERENCE: CO_2 SORPTION TESTS

Coal seams are naturally water saturated under in-situ conditions and this inherent moisture can be found in the bulk coal matrix and in the coal cleats (a network of fractures found in most coals). Additionally, large quantities of CH_4 (and to an extent, water) are generally sorbed to the coal matrix. The inherent coal moisture varies from coal seam to coal seam according to specific coal rank and type (Joubert *et al.,* 1973; Levy *et al*., 1997; Krooss *et al*., 2002; Ozdemir, 2004; Bromhala *et al*., 2005; Day *et al*., 2008; Viljoen *et al*., 2010; Kim *et al*., 2011). As discussed in section 2.12.5, previous studies have revealed that CO_2 molecules compete with water molecules for adsorption sites within the coal matrix. CO_2 molecules undergo volumetric displacement, so moisture- equilibrated coals would then adsorb less CO_2 gas than coal with "low moisture i.e. ~0% moisture". Some studies have estimated that the CO_2 adsorption capacity is reduced by about 7 kg/t for each 1% increase in moisture (Viljoen *et al*., 2010, Masterlez *et al*., 2009).

SA coals tested in this study show diverse inherent moisture contents across the different ranks (as discussed in section 4.2.1 and seen in Figure 4.1). For all ranks of coals studied here, the adsorbed amount of CO_2 decreased with the moisture content up to a critical value, which is characteristic of the coal type. The CO_2 sorption capacity experiments were performed on "as received, then dried and de-gassed" coals, 0% moisture and thereafter simulated moisture equilibrated samples (as described in methodology section 3.4.3.1). Moisture equilibrated adsorption isotherms of the three (3) samples, namely; SL (HRB), TN (MRB) and EM (MRC), are as shown in Figure 4.35(a), 4.35(b) and 4.35(c). The experiments were carried out at an isothermal temperature of 35^{o}C (308.15 K) and pressures ranging from 3.5 bars to 90 bars. The "as received" samples were used as standard test to compare the adsorption capacities of dry and moisture equilibrated coal samples since the main objective of the research is to study the influence of moisture on CO_2 adsorption capacity by the coal. The samples' moisture were simulated to different moisture percentages (ranges as discussed in Section 3.4.2.1) as outlined in Table 4.8.

Table 4.8: Moisture (simulated) percentages and CO_2 sorption capacities

Sample ID.	*Moisture (%)*	*Pressure (bar)*	*CO_2 Adsorbed (mmol/g)*	*Decreased Sorption (%)*	
SL	0	86.04	4.46	75	60
SL	0.51	86.73	3.31		
SL	1.55	88.20	2.51		
SL	2.43	86.13	1.79		
SL	4.42	84.34	1.12		
TN	0	86.12	4.43	77	67
TN	0.53	87.24	2.84		
TN	1.51	84.31	2.19		
TN	2.40	88.13	1.39		
TN	4.45	88.31	0.99		
EM	0	86.25	3.06	64	
EM	1.53	86.13	1.80		
EM	2.44	86.13	1.11		

The adsorption isotherms are clearly classified as the Type I: Langmuir isotherm according to the IUPAC classifications (Gregg & Sing, 1982; Birdi, 2010). It can be seen that the curve of the adsorbed volume of CO_2 versus the gas pressure exhibits a steep start and then slowly flattens above the sub-critical range of ~45 bar for the majority of the moisture conditions. The maximum capacity that can be seen from ~60 bar onwards, is due to the steep increase in the specific density of supercritical CO_2 in this pressure range (Bae and Bhatia, 2006; Saghafi *et al*., 2008; Gensterblum *et al*., 2010; Dutta, *et al*., 2011). From Figures 4.35(a), (b) and (c) it is clear that there is much less CO_2 is being adsorbed by the moisture (simulated) equilibrated coal than on the degassed and dry coal samples. The experimental results agree with the literature and previous studies; an increase in coal moisture content will result in the decrease of CO_2 adsorption capacity by the coal (Krooss *et al*., 2002; Ozdemir, 2004; Day *et al*., 2008b). From the Figures, the "as received, dried and degassed" samples have a very high number of mmol/g of CO_2 compared to the moisture-equilibrated coals which shows that indeed, moisture in coal has a negative effect on the adsorption capacity.

Theoretically, it is explained that coal sorption capacity for CO_2 is reduced by the coal moisture content due to the adsorbed "water" occupying some of the sorption sites and reduces the available surface area for gas molecules adsorption on the coal internal

surfaces, such as micro and meso-pores. Some of the adsorbed water blocks the gas path to the micro-pore system. The presence of water in the coal internal surfaces, where the gas phase is mostly adsorbed and stored, affects the ability of the coal to adsorb the CO_2 (Gentzis, 2000; Krooss *et al*., 2002; Busch *et al*., 2003; Goodman *et al*., 2004; Goodman *et al*., 2007; Day *et al*., 2008(b); Prusty, 2008; Gensterblum *et al*., 2009).

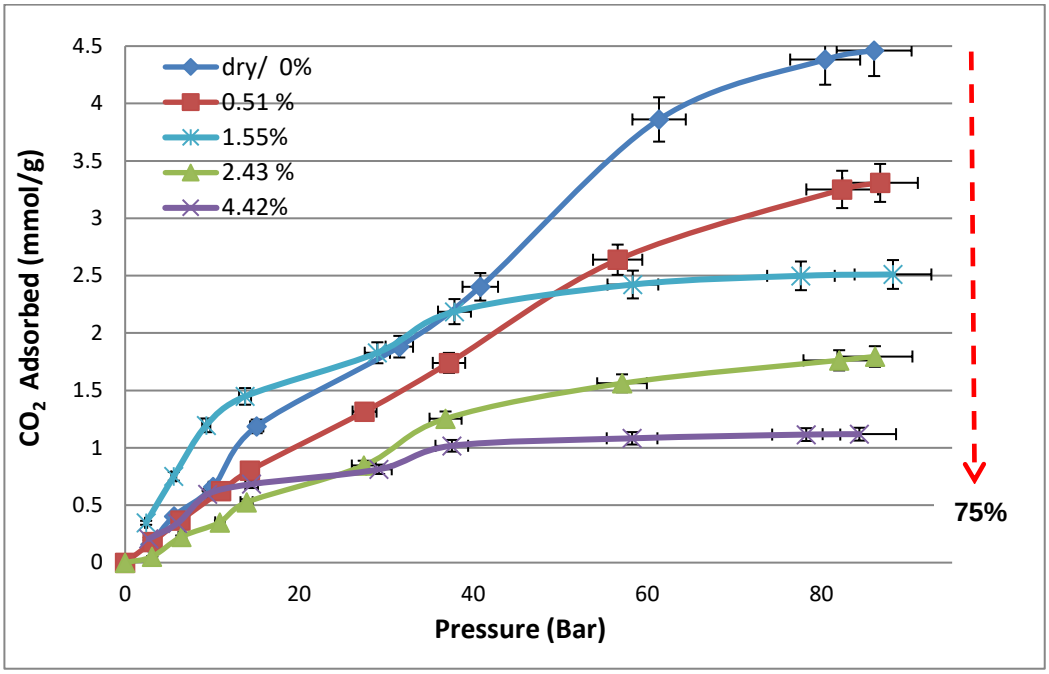

Figure 4.35(a): Comparison of adsorption capacities of dry and moisture-equilibrated coal (SL sample)

In Figure 4.35(a), the adsorption capacity of "0.51% moisture" curve for the SL sample at ~86 bar is 3.31 mmol/g, and for "dry/o%" curve at the same pressure it is 4.46 mmol/g. This shows that the adsorption capacity drops by 27.26 % for a 0.51% increase in moisture. It also does decrease up to 59.9% when the moisture is increased by 2.43%. Sorption decreased by 75% with the highest moisture content of 4.42% as compared to the 0% (dry) sample. The same observation was noted for the TN sample (Figure 4.35(b), the total decrease in sorption was found to be 77%.

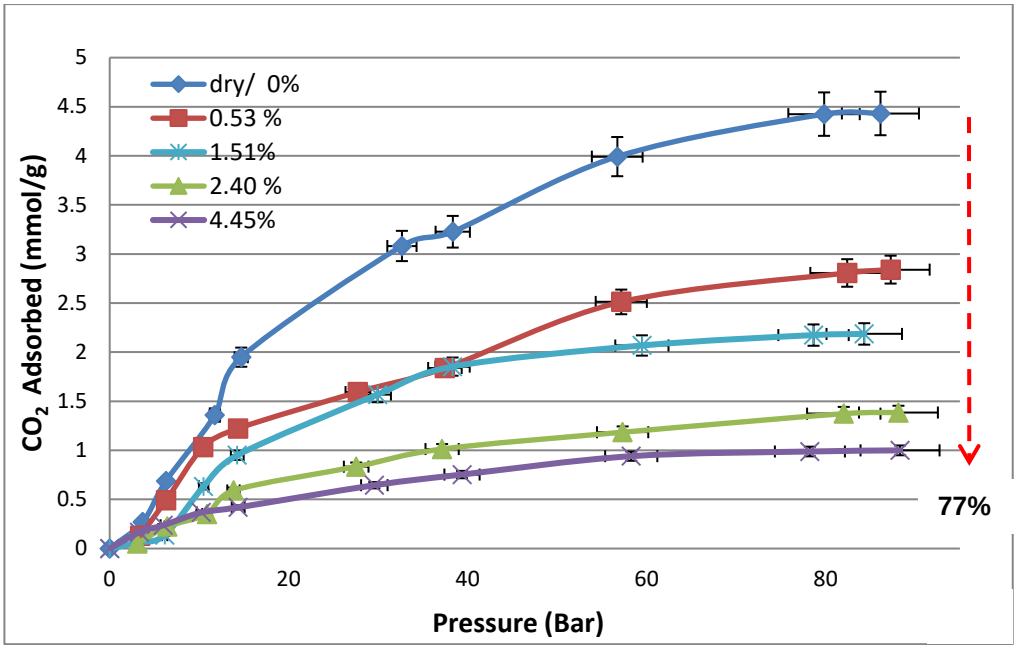

Figure 4.35(b): Comparison of adsorption capacities for dry and moisture-equilibrated coals (TN sample)

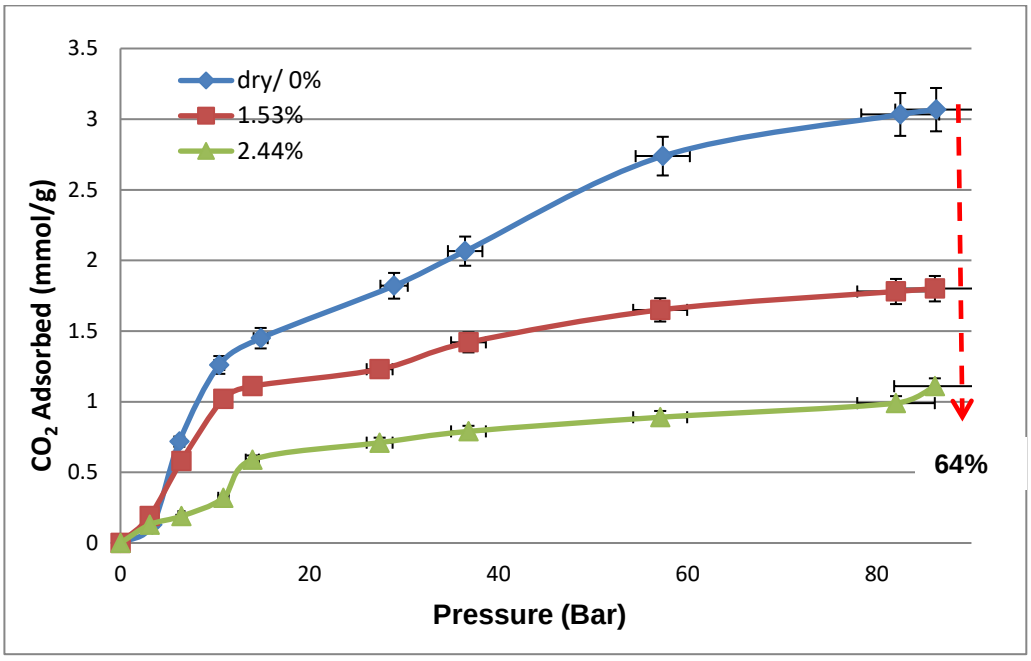

Figure 4.35(c): Comparison of adsorption capacities for dry and moisture-equilibrated coals (EM coal sample)

Figure 4.35(c) depicts the difference in sorption that was observed for the low rank EM coal. Due to insufficient sample, the higher moisture simulation of ~4% could not be carried

out. However, the trend is comparable to the TN and SL samples as can be clearly observed from Figure 4.36. Regression analysis shows good second order polynomial fits; R^2; SL= 0.983, TN=0.958 and EM = 1. Sorption decreases almost linearly for every 1% of moisture increase, until the maximum coal saturation is approached at around 4%.

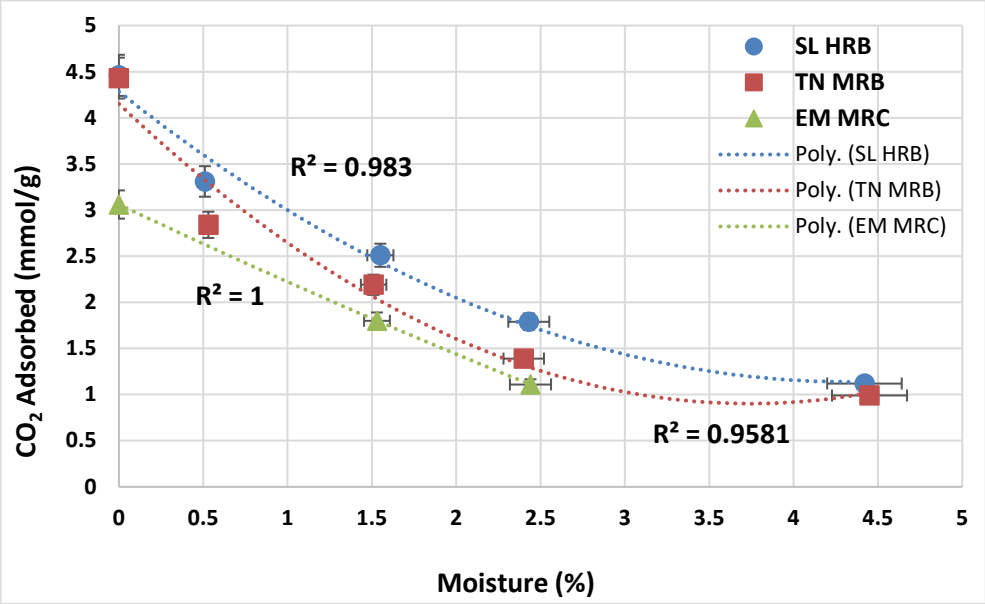

Figure 4.36: Trend of adsorption capacities of CO_2 vs dry to moisture-equilibrated coals

In addition to confirming the negating effect that moisture has on CO_2 adsorption, Figures 4.35(a) – 4.35(c) also clearly show that pressure increase does indeed cause the coal adsorption capacity to increase. At pressure ~20 bars, the adsorption rate increases for both wet and dry coal samples. Between 20 bars and 80 bars, the adsorption rate gradually changes to a high adsorption rate which means between those pressures more CO_2 is adsorbed. Above 80 bars, the adsorption rate is constant or very little adsorption occurs. This change in pressure represents the CO_2 molecules that have left the gas phase and adsorbed onto the coal.

These results show a comparative trend; however, they are more than double the findings of Day *et al*., (2008b), who averaged a decrease in sorption of approximately 30% for a 3% moisture increase. Again, this degree of variance is most definitely due to the adsorption methodology / technique, sample size, coal types and heterogeneity of samples

tested, i.e. differences in both rank and variances in maceral and mineral matter as discussed in sections 4.5.1, 4.5.3.1 and 4.5.3.2, respectively. Another important point to note is that coals generally show even more complex sorption behaviour for a few reasons: physical properties of coal may be anisotropically altered by CO_2 and its acidic solution in water, may react with the organic or mineral matter present in the coal matrix (Sakanishi *et al*., 2001).

The study of moisture effects are very integral to evaluation of coal-CO_2 sorption sites. As, even if initially dry, the seam will certainly become wet as a result of drilling operations, fracturing of the coal bed and over-lying strata, and the deposition of a combustion gas which may contain residual water of combustion. Thus, an aqueous phase will be present and will vary in composition according to its source and the nature of the coal bed and the surrounding minerals with which it is in contact (Schroeder and Ozedemir, 2009).

4.7 RESULTS FOR TEMPERATURE DIFFERENCE: CO_2 SORPTION TESTS

Temperature has been found by many researchers to have a considerable impact on gas adsorption calculations and adsorption behaviour (Saunders and Yang, 1985; Levy *et al*., 1997; Krooss *et al.,* 2002; Ozdemir, 2004; Azmi *et al*., 2006; Crosdale *et al*., 2008; Qing-Ling *et al.,* 2008; Deishad *et al*., 2009). While adsorption rate controls the equilibrium time, adsorption capacity determines the magnitude of swelling and shrinkage of the coal sample (Pan and Connell, 2007; Qu *et al*., 2010). It was found that the adsorption rate in some instances increases with increasing temperature, but the effect of temperature on sorption capacity is related to coal rank (Crosdale *et al*., 2008).

In the absence of external factors, underground temperatures tend to be fairly constant, but increases with depth are in contrast with injection of CO_2 due to its' supercritical nature. Because the adsorption of CO_2 is exothermic, it will provide a heat source, at least during the active pumping phase of sequestration. Also, some sequestration scenarios would provide additional heating mechanisms, such as by the dissolution of co-sequestered acid gases (SOx, NOx) or by reaction with residual oxygen in the flue gas (Bustin, 2002). Therefore, temperature is a very important parameter to consider in the adsorption capacity of coals.

Five (5) SA coals were assessed to determine the effect that temperature has on adsorption behaviour of CO_2 at two different temperatures (35°C and 55°C), up to a pressure of 80 bars. Table 4.9 summarises the final amounts of CO_2 adsorbed (mmol/g) for both temperatures tested and the calculated percentage reduced (decreased) adsorption between temperature of 35 to 55 ^oC.

Table 4.9: Temperature difference and CO_2 sorption capacities

Sample ID.	V_oR_{mr} (%)	Micro-pore area (m^2/g)	Max Pore volume (m^2/g)	Pressure (bar)	CO_2 Adsorbed (mmol/g)		Decreased Adsorption (%)
					35 °C	55 °C	
SF	0.65	153.54	0.035	79	2.63	2.28	35
BL	0.70	149.67	0.034	81	2.58	2.05	53
TN	1.26	108.41	0.019	80	3.47	2.75	72
AN	2.91	199.19	0.046	78	2.55	2.08	47
SL	3.49	170.67	0.039	78	3.25	2.76	49

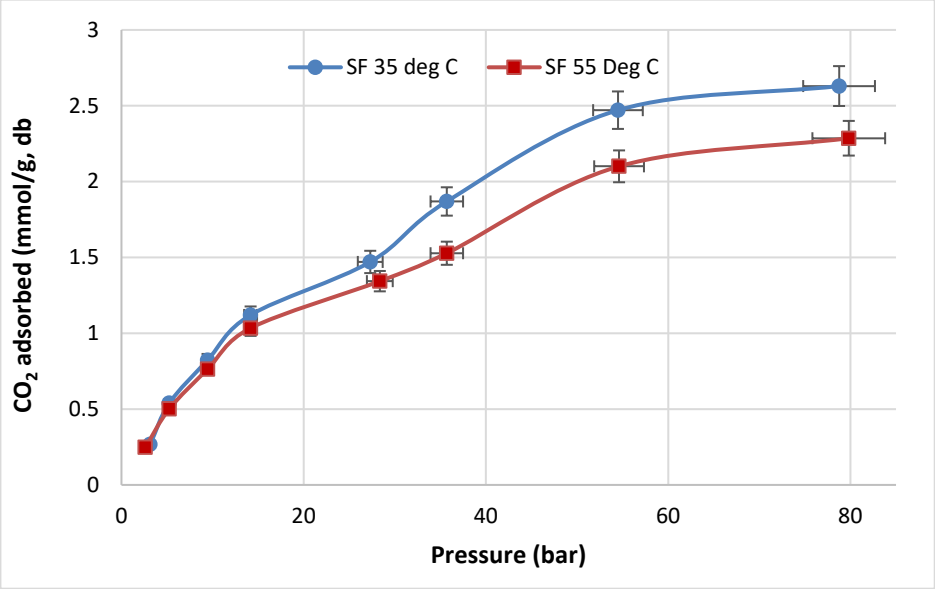

Figure 4.37(a): Temperature vs adsorption capacity (mmol/g) of SF coal ($\%R_oV_{mr}$ =0.65)

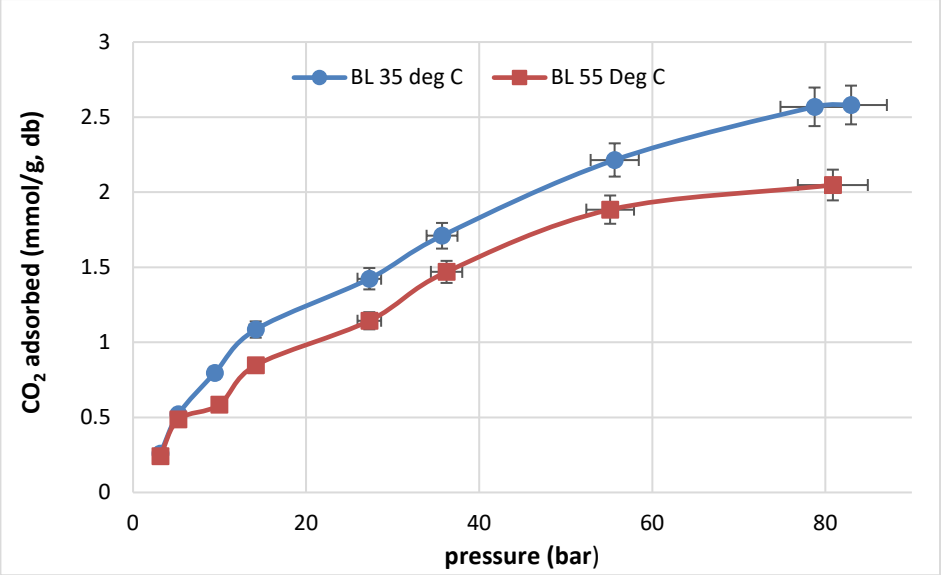

Figure 4.37(b): Temperature vs adsorption capacity (mmol/g) of BL coal (%R_oV_{mr} =0.7)

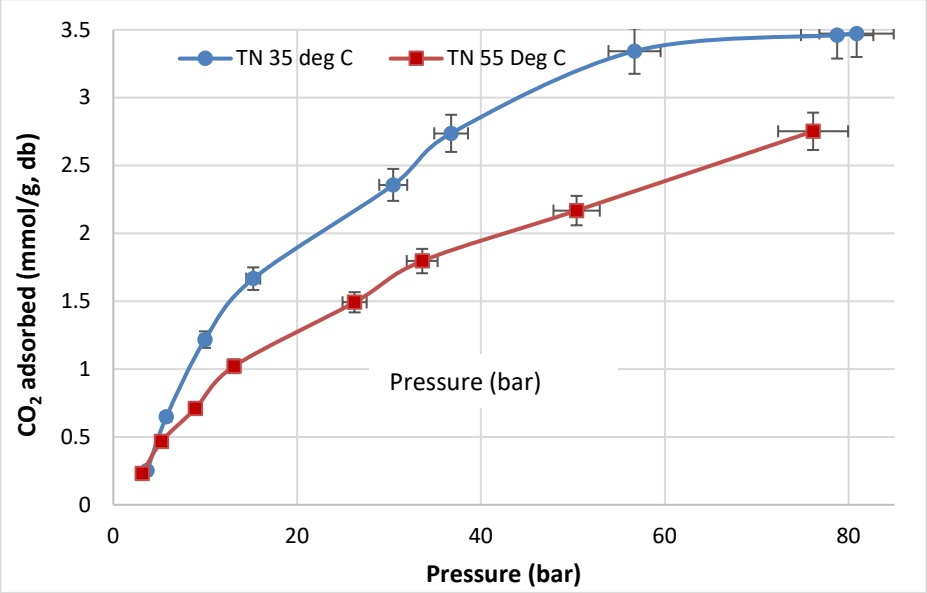

Figure 4.37(c): Temperature vs adsorption capacity (mmol/g) of TN coal (%R_oV_{mr}=1.26)

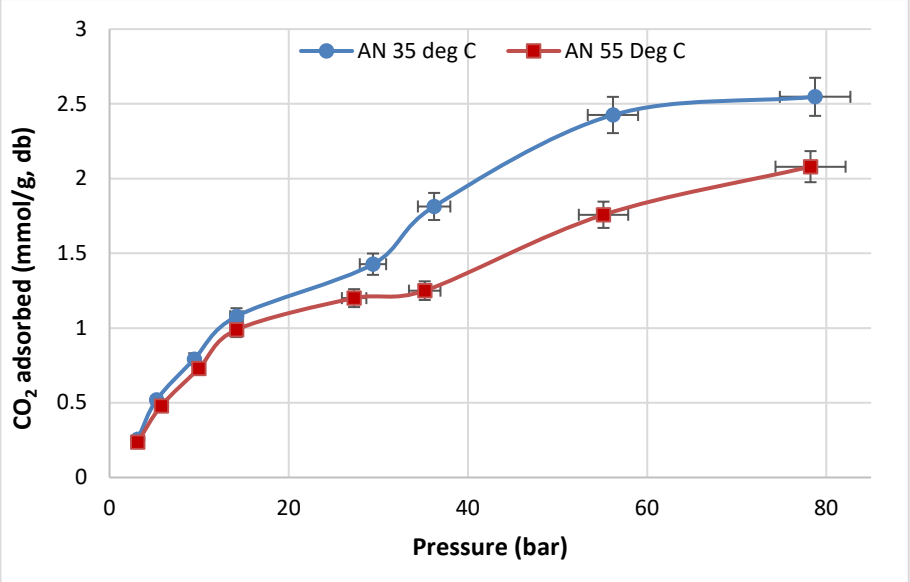

Figure 4.37(d): Temperature vs adsorption capacity (mmol/g) of AN coal (%R_oV_{mr}=2.91)

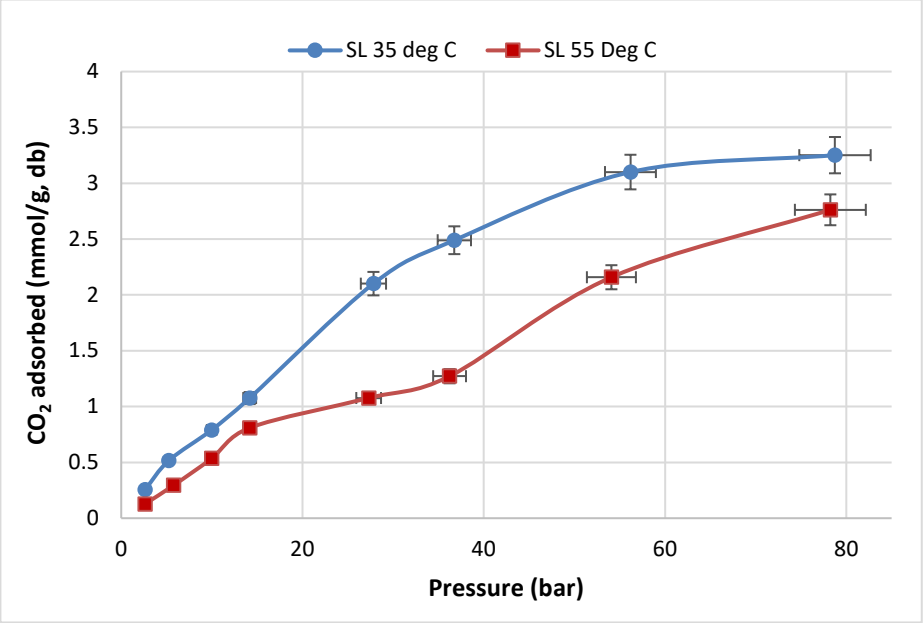

Figure 4.37(e): Temperature vs adsorption capacity (mmol/g) of SL coal (%R_oV_{mr} =3.49)

From Figures 4.37(a) to 4.37(e), it can clearly be seen from experimental test work conducted on these five (5) SA coal types, that an increase in temperature hinders the amount of CO_2 adsorbed per each coal type; apparently irrespective of coal type or rank. Table 4.9 summarised the amounts adsorbed and average decreased sorption (mmolg)

noted. These results exhibiting decreased sorption with increased temperature are in agreement with discussions from other researchers mentioned in section 2.12.4 (For MRC coals; Azmi *et al.,* 2006*;* Qing-Ling, 2008; Deishad *et al.*, 2009; Levy *et al*., 1997; Ozdemir, 2004; Oldenburg, 2007; Sakurovs, *et al.,* 2008 and for HR coals; Yang and Saunders, 1985; Krooss *et al*., 2002).

It is prominent that TN sample had the most marked decrease in sorption (72%) at the higher temperature of 55 ^{o}C compared to the other samples tested. This is most likely due to it having the lowest evaluated micro pore area (108.41 m^2/g) and displayed the least Langmuir monolayer capacity (70.16 m^2/g). Thermodynamically, this is due to the fact that the increased kinetic energy of the CO_2 molecules due to increased temperature, makes it difficult for CO_2 to remain physically adsorbed on larger macro and mesoporous coal such as TN (Deishad *et al*., 2009). This could be indicative that the adsorption volume of gas mainly concentrates in micro pores and it is influenced by meso pores at the same time for different coals.

Macroscopic mass transport is obtained through the gas flow equations incorporated with porosity and permeability models. The fluid properties, like viscosity and density, are defined as a function of temperature, and the effect of temperature on the gas adsorption and thermal expansion is taken into account through the Langmuir coefficient and Joule–Thomson process. It is quite obvious from thermodynamic principles that an increased temperature with increasing pressure will display an inverse relationship, and hence lower overall CO_2 sorption will occur. The reason for such trend is due to the fact that thermodynamically, at higher temperatures, molecules always favour the gas phase compared to the adsorbed phase (Zhang *et al.,* 2011). It is for this reason that the governing field equations need to be solved to obtain the general field variables like reservoir pressure and temperature, and to predict the effect of temperature on the coal porosity and permeability change during the CO_2 injection and adsorption processes (Qu *et al.,* 2012).

4.7.1. Isosteric Heat of adsorption

The isosteric heats of adsorption has been calculated for the two temperatures tested to evaluate the fundamental thermodynamic characteristics of CO_2 adsorption on the five (5) coals tested, using the fundamental theory based on the Clausius-Clapeyron equation. The isosteric heat of adsorption calculation methodology as detailed in section 3.4.2.2 was employed (Ma *et al*., 2014).

The relationship of pressures (logarithmic); ln (P/n) and adsorption capacity; n (mmolg) in the adsorption process are presented in Figure 4.38(a) – (e) showing that the linear curves fit the experimental test data within this pressure and low temperature range, which confirms Henry's law (Ma *et al*., 2014). Linear regression fits (slopes and intercepts) from Figures 4.38(a) – (e) were used to determine the Isosteric adsorption line in the adsorption process data, which is presented in Appendix C (Figures C1 – C5).

Table 4.10 summarises the calculated theoretical heats of adsorption (KJ/mol) and CO_2 adsorbed (mmol/g) data of the five coals evaluated at temperatures of 35 and 55 ^oC.

Table 4.10: Calculated Heat of adsorption

No.	***Sample ID***	***R_oV_{mr} (%)***	***Volatile Matter (%)***	***Mineral Matter (Vol%)***	***Heat of Adsorption (KJ/mol)***		***Δ KJ/mol***
					35	***55***	
1.	SF	0.65	30.1	12.4	-26.5	-21.9	-4.6
2	SL	3.49	5.8	1.5	-34.5	-24.2	-10.3
3	AN	2.91	5.7	4.6	-35.5	-28.7	-6.8
4	TN	1.26	22.2	8.3	-35.4	-27.0	-8.4
5	BL	0.70	29.1	6.2	-39.9	-32.0	-7.9

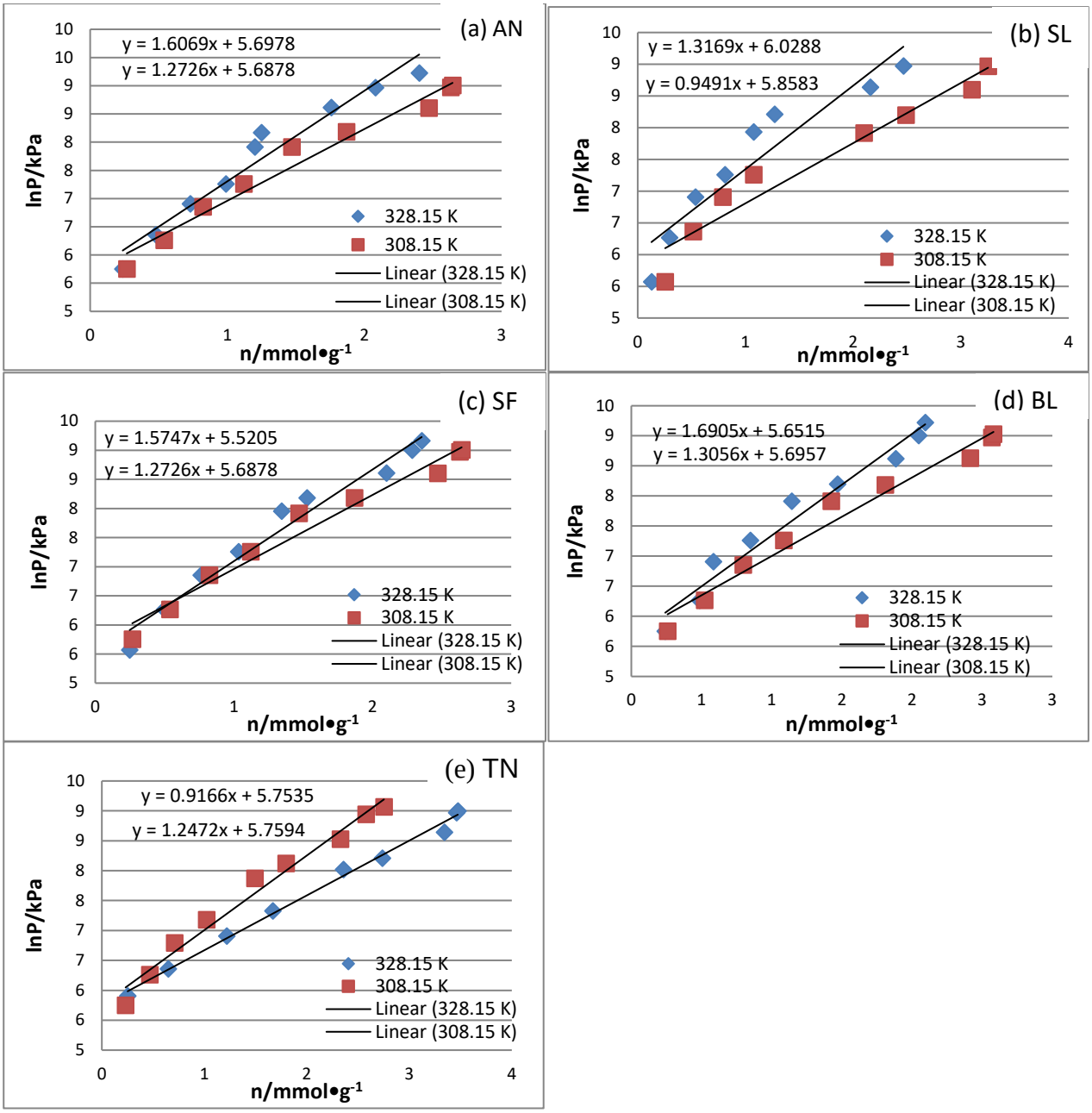

Figure 4.38 (a) - (e): Relationship of pressures (logarithmic) and adsorption capacity (mmol/g) in the adsorption process

According to the kinetic theory of gas, a higher temperature means that the average kinetic energy of the CO_2 molecule is higher, and therefore, the interaction among CO_2 molecules in a higher temperature system cannot be neglected. For a low-temperature system (~303.15-308.15 K), the interaction energy between a CO_2 molecule and coal surfaces dominates the process instead of the interaction of CO_2 molecules within Henry's region. This process can be treated as a monolayer adsorption process (Tang *et al*., 2015).

Results confirm that the calculated heat of adsorption (KJ/mol) and the adsorption capacity (mmol/g) are positively correlative (Figure 4.39). Also, the adsorption heat increases linearly with rising pressure. These calculations indicate that the maximum heat of adsorption in process of elevated pressure (adsorption) belongs to physical adsorption. The negative value indicates that the adsorption of CO_2 is an exothermic process

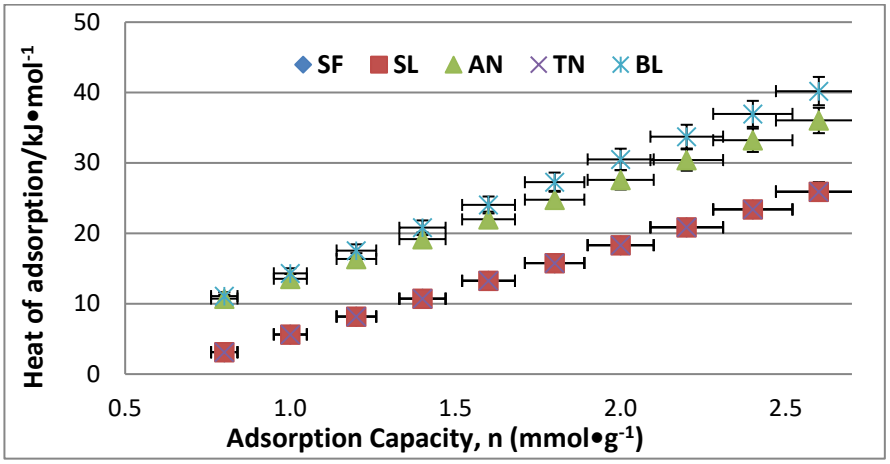

Figure 4.39: Isosteric heat of adsorption (KJ/mol) versus adsorption capacity (mmol/g)

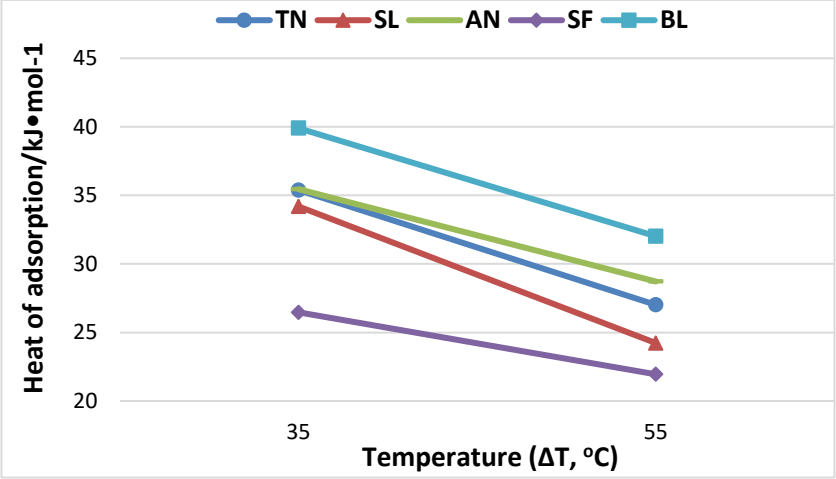

Figure 4.40: Isosteric heat of adsorption (KJ/mol) versus temperature change (°C)

The effect of increasing temperature is to decrease the equilibrium adsorption capacity of the coal. This is expected because higher temperatures increasingly favour the gas-phase

due to the T∆S entropy term in the free energy expression. This means that otherwise equivalent, but deeper, warmer seams will adsorb less CO_2 at a given pressure than shallower, cooler ones. Thermodynamics would suggest that the most active sites would be occupied first and provide the greatest heat of adsorption. Thus, it is to be expected that the heat evolved per mole of CO_2 at low coverage would be higher than the heat evolved at high coverage (Nodenski, 1998; Nishino, 2001).

The range of heats of adsorption for these coals was between 21.9 and 39.9 kJ/mol (Table 4.10), regardless of the coal rank. Comparing the differences in mineral matter and volatile matter for the 5 coals also showed no obvious related correlation. The influence of differing maceral matter content could be possibly the reason for the results in variable heats of adsorption as variable vitrinite, inertinite and liptinite macerals have variable porosity (as was discussed in detail in Section 4.5.3.3).

Coal has been proven to contain a wide variety of adsorption sites which are dependent on coal type and in turn the porosity and permeability due to the varying macro, meso and micro-pores of a specific coal (as discussed in Section 4.5). From Figure 4.41, it is observed that as maximum pore volume (0.035-0.046 m^2/g) and micro pore surface area 153.54 – 199.19 m^2/g) increases an increase in heat of adsorption can be seen (at a temperature of 35 ^oC: 26.5 – 35.5 KJ/ mol and at 55^oC: 21.9 – 28.7 KJ/mol) i.e. isosteric heat of adsorption increases with increasing pore surface area, as expected from the enhanced solid-fluid interaction potential in smaller pores (Sakurovs, *et al.,* 2008; Marsh 2001). This is attributed to the increase of higher micro-porosity as expected from the enhanced solid-fluid interaction potential in smaller pores. Although the structure of the coal is probably the most important factor affecting the primary adsorption process, the surface chemistry is another important factor which can affect the characteristic adsorption energy difference between the organic and inorganic adsorption process (Marsh 2001).

However, coals BL (32 KJ/mol) and TN (27 KJ/mol) exhibited higher adsorption energy, but do not show the apparent correlation with regard to the micro pore surface area and maximum pore volume, as determined from BET results (Section 4.3). This could mean that it is very likely that the microporous networks within coals, in which most of the sorption occurs, can be considered to be imperfectly connected, limiting the accessibility of

adsorbing molecules to some pore spaces that are otherwise large enough to accommodate them (Bae *et al*., 2009).

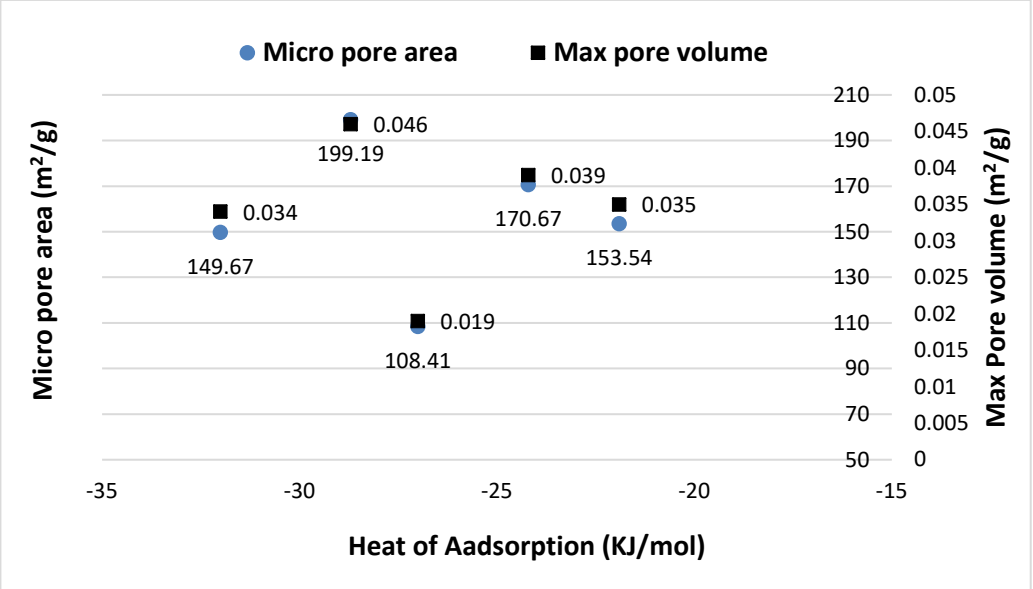

Figure 4.41: Isosteric heat of adsorption (KJ/mol) versus micro pore area and maximum pore volume (m^2/g)

The range and magnitude of these isosteric heats of adsorption values suggests a physical adsorption mechanism (physisorption), most possibly multilayer formation, rather than a chemisorption mechanism occurred as it has low enthalpy of adsorption i.e. ΔH adsorption is in the range of between 20-40KJ/mol (Nodenski, 1998; Schroeder & Ozdemir, 2009; Zeng *et al*., 2009; Ma *et al*., 2014). It should be noted that this approach is strictly only valid for an ideal gas. Since the isosteres used for the calculation are derived from isotherms measured at pressures between 3 – 80 bar, calculated heats of adsorption should be viewed with caution and were only used here to confirm that the observed process was physisorption rather than chemisorption.

This study on temperature variance is very pertinent to CO_2 sequestration as the geothermal gradient increases with coal seam depth (Azmi *et al.,* 2006; Zhang *et al.,* 2011), (Figures 2.14 and 2.15, and Section 2.71). In undertaking coal seam adsorption capacity calculations it is vital that increases in geothermal temperature with coal seam depth be

considered and evaluated carefully to maximise sorption potential injection and storage capacity of a particular seam or sink.

4.8 Modelling of all CO_2 experimental adsorption data

The CO_2 (natural gas) isotherms generated for SA coals tested, can be considered to be representative of in-situ coal seam reservoir P-T conditions, and conform to the Type 1 isotherm shape (Gregg & Sing, 1985), as discussed in Section 2.10 and 4.5. The theoretical Langmuir, Freundlich and Temkin adsorption models (as discussed in section 2.11) were used in modelling of the experimental data obtained for SA coals and the different conditions tested (i.e. experimental results detailed for CO_2 adsorption on dry, degassed coals (Section 4.5), moisture simulated coals (Section 4.6), and effect of temperature on adsorption (Section 4.7) to determine the optimum sorption equation to be applied to adsorption isotherm data.

The models are most commonly used for micro-porous solids such as natural coal and are also most extensively used in cases of single or pure gas adsorption systems where no other competing gases might cause interferences in the sorption process. Experimental data and modelling data are tabulated in Table C1 (Appendix C). All measured CO_2 isotherms were approximated by the excess sorption function given in equation (3). Maximum excess sorption (mmol/g), as well as the fitting parameters for the respective model equations were determined and adjusted by a least-squares optimization procedure, for the individual isotherms.

Linear regression plots for the three models were parameterised:

1) Langmuir: P/N_s (Pressure vs excess amount CO_2 adsorbed in mmol/g) versus P (pressure) where carried out to obtain the gradient and intercept to calculate the Langmuir volume which can be found in Appendices D, E, F and G.
2) Freundlich: a logarithmic plot of log q (amount CO_2 adsorbed) versus log P (pressure) was done to determine the isotherm constants, *n* and A. Regression plots can be found in Appendices D, E, F and G.

3) Temkin: q_e (amount CO_2 adsorbed) versus ln P (pressure) where plotted (can be found in Appendices D, E, F and G) out to obtain the gradient and intercept to determine the isotherm constants, b_T and A_T.

4.8.1 Modelling of CO_2 Adsorption Data

The fitting parameters for the three sorption models, Langmuir, Freundlich and Temkin, used to characterise the experimental CO_2 adsorption data is summarised in Table 4.11.

Figures 4.42 (a) – (j), shows the fitting of the experimental adsorption data obtained for the 10 SA coals, compared with the theoretical adsorption models; Langmuir, Freundlich and Temkin. Linear Regression analysis data and their corresponding plots can be found in Appendix E.

Table: 4.11: Summary of adsorption model parameter data for CO_2

Coal ID	CO_2 (mmol/g)	Langmuir			Freundlich			Temkin		
		R^2	b	a	R^2	n	K_F	R^2	b_T	A_T
AN	2.17	0.994	2.84	0.032	0.915	1.31	0.098	0.991	5889.5	1.69
IN	1.82	0.991	2.30	0.049	0.912	1.76	0.182	0.980	7740.0	2.85
GN	1.33	0.994	1.62	0.058	0.864	3.53	0.387	0.982	11645	4.65
SF	1.64	0.995	1.88	0.083	0.903	3.29	0.419	0.985	9084.9	3.29
SM	1.79	0.994	2.38	0.037	0.828	2.71	0.375	0.916	7535.2	2.49
TN	1.99	0.997	2.53	0.047	0.961	4.31	0.742	0.978	6149.7	1.82
EM	1.19	0.994	1.39	0.048	0.855	4.25	0.378	0.986	8280.4	0.48
SL	1.95	0.994	2.38	0.053	0.949	3.45	0.554	0.979	6569.1	1.77
WG	1.10	0.994	1.41	0.056	0.763	4.35	0.407	0.916	7535.2	2.49
BL	1.78	0.994	2.13	0.057	0.881	2.92	0.387	0.968	7544.1	2.15

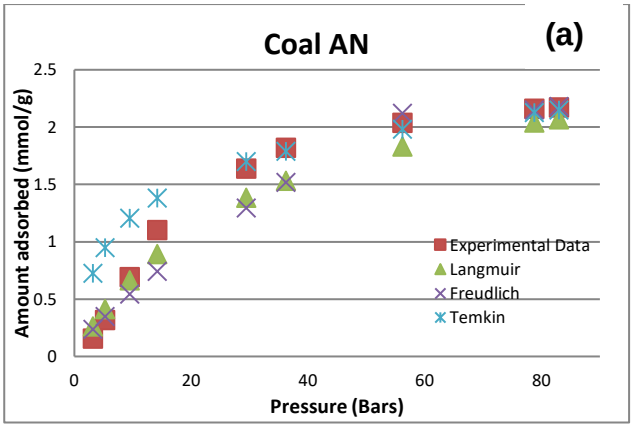
Coal AN
(a)
Amount adsorbed (mmol/g)
Pressure (Bars)
Experimental Data
Langmuir
Freudlich
Temkin

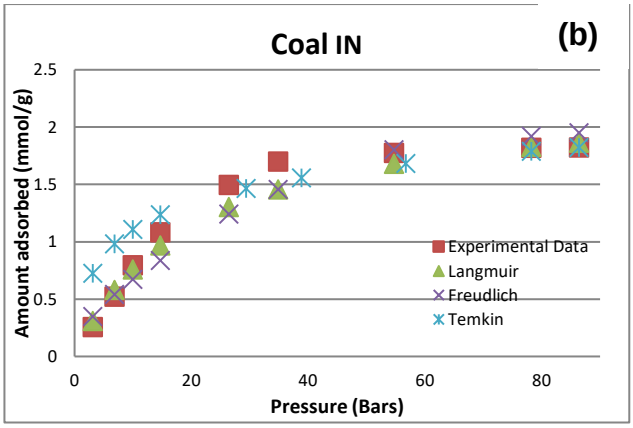
Coal IN
(b)
Amount adsorbed (mmol/g)
Pressure (Bars)
Experimental Data
Langmuir
Freudlich
Temkin

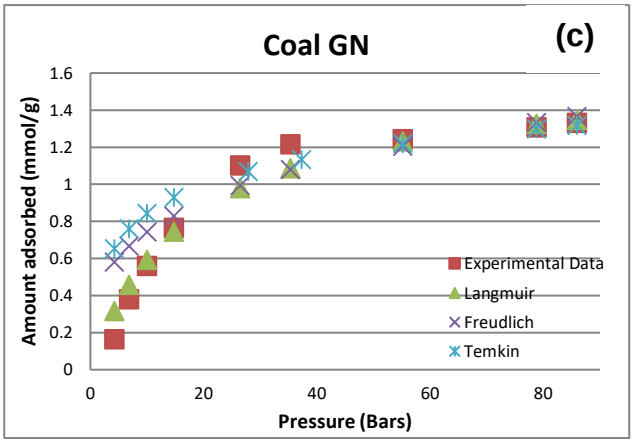
Coal GN
(c)
Amount adsorbed (mmol/g)
Pressure (Bars)
Experimental Data
Langmuir
Freudlich
Temkin

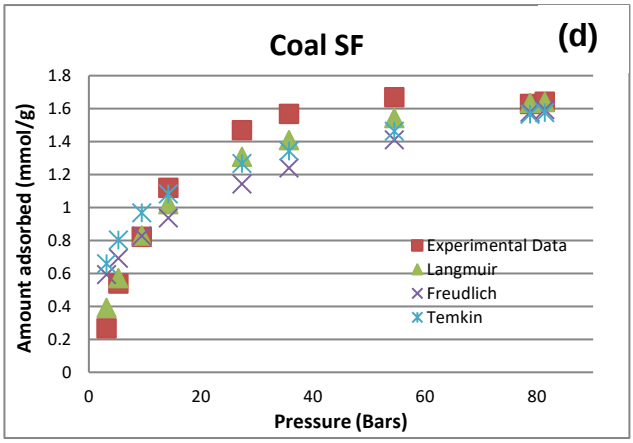
Coal SF
(d)
Amount adsorbed (mmol/g)
Pressure (Bars)
Experimental Data
Langmuir
Freudlich
Temkin

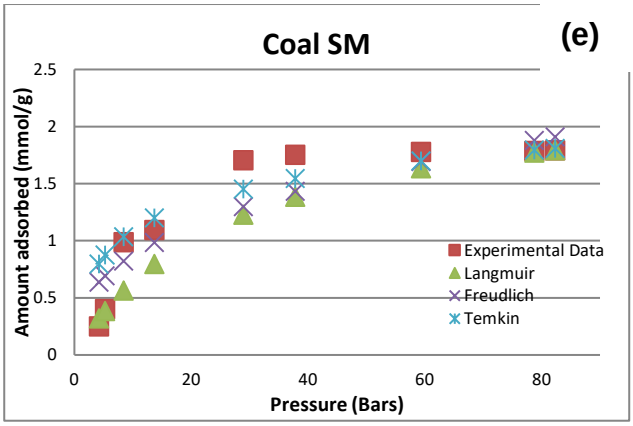
Coal SM
(e)
Amount adsorbed (mmol/g)
Pressure (Bars)
Experimental Data
Langmuir
Freudlich
Temkin

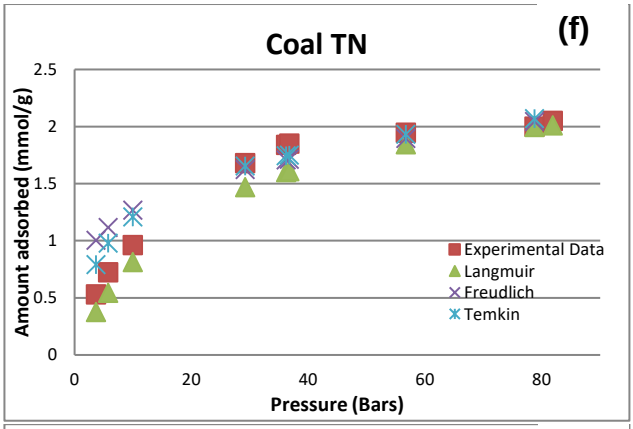
Coal TN
(f)
Amount adsorbed (mmol/g)
Pressure (Bars)
Experimental Data
Langmuir
Freudlich
Temkin

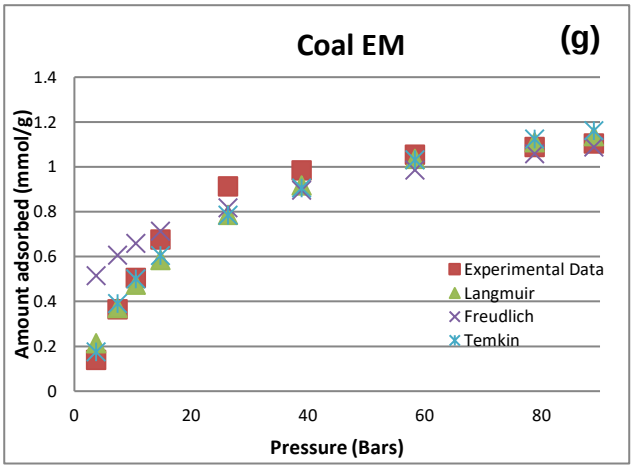
Coal EM
(g)
Amount adsorbed (mmol/g)
Pressure (Bars)
Experimental Data
Langmuir
Freudlich
Temkin

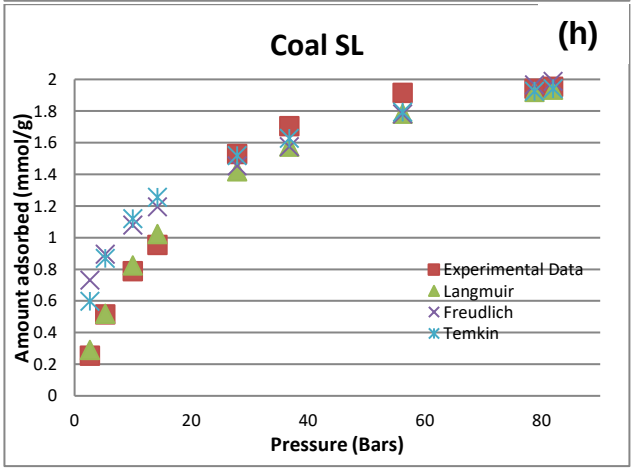
Coal SL
(h)
Amount adsorbed (mmol/g)
Pressure (Bars)
Experimental Data
Langmuir
Freudlich
Temkin

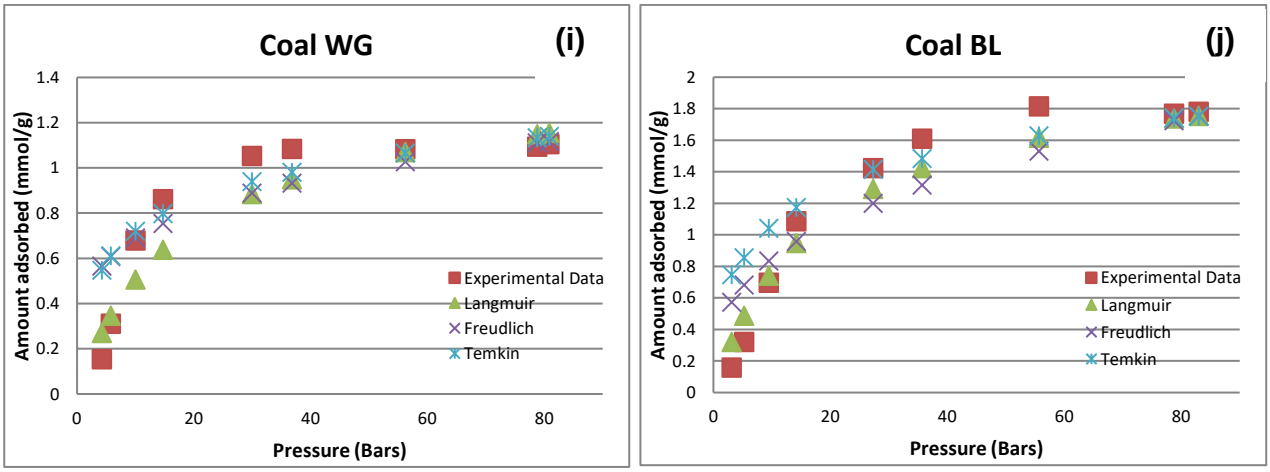

Figure 4.42 (a) – (j): Comparing experimental CO_2 data and adsorption models of all SA coals (10)

- ***Langmuir:***

The suitability of this model is validated from the good correlation coefficient values achieved i.e. R^2 values > 0.99. Langmuir monolayer coverages range from 1.39 mmol/g (for low rank coal EM, having a very high volatile matter, 49.8%)) to a maximum of 2.84 mmol/g (for high rank coal AN). The second lowest monolayer coverage was found for the WG coal, 1.41 mmol/g, which reported the highest ash content of 39.35%. The consequent lower monolayer amounts may therefore be attributed to surface heterogeneity (Marsh, 2001).

- ***Freundlich:***

Correlation coefficients, R^2 ranged from 0.763 (WG) – 0.961 (TN), showing unsuitability of the Freundlich model for CO_2 adsorption estimation. The high adsorbing coal AN had the lowest K_F value of 0.098. Also noted, was that R^2 values decrease with decreasing sorption potential of the specific coal.

- ***Temkin:***

Calculated correlation coefficients, R^2 are greater that 0.97 (with the exception of SM and WG, both at 0.916), indicating that it is more or less an appropriate model for CO_2 adsorption estimation. The A_T values range from 0.48 (EM) – 4.65 (GN). While b_T values were found to range from 5889.5 J/mol (5.89 KJ/mol) for coal AN to a maximum of 11 645 J/mol (11.645 KJ/mol).

Overall, the Langmuir model, had the best fit to the experimental CO_2 adsorption data. For all coals, both the Temkin and Freundlich models seem to over-estimate the sorption amounts at sub-critical pressures ranging less than 30 bar. Temkin however overlays very well at super-critical pressure in excess of 75 bar.

4.8.2 Modelling of CO_2 Adsorption data: Effect of Moisture

Fitting parameters of the three sorption models used to characterise the experimental CO_2 adsorption data for moisture simulated coal samples is summarised in Table 4.12.

Table: 4.12: Summary of adsorption model parameter data for moisture simulated samples

Model	**Langmuir**			**Freundlich**			**Temkin**		
Parameter	**R^2**	**b**	**a**	**R^2**	**n**	**K_F**	**R^2**	**b_T**	**A_T**
SL dry/0%	0.994	15.27	0.004	0.994	1.134	0.09	0.98	1862.84	0.21
SL 0.51%	0.991	7.64	0.007	0.912	1.145	0.07	0.98	2564.01	0.22
SL 1.55%	0.994	4.55	0.021	0.926	1.940	0.30	0.98	4031.40	0.69
SL 2.43%	0.992	9.02	0.003	0.958	1.015	0.03	0.98	4489.15	0.23
SL 4.42%	0.994	1.32	0.069	0.93	2.119	0.16	0.99	9133.54	0.74
TN dry/0%	0.732	24.69	0.003	0.99	1.045	0.07	0.98	1916.47	0.23
TN 0.53%	0.994	5.066	0.014	0.87	1.227	0.09	0.98	2198.35	0.18
TN1.51%	0.982	3.214	0.028	0.96	1.485	0.13	0.98	3573.63	0.28
TN 2.40%	0.993	1.869	0.032	0.98	1.694	0.11	0.92	6052.35	0.28
TN 4.45%	0.994	1.321	0.036	0.99	1.790	0.09	0.98	9265.67	0.41
EM dry/0%	0.997	5.75	0.015	0.82	1.272	0.12	0.98	2899.13	0.35
EM 1.53%	0.997	2.24	0.048	0.83	1.774	0.18	0.98	5526.23	0.60
EM 2.44%	0.997	1.47	0.030	0.93	1.572	0.07	0.98	8614.52	0.38

Fitting of the experimental adsorption data obtained for three (3) selected moisture equilibrated SA coals are compared with the theoretical adsorption models; Langmuir, Freundlich and Temkin and are presented for coal SL in figure 4.43 (a) – (e), coal TN in Figure 4.44 (a) – (e) and coal EM in Figure 4.45 (a) – (e).

Coal SL Experimental data and Adsorption Models Compared

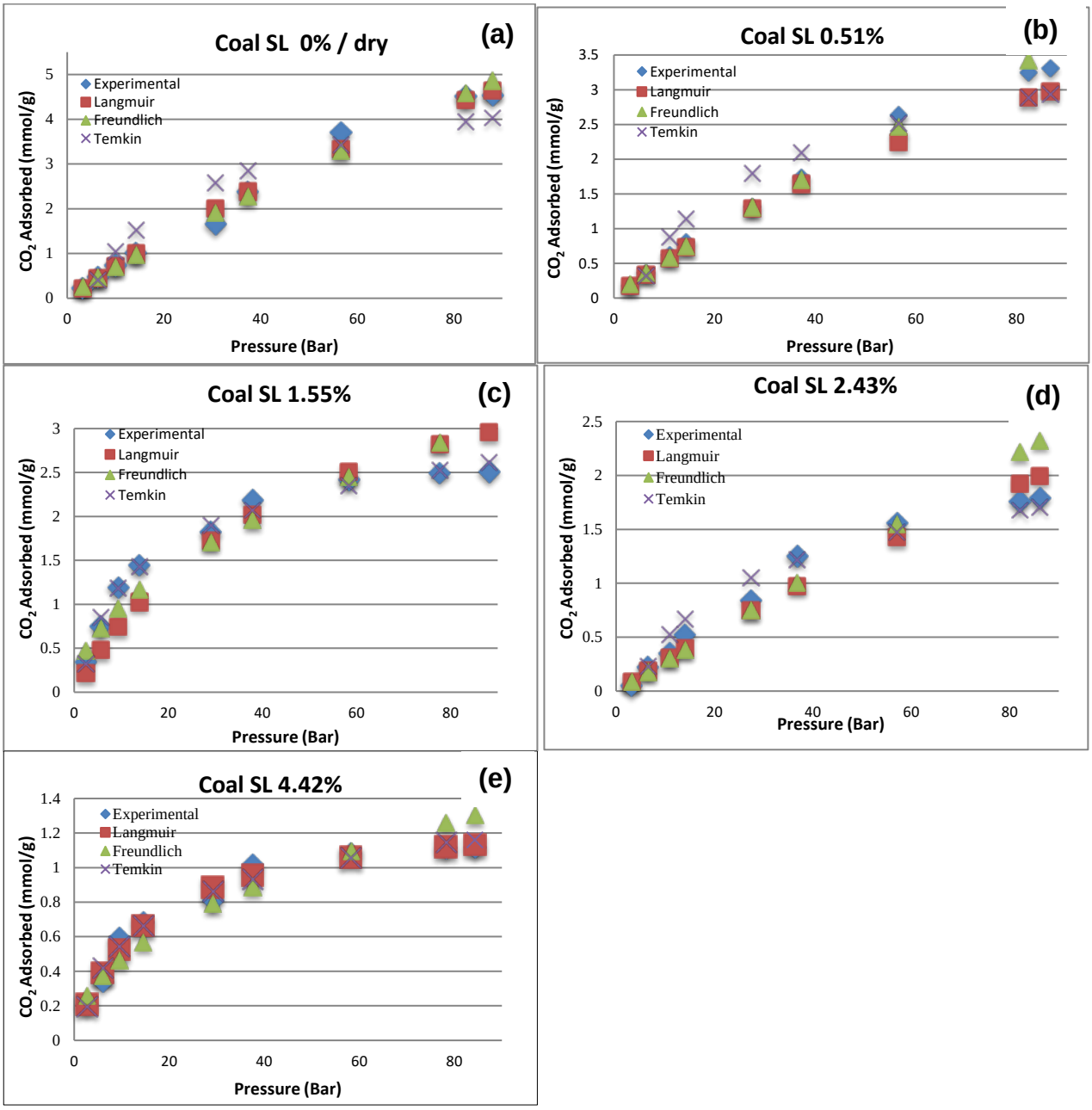

Figure 4.43 (a), (b), (c), (d), (e): Comparing experimental moisture simulated data of CO_2 adsorption and adsorption models for coal SL

Coal TN Experimental data and Adsorption Models Compared

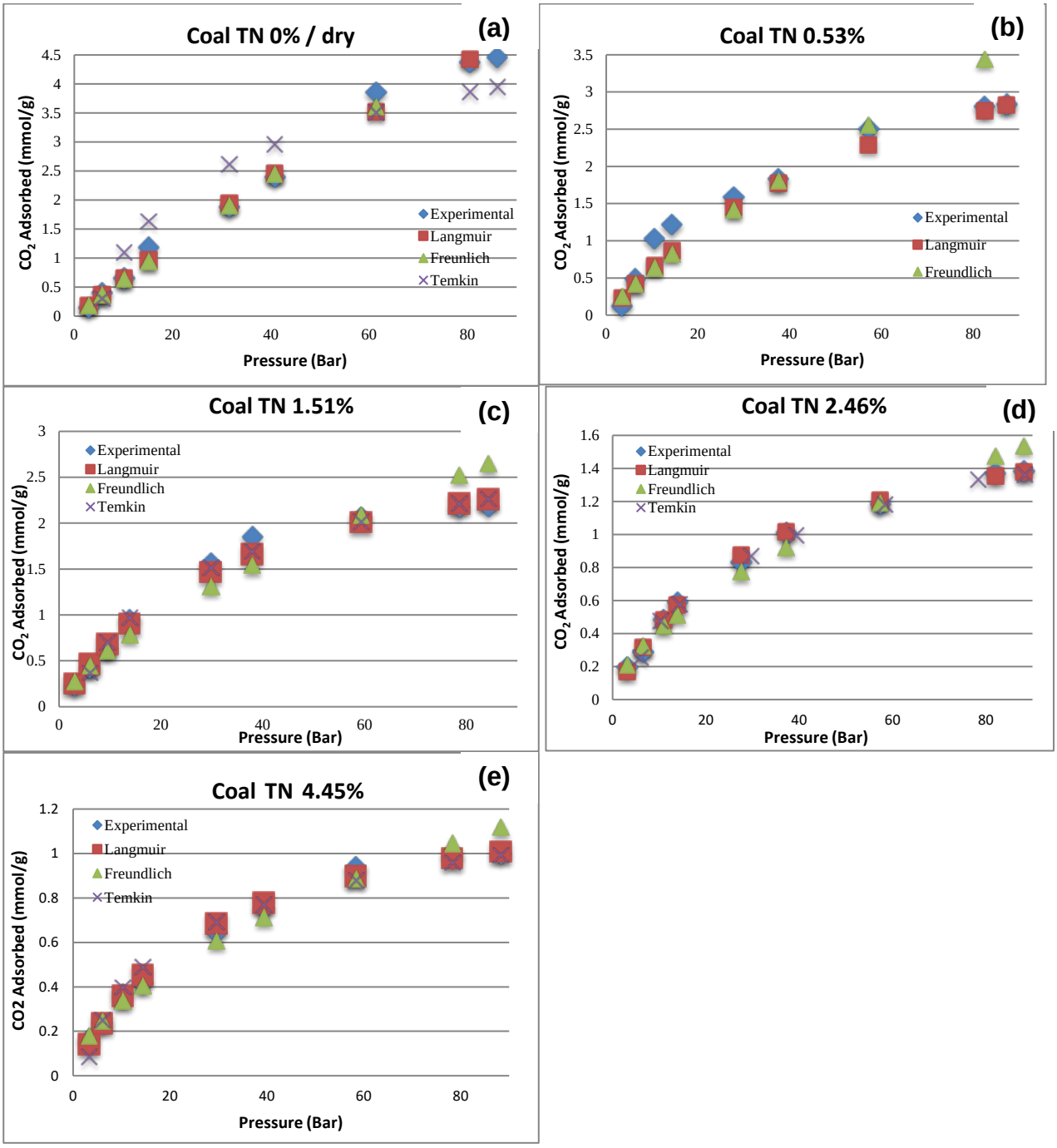

Figure 4.44: (a), (b), (c), (d), (e): Comparing experimental moisture simulated data of CO_2 adsorption and adsorption models for coal TN

Coal EM Experimental data and Adsorption Models Compared

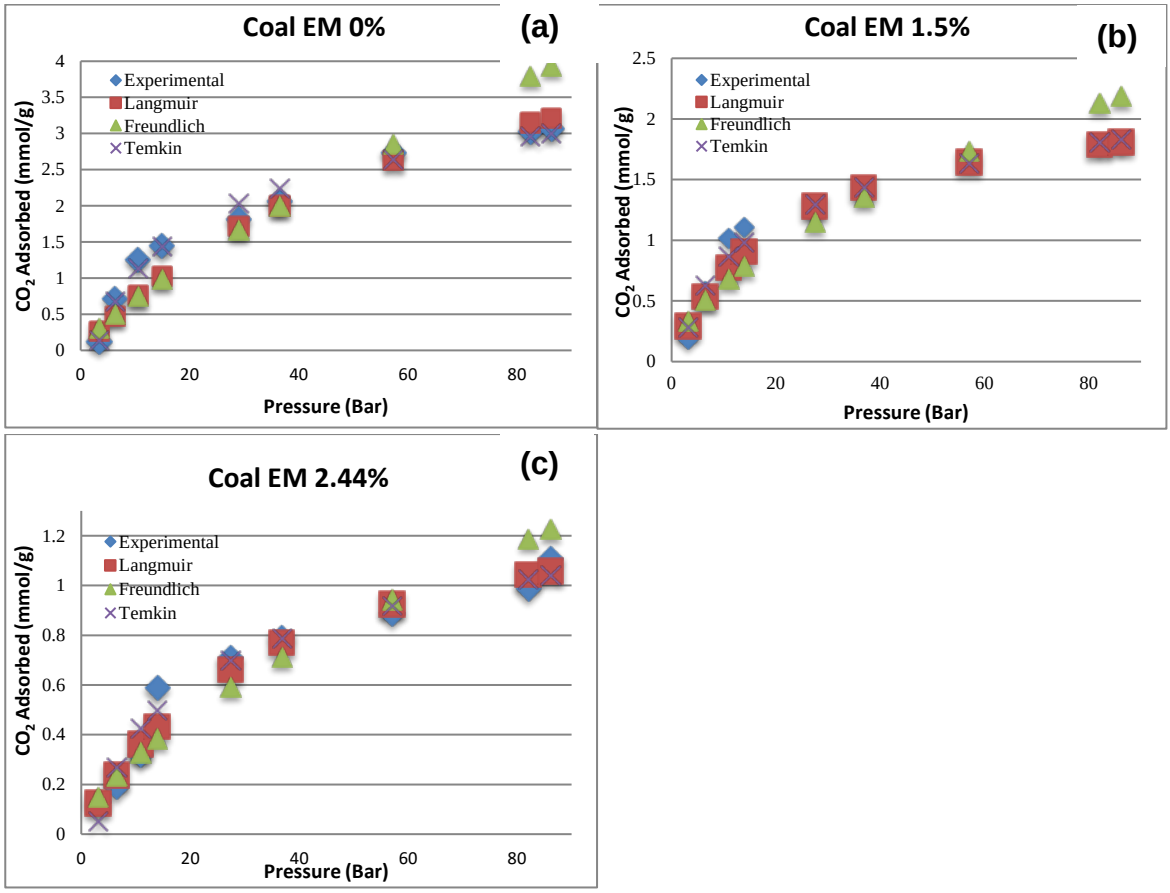

Figure 4.45 (a), (b) and (c): Comparing experimental moisture simulated data of CO_2 adsorption and adsorption models for coal EM

The equations used, are as detailed in section 2.11 (Theoretical adsorption Models). Comparison of the different models was done for three (3) of the different coal moistures tested: lowest (0%), intermediate (~1.51-1.55%) and highest (~4.42-4.45%) for two coals: TN and SL. Regression analysis data and the respective plots can be found in Appendix F.

As observed from Figures 4.43, 4.44 and 4.45, Langmuir and Temkin models seem to be the best fit as compared to the Freundlich model. The Freundlich model data for all samples and moistures is seen to overestimate the experimental data. From Table 4.12, it can be observed that the calculated Langmuir volume, b, showed incremental decrease with increased moisture content (Sakurovs *et al*., 2008).

In all comparative plots, for the different moisture equilibrated sorption tests, the Langmuir and Temkin proved more suited to modelling the moisture simulated experimental data as compared to the Freundlich model. The Freundlich model isotherm regression seems to hold better at sub-critical pressures and then starts to deviate as supercritical pressures are achieved. This proves that the Freundlich isotherm model cannot be used to model supercritical sorption for moist coals i.e. coals that generally exhibit greater inherent coal seam moisture (Ozdemir 2004).

4.8.3 Modelling of CO_2 Adsorption data: Effect of Temperature

Experimental sorption CO_2 data at the two tested temperatures (35 and 55^oC) were used to calculate the theoretical sorption employing commonly used empirical models to determine best model fit data. Tables 4.13 and 4.14 summarise the model fitting parameters data. Model regression plots for both temperatures; 35 and 55^oC can be found in Appendix G.

Table 4.13 Summary of model data at 35 ^oC

Model	***Langmuir***			***Freundlich***			***Temkin***		
Parameter	**R^2**	**b**	**a**	**R^2**	**n**	**K_F**	**R^2**	**b_T**	**A_T**
TN	0.98	4.21	0.017	0.86	1.31	0.148	0.99	2096	0.37
SL	0.99	4.24	0.018	0.91	1.47	0.377	0.92	2016	3.14
BL	0.98	3.81	0.016	0.97	1.51	0.159	0.91	2391	3.21
SF	0.98	3.91	0.015	0.97	1.51	0.075	0.97	3325	3.25
AN	0.98	4.58	0.026	0.97	2.15	0.159	0.91	2403	3.40

Fitting of the experimental adsorption data obtained for the five (5) selected SA coals are at temperature of 35 and 55 ^oC respectively, are compared with the theoretical adsorption models; Langmuir, Freundlich and Temkin and are presented for coals in Figures 4.46 (a) – (e) and Figures 4.47 (a) – (e).

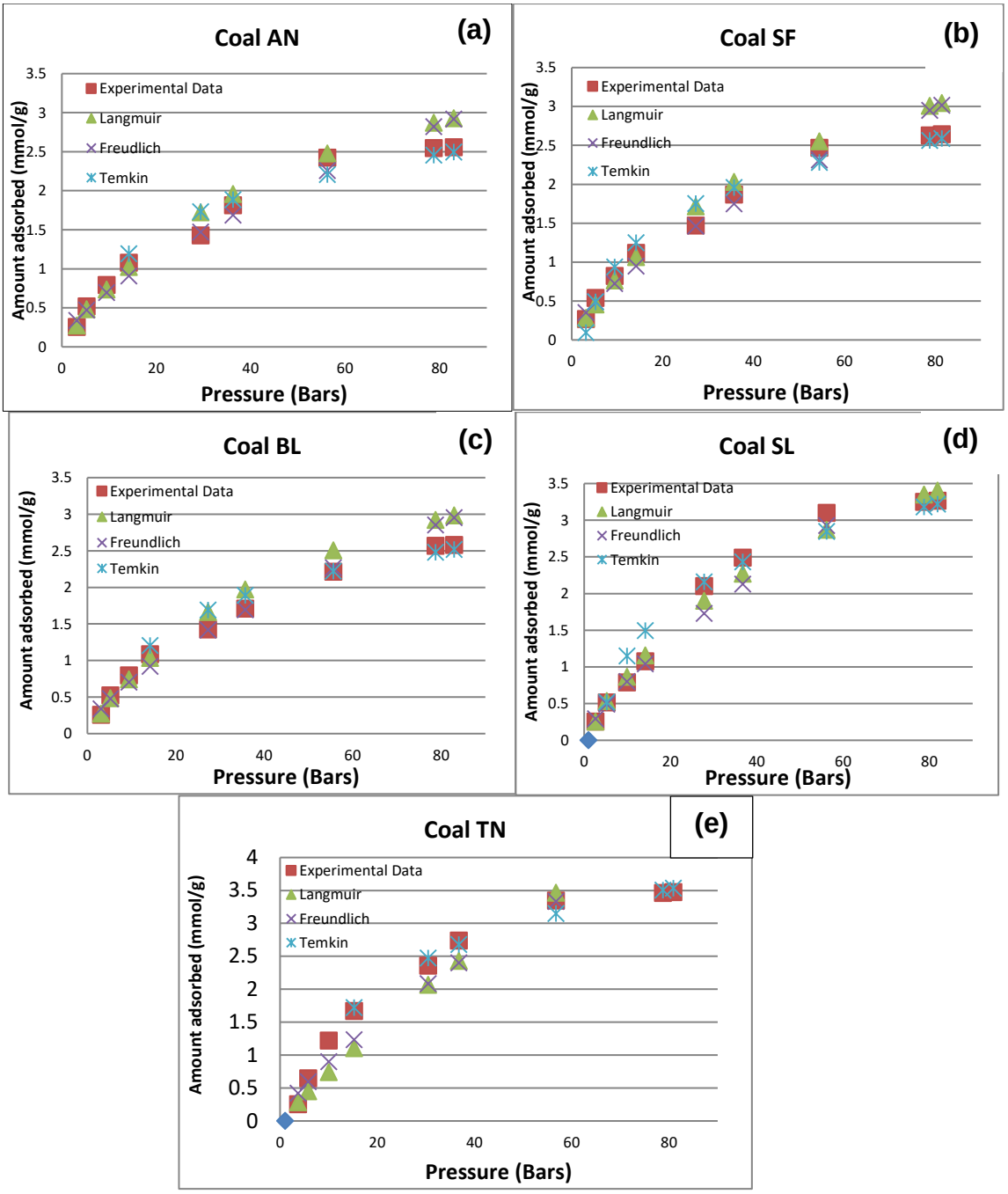

Figure 4.46 (a), (b), (c), (d and (e): Comparing experimental data of CO_2 adsorption and adsorption models for coals tested at 35°C

Table 4.14 Summary of compared model data at 55 ^{o}C

Model	*Langmuir*			*Freundlich*			*Temkin*		
Parameter	**R^2**	**b**	**a**	**R^2**	**n**	**K_F**	**R^2**	**b_T**	**A_T**
TN	0.99	2.55	0.027	0.93	1.36	0.074	0.84	2257	-
SL	0.98	2.63	0.028	0.91	1.48	0.075	0.98	3.047	0.16
BL	0.97	3.65	0.051	0.96	3.63	0.187	0.92	1031	3.83
SF	0.99	2.62	0.028	0.97	1.45	0.075	0.97	3048	0.17
AN	0.97	2.65	0.023	0.95	1.62	0.007	0.97	90849	0.38

Figures 4.47 (a) – (e) show the comparative fits of the theoretical models with the experimental data.

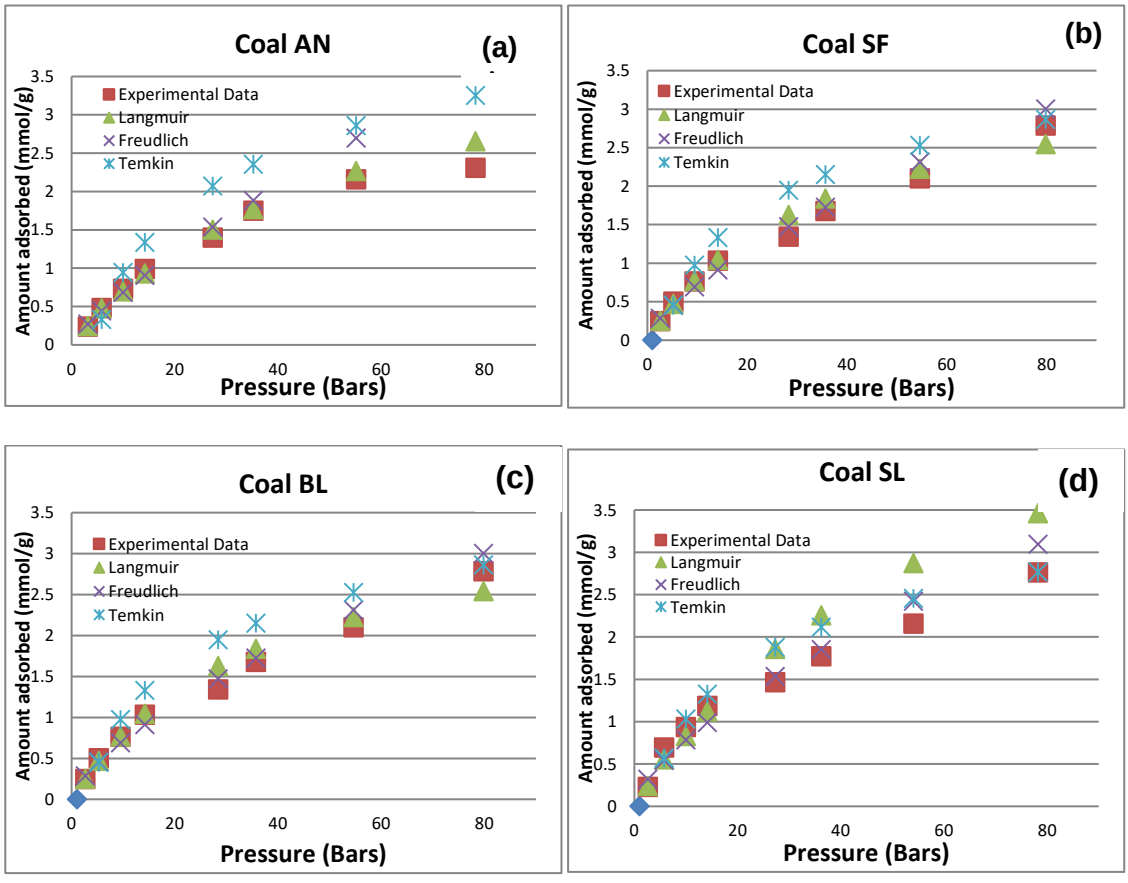

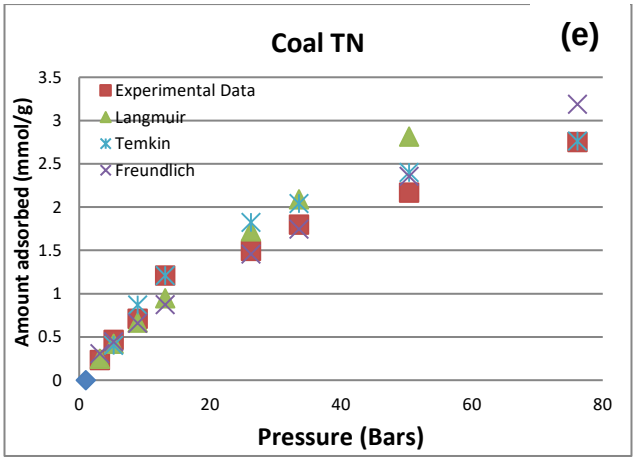

Figure 4.47(a), (b), (c), (d), (e): Comparing experimental data of CO_2 adsorption and adsorption models for coals tested at 55°C

- ***Langmuir:***

The suitability of this model, for both 35 and 55 ^{0}C, is validated from the good correlation coefficient values achieved i.e. R^2 values > 0.98 (Tables 4.13 and 4.14). Langmuir monolayer coverages (b) range from 3.81 mmol/g to a maximum of 4.58 mmol/g (for high rank coal AN) for 35 ^{O}C CO_2 adsorption, while a decreased sorption monolayer coverage is noted for the 55 ^{o}C adsorption, with ranges from 2.55 – 3.65 mmol/g. The monolayer volume and hence the slope of the Langmuir plot is temperature invariant. The fitting parameter b, decreases exponentially with an increase in temperature. Experiments were performed in the same pressure range and hence at higher temperature of 55^{o}C the isotherms represent less surface coverage (Day *et al*., 2008; Deishad *et al*., 2009; Zhang *et al*., 2011).

- ***Freundlich:***

Correlation coefficients, R^2 ranged from 0.86 – 0.97 for 35 ^{o}C and from 0.91 - 0.97 for 55 ^{o}C sorption, showing unsuitability of the Freundlich model for CO_2 adsorption estimation. Also noted, was that R^2 values decrease with decreasing sorption potential of the specific coal.

- ***Temkin:***

Calculated correlation coefficients, R^2 range from 0.91 – 0.99 for 35 ^oC, while for 55 ^oC, they ranged from 0.84 – 0.97, indicating that it is more or less an appropriate model for CO_2 adsorption estimation. The A_T values range from 0.38 (AN) – 3.83 (BL). While b_T values for 35 ^oC adsorption were found to range from 2016-3325 J/mol (2.02 – 3.325 KJ/mol) and for 55 ^OC ranged from 1031- 90 849 J/mol (1.03 – 90.85 KJ/mol).

The Freundlich isotherm showed deviations from the experimental data around the saturation pressure. The model parameters obtained from the Freundlich showed that the adsorption of CO_2 was not entirely comparable to the experimental data; in some case slightly over or under estimating the experimental sorption data. The Temkin isotherm deviated completely for HR coals from the experimental data in most cases, showing that for the modelling parameters there is a need to incorporate temperature increase parameter to account for increased pressure as well as temperature dependence thereof. Hence, for the theoretical CO_2 sorption capacity, comparison could not be met entirely from the results.

4.9 METHANE DESORPTION TESTS:

Cyclic injection of CO_2: CO_2 sorption capacity versus CH_4 desorption for CH_4 saturated samples at supercritical pressure

As discussed earlier, if CCS/CCUS can be linked to ECBM, and there is an economic benefit to CO_2 storage, then the whole process suddenly becomes viable. If CH_4 is present in coal seams, it will be displaced by CO_2 anyway, and potentially could be released to the environment if moved out of the coal seam. This would be highly negative towards GHG reduction as CH_4 is a more potent GHG than CO_2. Where CH_4 occurs in concentrations feasible for extraction and utilisation as an energy source, ECBM enables an excellent synergy with CCS. Much literature has to date been published with regards to investigating CH_4 and CO_2 adsorption to establish their respective selectivity in coals under various conditions of simulated elevated pressures, temperatures, moisture, etc., (Clarkson *et al.,* 1997; Bustin & Clarkson, 1998; Clarkson & Bustin, 2000; Busch *et al.*, 2003; 2004; 2006; Masterlez *et al*., 2004; Shimada *et al.,* 2005; Bromhal *et al*., 2005; Ceglarska-Stefanska & Zarebska, 2006; Bae & Bhatia, 2006; Busch & Gensterblum, 2007; Day *et al.,* 2008; Prusty, 2008; Sakurovs *et al*., 2008; Rivera-Ramos *et al*., 2008; Ottiger *et al*., 2008; Gensterblum *et al.,* 2009; Bae *et al*., 2009; Pone *et al*., 2009; Charriére *et al*, 2010; Dutta *et al*., 2011; Busch & Gensterblum, 2011; Zang *et al*., 2014; Merkel *et al*., 2015).

To address the issue of the potential of CH_4 release during CO_2 storage on SA coals, specifically, relating to objectives 7-11 as outlined in Section 1.1, tests were conducted using the same experimental methodology, sample preparation and system as discussed in Sections 3.4.1 and 3.4.3, respectively. Results, presented here, pertain to potential CH_4 desorption with CO_2 injection and respective adsorption. Unlike, for the most literature published, CH_4 *adsorption* has not been investigated in this study, only *desorption* of CH_4 has been considered for these SA coals.

Seven (7) different representative SA coals, namely: AN, EM, TN, WG, SL, BL and SF were studied. Sample preparation and the experimental methods conducted have been described in detail in Section 3.4.2.3 and 3.4.3.1, respectively. After each CO_2 injection step, the system was left to equilibrate, and thereafter a desorbed gas sample was recorded/analysed using the online GC. The values recorded in ppm were then converted

to mmol/gram. These sorption isotherms for the seven (7) CH_4 saturated samples are compared with those presented in Section 4.5, which details the pure CO_2 adsorption tests conducted on only dried and degassed samples. Table 4.15 summarises the total amount of CH_4 desorbed per amount of CO_2 adsorbed during injection at the respective final pressures attained.

Table 4.15 Summary of CH_4 desorbed versus CO_2 adsorbed

Sample ID	***Final Pressure (bar)***	***CH_4 Desorbed (mmol/g)***	***CH_4 Desorbed (ppm)***	***CO_2 Adsorbed (mmol/g)***
WG	79.6	0.85	515.26	2.10
BL	80.8	0.81	488.51	3.25
TN	79.6	0.80	484.44	5.37
SL	79.5	0.68	410.83	4.73
AN	80.1	0.67	406.73	3.43
EM	81.9	0.54	324.35	2.49
SF	79.8	0.44	263.50	2.49

Figure 4.48 displays the comparison between the summarised amounts (Table 4.15) of CO_2 (mmol/g) adsorbed versus the CH_4 desorbed (mmol/g) for the 7 coals tested over the entire range of incremental CO_2 injections and gives the total summative values of CH_4 desorbed per sample after maximum pressure of CO_2 injection was achieved.

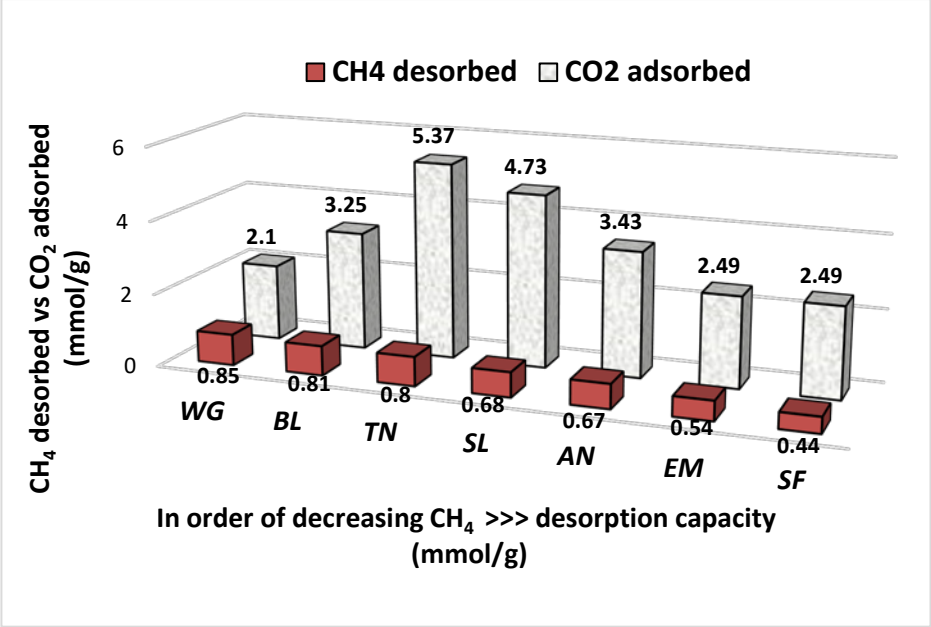

Figure 4.48 CO_2 Adsorbed versus CH_4 Desorbed vs Pressure for CH_4 simulated Saturated Coal samples

The total amount of CH_4 desorbed for the seven coals tested is in the range of 0.44 – 0.85 mmol/g. Of interest, the highest desorbing CH_4 amount (0.85 mmol/g) was reported for coal WG (MRC), which inversely reported the lowest CO_2 adsorption (2.1 mmol/g) as well as in section 4.5 (1.1 mmol/g) for dried, degassed only samples. This sample has the highest ash yield (39.35%) and inertinite matter content (90.8%) of all coals tested. Specific details relating to coal rank and type for CH_4 desorption will be discussed in further sections.

4.9.1 Break-Through curves: CO_2 adsorption versus CH_4 desorption

Using the CO_2 adsorption data and the CH_4 desorption data summarised in Table 4.15 and as depicted in Figure 4.48 and, “break-through” (BT) sorption curves were plotted for each of the seven (7) SA coals tested as depicted in Figure 4.49 (a – g). These BT sorption curves exhibit the lowest / highest pressures at which CH_4 will most likely be easily desorbed for the different coals tested.

Table 4.16 Break through pressure & regression fits - CH_4 desorbed vs CO_2 adsorbed

Sample ID	*Break-through Pressure (bar)*	*R^2: CH_4 Desorbed*	*R^2: CO_2 Adsorbed*
WG	20.1	0.97	0.94
BL	29.6	0.97	0.99
TN	28.3	0.97	0.98
SL	37.2	0.94	0.95
AN	30.9	0.97	0.99
EM	29.4	0.97	0.99
SF	27.8	0.97	0.99

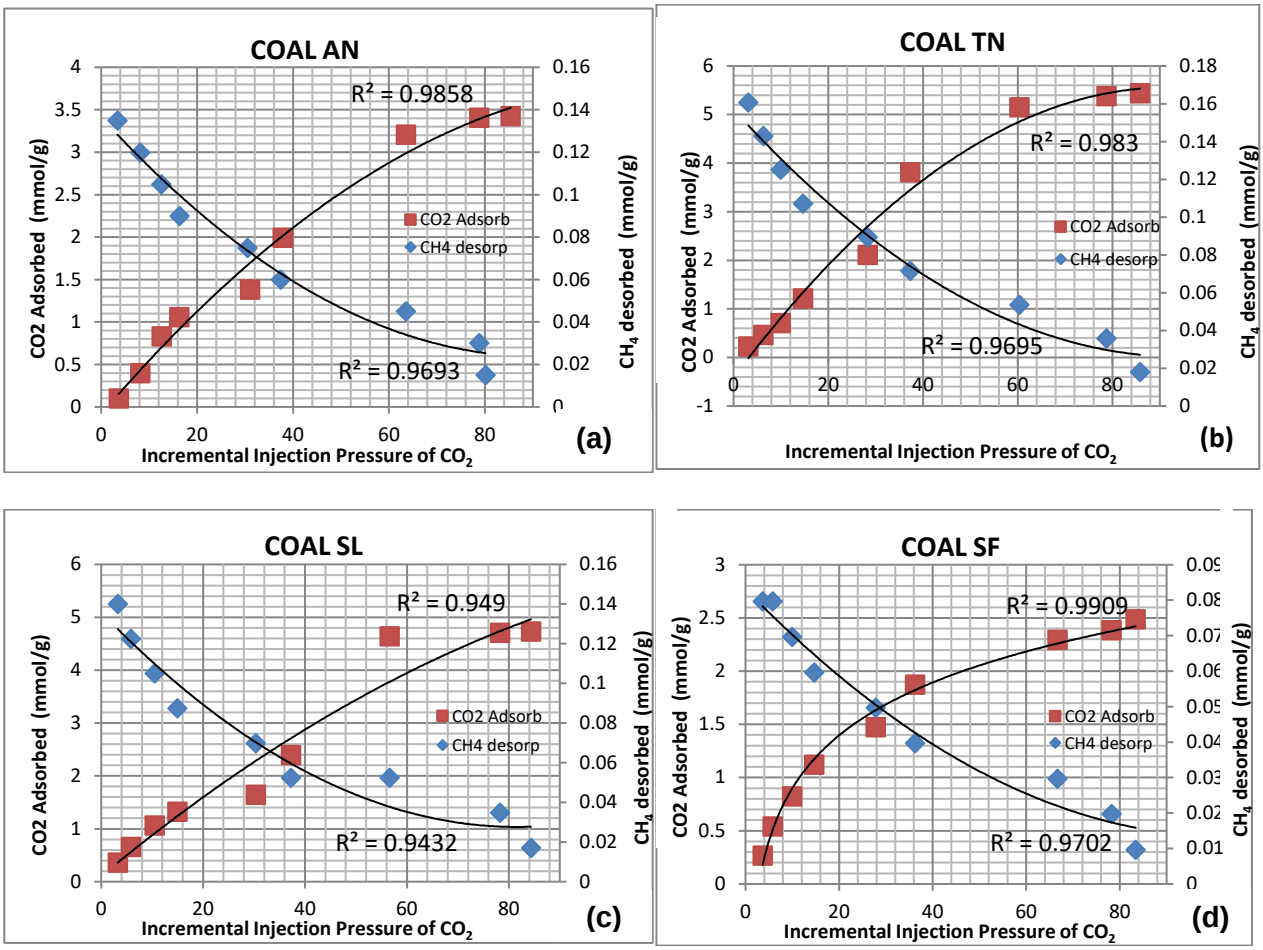

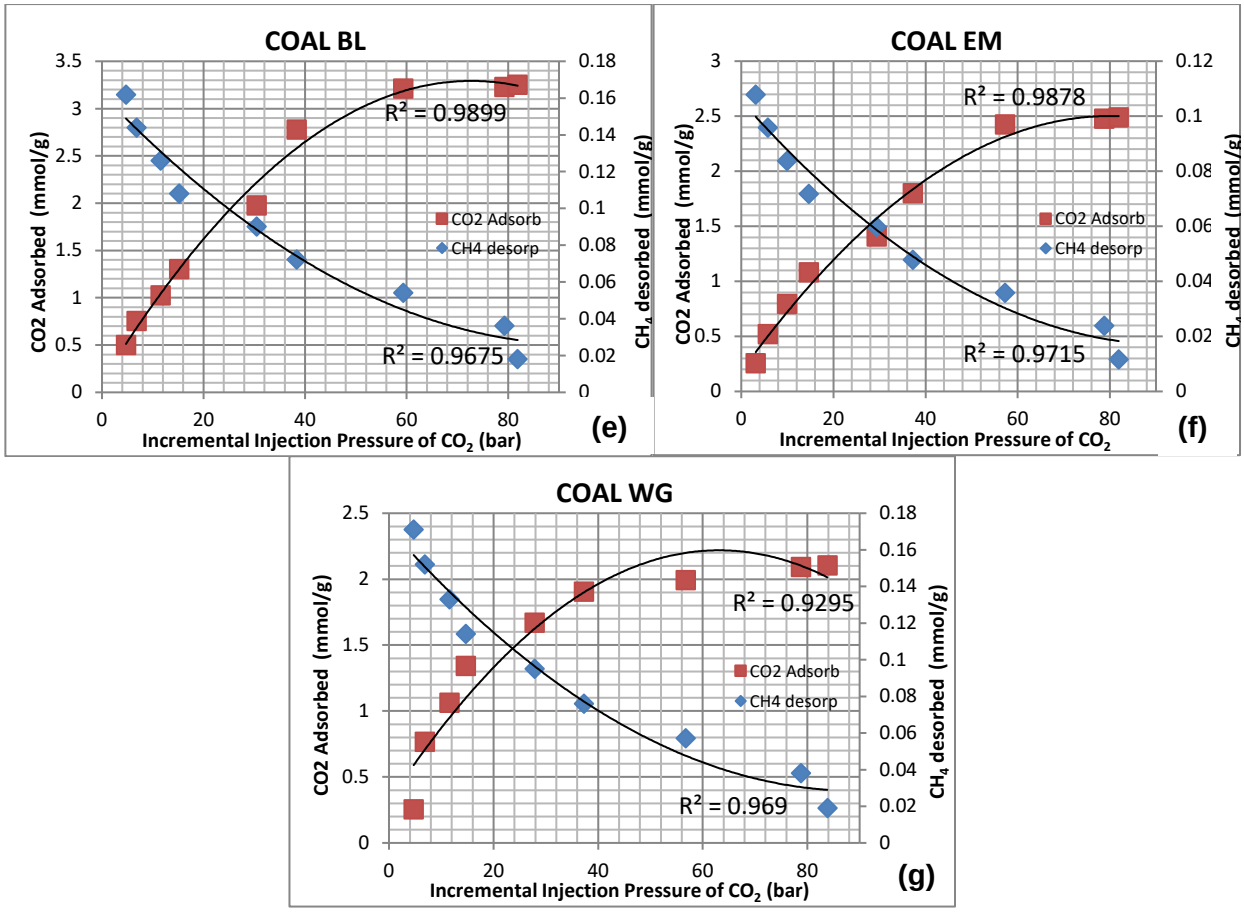

Figure 4.49: (a-g) Comparison of CO_2 adsorption versus CH_4 desorption

The exact ratio of number of moles of injected CO_2 adsorbed to number of moles of exact CH_4 desorbed (CO_2 : CH_4) could not be defined at each CO_2 injection from these results due to the method used of continued sampling and evacuation of GC lines with each incremental CO_2 pressure injection step.

The experimental data shows very good polynomial regression fits have been established for both CH_4 desorption and CO_2 adsorption isotherms. Quadratic polynomial fits show R^2 values in the range of 0.94 – 0.99 (Table 4.16). From Figures 4.49 (a) – (g)), it can be clearly seen that for HR samples AN (30.9 bar) and SL (37.2 bar), a higher BT pressure for CH_4 desorption was needed. This need for this higher BT pressure can possibly be attributed to the rank of samples corresponding to their increased vitrinite content and hence greater micro-porosity. While the highest CH_4 desorption sample WG MRC (20.1 bar) exhibited fasted BT pressure. This highlights the difference that is exhibited for CH_4 desorption in different coal types. This trend can most certainly be attributed to variance in

coal rank and its individual properties such mineral/ash content and maceral type i.e. ratios of inertinite to vitrinite, which will be discussed further in the next sections

4.9.2 CO_2 Adsorption for CH_4 saturated coals using CO_2 injection

Total amount of CO_2 adsorbed (mmol/g) (onto the CH_4 saturated coals) and the petrographic details of all 7 coals are compared and summarised in Table 4.17. Figure 4.50 shows a comparison of all the experimentally obtained CO_2 adsorption isotherms for the seven CH_4 saturated samples. The sample that recorded the highest CO_2 adsorption capacity was TN MRB with a total of 5.44 mmol/g. While WG MRC sample recorded the lowest CO_2 adsorption of 2.10 mmol/g as was observed for results presented in Section 4.5.

Table 4.17: Total CO_2 adsorbed versus Petrographic data for CH_4 saturated coals

Sample ID	*CO_2 (mmol/g)*	*Vitrinite (Vol%, mmf)*	*Inertinite (Vol%, mmf)*	*Liptinite (Vol%, mmf)*	*R_oV_{mr} (%)*
TN	5.44	71.6	28.1	0.3	1.26
SL	4.73	56.1	43.9	0.0	3.49
AN	3.43	33.4	66.6	0.0	2.91
BL	3.25	32.2	62.3	5.5	0.70
EM	2.49	13.9	82.2	3.6	0.64
SF	2.48	20.8	43.9	2.5	0.65
WG	2.10	5.0	90.8	4.3	0.51

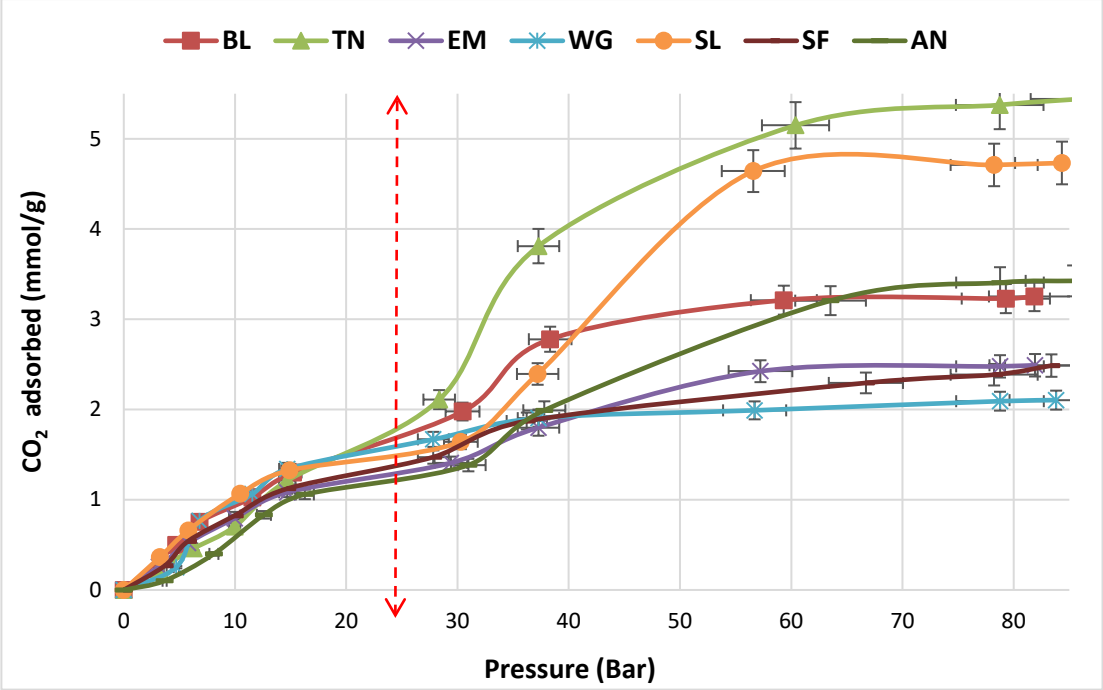

Figure 4.50: CO_2 Adsorbed vs Pressure for CH_4 simulated saturated coal samples

Figure 4.50 shows a distinguished deviation of CO_2 sorption rate that starts just after ~25 bar for all coals. This trend merely re-emphasises the fact that the increased injection pressures is actually one of the main and crucial driving parameters to achieve greater sorption in all different coals. From around 60 bar onwards it can be noted that coals seem to have reached a plateau showing saturation limits have been reached, as was determined in Section 4.5., confirming to the definite Type I sorption theory mechanism (Gregg & Sing, 1982). Also, observation of the isotherms, display concavities that are very variable, as is expected, due to the differences in samples tested. The strongest concavities provide evidence of a strong affinity of the coal for CO_2, while the "flat" shape isotherms for WG and EM demonstrate low affinity as was also observed for pure CO_2 tests (as was also observed for results in Section 4.5).

HRC samples, AN, SL and TN showed higher CO_2 sorption capacities. While lower MRC samples showed a similar trend of lower CO_2 sorption capacities as was also presented in Section 4.5. From summarised R_oV_{mr} (%) values in Table 4.17, it can be noted that a decrease in coal rank (with the exception of TN) is directly proportional to the amount of CO_2 adsorbed (mmol/g). Higher CO_2 sorption amounts observed are also as a result of

retention of adsorbed CO_2 on the coal surface, which is significant with extreme pressure CO_2 cycling (Gruszkiewicz *et al.,* 2009).

The effects of coal type, ash/mineral content, maceral matter content, effect of moisture and temperature differences on CO_2 adsorption of these coals have been discussed fully in Sections 4.5.1, 4.5.2 and 4.5.3, 4.6, 4.7, and will not be re-examined here to avoid repetition of discussions already made in said sections.

However, it should be noted here that, on comparing these CO_2 adsorption results for CH_4 saturated samples, (Figure 4.50, with CO_2 sorption results (Figure 4.11, Section 4.5), for dried and degassed samples, the CO_2 sorption was noted to diverge around a lower pressure of ~16 bar. For these CH_4 saturated samples, a divergence was only initiated at an increased pressure of ~25 bar. This result is most probably due to the fact that CH_4 was saturated in the macro, meso and most probably micro pores, which needed a greater injection of pressure of CO_2 to firstly expel or displace the CH_4 molecules in order to proceed to adsorbing into the porous coal matrix (Ohga *et al.,* 2003; Bae & Bhatia, 2006; Busch & Gensterblum, 2011).

In order to assess the difference noted, a separate study was conducted to establish this effect. A comparison of dried and degassed SA coal samples versus dried, degassed and CH_4 saturated samples were tested to determine CO_2 adsorption comparisons at sub – critical pressures up to a maximum of approximately ~60 bar (Results are presented in Appendix H1).

A large reduction in CO_2 adsorption amounts in the range of 75 – 85% were calculated. From these results it is evident that CO_2 sorption data for the typically dried and degassed coals, as is widely prepared for laboratory experiments to evaluate sorption capacity, do not give a true representation for the CO_2 sorption rates or capacities that may typically be found in a real-time injection scenario and, may very well-be overstated values and not exactly what would be expected in-situ (Crosdale *et al*., 1998; Ohga *et al.,* 2003; Busch *et al*., 2003).

4.9.3. CH_4 desorption from CH_4 saturated coals using CO_2 injection

Total desorbed amounts of CH_4, (mmol/g), vitrinite reflectance (R_oV_{mr}, %), volatile matter content (%, daf), ash content (%, adb) and BET determined average micro pore diameter (Å) are summarised in Table 4.18.

Figure 4.51 shows the CH_4 desorption isotherms for the seven (7) CH_4 saturated coals injected with incremental pressure of CO_2.

Table 4.18: Total CH_4 desorbed versus Rank, proximate, BET and diffusivity data for CH_4 saturated coals

Sample ID	*CH_4 (mmol/g)*	*R_oV_{mr} (%)*	*Volatile matter (%, daf)*	*D ($x10^{-10}$ (m^2/s)*	*Micro pore diameter (Å)*	*Ash (%,daf)*
WG	0.85	0.51	41.6	974.64	-	64.9
BL	0.81	0.70	29.1	316.06	3.88	17.2
TN	0.80	1.26	22.2	2.02	4.13	24.2
SL	0.68	3.49	5.8	3.49	3.80	9.6
AN	0.67	2.91	5.7	1.54	3.78	8.80
EM	0.54	0.64	47.5	451.04	3.84	21.9
SF	0.44	0.65	30.1	425.08	3.83	23.9

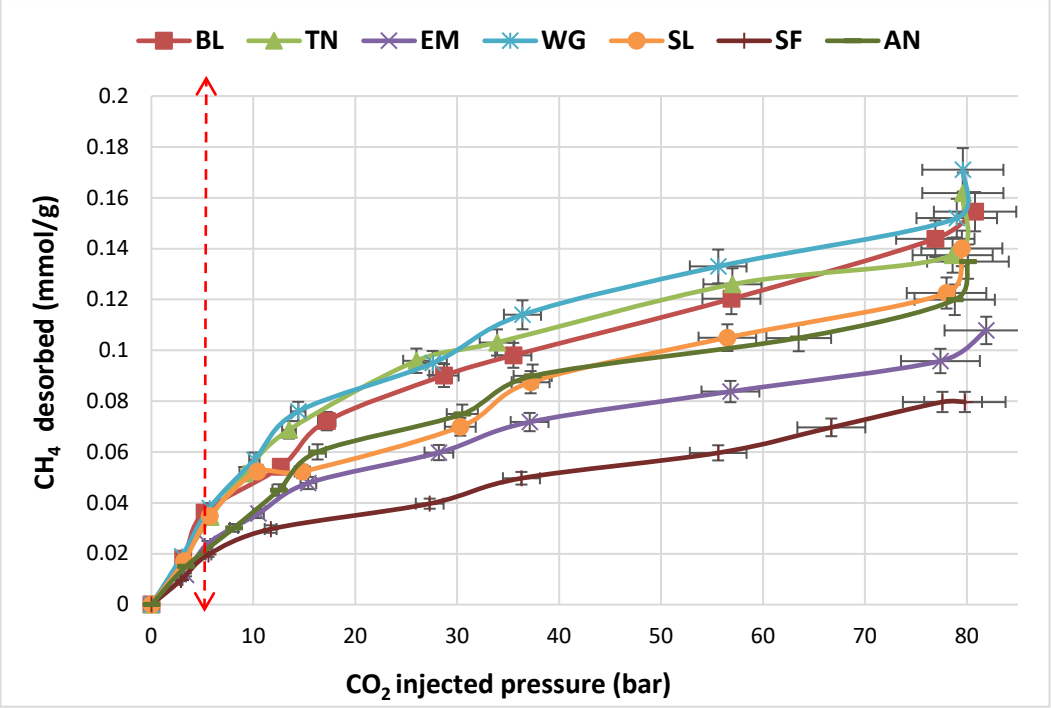

Figure 4.51: CH_4 desorbed (mmol/g) vs CO_2 injection pressure for CH_4 saturated samples

The sample with the highest CH_4 desorption at final CO_2 injection pressure was the inertinite rich (90.8%) WG (MRC), which desorbed 0.85 mmol/g. The second highest inertinite sample was BL (62.3%) with 0.81 mmol/g CH_4 desorbed at last CO_2 injection pressure. The two lowest CH_4 desorbing samples were EM and SF (MRC) with 0.54 and 0.44 mmol/g of desorbed CH_4 respectively. High rank samples, TN (0.80 mmol/g), SL (0.68 mmol/g) and AN (0.67 mmol/g), desorbed similar amounts of CH_4. Of interest, from Figure 4.50 for CH_4 desorption isotherms, is that, with CO_2 injection pressures exceeding ~79 bar, desorption rates start to exhibit an increase. This is an indication that for greater CO_2 injection pressures, as well as, the preferential sorbing nature and affinity for CO_2 (to be discussed further in Section 4.9.3.1) that coal holds, these combined properties will certainly enhance CH_4 desorption rates (Ohga *et al.,* 2003; Masterlez *et al.,* 2004; Shimada *et al.,* 2005; Ottiger *et al*., 2008). Hence, the greater sorption potential of CO_2 and displaced CH_4 can be observed from these results.

4.9.3.1 Effect of Rank: CH_4 desorption

The relationship between coal rank and CH_4 diffusivity (*D* x10^{-10}, m^2/s) has been reported by a number of authors (Zhang *et al*., 2011; Meng & Li, 2016; Xu *et al.,* 2015). Diffusivity of CH_4, was calculated for the seven (7) different coals (ranks) used in this study, using the "controlled mechanism of CH_4 gas diffusion model" developed by Meng & Li (2016). Calculated theoretical diffusion coefficients for this set of SA coals are summarised in Table 4.18.

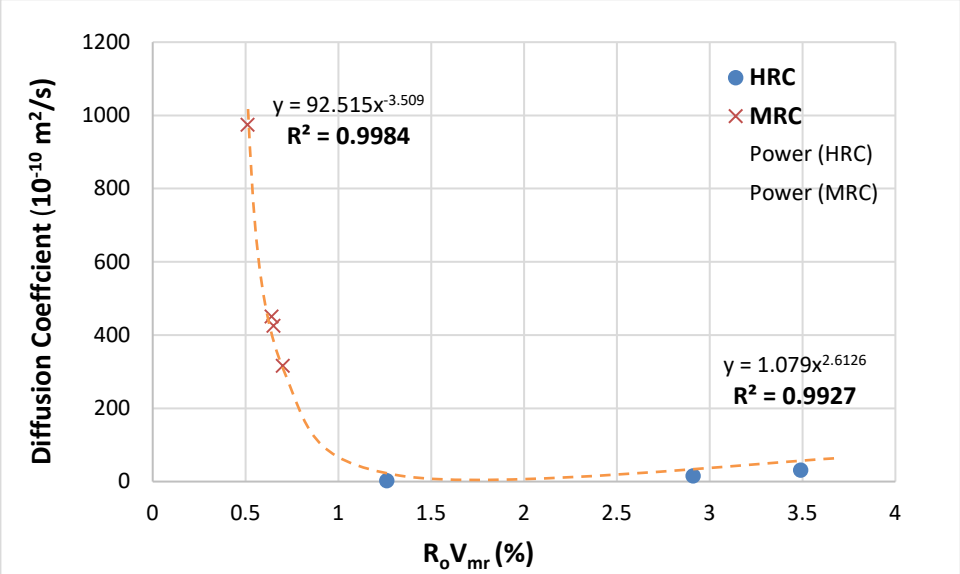

Figure 4.52: Diffusion coefficient (10^{-10} m^2/s) of CH_4 in coals vs Rank (R_oV_{mr}, %)

From Figure 4.52, results indicate that under isothermal temperature, gas and confining pressure, the diffusion coefficient (*D*) of CH_4 gas in the different rank coals exhibit a trend of first dropping rapidly and then rising slowly (asymmetric ''U" shape) with the metamorphic degree of coal increases i.e. as R_oV_{mr} increases from 0.51% to 3.49%. Lowest MRC WG (0.51%) had the highest diffusion coefficient (974.4 x10^{-10} m^2/s) followed by EM, SF and BL. Highest rank coal, AN, had the lowest diffusion coefficient (1.54 x10^{-10} m^2/s), followed by coals TN and SL (Table 4.18). In MR coals, the diffusion coefficient of CH_4 gas decreases by negative exponential function as the metamorphism degree of coal increased. While in HR coals, the diffusion coefficient of CH_4 gas increases by exponential

function with the metamorphism degree of coal increased. Regression analysis exhibits a correlation of power function that fits the data most appropriately. These findings approximate well with reporting's from other studies (Zhang *et al*., 2011; Meng & Li, 2016; Xu *et al.,* 2015).

The relationship between the diffusion coefficient of CH_4 gas and coal rank reflects pore structure of coal influencing on diffusion coefficient of CH_4 gas. Coal reservoirs have a double pore structure composed of pores and fissures. The diffusion property is not only related to the gas pressure, but also related to the degree of coalification i.e. coal rank (Zhang *et al*., 2011). Furthermore, the larger molecules have difficulty flowing through the smaller micro pore regions (as discussed in Section 4.9.1.2); as a result, the permeability of the fluid (CH_4) through the coal is affected.

Final amounts of CH_4 desorbed were plotted against vitrinite reflectance (R_oV_{mr}) (figure 4.53a) and volatile matter (figure 4.54a). No appreciable trend of rank or volatile matter for CH_4 desorption can be observed, exhibiting very poorly for second order polynomial regression fits of $R^2 = 0.0227$ and 0.1991, respectively. Low rank coal WG (R_oV_{mr}: 0.51%) reported the highest amount of CH_4 desorbed (0.85 mmol/g), while also having the highest volatile matter (49.8%).

Taking into account the results relating to potential diffusivity of CH_4 with relation to rank (Figure 4.52), rank / vitrinite reflectance (Figure 4.53(a)) and volatile matter (Figure 4.54(a)) graphs were separated into HR and MRC coals. Plots showing separated coal rank, HR and MRC, exhibit significantly different trends shown in Figures 4.53(b) and 4.54(b).

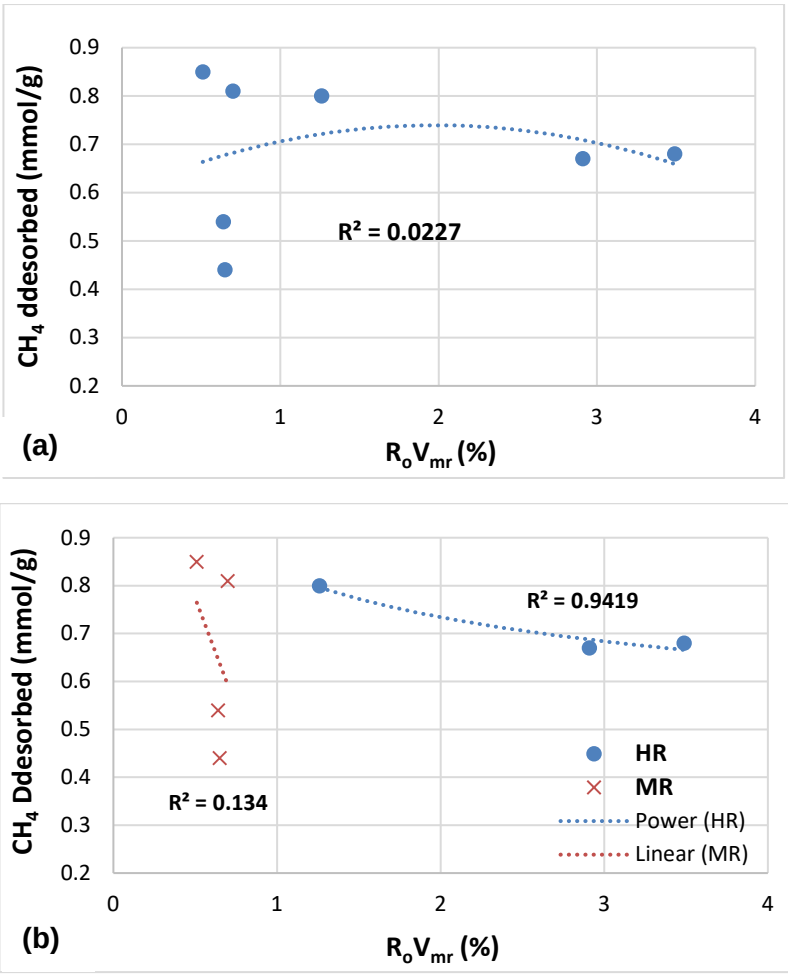

Figure 4.53 (a), (b): CH_4 desorbed (mmol/g) vs Vitrinite Reflectance, R_oV_{mr} (%)

It is observed that HR coals display a gradually decreasing relationship of CH_4 desorbed as vitrinite reflectance increases (good polynomial regression fit R^2 =0.9419). Misra *et al*. (2006) reported that desorption rates of low rank (dull) coals reduces with increasing rank. The lowest rank coal, WG (0.85 mmol/g) exhibited the highest amount of desorbed CH_4. This finding is in agreement with reporting's' from Crosdale *et al*., (1998), Laxminarayana and Crosdale, (1999) and Misra (2006), who concluded that desorption rates are faster in dull coals. However, no apparent trend can be found from the rest of the MRC coals though (R^2 = 0.134). Coals EM (0.64) and SF (0.65%) have relatively similar R_oV_{mr}, however report a difference in the total amounts of CH_4 desorbed, 0.54 mmol/g and 0.44 mmol/g, respectively.

For volatile matter (Figure 4.54(b)), it is shown that increased CH_4 desorption amounts was observed for HR coals with increased volatile matter content, it has been proposed that this phenomenon could be due to extraction of volatile coal components by the high pressure super-critical injected CO_2 (Busch *et al*., 2003). While, MRC coals showed no apparent trend (R^2 = 0.1385). Coals BL (24.8) and SF (24.3%) have relatively similar volatile content, however, report a huge difference in the total amounts of CH_4 desorbed, 0.81 mmol/g and 0.44 mmol/g, respectively. This difference could only be attributed to effects of ash content and maceral matter compositions which will be discussed in the following sections.

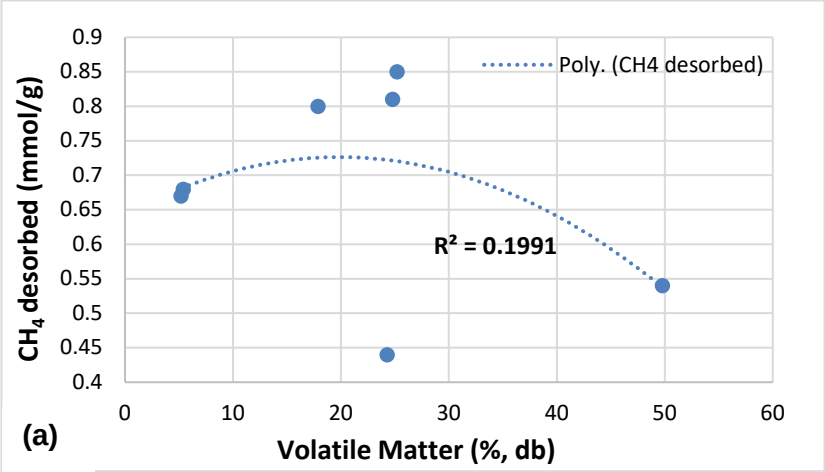

Figure 4.54(a): CH_4 desorbed (mmol/g) vs Volatile Matter (%, db)

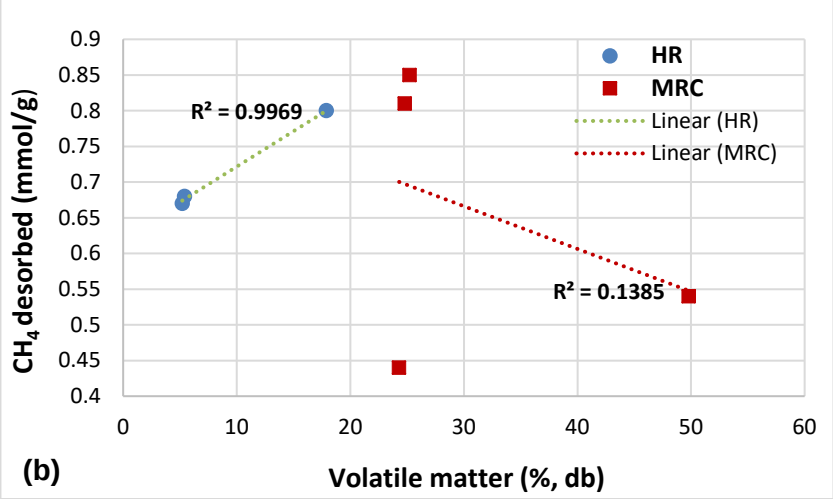

Figure 4.54(b): CH_4 desorbed (mmol/g) vs Volatile Matter (%, db)

The reduction of coal permeability with rank is due to the fact that increasing of rank causes the coal mass porosity to reduce, which makes more tortuous pathways for gas flow in the coal mass, resulting in permeability reduction. However, coal WG, with the lowest R_oV_{mr} (0.51%), reported the highest CH_4 desorption of all coals compared. This coal does not seem to confirm to the trends reported with regard to low rank coals and decreased permeability. This effect of cleating will be looked at in terms of vitrinite to inertinite content in the Section 4.9.3.3.

With regard to coal porosity, using the determined average maximum pore size (Å) data from BET analysis (Section 3.3.4), Figure 4.55, displays a weak correlation (R^2 = 0.4959 to the final amounts of CH_4 desorbed. While, Figure 4.56, depicts a very vague trend between average pore size in relationship to coal rank (R_oV_{mr}). Coal microstructure (porosity system) is relevant for gas flow behaviour in coal and, consequently, directly influences gas recovery from the coalbed (Rodrigues *et al*., 2002). Pore geometry significantly influences the gas desorption potential as the injected CO_2 cannot access micro pores with narrow tortuous pore throats. Considering the kinetic molecular diameters of CH_4 and CO_2, which are 3.8 and 3.3 Å (0.38 nm and 0.33 nm), respectively, this suggests that the CO_2 molecules interacts more favourably with the coal matrix, be it macro, meso or micro porous, as the larger CH_4 molecules have greater difficulty in flowing through the smaller micro-pore regions of the coal matrix (Shen *et al*., 2011). Thus pore geometry allows CO_2 to very easily diffuse through the heterogeneous porous, bi/tri-modal coal structure and displace any physically adsorbed CH_4, while adsorbing more favourably (Ciu *et al*., 2004; Rivera-Ramos *et al*., 2008; Perera *et al*., 2011). Also, depending on the specific coal rank or/and coal type, this opens up the “gate” to enhanced sorption of CO_2 due to its large polarizability and presence of a permanent quadrupole moment as compared to CH_4. Thus making the electrostatic forces a significant contributor to gas sorption (Sharkey and McCartney, 1981; Gregg and Sing, 1982; Hong & Suh, 2012). The accessibility of pore spaces is known to become limited if the pore spaces are connected with narrow necks or have small pore mouths, a likely arrangement for more structured HR coals due to their complex pore structure, as is the case with coals AN and SL (Bae *et al*., 2009).

The lower HR TN sample reported the largest average micro pore size of 4.3 Å, while exhibiting the highest CH_4 desorbed amount, compared to other HR samples AN and SL. While the MRC BL sample had the second highest CH_4 desorbed (0.81 mmol/g) and reported the largest average micro pore size of 3.88 Å as compared to all other MRC coals. This is evident that these samples have a very high macro porosity, and in being meso- and macroporous, it was able to hold substantial CH_4 gas in adsorbed free-state during the CH_4 injection simulation (Misra *et al*., 2006). It has been shown that a very heterogeneous pore geometry exists, from slit-shaped pores, conical pores and cylindrical pores, etc., so coal is very highly porous with numerous bottle-shaped pores evident (Liu & He, 2016).

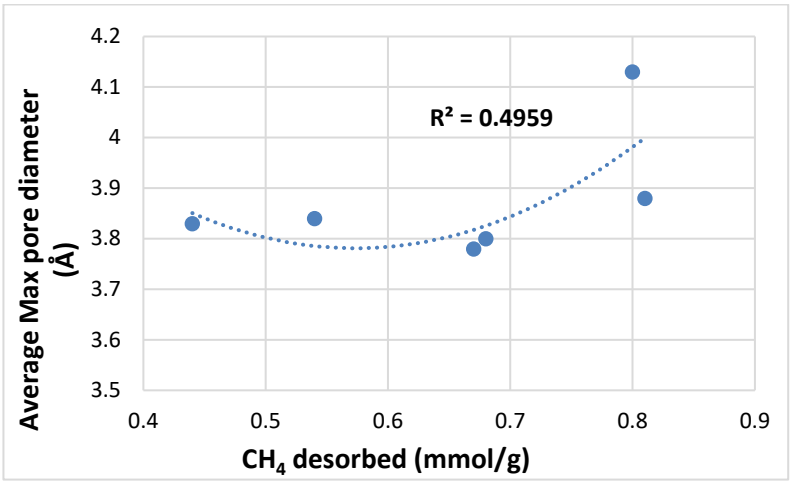

Figure 4.55: Average maximum pore diameter (Å) vs CH_4 desorbed (mmol/g)

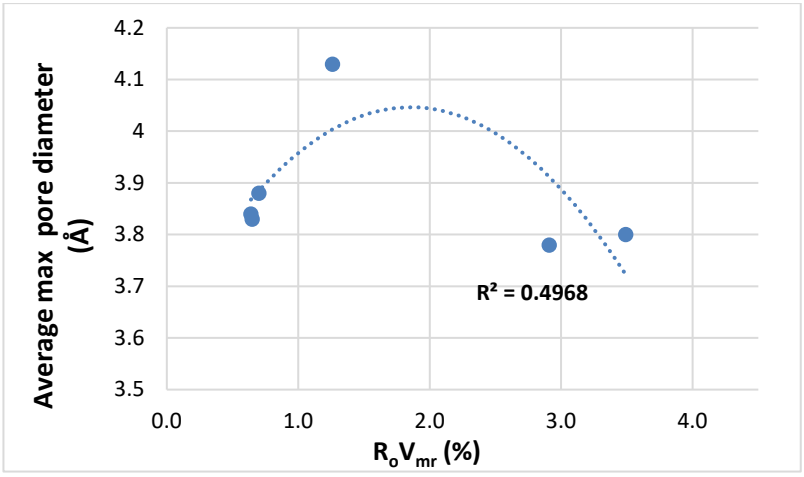

Figure 4.56: Average maximum pore diameter (Å) vs R_oV_{mr} (%)

However, it should be also be noted, that findings may exhibit conflicting views as consequence of several opposing effects. On one hand, as coal rank increases, micro pores of smaller size do develop. On the other hand, however, as coal rank increases so does the inability of the adsorbate (CH_4) to probe the highly constricted microporous structure (using conventional adsorbates, equilibration times and adsorption temperatures); this leads to the detection of pores of larger effective size for higher-rank coals. The existence of an interconnected but highly constricted pore system imposes severe limitations on our current ability to properly quantify these influences of coal sorption (Masterlez *et al*., 2004; Radovic *et al*., 1997).

4.9.3.2 Effect of Ash: CH_4 desorption

The effect of ash content (%) for all coals compared shows no appreciable trend (Figure 4.57(a) with regards to CH_4 desorption. As was done, for vitrinite reflectance and volatile matter data, Figure 4.55(b) depicts HR and MRC coals with relation to ash content separately. HR coals show gradual increased CH_4 desorbed amount in relation to increasing ash (%). Regression analysis shows a good quadratic polynomial fitting R^2= 0.9335. Coals with low ash content tend to have smaller cleat spacing's than do coals with high ash content (Levine, 1993).

The MRC coals (with the exception of WG) exhibit a very dramatic decline in desorbed CH_4 amounts for increased ash contents. A very good correlation coefficient was also found, R^2= 0.9992. These results are in very good agreement with findings from Wang (2007), Ward (2002) and Weniger (2010), who reported a reduction of coal mass permeability with increasing dry ash content for high rank coal. Findings from Robertson (2005) and Misra (2006) showed a reduction for increased ash content for low rank coal. However, it has been reported that meso porosity is exceptionally high for extreme ash rich coals, such as the WG sample (39.5%) (Masterlez *et al*., 2004); this could possibly explain the significantly huge CH_4 amount desorbed.

These results, regarding the effect of higher ash content, were also mirrored for the CO_2 adsorption data presented in Section 4.5.2. It is presumed that fine-grained and fine-

precipitated (secondary) mineral matter tend to clog the pore spaces and cracks (cleat in-fillings) in earlier stage of coal formation, and thus retard the gas-holding capacity of coals by depleting pore volume and limit the diffusion and migration within the coal matrix (Clarkson & Bustin, 1999; Stach *et al*., 1982; Ettinger *et al*., 1966).

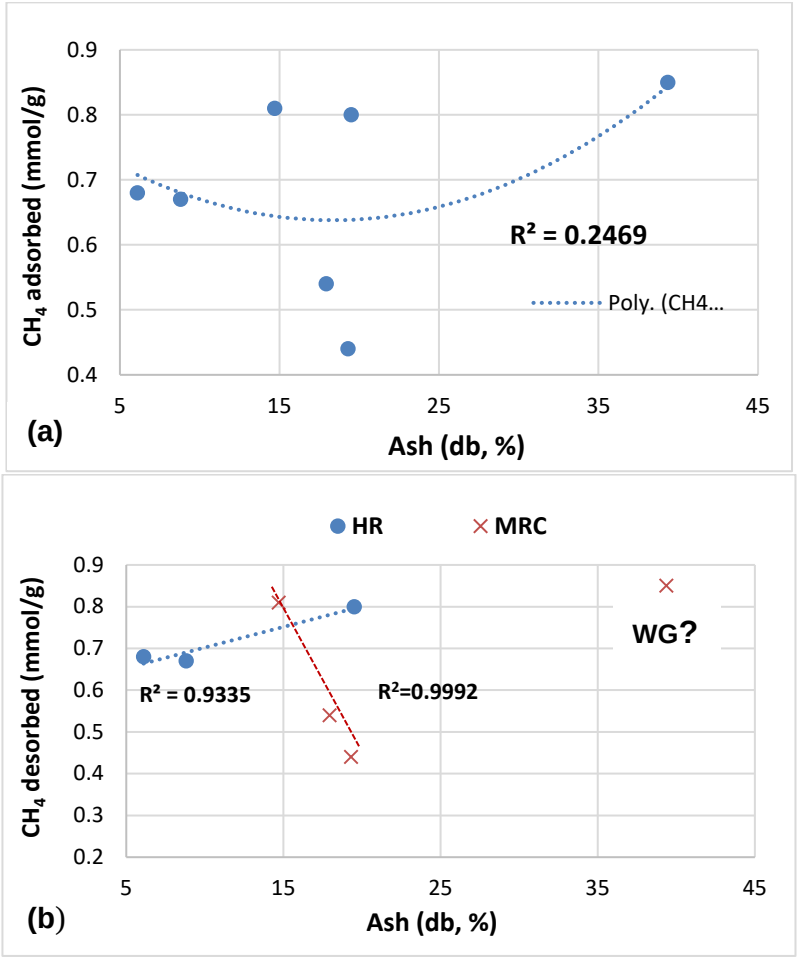

Figure 4.57(a), (b): CH_4 desorbed (mmol/g) vs Ash (db%)

While the porous structure of the coal dictates how much surface area is available for adsorption/desorption, the chemical structure and surface chemistry (maceral components) of the coal determines the kinetics of the fluid-coal reaction at the surface, and what role mass transfer will play in the overall rate of sorption (Du & Wu, 2016). The maceral components of the coal play a vital role which can affect the characteristic adsorption energy difference between the organic and inorganic adsorption process (Marsh, 2001).

4.9.3.3 Effect of Maceral matter: CH_4 desorption

The comparison of the overall effect of coal maceral and mineral composition on total CH_4 desorption is shown in Figure 4.58. As mentioned, and surprisingly noted, was that sample WG with the highest mineral matter content had the greatest CH_4 desorption as compared to the higher rank coals with the lowest mineral matter content.

As was discussed for pure CO_2 sorption studies earlier in Section 4.5.3, hereto the argument about the influence of coal maceral composition on sorption continues. Ryan & Lane (2002) argued that inertinite may preferentially adsorb CO_2, whereas vitrinite may preferentially adsorb CH_4. Further, they assume that CO_2 may layer fill the larger pores in inertinite, whereas CH_4 may volume fill the smaller pores in vitrinite. They also stated that larger CO_2-surface interactions occur in inertinite than in vitrinite macerals, which results in a greater affinity of CO_2 towards inertinite. From results presented here, it is evident that the samples TN, SL and AN with the higher vitrinite contents and higher rank exhibited decreasing CH_4 desorption rates compared to the very high mineral matter WG coal sample. It is proposed that the shrinkage of the coal matrix due to desorption of gas tends to open the cleat fractures and thereby increase coal permeability in lower rank coals; however the opposite is said to be true for higher rank coals, where a correlation was noted between rank increase and the swelling[3] capacity during gas adsorption (Gaucher *et al.* 2011). On just the comparison of vitrinite, inertinite and liptinite matter, no definite correlation could be found concerning CH_4 desorption rates from these results. Hence, the observations made in Section 4.5.1.2 for pure CO_2 adsorption with regard to specific maceral compositions might be needed to explain this finding further. The different coal macerals must be further identified to establish their contribution to the difference in CH_4 desorption results.

---

[3] The investigation of coal swelling and/or shrinkage effects is beyond the scope of this study and hence will not be discussed in any further detail. Further reading refer to: Reucroft and Patel.,1986; Larsen et al., 1997; Holloway, 1997; Opaprakasit and Painter, 2003; Karacan, 2003; White et al., 2005; Mazumder et al., 2005; Wang et al., 2007; Mazzotti et al., 2009; Day et al (2008a); Pone et al., 2010; Gensterblum et al., 2010.

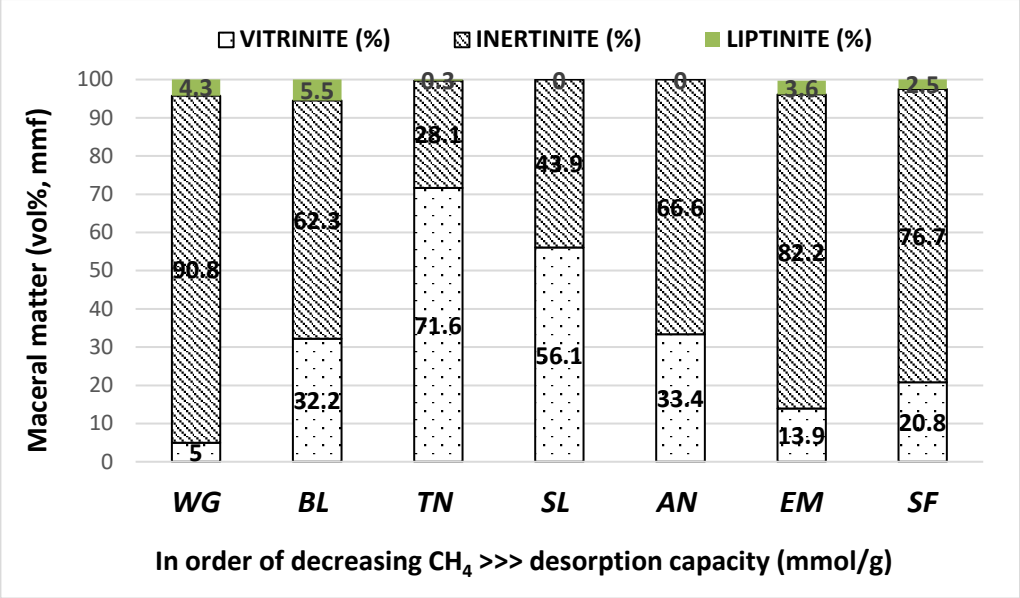

Figure 4.58: Effect of maceral composition (vol%) on CH_4 desorbed (mmol/g)

Recent work by Masterlez *et al* (2012) is also in agreement that the inertinite-rich low rank coals desorb more than higher rank coals because of better connection between the pores, hence better gas transmissibility in the network compared to the relatively "tight" vitrinite bearing coals. This is was also found by Laxinarayan & Crosdale (1999) who concluded that desorption rates studies showed that dull coals desorb more rapidly than bright coals (high rank coals), and that desorption rate is also a function of rank. Yang *et al.* (2011) further agreed that, when CH_4 is replaced by CO_2, the changes in the volumetric strain of meso pores are negligible, while in microporous domains a significant deformation occurs, which may strongly influence the structure and permeability of the coal matrix during CO_2 injection/sequestration. This was more recently found in the work carried out by Maphala (2012) for SA coals; it was concluded that inertinite has a higher degree of crystallinity and a higher fraction of aromatic carbon compared to vitrinite. Thus a material with a high crystalline structure will generally have a more porous structure and is less prone to structural changes than a material with a less crystalline structure.

Although meso and macro-pores present in inertinites are said to facilitate the displacement of CH_4 gas in place (Unsworth *et al*., 1989; Clarkson & Bustin, 1996; Laxminarayana & Crosdale, 1999), the observation seems to only be partially verified in this study for some of the HRC and some of the MRC coals. The two high inertinite rich

samples, HRC AN (66.6%) and MRC SF (76.7%), exhibited poor desorption results. Hence no exact correlation between total vitrinite or total inertinite group content with CH_4 desorption could be definitely concluded from Figure 4.59 exhibiting very poor quadratic regression fits, R^2 = 0.2478 and 0.2401, respectively. This could mean that a specific or ideal ratio between *only* the maceral components, in similar rank coals (i.e. effect of porosity, as discussed in Section 4.9.3.1), is the controlling factor for best CH_4 desorption required, depending also on the effect of mineral matter / ash content (as discussed in Sections 4.5.2, 4.5.3.1 and 4.9.3.2). Section 4.9.4, will look into comparing the detailed maceral compositions of these SA coals and identifying a possible correlation to the sorption capacity of CO_2 from the results presented.

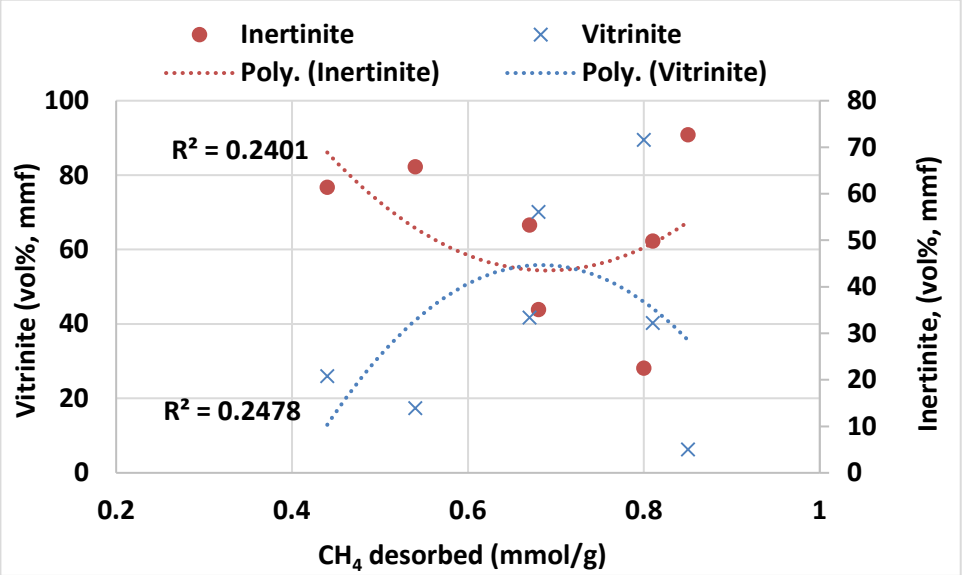

Figure 4.59: Vitrinite & inertinite (Vol%, mmf) versus CH_4 desorbed (mmol/g)

As also discussed in Section 4.5.3.2, seams with higher V/I ratio, are alleged to have high cleat density as well as high permeability (Stach *et al*., 1982; Laubach *et al*. 1998). The comparison between the vitrinite to inertinite ratio (V : I) for the HR and MRC coals, to both the coal and total amount of CH_4 desorbed (mmol/g) is illustrated in Figure 4.60.

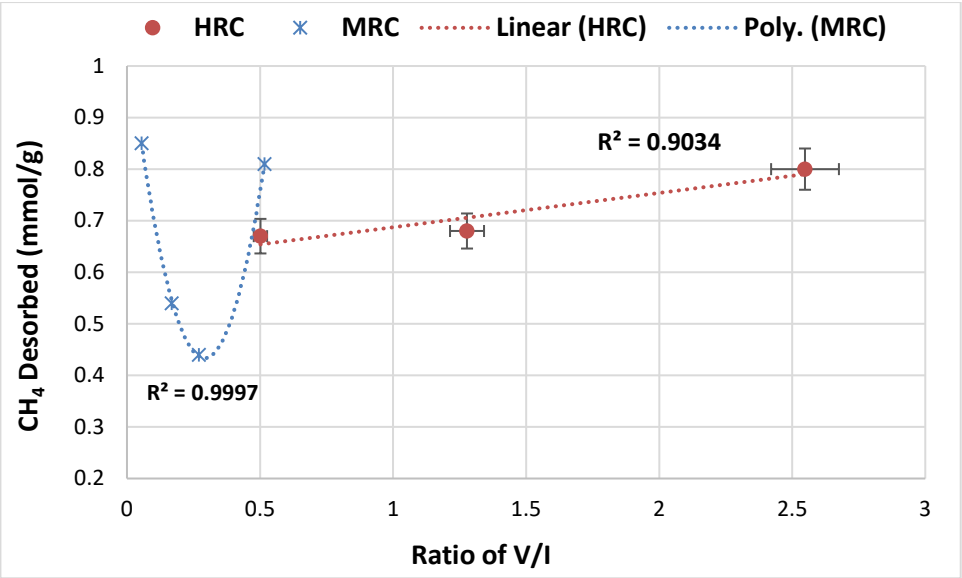

Figure 4.60: Comparison of vitrinite to inertinite ratio (V:I) versus CH_4 desorbed (mmol/g)

The association of V:I ratio to CH_4 desorbed amounts presented in Figure 4.60, shows a good linear relationship for HR coals (R^2= 0.9034), while for MRC coals, V:I correlates to a second order polynomial regression fit, shows good fitting to validate this trend (R^2=0.9997). While for the MRC coals, an increasing V:I ratio (up to ~0.27), shows a steady decrease in CH_4 desorbed and thereafter an increased V:I ratio of 0.517 exhibits an increased CH_4 desorption amount. This bell-shaped trend, has also been established by a number of others (Stach *et al*., 1982; Laubach *et al*., 1998; Levine, 1993). This confirms that rank is not the main parameter (vitrinite reflectance i.e. rank of the coal) and is not controlled solely by petrographic (maceral) composition (Faiz *et al*., 2007; Masterlez *et al*., 2004; Sen & Banerjee, 2015).

Although coals AN (HR) having greater micro porosity and BL (MRC) having greater macro porosity, show comparable V:I ratios, 0.5015 and 0.5168, respectively, it can be seen that they desorbed very different amounts of CH_4, 0.67 and 0.81 mmol/g, respectively. The macro-pore system is established by the fracture network that is currently designated by the cleat system (Rodrigues *et al*., 2002) and the macro pores (the primary porosity) predominates in lower rank coals, such as samples BL and WG. This is an indication, that in terms of porosity, rank dominates displaying that the macro or micro porosity will be a

key factor with regards to migration and diffusion of CH_4 through the respective coal matrices (porosity details discussed in Section 4.3).

4.9.3.4 Evaluation of detailed coal maceral composition on CH_4 desorption

Table 4.7 (Section 4.5.3.3) gives details of the respective compositions of individual macerals (vol%, mmf) (summarised from the detailed petrographic data presented in Appendix A). Background details of the specific macerals evaluated are detailed in discussions in section 4.5.3.3. The detailed individual macerals of the vitrinite group are graphically represented in Figures 4.61 (a): collodetrinite, (b): corpogelinite & gelinite, (c) collotelinite.and (d): pseudovitrinite. Figure 4.61 shows the comparison of individual inertinite maceral compositions on CO_2 adsorption; (a) Fusinite (b) Inertodetrinite, (c) Semi-fusinite, while Figure 4.62, depicts the comparison of liptinite maceral compositions; (a) sporinite and (b) cutinite, respectively, with regards to the CH_4 desorption (mmol/g) capacities of the seven (7) coals tested in this study.

4.9.3.4.1 Effect of Vitrinite macerals

- **Collodetrinite:**

From Figure 4.61(a), as collodetrinite increases in content, the amount of CH_4 desorbed (mmol/g) decreased sharply for MR coals: (SF and EM). Coal WG and BL reported the highest desorbed amounts of CH_4, however, have the lowest collodetrinite contents of all MRC coals, 0.7 and 0%, respectively. While for HR coals, an increase in collodetrinite content showed a small increase in the amount of CH_4 desorbed (SL and TN). This finding is in contrast to findings for amounts of CO_2 adsorbed.

- **Corpogelinite & gelinite**

All HR coals tested here have 0% corpogelinite & gelinite contents. MRC EM had 0%, while coals WG (1.1%), SF (1.6%) and BL (2.1), showed increased CH_4 desorbed amounts

as compared to coal EM. Of interest is the comparison of MRC EM and WG samples have very low vitrinite contents, 13.9% and 5% respectively, the desorbed capacity of EM (0.54 mmol/g) was much lower than WG (0.85 mmol/g) and other coals, SF and BL. WG has corpogelinite and gelinite of 1.1% as compared to EM (0%). This could mean that these gel-filled bodies (infillings) have a positive effect by enhancing the desorption capacity of CH_4 to some little extent.

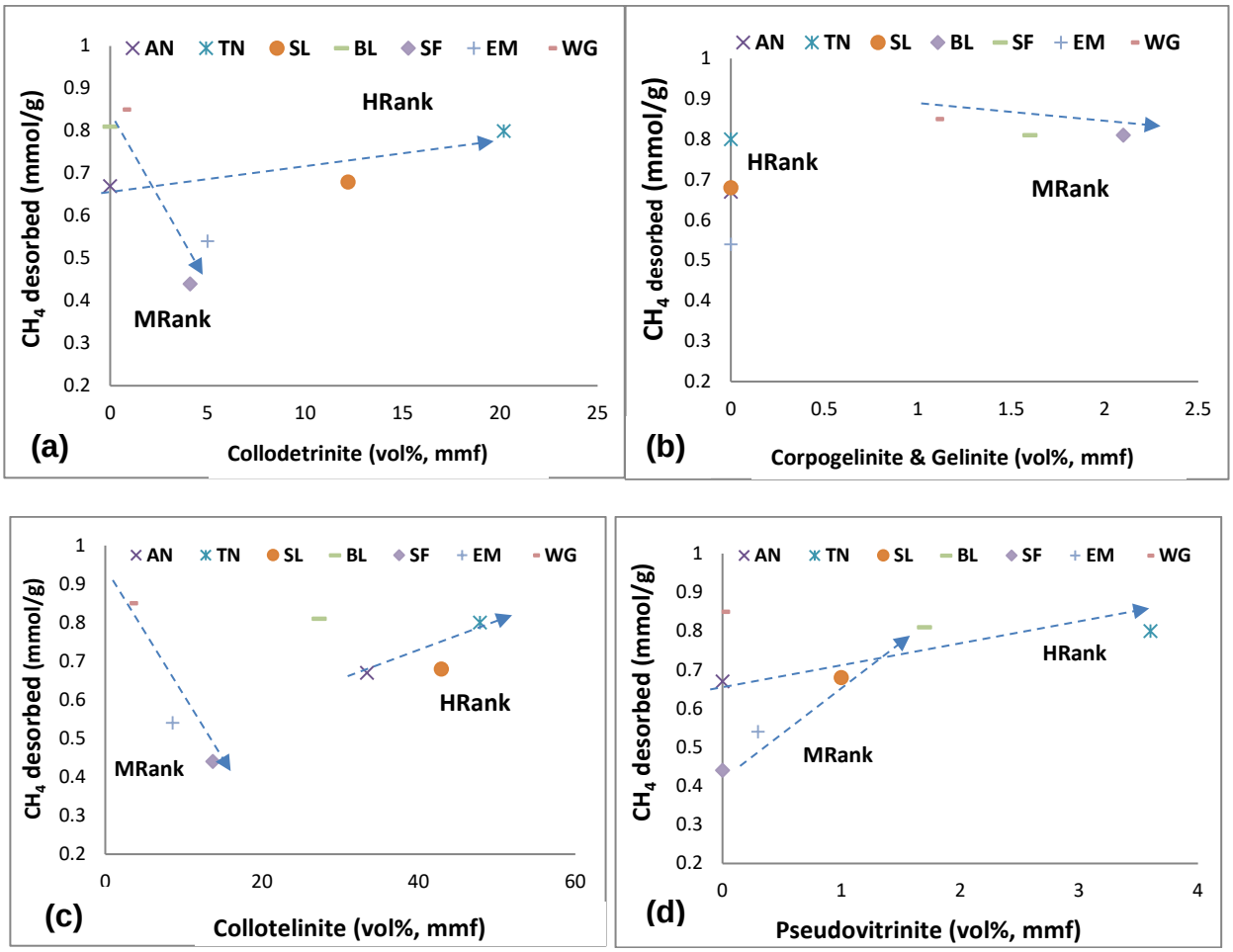

Figure 4.61: Comparison of vitrinite individual maceral compositions on CO_2 adsorption: (a): Collodetrinite; (b): corpogelinite & gelinite; (c): collotelinite & (d): pseudovitrinite

- **Collotelinite**

Figure 4.61(c) shows a possible correlation, revealing a trend of increasing CH_4 desorption for HRC coals with increasing collotelinite maceral content observed from coals AN (0.67 mmol/g) to sample TN (0.8 mmol/g), reporting the highest collotelinite content (47.8 vol%). This was in stark contrast to the CO_2 adsorption observations, where the inverse was observed. The highest CO_2 sorbing coal, AN (33.4%) had the lowest percentage of collotelinite of all HR coals. This observation is in agreement to reportings of Chalmers & Bustin (2007), who concluded that higher desorption capacities were found in high-rank, vitrinite-rich coals with higher telovitrinite (collotelinite & telinite) content.

The inverse was observed for the MRC coals. Increasing collotelinite contents exhibited decreased CH_4 desorbed. The highest CH_4 desorbing MRC coal, WG (0.85 mmol/g) had the lowest collotelinite content (3.2%) followed by EM (8.6%) and SF (13.7%), showing sharp decline in CH_4 desorbed. The inverse was found from the CO_2 adsorbed observations, where the inverse was observed MRC BL sample did not follow this observed trend, having a large collotelinite content of 27.3%. This outcome needs further study with more samples to make a more concise deduction. For a given rank level, the collotelinite, has the lowest carbon and highest oxygen contents (Meyers, 1982; Suárez-Ruiz & Crelling, 2008).

- **Pseudovitrinite**

Only two of the HR coals reported pseudovitrinite contents, i.e. coals SL (1%) and TN (3.6%). From figure 4.61(d), it is evident that this maceral, does not seem to have any negative effect on the total CH_4 desorption capacity for HR coals. However, more samples HR need to be further examined to make a conclusive decision. MRC coals show a progressive incremental amount of CH_4 desorbed with increasing pseudovitrinite contents.

Although, very noticeable, trends have been identified for these selected vitrinite macerals, it must be mentioned that in iso-rank coals, vitrinite with the same textural and optical

characteristics might not be homogeneous with respect to its chemical properties (Jimenez *et al*., 1998).

4.9.3.4.2 Effect of Inertinite macerals

- **Fusinite**

Both HR and MRC coals showed on average an increasing desorption as fusinite content increased, with the exception of MRC WG sample, having the least fusinite content of 3.5% of all samples tested. Fusinite has been found to have no micro porosity due to very diminished volatile matter (CIarkson & Bustin, 1996), hence MRC coals, WG and BL, having very diminished volatile matter, 25.21% and 24.8%, display increased CH_4 desorption potential.

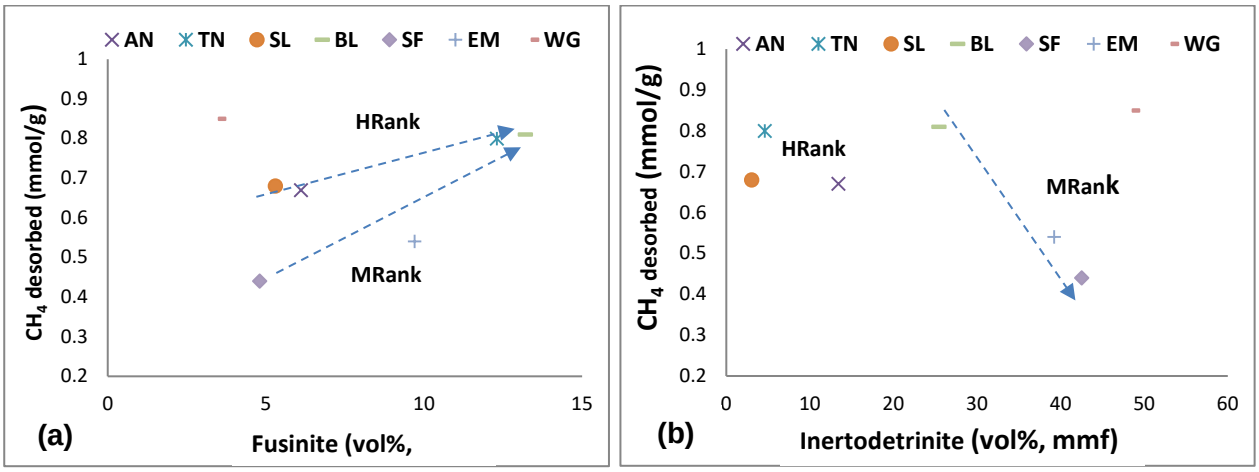

Figure 4.62: Comparison of inertinite macerals' compositions on CO_2 adsorption; (a) fusinite (b) inertodetrinite

- **Inertodetrinite**

Reactive inertodetrinite was found to be 0% for most coals, and in very low proportion for TN (0.5) and EM (7.5%) coals. Inert inertodetrinite is more dominant, ranging from 4.1 - 42.5%. Reactive inertodetrinite and inert inertodetrinite data have therefore, been combined (for simplicity of comparison and are presented in Figure 4.62(b). HR coals

exhibit no specific trend, results are scattered. However, sample AN, at 13.4% and SL at 3% report very similar CH_4 desorbed amounts, 0.67 and 0.68 mmol/g.

MRC coals show a decreasing desorption trend with increasing inertodetrinite content, with the exception of WG (48.6%) having the greatest amount of inertodetrinite and reporting the highest desorbed amount of CH_4. But this, however, could be attributed to other discussed macerals such as the low proportion of collodetrinite and collotelinite contents.

- **Semi-fusinite**

Reactive semi-fusinite (RSF) is found to be in very low proportion for all coals, ranging from 0-5.3%. ISF (inert semi-fusinite) is more dominant, ranging from 8 – 46.8%. RSF and ISF data have therefore been combined (for simplicity of comparison) and are presented in Figure 4.62(c). As semi-fusinte content increases in HRC coals, there is a gradual, linear decrease in the CH_4 desorption amount. It can be observed that the AN sample, had a very high semi-fusinite (46.80%) content as compared to both SL (35%) and TN (8.2%).

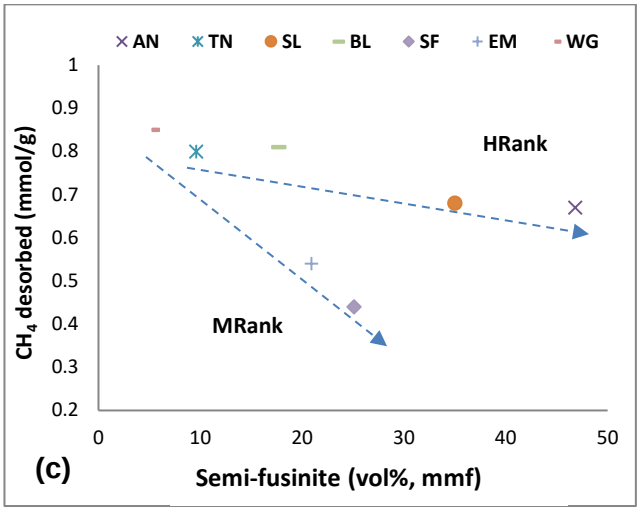

Figure 4.62(c): Comparison of inertinite macerals' compositions on CO_2 adsorption: (c) semi-fusinite

CIarkson & Bustin (1996) hypothesised that, the loss of volatile matter as a result of partial charring during the formation of semi-fusinite may open up the pore structure, allowing additional desorption. It is believed to occur, whereby micro porosity is created by the removal of walls between adjacent micro pores through coalification process and creates additional micro porosity in semi fusinite. This theory is supported here by the fact that HRC coals (AN and SL) have the lowest volatile matter (as presented in Section 4.2.1, Figure 4.3), and the greatest total number of micro pore surface areas, 199.19 and 170.67 m^2/g, respectively (as determined from BET determinations discussed in section 4.3), even though they do not have the highest total vitrinite contents (AN: 33.4% and SL: 56.1%).

The same trend is observed for MRC coals. A steady increase in semi-fusinite exhibits a decrease in sorption for MRC coals (Figure 4.62(c)). WG has the highest RSF (5.3%) as compared to all coals. There is a positive relationship between reactive inertinite content and CH_4 desorption capacity occurs within the subbituminous to medium volatile bituminous coals because the reactive inertinite is structurally similar to vitrinite and is believed to have a higher micro porosity than non-reactive inertinite (Masterlez & Bustin, 1997; Chalmers & Bustin, 2007).

4.9.3.4.3 Effect of Liptinite macerals:

The main liptinite macerals examined in this study are classified as sporinite and cutinite. In general, an increased liptinite content, seems to relate to an increase in CH_4 desorption. For this suite of SA coals, other macerals in this group are considered negligible as percentages is at zero. In general, an increased liptinite content, seems to relate to an increased CH_4 desorption. It seems most likely that sporinite could be responsible for this. This was observed for MRC: (SF, BL and EM) and HRC (AN, TN and SL samples) (Figure 4.63 (a)).

- **Sporinite**

As sporinite dominates the liptinite maceral group, it could be assumed, that it is solely responsible for increased CH_4 desorption. This was observed for both MRC and HRC coals (Figure 4.63(a) and (b)). Coal WG seems to be at odds with this trend. Comparing MRC WG and SF samples, although they have very similar sporinite contents, 2.1% and 2.3% respectively, the desorbed amount of CH_4, WG (0.85 mmol/g) was much greater than SF (0.44 mmol/g). This observation could most probably be attributed to the fact that it exhibited very low amounts of fusinite, semi-fusinite, vitrodetrinite and collotelinite, collectively.

- **Cutinite**

Cutinite maceral is non-existent in this suite of HRC SA coals, AN, SL and TN (0%). For MRC coals, an increase in cutinite, correlates to an increase in CH_4 desorption, an exception is noted for coal WG following the trend of other MRC coals. Although, WG does exhibit a very low fusinite and semi-fusinite and structure collotelinite amounts.

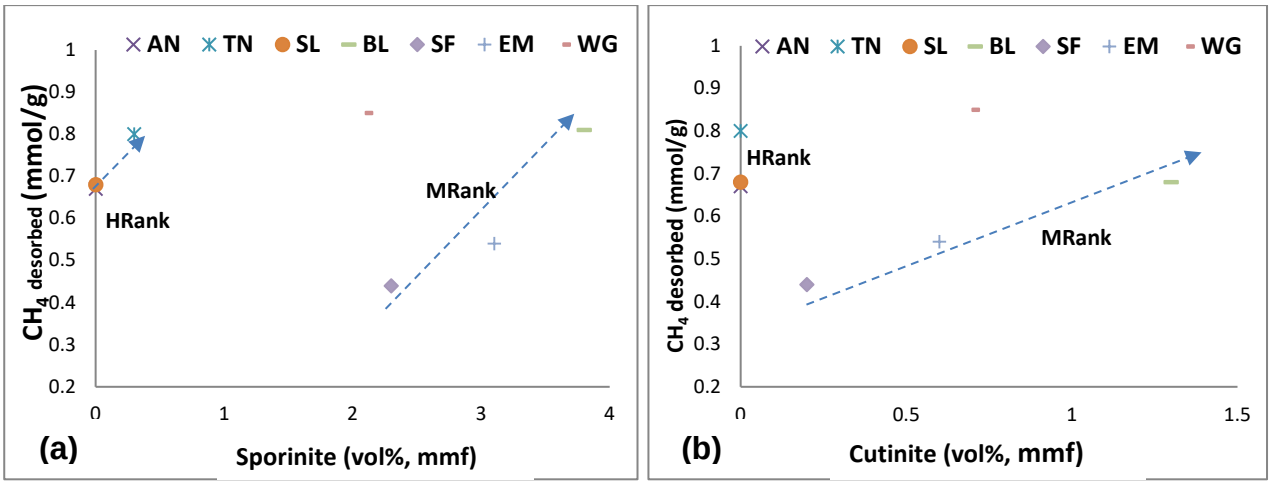

Figure 4.63: Comparison of liptinite macerals' compositions on CO_2 adsorption; (a) sporinite (b) cutinite

4.9.3.4.4 Summary of maceral correlations

These comparative correlations relating different macerals to CH_4 sorption capacity, do indeed show, that details of maceral compositions are essential and need to be identified and considered as well when evaluating the sorption/desorption capacity of the coal. It can be noted that a certain ratio of reactive maceral components to the inert ones in terms of petrographic composition is pertinent when gas sorption processes are to be considered (Holuszko & Masterlez, 2015). It is evident that only selected maceral constituents are seemingly responsible for gas transport and movement in the coal matrix.

Although, very noticeable, trends have been identified for these selected vitrinite macerals, it must be mentioned that in iso-rank coals, vitrinite with the same textural and optical characteristics might not be homogeneous with respect to its chemical properties. This is because variations are not only affected by rank but also by paleo environmental conditions and post-sedimentary history (Jimenez.*et al*., 1998).

Also to note, is that dual-porosity representations may include the response of the two principle components only; i.e. the release from storage in the porous matrix and transport in the fractured network (Wu *et al.,* 2010). This specific change in surface area due to CH_4 desorption results in an increase in effective stress. This indicates that the shrinking/swelling[3] of the coal matrix may be another factor to consider in understanding the CO_2-CH_4 sorption-desorption characteristics of the coal dynamic and flow kinetics.

The correlations from Figure 4.61 - 4.63, regarding the effect of the different maceral compositions for CH_4 desorption results do indeed show that details of maceral compositions are essential and need to be identified and considered as well when evaluating the sorption or desorption capacity of coal. The various constituents are responsible for gas transport and movement in the coal matrix. The ratios of the different macerals can either hinder sorption or desorption depending on their appreciable quantities

4.9.4 Effect of temperature on CH_4 desorption for CH_4 saturated samples

As discussed earlier in Section 4.5.3, for dry and degassed adsorption tests, in different coal basins the variations in temperature and pressure vary. In a particular basin, the same coal seam with identical degree of metamorphism (rank / metamorphism maturity attained) may be buried at different depths and it may also result in large in seam variation in temperature and pressure. Temperature and pressure of the reservoir are ever changing, thus resulting in differences in the adsorption capacity of coal (Zhong *et al*, 2002; Qing-Ling, 2008). The greater the burial depth, the larger the pressure and the higher the temperature will be. Pressure is an important condition for increasing the amount of adsorption of coal, while an increase in the temperature decreases the amount of adsorption (as discussed in detail in Section 4.7). This phenomenon poses a problem for predicting the amount of the gas adsorption or desorption of coals. Inaccurate prediction of the amount of adsorption also indicates that the prediction of its gas content is inaccurate. This inaccuracy can have an effect on a series of problems such as the reliability of the predicted amount of coal bed methane (CBM) resource, as well as the reliability of the predicted gas productivity and on the CO_2 storage capacity (Scott, 2002).

The effect is caused by changes in the porous system which occurs with changes in temperature. The properties and behavior of CO_2 at elevated temperatures change when kinetic energy of the gas molecules increases as temperature is increased. This limits number of pores, which can be completely filled because of CO_2 that will be more mobile due to the high levels of kinetic energy at elevated temperatures (Sakurovs *et al*. 2008).

Three (3) SA coals of different rank were chosen for this study: samples, TN (HRB), BL (MRC) and EM (MRC). From Figure 4.64, it is shown that sample TN had, overall the highest CH_4 total desorbed amount of 1.01 mmol/g. BL being the second highest with a maximum of 0.93 mmol/g. The least CH_4 desorbed was observed for EM which had a high of 0.61 mmol/g. Comparing the coals petrographic information and rank it shows that there is a visible correlation between CH_4 desorbed versus rank (as already discussed in section 4.9.3.1).

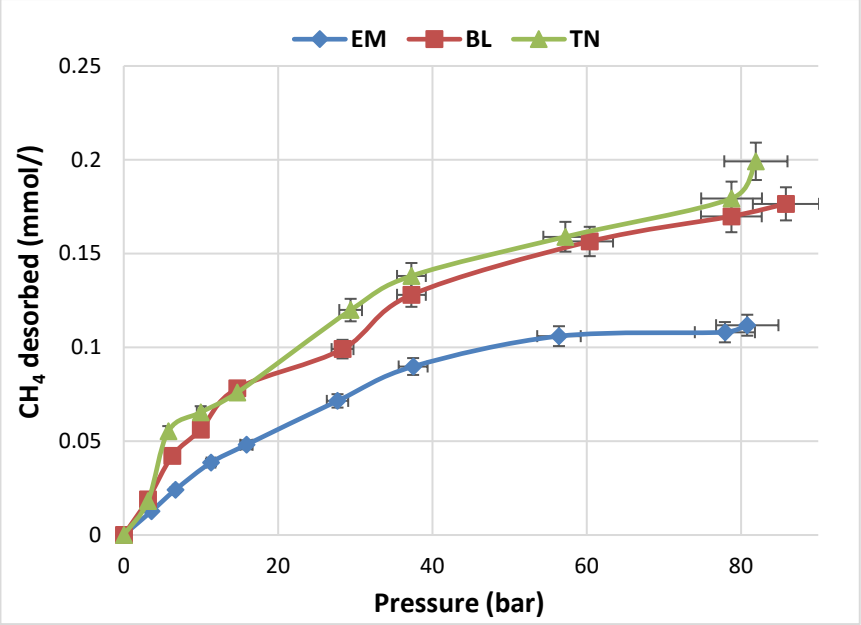

Figure 4.64: Comparison of CH_4 desorption @ 55 °C for different SA coals

Table 4.19 summarises the differences in CH_4 desorption with regard to temperature differences, i.e. the two tested (35 and 55 °C), pressure and vitrinite reflectance and BET data. Figures 4.65 (a) – (c) depict plots representing the evaluation of difference in temperature of the three (3) coals tested.

Table 4.19: Temperature difference and CH_4 desorption capacities

Sample ID.	*V_oR_{mr} (%)*	*Micro-pore area (m^2/g)*	*Max Pore volume (m^2/g)*	*Pressure (bar)*	*CH_4 desorbed (mmol/g)*		*Increased desorbed (%)*
					35 °C	*55 °C*	
EM	0.64	124.13	0.028	80.8	0.108	0.112	0.4
BL	0.70	149.67	0.034	84.8	0.154	0.176	2.2
TN	1.26	108.41	0.019	81.9	0.137	0.199	6.2

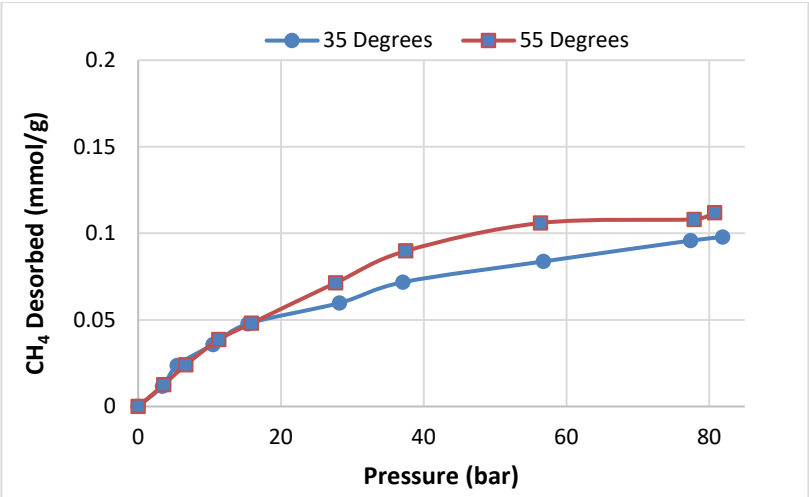

Figure 4.65 (a): Desorption of CH_4 in EM at 35 and 55 °C

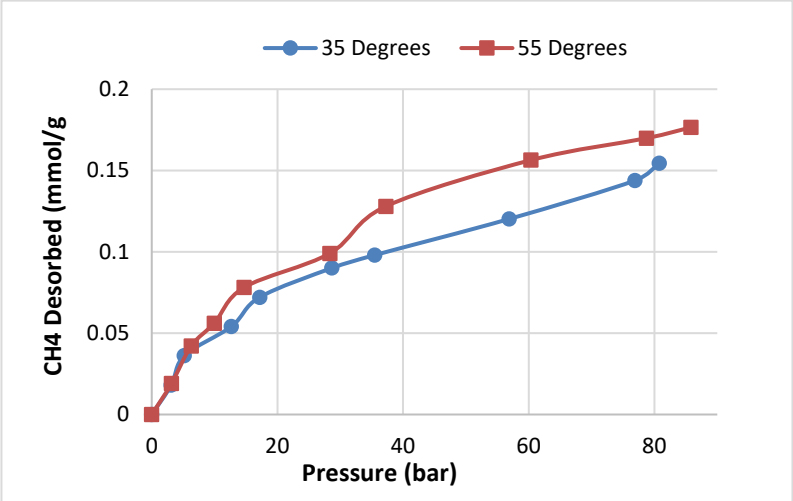

Figure 4.65 (b): Desorption of CH_4 in BL at 35 and 55 °C

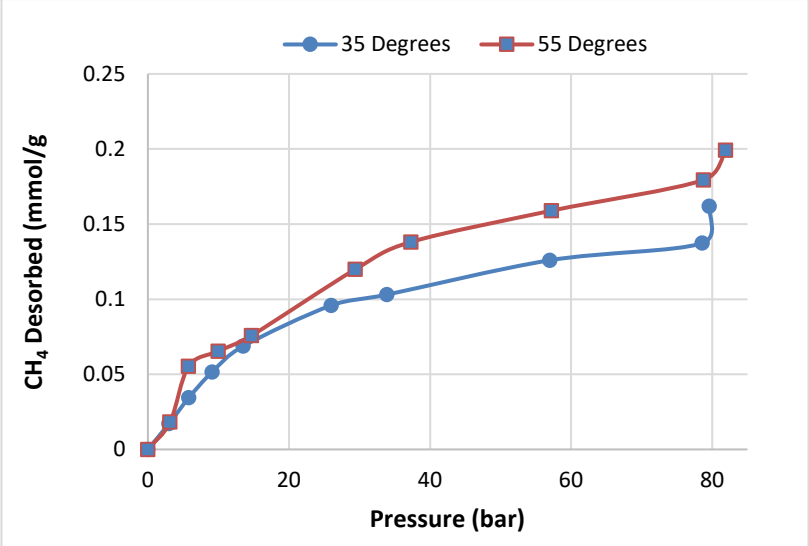

Figure 4.65(c): Desorption rates of CH_4 in TN at 35 and 55 ^oC

Generally there is an observed increase in the rate of CH_4 desorption for all three coals tested at 35 and 55 ^oC. This can as well be attributed to the fact that the increase in temperature causes the adsorbed CH_4 molecules to vibrate more due to the increased kinetic energy of the molecules. This consequently leads to ease of desorption when CO_2 is pumped under pressure into the coal structure. These results, for all three samples, clearly show that from a pressure injection exceeding ~30 bar, the CH_4 desorbed for the 55 ^oC experiment suddenly starts to increase as compared to the amount for the 35^oC test. Very limited studies on CO_2 adsorption versus CH_4 desorption are available to date, more especially with determining the effects of changes in temperature. It is believed from these results for desorption that the effect of temperature most certainly affects the desorbing gas rate and needs further investigation, considering the temperature-depth profile of coal seams.

4.9.5 Model fitting for CH_4 desorption experimental data

The experimental CO_2 adsorption and CH_4 desorption data was mathematically modelled. Only the CH_4 desorption data will be discussed here to avoid repetition of trends and findings already discussed in Section 4.8.3. for CO_2 adsorption. Table 4.20 shows the three isotherm's model parameters that were calculated after obtaining the respective plots using the equations outlined in Table 2.3, Section 2.11. All the models fitted the experimental adsorption and desorption data very well as seen by the linear regressions R^2 in Table 4.20. The plots for all the linear regressions are shown in Appendix H2. Appendix H3 contains modelling data for 55 ^oC experiments.

Table 4.20 Langmuir, Freundlich and Temkin model parameters **CH_4 desorption at 35^oC**

Model	***Langmuir***			***Freundlich***			***Temkin***		
Parameter	**R^2**	**a**	**b**	**R^2**	**n**	**K_F**	**R^2**	**b_T**	**A_T**
SL CH_4	0.973	0.158	0.041	0.9594	1.769	0.0112	0.9308	74911.1	0.418
AN CH_4	0.997	0.177	0.027	0.9726	1.551	0.008	0.9583	69998.9	0.325
TN CH_4	0.989	0.233	0.028	0.9616	1.642	0.0116	0.9741	61437.9	0.403
BL CH_4	0.991	0.261	0.021	0.965	1.566	0.0102	0.9754	58226.3	0.341
SF CH_4	0.988	0.091	0.042	0.9791	1.721	0.0062	0.9352	125586	0.424
EM CH_4	0.971	0.168	0.024	0.9588	1.621	0.0074	0.9736	90849	0.384
WG CH_4	0.993	0.231	0.031	0.9657	1.660	0.0125	0.971	58626	0.414

Figures 4.66 to 4.72 that follow show the comparison of all experimental CH_4 desorption data for the CH_4 saturated coals for the three (3) isotherm model isotherm fits that are most widely used to evaluate gas sorption and desorption isotherms.

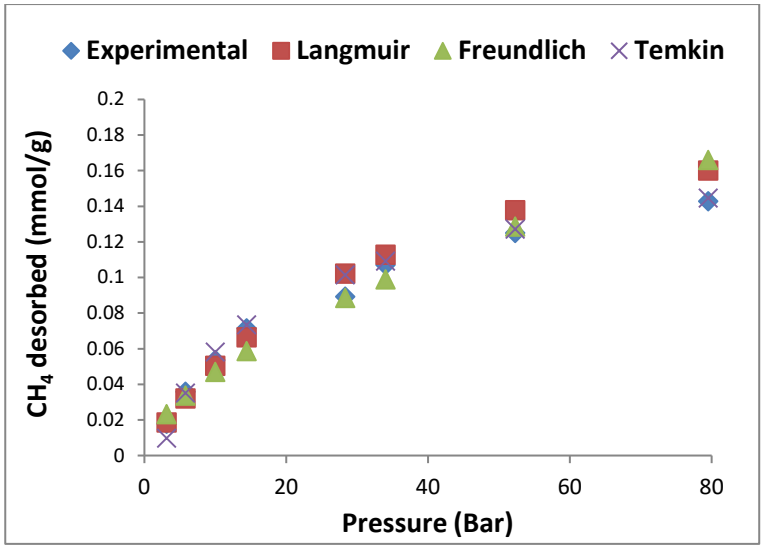

Figure 4.66: Model fit - TN CH_4 desorption isotherm

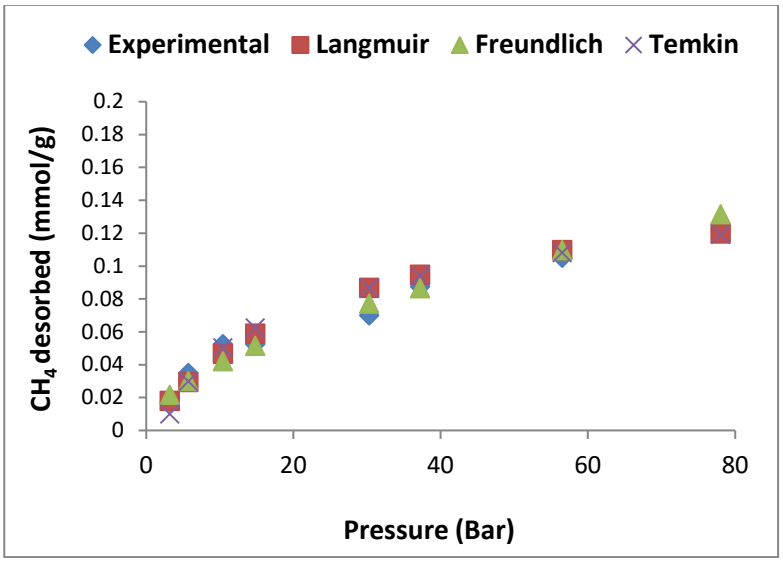

Figure 4.67: Model fit- SL CH_4 desorption isotherm

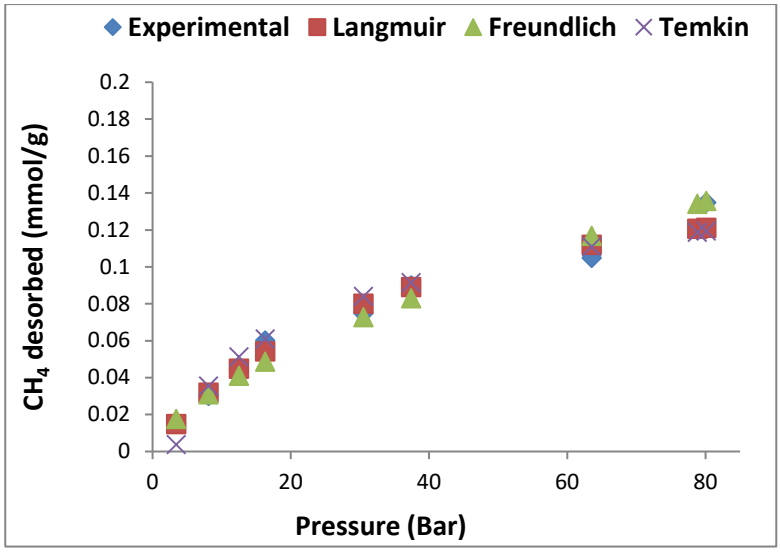

Figure 4.68: Model fit -AN CH_4 desorption isotherm

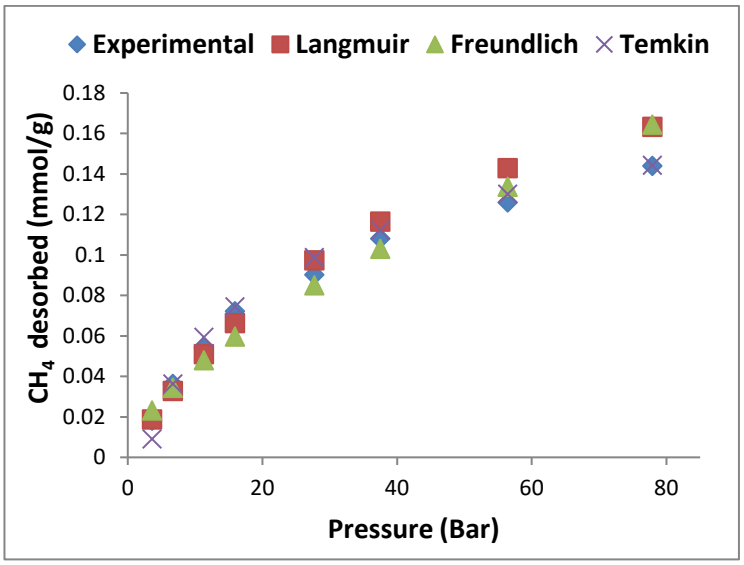

Figure 4.69: Model fit - BL CH_4 desorption isotherms

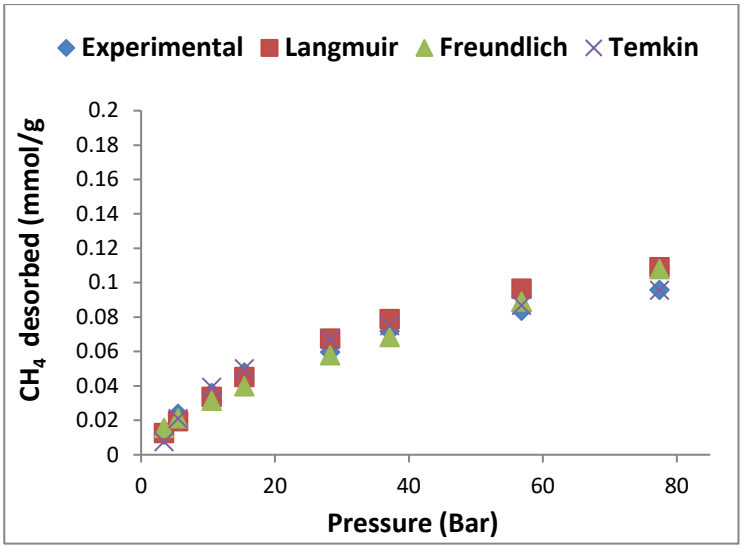

Figure. 4.70: Model fit- EM CH_4 desorption isotherm

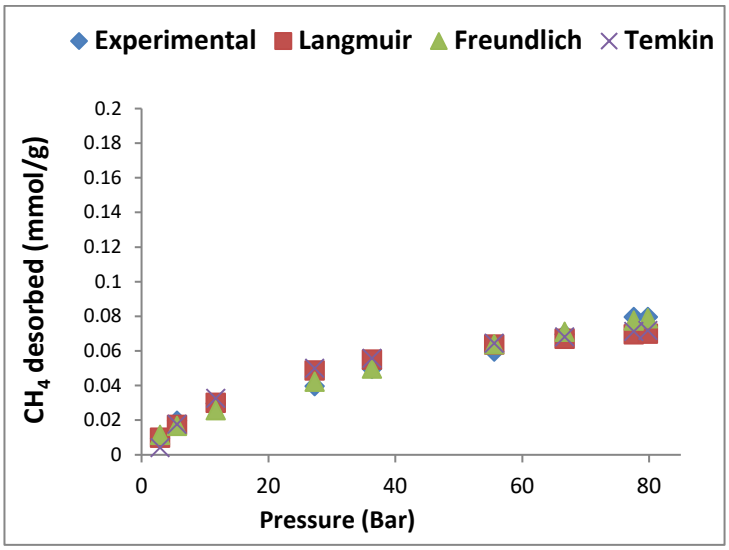

Figure 4.71: Model fit-SF CH_4 desorption isotherm

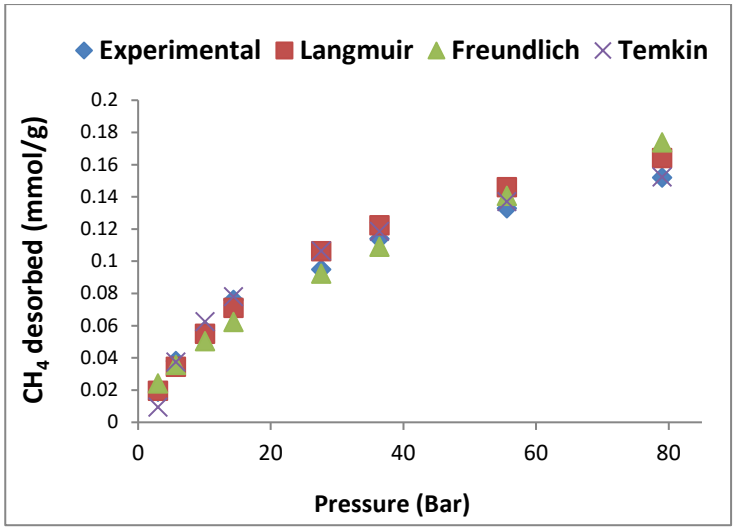

Figure 4.72: Model fit- WG CH_4 desorption isotherm

The comparison of all models for CO_2 sorption data showed quite increased theoretical calculated sorption for especially the Langmuir isotherm model (except for the SL sample). This is in contradiction with Langmuir characteristic sorption data calculated for pure CO_2 experimental sorption data (dried and degassed) samples as discussed in Section 4.8.1. This deviation could be attributed to the dual (binary)-component system and the effect of a binary sorption – desorption system that is occurring as the coal already has CH_4 that is diffusing (desorbing) due to the affinity of CO_2 sorption in the coal matrix over the CH_4 present in the coal matrix. Deviation in the traditional model seems to occur around 30 – 40 bars in sub-critical CO_2 conditions.

This concludes that the general Langmuir model is not equipped to model a binary sorption-desorption environment, where one gas is competing for sorption over another.

From modelling of experimental desorption CH_4 data, it can clearly be seen that the best regression fit seems to be more suitable to the Temkin theoretical parameters as compared to both the Langmuir and Freundlich models. These later two theoretical models show considerable deviation as pressure increased from sub-critical (~30-40 bars).

CHAPTER 5: SUMMARY AND CONCLUSIONS

The main aim of this research project was to firstly assess a variety of SA coals in terms of their CO_2 adsorption capacity, and secondly to consider CH_4 desorption capacity as per CO_2 injection using pure CO_2 for various parameters, such; incremental pressures (sub and super-critical), variable temperatures and moistures at a laboratory scale. A high pressure volumetric sorption apparatus (HPVAS) was designed and constructed (objective 1) in order to perform experiments to evaluate the sorption capacities of the ten (10) selected coals (with variable type and rank) and sorption capacities of CO_2 (pure) to produce sorption isotherms. As this project grew from the initial concept, as it became necessary to check a number of issues relating to the diversity of the coal properties and to simulate in-situ conditions (as far as possible), in order to effectively achieve the aims and objectives. A vast dataset on the interaction of CO_2 with different SA coals using the volumetric method (super-critical) for determining adsorption capacity has been produced.

In order to access the CO_2 sorption capacities and potential CH_4 characteristics of SA coals, the investigation to identify the fundamental differences around the effects of increased pressure under simulated in-seam conditions including super-critical pressures up to ~90 bar for gaseous and supercritical CO_2 addressing, objective 2. The effect of difference in coal moisture contents, were simulated in the range from ~0.5 – 4.4% and the influence of increased temperatures in the range of 35 to 55 ˚C (addressing objectives 3, 4, 5 and 6, outlined in chapter 1) were carried out on ten (10) SA coals. These results were then accessed to understand how CH_4 desorption would be influenced by the parameters compared to CO_2 sorption only (addressing objectives 7, 8 and 9).

Key findings have been summarised here for each tested section of parameters that were explored which address research the questions posed in Chapter 1:

1. *Can fundamental differences in CO_2 adsorption be observed in the different South African coal samples?*

Tests conducted, where the simulated pressures, moisture and temperatures could be considered to be more representative of underground storage conditions, have shown that there are most definitely differences in adsorption rates and capacities for different coal types, grade, and rank. Overall, many fundamental differences in CO_2 adsorption was observed in the different SA coal samples. From subcritical to supercritical tests with single component injection of CO_2, adsorption isotherms were produced for a variety of parameters; variable pressure, temperature and moisture content and these were compared to literature.

A very positive correlation was found to exist between adsorption of CO_2 (and desorption of CH_4), with increased pressure injection irrespective of coal moisture or temperature effects. The results also indicate that there is most certainly a correlation between CO_2 adsorption behaviour and coal rank, grade and coal type. The higher rank anthracitic coal samples (HRC and HRB), absorbed more CO_2 than bituminous MRC coals with a comparable maceral composition and ash content. Tests were conducted with the pressures, simulated moisture differences and increased temperatures which are more representative of underground storage conditions. Results have shown that there are most definitely differences in adsorption rates and capacities for different coal rank, maceral, mineral, ash, and varying moisture contents.

2. *Is there a correlation between coal rank and the ability to adsorb CO_2 gas in South African coals?*

According to the results from this study (Section 4.5.1), higher rank coals adsorbed more CO_2 than lower rank coals. Higher rank coals: AN, (HRC), TN (MRB), and SL (HRB) recorded higher CO_2 adsorption rates compared to the lower MRC; GN, IN, BL, EM, SF and WG samples. It is clear that samples in the range greater than 0.7% R_oV_{mr} exhibits increased CO_2 uptake due to larger macro, increasing meso porosity and micro-pore volumes. For CO_2 adsorption, behaviour of HRC and MRC coals suggests that microstructures play a rate-limiting role between diffusion in micro-pores and laminar flow (macro-pore). The flow behaviour of CO_2 in such coals is therefore not solely dependent on the cleat network and fracture system, but on a combination of cleat, macro-structure,

microstructure and mineralization in coal. As coals increase in rank, there is a general decrease in moisture, and an overall increase in density and structural arrangement which increases the micro porosity of the coal, the coal pore diameter decreases significantly, creating fine pores, i.e., the micro-pore proportion increases and hence pore porosity, and the physical structure of the coal gradually becomes more compact having a greater surface area thereby enhancing the adsorption capacity of CO_2 (Crosdale *et al.*, 1998; Ceglarska-Stefańska and Zarębska's, 2005; Zhao *et al*., 2014).

3. *Do inertinite-rich coals have the ability to adsorb a greater amount of CO_2 than vitrinite-rich coals?*

The distinction between coal rank and CO_2 adsorption is relatively easy to understand; however, the various types of compositions and ratios of vitrinite and inertinite maceral compositions, as well as the difference in mineral matter, is quite complex to compartmentalise.

The overall comparison of the maceral groups; vitrinite, inertinite and liptinite (vol%, mmf) versus the excess CO_2 adsorption capacity (mmol/g) for all SA coals tested in this study showed no apparent, direct relationship with relation to decreased CO_2 sorption potential. The slightly increasing liptinite content of coals; BL, GN, EM & WG, did however, correlate to a decrease with the CO_2 sorption capacity, although liptinite was a minor component (~<5%).

The effect of each maceral group was accessed separately, against CO_2 adsorption. Sorption capacity was found to decrease steadily with a decrease in vitrinite content for HR coals, AN, TN, SL & SM (R^2=0.8603), while increasing vitrinite content for MRC (R^2=0.8566) coals exhibit increasing sorption potential. Conversely, increased inertinite content for HR coals, exhibits increased CO_2 sorption capacities; while the opposite is noted for MRC coals, as inertinite decreases, the sorption also shows a decrease. This could be related to the fact that inertinite has been found to contain more macro-porosity (30 nm to 10 µm pore diameter) than vitrinite. Results presented here show that the vitrinite seems to be more of a controlling parameter than the inertinite for MRC coals while the

inertinite content increase seems to be more of a controlling factor for HR coal samples. Noted general trends are summarised below:

- MRC coals:
  1. High adsorbing: Inertinite-low, open lumen, less mineralized.
  2. Low adsorbing: higher proportion of inertinite band and higher vitrinite and/or unstructured inertinite bands, mineralized cell lumens/closed-tightly compressed or broken and pushed together.

- HRC coals:
  1. High adsorbing: low vitrinite and high inertinite content, well-defined cleat network, moderately in-filled with minerals.
  2. Low adsorbing: Greater vitrinite content, exhibiting tightly in-filled micro-cleats and other micro-fractures, and/or no micro-fractures.

.

The comparison between the vitrinite to inertinite ratio (V : I) for the HR and MRC coals to total amount of CO_2 adsorbed (mmol/g) exhibited the following:

1. HRC – Total adsorbed CO_2 decreases gradually with a decrease in the V: I ratio
2. MRC - Total adsorbed CO_2 shows a steady increase with increasing V:I ratio (up to R_oV_{mr} ~1.08%) and thereafter a small drop in sorption capacity for V:R ratio of 1.06 to 1.17.

The sorption capacity of CO_2 is most undoubtedly as a result of the coal make-up/composition. It is therefore proposed from this study that the sorption capacity of CO_2 is dictated by a myriad of complex heterogeneous coal compositions, individual macerals within the vitrinite and inertinite groups in different ratios/proportions are seemingly responsible for varied sorption capacities. The findings for this suite of coals are summarised here:

Vitrinite macerals:

1. *Collodetrinite:* Increase in content exhibits decrease in CO_2 adsorbed for both HR and MRC coals.

2. *Gelovitrinite*: : Increase in content exhibits decrease in CO_2 adsorbed for both HR and MRC coals
3. *Collotelinite*: increased content in HRC coals shows decrease in CO_2 adsorption whilst inverse was found for MRC coals.
4. *Pseudovitrinite:* increased content in HRC coals shows decrease in CO_2 adsorption whilst inverse was found for MRC coals.

Inertinite macerals:

1. ***Fusinite:*** increased content exhibits decreased CO_2 adsorption for HRC coals, while the inverse was found for MRC coals.
2. ***Inertodetrinite:*** increased content exhibits increased CO_2 adsorption for HRC coals, while the inverse was found for MRC coals.
3. ***Semi-fusinite:*** increased content exhibits increased CO_2 adsorption for both HRC and MRC coals.

***Liptinite macerals*:**

1. ***Sporinite:*** Increased content exhibits a decrease in CO_2 adsorption for both HRC and MRC coals.
2. ***Cutinite:*** increased content shows decrease in CO_2 adsorption for MRC coals. No visible cutinite observed in HRC coals.

Results (Section 4.5.3.2) indicate that the difference in source material i.e. the amounts of individual maceral components, results in different porosity, pore structure and therefore also in different adsorption rates (Laxminarayana & Crosdale, 2002). Each maceral has a specific and distinctive set of physical and chemical properties that control the adsorptive behaviour of coal. These findings suggests that a specific or ideal ratio between *only* the maceral components, in similar rank coals, is the controlling factor for best CO_2 adsorption required.

4. *Does the mineral composition in coal have an impact on the CO_2 adsorption capacity of the coal?*

Ash (proximate determination) and observable mineral matter (petrographic determination) of coals are analogous. It is concluded that mineral matter / ash is also a contributing factor to poor CO_2 adsorption. Results presented (Section 4.5.2 and 4.5.3) show that there is generally a negative correlation with ash content to CO_2 sorption capacity, as can be seen for the HRC, HRB and for MRC coals, where a linear decrease is observed. The two coals with the lowest ash% (AN (8.8%) and SL (6.1)) reported higher CO_2 sorption capacities. On average, for a 1% increase in ash content in HRC and MRC coals, a decrease of CO_2 adsorption capacity of 1.1 mmol/g and 0.018 mmol/g was observed respectively.

In addition, evaluation showed that there is also a negative relationship with mineral matter content to CO_2 sorption capacity. A linear decrease in CO_2 adsorption was observed which is in agreement with other investigators (Ward, 2002; Gürdal & Yalçin, 2001; Weniger *et al*., 2010; Dutta *et* al., 2011). On average, for a 1% increase in mineral matter content in coal, a decrease of CO_2 adsorption capacity of ~0.02 mmol/g is expected. Typically, the results indicate that coals high in mineral matter, greatly hinders the adsorption of CO_2 in coals. This ties in well with the observed ash content results.

5. *How does coal moisture and temperature affect CO_2 adsorption capacity?*

A marked decrease in CO_2 adsorption capacity results was observed for the moisture simulated coals ranging from sub-critical to supercritical pressures. It is concluded that the adsorbed water occupies some of the sorption sites and blocks the gas path to the micro-pore system thereby reducing the available surface for CO_2 gas molecule adsorption on the coal internal surfaces (Gentzis, 2000; Busch *et al*., 2003; Goodman *et al.*, 2004; Goodman *et al*., 2007; Day *et al*., 2008(b); Prusty, 2008; Gensterblum *et al*., 2009). Results presented (Section 4.6) show a steady decline in sorption ability as the moisture content increased gradually. A decrease of sorption of CO_2 was as great as 77% from dry (0%) to the maximum moisture simulated value of ~4.4%. Sorption decreased almost

linearly for every 1% of coal moisture increase, until the maximum coal saturation was approached at around 4%.

It is noted that this finding is vital for CO_2 sequestration, as even if initially dry, the coal seam will certainly become increasingly wet a result of drilling operations, fracturing of the coal bed and over-lying strata, and the deposition of a combustion gas which may contain residual water of combustion. Thus, an aqueous phase will be present and will vary in composition according to its source and the nature of the coal bed and the surrounding minerals with which it is in contact.

In terms of temperature, results (Section 4.7) from this study it was shown that CO_2 sorption capacity and rates tend to decrease with increasing temperatures (35 – 55 ^oC). An increase in temperature with increasing pressure displayed an inverse relationship, resulting in much lower overall CO_2 sorption capacities. The amount of CO_2 that can be adsorbed for any coal type is severely affected by temperature increases. Coal TN had the most marked decrease in sorption (72%) at the higher temperature of 55 ^oC compared to the other samples tested. This could be due to it having the lowest evaluated micro pore area (108.41 m^2/g) and displayed the least Langmuir monolayer capacity (70.16 m^2/g). And hence the increase in temperature causes the adsorbed CO_2 molecules to vibrate more due to the increased kinetic energy of the molecules, hence making fixed sorption difficult on the coal surface. The monolayer cannot be properly established and pore-filling sorption is also affected by increased temperatures.

From Isosteric results (Section 4.7.1), the range of heats of adsorption for these coals was found to be between 21.9 and 39.9 kJ/mol. Results confirm that the calculated heat of adsorption (KJ/mol) and the adsorption capacity (mmol/g) are positively correlative and that the nature of adsorption belongs to that of physical adsorption. Also, the adsorption heat increases linearly with rising CO_2 pressure. These results exhibiting decreased sorption with increased temperature are in agreement with discussions from other researchers mentioned in Section 2.12.4 (For MRC coals; Azmi *et al.,* 2006*;* Qing-Ling, 2008; Deishad *et al*, 2009; Levy *et al*., 1997; Ozdemir, 2004; Oldenburg, 2007; Sakurovs, *et al.,* 2008 and for HR coals; Saunders and Yang, 1985; Krooss *et al*., 2002).

6. *What is the CH_4 release rate relative to CO_2 adsorption rate?*

The exact ratio of number of moles of injected CO_2 adsorbed to number of moles of exact CH_4 desorbed (CO_2 : CH_4) could not be defined at each CO_2 injection from these results due to the method used of continued sampling and evacuation of GC lines with each incremental CO_2 pressure injection step.

However, the results do indicate that, under isothermal temperature, gas and confining pressure, the diffusion coefficient (*D*) of CH_4 gas for the different rank coals exhibited a trend of first dropping rapidly and then rising slowly (asymmetric ‘‘U” shape) with the increase in coal rank i.e. as R_oV_{mr} increases from 0.51% to 3.49%.

For MRC coals, the diffusion coefficient of CH_4 gas decreases by negative exponential function as the metamorphism degree (rank) of coal increased. While in HRC coals, the diffusion coefficient of CH_4 gas increases by exponential function with the metamorphism degree of coal increased. HR coals, displayed a gradually decreasing relationship of CH_4 desorbed as vitrinite reflectance increases (good polynomial regression fit $R^2 = 0.9419$). Results show that HRC samples TN, SL and AN with the higher vitrinite contents and higher rank exhibited decreasing CH_4 desorption rates compared to the very high mineral matter WG coal sample.

Pore geometry significantly influences the gas desorption potential as the injected CO_2 cannot access micro pores with narrow tortuous pore throats. Considering the kinetic molecular diameters of CH_4 and CO_2, which are 3.8 and 3.3 Å (0.38 nm and 0.33 nm), respectively, this suggests that the CO_2 molecules interacts more favourably with the coal matrix, be it macro, meso or micro porous, as the larger CH_4 molecules have greater difficulty in flowing through the smaller micro-pore regions of the coal matrix (Shen *et al*., 2011). Thus pore geometry allows CO_2, to very easily diffuse through the heterogeneous porous, bi/tri-modal coal structure and displace any physically adsorbed CH_4, while adsorbing more favourably. . This is an indication, that in terms of porosity, rank dominates displaying that the macro or micro porosity will be a key factor with regards to migration and diffusion of CH_4 through the respective coal matrices.

7. *What are the implications for CH_4 desorption from these results?*

Results revealed that incremental CO_2 injection pressures yielded higher CH_4 desorption rates, for both the HRC and MRC coals. A marked increase in CH_4 desorption using cyclic CO_2 injections is evident. Most importantly to note, is that the dual-porosity representations may include the response of the two principle components only i.e. the release from storage in the porous matrix and transport in the fractured network (Wu *et al.,* 2010). This specific change in surface area due to CH_4 desorption results in an increase in effective stress. This indicates that the shrinking/swelling of the coal matrix may be another factor to consider in understanding the CO_2-CH_4 sorption-desorption characteristics of the coal dynamic and flow of adsorbate gas diffusion kinetics.

Generally there is an observed increase in the rate of CH_4 desorption for all coals tested at 35 and 55 ^oC. This can be attributed to the fact that the increase in temperature causes the adsorbed CH_4 molecules to vibrate more due to the increased kinetic energy of the molecules. This consequently leads to ease of desorption when CO_2 is pumped under pressure into the coal structure.

The correlations regarding the effect of the different maceral compositions for CH_4 desorption results do indeed show that details of maceral compositions are essential and need to be identified and considered as well when evaluating the sorption or desorption capacity of coal. The various constituents are responsible for gas transport and movement in the coal matrix. The ratios of the different macerals can either hinder sorption or desorption depending on their appreciable quantities.

The data gathered using simulated CH_4 desorption tests have been used as a way forward to gain an understanding of CH_4 desorption in contrast to CO_2 adsorption for the various SA coals and their respective ranks and composition. Data has shown that there is indeed a greater affinity for CO_2 than CH_4. It must be noted that only tests with fresh bore samples can indicate a way forward in terms of the validity of enhanced coalbed CH_4 (ECBM) for any particular coal type. It would be advantageous if mass spectrometer attached to the adsorption equipment could be used to determine the exact volume / amount of CH_4 that

can be desorbed for varying CO_2 injection temperatures and pressures. There is definitely a contrast here for CH_4 desorption in contrary to CO_2 adsorption.

8. *Do the findings on South African coals differ from those previously reported in literature?*

To some extent there is very close similarity in the trend of results received thus far. In terms of more common aspects, like that of incremental pressure ranges, effects of coal moisture and, temperature differences, one can say that SA coal test results gave very similar outcomes in terms of matching previously reported work. For example, with increased pressures, it was observed that coal adsorption showed that more adsorption takes place at high pressure than at lower pressures for most coals types; this is due to the adsorbate being forced at high pressure to the surface adsorption and pore (micro and meso-pores) volumes on the coals, yet at low pressures there is very little pressure of the adsorbate into the coal pores. This is also the same with the testing of particle size. As particle size decreases, an increase is noted in the amount of CO_2 adsorbed, obviously due to the increased surface area. A difference can only be noted with large, core samples, as this will be able to give distinction between internal coal matrix structure for pore and network arrangement of the coal.

Other aspects that deal with coal type, rank, maceral, mineral composition, ash content and moisture have indicated very comparable results to most published literature. Experimental test work has been done using CO_2 from a sub-critical to super critical level, and do show very good repeatability and tendencies, not very different to global coals. Although the range of coal types has been fairly limited, all data thus far gave good correlations.

It is hoped, that the sum of results presented in this thesis, are of importance for the selectivity and technical modelling for CO_2 onshore coalbed storage and ECBM projects to be implemented in SA in the near future so as to meet the demands required to reduce CO_2 emissions in SA as part of the global community.

REFERENCES

ADAM, N. 1998. Sorption and desorption of gases (CH_4, CO_2) on hard coal and active carbon at elevated pressures. *Fuel,* 77(11):1243-1246.

ACCELERATED SURFACE AREA AND POROSIMETRY SYSTEM (ASAP 2020). Micromeritics. Operator's manual v3.01. 2006. Norcross (Georgia, US): Micromeritics Instrument Corporation. p. 4:15–25; C:11–44.

ASTM 1981. Standard specification for classification of coals by rank; Standard D388-77. In: 1981 Annual Book of ASTM Standards, Part 26, Gaseous Fuels, Coal and Coke, Atmospheric Analysis, p. 214-218.

ATKINS, P., W. 1998. *Physical Chemistry*. 6th ed. Oxford: Oxford.

AZMI, A. S., 2006. The influence of temperature on adsorption capacity of Malaysian coal"; Chemical Engineering and processing; Vol.45, pp: 392-396.

BACHU, S. 2000. Sequestration of CO_2 in geological media: criteria and approach for site selection in response to climate change. *Energy Conversion and Management,* 41(9):953-970.

BACHU, S. 2003. Screening and ranking of sedimentary basins for sequestration of CO_2 in geological media in response to climate change. *Environmental Geology,* 44:277-289.

BACHU, S. & ADAMS, J. J. 2003. Sequestration of CO_2 in geological media in response to climate change: capacity of deep saline aquifers to sequester CO_2 in solution. *Energy Conversion and Management,* 44(20):3151-3175.

BAE, J., S., BHATIA, S., K., RUDOLPH, V. & MASSAROTTO, P. 2009. Pore Accessibility of Methane and Carbon Dioxide in Coals, *Energy & Fuels,* 23-3319-3327.

BAE, J., S. & BHATIA, S., K. 2006. High-pressure adsorption of methane and carbon dioxideon coal. *Energy & Fuels,* 20(6): 2599-2607.

BELMABKHOUT, Y., FRÈRE, M & De WEIRELD, G. 2004. High-Pressure adsorption measurement. A comparative study of the volumetric and gravimetric methods. *Measurement Science and Technology,* 15: 848-858.

BIRDI, K., S. 2010. *Surface and colloid chemistry: principles and applications*. United State of America: Taylor and Francis Group, LLC.

BLAKEMORE, E., 2017. Six irrefutable pieces of evidence that prove climate change is real. *Popular Science.* Online: https://www.popsci.com/evidence-climate-change-is-real. Accessed: May 2017.

BOM. 2003. The Greenhouse Effect and Climate Change [Online]. Available from: http://www.bom.gov.au/info/GreenhouseEffectAndClimateChange.pdf. [Accessed: 12 December 2011].

BRADLEY, R. H. & RAND, B. 1995. On the Physical Adsorption of Vapors by Microporous Carbons. *Journal of Colloid and Interface Science,* 169(1):168-176.

BROMHALA, G., S., SAMS, W. N., JIKICHC, S., ERTEKIND, T. & SMITH, D., H. 2005. Simulation of CO_2 sequestration in coal beds: The effects of sorption isotherms, *Chemical Geology,* 217: 201– 211.

BRUNNAUER, S. 1945. *The Adsorption of Gases and Vapors*. (1). Princeton: Reinhold.

BUSCH, A. & GENSTERBLUM, Y. 2011. CBM and CO2-ECBM related sorption processes in coal: A review. *International Journal of Coal Geology,* 87(2):49-71.

BUSCH, A., GENSTERBLUM, Y. & KROOSS, B. M. 2003. Methane and CO_2 sorption and desorption measurements on dry Argonne coals: pure components and mixtures, *Int. Journal Coal Geology,* 55: 205-224.

BUSCH, A., KROOSS, B. M., GENSTERBLUM, Y., van BERG, F. & PAGNIER, H. J. M. 2003. High-pressure adsorption of methane, carbon dioxide and their mixtures on coals with special focus on the preferential sorption behaviour. *Journal of Geochemical Exploration,* 79, 671-674.

BUSCH, A., GENSTERBLUM, Y. & KROOSS, B. M. 2004. CH_4 and CO_2 sorption and desorption measurements on dry Argonne premium coals: pure components and mixtures. *International Journal of Coal Geology,* 45(1):5.

BUSCH, A., GENSTERBLUM, Y., KROOSS, B. M. & LITTKE, R. 2004. Methane and Carbon dioxide adsorption-diffusion experiments on coal: upscaling and modelling, *International Journal of Coal Geology,* 60: 151-168.

BUSCH, A., GENSTERBLUM, Y., KROOSS, B. M. & SIEMONS, N. 2006. Investigation of high-pressure selective adsorption/desorption behaviour of CO_2 and CH_4 on coals: An experimental study, *International Journal of Coal Geology,* 66: 53-68.

BUSCH, A., & KROOSS, B., M. 2014. Molecular concept and experimental evidence of competitive adsorption of H_2O, CO_2 and CH_4 on organic material, *Fuel 115 (2014) 581–588.*

BUSTIN, R. M & CLARKSON, C. R. 1998. Geological controls on coalbed methane reservoir capacity and gas content. *International Journal of Coal Geology,* 38, 3-26.

CARBON BRIEF, 2018. South Africa CO_2 Update, available online: Retrieved 21 April 2019 from https://www.carbonbrief.org/wp-content/uploads/2018/10/South-Africa-update-2.jpg

CARROLL, R., E. & PASHIN, J., C. 2003. Relationship of sorption capacity to coal quality: CO_2 sequestration potential of coalbed methane reservoirs in the Black Warrior Basin, International Coalbed Methane Symposium, Tuscaloosa, Al.

CEGLARSKA-STEFAŃSKA, G & ZARĘBSKA, K. 2008. Sorption of carbon dioxide - methane mixtures, *International Journal of Coal Geology,* 62: 211-222.

CHALMERS, G. R. L. & BUSTIN, R., M. 2007. On the effects of petrographic composition on coalbed methane sorption. *International Journal of Coal Geology,* 69: 288-304.

CHARRIÉRE, D., POKRYSZKA, Z. & BEHRA, P. 2010. Effect of pressure and temperature on diffusion of CO_2 and CH_4 into coal from the Lorraine basin (France). *International Journal of Coal Geology*. 81:373-380.

CHEN, S., G, LU, Y. & ROSTAM-ABADI, M. 2004. *CO_2 Capture and Transportation Options in the Illinois Basin*. Illinois: Illinois State Geological Survey.

CHEN, Y., MASTALERZ, M. & SCHIMMELMANN, A. 2012. Characterization of chemical functional groups in macerals across different coal ranks via micro-FTIR spectroscopy, *International Journal of Coal Geology*, 104: 22–33.

CHEMICAL TECHNOLOGY. 2006. CO_2 utilisation and storage, *Chemical Technology* July 2006, 20-27, Crown Publications, South Africa.

CLARKSON, C. R., BUSTIN, R. M. & LEVY, J. H. 1997. Application of the mono/multilayer and adsorption potential theories to coal CH_4 adsorption isotherms at elevated temperature and pressure. *Carbon,* 35(12):1689-1705.

CLARKSON, C. R. & BUSTIN, R. M. 1997. The effect of methane gas concentration, coal composition and pore structure upon gas transport in Canadian coals: implications for reservoir characterisation**,** *International Coalbed Methane Symposium, Tuscaloosa, AL, USA, May 12-16.*

CLARKSON, C. R. & BUSTIN, R. M. 1999. The effect of pore structure and gas pressure upon the transport properties of coal: a laboratory and modeling study. 1. Isotherms and pore volume distributions. *Fuel,* 78(11):1333-1344.

COALIFICATION PROCESS: from swamp to coal (image). 2011. Retrieved 26 February 2012 from http://www.christianforums.com/threads/creationist-explain-the-miocene-please.7263729/page-21

CLOETE, M. 2010. *Atlas on geological storage of carbon dioxide in South Africa* (No. ISBN:978-1-920226-24-4). Silverton, Pretoria, South Africa: Council for Geoscience.

CO2CRC. 2008. *Storage Capacity Estimation, Site Selection and Characterisation for CO_2 Storage Projects* (No. RPT08-1001). Canberra: Australia.

COSTA, E., SOTELO, J., L, CALLEJA, G. & MARRÓN, C. 1981. Adsorption of binary and ternary hydrocarbon gas mixtures on activated carbon: Experimental determination and theoretical prediction of the ternary equilibrium data. *AIChE Journal,* 27(1):5-12.

CROSDALE, P. J., BEAMISH, B. B. & VALIX, M. 1998. Coalbed methane sorption related to coal composition, *International Journal of Coal Geology,* 35: 147-158.

CUI, X. J., BUSTIN, R. M & CHIKATAMARLA, L. 2007. Adsorption-induced coal swelling and stress: implications for methane production and acid gas sequestration into coal seams, *Journal of Geophysics Resources [solid earth],* 12: 1-16.

DAY, S., FRY, R. & SAKUROVS, R. 2008a. Swelling of Australian coals in supercritical CO_2, *International Journal of Coal Geology,* 74(1): 41-52.

DAY, S., SAKUROVS, R., & WEIR, S. 2008b, Supercritical gas sorption on moist coals, *International Journal of Coal Geology,* 74(3-4): 203-214.

DAY, S., FRY, R. & SAKUROVS, R. 2012. Swelling of coal in carbon dioxide, methane and their mixtures. *International Journal of Coal Geology,* 93: 40-48.

DAY, S., DUFFY, G., SAKUROVS, R. & WEIR, S. 2008. Effect of coal properties on CO_2 sorption capacity under supercritical conditions. *International Journal of Greenhouse Gas Control,* 2: 342-352.

DEAT (Department of Environmental Affairs and Tourism, Souh Africa). 2007. Long term mitigation mitigating scenarios. Strategic options for South Africa. [Electronic Version]. Retrieved on 11 August 2011 from

http://www.environment.gov.za/HotIssues/2008/LTMS/A%20LTMS%20Scenarios%20for%20SA.pdf

DEISHAD, M., THOMAS, S. G. & WHEELER, M. F. 2009. Parallel numerical reservoir simulations of non-isothermal compositional flow and chemistry, SPE Reservoir simulation Symposium Proceedings, The Woodlands, TX.

DIFFERENT RANKS OF COAL, Alberta Energy (image) Retrieved 15 June 2012 from http://history.alberta.ca/energyheritage/coal/early-coal-history-to-1900/global-coal-formation/coal-properties.aspx#page-1

DONOHUE, M. D. & ARANOVICH, G. L. 1998. Classification of Gibbs adsorption isotherms. *Advances in Colloid and Interface Science,* 76–77(0):137-152.

DU, X. & WU, E. (2007). Porosity of Microporous Zeolites A, X and ZSM-5 Studied by Small Angle X-Ray Scattering and Nitrogen Adsorption. *Journal of Physics and Chemistry of Solids*, 68, 1692-1699.

DUBININ, M., M. 1966. *In Chemistry and Physics of Carbon*. (2). P. L. Walker, Jr. ed. New York: Edward Arnold, Ltd.DUTTA, P., BHOWMIK, S. & DAS, S., 2011. Methane and carbon dioxide sorption on a set of coals from India, *Journal of Coal Geology,* 85: 289-2.

DUTTA, P, HARPALANI, S. and PRUSTY, B., 2008. Modeling of CO_2 sorption in coal. *Fuel,* 87: 2023-2036.

DUTTA, P., BHOWMIK, S. and DAS, S., 2011. Methane and carbondioxide sorption on a set of coals from India, *International Journal of Coal Geology,* 85: 289-299.

EC. 2009. Climate change-what is it all about?, *An introduction to young people*.

Ecoal, 2002. A pathway to decreasing carbon intensity. *World Coal Institute, Vol. 44.*

ELDER, W. Greenhouse Gas Effect. National Park Services.Retrieved 11 April 2012 from http://www.nps.gov/goga/learn/nature/climate-change-causes.htm

ENNIS-KING, J. & PATERSON, L. 2000. Reservoir engineering issues in the geological disposal of CO2. Paper presented at the *Greenhouse Gas Control Technologies: Proceedings of the 5th International Conference on Greenhouse Gas Control Technologies (GHGT-5)*, Collingwood, Victoria, Australia.

ENNIS-KING, J. & PATERSON, L. 2001. Reservoir engineering issues in the geological disposal of CO_2. Paper presented at the *Greenhouse Gas Control Technologies: Proceedings of the Fifth International Conference on Greenhouse Gas Control Technologies*, Cairns: Australia.

FAIZ, M., A. SAGHAF, N. SHERWOOD, AND I. WANG. 2007. The influence of petrological properties and burial history on coal seam methane reservoir characterisation, Sydney Basin, Australia. *International Journal of Coal Geology* 70(1–3): 193–208.

FINDENEGG, G., H. 1984. Fundamentals of Adsorption. New York: United Engineering Trustees Inc.

FITZGERALD JE, PAN Z, SUDIBANDRIYO M, ROBINSON JR RL, GASEM K. A. M., REEVES SR. 2005. Adsorption of methane, nitrogen, carbon dioxide and their mixtures on wet Tiffany coal. *Fuel*: 84: 2351–2363.

FOO, K. Y. & HAMEED, B. H. 2010. Insights into the modelling of adsorption isotherm systems.*Chemical Engineering Journal,* 156(1): 2-10.

GENTZIS, T. 2000. Sub-surface sequestration of carbon dioxide – an overview from Alberta (Canada) perspective, *International Journal of Coal Geology,* 43(1-4): 287-305.

GERTENBACH, R., M. 2009. Methane and Carbon Dioxide sorption studies on South African coals, MSc Dissertation, University of Stellenbosch.

GLOBAL CCS Institute, 2012. CO_2 Phase diagram: Temperature versus Pressure, http://decarboni.se/publications/co2-liquid-logistics-shipping-concept-llsc-overall-supply-chain-optimization/31

GLOBAL CCS Institute, Global Status of CCS: 2016 Summary Report, Retrieved 11 January 2017 from https://www.globalccsinstitute.com/projects/large-scale-ccs-projects

GLOBAL CO_2 EMISSIONS JUMPED 3% IN 2011. *Environmental Leader: Environmental and Energy Management News.* [Electronic Version]. Retrieved on 23 July 2012 from http://www.environmentalleader.com/2012/07/23/global-co2-emissions-jumped-3-in-2011/

GOODMAN, A. L., BUSCH, A., DUFFY, G. J., FITZGERALD, J. E., GASEM, K. A. M., GENSTERBLUM, Y., et al. 2004. An Inter-laboratory Comparison of CO_2 Isotherms Measured on Argonne Premium Coal Samples. *Energy & Fuels,* 18(4):1175-1182.

GOODMAN, A. L., BUSCH, M., BUSTIN, L., CHIKATAMARLA, S., DAY, G. J. DUFFY, J. E., FITZGERALD, J. E., GASEM, K. A. M., GENSTERBLUM, Y., HARTMAN, C., JING, C., KROOSS, B. M., MOHAMMED, S., T., PRATT, T., ROBINSON, R. L., ROMANKOV, V., SAKUROVS, R., SCHROEDER, K. & WHITE, C. M. 2007. Inter-laboratory comparison II: CO_2 isotherms measured on moisture-equilibrated Argonne premium coals at 55 ^{0}C and up to 15 MPa, *International Journal of Coal Geology,* 72(3-4): 153 – 164.

GREGG, S.J. and SING, K.S.W., 1982. Adsorption, Surface Area and Porosity. Academic Press, London.

GROENEWALD, Y. 2011. SA policy sets the example at COP17. *Mail & Guardian News*. [Electronic Version]. Retrieved on 4 October 2012 from Http://mg.co.za/article/2011-10-21-sa-policy-sets-the-example-at -cop17/

GRUSZKIEWICZ, M. S., NANEY, M. T., BLENCOE, J. G., COLE, D. R., PASHIN, J. C. & CARROLL, R. E. 2009. Adsorption kinetics of CO_2, CH_4, and their equimolar mixture on

coal from the Black Warrior, West-Central Alabama, *International Journal of Coal Geology,* 77: 23-33.

GÜRDAL, G. and YALÇIN, M., N. 2000. Gas adsorption capacity of Carboniferous coals in the Zonguldak basin (NW Turkey) and its controlling factors. *Fuel,* 79: 1913-1924.

GÜRDAL, G. and YALÇIN, M., N. 2001. Pore volume and surface area of the Carboniferous coals from the Zonguldak basin (NW Turkwy) and their variations with rank and maceral composition, *Coal Geology*, 48: 133-144.

HALMANN, M. M., & STEINBERG, M., 1999, Greenhouse gas carbon dioxide mitigation: Science and Technology, Lewis Publishers, Boca Raton-FL.

HAMELINCK, C. N., FAAIJ, W. C., TURKENBURG, F. van BERGEN, PAGNIER, H. J. M., BARZANDJI, O. H. M., WOLF, K-H. A. A. & RUIJG, G. J., 2002. CO_2 Enhanced coal bed methane production in the Netherlands, *Energy,* 271: 647-674.

HARPALANI S., PRUSTY B.K. & DUTTA P. 2006. Methane/CO_2 sorption modeling for coalbed methane production and CO_2 sequestration. *Energy Fuel*; 20: 1591-1599.

HASSAN, S., M, N. 2005. Techno-Economic Study of CO_2 Capture Process for Cement. Master of Applied Science: Chemical Engineering, Waterloo, Ontario, University of Waterloo.

HE, J., SHI, Y., AHN, S., KANG, J. W. & LEE, C.-H. 2010. Adsorption and Desorption of CO_2 on Korean Coal under Subcritical to Supercritical Conditions. *The Journal of Physical Chemistry B,* 114(14):4854-4861.

HE, L., MELNICHENKO, Y., B., MASTALERZ, M., SAKUROVS, R., RADLINSKI, A., P. & BLACH, T. 2012. Pore Accessibility by Methane and Carbon Dioxide in Coal as Determined by Neutron Scattering, *Energy Fuels, 26:1975−1983*.

HENDRIKS, C., GRAUS, W. & VAN BERGEN, F. 2004. *Global CO_2 storage potential and costs*. Ecofys in cooperation with TNO.

HERZOG, H. & GOLOMB, D. 2004. Carbon Capture and Storage from Fossil Fuel Use. *Encyclopedia of Energy* (pp. 1-19). Massachusetts Institute of Technology, Laboratory for Energy and the Environment.

HIDNERT, P. & PEFFER, E., L. 1950. *Density of Solids and Liquids*. USA: Washington: United States Department of Commerce.

HIETKAMP, S., ENGELBRECHT, A., SCHOLES, B. & GOLDING, A. 2004. *The Potential for Sequestration of CO_2 in South Africa*. Pretoria: CSIR.

HOFFERT, M., I & CALDEIRA, K. 2004. Climate Change and Energy, Overview. *Encyclopedia of Energy* (Vol. 1, pp. 359-380). New York.

HOLLOWAY, S. & SAVAGE, D. 1993. The potential for aquifer disposal of CO_2 in the UK. *Energy Conversion and Management,* 34(9–11):925-932.HOLLOWAY, S. 1997. An overview of the underground disposal of carbon dioxide, *Energy Conversion and Management,* 38: 193-198.

HOLUSZKO, M., E. & MASTERLEZ, M., D. 2015. Coal macerals chemistry and its implications for selectivity in coal floatability, *International Journal of Coal Preparation and Utilisation,* 35:2, 99-110.

HONG, D. H. & SUH, M., P. 2012. Selective CO_2 adsorption in a metal–organic framework constructed from an organic ligand with flexible joints, *Chemical Communique,* 48: 9168–9170.

HSIEH, S. T. and DUDA, J. L. 1987. Probing coal structure with organic vapour sorption, *Fuel,* 66: 170-177.

HUMAYUN, R., TOMASKO, D.L., 2000. High-resolution adsorption isotherms of supercritical carbon dioxide on activated carbon, *AICHE Journal*, 10: 2065–2075.

ICCP. 1998. The new vitrinite classification (ICCP system 1994). *Fuel,* 77:349–358.

ICCP. 2001. The new inertinite classification (ICCP System 1994). *Fuel,* 80:459–471.

IEA Greenhouse Gas R and D Programme, (IEA GHG). 2007. "Storing CO_2 in Unmineable Coal Seams"**,** July 2007.

IEA. 2010. *ETSAP: Energy Technology Systems Analysis Programme*. Paris: France.

IEA. World Energy Outlook. 2006. [Electronic Version]. Retrieved on 8 November 2009 from Http://www.worldenergyoutlook.org/2006.asp

INGLEZAKIS, V., J & POULOPOULOS, S., G. 2006. *Adsorption, Ion Exchange and Catalysis: Design of Operations and Environmental Applications*. Amsterdam, Netherlands: ELSEVIER.

IPCC (Intergovernmental Panel on Climate Change). 1971. *International hand-book of coal petrography*. 1st supplement to 2nd ed. Paris: CNRS.

IPCC (Intergovernmental Panel on Climate Change). 1998. The new vitrinite classification (ICCP system 1994). *Fuel,* 77:349-358.

IPCC (Intergovernmental Panel on Climate Change). 2005. *IPCC Special Report on CO_2 Capture and Storage*. Cambridge, UK and New York, USA.

IPIECA, COP 22 - Highlights and Outcomes, Retrieved on 10 February 2017, from http://www.ipieca.org/news/cop-22-highlights-and-outcomes/

ISO. Solid mineral fuels. Hard coal – determination of moisture in the general analysis test sample by drying in nitrogen, in ISO 11722:2013. International Organisation for Standardisation, Geneva, Switzerland; 2013. 5p.

ISO. Solid mineral fuels: determination of ash, in ISO 1171:2010. International Organisation for Standardisation, Geneva, Switzerland; 2010. 4p.

ISO. Hard coal and coke- Determination of volatile matter, in ISO 562:2010. International Organisation for Standardisation, Geneva, Switzerland; 2010. 8p.

ISO. Coal Ultimate analysis, in ISO 17247:2013. International Organisation for Standardisation, Geneva, Switzerland; 2013. 5p.

ISO. Solid mineral fuels – determination of sulfur by IR spectrometry, in ISO 19579:2006. International Organisation for Standardisation, Geneva, Switzerland; 2006. 4p.

ISO. Methods for the petrographic analysis of coals. Part 2: Methods of preparing coal samples, in ISO 7404-2:2009. International Organisation for Standardisation, Geneva, Switzerland; 2009. 12p.

ISO. Methods for the petrographic analysis of coals. Part 5: Method of determining microscopically the reflectance of vitrinite, in ISO 7404-5:2009. International Organisation for Standardisation: Geneva, Switzerland; 2009.14p.

ISO. Classification of coals, in ISO 11760:2005. International Organisation for Standardisation, Geneva, Switzerland; 2005. 9p.

ISO. Methods for the petrographic analysis of coals. Part 3: Method of determining maceral group composition, in ISO 7404-3:2009. International Organisation for Standardisation, Geneva, Switzerland; 2009. 7p.

ISO 7404 - 2, “Methods for the petrographic analysis of bituminous coal and anthracite, Part 2: Method of preparing coal samples.,” *International Standards Organization*. Standards Organization International, South Africa, 1985.

JESSEN, K., TANG, G-Q, & KOVSCEK, A. R. 2008. Laboratory and Simulation investigation of enhanced coalbed methane Recovery by gas injection, *Transport in Porous Media,* 73(2): 141-159.

JOUBERT, J.I., GREIN C.T., and BIENSTOCK D., 1973, Sorption of Methane in Moist Coal, *Fuel*, 52:181-185.

JOSEPH, J. T. & FORRAI, T. R. 1992. Effect of Exchangeable Cations on Liquefaction of Low Rank Coals, *Fuel*, Vol.71:75-80.

JILLAVENKATESA, A., DAPKUNAS, S., J & LUM, L., H. 2001. *Particle Size Characterization*. USA: Washington, DC: Special Publication 960-1.

JIMENEZ, A., IGLESIAS, M., J., LAGGOUN DE-FARGE, F. & SUAREZ-RUIZ, I. 1998. Study of physical and chemical properties of vitrinites: Inferences on depositional and coalification controls, *Chemical Geology Elsevier*, 150 (3-4):197-221.

KAPOOR, A., RITTER, J., A & YANG, R., T. 1989. On the Dubinin-Radushkevich Equation for Adsorption in Microporous Solids in the Henry's Law Region. *Langmuir,* 5:1118-1121.

KARACAN, C., O., & MITCHELL, G., D. 2003. Swelling-induced volumetric strains internal to a stressed coal associated with CO_2 sorption, *International Journal of Geology,* 53:201-217.

KELEMEN, S.R., KWIATEK, L.M., & LEE, A.G.K. 2006. Swelling and sorption response of selected Argonne premium bituminous coals to CO_2, CH_4, and N_2, International CBM Symposium, Tuscaloosa, Alabama.

KHALFAOUI, M., KNANI, S., HACHICHA, M. A. & LAMINE, A. B. 2003. New theoretical expressions for the five adsorption type isotherms classified by BET based on statistical physics treatment. *Journal of Colloid and Interface Science,* 263(2):350-356.

KHALFAOUI, M., M.H.V. BAOUAB, M., H, V, GAUTHIER, R. & LAMINE, A., B. 2002. *Adsorption Science and Technology,* 20.

KHANEKO, K & MURATA, K. 1997. An analytical method of micropore filling of a supercritical gas, *Adsorption,* 3: 197-208.

KIM, H. J., SHI, Y., HE, J., LEE, H.-H. & LEE, C.-H. 2011. Adsorption characteristics of CO_2 and CH_4 on dry and wet coal from subcritical to supercritical conditions. *Chemical Engineering Journal,* 171(1):45-53.

KORRE, A., SHI, J. Q., IMRIE, C., GRATTONI, C. & DURUCAN, S., 2007. Coalbed methane reservoir data and simulator parameter uncertainty modelling for CO_2 storage performance, *Int. Journal of Greenhouse Gas Control,* 1: 492- 501.

KROOSS, B. M., VAN BERGEN, F., GENSTERBLUM, Y., SIEMONS, N., PAGNIER, H. J. M. & DAVID, P. 2002. High-pressure CH_4 and CO_2 adsorption on dry and moisture-equilibrated Pennsylvanian coals. *International Journal of Coal Geology,* 51(2):69-92.

LABUSCHAGNE, B. C. J. 1986. Relationships Between Oil and Agglomeration and Surface Properties of Coal: Effect of pH and oil composition, *Coal Preparation*, Vol.3:.1-13.

LAMBERSON, M.N. and BUSTIN, R.M., 1993. Coalbed methane characteristics of Gates Formation coals, northeastern British Columbia: Effect of maceral composition. *American Assoc. Petrology: Geol*. Bull. 77, 2062–2076.

LARSEN, J. W., FLOWERS II, R. A., HALL, P & CARLSON, G. 1997. Structural rearrangement of strained coals, *Energy Fuels,* 11: 998-1002.

LARSEN, J. W. 2004. The effects of dissolved CO_2 on coal structure and properties, *International Journal of Coal Geology,* 57: 63-70.

LARSEN, J. W., HALL, P., and WERNET, P. C. 1995, Pore Structure of Argonne Premium Coals, *Energy & Fuels*, Vol.9: 324-330.

LASAGA, A. C. & R. A. BERNER 1998. Fundamental Aspects of Quantitative Models for Geochemical Cycles., *Chemical Geology* 145 (3-4), 161-175.

LATONA CONSULTING SA (Pty) Ltd. 2011. SA's mine boundaries for CH_4 highest emissions, provided by Cook. A.

LAXMINARAYANA, C & CROSDALE, P., J. 1999. Role of coal type and rank on methane sorption characteristics of Bowen basin, Australia coals, *International Journal of Coal Geology,* 40: 309-325.

LAXMINARAYANA, C & CROSDALE, P., J. 2002. Controls on methane sorption capacity of Indian coals, AAPG Bulletin 86 (2), 201-2012.

LETETE, T., MONDLI, G. & MARQUARD. 2010. *Information on climate change in South Africa: greenhouse gas emissions and mitigating options*. Cape Town: University of Cape Town, Energy Research Centre.

LEVINE, J., 1993. Coalification: the evolution of coal as source rock and reservoir. In: LAW, B.E., RICE, D.D. (Eds.), Hydrocarbons from Coal. American Association of Petroleum geologists, *Studies in Geology Series*, 38: 39–77.

LEVY, J.H., DAY S.J., and KILLINGLEY J.S., 1997. Capacities of Bowen Basin Coals Related to Coal Properties. *Fuel,* 76: 813-819.

LI, K. 2011. *Carbon Capture by Adsorption*. Cooperative Research Centre for Greenhouse Gas Technology (CO_2CRC): Monash University.

LI, Z., LIU, D., CAI, Y. & SHI, Y. 2016. Investigation of methane diffusion in low-rank coals by a multiporous diffusion model, *Journal of Gas Science and Engineering*, 33: 97-107.

LIU, X. & HE, X. 2016. Effect of pore characteristics on coalbed methane adsorption in middle-high rank coals, Adsorption, Springer Science: DOI 10.1007/s10450-016-9811-z.

LMS. 2011. Endecotts Test Sieve Shakers. *Vacuum, Pressure & Laboratory Equipment, 30*: 5.

LOTZ, M. & BRENT, A., C. 2008. A review of CO_2 capture and sequestration and Kyoto Protocol's clean development mechanism and prospects for Southern Africa. *Journal of Energy in Southern Africa,* 19(1):13-24.

MA, D., ZHANG, J., BAI, J. & ZHANG, H. 2014. Thermodynamic Characteristics of Adsorption-Desorption of Methane in 3# Coal Seam of Sihe, *Natural Resources,* 5: 782-794. Published Online: September 2014 in SciRes. http://www.scirp.org/journal/nr, http://dx.doi.org/10.4236/nr.2014.512067.

MABUZA M. M., 2013. Evaluating the Adsorption Capacity of Supercritical CO_2 on South African Coals using a Simulated Flue Gas. Magister Techonologiae, Pretoria: South Africa, Tshwane University of Technology.

MAPHALA, T. 2012. Effects of Carbon Dioxide Storage in Coal on the Physical and Chemical Properties of Coal. PhD Degree, Johannesburg, University of the Witwatersrand.

MARSH, H. (Ed.). 2001. Activated Carbon Compendium: A collection of papers from the journal *Carbon:* 1996-2000, Elsevier Science Ltd.

MASEL, R., I. 1996. *Principles of Adsorption and Reaction on Solid Surfaces*. Canada: Wiley.

MASTALERZ, M. & BUSTIN, R., M. 1997. Variation in the chemistry of macerals in coals of the Mist Mountain Formation, Elf Valley coalfield, British Columbia, Canada. *International Journal of Coal Geology*, 33: 43–59.

MASTERLEZ, M., GOODMAN, A & CHIRDON, D. 2004. Coal lithotypes before, during and after exposure to CO_2; Insighs from Direct Fourier Transform Infrared investigation, USA, *Energy & Fuels, 2*6: 3586-3591.

MASTERLEZ M., GLUSKOTER, H. & RUPP, J. 2012. Carbon dioxide and methane sorption in high volatile bituminous coals from Indiana, USA, *International Journal Coal of Geology,* 60: 43-56.

MATJIE, R.H, LI, Z., WARD, C. R., BUNT, J. R. & STRYDOM, C. A. 2016. Determining of mineral matter and elemental composition of individual macerals in coals from Highveld mines, *Journal of Southern African Institute of Mining and Metallurgy,* 116: 168-180.

MAZZOTTI, M., PINI, R. & STORTI, G. 2009. Enhanced Coalbed methane recovery, *Journal of Supercritical Fluids,* 47: 619-627.

MCCARTY, R., D. 1972. *Thermophysical properties of helium-4 from 2 to 1500 K with pressures to 1000 atmosphere. NBS Technical note 631*. US Department of Commerce.

MCCOY. 2008. The Economics of CO_2 Transport by Pipeline and Storage in Saline Aquifers and Oil Reservoirs. PhD, Pittsburgh, Carnegie Mellon University.

MENG, Y. & LI, Z. 2016. Experimental study on diffusion property of methane gas in coal and its influencing factors, *Fuel,* 185: 219–228.

METZ, B., DAVIDSON, O., DE CONINCK, H., LOOS, M. & MEYER, L. 2005. *IPCC Special Report: Carbon Capture and Storage*. Cambridge: Cambridge University.

MERKEL, A., GENSTERBLUM, Y., KROOSS, B. M. & AMANN, A. 2015. Competitive sorption of CH_4, CO_2 and H_2O on natural coals of different rank, *International Journal of Coal Geology*, 150-151: 181-192.

MEYERS, R., A. (Ed.) 1982. *Coal Structure*. California: Academic Press.

MISRA, B., K., SINGH, B., D. & SINGH, A. 2006. Significance of coal petrological investigations in coal bed methane exploration – Indian context, *Current Science,* 91: 10.

NALAWADE, S., P, PICCHIONI, F. & JANSSEN, L. P. B. M. 2006. Supercritical CO_2 as a green solvent for processing polymer melts: Processing aspects and applications. *Progress in Polymer Science,* 31(1):19-43.

NANDI, B., N., BROWN, T., D., & LEE, G., K. 1977. Inert coal macerals in combustion. *Fuel,* 56(2):125–30.

NASA's Global Climate Change newsletter, For first time, Earth's single-day CO_2 tops 400 ppm. May 2013. Retrieved on 16 October 2013 from http://climate.nasa.gov/news/916/

NEAVEL, R. C. 1981. Coal Structure and Coal Science: Overview and Recommendations, *American Chemical Society*, http://pubs.acs.org | doi: 10.1021/ba-1981-0192.ch001.

NISHINO, J., 2001. Adsorption of Water Vapour and Carbon Dioxide at Carboxylic Functional Groups on the Surface of Coal, *Fuel*, 80:757-764.

NIST, 2007. NIST Standard Reference Database 23. NIST Reference fluid Thermodynamic and Transport properties - REFPROP Version 8.0. Physical and Chemical Properties Division, National Institute of Standards and Technology, Colorado.

NODZENSKI., A. 1998. Sorption and desorption of gases (CH_4, CO_2) on hard coal and active carbon at elevated pressures. *Fuel*, 77: 1243-1246.

OHGA, K., SASAKI, K., DEGUCHI, G. and FUJIOKA, M. 2003. Fundamental tests on carbon dioxide sequestration into coal seams, *Greenhouse Gas control Technologies,* 1: 531-537.

O'KEEFE, J., M., K., BECHTEL, A., CHRISTIANIS, K., DAI, S., DIMICHELE, W., A., EBLE, C., F., ESTERLE, J., S., MASTERLEZ, M., RAYMOND, A., L., VALENTIM, B., V., WAGNER, N., J., WARD, C. R. and HOWER, J., C. 2013. On the fundamental difference between coal rank and coal type, *International Journal of Coal Geology,* 118: 58-87.

OKOLO, G. N, EVERSON, R. C., NEOMAGUS, H. W.J.P, ROBERTS, M. J., SAKUROVS, R. 2015. Comparing the porosity and surface areas of coal as measured by gas adsorption, mercury intrusion and SAXS techniques, *Fuel,* 14: 293-304.

OLADOJA, N., A, ABOLUWOYE, C., O & OLADIMEJI, Y., B. 2008. Kinetics and Isotherm Studies on Methylene Blue Adsorption onto Ground Palm Kernel Coat. *Turkish Journal of Engineering and Environmental Sciences,* 32(0):303-312.

OLAJIRE, A., A. 2010. CO_2 capture and separation technologies for end-of-pipe applications - A review [Electronic Version]. *Energy*, 35: 2610-2628. Retrieved on 11 August 2011 from www.elsevier.com/locate/energy.

OLDENBURG, C. 2007. Joule-Thomson Cooling Due to CO_2 Injection into Natural Gas Reservoirs, *Energy Conversion and Management*, 48: 1808-1815.

OPAPRAKASIT, P. & PAINTER, P. 2003, Concerning glass transition temperature of coal, *Energy Fuels,* 17: 354-358.

ORREGO-RUIZ, R. A.; CABANZO, R.; MEJIA-OSPINO, E. 2011. Study of Colombian coals using photoacoustic Fourier transform infrared spectroscopy. *International Journal of Coal Geol*ogy, 85: 307−310.

OTTIGER, S., PINI, R., STORTI, M & MAZZOTTI, M. 2008. Competitive adsorption equilibria of CO_2 and CH_4 on a dry coal, *Adsorption,* 14(4-5): 539-556.

OZDEMIR, E. 2004. Chemistry of the adsorption of CO_2 by Argonne Premium coals and a model to simulate CO_2 sequestration in coal. PhD, Pittsburgh, University of Pittsburgh.

OZDEMIR, E. & SCHROEDER, K. 2009. Effect of Moisture on Adsorption Isotherms and Capacities of CO_2 on coals, *Energy & Fuels*, 23: 2821-2831.

PERERA, M., S., A., RANJITH, P., G., CHOI, S., K., BOUAZZA, A., KODIKARA, D. & AIREY, D. 2011. A review of coal properties pertinent to carbon dioxide sequestration in coal seams: with special refernce to Victorian brown coals, *Environmental Earth Sciences*, 64: 223-235.

PINI, R., OTTIGER, S., STORTI, G. & MAZZOTTI, M. 2009. Pure and competitive adsorption of CO_2, CH_4 and N_2 on coal for ECBM. *Energy Procedia,* 1(1):1705-1710.

PINI, R., OTTIGER, S., BURLINI, L., STORTI, G., & MAZZOTTI, M. 2010. Sorption of carbon dioxide, methane and nitrogen in dry coals at high pressure and moderate temperature. *International Journal of Greenhouse Gas Control*, 4(1):90–101

PIRES, J. C. M., MARTINS, F. G., ALVIM-FERRAZ, M. C. M. & SIMÕES, M. 2011. Recent developments on carbon capture and storage: An overview. *Chemical Engineering Research and Design,* 89(9):1446-1460.

PONE, J., D., N., HALLECK, P., M. & MATHEWS, J., P. 2009. Sorption capacity and sorption kinetic measurements of CO2 and CH4 in confined and unconfined bituminous coal. *Energy and Fuels,*23: 4688-4695.

PRINZ, D., PYCKHOUT-HINTZEN, W., KROOSS, B., LITTKE, R., 2001. Investigations on the micro-and mesoporous structure of coals of varying rank: a combined small angle neutron scattering (SANS) and gas adsorption experiments study. Proceedings of the 2001 International Coalbed Methane Symposium, Tuscaloosa, Alabama, May 14– 18.

PRUSTY, B., K. 2007. Sorption of methane and CO_2 for enhanced coalbed methane recovery and carbon dioxide sequestration. *International Journal of Natural Gas Chemistry,* 17: 29-38.

QING-LING, Z. 2008. Adsorption mechanism of different coal ranks under variable temperature and pressure conditions. *Journal of China University of Mining and Technology,* 18(3):395-400.

QU, H. LIU, J, CHEN, Z., WANG, J., PAN, Z., CONNELL, L. & ELSWORTH, D. 2012. Complex evolution of coal permeability during CO_2 injection under variable temperatures. *International Journal on Greenhouse Gas Control,* 9: 281-293.

RAMASAMY, S., SRIPADA, P., P., KHAN, M., M., TIAN, S., TRIVEDI, J. & GUPTA, R. 2014. Adsorption behaviour of CO_2 in Coal and Coal Char, *Energy & Fuels,* 28, 5241-5251.

RADOVIC, L., R., MENON, V.C. LEON, C., A., LEON, Y., KYOTANI, T., DANNER, R., E., ANDERSON, S. & HATCHER P.,G. 1997. On the Porous Structure of Coals: Evidence for an Interconnected but Constricted Micro-pore System and Implications for Coalbed Methane Recovery, *Adsorption*, 3: 221-232.

REEVES, S., TAILLEFERT, A. and PEKOT, L. 2003, The Allison Unit CO2 - ECBM Pilot: A Reservoir Modelling Study, Topical Report, US Department of Energy. Electronic version available: http://www.adv-res.com/pdf/Topical%20Report%20-%20Allison%20Unit.pdf Date accessed: March 2009.

REUCROFT, P. J. & PATEL, H. 1986. Gas-induced swelling in coal, *Fuel,* 65: 816-820.

RIVERA-RAMOS, M., E, RUIZ-MERCADO, G., J & HERNANDEZ-MALDONADO, A., J. 2008. Separation of CO_2 from light gas mixtures using ion-exchanged Silico-alumino-phosphate nano-porous sorbents. *Industrial Engineering Chemical Resources,* 47:5602–5610.

ROBERTSON, E. P. 2005. Measurement and modeling of sorption-induced strain and permeability changes in coal, Idaho National Laboratory, *INL/EXT-06-11832.*

ROBERTS, M., J., EVERSON, R., C., NEOMAGUS, H. W.J., DANIEL VAN NIEKERK, D., MATHEWS, J. P. & BRANKEN., D., J. 2015. Influence of maceral composition on the structure, properties and behaviour of chars derived from South African coals, *Fuel*, 142: 9–20.

ROMANOV, V. N., GOODMAN, A., L & LARSEN, J. W. 2006. Errors in CO_2 adsorption measurements caused by coal swelling, *Energy Fuels,* 20(1): 415-416.

RØKKE, N. UNFCCC (UNITED NATIONS FRAMEWORK CONVENTION ON CLIMATE CHANGE) COP 21 - We can deliver. SINTEF Energy. Paris, 2015. http://blog.sintefenergy.com/energy-efficiency/cop21-will-it-deliver/

RUTHVEN, D., M & WONG, F. 1985. Generalized Statistical Model for the Prediction of Adsorption Equilibria in Zeolite. *Industrial and Engineering Chemistry Fundamentals,* 24:27-32.

RYAN, B. & LANE, B. 2002. Adsorption characteristics of coals with special reference to the Gething Formation. *British Columbia Ministry of Energy and Mines* (2002-1):83-90.

SAGHAFI, A., FAIZ, M. & ROBERTS, D. 2007. CO_2 storage and gas diffusivity properties of coals from Sydney Basin, Australia. *International Journal of Coal Geology,* 70(1–3):240-254.

SAGHAFI, A., PINETOWN, K. L., GROBLER, P. G. & van HEERDEN, J. H. P. 2008. CO_2 storage potential of South African coals and gas entrapment enhancement due to igneous intrusions, *International Journal of Coal Geology,* 73:74-87.

SAKANISHI, K., WATANABE, I., NONAKA, T., KISHINO, M. & MOCHIDA, I. 2001. Effects of Organic Acid Pretreatment on the Structure and Pyrolysis Reactivity of Coals, *Fuel*, 80:273-281.

SAKUROVS, R., DAY, S., WEIR, G. & DUFFY, G. 2007. Application of a modified Dubinin-Radushkevich equation to adsorption of gases by coals under supercritical conditions. *Energy Fuels,* 21:992-997.

SAKUROVS, R., DAY, S., WEIR, S. & DUFFY, G. 2008. Temperature dependence of sorption of gases by coals and charcoals, *International Journal of Coal Geology,* 73: 250-258.

SAVAGE, P., E, GOPALAN, S., MIZAN, T., I, MARTINO, C., J & BROCK, E., E. 1995. Reactions at supercritical conditions: Applications and fundamentals. *AIChE Journal,* 41:1723-1778.

SEN, S. & BANERJEE, S. 2015. Identifying Relationship Amongst Vitrinite/Inertinite Ratio (V/I), Cleat Parameters, Vitrinite Reflectance, O/C Ratio and Permeability of Coal Seams and V/I Ratio as Exploration Tool: Study from Raniganj Coal Bed Methane Block, Essar Oil Limited, India, *Petroleum Geosciences: Indian Contexts, Springer Geology*, Springer International Publishing Switzerland, 205 – 217

SCOTT, A., R. 2002. Hydrogeologic Factors Affecting Gas Content Distribution in Coal beds. *International Journal of Coal Geology*, 50: 363–387.

SHAFEEN, A., CROISET, E., DOUGLAS, P. L., CHATZIS, I., 2004. CO_2 sequestration in Ontario, Canada - Part 1: Storage evaluation of potential reservoirs, *Energy Conservation Management,* 45(17), 2645 – 2659.

SHARKEY, A.G., Jr, AND MCCARTNEY, J.T., 1981. Physical Properties of Coal and Its Products: in Elliott, M.A. (ed), Chemistry of Coal Utilization, Second Supplementary Volume, John Wiley and Sons, New York, pp. 159-283.

SHAW, D., J. 1983. *Introduction to Colloid & Surface Chemistry*. 3rd ed. London: Butterworths.

SHEN, J., Qin, Y., Wang, G. X., Fu, X., Wei, C. & Lei., B. 2011. Relative permeabilities of gas and water for different rank coals, *International Journal of Coal Geology*, 86: 266–275.

SHI, J. Q., MAZUMDER, S. & WOLF, K-H., 2008. Competitive methane desorption by supercritical CO_2 injection in coal, *Transport in porous media,* 75(1): 35-54.

SHIMADA, S., LI, H., OSHIMA, Y. & ADACHI, K., 2005. Displacement behaviour of CH_4 adsorbed on coals by injecting pure CO_2, N_2 and CO_2-N_2 mixture, *Environmental Geology,* 49: 44-52.

SIDDIQI, K. S. & THOMAS, W. J. 1982. The adsorption of CH_4-ethane mixtures on activated carbon. *Carbon,* 20(6):473-479.

SIEMONS, N. & BUSCH, A. 2007. Measurement and interpretation of supercritical CO_2 sorption on various coals, *International Journal of Coal Geology,* 69: 229-242.

SIMBECK, D. R., 2004. CO_2 capture and storage – The essential bridge to the hydrogen economy, *Energy,* 29(9-10): 1633 – 1641.

SMITH, W. H., ROUX, H., J. & STEYN J. G. H. 1983. The classification of coal macerals and their relation to certain chemical and physical parameters of coal. *Spec Publ Geol Soc* South Africa, 7:111–5.

SMOLINSKI, A. & HOWANIEC, N. 2010. Environment friendly coal processing technologies for sustainable development of polish energy sector. *Journal of Ecological Chemistry and Engineering Science,* 17(3):297-308.

SOARES, J. L., OBERZINER, A. L. B., JOSÉ, H. J., RODRIGUES, A. E. & MOREIRA, R. F. P. M. 2007. Carbon dioxide adsorption in Brazilian coals, *Fuels,* 21: 209-215.

SOBOLIK, J. L., LUDLOW, D. K. & HESSEVICK, T. L. W. L. 1992. Parametric sensitivity comparison of the BET and Dubinin-Radushkevich models for determining char surface area by CO2 adsorption. *Fuel,* 71(10):1195-1202.

SOLANO-ACOSTA, W., MASTERLEZ, M. & SCHIMMELMANN, A. 2004. Experimental CO_2 adsorption in coal versus particle size: Implications for CO_2 sequestration. [Electronic Version]. Retrieved on 27 January 2009 from http://www.searchanddiscovery.net/documents/abstracts/2004eastern/solano_acosta.htm

SORIAL, G. A., GRANVILLE, W. H. & DALY, W. O. 1983. Adsorption equilibria for oxygen and nitrogen gas mixtures on 5a molecular sieves. *Chemical Engineering Science,* 38(9):1517-1523.

SOUTH AFRICA'S MINERAL INDUSTRY (SAMI) 2005/2006, Department of Minerals and Energy (DME), Republic of South Africa, *23rd Revised Edition, December 2006,* 49-50.

SPAN, R. & WAGNER, W. 1996. A new equation of state for carbon dioxide covering the fluid region from the triple-point temperature to 1100 K at pressures up to 800 MPa. *Journal of Physical and Chemical Reference Data,* 25:1509-1596.

STACH, E., MACKOWSKY, M., -TH, TEICHMULLER, M., TAYLOR, M., CHANDRA, D. & TEICHMULLER, R. 1982. *Stach's textbook of coal petrology*. Germany: Berlin: Borntraeger.

STANTON, R.W., FLORES, R.M., WARWICK, P.D., GLUSKOTER, H.J. 2002. Sequestration of carbon dioxide in low-rank coals (abstract). *TSOP Abstracts and Program v. 18, 111.*

STANTON, R. W., FLORES, R., WARWICK, P.D., GLUSKOTER, H. & STRICKER, G. D. Coal bed sequestration of carbon dioxide. [Electronic Version]. Retrieved on 05 February 2009. 2011 from http://www.netl.doe.gov/publications/procceedings/01/carbonseq/3a3pdf

STEVENS, S.H. and GALE, J.J., 2000. Geologic CO_2 Sequestration, *Oil and Gas Journal*, 98(15): 40-44.

SUÁREZ-RUIZ, I. & WARD, C. R. 2008. Basic Factors Controlling Coal Quality and Technological Behavior of Coal. In: SUÁREZ -RUIZ, I. & CRELLING, J., C (Eds.). *Applied Coal Petrology: The Role of Petrology in Coal Utilization*. USA: California: Academic Press: 19-59.

SUÁREZ-RUIZ, I. & CRELLING, J. C. 2008. Applied Coal Petrology: *The Role of Petrology in Coal Utilization*. Elsevier Publishing, USA; pp: 10-31.

SUDIBANDRIYO, M. 2010. A Simple Technique for Surface Area Determination Through Supercritical CO_2 Adsorption. *Makara of Technology Series,* 14(1):1-6.

SURRIDGE, T. 2005. South African Activities Related to Carbon Capture and Storage. Department of Minerals and Energy.

SÝKOROVÁ, I., PICKEL, W., CHRISTIANIS, K., WOLF, M., TAYLOR, G., H & FLORES, D. 2005. Classification of huminite: ICCP System 1994. *International Journal of Coal Geology,* 62:689-700.

TANG, X, WANG, Z., RIPEPI, KANG, B. AND YUE, G. 2015. Adsorption Affinity of Different Types of Coal: Mean Isosteric Heat of Adsorption*, Energy Fuels*, 29:3609−3615.

THAKUR, P. C., GRAHAM-BRYCE, I. J., KARIS, W. G. & SULLIVAN, K. M., 1994. Global Methane emissions from the world coal industry, *Environmental Monitoring and Assessment,* 31: 73-91.

TAYLOR, G.H., TEICHMÜLLER, M., DAVIS, A., DIESSEL, C.F.K., LITTKE, R., ROBERT, P., 1998. *Organic Petrology*, Gebrüder Borntraeger, Berlin (704 pp.).

TESTO. 2006. Flue Gas Analyisi in Industry [Electronic Version]. *Practical guide for Emission and Process Measurements*, Retrieved on 27 November 2011 from http://pdfbrief.com/pdf/practical-guide-for-emission-and-process-measurements.html.

TSCHINO, W., TAMURA, M., Li, H. & SHIMADA, S., 2003. Adsorption behaviour of supercritical CO_2 to coal. In: *Proceedings of 12th International Conference on Coal Science*, Cairns, Australia, November 2–6, 2006.

UNFCCC (UNITED NATIONS FRAMEWORK CONVENTION ON CLIMATE CHANGE) COP 19 - Warsaw, Poland, November 2013. http://unfccc.int/meetings/warsaw_nov_2013/session/7767.php

UNFCCC (UNITED NATIONS FRAMEWORK CONVENTION ON CLIMATE CHANGE) COP 20 - Lima, Peru, December 2014. http://www.c2es.org/international/negotiations/cop-20-lima/summary

UNSWORTH, J. F., FOWLER, C. S. & JONES, L. F. 1989. Moisture in coal 2. Maceral effects on pore structure, *Fuel*, Butterworth & Co. 68: 18-12.

VAN DER MEER, L. G. H. 1993. The conditions limiting CO2 storage in aquifers. *Energy Conversion and Management,* 34(9–11):959-966.

Van NIEKERK, D. & MATHEWS, J. P. 2010. Molecular representations of Permian-aged vitrinite-rich and inertinite-rich South African coals. *Fuel*, 89(1):73–82.

VASSILEV, S., V., VASSILEVA, C., G. & BAXTER, D. 2010. Relationships between chemical and mineral composition of coal and their potential applications as genetic indicators, *Geologica Balcania,* 39(3): 21-41.

VILJOEN, J., H, A, STAPELBERG, F., D, J & CLOETE, M. 2010. *Technical Report on th Geological Storage of CO_2 in South Africa*. Silverton: Pretoria: Council for Geoscience.

VYACHESLAV N. ROMANOV, ANGELA L. GOODMAN, A. & SOONG, Y. 2005. Effects of moisture and pressure cycling on sorption capacity of coals. *National Energy Technology Laboratory, U.S. Department of Energy* (15236): 217

WANG, F., Y., ZHU, P., ZH & RUDOLPH, M., V. 2007. Mass transfer in coal seams for CO_2 sequestration. *AIChE Journal,* 53:1028-1049.

WANG, Z. 2007. Influence of coal quality factors on seam permeability associated with coal bed methane production. Dissertation. University of New South Wales.

WANG, L., CHENG, Y. & WANG, Y. 2014. Laboratory study of the displacement coal bed CH_4 process and efficiency of CO_2 and N_2 injection, *The Scientific World Journal,* 242947: 1-9.

WANG, X., ZHANG, L., JIANG, Y., WEI, J. & CHEN, Z. 2016. Mineralogical and Geochemical Characteristics of the Early Permian Upper No. 3 Coal from Southwestern Shandong, China. *Minerals,* 6(58): 1-20.

WARD, C.R. 2002. Analysis and Significance of Mineral Matter in Coal Seams. *International Journal of Coal Geology*, **50**:135-168. http://dx.doi.org/10.1016/S0166-5162(02)00117-9

WENIGER, P., FRANCŮ, J., HEMZA, P. & KROOSS, B. M. 2012. Investigations on the methane and carbon dioxide sorption capacity of coals from the SW Upper Silesian Coal Basin, Czech Republic. *International Journal of Coal Geology,* 93(0):23-39.

WEUBBLES, D. J. & JAIN, A.K., 2001, Concerns about climate change and the role of fossil fuel use, *Fuel Processing Technology,* 71, 99-119.

WHITE, C., M., SMITH, D., H., JONES, K., L., GOODMAN, A., L., JIKICH, S., A., LACOUNT, R., B., DUBOSE, S., B., OZDEMIR, E., MORSI., B., I. & SCHROEDER, K., T. 2005. Sequestration of carbon dioxide in coal with enhanced methane recovery – a review, *Energy and Fuels,* 19: 659-724.

WILLS, B., A. 1992. *Mineral Processing Technology - An Introduction the Practical Aspects of Ore Treatment and Mineral Recovery*. 5th ed. Oxford: Pergamon Press.

WINKLER, H., MARQUARD, A. & JOOSTE, M. 2010. Economic instruments to mitigate climate changen in South Africa and other developing countries. Paper presented at the *Putting a price on carbon*, University of Cape Town.

WORLD COAL INSTITUTE. 2007. Coal conversion facts, info from: www.worldcoal.org; [Online: Http://www.drummondoco.com/wp-coalconversionfacts200704_06_2009.pdf; Accessed: August 2018.

WU, Y., LIU, J,ELSWORTH, D.,MIAO, X & MAO, X. 2010. Development of anisotropic permeability during coalbed methane production. *Jnl of Natural Gas & Science,* vol. 2: 197-210.

XIE, K.-C., 2015. Structure and Reactivity of Coal: A survey of selected Chinese coals, http://www/springer.com/978-3-662-47336-8.

XU, H., TANG, D.Z., ZHAO, J.L., LI, S., TAO, S., 2015. A new laboratory method for accurate measurement of the methane diffusion coefficient and its influencing factors in the coal matrix. *Fuel,* 158: 239-247.

YANG, T., R. 1997. *Gas Separation by Adsorption Processes*. (1). United Kingdom: London: Butterworth.

YANG, K., LU, X., LIN, Y & Neimark, A. V. 2011. *Effects of CO_2 adsorption on coal deformation during geological sequestration*. *Journal of Geophysical Research,* vol. 116: 1-11.

ZARĘBSKA, K. & CEGLARSKA-STEFAŃSKA, G. 2008. The change in effective stress associated with swelling during carbon dioxide sequestration on natural gas recovery, *International Journal of Coal Geology,* 74: 167-174.

ZENG, F. 1997. *Coal, Oil Shale, Natural Bitumen, Heavy Oil and Peat*. Shanxi, China: Taiyuan University of Technology.

ZHANG, D-F., CUI, Y-J., LIU, B., LI, S-G., SONG, W-L., & LIN, W-G. 2011. Supercritical pure methane and CO_2 adsorption on various rank coals of China: Experiments and modelling, *Energy and Fuels,* 25: 1891-1899.

ZHANG DF, CUI, Y., J., LI, S., G. 2011. Adsorption and diffusion behaviours of methane and carbon dioxide on various rank coals. *Journal of Chinese Coal Society*, 10:1693–8.

ZHANG, L., AZIZ, N. & REN, T. X T. X. 2011. Influence of Temperature on coal sorption characteristics and the theory of coal surface free energy. *Procedia Engineering,* 26: 1430-1439.

ZHAO, Y, LIU, S., ELSWORTH, D., JIANG Y. & ZHU, J., 2014. Pore Structure Characterization of Coal by Synchrotron Small-Angle X‑ray Scattering and Transmission Electron Microscopy, *Energy Fuels*, 28:3704−3711

ZHOU, L. 2001. Adsorption Isotherms for the Supercritical Region. In: TOTH, J. (Ed.). *ADSORPTION: Theory, Modeling, and Analysis*. USA: New York: Marcel Dekker, Inc.:211

ZHU, J., JESSEN. K., KOVSCEK, A. R. & ORR, F. M. Jr. 2003. Analytical theory of coalbed methane recovery by gas injection, *Society of Petroleum Engineering,* 8(4): 371-379

APPENDIX A: DETAILED PETROGRAPHIC DATA OF SA COALS

Petrographic analysis of all SA coals tested in the study was conducted as per detailed methodology outlined in section 3.3.2. Full maceral analysis (percent by volume %) and rank determination (%R_oV_{mr}) was undertaken.

Project: Premlall, K – PhD study – CO_2 Adsorption Study

Date: 07-January-2013

Analyst: Prof. N. J. Wagner

Department: Coal & Carbon Research Group, School of Chemical & Metallurgical Engineering, University of the Witwatersrand, SA

ICCP Accreditation: ICCP/SCAP-056/AB; ICCP/CBAP/056

Table A1: Detailed petrographic data of South African coals tested

Sample no:		1252		1253		1254		1255		1256		1257		1258		1269		1260		1261	
Sample identification:		***SM***		***TN***		***EM***		***SL***		***AN***		***IN***		***SF***		***GN***		***BL***		***WG***	
		inc. mm	mmf	inc. mm	mmf	inc. mm	mmf	inc. mm	mmf	inc. mm	mmf	inc. mm	mmf	inc. mm	mmf	inc. mm	mmf	inc. mm	mmf	inc. mm	mmf
MACERAL GROUP	MACERAL (vol%)	vol%	vol%	vol%	vol%	vol%	vol%	vol%	vol%	vol%	vol%	vol%	vol%	vol%	vol%	vol%	vol%	vol%	vol%	vol%	vol%
Vitrinite	telinite	0.0	0.0	0.0	0.0	0.3	0.3	0.0	0.0	0.0	0.0	2.6	2.9	0.8	0.9	2.8	3.2	1	1.1	0.0	0.0
	collotelinite	54.75	57.3	43.9	47.8	7.8	8.6	42.3	42.9	32.0	33.4	35.2	39.3	12	13.7	29.2	32.9	25.6	27.3	1.8	3.2
	collodetrinite	29.25	30.6	18.5	20.2	4.5	5.0	12.0	12.2	0.0	0.0	1	1.1	3.6	4.1	4	4.5	0	0.0	0.4	0.7
	vitrodetrinite	0.0	0.0	0.0	0.0	0.0	0.0	0.0	0.0	0.0	0.0	0.2	0.2	0.4	0.5	1	1.1	0	0.0	0.0	0.0
	corpogelinite	0.0	0.0	0.0	0.0	0.0	0.0	0.0	0.0	0.0	0.0	1.8	2.0	1.2	1.4	4.2	4.7	1.4	1.5	0.0	1.5
	gelinite	0.0	0.0	0.0	0.0	0.0	0.0	0.0	0.0	0.0	0.0	0	0.0	0.2	0.2	1.2	1.4	0.6	0.6	0.6	1.1
	pseudovitrinite	0.0	0.0	3.3	3.6	0.3	0.3	1.0	1.0	0.0	0.0	4.2	4.7	0.0	0.0	3.2	3.6	1.6	1.7	0.0	0.0
		SM		***TN***		***EM***		***SL***		***AN***		***IN***		***SF***		***GN***		***BL***		***WG***	
Inertinite	fusinite	6.0	6.3	11.3	12.3	8.8	9.7	5.3	5.3	5.8	6.1	7.0	7.8	4.2	4.8	17.8	20.0	12.4	13.2	2.0	3.5
	reactive semifusinite	0.0	0.0	1.3	1.4	2.8	3.1	0.0	0.0	0.0	0.0	1.2	1.3	2.2	2.5	6.2	7.0	3.4	3.6	3.0	5.3
	inert semifusinite	4.5	4.7	7.5	8.2	16.0	17.8	34.5	35.0	44.8	46.8	12.6	14.1	19.8	22.6	9.0	10.1	13.2	14.1	16.6	29.4
	micrinite	0.0	0.0	0.0	0.0	1.5	1.7	0.0	0.0	0.0	0.4	3.4	3.8	1.4	1.6	1.4	1.6	0.8	0.9	0.0	0.0
	macrinite	0.25	0.3	1.5	1.6	4.5	5.0	0.0	0.0	0.0	0.0	0.2	0.2	1	1.1	0.8	0.9	0.6	0.6	0.2	0.4
	secretinite	0.0	0.0	0.0	0.0	5.3	5.8	0.5	0.5	0.0	0.0	0.8	0.9	1.4	1.6	0.2	0.2	4.2	4.5	2.0	3.5
	funginite	0.0	0.0	0.0	0.0	0.0	0.0	0.0	0.0	0.0	0.0	0.0	0.0	0.0	0.0	0.0	0.0	0.0	0.0	0.0	0.0
	inertodetrinite R	0.0	0.0	0.5	0.5	6.8	7.5	0.0	0.0	0.0	0.0	0.0	0.0	0.0	0.0	0.0	0.0	0.0	0.0	0.0	0.0
	inertodetrinite I	0.75	0.8	3.8	4.1	28.6	31.7	3.0	3.0	12.8	13.4	17.2	19.2	37.2	42.5	3.6	4.1	23.8	25.4	27.4	48.6
		SM		**TN**		**EM**		**SL**		**AN**		**IN**		**SF**		**GN**		**BL**		**WG**	
Liptinite	sporinite	0.0	0.0	0.3	0.3	2.8	3.1	0.0	0.0	0.0	0.0	1.8	2.0	2	2.3	3.2	3.6	3.6	3.8	1.2	2.1
	cutinite	0.0	0.0	0.0	0.0	0.5	0.6	0.0	0.0	0.0	0.0	0.2	0.2	0.2	0.2	1	1.1	1.2	1.3	0.4	0.7
	resinite	0.0	0.0	0.0	0.0	0.0	0.0	0.0	0.0	0.0	0.0	0.2	0.2	0.0	0.0	0.0	0.0	0.2	0.2	0.4	0.7
	alginite	0.0	0.0	0.0	0.0	0.0	0.0	0.0	0.0	0.0	0.0	0.0	0.0	0.0	0.0	0.0	0.0	0.0	0.0	0.0	0.0
	liptodetrinite	0.0	0.0	0.0	0.0	0.0	0.0	0.0	0.0	0.0	0.0	0.0	0.0	0.0	0.0	0.0	0.0	0.0	0.0	0.4	0.7
	suberinite	0.0	0.0	0.0	0.0	0.0	0.0	0.0	0.0	0.0	0.0	0.0	0.0	0.0	0.0	0.0	0.0	0.0	0.0	0.0	0.0

	exsudatinite	0.0	0.0	0.0	0.0	0.0	0.0	0.0	0.0	0.0	0.0	0.0	0.0	0.0	0.0	0.0	0.0	0.2	0.2	0.0	0.0
		SM		**TN**		**EM**		**SL**		**AN**		**IN**		**SF**		**GN**		**BL**		**WG**	
Mineral matter	silicate	4.25		7.5		9.5		1.0		3.2		2.2		7.0		3.0		3.0		17.4	
	sulfide	0.25		0.3		0.0		0.5		0.8		3.2		0.0		1.4		0.2		5.8	
	carbonate	0.0		0.5		0.3		0.0		0.2		4.2		4.6		0.0		1.6		3.8	
	quartz																			16.2	
	OTHER	0.0		0.0		0.0		0.0		0.4		0.0		0.0		0.2		0.0		0.4	
		SM		**TN**		**EM**		**SL**		**AN**		**IN**		**SF**		**GN**		**BL**		**WG**	
MACERAL GROUP TOTALS	VITRINITE	84.0	88.0	65.7	71.6	12.5	13.9	55.3	56.1	32.0	33.4	45	50.2	18.2	20.8	45.6	51.4	30.2	32.2	2.8	5.0
(vol%)	INERTINITE	11.5	12.0	25.8	28.1	74.2	82.2	43.3	43.9	63.4	66.6	42.4	47.3	67.2	76.7	39	43.9	58.4	62.3	51.2	90.8
	LIPTINITE	0.0	0.0	0.3	0.3	3.3	3.6	0.0	0.0	0.0	0	2.2	2.5	2.2	2.5	4.2	4.7	5.2	5.5	2.4	4.3
	MINERAL MATTER	4.5		8.3		9.8		1.5		4.6		10.4		12.4		11.2		6.2		43.6	
	TOTAL INERTINITE	11.5	12.0	25.8	28.1	74.2	82.2	43.3	43.9	63.4	66.6	42.4	47.3	67.2	76.7	39	43.9	58.4	62.3	58.4	62.3
	TOTAL REACTIVE MACERALS	84.0	88.0	67.7	73.8	25.3	28.1	55.3	56.1	32	33.4	45	50.2	18.2	20.8	45.6	51.4	30.2	32.2	30.2	32.2
(RoV%)	Rrandom	**2.24**		**1.26**		**0.64**		**3.49**		**2.91**		**0.81**		**0.65**		**0.7**		**0.7**		**0.51**	
	st. dev.	0.433		0.16 1		0.09 7		0.31 4		0.32		0.04		0.06		0.05		0.06		0.08	
	RANK	**high rank C**		**med rank B**		**med rank C**		**high rank B**		**High rank C**		**med rank C**		**med rank C**		**med rank C**		**med rank C**		**med rank C**	

APPENDIX B 1: COAL DENSITIES DETERMINED BY VOLUME DISPLACEMENT AND HELIUM DISPLACEMENT

Initial densities of all the coal samples were determined using a simple volume displacement method using de-ionised water as displacement medium in order to do the adsorption capacity calculations. Density displacement measurements were carried out three times for each sample and the averaged density was used and compared with Helium Stereo-pycnometer results.

The Stereopycnometer is the standard model of the series of manually operated pycnometers. It offers a choice of two interchangeable sample cells used in conjunction with a single reference volume. A sample is placed in the sample cell and degassed by purging with a flow of dry gas, by vacuum, or by a series of pressurization cycles. The standard analysis is performed by pressurizing the sample cell to approximately 17 psi (117.21 kPa) and recording the value. The selector valve is rotated so the gas expands into the reference or added volume and that lower pressure is recorded. From these two readings, the sample volume can be quickly and accurately calculated (QI, 2007).

The state of the system is then defined as

$$P_a V_c = nRT_a \qquad \text{(B.1)}$$

where n is the number of moles of gas occupying volume V_c at P_a, R is the gas constant and T_a is ambient temperature in degrees Kelvin. When a solid sample of volume V_p is placed in the sample cell Equation (F.1) can be rewritten as

$$P_a\left(V_c - V_p\right) = n_1 RT_a \qquad \text{(B.2)}$$

when pressurized to about 17 psi (117.21 kPa) above ambient, the state of the system is given by

$$P_2\left(V_c - V_p\right) = n_2 RT_a \qquad \text{(B.3)}$$

here P_2 indicates a pressure above ambient and n_2 represents the total number of moles of gas contained in the sample cell. When the rotary valve is turned to connect the added volume V_A to that of the cell, the pressure will fall to a lower value P_3 given by

$$P_3\left(V_c - V_p + V_A\right) = n_2 RT_a + n_a RT_a \qquad \text{(B.4)}$$

where n_a is the moles of gas contained in the added volume at ambient pressure. The term $P_a V_A$ can be used in place of $n_a RT_a$ in Equation (F.4) which gives Equation (F.5).

$$P_3\left(V_c - V_p + V_A\right) = n_2 RT_a + P_a V_A \qquad \text{(B.5)}$$

Substituting $P_2\ (V_c - V_p)$ from Equation (F.3) for $n_2 RT_a$ changes Equation (F.5) to

$$P_3\left(V_c - V_p + V_A\right) = P_2(V_c - V_p) + P_a V_a \qquad \text{(B.6)}$$

or

$$(P_3 - P_2)(V_c - V_p) = (P_a - P_3)V_A \qquad \text{(B.7)}$$

then

$$V_c - V_p = \frac{P_a - P_3}{P_3 - P_2} V_A \qquad \text{(B.8)}$$

Equation (F.8) is further reduced by adding and subtracting P_a from P_3 and P_2 in the denominator giving

$$V_p = V_c - \frac{(P_a - P_3)V_a}{(P_3 - P_a) - (P_2 - P_a)} = V_c + \frac{V_A}{1 - \dfrac{P_2 - P_a}{P_3 - P_a}} \qquad \text{(B.9)}$$

Since P_a is made to read zero, that is all pressure measurements are relative to P_a which is zeroed prior to pressurizing, Equation (F.9) becomes

$$V_p = V_c + \frac{V_A}{1 - P_2/P_3} \qquad \text{(B.10)}$$

Equation (F.10) is the working equation employed in the Stereo pycnometer.

Table B1 summarises the densities calculated by both the different methods that were employed

Table B1: Coal Densities of all coals tested – Comparing Displacement and Helium Pycnometer methods

Coal	***Water Volume Displacement***	***Stereo Pycnometer***	***% diff***
EM	1.454	1.641	11.41
GN	1.539	1.479	3.85
AN	1.411	1.591	11.34
Bit (1)	1.359	1.845	26.38
Bit (2)	1.327	1.559	14.93
IN	1.463	1.472	0.60
BL	2.0917	2.230	6.22
SM	-	1.798	-
SL	-	1.553	-
SF	1.668	1.599	4.12
TN	1.387	1.472	5.80
WG	1.904	2.308	17.49

APPENDIX B 2: BET DETAILED SAMPLE REPORTS (example of coals SL and SM)

SAMPLE: 429- SL
Operator: Gregory
Submitter: Premlall, K
File: C:\2020\DATA\429.SMP

Started:	12/11/2014 10:26:54AM	Analysis Adsorptive:	CO2
Completed:	12/11/2014 5:04:41PM	Analysis Bath Temp.:	0.000 °C
Report Time:	12/16/2014 6:44:12PM	Thermal Correction:	No
Sample Mass:	0.2216 g	Warm Free Space:	27.4582 cm^3 Measured
Cold Free Space:	29.6673 cm^3	Equilibration Interval:	15 s
Ambient Temperature:	22.00 °C	Low Pressure Dose:	3.000 cm^3/g STP
Automatic Degas:	Yes		

Table B2: COAL SL: Summary Report

Dubinin-Astakhov	
Micropore surface area:	169.9334 m^2/g
Limiting micropore volume:	0.067079 cm^3/g
Surface Area	
Single point surface area at P/Po = 0.032980639:	94.9264 m^2/g
BET Surface Area:	108.8291 m^2/g
Langmuir Surface Area:	115.3104 m^2/g
Horvath-Kawazoe	
Maximum pore volume at P/Po = 0.032980639:	0.039337 cm^3/g
Median pore width:	0.000 Å

Table B3: Isotherm Tabular Report

Relative Pressure (P/Po)	Absolute Pressure (mmHg)	Quantity Adsorbed (cm^3/g STP)	Elapsed Time (h:min)
0.00031	8.10932	1.612311	02:57
0.000428	11.18215	2.075668	03:19
0.000784	20.48926	3.228853	03:47
0.001578	41.25761	5.103606	04:11
0.001945	50.84428	5.822517	04:25
0.003494	91.35194	8.115483	04:42
0.005209	136.176	9.959958	04:54
0.006928	181.1215	11.45157	05:04
0.007883	206.0789	12.17843	05:10
0.008688	227.1223	12.74763	05:15
0.010434	272.7558	13.78118	05:21
0.011044	288.7202	14.16326	05:25
0.012174	318.2656	14.75046	05:29
0.013891	363.1296	15.53249	05:34
0.015632	408.6584	16.25733	05:38
0.016339	427.1418	16.58686	05:41
0.017389	454.5792	17.00037	05:44
0.019103	499.3892	17.58639	05:47
0.02052	536.4438	18.05501	05:51
0.020842	544.8539	18.23735	05:54
0.022598	590.7473	18.73816	05:57
0.024834	649.2147	19.33067	06:00
0.025253	660.1599	19.53697	06:03
0.026082	681.8307	19.79585	06:06
0.02777	725.9708	20.21029	06:10
0.029514	771.5458	20.62878	06:13
0.029998	784.1983	20.80175	06:16
0.031286	817.8779	21.10679	06:19
0.032981	862.1799	21.48866	06:23

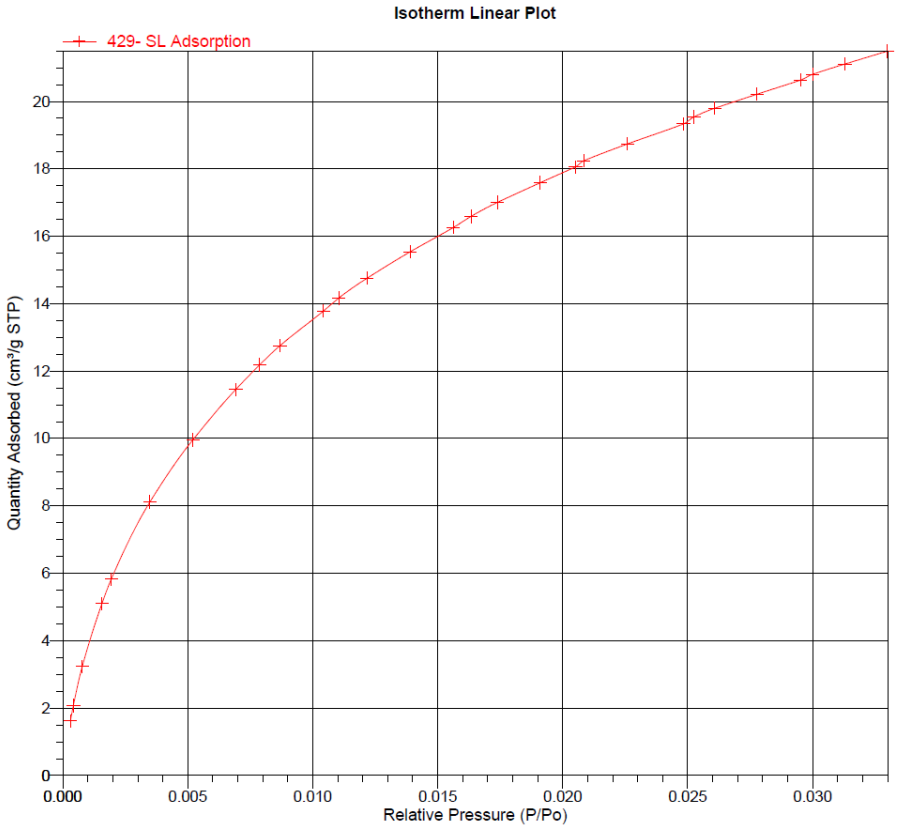

SAMPLE SL: Langmuir Surface Area Report

Langmuir Surface Area:	115.3104 ± 3.7539 m²/g
Slope:	0.039616 ± 0.001290 g/cm³ STP
Y-Intercept:	7.593427 ± 0.625581 mmHg·g/cm³ STP
b:	0.005217 1/mmHg
Qm:	25.2421 cm³/g STP
Correlation Coefficient:	0.992663
Molecular Cross-Sectional Area:	0.1700 nm²

Table B4: Langmuir Surface Area data

Pressure (mmHg)	Quantity Adsorbed (cm^3/g STP)	P/Q (mmHg·g/cm^3 STP)
8.10932	1.612311	5.029625
20.48926	3.228853	6.345678
50.84428	5.822517	8.732354
136.176	9.959958	13.67234
181.1215	11.45157	15.81631
227.1223	12.74763	17.81683
272.7558	13.78118	19.79191
318.2656	14.75046	21.57666
408.6584	16.25733	25.13687
454.5792	17.00037	26.73937
536.4438	18.05501	29.71164
590.7473	18.73816	31.52643
681.8307	19.79585	34.44312
771.5458	20.62878	37.40143
817.8779	21.10679	38.74952
862.1799	21.48866	40.12256

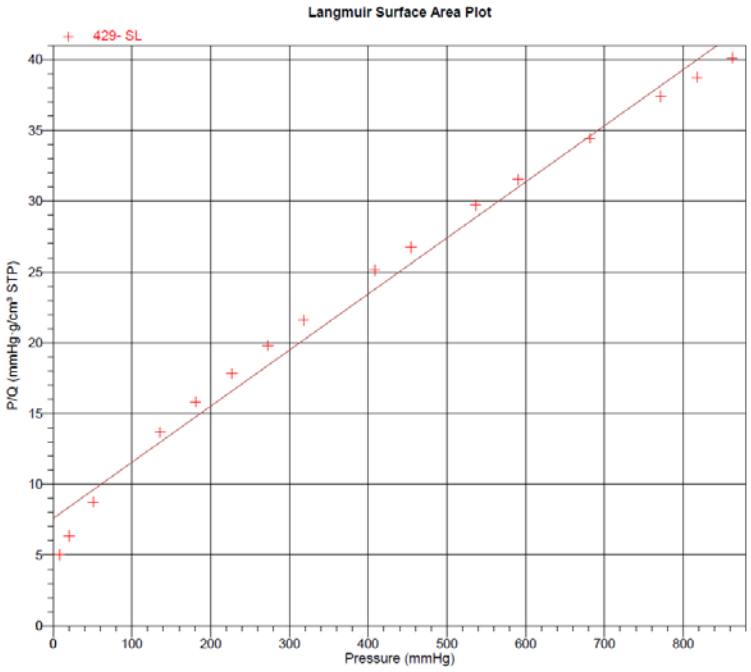

SAMPLE: SL:

BET Surface Area Report

BET Surface Area:	108.8291 ± 2.5440 m^2/g
Slope:	0.041699 ± 0.000981 g/cm^3 STP
Y-Intercept:	0.000276 ± 0.000017 g/cm^3 STP
C:	151.983229
Qm:	23.8233 cm^3/g STP
Correlation Coefficient:	0.9942380
Molecular Cross-Sectional Area:	0.1700 nm^2

Table B5: BET Surface Area data

Relative Pressure (P/Po)	Quantity Adsorbed (cm^3/g STP)	1/[Q(Po/P - 1)]
0.00031	1.612311	0.000192
0.000428	2.075668	0.000206
0.000784	3.228853	0.000243
0.001578	5.103606	0.00031
0.001945	5.822517	0.000335
0.003494	8.115483	0.000432
0.005209	9.959958	0.000526
0.006928	11.45157	0.000609
0.007883	12.17843	0.000652
0.008688	12.74763	0.000688
0.010434	13.78118	0.000765
0.011044	14.16326	0.000788
0.013891	15.53249	0.000907
0.015632	16.25733	0.000977
0.017389	17.00037	0.001041
0.02052	18.05501	0.00116
0.020842	18.23735	0.001167
0.024834	19.33067	0.001317
0.025253	19.53697	0.001326
0.02777	20.21029	0.001413
0.029998	20.80175	0.001487
0.031286	21.10679	0.00153
0.032981	21.48866	0.001587

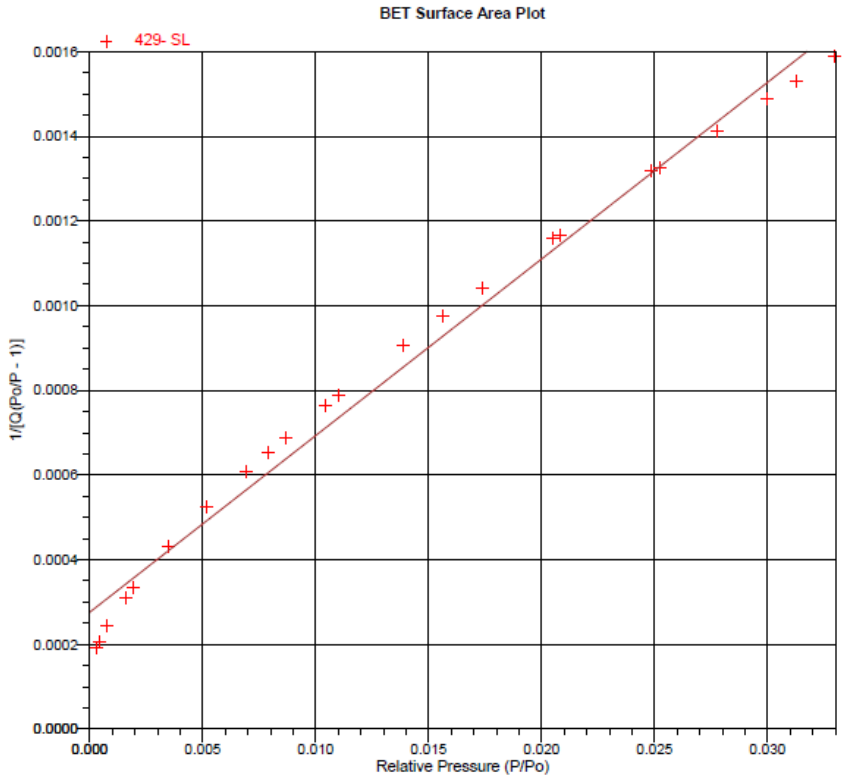

Sample:	**431- SM**
Operator:	Gregory
Submitter:	Premlall, K
File:	C:\2020\DATA\431.SMP

Started:	12/11/2014 7:29:00PM	Analysis Adsorptive:	CO2
Completed:	12/12/2014 1:35:16AM	Analysis Bath Temp.:	0.000 °C
Report Time:	12/16/2014 6:48:25PM	Thermal Correction:	No
Sample Mass:	0.2370 g	Warm Free Space:	27.1529 cm^3 Measured
Cold Free Space:	29.2769 cm^3	Equilibration Interval:	15 s
Ambient Temperature:	22.00 °C	Low Pressure Dose:	3.000 cm^3/g STP

Table B6: Coal SM: Summary Report

Dubinin-Astakhov	
Micropore surface area:	184.3454 m^2/g
Limiting micropore volume:	0.074708 cm^3/g
Surface Area	
Single point surface area at P/Po = 0.032980016:	95.8571 m^2/g
BET Surface Area:	114.3497 m^2/g
Langmuir Surface Area:	121.8101 m^2/g
Horvath-Kawazoe	
Maximum pore volume at P/Po = 0.032980016:	0.039723 cm^3/g
Median pore width:	0.000 Å

Table B7: Isotherm Tabular Report

Relative Pressure (P/Po)	Absolute Pressure (mmHg)	Quantity Adsorbed (cm^3/g STP)	Elapsed Time (h:min)
0.000365	9.549105	1.455925	02:45
0.000435	11.37853	1.704355	03:02
0.000812	21.23768	2.757315	03:25
0.001585	41.42718	4.426933	03:45
0.001937	50.64788	5.082864	03:58
0.003502	91.5556	7.338207	04:13
0.005212	136.2507	9.212153	04:25
0.006939	181.4113	10.7205	04:33
0.007881	206.0204	11.47418	04:39
0.008692	227.2391	12.07503	04:43
0.010436	272.8243	13.18323	04:49
0.01105	288.8592	13.58041	04:53
0.012176	318.3104	14.2127	04:57
0.013898	363.3321	15.08072	05:02
0.015632	408.6474	15.88512	05:06
0.015765	412.138	16.01622	05:09
0.017426	455.5478	16.6892	05:12
0.019603	512.4611	17.50241	05:16
0.020524	536.5507	17.88086	05:19
0.020849	545.028	18.05919	05:22
0.022582	590.3275	18.6237	05:26
0.024282	634.7916	19.1662	05:29
0.025263	660.4197	19.50829	05:32

0.026054	681.0919	19.78027	05:35
0.027791	726.5197	20.27004	05:38
0.029516	771.6038	20.75216	05:42
0.029991	784.0264	20.9351	05:45
0.031287	817.8963	21.27919	05:48
0.03298	862.1636	21.69934	05:51

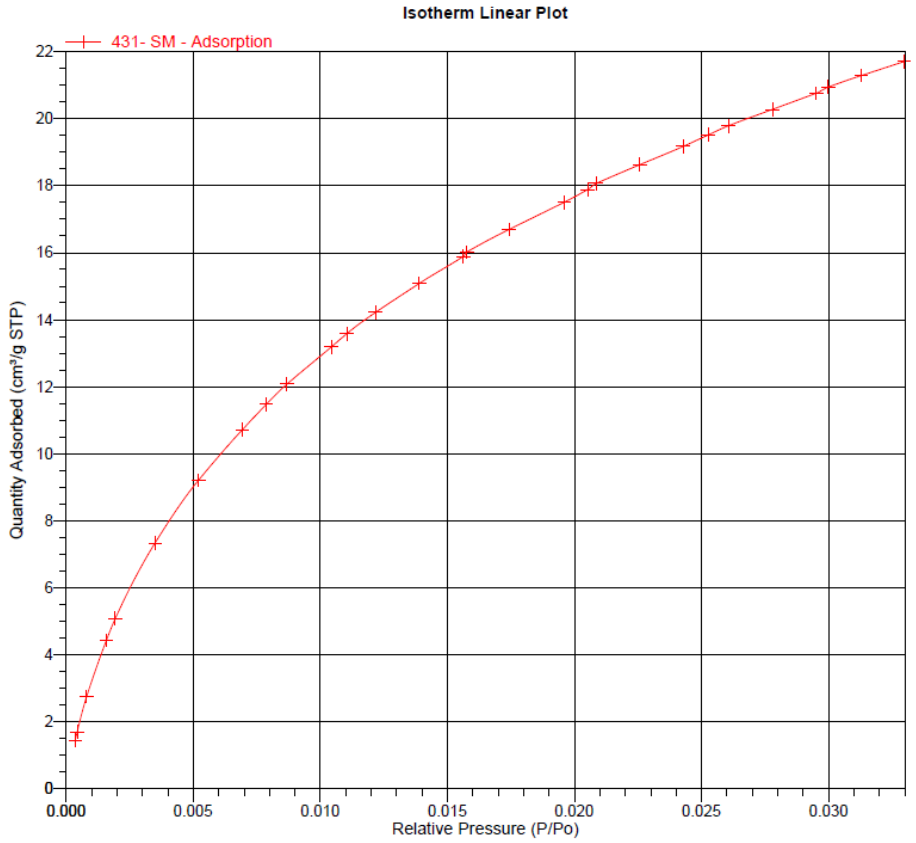

Langmuir Surface Area Report: Coal SM

Langmuir Surface Area:	121.8101 ± 4.2466 m²/g
Slope:	0.037502 ± 0.001307 g/cm³ STP
Y-Intercept:	9.033928 ± 0.634173 mmHg·g/cm³ STP
b:	0.004151 1/mmHg
Qm:	26.6649 cm³/g STP
Correlation Coefficient:	0.991599
Molecular Cross-Sectional Area:	0.1700 nm²

Table B8: Langmuir Surface Area data

Pressure (mmHg)	Quantity Adsorbed (cm^3/g STP)	P/Q (mmHg·g/cm^3 STP)
9.549105	1.455925	6.558788
21.23768	2.757315	7.702303
50.64788	5.082864	9.964437
136.2507	9.212153	14.79032
181.4113	10.7205	16.92192
227.2391	12.07503	18.81892
272.8243	13.18323	20.6948
318.3104	14.2127	22.3962
408.6474	15.88512	25.72518
455.5478	16.6892	27.29597
536.5507	17.88086	30.00699
590.3275	18.6237	31.69765
681.0919	19.78027	34.43289
771.6038	20.75216	37.18186
817.8963	21.27919	38.43644
862.1636	21.69934	39.73225

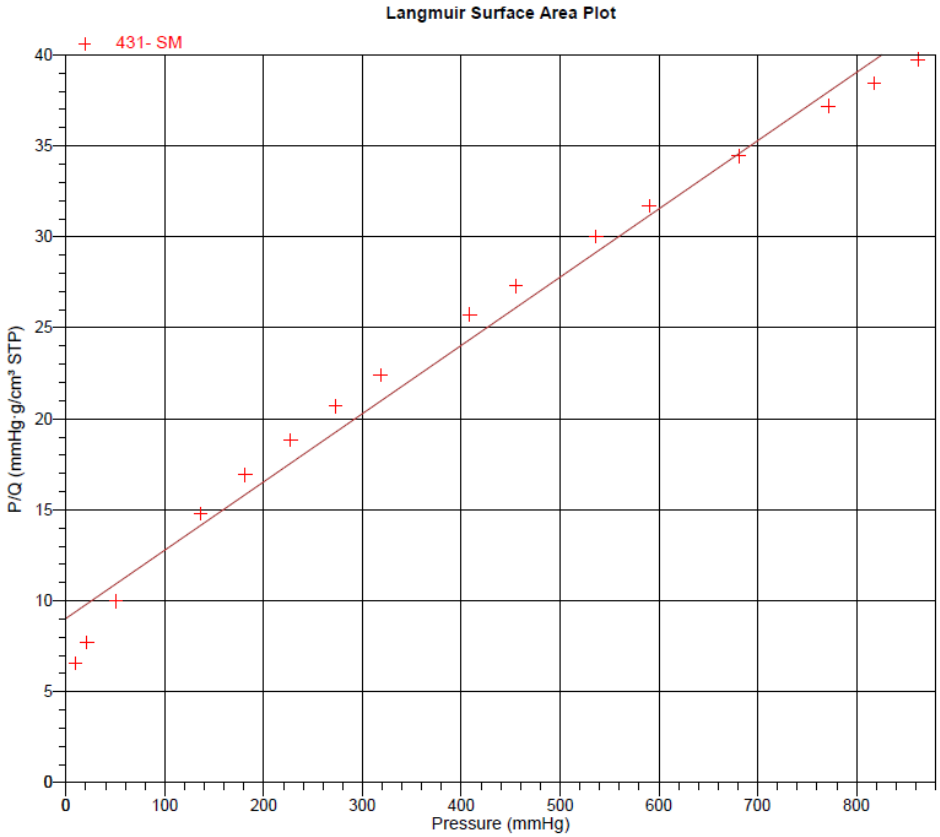

BET Surface Area Report: Coal SM

BET Surface Area:	114.3497 ± 2.8916 m^2/g
Slope:	0.039618 ± 0.001010 g/cm^3 STP
Y-Intercept:	0.000331 ± 0.000018 g/cm^3 STP
C:	120.823818
Qm:	25.0318 cm^3/g STP
Correlation Coefficient:	0.9932442
Molecular Cross-Sectional Area:	0.1700 nm^2

Table B9: BET
Surface Area data

Relative Pressure (P/Po)	Quantity Adsorbed (cm^3/g STP)	1/[Q(Po/P - 1)]
0.000365	1.455925	0.000251
0.000435	1.704355	0.000255
0.000812	2.757315	0.000295
0.001585	4.426933	0.000359
0.001937	5.082864	0.000382
0.003502	7.338207	0.000479
0.005212	9.212153	0.000569
0.006939	10.7205	0.000652
0.007881	11.47418	0.000692
0.008692	12.07503	0.000726
0.010436	13.18323	0.0008
0.01105	13.58041	0.000823
0.013898	15.08072	0.000935
0.015632	15.88512	0.001
0.017426	16.6892	0.001063
0.020524	17.88086	0.001172
0.020849	18.05919	0.001179
0.024282	19.1662	0.001298
0.025263	19.50829	0.001329
0.027791	20.27004	0.00141
0.029991	20.9351	0.001477
0.031287	21.27919	0.001518
0.03298	21.69934	0.001572

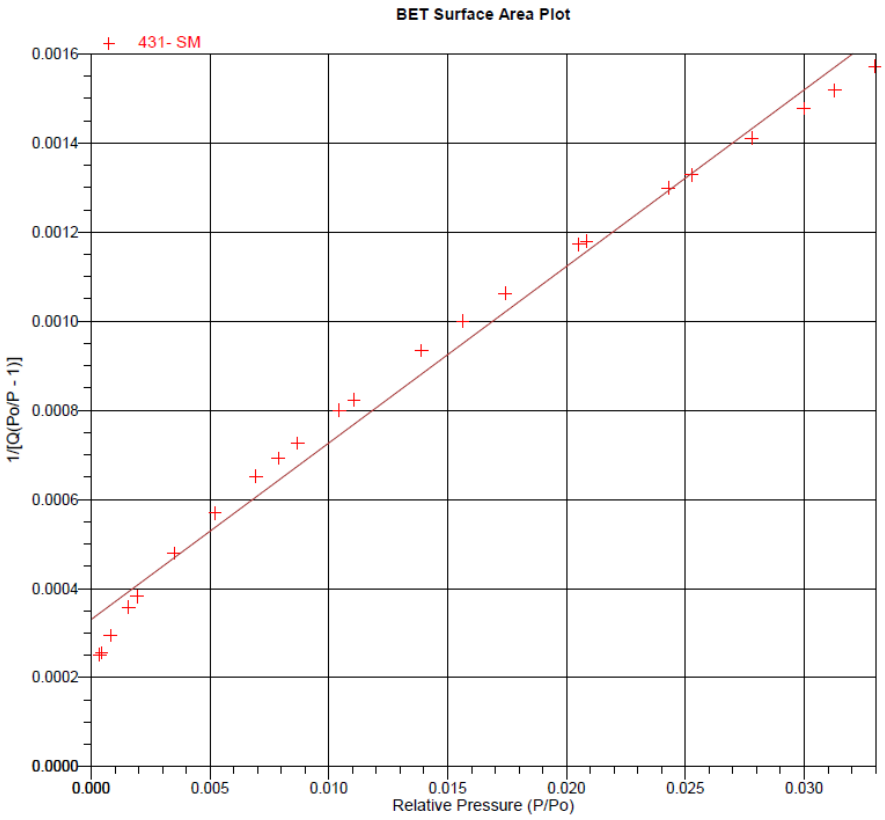
BET Surface Area Plot
431- SM
0.0016
0.0014
0.0012
0.0010
0.0008
0.0006
0.0004
0.0002
0.0000
1/[Q(Po/P - 1)]
0.000
0.005
0.010
0.015
0.020
0.025
0.030
Relative Pressure (P/Po)

APPENDIX C: ISOSTERIC ADSORPTION LINE IN THE ADSORPTION PROCESS

Using the fundamental theory based on the Clausius-Clapeyron equation and methodology employed (Ma *et al*., 2014). The isosteric heat of adsorption calculation methodology as detailed in section 3.4.2.2 was employed (Ma *et al*., 2014). Calculation process: ln*P* correlates with *n*, adsorption capacity; fit ln*P* − *n* data and then to get ln*P* − *n* relation. Having several fixed adsorption capacity points, *n* (mmol/g), the corresponding ln*P* can then be got with the fitting formulas. Then, a plot of ln*P* with 1/*T*, at fixed adsorption capacity *(n)* and conducting a linear regression fitting (Figures C1 – C5), so that the adsorption isostere is achieved, based on these slopes, the isosteric heat of adsorption (KJ/mol) is calculated.

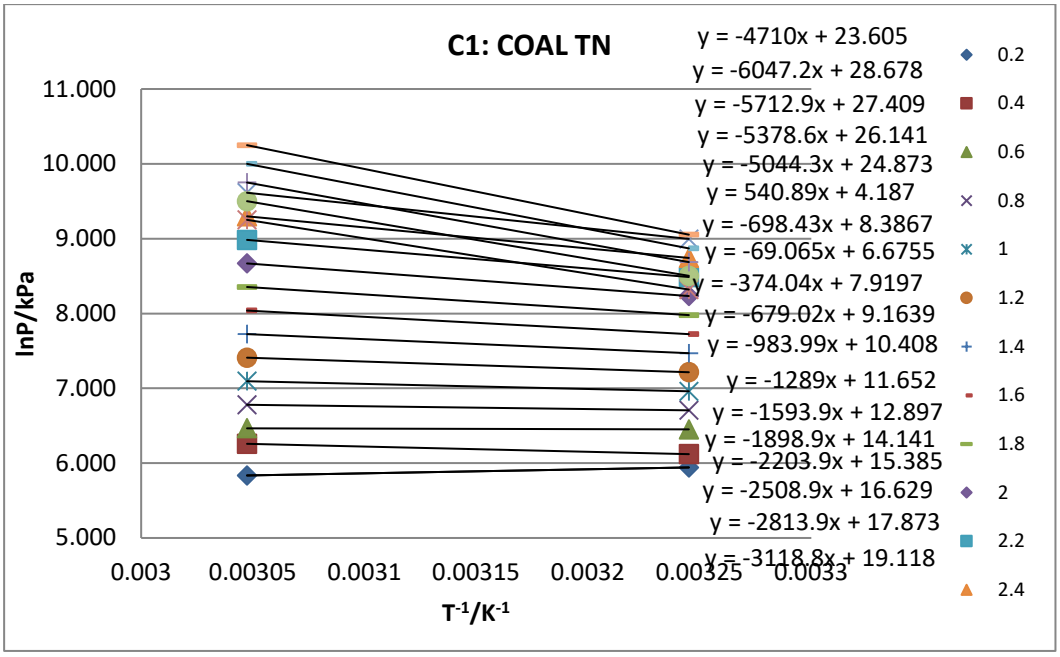

Figure C1: Isosteric adsorption line in the adsorption process

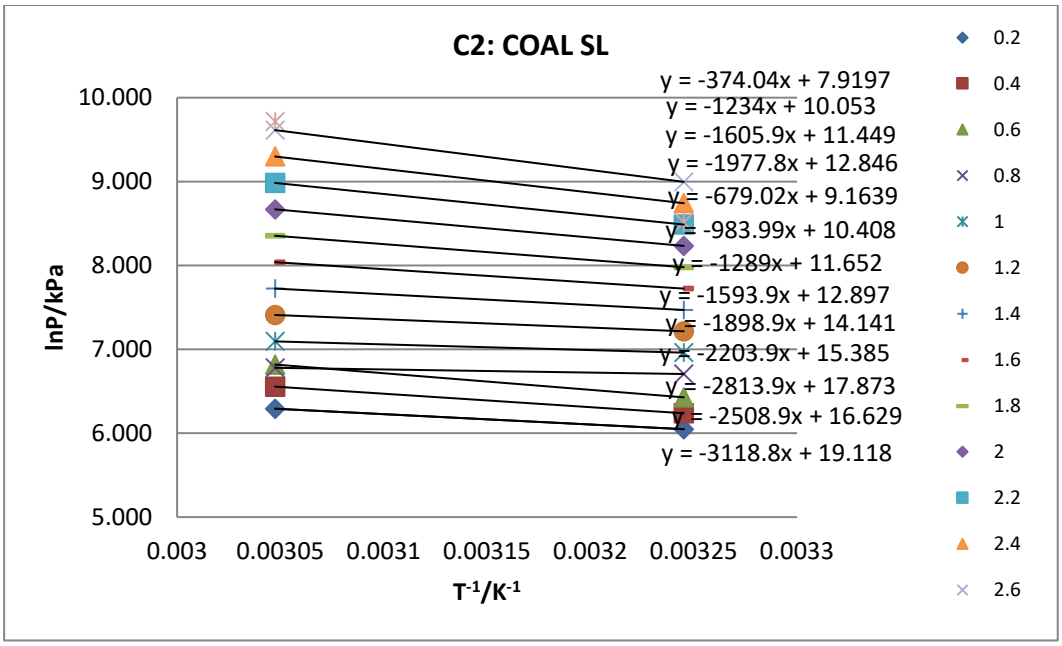

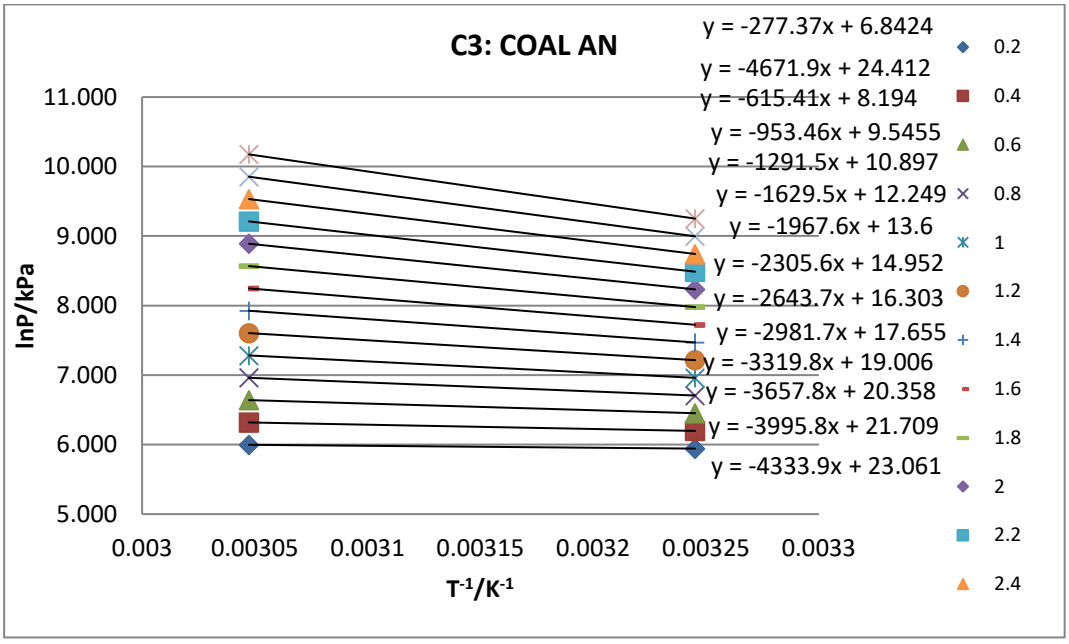

Figure C2 – C3: Isosteric adsorption line in the adsorption process

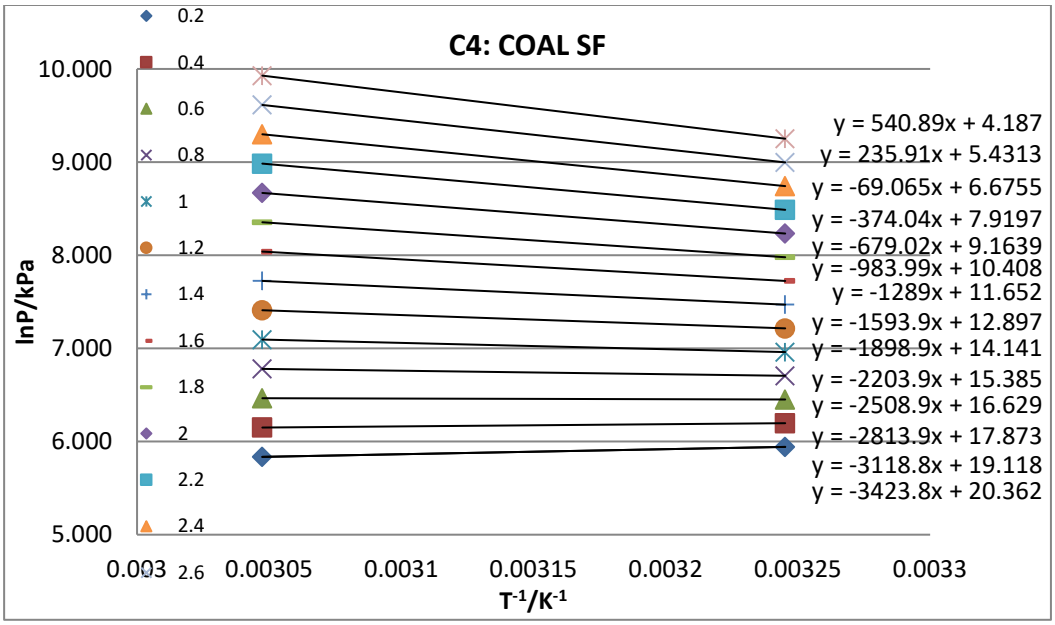

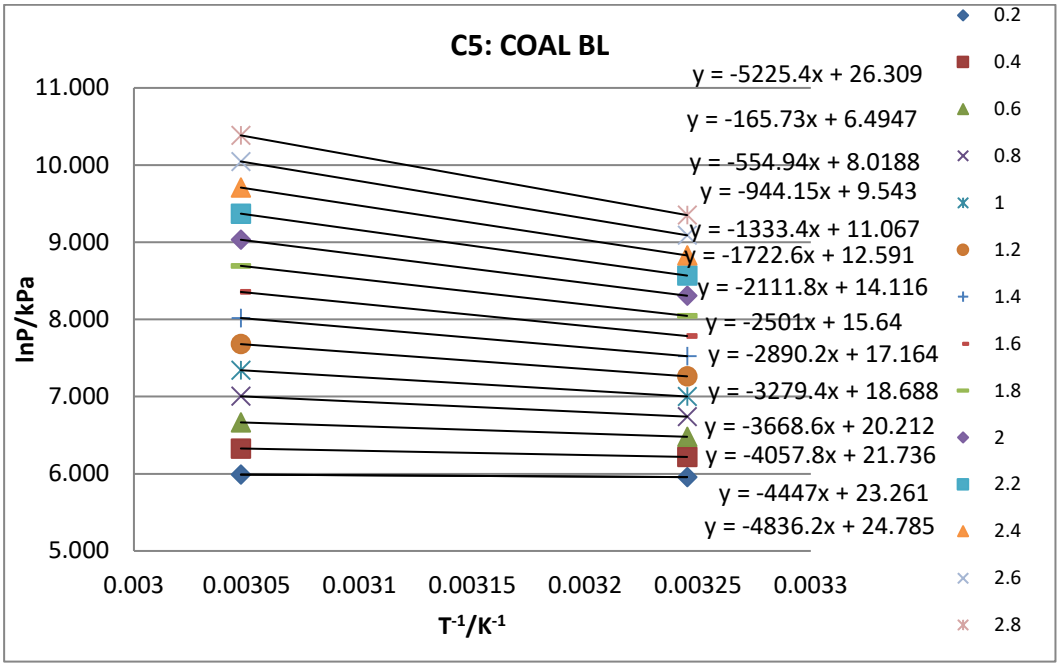

Figure C4 – C5: Isosteric adsorption line in the adsorption process

APPENDIX D: CO_2 ADSORPTION EXPERIMENTAL AND MODELLING DATA

Table D1: Three (of 10) sample examples for TEMKIN Modelling

Coal AN

P	q	ln(P)			T - Value
3.1442178	0.1567231	1.1455651	R^2=	0.988	0.7263208
5.244817	0.3185467	1.6572404	m=	0.435	0.9488996
9.4460155	0.6915427	2.245593	c=	0.228	1.204833
14.172364	1.1027922	2.6512939	b_T=	5889.5611	1.3813128
29.401708	1.6376344	3.3810528	A_T=	1.6890022	1.698758
36.228656	1.8204552	3.5898504			1.7895849
56.184349	2.0385823	4.0286382			1.9804576
78.754064	2.1600218	4.3663299			2.1273535
82.965036	2.1721658	4.4184193			2.1500124

R=	8.314
T=	308.15

Coal IN

P	q	ln(P)			T - Value
3.144218	0.2562749	1.145565136	R^2=	0.98	0.72618206
6.820266	0.5215633	1.919898542	m=	0.331	0.982486417
9.971165	0.7953779	2.299697463	c=	0.347	1.10819986
14.69751	1.0832	2.687678342	b_T=	7740.0577	1.236621531
29.40171	1.4948964	3.381052784	A_T=	2.8529067	1.466128471
38.85441	1.5983085	3.659821459			1.558400903
56.7095	1.7750448	4.037941724			1.683558711
78.24064	1.8188941	4.359789221			1.790090232
86.39154	1.8224264	4.458889755			1.822892509

R=	8.314
T=	308.15

Coal GN

P	q	ln(P)			T - Value
4.1945174	0.1656381	1.4337783	R^2=	0.982	0.6534312
6.8202266	0.3801509	1.9198927	m=	0.22	0.7603764
9.9711653	0.5609024	2.2996975	c=	0.338	0.8439334
14.697514	0.7654209	2.6876783	b_T=	11645.269	0.9292892
27.826259	1.0530349	3.3259801	A_T=	4.6476589	1.0697156
37.278956	1.1163854	3.618429			1.1340544
55.134049	1.2444183	4.0097675			1.2201488
78.765791	1.3077971	4.3664788			1.2986253
85.86639	1.3322955	4.4527925			1.3176143

R=	8.314
T=	308.15

Table D2: Three (of 10) sample examples for LANGMUIR Modelling

Coal AN					
P	**N_s**	**P/N_s**			**L - Value**
3.1442178	0.1567231	20.062246	R^2=	0.9945	0.2622868
5.244817	0.3185467	16.46483	m=	0.3523	0.4120773
9.4460155	0.6915427	13.659338	c=	10.88	0.6648457
14.172364	1.1027922	12.851346	N_{sm}=	2.8384899	0.8928641
29.401708	1.6376344	17.953768	a=	0.0323805	1.3843771
36.228656	1.8204552	19.900877			1.5322976
56.184349	2.0385823	27.560501			1.8316755
78.754064	2.1600218	36.459847			2.0389372
82.965036	2.1721658	38.194615			2.0685108

Coal IN					
P	**N_s**	**P/N_s**			**L - Value**
3.144218	0.2562749	12.26892559	R^2=	0.991	0.308844341
6.820266	0.5215633	13.07658468	m=	0.434	0.579166864
9.971165	0.7953779	12.53638693	c=	8.816	0.758639339
14.69751	1.0832	13.568606	N_{sm}=	2.3041475	0.967277632
26.40171	1.4948964	19.66805816	a=	0.0492287	1.302222738
34.85441	1.6983085	22.8782967			1.455735666
54.7095	1.7750448	31.9482074			1.680271163
78.24064	1.8188941	43.01550112			1.829230325
86.39154	1.8224264	47.40467971			1.865507961

Coal GN					
P	**N_s**	**P/N_s**			**L - Valuae**
4.1945174	0.1656381	25.323392	R^2=	0.994	0.3167535
6.8202266	0.3801509	17.094084	m=	0.618	0.4588142
9.9711653	0.5609024	17.777007	c=	10.65	0.5930917
14.697514	0.7654209	19.201872	N_{sm}=	1.618123	0.7448166
26.426259	1.1030349	25.226999	a=	0.0580282	0.979424
35.278956	1.2163854	30.647322			1.0870987
55.134049	1.2444183	44.305076			1.2327939
78.765791	1.3077971	60.227835			1.3276493
85.86639	1.3322955	64.44996			1.3476546

Table D3: Three (of 10) sample examples for FREUNDLICH Modelling

Coal AN						
P	**q**	**log P**	**log q**			**F - Value**
3.1442178	0.1567231	0.4975126	-0.8048669	R^2=	0.9153	0.235751
5.244817	0.3185467	0.7197303	-0.4968269	m=	0.7621	0.348182
9.4460155	0.6915427	0.9752487	-0.160181	c=	-1.0067	0.545176
14.172364	1.1027922	1.1514423	0.0424937	n=	1.3121638	0.742701
29.401708	1.6376344	1.4683726	0.214217	A=	0.0984691	1.29523
36.228656	1.8204552	1.5590522	0.26018			1.518636
56.184349	2.0385823	1.7496154	0.3093283			2.12169
78.754064	2.1600218	1.896273	0.3344581			2.15
82.965036	2.1721658	1.9188951	0.336893			2.18

Coal IN						
P	**q**	**log P**	**log q**			**F - Value**
3.1442178	0.256274907	0.4975126	-0.591293915	R^2=	0.9124	0.3489693
6.8202665	0.521563285	0.8338013	-0.282692988	m=	0.568	0.5417503
9.9711653	0.795377919	0.9987459	-0.09942647	c=	-0.7398	0.6721832
14.697514	1.083199975	1.1672439	0.034708641	n=	1.7605634	0.8379045
29.401708	1.494896356	1.4683726	0.174611083	A=	0.1820539	1.2423261
38.854405	1.698308473	1.5894403	0.230016576			1.455466
56.709499	1.775044781	1.7536558	0.249209314			1.804166
78.240641	1.8188941	1.8934324	0.259807414			1.92
86.39154	1.822426406	1.9364712	0.260649999			1.95

Coal GN						
P	**q**	**log P**	**log q**			**F - Value**
4.1945174	0.1656381	0.622682	-0.7808399	R^2=	0.8638	0.5814944
6.8202266	0.3801509	0.833798807	-0.420044	m=	0.2832	0.6673195
9.9711653	0.5609024	0.998745918	-0.2511127	c=	-0.9482	0.7430992
14.697514	0.7654209	1.167243873	-0.1160997	n=	3.5310734	0.8294027
27.826259	1.1030349	1.444454824	0.0425892	A=	0.3874378	0.9937373
37.278956	1.2163854	1.571463738	0.0850712			1.0795444
55.134049	1.2444183	1.741419891	0.0949664			1.2060688
78.765791	1.3077971	1.896337639	0.1165404			1.3342733
85.86639	1.3322955	1.933823206	0.1246006			1.3672902

APPENDIX E: CO_2 SORPTION MODELLING: REGRESSION PLOTS

LANGMUIR REGRESSION PLOTS:

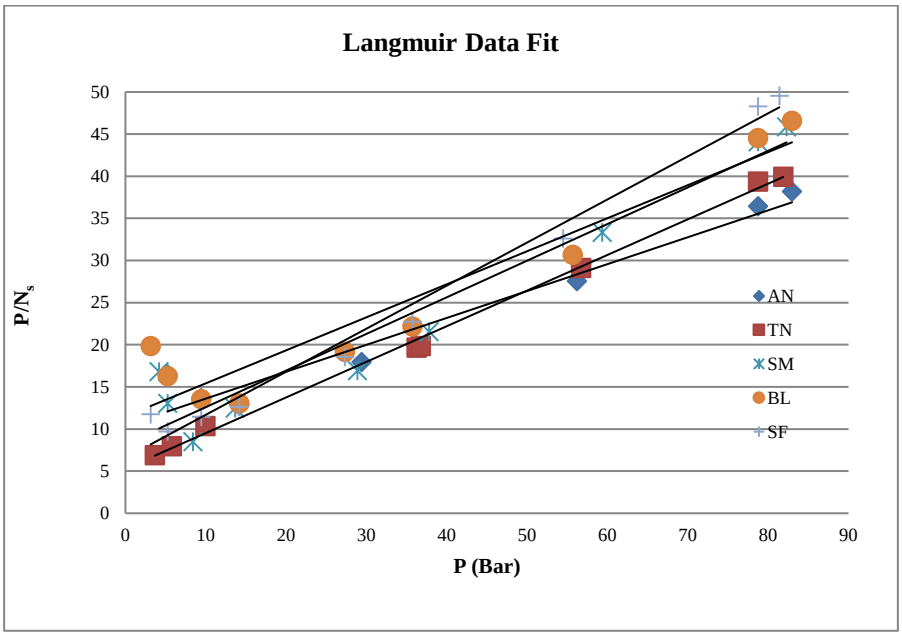

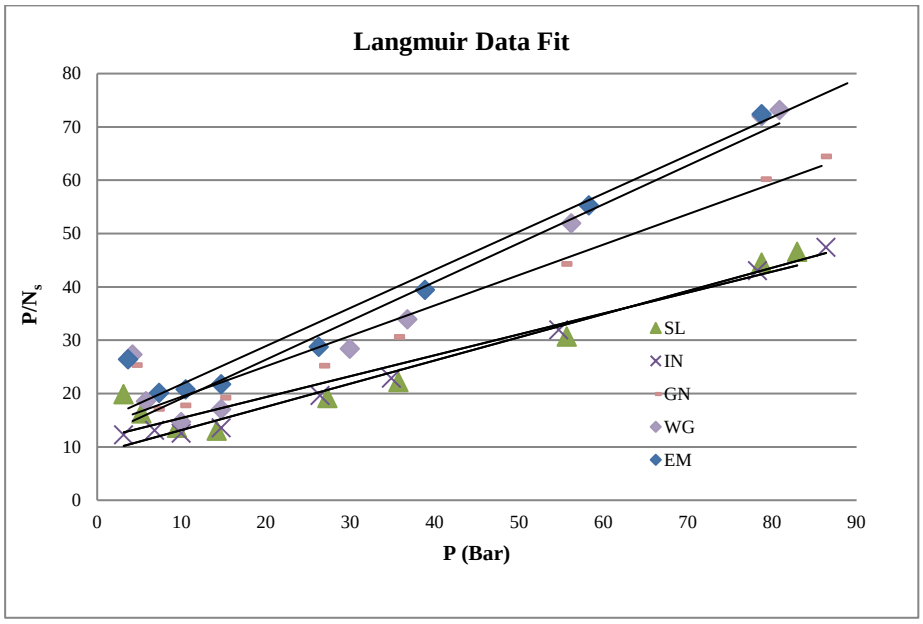

Figure E1 (a), (b): Langmuir Regression Plots for all coals

FREUNDLICH REGRESSION PLOTS:

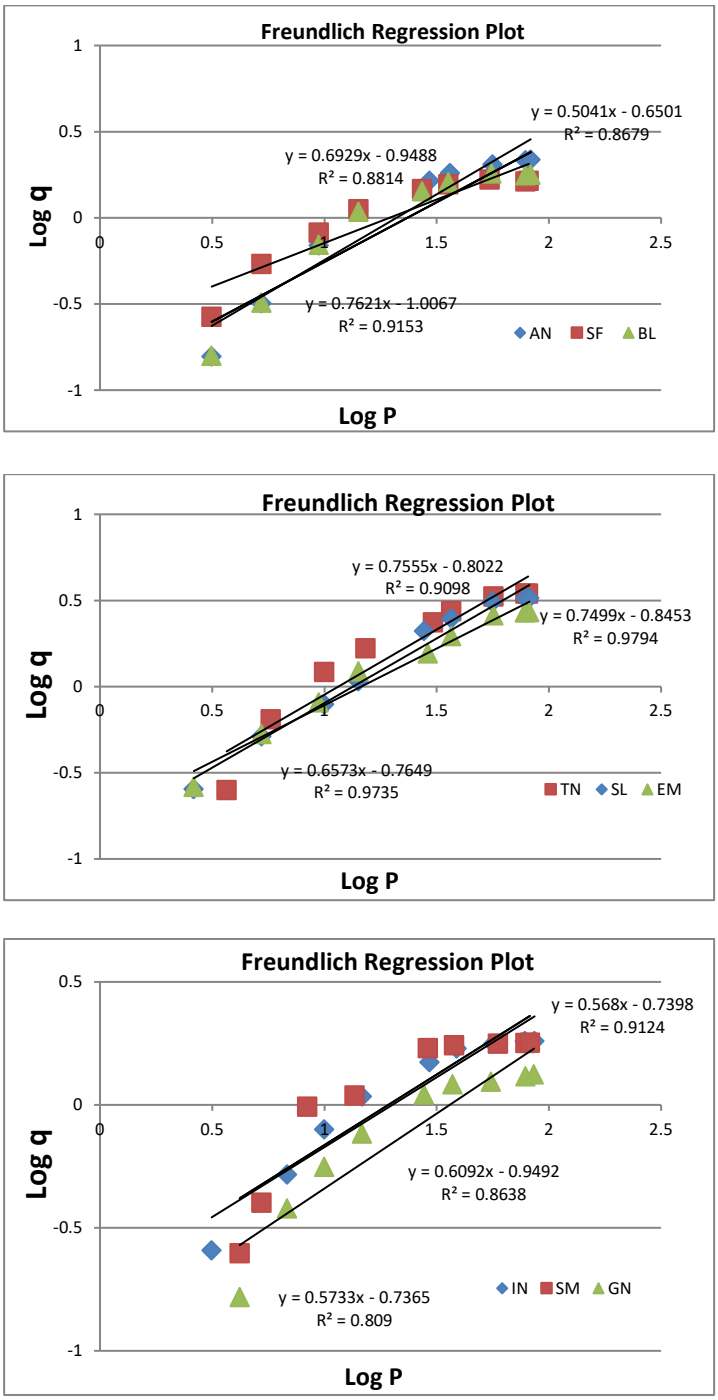

Figure E2 (a), (b), (c): Freundlich Regression Plots for all coals

TEMKIN REGRESSION PLOTS

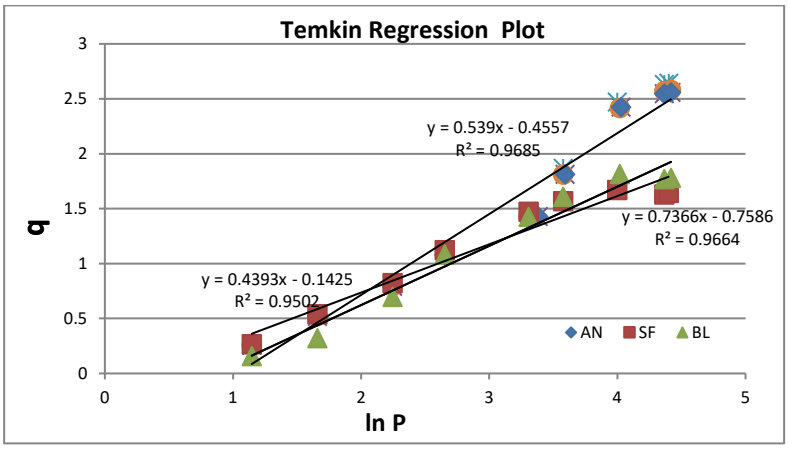

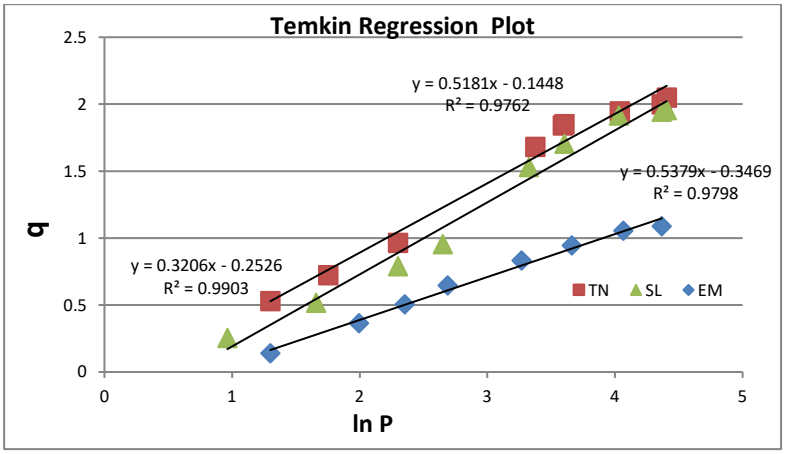

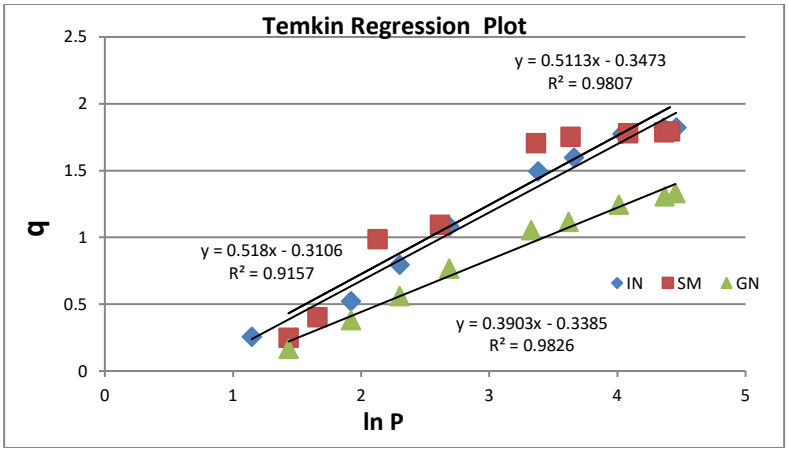

Figure E3 (a), (b), (c): Temkin Regression Plots for all coals

APPENDIX F: CO_2 SORPTION MODELLING DATA: SIMULATED MOISTURE TESTS

Table: F1 – Experimental and LANGMUIR Model Data

SL dry 0%					
P	N_s	P/N_s			L - Value
3.1442178	0.2398327	13.110044	R^2=	0.9945	0.2346966
6.2951167	0.4869263	12.928275	m=	0.0655	0.4627629
9.9711653	0.7433227	13.414317	c=	13.191	0.720246
14.154	1.0205938	13.868397	N_{sm}=	15.267176	1.0025438
30.611	1.6672573	18.360094	a=	0.0049655	2.014409
37.321	2.3774526	15.697894			2.3869361
56.565	3.708218	15.253958			3.3478323
82.345013	4.5137111	18.243306			4.4308201
87.96	4.547746	19.34145			4.6411058

SL 0.51%					
P	**N_s**	**P/N_s**			**L - Value**
3.14462	0.180272987	17.44365611	R^2=	0.991	0.173538109
6.3339	0.36723956	17.24732489	m=	0.1309	0.34166918
11.027	0.623978245	17.67209048	c=	17.709	0.575749267
14.347	0.803116726	17.8641529	N_{sm}=	7.6394194	0.732474788
27.5	1.315913393	19.66805816	a=	0.0073917	1.290549657
37.198	1.7402186	22.8782967			1.647517075
56.576	2.638747272	31.9482074			2.252695765
82.367	3.251380458	25.33293198			2.890999322
86.724	3.308105753	26.2156069			2.984188015

SL 2.43%					
P	**N_s**	**P/N_s**			L - Value
3.09258	0.0523002	59.131271	R^2=	0.1018	0.0911702
6.44661	0.2250023	28.651303	m=	0.1109	0.1879866
10.8862	0.3508568	31.027477	c=	33.578	0.3129542
13.946	0.5262295	26.501745	N_{sm}=	9.0171326	0.3970435
27.409	0.8455948	32.413869	a=	0.0033028	0.7485186
36.805	1.2539819	29.350505			0.9773053
57.078	1.5622195	36.53648			1.4302413
82.022	1.7625183	46.536822			1.9220495
86.13	1.7959014	47.959203			1.9969943

SL 4.42%					
P	**N_s**	**P/N_s**			L - Value
2.7068725	0.2068399	13.086798	R^2=	0.994	0.2093209
6.0115679	0.3430811	17.522293	m=	0.755	0.3896851
9.4756872	0.5957846	15.904551	c=	10.888	0.5251974
14.529364	0.6839749	21.242539	N_{sm}=	1.3245033	0.6647261
29.163459	0.813119	35.866164	a=	0.0693424	0.8862546
37.520956	1.017888	36.861577			0.9567689
58.231248	1.0830417	53.766394			1.0615952
78.236641	1.1156186	70.128483			1.1183587
84.33924	1.119109	75.362848			1.1310967

TN dry 0%

P	N_s	P/N_s			L - Value
2.9	0.1573548	18.429691	R^2=	0.7329	0.1932374
5.6	0.4044483	13.846022	m=	0.0405	0.3704488
10.1	0.6608447	15.28347	c=	14.89	0.6601717
15.109	1.1869111	12.729681	N_{sm}=	24.691358	0.9746538
31.494	1.8812235	16.741233	a=	0.0027199	1.9482222
40.794	2.4030923	16.975628			2.4660629
61.336	3.8609213	15.886364			3.5303107
80.413	4.3827901	18.347445			4.4312675
86.039	4.4622049	19.281723			4.6825017

TN 0.53%

P	N_s	P/N_s			L - Value
3.3884	0.128426068	26.384052	R^2=	0.994	0.23630872
6.2951166	0.490787252	12.826569	m=	0.1974	0.42213249
10.444	1.033534875	10.105126	c=	13.67	0.66388478
14.327	1.22299736	11.714661	N_{sm}=	5.0658561	0.86840041
27.737	1.593980789	17.401088	a=	0.0144404	1.44876411
37.455	1.839034064	20.36667			1.77818463
57.161	2.511796062	22.757023			2.29069323
82.405	2.806767596	29.359396			2.75263709
87.25431	2.840802773	30.714667			2.82431242

TN 1.51%

P	N_s	P/N_s			L - Value
3.0131665	0.2341	12.871279	R^2=	0.982	0.252034
5.9855677	0.425	14.083689	m=	0.3111	0.464714
9.5233693	0.632812	15.049287	c=	11.018	0.6811787
13.857214	0.9502289	14.583028	N_{sm}=	3.2144005	0.903988
29.770497	1.5686507	18.978411	a=	0.0282356	1.4680021
37.935106	1.8528869	20.473514			1.6623905
59.294854	2.0681452	28.670547			2.012408
78.630485	2.1739905	36.168735			2.2161953
84.310862	2.1858832	38.570616			2.2635545

TN 2.40%

P	N_s	P/N_s			L - Value
3.09258	0.198	15.619091	R^2=	0.993	0.1682988
6.44661	0.289	22.306609	m=	0.535	0.3196148
10.8862	0.485	22.445773	c=	16.721	0.4828629
13.829	0.5915492	23.3776	N_{sm}=	1.8691589	0.5733532
27.541	0.8341333	33.017505	a=	0.0319957	0.8755562
37.142	1.0132894	36.654877			1.0150314
57.311	1.1846562	48.377749			1.2095423
82.023	1.3738273	59.70401			1.353441
88.132	1.3851616	63.62579			1.3798304

TN 4.45%

P	N_s	P/N_s			L - Value
3.3131665	0.1658371	19.978444	R^2=	0.994	0.1423605
5.9855677	0.2371909	25.235229	m=	0.7567	0.2366279
10.233693	0.3681028	27.801185	c=	20.766	0.3589531
14.357214	0.4193342	34.238122	N_{sm}=	1.3215277	0.4539098
29.570497	0.6448448	45.856765	a=	0.0364394	0.6854226
39.365106	0.7535525	52.239366			0.7786809
58.274854	0.9408998	61.935238			0.8984356
78.236485	0.9883149	79.161497			0.9783529
88.310302	0.9998795	88.320942			1.0082189

EM dry 0%

P	N_s	P/N_s			L - Value
3.36740	0.1284	26.225857	R^2=	0.9974	0.2713254
6.22512	0.71756	8.6753493	m=	0.174	0.4822617
10.45400	1.26022	8.2953946	c=	11.825	0.7661978
14.82700	1.44965	10.228008	N_{sm}=	5.7471264	1.0293027
28.93700	1.8205	15.895084	a=	0.0147146	1.7163069
36.45500	2.06558	17.648824			2.0065312
57.35100	2.73822	20.944613			2.6302883
82.46500	3.03314	27.187997			3.1506565
86.25431	3.06717	28.12179			3.2144563

Ermelo 1.53%

P	N_s	P/N_s			L - Value
3.09258	0.1903	16.276737	R^2=	0.9974	0.292571
6.44661	0.5823	11.114845	m=	0.4467	0.5341638
10.88620	1.0215	10.672745	c=	9.1889	0.7747212
13.94600	1.1121	12.563964	N_{sm}=	2.2386389	0.9044933
27.40900	1.2352	22.28374	a=	0.048613	1.2788522
36.80500	1.4221	25.919014			1.4360297
57.07800	1.6532	34.592727			1.64558
82.02200	1.7821	46.079775			1.7897742
86.13000	1.8121	47.85			1.8070556

EM 2.44%

P	N_s	P/N_s			L - Value
3.09258	0.13	23.789077	R^2=	0.9974	0.1246448
6.44661	0.19	33.929526	m=	0.682	0.2378947
10.88620	0.32	34.019375	c=	22.702	0.361351
13.94600	0.59	23.637288	N_{sm}=	1.4662757	0.4329285
27.40900	0.71	38.604225	a=	0.0300414	0.6621341
36.80500	0.79	46.588608			0.7699306
57.07800	0.89	64.132584			0.9261519
82.02200	0.99	82.850505			1.0429928
86.13000	1.11	77.594595			1.0575539

Linear Regression Plots

LANGMUIR REGRESSION PLOTS

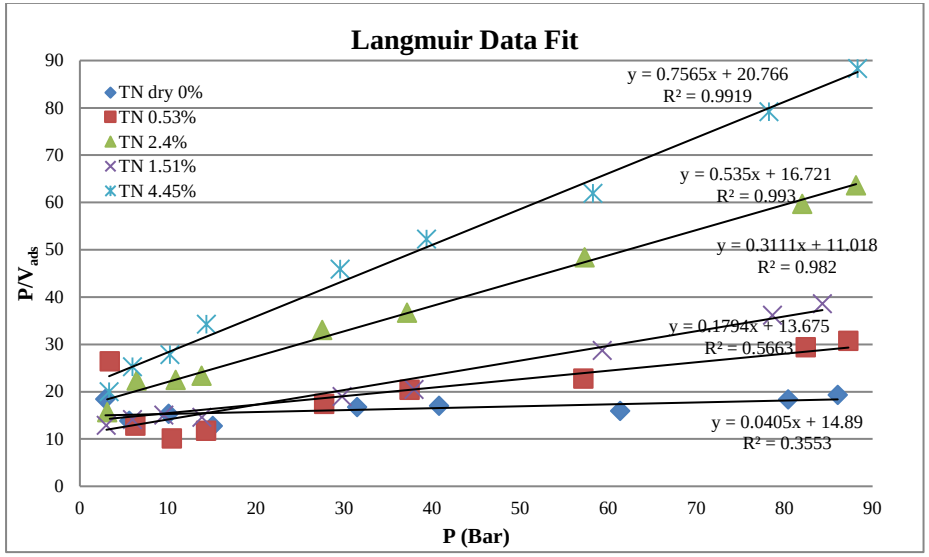

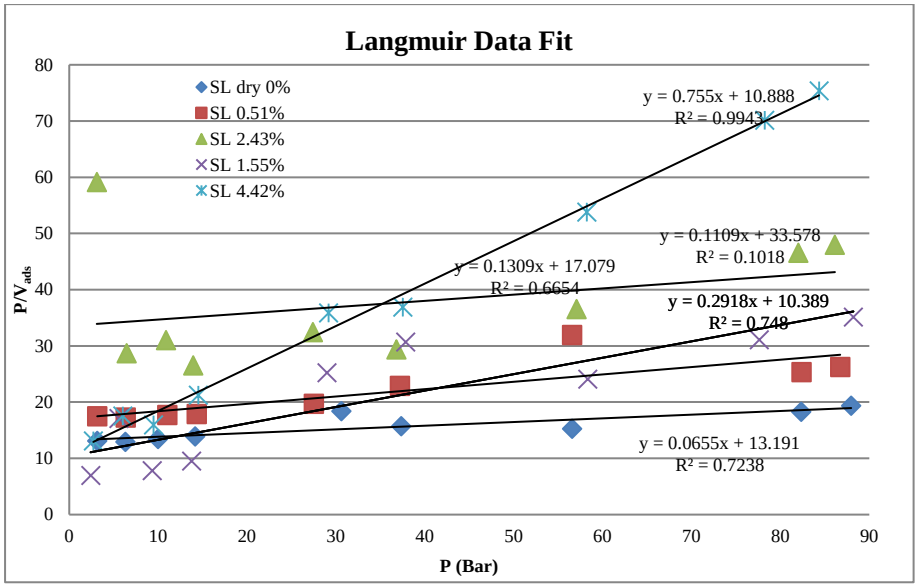

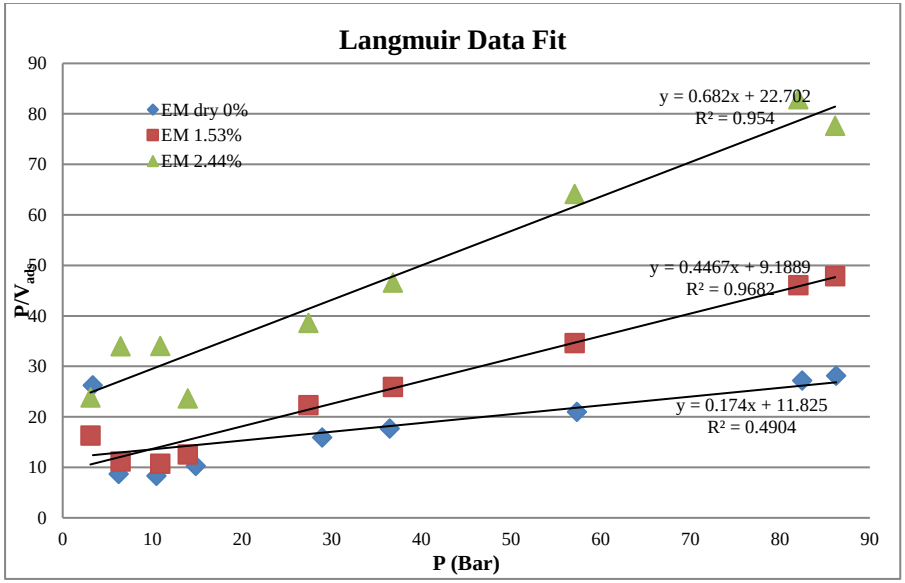

Figure F1: (a), (b) and (c) Coals TN, SL and EM: Langmuir Modelling

Table: F2 – Experimental and FREUNDLICH Model Data

SL 0%/dry						
P	**q**	**log P**	**log q**			**F - Value**
3.1442	0.23983	0.4975126	-0.620091	R^2=	0.994	0.255888
6.295	0.48692	0.7990038	-0.312536	m=	0.8843	0.47278
9.971	0.74332	0.9987459	-0.128822	c=	-1.0319	0.710053
14.154	1.02059	1.1508792	0.008852	n=	1.130838	0.967882
30.611	1.66725	1.4858775	0.222002	A=	0.092918	1.914527
37.321	2.37745	1.5719533	0.376111			2.281278
56.565	3.7082	1.7525478	0.56916			3.295171
82.345	4.5137	1.9156373	0.654533			4.593017
87.96	4.5477	1.9442852	0.657796			4.868906

SL 0.51%						
P	**q**	**log P**	**log q**			**F - Value**
3.14462	0.180272	0.4975682	-0.74406	R^2=	0.9124	0.19786
6.3339	0.36723	0.8016712	-0.43505	m=	0.873	0.36463
11.027	0.623978	1.0424574	-0.20483	c=	-1.138	0.59165
14.347	0.803116	1.1567611	-0.0952	n=	1.1454754	0.7444
27.5	1.315913	1.4393327	0.11922	A=	0.072778	1.31382
37.198	1.74021	1.5705196	0.24060			1.71026
56.576	2.638747	1.7526322	0.42139			2.46631
82.367	3.251380	1.9157532	0.51206			3.42336
86.724	3.308105	1.9381393	0.5195			3.58092

SL 1.55%						
P	**q**	**log P**	**log q**			**F - Value**
2.4032	0.3468	0.380798	-0.459842	R^2=	0.926	0.4744
5.5854	0.75175	0.747059	-0.12392	m=	0.5152	0.7326
9.313	1.19621	0.969105	0.077809	c=	-0.52	0.9534
13.77	1.44823	1.139008	0.160840	n=	1.94099	1.1663
28.9704	1.82831	1.461955	0.262050	A=	0.30199	1.7108
37.8304	2.18680	1.577841	0.339810			1.9629
58.3238	2.42300	1.765846	0.384354			2.4533
77.6304	2.49854	1.890032	0.397686			2.8427
88.2048	2.51053	1.945492	0.399765			3.0361

SL 2.43%						
P	**q**	**log P**	**log q**			F - Value
3.0925	0.052300	0.4903209	-1.28149	R^2=	0.9581	0.0879
6.446	0.22500	0.8093314	-0.6478	m=	0.9847	0.181
10.886	0.350856	1.0368763	-0.45487	c=	-1.5388	0.3035
13.94	0.526229	1.1444497	-0.27882	n=	1.0155377	0.3873
27.40	0.845594	1.4378932	-0.07283	A=	0.0289201	0.7535
36.80	1.253981	1.5659068	0.09829			1.0072
57.07	1.56221	1.7564687	0.1937			1.5516
82.02	1.76251	1.9139304	0.24613			2.2174
86.13	1.79590	1.9351544	0.25428			2.3267

SL 4.42%

P	q	log P	log q			F - Value
2.7068	0.20683	0.4324678	-0.68436	R^2=	0.9258	0.2575106
6.01156	0.34308	0.7789878	-0.46460	m=	0.4717	0.3751876
9.47568	0.59578	0.9766107	-0.22491	c=	-0.7932	0.4650153
14.5293	0.68397	1.1622466	-0.16495	n=	2.1199915	0.5688945
29.1634	0.8131	1.464839	-0.08984	A=	0.1609904	0.7902501
37.5209	1.0178	1.5742739	0.007			0.8899897
58.2312	1.08304	1.7651561	0.034645			1.0950252
78.2366	1.11561	1.8934102	0.047515			1.2586981
84.3392	1.1191	1.9260297	0.048872			1.3040919

TN 0% /dry

P	q	log P	log q			F - Value
2.9	0.15735	0.4623	-0.803120059	R^2=	0.9881	0.1947219
5.6	0.40444	0.7481	-0.393136986	m=	0.957	0.365524
10.1	0.66084	1.00432	-0.17990059	c=	-1.1531	0.6427403
15.109	1.18691	1.17923	0.074418196	n=	1.0449321	0.944993
31.494	1.88122	1.49822	0.274440391	A=	0.070291	1.9085521
40.794	2.40309	1.61059	0.380770444			2.4447849
61.336	3.86092	1.78771	0.586690953			3.6119663
80.413	4.38279	1.90532	0.641750672			4.6805537
86.039	4.46220	1.93469	0.649549511			4.9934816

TN 0.53%

P	q	log P	log q			F - Value
3.3884	0.12842	0.5299947	-0.89134	R^2=	0.8774	0.25579
6.29511	0.49078	0.7990038	-0.30910	m=	0.8147	0.42369
10.444	1.03353	1.0188669	0.01432	c=	-1.0239	0.63998
14.327	1.22299	1.1561553	0.08742	n=	1.2274457	0.82797
27.737	1.59398	1.4430595	0.20248	A=	0.0946455	1.41827
37.455	1.83903	1.5735098	0.2645			1.81150
57.161	2.51179	1.7570998	0.39998			2.5562
82.405	2.80676	1.9159536	0.44820			3.44371
87.25431	2.84080	1.9407869	0.45344			3.60793

TN 1.51%

P	q	log P	log q			F - Value
3.0131	0.2341	0.4790	-0.6305	R^2=	0.9631	0.28107
5.9855	0.425	0.7771	-0.3716	m=	0.6733	0.44619
9.52336	0.6328	0.9787	-0.1987	c=	-0.8737	0.60998
13.8572	0.95022	1.1416	-0.02217	n=	1.485222	0.78521
29.7704	1.56865	1.4737	0.19552	A=	0.1337519	1.31401
37.9351	1.85288	1.5790	0.26784			1.54692
59.2948	2.06814	1.773	0.3155			2.08964
78.6304	2.17399	1.895	0.3372			2.52697
84.3108	2.18588	1.9258	0.3396			2.64848

TN 2.40%						
P	**q**	**log P**	**log q**			F - Value
3.092	0.198	0.4903209	-0.70333	R^2=	0.9802	0.21297
6.446	0.289	0.8093314	-0.53910	m=	0.5903	0.32858
10.88	0.485	1.0368763	-0.31425	c=	-0.9611	0.44768
13.82	0.59154	1.1407908	-0.22800	n=	1.694053	0.51559
27.54	0.83413	1.4399797	-0.07876	A=	0.109370	0.77431
37.14	1.01328	1.5698653	0.005733			0.92382
57.31	1.18465	1.758238	0.073592			1.19340
82.02	1.37382	1.9139356	0.13793			1.4746
88.13	1.38516	1.9451336	0.141500			1.53855

TN 4.45%						
P	**q**	**log P**	**log q**			F - Value
3.3131	0.1658	0.52024	-0.78031	R^2=	0.9874	0.17898
5.9855	0.2371	0.77710	-0.62490	m=	0.5586	0.24905
10.233	0.3681	1.01003	-0.43403	c=	-1.0378	0.33605
14.357	0.4193	1.15707	-0.37743	n=	1.79018	0.40601
29.570	0.6448	1.47085	-0.19054	A=	0.09163	0.60788
39.365	0.7535	1.59511	-0.12288			0.71322
58.274	0.9408	1.76548	-0.02645			0.8879
78.236	0.9883	1.89340	-0.00510			1.04678
88.310	0.9998	1.94601	-5.232E-			1.12006

EM 0%/ Dry						
P	**q**	**log P**	**log q**			F - Value
3.367	0.1284	0.52729	-0.8914	R^2=	0.8212	0.30740
6.225	0.71756	0.79414	-0.14413	m=	0.7863	0.49835
10.454	1.26022	1.01928	0.10044	c=	-0.9269	0.7491
14.827	1.44965	1.17105	0.16126	n=	1.27177	0.98605
28.937	1.8205	1.46145	0.26019	A=	0.11833	1.66817
36.455	2.06558	1.56175	0.31504			2.00036
57.35	2.73822	1.7585	0.43746			2.85654
82.465	3.03314	1.91626	0.48189			3.80069
86.254	3.06717	1.93578	0.48673			3.93735

EM 1.53%						
P	**q**	**log P**	**log q**			F - Value
3.092	0.19	0.4903	-0.72124	R^2=	0.8308	0.33577
6.446	0.58	0.80933	-0.2365	m=	0.5636	0.50797
10.886	1.02	1.03687	0.0086	c=	-0.7503	0.68246
13.946	1.11	1.14444	0.0453	n=	1.774308	0.78471
27.409	1.23	1.43789	0.0899	A=	0.1777051	1.1484
36.805	1.42	1.56590	0.1522			1.35595
57.078	1.65	1.75646	0.2174			1.7363
82.022	1.78	1.91393	0.250			2.13005
86.13	1.8	1.93515	0.2552			2.18954

FREUNDLICH REGRESSION PLOTS:

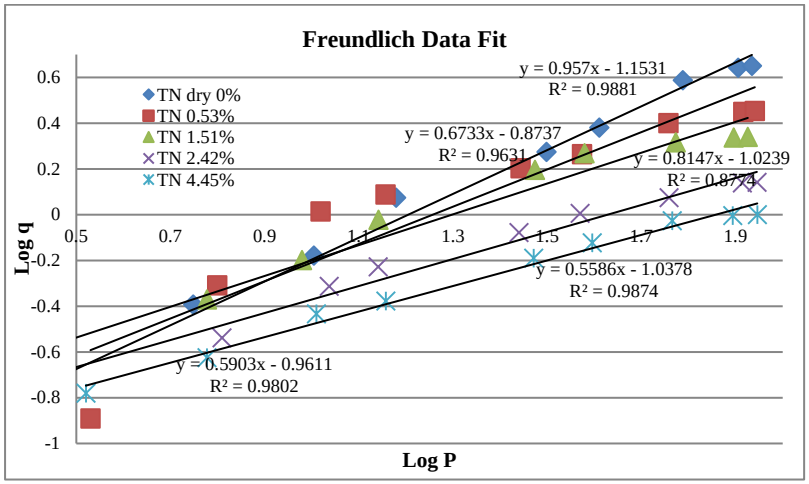

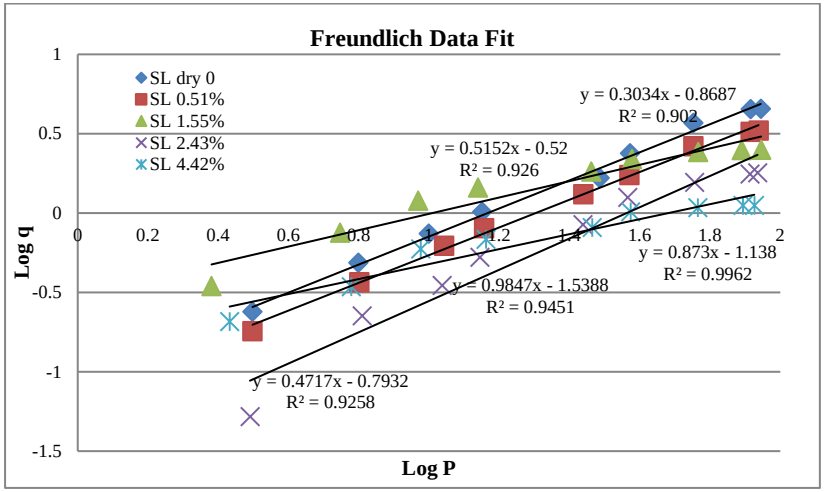

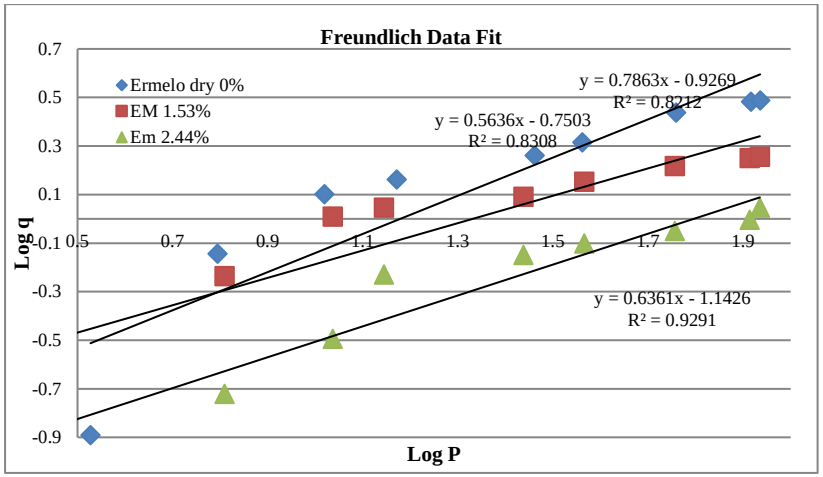

Figure F2: (a), (b) and (c) Coals TN, SL and EM: FREUNDLICH Modelling

Table: F3 – Experimental and Temkin Model Data

SL Dry / 0%

P	q	ln(P)			T - Value
3.1442	0.23983	1.14556	R^2=	0.988	-0.54260
6.2951	0.48692	1.83977	m=	1.3753	0.41214
9.9711	0.74332	2.29969	c=	-2.1181	1.04467
14.154	1.02059	2.64999	b_T=	1862.83	1.52644
30.611	1.66725	3.42135	A_T=	0.21435	2.58729
37.321	2.37745	3.61955			2.85987
56.565	3.70821	4.03539			3.43177
82.345	4.5137	4.41091			3.94823
87.96	4.5477	4.47688			4.03895
R=	8.314				
T=	308.15				

SL 0.51%

P	q	ln(P)			T - Value
3.1446	0.18027	1.145693	R^2=	0.98	-0.371323
6.333	0.36723	1.845916	m=	0.9992	0.328339
11.028	0.623978	2.400346	c=	-1.5161	0.882326
14.347	0.803116	2.663540	b_T=	2564.01	1.145310
27.5	1.315913	3.314186	A_T=	0.21930	1.795434
37.198	1.74021	3.616254			2.097261
56.576	2.638747	4.035584			2.516256
82.367	3.251380	4.411184			2.891555
86.724	3.308105	4.462730			2.943060
R=	8.314				
T=	308.15				

SL 1.55%

P	q	ln(P)			T - Value
2.40324	0.3468	0.8768	R^2=	0.982	0.32301
5.58546	0.7517	1.7201	m=	0.6355	0.85896
9.31334	1.19621	2.2314	c=	-0.2342	1.18388
13.7723	1.44823	2.6226	b_T=	4031.40	1.4325
28.9704	1.82831	3.3662	A_T=	0.69175	1.90506
37.8304	2.18680	3.6331			2.07464
58.3238	2.42300	4.0660			2.34975
77.6304	2.49854	4.3519			2.53147
88.2048	2.51053	4.4796			2.61262
R=	8.314				
T=	308.15				

SL 2.43%

P	q	ln(P)			T - Value
3.092	0.0523	1.12900	R^2=	0.985	-0.19057
6.446	0.2250	1.86355	m=	0.5707	0.22863
10.88	0.3508	2.38749	c=	-0.8349	0.52764
13.94	0.5262	2.63519	b_T=	4489.15	0.66900
27.40	0.8455	3.31087	A_T=	0.23155	1.05461
36.80	1.2539	3.60563			1.22283
57.07	1.5622	4.04441			1.47324
82.02	1.7625	4.40698			1.68016
86.13	1.7959	4.45585			1.7080
R=	8.314				
T=	308.15				

SL 4.42%

P	q	ln(P)			T - Value
2.706	0.2068	0.99579	R^2=	0.986	0.19552
6.0115	0.34308	1.79368	m=	0.2805	0.41932
9.4756	0.59578	2.24872	c=	-0.0838	0.54696
14.529	0.68397	2.67617	b_T=	9133.54	0.66686
29.163	0.8131	3.37291	A_T=	0.74174	0.86230
37.520	1.0178	3.62489			0.93298
58.231	1.0830	4.06442			1.05627
78.236	1.1156	4.35973			1.14680
84.33924	1.1191	4.43484			1.16017
R=	8.314				
T=	308.15				

TN Dry / 0%

P	q	ln(P)			T - Value
2.9	0.1573548	1.0647107	R^2=	0.9798	-0.5700947
5.6	0.4044483	1.7227666	m=	1.3368	0.3095944
10.1	0.6608447	2.3125354	c=	-1.9934	1.0979974
15.109	1.1869111	2.7152906	b_T=	1916.4865	1.6364005
31.494	1.8812235	3.4497971	A_T=	0.2251085	2.6182887
40.794	2.4030923	3.708535			2.9641696
61.336	3.8609213	4.1163669			3.5093593
80.413	4.3827901	4.3871759			3.8713767
86.039	4.4622049	4.4548007			3.9617776
R=	8.314				
T=	308.15				

TN 0.53%

P	q	ln(P)			T - Value
3.3884	0.128426	1.22035	R^2=	0.9834	-0.68957
6.29511	0.490787	1.83977	m=	1.1654	0.110309
10.444	1.033534	2.34602	c=	-1.975	0.651518
14.327	1.222997	2.66214	b_T=	2198.3517	1.088610
27.737	1.593980	3.32276	A_T=	0.1836548	1.979805
37.455	1.839034	3.62314			2.262251
57.161	2.511796	4.04587			2.782771
82.405	2.80676	4.41164			3.111690
87.254	2.840802	4.46882			3.1929787
R=	8.314				
T=	308.15				

TN 1.51%

P	q	ln(P)			T - Value
3.01316	0.06255	1.10299	R^2=	0.9685	-0.1221654
5.98556	0.13593	1.78935	m=	0.7169	0.3698859
9.52336	0.6328	2.25374	c=	-0.9129	0.7028124
13.8572	0.95022	2.6288	b_T=	3573.6631	0.971691
29.7704	1.56865	3.39351	A_T=	0.2798786	1.519913
37.9351	1.85288	3.6358			1.6936602
59.2948	2.06814	4.08252			2.0138604
78.6304	2.17399	4.36475			2.2161961
84.3108	2.18588	4.43451			2.2662007
R=	8.314				
T=	308.15				

TN 2.40%					
P	**q**	**ln(P)**			**T - Value**
3.092	0.05230	1.12900	R^2=	0.9157	-0.0539
6.446	0.22500	1.86355	m=	0.4233	0.2569
10.88	0.35085	2.38749	c=	-0.5319	0.4787
13.82	0.59154	2.62676	b_T=	6052.34	0.58001
27.54	0.83413	3.31567	A_T=	0.284632	0.87162
37.14	1.01328	3.61474			0.9982
57.31	1.18465	4.04849			1.1818
82.02	1.37382	4.40699			1.3335
88.13	1.38516	4.47883			1.36399
R=	8.314				
T=	308.15				

TN 4.45%					
P	**q**	**ln(P)**			**T - Value**
3.3131	0.16583	1.19790	R^2=	0.9783	0.08602
5.985	0.23719	1.78935	m=	0.2765	0.24955
10.233	0.36810	2.32568	c=	-0.2452	0.3978
14.357	0.41933	2.66425	b_T=	9265.6749	0.49146
29.570	0.64484	3.38677	A_T=	0.4119723	0.69124
39.36	0.75355	3.67287			0.77035
58.274	0.94089	4.06517			0.87881
78.236	0.98831	4.35973			0.9602
88.310	0.99987	4.48085			0.99375
R=	8.314				
T=	308.15				

EM 1.53%					
P	**q**	**ln(P)**			**T - Value**
3.092	0.19	1.12900	R^2=	0.9783	0.2873
6.446	0.58	1.86355	m=	0.4636	0.62784
10.886	1.02	2.38749	c=	-0.2361	0.87074
13.946	1.11	2.63519	b_T=	5526.22	0.98557
27.409	1.23	3.31087	A_T=	0.600931	1.29882
36.805	1.42	3.60563			1.43547
57.078	1.65	4.04441			1.63889
82.022	1.78	4.40698			1.80697
86.130	1.8	4.45585			1.82963
R=	8.314				
T=	308.15				

EM Dry / 0%					
P	**q**	**ln(P)**			**T - Value**
3.367	0.1284	1.21414	R^2=	0.9783	0.13583
6.225	0.7175	1.82859	m=	0.8837	0.67882
10.45	1.2602	2.34698	c=	-0.9371	1.136934
14.82	1.4496	2.69644	b_T=	2899.12	1.44577
28.93	1.8205	3.36512	A_T=	0.34630	2.03665
36.455	2.0655	3.59607			2.24077
57.35	2.7382	4.04919			2.64115
82.46	3.0331	4.4123			2.96219
86.25	3.0671	4.4573			3.0016
R=	8.314				
T=	308.15				

EM 2.44%					
P	**q**	**ln(P)**			**T - Value**
3.092	0.13	1.1290	R^2=	0.9783	0.05146
6.446	0.19	1.86355	m=	0.2974	0.26992
10.88	0.32	2.38749	c=	-0.2843	0.42574
13.946	0.59	2.63519	b_T=	8614.52	0.49940
27.409	0.71	3.31087	A_T=	0.38444	0.70035
36.805	0.79	3.60563			0.78801
57.078	0.89	4.04441			0.91851
82.022	0.99	4.40698			1.02633
86.130	1.11	4.45585			1.04087
R=	8.314				
T=	308.15				

TEMKIN REGRESSION PLOTS

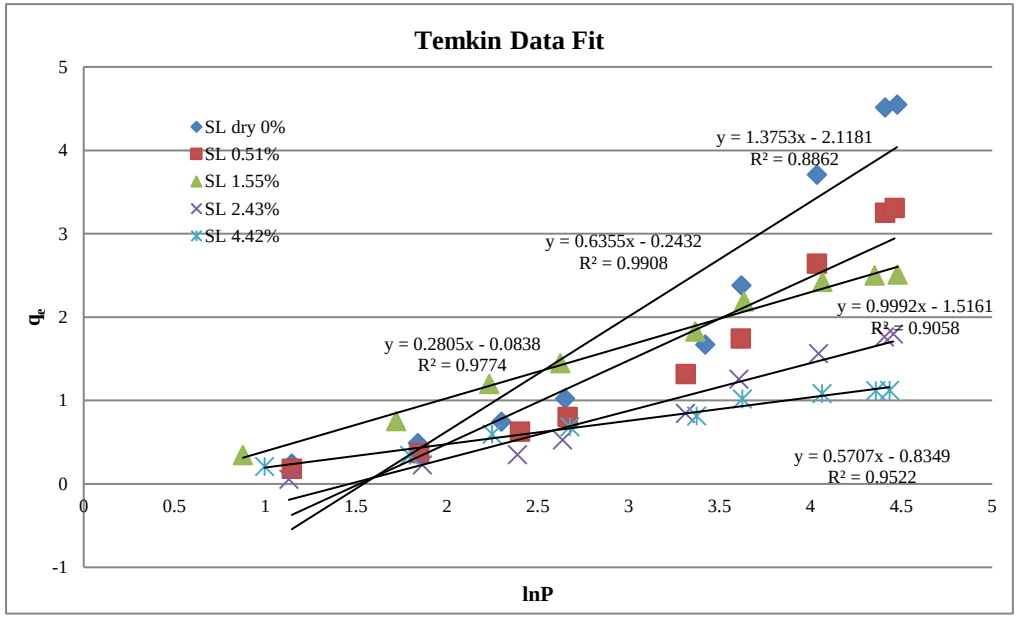

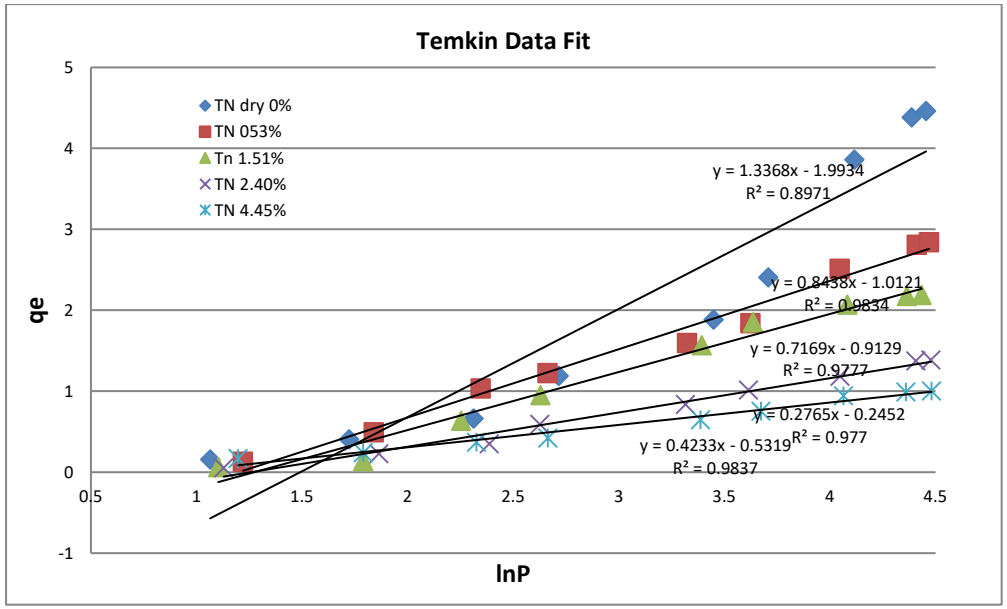

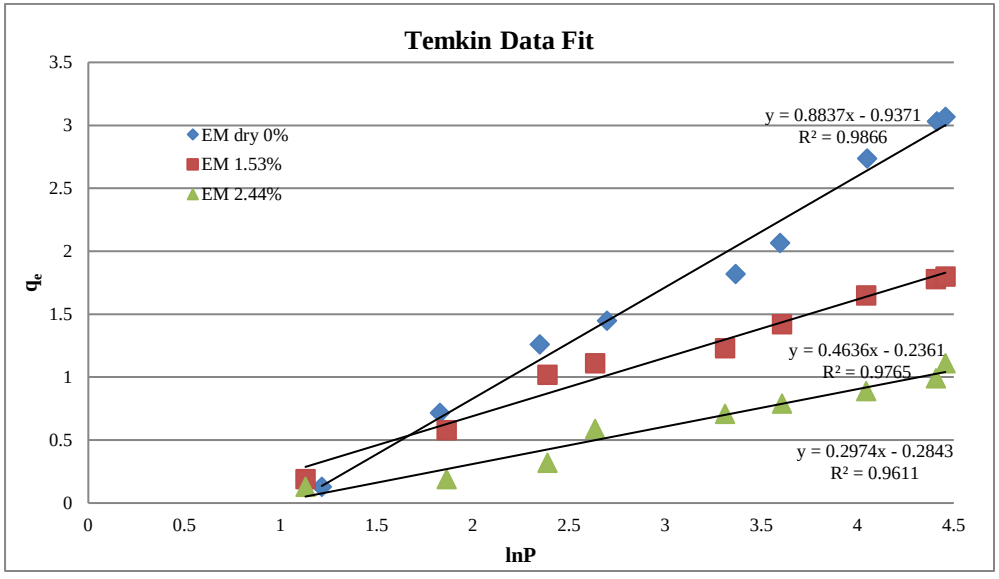

Figure F3: (a), (b) and (c) Coals TN, SL and EM: Temkin ModellinG

APPENDIX G: CO_2 SORPTION MODELLING DATA: TEMPERATURE TESTS

Linear Regression Plots:

MODELS REGRESSION DATA PLOTS AT 35ºC

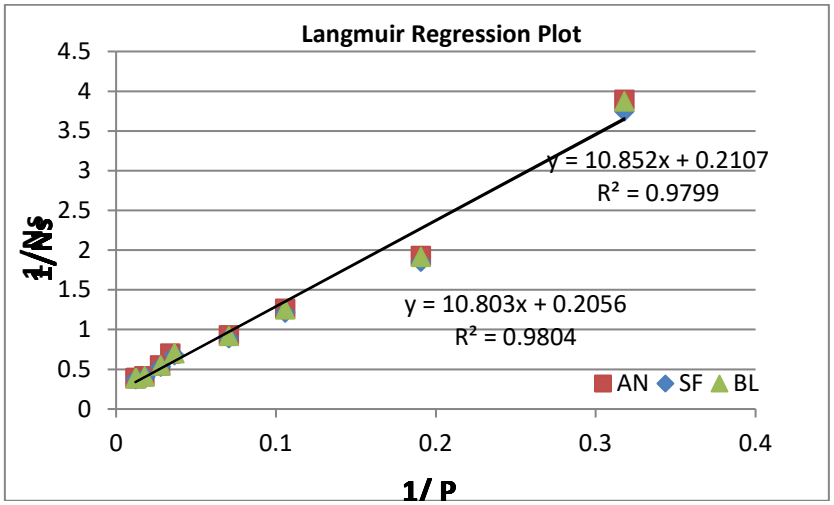

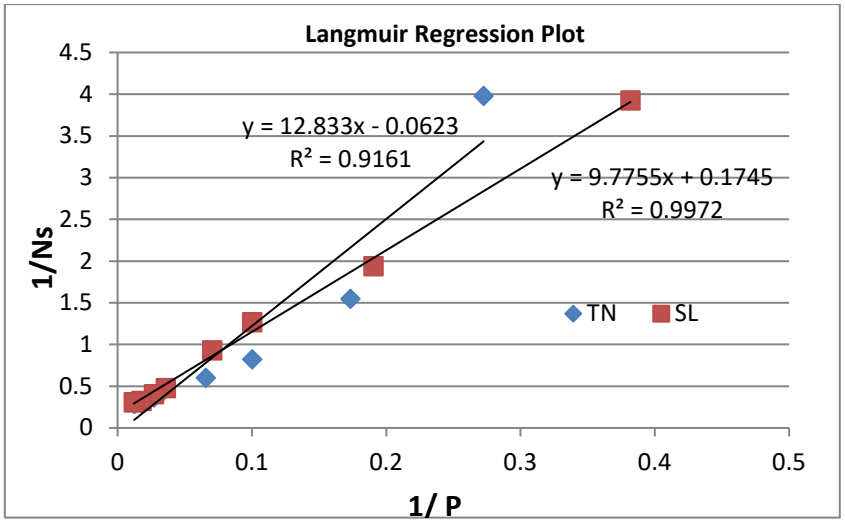

Figure G1 CO_2 Langmuir Model regressions for all coals at 35°C

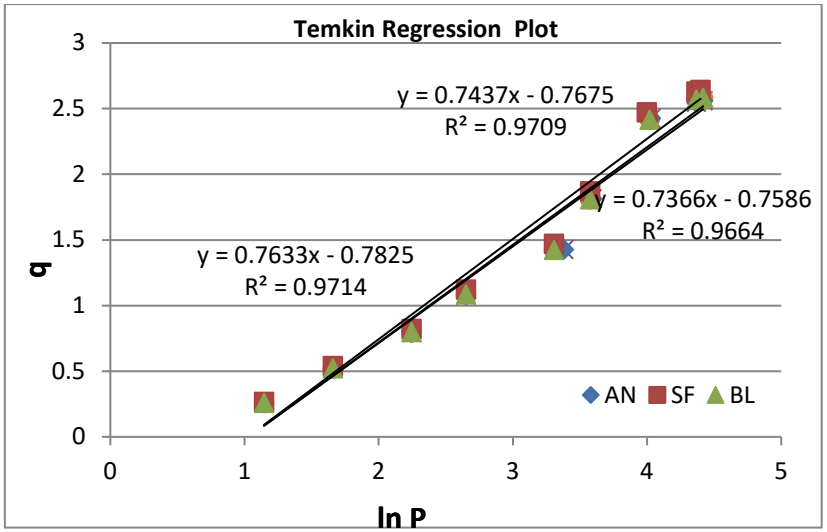

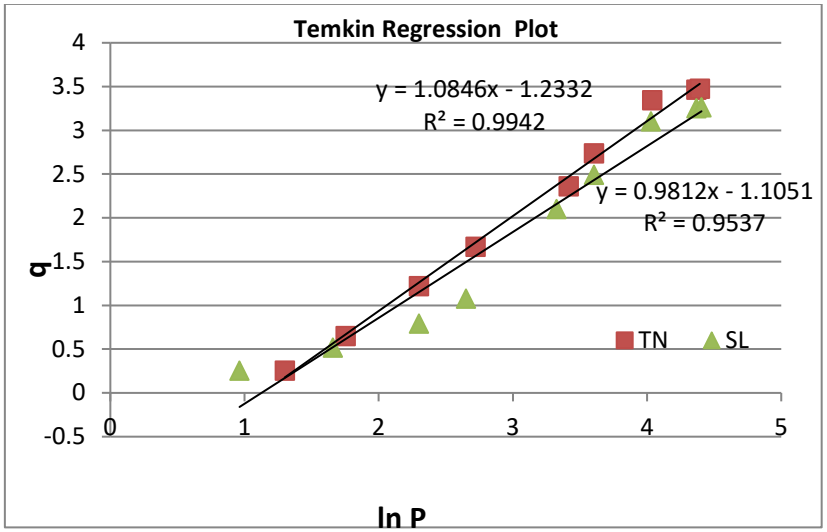

Figure G2 CO_2 Temkin model regressions for all coals at 35°C

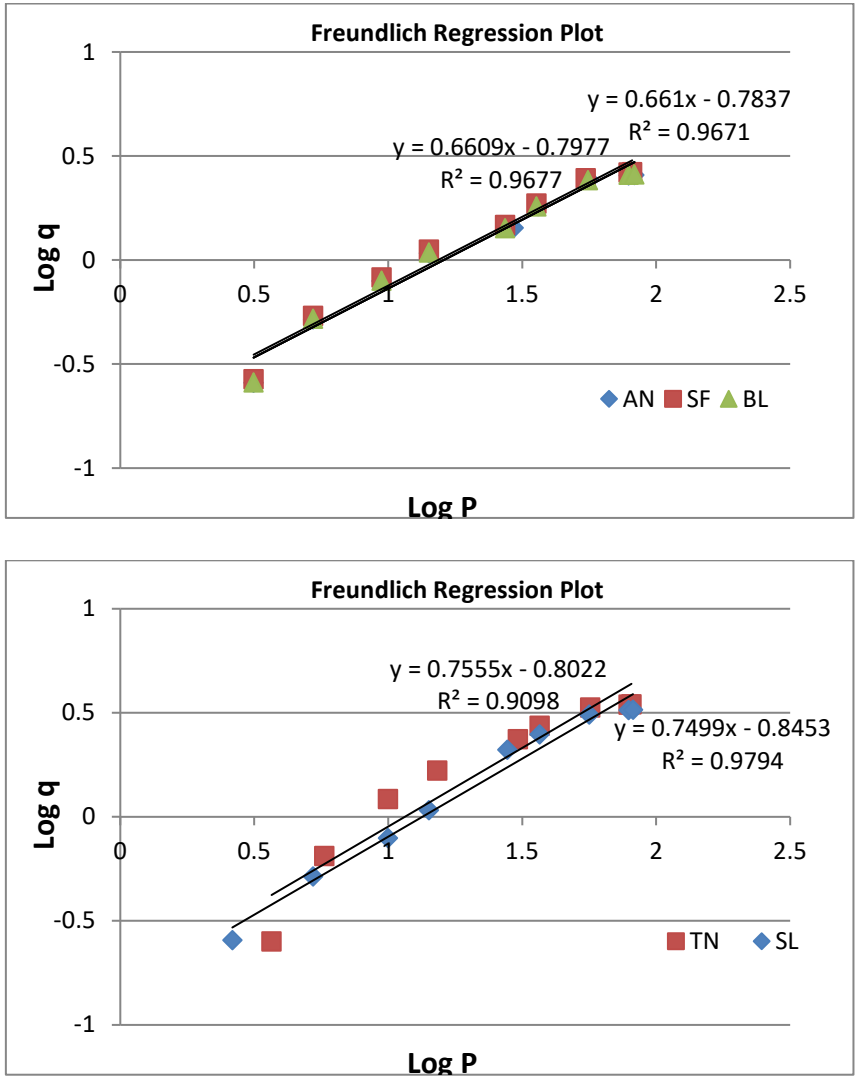

Figure G3 CO_2 Freundlich model regressions for all coals at 35°

Table G1: Experimental and LANGMUIR Modelling data

AN 55 Degrees						
P	**N_s**	**1/P**	**1/Ns**			L - Value
3.1442	0.23739	0.31804	4.21233	R^2=	0.9866	0.24741
5.7699	0.47948	0.17331	2.08556	m=	11.774	0.4900
9.9711	0.7296	0.10028	1.3705	c=	0.2972	0.67658
14.17	0.98867	0.070	1.011	N_{sm}=	3.3647376	0.88654
27.30	1.19997	0.036	0.8333	a=	0.0252421	1.37275
35.17	1.34993	0.028	0.7407			1.58254
55.13	1.75762	0.018	0.5689			1.95789
78.240	2.07954	0.012	0.4808			2.23371

SF 55 degrees						
P	**N_s**	**1/P**	1/Ns			**L - Value**
2.6190	0.2480	0.3818	4.031	R^2=	0.9962	0.25252
5.2448	0.5010	0.1906	1.9957	m=	9.5239	0.46740
9.4460	0.7625	0.1058	1.3114	c=	0.3236	0.7508
14.1723	1.0343	0.0705	0.9668	N_{sm}=	3.09023	1.00441
28.3514	1.3434	0.0352	0.7443	a=	0.03397	1.51624
35.7035	1.5276	0.0280	0.6545			1.6939
54.608	2.1006	0.0183	0.4760			2.00802
79.8160	2.2858	0.0125	0.4374			2.25772

BL 55 Degrees						
P	**N_s**	**1/P**	1/Ns			**L - Value**
3.1442	0.241	0.31804	4.14090	R^2=	0.9962	0.253475
5.244	0.487	0.19066	2.05432	m=	11.242	0.466537
9.9711	0.584	0.10028	1.71222	c=	0.3697	0.667935
14.172	0.848	0.07055	1.17987	N_{sm}=	2.70489	0.859894
27.30	1.144	0.03662	0.87442	a=	0.03288	1.279626
36.228	1.469	0.02760	0.68072			1.470573
55.134	1.884	0.01813	0.53085			1.743365
80.866	2.048	0.01236	0.48835			1.965720

TN 55 Degrees						
P	**N_s**	**1/P**	**1/Ns**			L - Value
3.14421	0.2315	0.3180	4.3181	R^2=	0.9819	0.2084
5.2448	0.4668	0.1906	2.1422	m=	14.69	0.3570
8.9208	0.7088	0.1120	1.4107	c=	0.1247	0.5645
13.1220	1.0210	0.0762	0.9793	N_{sm}=	8.01924	0.8037
26.250	1.4922	0.0380	0.6701	a=	0.00848	1.4613
33.602	1.7961	0.0297	0.5567			1.7797
50.407	2.16801	0.0198	0.4612			2.4031
76.140	2.75224	0.0131	0.3633			3.1482

SL 55 Degrees						
P	**N_s**	**1/P**	**1/Ns**			L - Value
2.6190	0.12741	0.38181	7.84817	R^2=	0.9833	0.12785
5.76996	0.29412	0.17331	3.3999	m=	20.078	0.28737
9.97116	0.53476	0.10028	1.86997	c=	0.1552	0.46108
14.1723	0.80969	0.07055	1.23502	N_{sm}=	6.4432	0.63617
27.3011	1.07639	0.03662	0.92902	a=	0.0077	1.12280
36.2286	1.27169	0.02760	0.78635			1.40963
54.083	2.15810	0.01848	0.46336			1.89955
78.2406	2.46578	0.01278	0.40555			2.42825

Table G2: Experimental and FREUNDLICH Modelling data

AN 55 Degrees						
P	**q**	**log P**	**log q**			F - Value
3.1442	0.2378	0.4975	-0.62452	R^2=	0.9535	0.3064
5.7699	0.4798	0.76117	-0.31922	m=	0.6223	0.44717
9.9711	0.7294	0.9987	-0.13689	c=	-0.8232	0.62852
14.172	0.9885	1.1514	-0.00494	n=	1.606942	0.78224
27.301	1.1996	1.4361	0.07917	A=	0.150245	1.17634
35.178	1.24999	1.5462	0.09688			1.37735
55.134	1.7571	1.7414	0.24492			1.82173
78.2406	2.07951	1.8934	0.317967			2.26507

SF 55 Degrees						
P	**q**	**log P**	**log q**			**F - Value**
2.6190	0.2480	0.41814	-0.60546	R^2=	0.984	0.27353
5.2441	0.5010	0.71973	-0.30011	m=	0.622	0.421393
9.4460	0.76252	0.97524	-0.11774	c=	-0.823	0.607711
14.1723	1.03433	1.15144	0.01466	n=	1.60694	0.782244
28.3514	1.34349	1.45257	0.12823	A=	0.15024	1.204307
35.7035	1.52766	1.55271	0.18402			
54.60	2.10063	1.73726	0.32234			
79.8160	2.28583	1.90209	0.35904			

BL 55 Degrees						
P	**q**	**log P**	**log q**			**F - Value**
3.1442	0.241	0.49751	-0.61709	R^2=	0.9742	0.29282
5.244	0.487	0.71973	-0.31266	m=	0.6372	0.40570
9.9711	0.584	0.99874	-0.23355	c=	-0.8504	0.61094
14.172	0.848	1.15144	-0.07183	n=	1.5693	0.76436
27.3011	1.144	1.43618	0.05827	A=	0.1411	1.16073
36.2286	1.469	1.55905	0.16702			1.39004
55.13409	1.884	1.74141	0.27502			1.81648
80.86639	2.048	1.90776	0.31126			2.31862

TN 55 Degrees						
P	**q**	**log P**	**log q**			F - Value
3.1442	0.2315	0.4975	-0.6352	R^2=	0.9649	0.2997
5.2448	0.46680	0.7197	-0.3308	m=	0.72	0.43331
8.9208	0.70882	0.9504	-0.1494	c=	-0.8814	0.63517
13.1220	1.21070	1.1180	0.0830	n=	1.38888	0.83861
26.250	1.49226	1.4191	0.17384	A=	0.13140	1.38160
33.6029	1.79611	1.5263	0.25433			1.6504
50.4077	2.16801	1.7024	0.33606			2.21002
76.1400	2.7522	1.88161	0.43968			2.97414
86.1178	3.50307	1.93509	0.54444			3.24987

SL 55 Degrees						
P	**q**	**log P**	**log q**			F - Value
2.619	0.1274	0.4188	-0.8947	R^2=	0.9814	0.1499148
5.7699	0.2941	0.76117	-0.5314	m=	0.8577	0.29516
9.9711	0.5347	0.99874	-0.2718	c=	-1.1828	0.47187
14.172	0.8096	1.15144	-0.0916	n=	1.16590	0.63795
27.301	1.07639	1.43618	0.0319	A=	0.06564	1.11946
36.228	1.27169	1.55905	0.10438			1.42691
54.083	2.15810	1.73306	0.33407			2.01210
78.2406	2.46578	1.89343	0.39195			2.76183

Table G3: Experimental and TEMKIN Modelling data

An 55 Degrees					
P	**q**	**ln(P)**			**T - Value**
3.14421	0.23738	1.14556	R2=	0.9605	0.1440438
5.76996	0.4798	1.75266	m=	0.5437	0.4741247
9.97116	0.72963	2.29969	c=	-0.4788	0.7715455
14.1723	0.98867	2.65129	bT=	5017.91	0.9627085
27.3011	1.19997	3.30692	AT=	0.41452	1.3191764
35.1783	1.24993	3.5604			1.4570063
55.1340	1.75762	4.00976			1.7013106
78.2406	2.07954	4.359789			1.8916174
101.347	4.47628	4.618552			2.032307

SF 55 Degrees					
P	**q**	**ln(P)**			**T - Value**
2.6190	0.24804	0.96281	R^2=	0.9615	0.08434
5.2448	0.50105	1.65724	m=	0.604	0.503773
9.44601	0.76252	2.24559	c=	-0.4972	0.859138
14.1723	1.03433	2.65129	b_T=	4516.92	1.104181
28.3514	1.34349	3.3446	A_T=	0.43908	1.522984
35.7035	1.52766	3.57524			1.662250
54.608	2.10063	4.00019			1.918918
79.8160	2.28583	4.37972			2.148153

BL 55 Degrees					
P	**q**	ln(P)			T - Value
3.1442178	0.241	1.1455651	R^2=	0.9548	0.1016247
5.244817	0.487	1.6572404	m=	0.5683	0.3924097
9.9711653	0.584	2.2996975	c=	-0.5494	0.7575181
14.172364	0.848	2.6512939	b_T=	4800.7023	0.9573303
27.301109	1.144	3.3069273	A_T=	0.3803198	1.3299268
36.228656	1.469	3.5898504			1.490712
55.134049	1.884	4.0097675			1.7293509
80.86639	2.048	4.3927983			1.9470273

TN 55 Degrees					
P	**q**	**ln(P)**			**T - Value**
3.14421	0.23158	1.14556	R2=	0.9696	0.0677301
5.2448	0.46680	1.65724	m=	0.7655	0.4594175
8.92086	0.70882	2.1883	c=	-0.8092	0.8660148
13.1220	1.21070	2.57429	bT=	3563.9962	1.1614229
26.250	1.49226	3.26769	AT=	0.3474666	1.6922219
33.6029	1.79611	3.51461			1.8812359
50.4077	2.16801	3.9201			2.1916702
76.1400	2.75224	4.33257			2.5073856
86.1178	3.5030	4.45571			2.6016515

SL 55 Degrees					
P	**q**	**ln(P)**			**T - Value**
2.6190	0.12741	0.98185	R2=	0.8854	-0.1206016
5.76996	0.29412	1.76663	m=	0.78	0.4954797
9.97116	0.53476	2.26975	c=	-0.8716	0.922164
14.1723	0.80969	2.62939	bT=	3497.7424	1.1964092
27.3011	1.07639	3.39273	AT=	0.3271175	1.7078033
36.2286	1.27169	3.58504			1.9284833
54.083	2.15810	3.95338			2.2410163
78.240	2.46578	4.37892			2.5290356

REGRESSION DATA PLOTS TO 55ºC

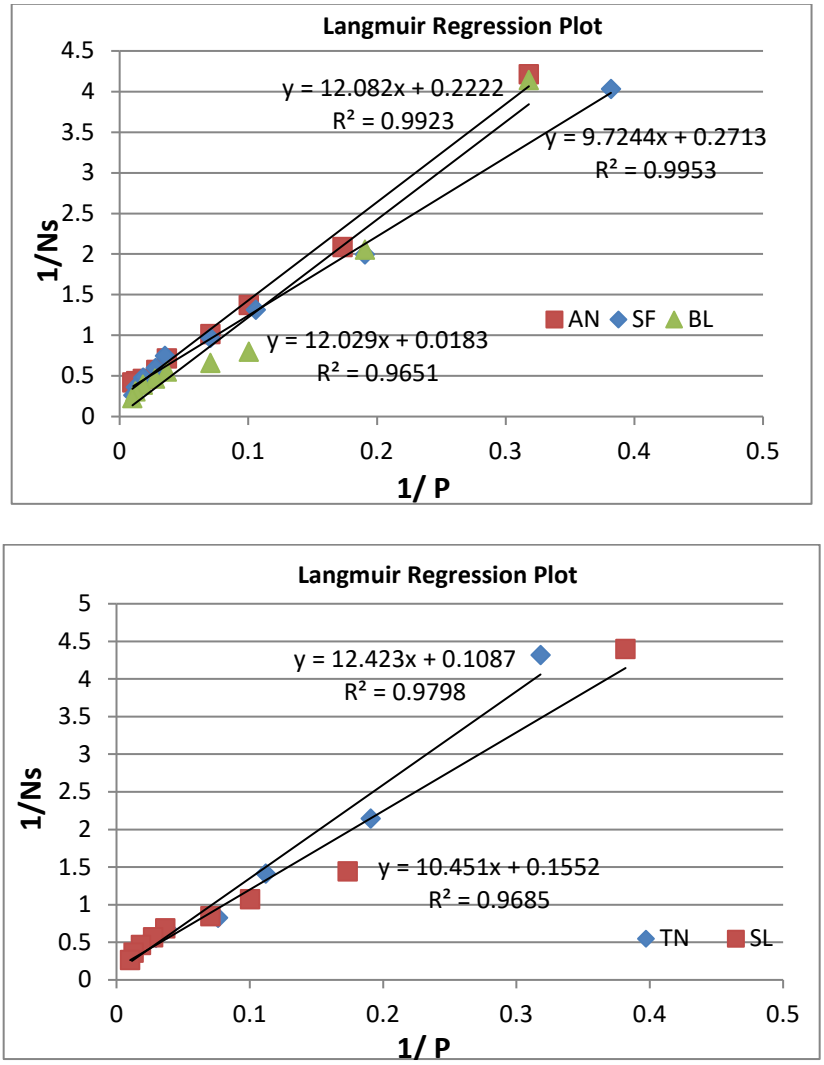

Figure G4 CO_2 Langmuir Model for all coals at 55ºC

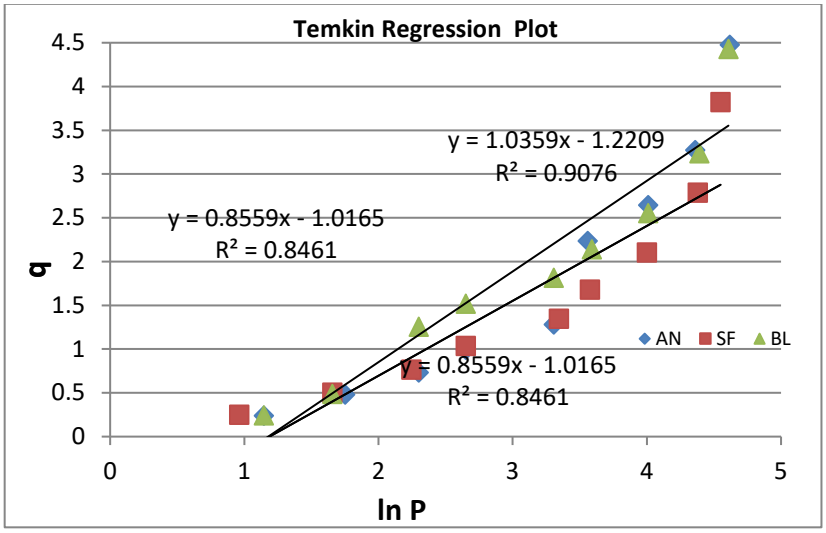

Figure G5 CO_2 Temkin Model for all coals at 55°C

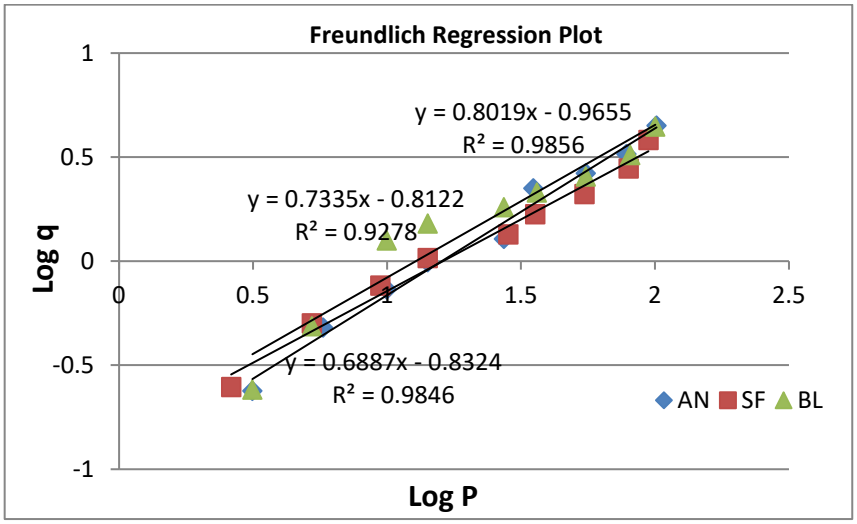

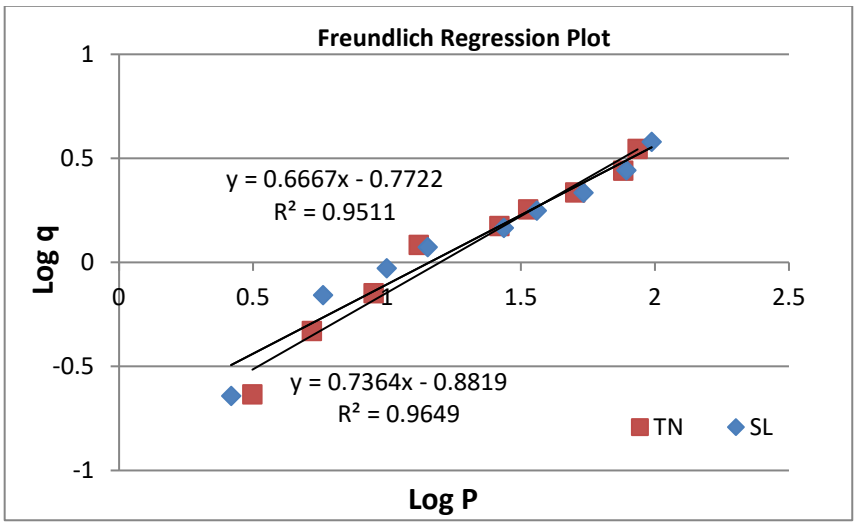

Figure G6 CO_2 Freundlich model regressions for all coals at 55°C

APPENDIX H1: CYCLIC INJECTION OF CO_2: CO_2 SORPTION CAPACITY FOR CH_4 SATURATED SAMPLES VS DRIED AND DEGASSED SAMPLES AT SUB-CRITICAL PRESSURE

The objective of these tests was to determine the difference between the CO_2 adsorption capacity for typically dried and degassed samples, compared to CH_4 saturated samples, discussed in Section 3.4.2.3. The data presented here gives a comparison of the CO_2 uptake using the pressure step method of cyclic injections of CO_2 to sub-critical conditions.

Experiments were conducted at isothermal conditions of 30^oC and using particle size +4.75-6.7 mm and mass of 5g each of the five different coals namely: AN, EM, GN, TN and IN. Samples were initially dried and degassed (described in section 3.4.2.3) and then injected with pure CH_4 gas at a pressure of 2 bar and allowed to saturate overnight. The samples were then placed in the HPVAS and cyclically injected (every hour and a half) with CO_2 until maximum highest sub-critical pressure that could be achieved was attained. These isotherms are compared with those as are presented in section 4.5., detailing the pure CO_2 adsorption tests. The same size fractions and masses were used for both tests.

The legends: CO_2 D&DG (Dried and degassed samples), while CO_2_CH_4 are those samples that have been dried and degassed and the saturated with CH_4 (as per preparation described for trial test) and then cyclically injected with CO_2.

From Figures H1 to H5, a clear trend can be noticed by the greatly reduced CO_2 adsorption capacities using the CH_4 saturated coal samples as compared to those that were just the died and degassed samples.

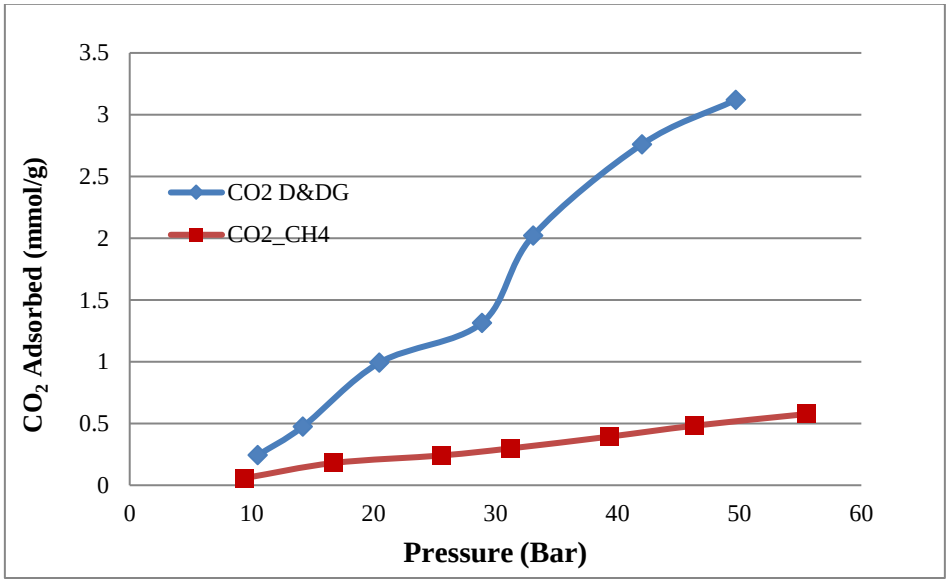

Figure H1: Comparison of CO_2 adsorption for D&DG & CH_4 saturated: AN

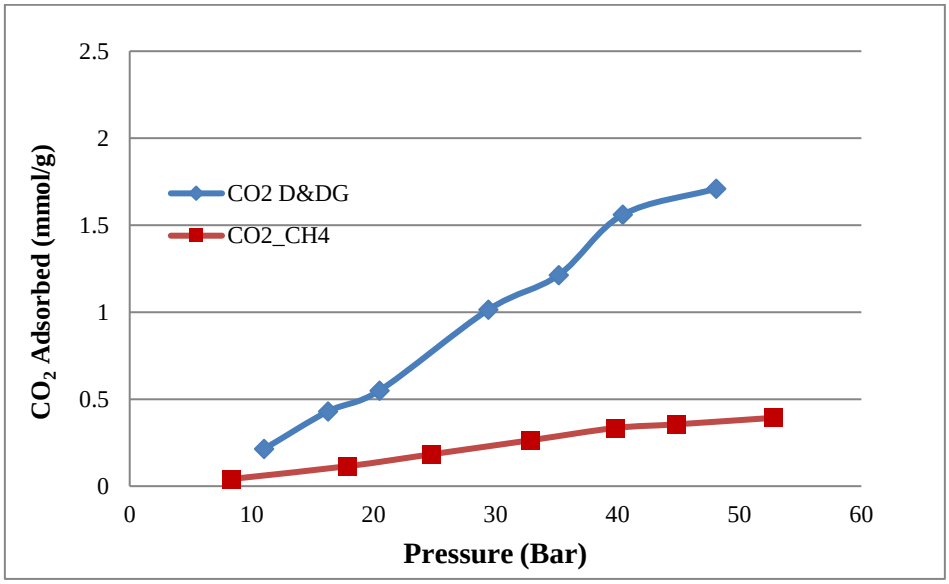

Figure H2: Comparison of CO_2 adsorption for D&DG and CH_4 saturated: EM

The AN and EM samples in Figures H1 and H2, respectively, show very marked differences in reduced CO_2 sorption as compared to the rest depicted below. Sorption in the AN sample reduced up to 10 times, while for the EM sample, it is noted to have reduced the CO_2 sorption

by up to approximately four (4) times (for the dried and degassed only) as compared to that that for a none-CH_4 saturated sample.

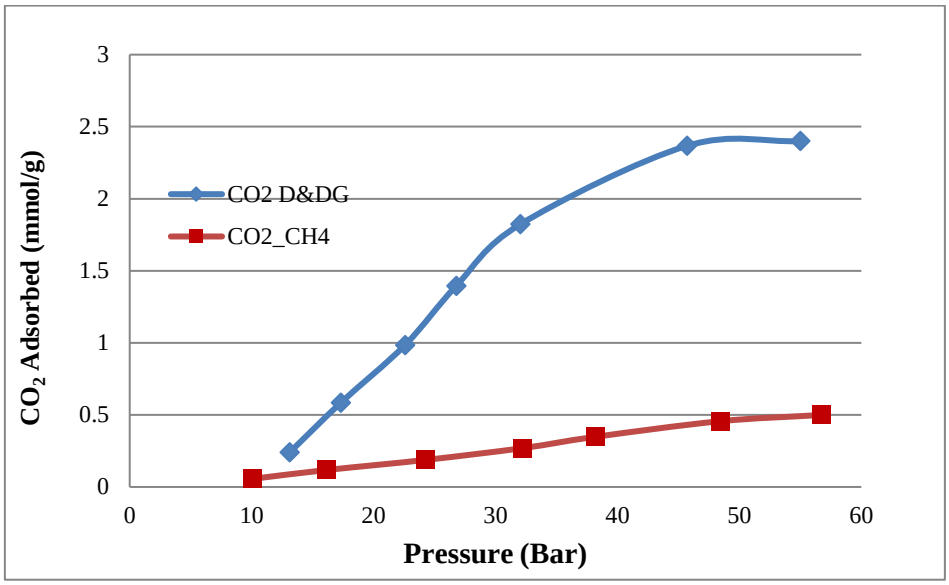

Figure H3: Comparison of CO_2 adsorption for D&DG and CH_4 saturated: GN

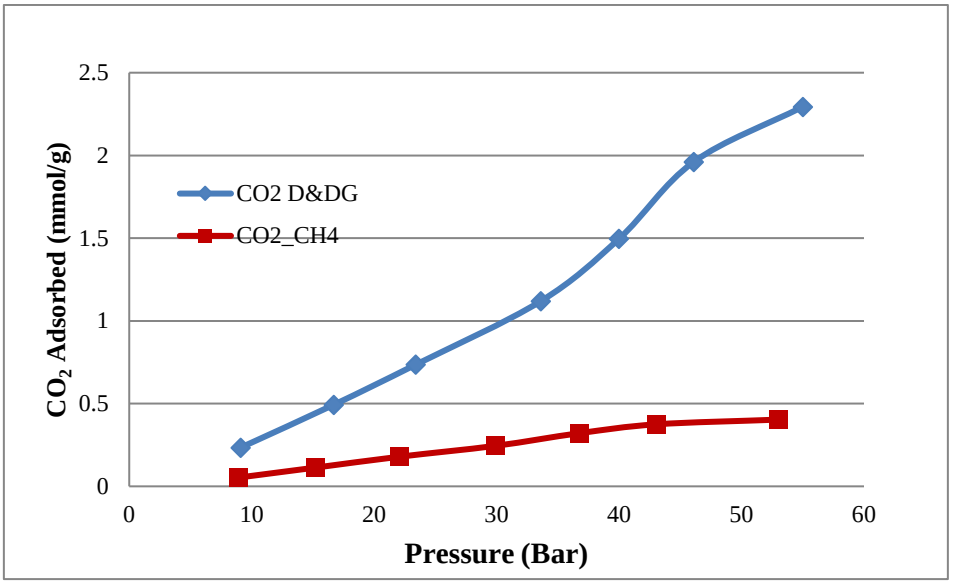

Figure H4: Comparison of CO_2 adsorption for D&DG and CH_4 saturated: TN

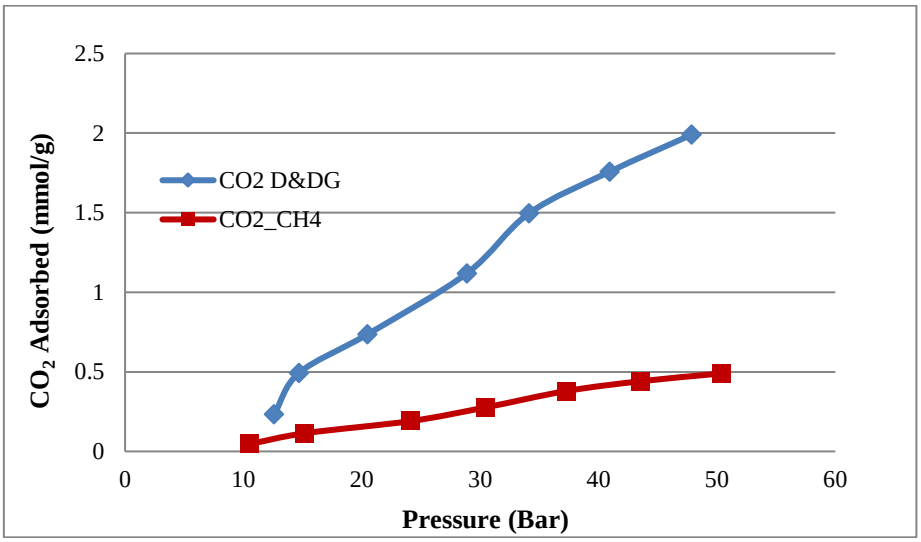

Figure H5: Comparison of CO_2 adsorption for D&DG and CH_4 saturated: IN

The GN, TN and IN samples all show very comparable reduction in the sorption rates at approximately six (6) times less CO_2 capacity rates for the CH_4 saturated samples tested. The focus of the current investigation was to evaluate the difference in CO_2 sorption for CH_4 saturated samples as compared to the conventional method of drying and degassing coal samples. Table H1 gives a summary of the reduction in adsorption rates that was observed for these coals tested.

Table H1 Summary of CO_2 adsorption capacities comparing dried and degassed samples with CH_4 saturated samples

Coal ID	*CO_2 adsorbed for D&D* (mmol/g)*	*CO_2 Sorption for CH_4 saturated (mmol/g)*	*CO_2 Sorbed Decrease (%)*
AN	3.1	0.58	81
EM	1.7	0.39	77
GN	2.4	0.35	85
TN	2.3	0.40	82
IN	1.9	0.49	75

D&D - Dried & degassed*

From these results it is evident that CO_2 sorption data for the, typically dried and degassed coals as is widely prepared for laboratory experiments to evaluate sorption capacity, do not give a true representation for the CO_2 sorption rates that may be found in a real-time injection scenario and may very well-be overstated values and not exactly what would be expected in-situ. The key factor that controls the fluid flow in coal seams is the permeability of fluid such as gas and water. It is a well-known fact that coal is a naturally fractured material comprising of both solid, fluid and gas components, which need to be taken into account in order to better understand the migration of CO_2 through coal and the mechanisms behind the multi dynamic interactions.

However, the trends that are found from them, do give direction in terms of addressing specific coals and further investigation of CO_2 uptake and other parameters that could also influence the sorption capacity. Furthermore, it can be concluded that due to lack of constant gas (CH_4) drainage from the system, a build-up in partial pressures of CH_4 and CO_2 could be the reasoning for the decreased sorption of the CO_2. It is clear that further test methods need to be evaluated and perfected as understanding the competitive sorption effects for CO_2-CH_4 system is essential for the implementation of ECBM undertakings.

APPENDIX H2: MODELLING DATA FOR CYCLIC INJECTION OF CO_2: CO_2 SORPTION CAPACITY VERSUS CH_4 DESORPTION FOR CH_4 SATURATED SAMPLES TO SUPERCRITICAL PRESSURE AT 35 ^oC

Linear Regression Plots:

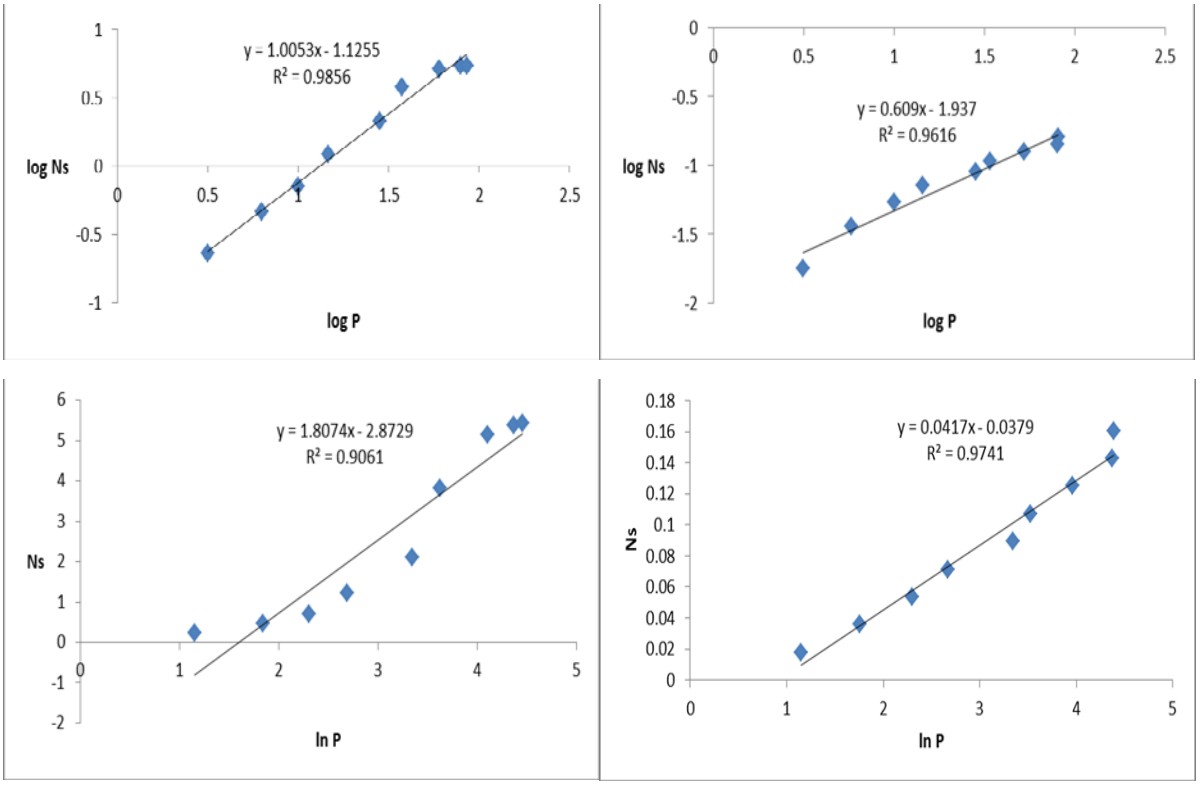

Figure H6 TN CO_2 and CH_4 Langmuir, Freundlich and Temkin model regressions

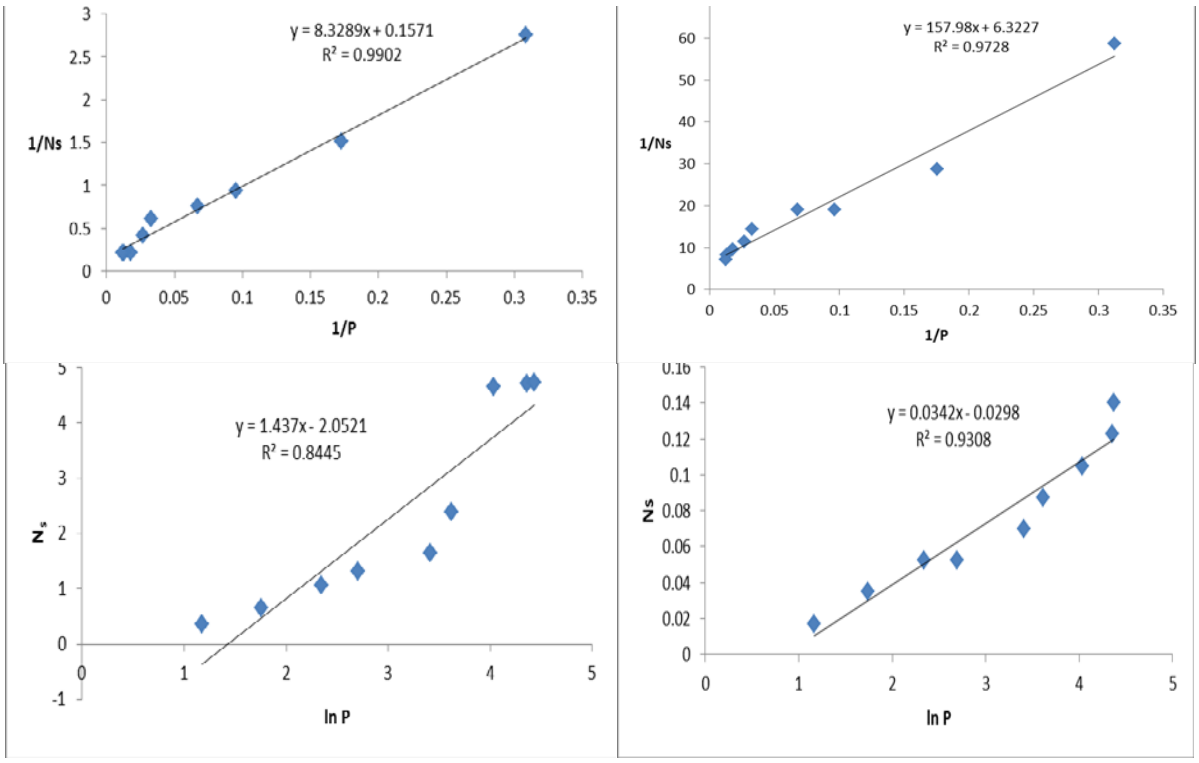

Figure H7: SL CO_2 and CH_4 Langmuir and Temkin model regressions

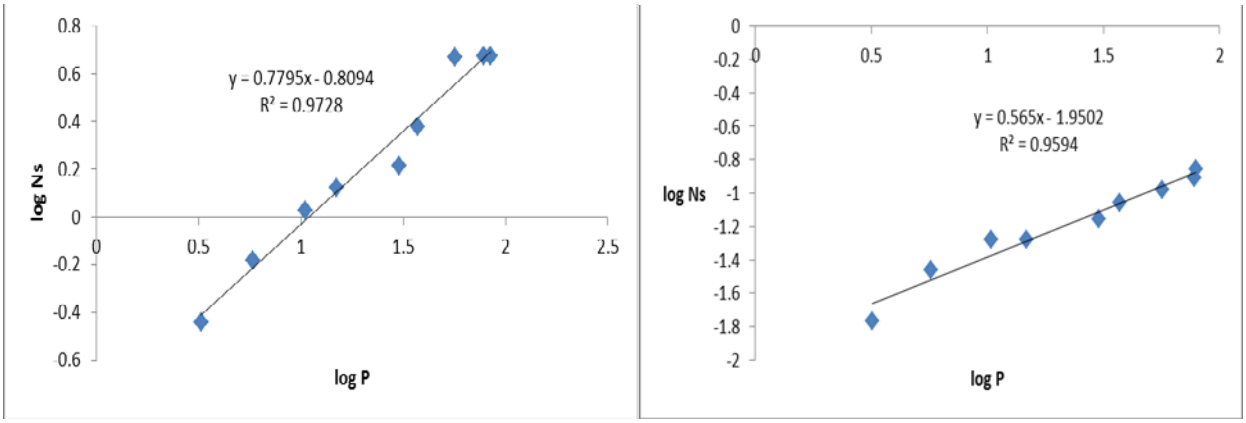

Figure H8: SL CO_2 and CH_4 Freundlich model regressions

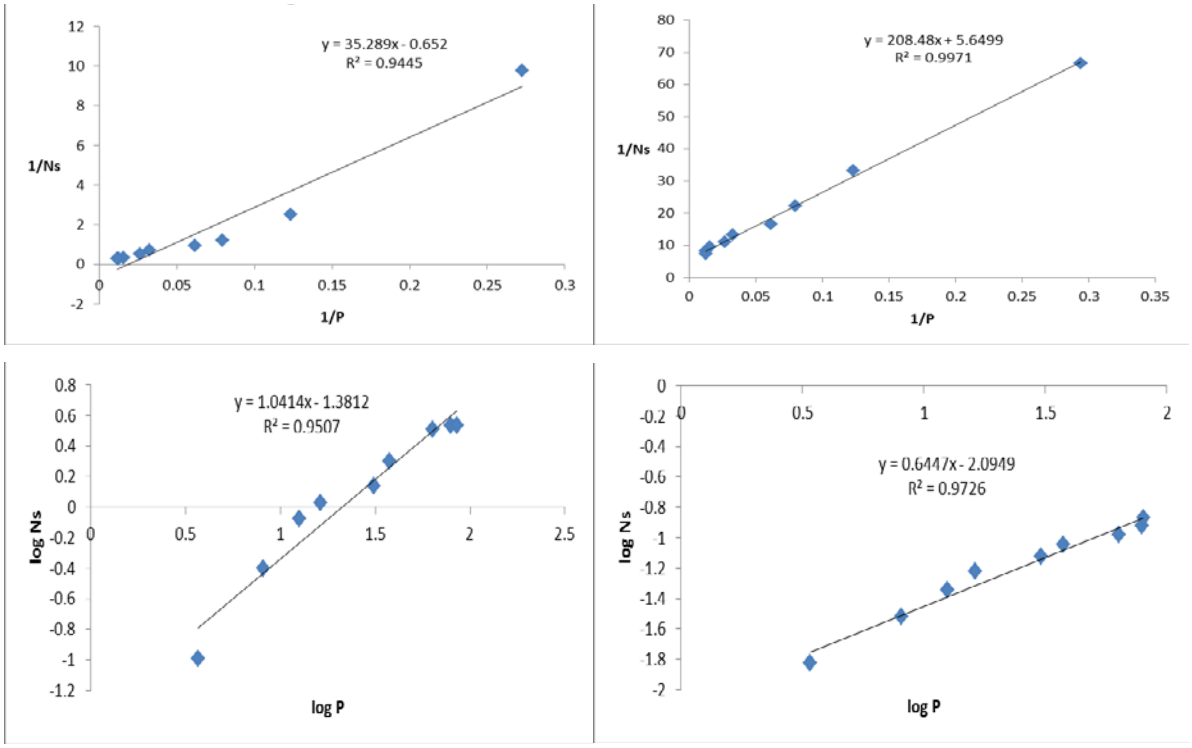

Figure H9: AN CO_2 and CH_4 Langmuir and Freundlich model regressions

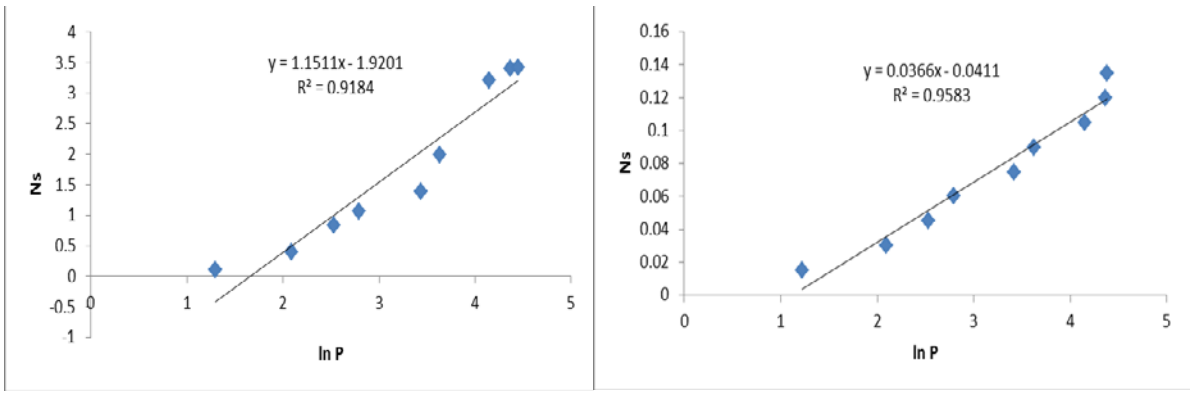

Figure H10: AN CO_2 and CH_4 Temkin model regressions

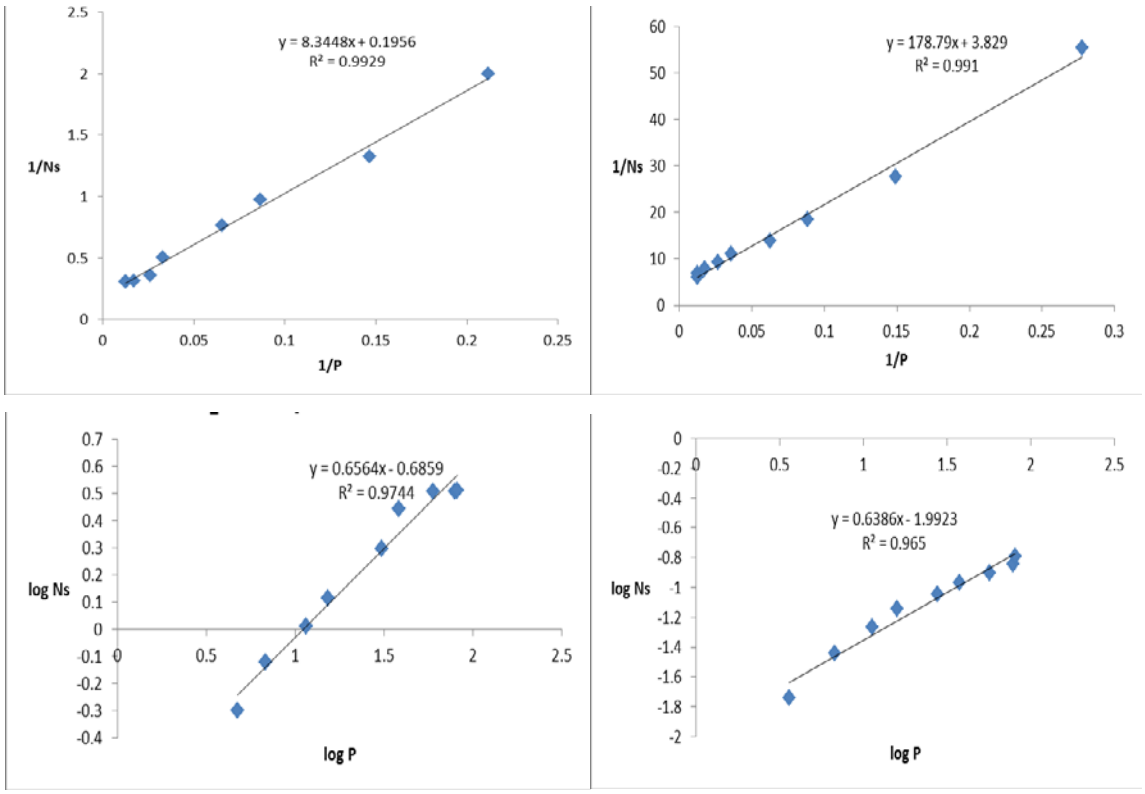

Figure H11: BL CO_2 and CH_4 Langmuir and Freundlich model regressions

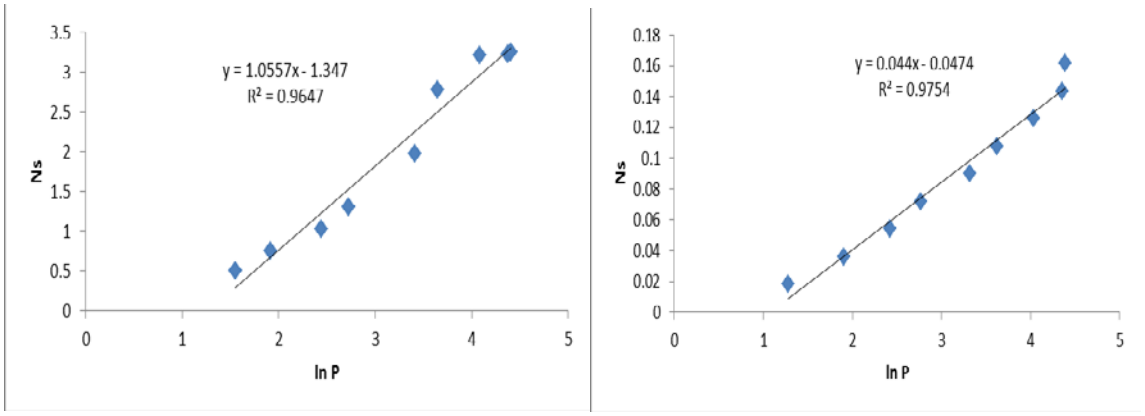

Figure H12: BL CO_2 and CH_4 Temkin model regressions

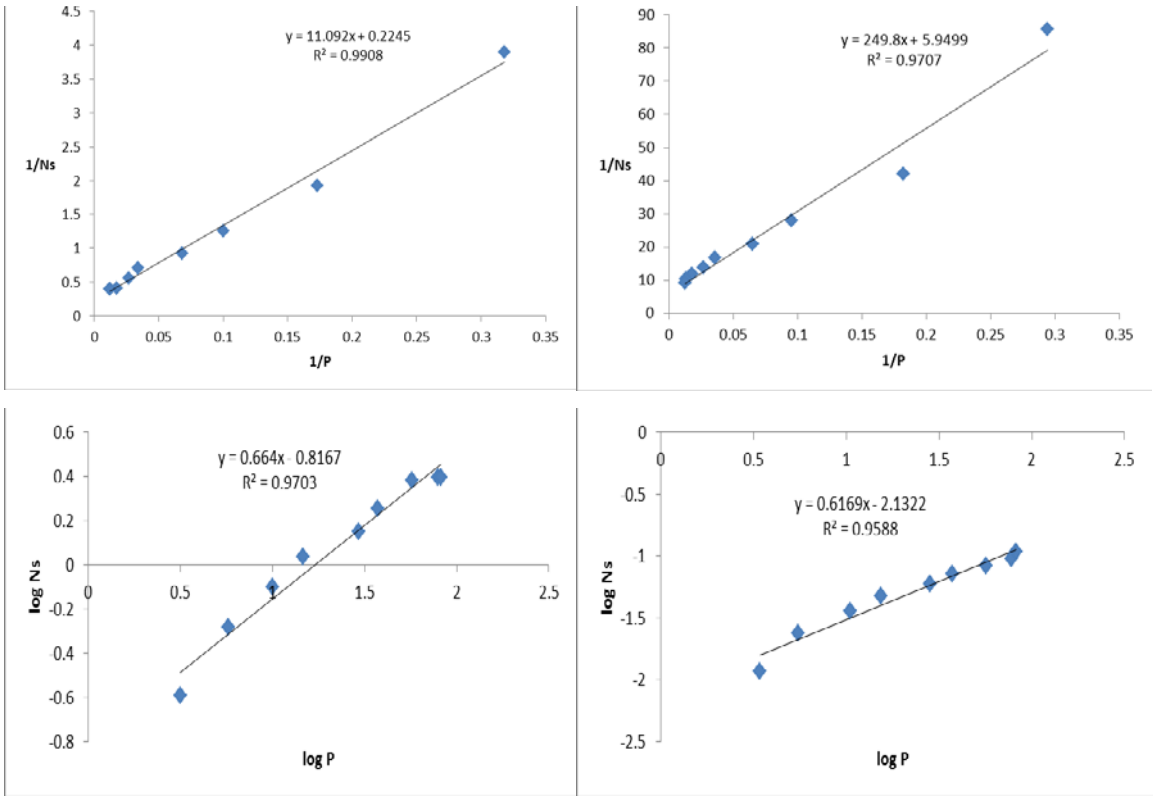

Figure H13: EM CO_2 and CH_4 Langmuir and Freundlich model regressions

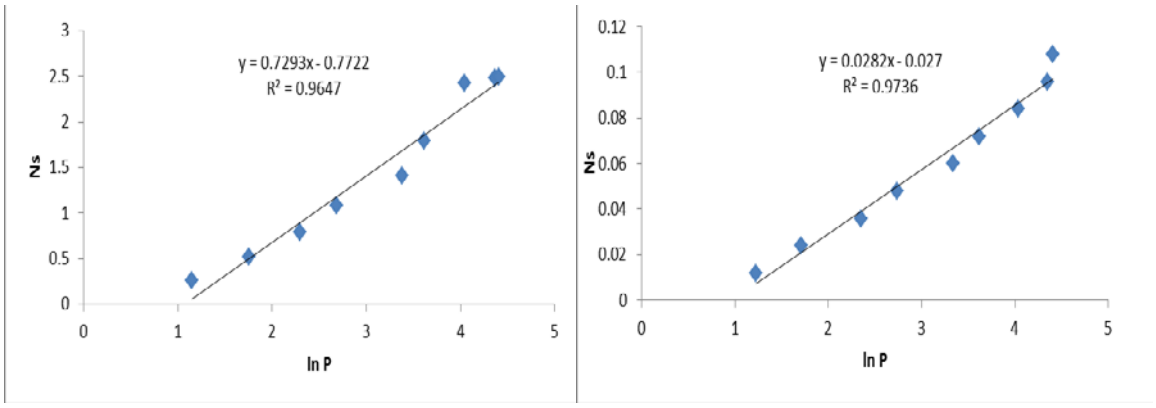

Figure H14: EM CO_2 and CH_4 Temkin model regressions

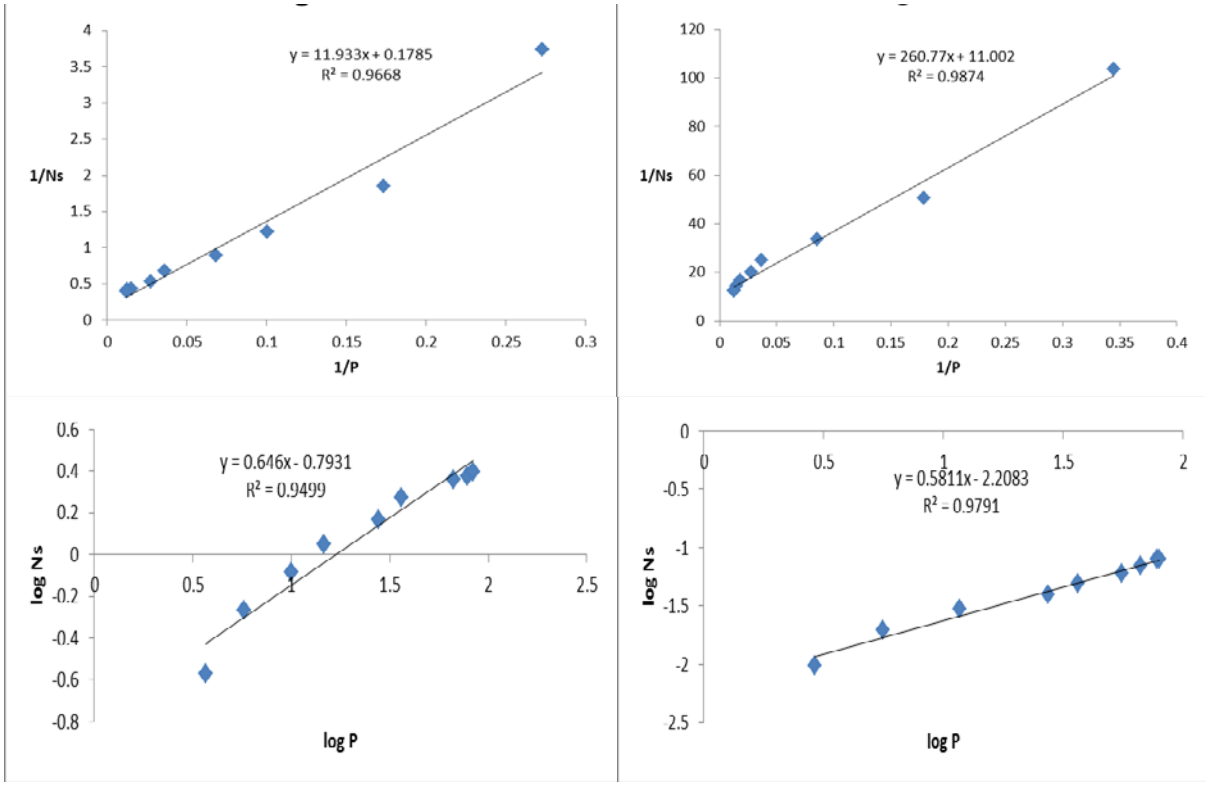

Figure H15: SF CO_2 and CH_4 Langmuir and Freundlich model regressions

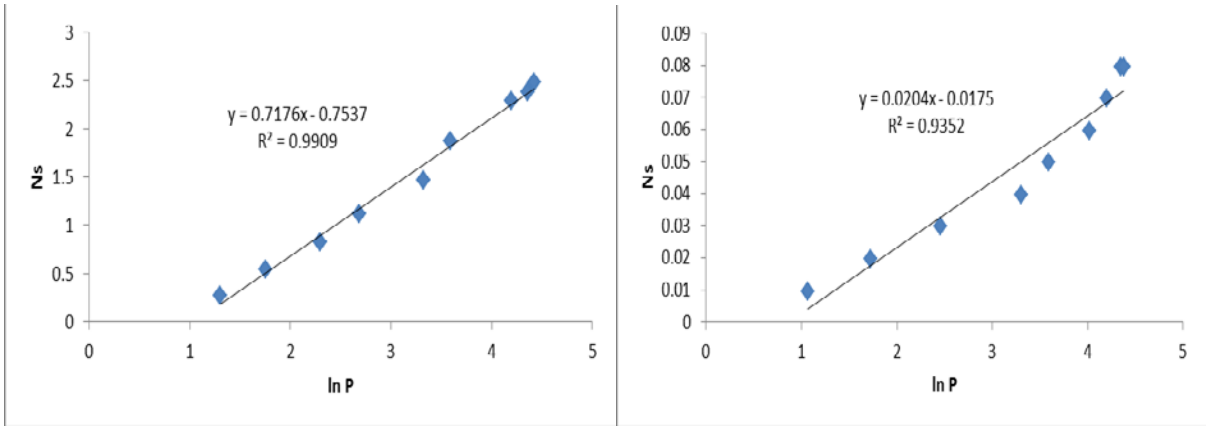

Figure H16: SF CO_2 and CH_4 Temkin model regressions

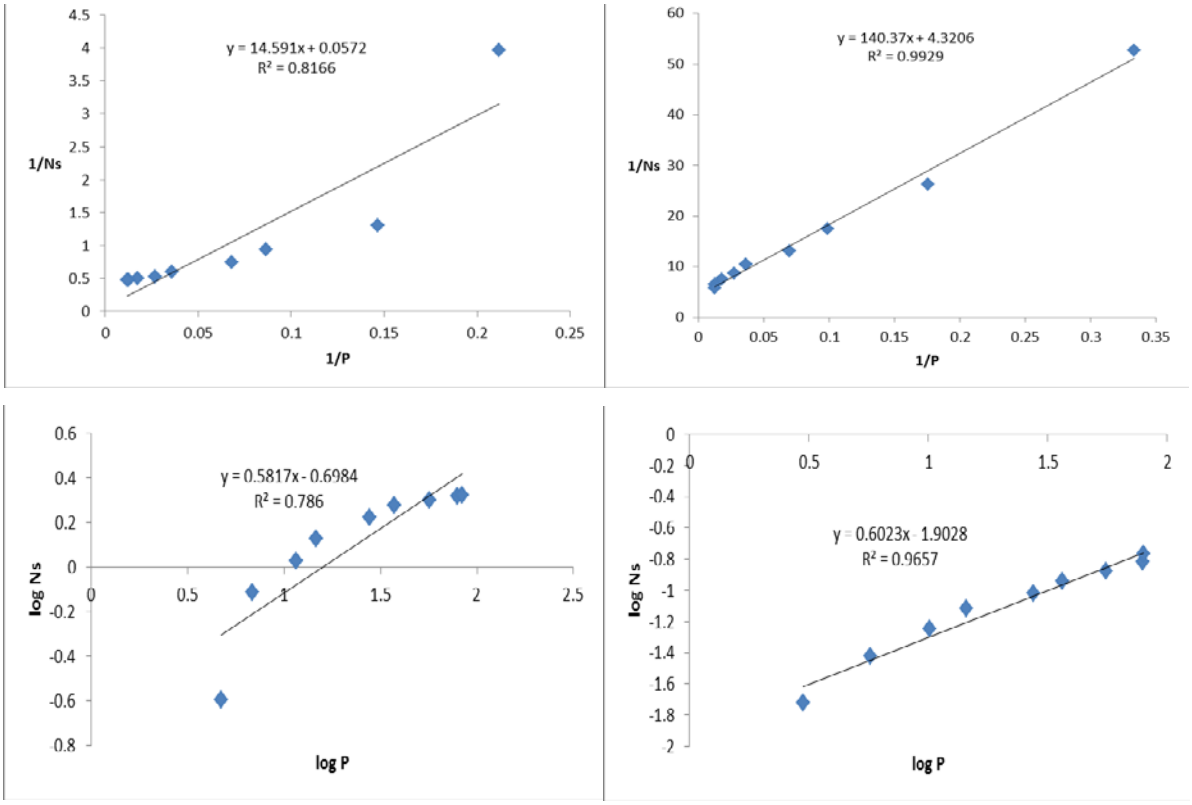

Figure H17: WG CO_2 and CH_4 Langmuir and Freundlich model regressions

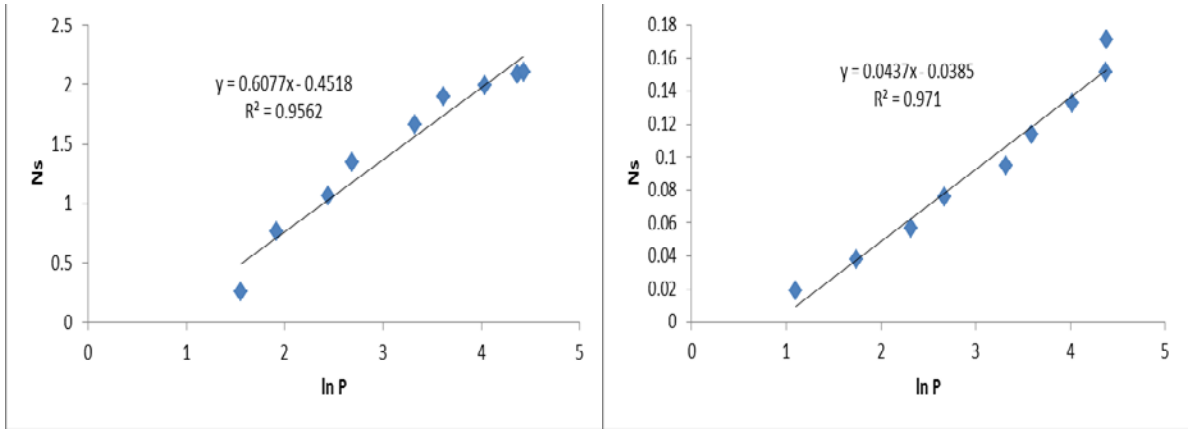

Figure H18: WG CO_2 and CH_4 Temkin model regressions

APPENDIX H3: MODELLING DATA FOR CYCLIC INJECTION OF CO_2: CH_4 DESORPTION FOR CH_4 SATURATED SAMPLES TO SUPERCRITICAL PRESSURE AT 55 ^oC

As done with other experimental results, the CH_4 desorption results at temperature of 55^oC was modelled using the three mathematical models. Only the CH_4 desorption results at 55 ^oC are presented here together with regression analysis plots. Model fitting for CO_2 adsorption at 55 ^oC has already been discussed and concluded in Section 4.8.3 and will not be included here to avoid repetition of discussion of the similar trends and findings.

Langmuir, Temkin and Freundlich. Traditionally Langmuir isotherms best fit adsorption and desorption data but other models like Temkin and Freundlich proved to fit data (Harpalani, et al 2006). As expected, the data fitted well as type one models' that best describe monolayer pore filling on the coal surface. Comparing the R^2 values for the model fits for the different coals it can clearly be seen that Langmuir best fits all the data for desorption with its lowest R^2 of 0.9707 recorded for model for Ermelo. Temkin and Freundlich also proved to be good models for the data since the R^2 values are all above 0.96 except the one for BL at 0.9588. At high pressures the data does not perfectly fit to the models which might be because the models were developed for incorporating the effect pressures and may need modification to account for incremental temperatures that were used in the experimental work for this project.

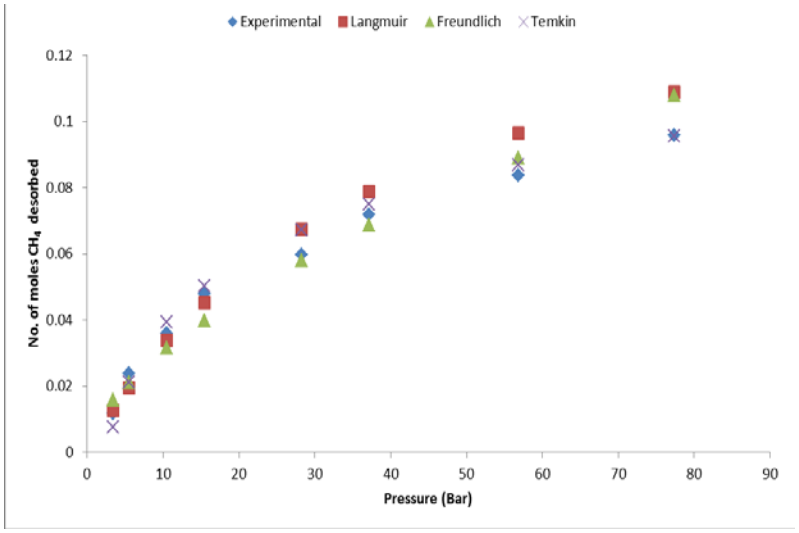

Fig: 4.62. Model fit for EM CH_4 desorption isotherm

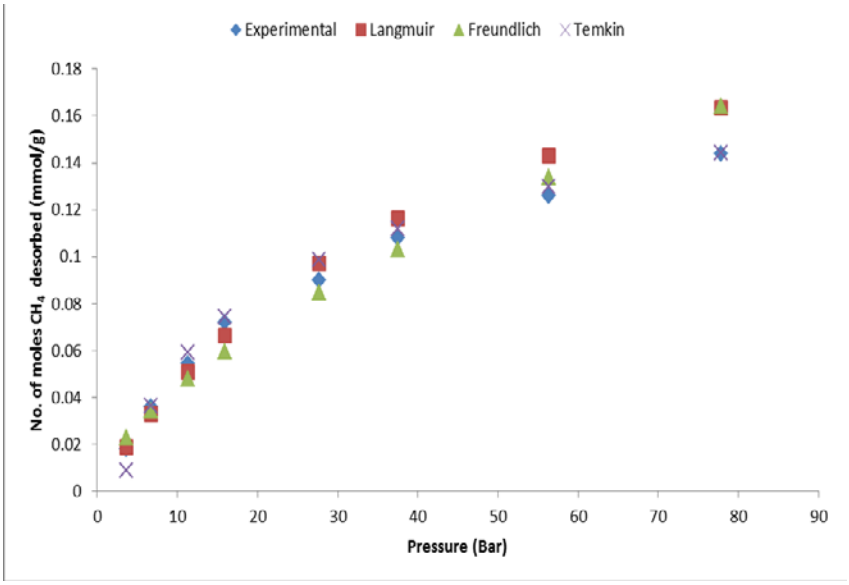

Fig 4.63 Model fit for BL CH_4 desorption isotherm

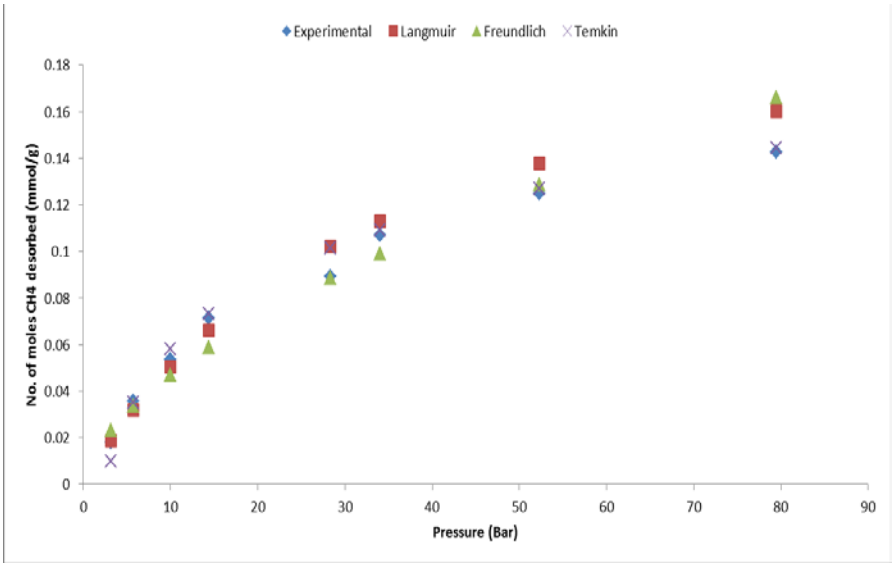

Fig. 4.64 Model fit for the TN CH_4 desorption isotherm

The experimental CH_4 desorption data obtained was fit to three models that are predictive of the sorption capacities for these conditions. The three models that were used are Langmuir, Temkin and Freundlich. Traditionally Langmuir isotherms best fit adsorption and desorption data but other models like Temkin and Freundlich proved to fit data (Harpalani, *et al*., 2006). As expected, the data fitted well as type one models' that best describe monolayer pore filling on the coal surface. Table H2 shows the correlation coefficients calculated for the model models and data.

Table H2: Langmuir, Freundlich and Temkin model parameters

Model	**Langmuir**			**Freundlich**			**Temkin**		
Parameter	**R^2**	**a**	**b**	**R^2**	**n**	**K_F**	**R^2**	**b_T**	**A_T**
TN CH_4	0.989	0.2329	0.0277	0.9616	1.642	0.0116	0.9741	61437.9	0.403
BL CH_4	0.991	0.26116	0.0214	0.965	1.5659	0.0102	0.9754	58226.3	0.341
EM CH_4	0.971	0.168	0.0238	0.9588	1.621	0.0074	0.9736	90849	0.384

Comparing the R^2 values for the model fits for the different coals it can clearly be seen that Langmuir best fits all the data for desorption with its lowest R^2 of 0.9707 recorded for model for Ermelo. Temkin and Freundlich also proved to be good models for the data since the R^2 values are all above 0.96 except the one for BL at 0.9588. At high pressures the data does not perfectly fit to the models which might be because the models were developed for incorporating the effect pressures and may need modification to account for incremental temperatures that were used in the experimental work for this project.

Linear Regression Plots:

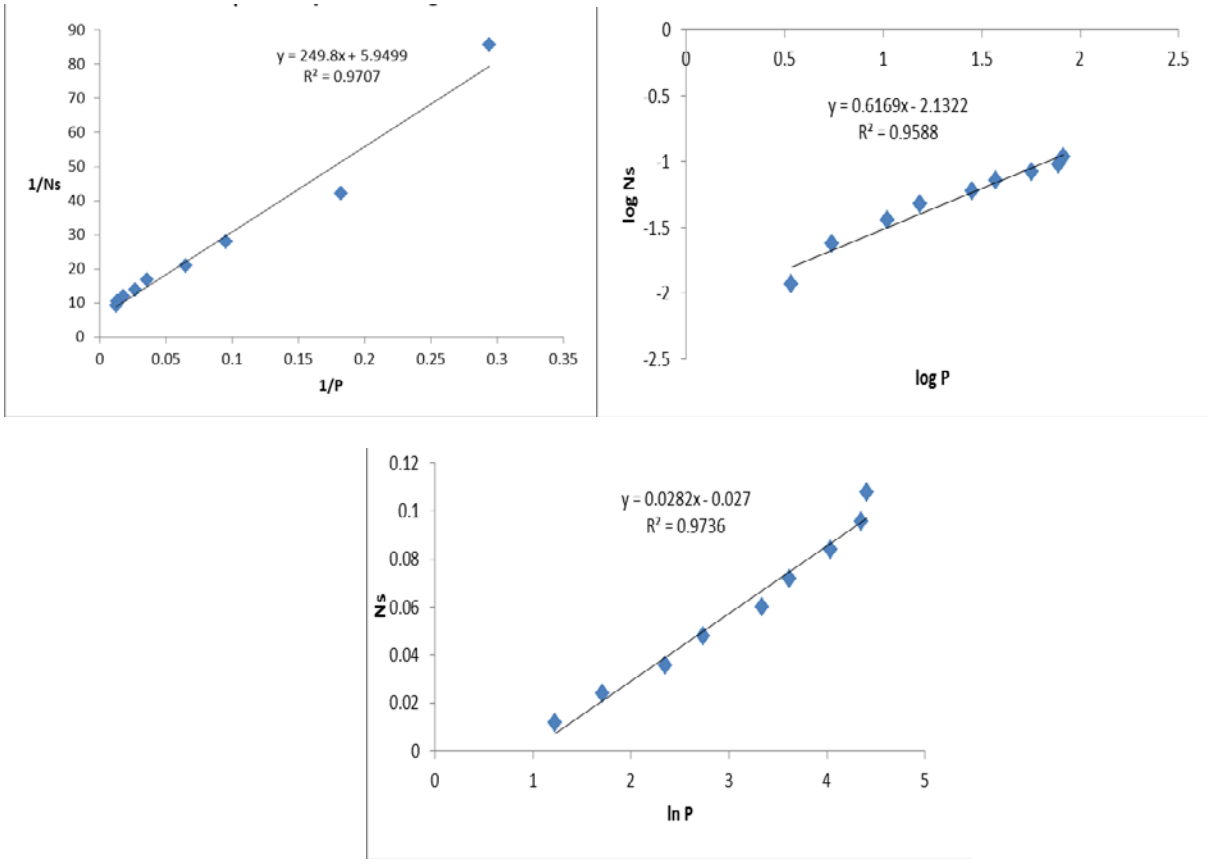

Figure H19: EM CH_4 Langmuir, Freundlich and Temkin model regressions

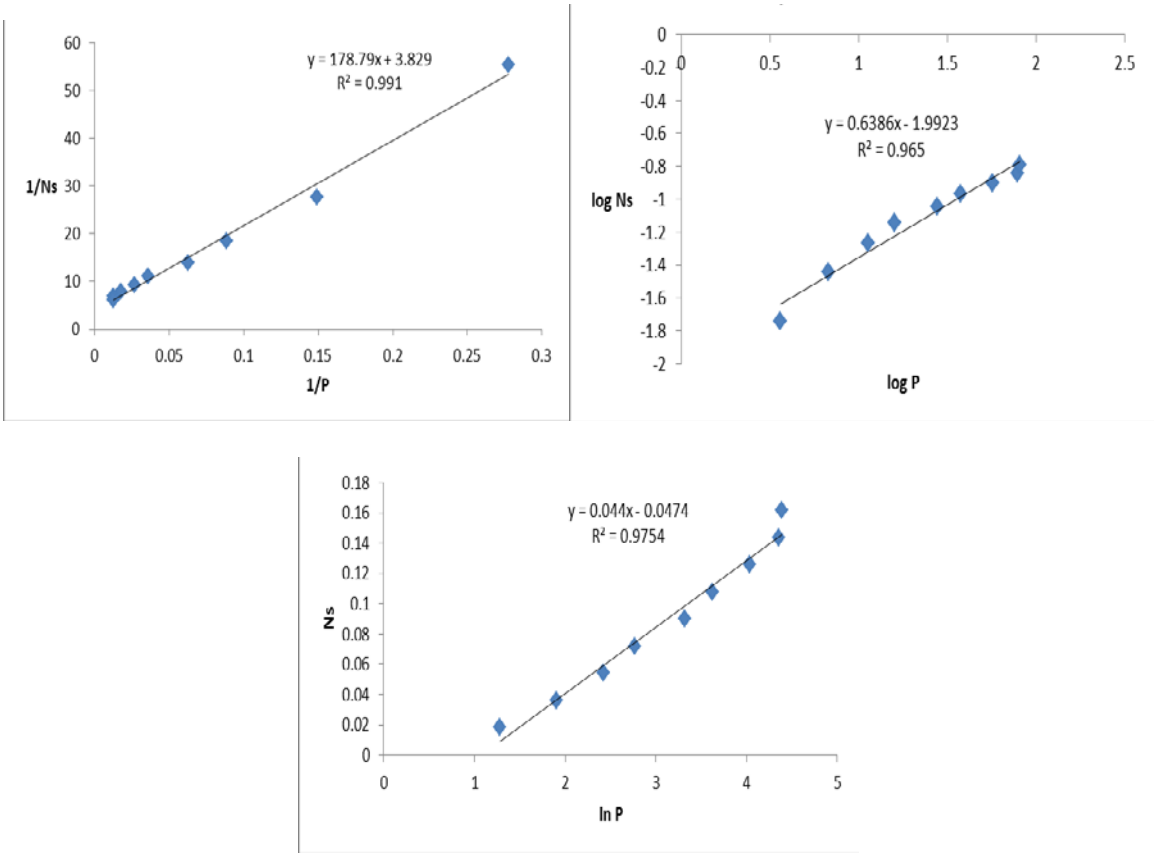

Figure H20: BL CH_4 Langmuir, Freundlich and Temkin model regressions

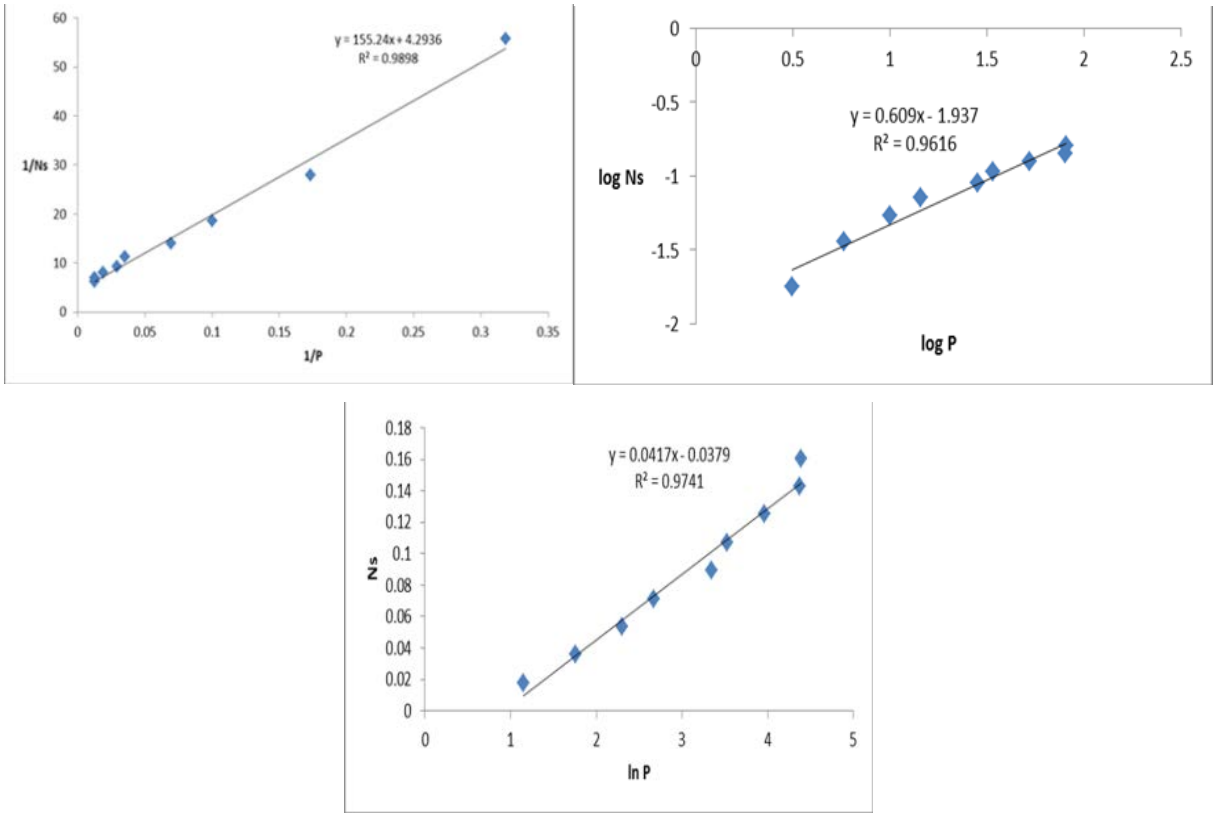

Figure H21: TN CH_4 Langmuir, Freundlich and Temkin model regressions